# CATALYTIC REARRANGEMENT OF ALPHA PINENE OXIDE USING SPINNING DISC REACTOR TECHNOLOGY

**by**

**Marija Vicevic BSc.**

**Thesis submitted for the degree of Doctor of Philosophy in the School of Chemical Engineering and Advanced Materials of the University of Newcastle Upon Tyne**



**Process Intensification and Innovation Centre (PIIC)**
**School of Chemical Engineering and Advanced Materials**
**University of Newcastle Upon Tyne**
**Newcastle Upon Tyne**
**U.K.**

**July 2004**

# ABSTRACT

This investigation explores the use of environmentally friendly solid acid catalysts based on immobilised Lewis acids in liquid phase organic reaction using the spinning disc reactor. The reaction studied was the rearrangement of α-pinene oxide to campholenic aldehyde, which is an important intermediate used by the fragrance industry in the synthesis of santalol (sandalwood). By focusing on liquid phase reactions and by addressing the particular problems associated with catalysis for such reaction systems the aim of this work is to develop new catalytic technology of value to the highly successful UK fine and speciality chemical industries, where acid catalysis is widely used but normally involves the use of corrosive and toxic reagents, unselective processes, and the production of unacceptable levels of hazardous waste.

The performance of a compact catalytic spinning disc reactor (SDR) with good heat and mass transfer characteristics for continuous conversion of α-pinene oxide to campholenic aldehyde using supported $Zn(OTf)_2$ catalysts was studied. The spinning disc runs were performed at various conditions and conversion and selectivity were monitored. A 100% conversion of α-pinene oxide was easily achieved for most of the conditions. Lower residence time enhanced selectivity towards aldehyde up to a maximum of 82%, at 60% conversion. SDR empirical models were developed and activation energies determined for each catalyst used. Comparison of SDR with batch process is also made.

Results suggest that the catalytic SDR can significantly enhance the reaction rates, reaction selectivity and improve process safety whilst eliminating the loss of catalyst. The findings of this investigation indicate that the vision of realising a truly intensified plant using green chemistry to achieve greener technology is a real possibility.

**Keywords**: Process Intensification, Green Chemistry, Spinning Disc Reactor, Rearrangement of α-pinene oxide, Campholenic aldehyde

# ACKNOWLEDGEMENTS

I would like to take this opportunity to thank my supervisors Dr R.J.J. Jachuck and Prof Keith Scott for giving me a chance to work with them. I would also like to thank Dr Boodhoo for constant support.

My sincere gratitude goes to fellow members of the Process Intensification and Innovation Centre, for creating a wonderful place to work in: Mileta, Natasha, Liza, Paul, Sarah, Matt – when I think of the time related to my studies I will always think of you.

This work would not be possible without extremely helpful and skilful people from our workshop. Therefore I would like to thank you all, Mr Eric Horsley, Mr Stuart Latimer, Mr Brian Glover, Ian, Jimmy, Brian D. and George.

Thanks to my family without whose support I would not be where I am today. Thanks mom and dad. Thanks to my sister for always being there for me.

Finally – thank you Mileta for everything.

# TABLE OF CONTENTS

# TABLE OF FIGURES

# LIST OF TABLES

# NOMENCLATURE

| | | Units |
|---|---|---|
| A | Pre-exponential factor (Arrhenius equation) | - |
| $A$ | Area | $m^2$ |
| $A_i$ | Peak area of the solute i | - |
| a | Parameter | - |
| $a_{Cor}$ | Coriolis acceleration | $m\ s^{-2}$ |
| b | Parameter | - |
| C | Integration constant (units as concentration); Constant | - |
| $\Delta C$ | Molar heat capacity | J/(mol K) |
| $C_p$ | Heat capacity | kJ/(kg K) |
| $C_x$ | Concentration of component x | $mol/m^3$ |
| c | Parameter | - |
| $c_p$ | Specific heat capacity | J/(kg K) |
| D | Diffusion coefficient | $m^2/s$ |
| d | Diameter | m |
| $d_e$ | Equivalent hydraulic diameter | m |
| $d$ | Channel width | m |
| E | Ekman's boundary layer thickness | m |
| $E_a$ | Activation energy | kJ/mol |
| $F_G$ | Correction factor | - |
| f | Frequency (rotation rate) | Hz |
| $\Delta G$ | Gibbs free-energy change | J/mol |
| g | Gravitational acceleration | $m\ s^{-2}$ |
| $\Delta H$ | Change in enthalpy | J/mol |
| I | Parameter | - |
| $j_h$ | Heat transfer factor | - |
| K | Equilibrium constant | - |
| $K$ | Overall mass transfer coefficient | m/s |
| k, $k_x$ | Rate constant | * |
| L | Characteristic length | m |
| l | Distance | m |
| M | Active site on the catalyst | - |
| $M_0$ | Total number of surface atoms | - |
| $M_x$ | Molar mass of component x | kg/mol |
| m | Mass | kg |
| $\dot{m}$ | Mass flowrate | kg/s |
| N | Rotational speed | rpm |
| N | Number of transfer units | - |
| $\Delta n$ | Mole change of reaction | - |
| n, $N_A$ | Number of moles | mol |
| $n$ | Number of times a catalyst is used | - |
| P | Pressure | Pa, bar |
| $P$ | Catalyst productivity | - |

| | | |
|---|---|---|
| p | Pressure or partial pressure | Pa, bar |
| Q, $Q_v$ | Volumetric flowrate | $m^3/s$ |
| $\dot{q}$ | Rate of heat flow | W |
| R | Universal gas constant = 8.314 | J/(mol K) |
| $R^2$ | Fitting factor | - |
| $R_i$ | Absolute response factor of solute i | - |
| $r_A$ | Reaction rate | * |
| r | Radial distance | m |
| $\Delta S$ | Change in enthropy | J/mol |
| S | Substrate molecule | - |
| *S* | Scaling factor | - |
| T | Temperature | $^0C$ or K |
| $\Delta T$ | Temperature rise | K |
| t | Reaction time; time | s |
| $t_{res}$ | Mean residence time | s |
| V | Volume | $m^3$ |
| U | Overall heat transfer coefficient | $WK^{-1}m^{-2}$ |
| v | Velocity | m/s |
| $\bar{v}$ | Average film velocity | m/s |
| W | Catalyst loading | wt% |
| $W_i$ | Solute quantity | - |
| x | Disc thickness | m |
| $x_A$ | Conversion | % |
| $Y_P$ | Yield | % |
| y | Thickness of the catalyst layer | m |
| z | Vertical upward distance | m |

Greek

| | | |
|---|---|---|
| $\alpha$ | Film heat transfer coefficient on disc surface | $kW/m^2K$ |
| $\alpha_m$ | Mass transfer coefficient | $kg/(m^2s)$ |
| $\alpha$ | Angle | $^0$ |
| $\beta$ | Coefficient of expansion | 1/K |
| $\delta$ | Average film thickness | m |
| $\phi$ | Rate of mass transfer | mol/s |
| $\dot{\gamma}$ | Shear rate | $s^{-1}$ |
| $\eta$ | Heat-transfer effectiveness | - |
| $\lambda$ | Thermal conductivity | $Wm^{-1}K^{-1}$ |
| $\mu$ | Dynamic viscosity | Pa s |
| $\nu$ | Kinematic viscosity | $m^2/s$ |
| $\nu_X$ | Stoichiometric coefficient for component X | - |
| $\nu$ | Circumferential velocity | m/s |
| $\theta$ | Angle of inclination of plane surface to the horizontal | - |
| $\rho$ | Density | $kg/m^3$ |
| $\sigma$ | Stefan-Boltzmann constant = $5.67x10^{-8}$ | $W/(m^2K^4)$ |
| $\sigma$ | Symmetry number | - |
| $\sigma_P$ | Selectivity | % |

| | | |
|---|---|---|
| $\tau_C$ | Contact time | s |
| $\varpi$ | Axial velocity component | m/s |
| $\omega$ | Angular velocity | $s^{-1}$ |
| $\omega_x$ | Mass fraction of component x | - |
| $\nabla$ | Del operator $(= i\frac{\partial}{\partial x} + j\frac{\partial}{\partial y} + k\frac{\partial}{\partial z})$ | $m^{-1}$ |

Dimensionless group

| | | |
|---|---|---|
| Gr | Grashof number | - |
| Pr | Prandtl number | - |
| Re | Reynolds number | - |
| Ta | Taylor number | - |

Symbols

| | |
|---|---|
| OTf | Triflate (Trifluoromethanesulphonyl group), $CF_3SO_3^-$ |
| KX | K stands for Kiesel (Silica), X for pore size |
| $HMS_x$ | Hexagonal mesoporous silica, with pore size x |

Subscripts

| | |
|---|---|
| ad | Adiabatic |
| av | Average |
| c | Cold |
| cat | Catalyst |
| D | Disc surface |
| e | Equvivalent |
| ext | External |
| f | Formation; also: fluid |
| h | Hot |
| HTF | Heat transfer fluid |
| i | Inlet |
| int | Internal |
| lm | Logarithmic mean |
| o | Outlet |
| p | Product |
| PF | Process fluid |
| res | Residence |
| r, $\theta$, z | Radial, angular and vertical directions respectively in cylindrical co-ordinates |
| x, y, z | x, y and z-directions respectively in rectangular Cartesian co-ordinates |
| w | Wall |

# CHAPTER 1

## INTRODUCTION

In a today's world it is becoming increasingly difficult to abide by the latest innovative processes and technologies in a very competitive market. Consumers not only demand a product to be reasonably cheap, which, for industrialised countries, is a problem in itself (since developing countries have an advantage of inexpensive workforce), but there is also an overwhelming concern about environment and safety issues which need to be addressed and resolved sooner rather than later. In order to stay on the market, industries need to act fast. It is a double challenge that they are facing now in order to evolve [1]:

1. Selecting processes only on the basis of economic exploitation is an old attitude which needs to be rejected. Implementation of novel non polluting processes is necessary with the intention of improving selectivity, overall safety, reduction of raw materials and energy losses, health and environmental aspects as well as materials recyclability. Only this will increase the final product saleability and ensure the sellers to stay on the global market.

2. Traditional chemistry needs to be surpassed and new speciality and active material chemistry employed to facilitate better end-product properties (such as its quality, shape or size) which could be easily controlled by new process parameters.

It is also very important to identify the latest demands and take action fast both in improving and promoting the product as soon as possible to be first on the market.

Better understanding of elementary phenomena makes it viable to envisage new operating modes of equipment, or to design novel equipment based on scientific principles. The way forward is to put Process Intensification (PI) into practice.

## 1.1 PROCESS INTENSIFICATION

A long time ago, when an idea of PI was just in a cradle, it was thought that by cutting down of the size of equipment in a chemical plant such as reactors, heat exchangers and separators by applying PI techniques, a *reduction in capital cost* of production system would be achieved [2]. Although it would be good to achieve this goal only, all the other immensely attractive advantages of PI technology were not foreseen at the beginning.

As mentioned above, money has always been a primary issue – if less material is present, capital cost decreases; vessels, pipes, structures and foundations become *smaller and cheaper*. The obvious advantage of using PI techniques – a small, compact, highly intensified plant could, in the near future, replace the existing plants, therefore create a far more attractive sight. A pilot plant in such a small size could be moved to manufacturer's sites, which would enable them to study the suitability of PI in real-time on their own processes [3]. As an example, traditionally, Caro's acid ($H_2SO_5$) has been produced by reacting concentrated sulphuric acid with hydrogen peroxide at sub-ambient temperatures to avoid product decomposition. The equipment was bulky and relatively costly – typically, a refrigerated 30-litre reactor vessel operating with a residence time of 30 minutes was needed to produce 300 kg of product per day. By applying the principle of intensification a continuous adiabatic reactor has been developed with an output three times greater than the previous unit, using a reactor volume of only 20 ml (equivalent to a size reduction of 1500:1). The residence time was less than a second and it was capable of operating without cooling [4]. Intensification is becoming a reality.

Lately, it became very important for the chemical process industries to remain cost competitive, but in an environmentally friendly, "green" manner. Every now and then you hear about disasters taking place all over the world. A number of fatal incidents have occurred involving large inventories of hazardous materials and exothermic runaways in batch reactors [5-7]. In the case of disaster in Bhopal (India) in 1984, material which leaked killed 2000 people and was in fact convenient intermediate. That is why process minimisation is very important, "*what you don't have, can't leak*" [8, 9]. Having an ultra-compact process plant, inherently *safer* designs can be accomplished by reducing the inventory of hazardous material and

hence the intrinsic safety of a process can be substantially improved [10]. Furthermore, novel reactor designs based on the PI concept will enable practising of the *"clean" technology*. High selectivity operations in intensified reactors will reduce or eliminate the formation of unwanted by-products, which can cause irreversible damage to the environment. Along with renewed interest for PI there is also a greater awareness for Green Chemistry, as the two cannot be separated these days.

Additionally, one of the objectives of PI is to move away from batch processing, often associated with inherent processing difficulties, to small semi-batch or *continuous* reactors [11], the latter giving more efficient overall operation especially in the case of hugely exothermic reactions whereby the heat can be removed continuously as it is being released. Another attractive benefit of the PI is the *improved energy efficiency* [12] envisaged in intensified unit operations. There is an enormous and urgent need for the development of new process technologies, which will utilise energy in an efficient way. Two of the most fundamental operations in chemical engineering processes, heat and mass transfer, as well as mixing, can be enhanced in intensified units [13-15], thus the interest from the industry is potentially enormous.

## 1.2 INTENSIFICATION STRATEGIES

In order to improve the performance of equipment, e.g. heat transfer, many techniques can be employed, which may be categorised as active or passive in nature. Surface roughening and surface extensions in the forms of fins are some of the passive methods which have long been used on a commercial basis [16] and have been proven to give better film heat transfer coefficients in evaporators. Some of the active methods are stirring, scraping, surface vibration and surface rotation. One of the simplest and most commonly met (wherever adequate heat and mass transfer rates are needed) is stirring (agitation). For more specific applications scraping and surface vibration can be implemented involving complex installation methods. Surface rotation has provoked an interest in academic workers for many years. First successful centrifugal evaporator used in sea-water desalination was developed in the 1950s as a result of Hickman's research efforts into two phase heat transfer on

spinning disc [17]. Some of the benefits from the exploitation of high centrifugal fields created by rotation are:

- The rotational speed of the spinning surface provides an additional degree of freedom which can be effortlessly controlled for optimum equipment performance;

- Extremely high gravity fields generated as a result are capable of producing very thin films in which heat transfer, mass transfer and mixing rates are expected to be greatly intensified;

- Applications, in which the solid content of a process fluid often poses a number of problems with regard to fouling in conventional devices, can be handled by the rotating equipment. The rotating action in itself provides a scraping or 'self-cleaning' mechanism strong enough to shift any solid deposit away from the surface of revolution, thereby ensuring maximum exposed area at all times during operation;

- The effect of very short and controllable residence times achieved under the centrifugal action will enable heat sensitive materials to be processed with minimised risk of degradation.

The practical implementation of intensified processes will engage the application of entirely ground-breaking designs. So far industrialists were hesitant to embrace the novel and therefore unestablished nature of the technology, even though the advantages could be enormous. But the interest in PI is nevertheless huge and there are more and more industries keen on exploring new and exciting opportunities that PI has to offer [18].

## 1.3 SPINNING DISC TECHNOLOGY

The spinning disc technology uses the centrifugal accelerations to create thin (100-200 μm), highly sheared films on rotating surfaces (Figure 1.1). Studies have indicated that the fluid dynamics within these films result in significant enhancement in heat and mass transfer rates. For that reason it is expected that a reactor based on this technology should allow rapid mixing in the liquid film, short liquid residence time, rapid solid/liquid heat/mass transfer and rapid liquid/vapour heat/mass transfer

[19]. This makes spinning disc reactors strong contenders for performing fast exothermic reactions and reactions which are limited by mass transfer rates. The Process Intensification and Innovation Centre (PIIC) at Newcastle University has studied and developed this technology (namely a spinning disc reactor) with possible applications in processes involving separation, heat transfer, gas liquid reactions, crystallisation etc. [17, 20]. Previous work carried out on rotating discs has concentrated mostly on understanding the hydrodynamics of thin film flow [21-24] and measuring heat and mass transfer rates from solid to liquid and liquid to vapour [22, 25-27].

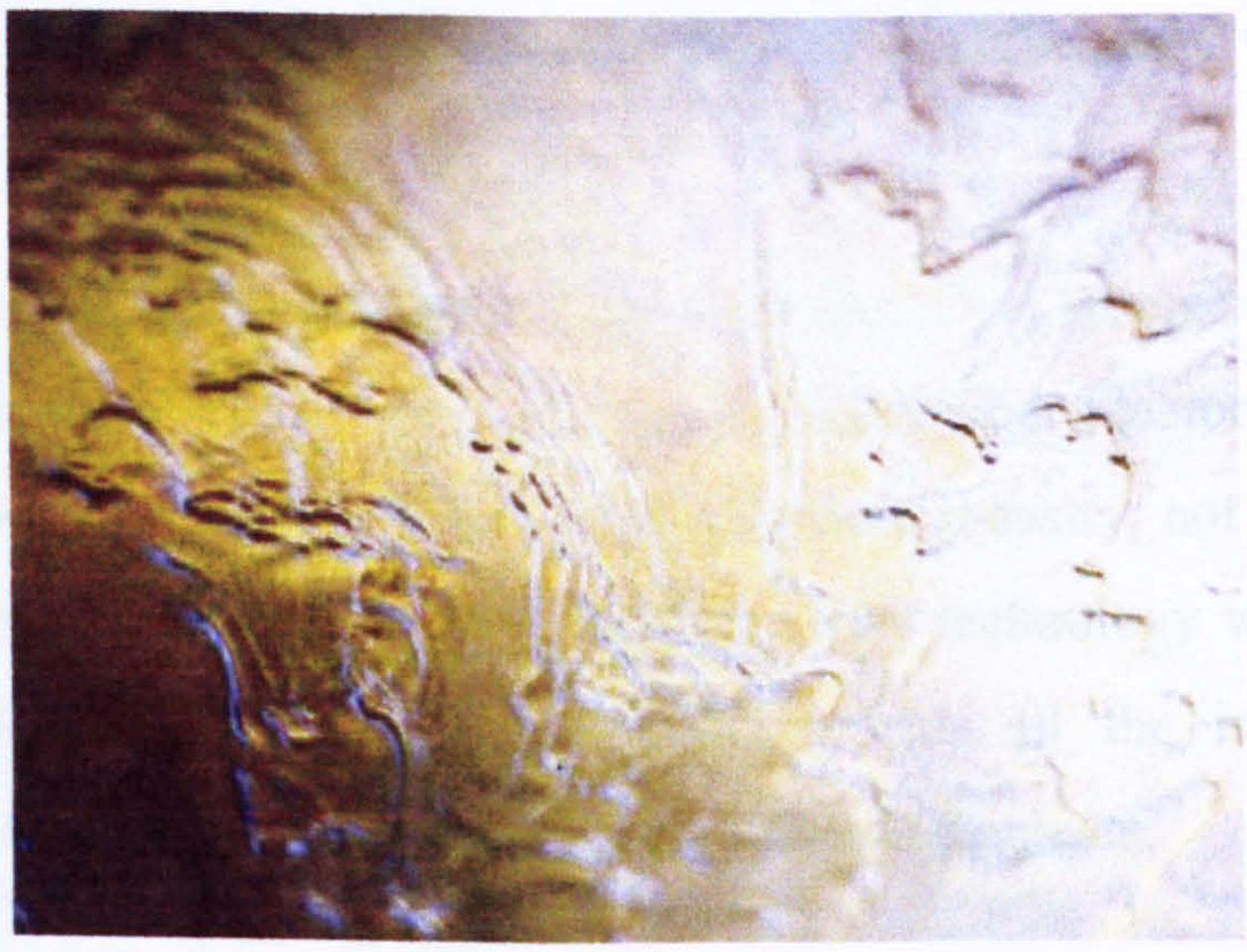

**Figure 1.1. Thin film on the surface of the rotating disc**

In addition to significant enhancement in the heat and mass transfer rates, it has also been demonstrated that a reactor based on this technology may have the following advantages:

- Rapid mixing in the liquid film;
- Short liquid residence time;
- Rapid solid/liquid heat/mass transfer and
- Rapid liquid/vapour heat/mass transfer.

A typical example for the mass transfer limited reaction is the polymerisation of unsaturated esters where the reaction is driven by the removal of water from the

reaction system. Previous studies [19] have shown that using spinning disc reactor systems can significantly reduce the total reaction time for the manufacture of unsaturated polyester. Studies carried out on the polymerisation of styrene have also indicated that, apart from increasing the rate of polymerisation, the disc reactor can also improve the product quality by tightening the molecular weight distribution of the polymers [28].

The sectors of the chemical industry being targeted with the spinning disc technology are the pharmaceutical and fine chemicals industries. Traditionally, reactions have been carried out in batch processes which are associated with inherent processing difficulties, especially in the case of hugely exothermic reactions [29]. As a result, there is a clear motivation to replace batch reactors with intensified, continuous units [11].

A process can be improved in many ways, but it is a reactor which is still the heart of it. This study will involve the use of spinning disc reactor with the aim of intensifying catalytic process utilised by the fragrance industry, not only to improve the product quality, but to find novel, greener, safer technology which can match today's thirst for carefully designed processes with all the issues mentioned previously well thought of; and essentially, quality end-products.

# CHAPTER 2

## LITERATURE REVIEW

### 2.1 INTRODUCTION TO INDUSTRIAL REACTORS

In the first part of this Chapter, reactors used for industrially utilised chemical reactions will be introduced. As said in previous section, reactor is the most important part of the process, therefore it is important to understand the capabilities of currently available technologies and see the potential for implementation of new ones.

Chemical reactions are classified from various viewpoints with individual characteristics. On the basis of their kinetic behaviour, reactors can be classified as follows [30] (Figure 2.1).

1. Batch type
2. Continuous flow type

    a) Tubular reactor, plug flow

    b) Tank reactor, mixed flow.

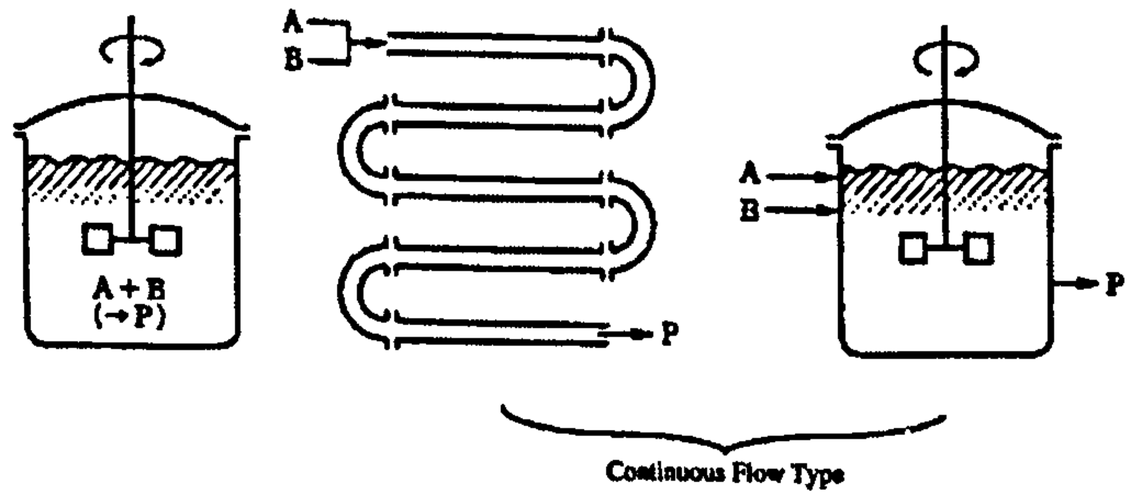


(a) (b) (c)

**Figure 2.1. Types of reactor: (a) Batch type, (b) Tubular reactor, (c) Tank reactor**

**Table 2.1. Comparison of characteristics of reactors**

| Comparison item \ Reactor | | Batch | Continuous flow | |
|---|---|---|---|---|
| | | | Tubular type | Tank type |
| Ideal conditions | 1. Temperature, pressure, composition in reactor | Uniform at each moment | • Concentration changes in the direction of flow<br>• No gradient of reaction rate and temperature in radial direction<br>• No mixing and diffusion in axial direction | • Complete mixing<br>• Uniform composition (equal to that at the outlet) |
| | 2. Residence time distribution of reactant | None | None | Yes |
| Kinetic characteristics | 1. Required reaction volume (Equal conversion basis) | Relatively small | Relatively small | Large |
| | 2. Distribution of products (Consecutive reaction) | Large yield of intermediate product | Large yield of intermediate product | Small yield of intermediate product |
| | 3. Probability of reaction with specific composition ratio | Impossible | Impossible | Possible |
| Features | 1. Flexibility | Large | Small | Medium |
| | 2. Application | Multi-purpose and small-scale production | Mass production | Medium |

Operation in batch reactor starts by feeding the raw materials into the reaction vessel, followed by sealing or heating if necessary. After several hours or days of operation, the reaction proceeds nearly to completion and it is terminated by cooling of reactor, followed by the recovery of the product from the reactor. This type is generally used for liquid-phase systems with relatively slow reaction rate. Commercially it is suitable for small-scale plants (dyes and pharmaceuticals).

In the continuous type raw materials are continuously fed and products taken out making it suitable for large-scale chemical processes with relatively high reaction rate at substantially constant operating conditions. In the case of the tubular reactor, highest concentration of raw materials is at the inlet of the reactor, gradually decreasing along the reactor, without back-mixing or diffusion of reacting molecules along the direction of the material flow, making the residence time of the molecules passing through the reactor equal (for all the molecules). In a tank reactor, however,

reactants are vigorously stirred, making this reactor completely mixed (if operated ideally), where the chemical composition and temperature are kept constant throughout the reactor vessel. In tank reactors molecules do not have the same residence time; average residence time can be determined instead by dividing the volume of the reactor by the feed rate in the volume under the reacting conditions, but it has to be kept in mind that some molecules remain in the reactor for a long time and others for short time only. Characteristics of each reactor can be observed in a comparison Table 2.1.

Furthermore, reactors can be classified into homogeneous and heterogeneous depending on their internal states. In the former type gas, liquid or solid (homogeneous) phase is present and in many cases materials are mixed uniformly before they are supplied to the reactor, hence changes in behaviour involving mass transfer do not normally take place. The later can contain two or more phases.

### 2.1.1 HOMOGENEOUS REACTORS

#### *2.1.1.1 Tubular reactors*

Tubular reactors and their modes (depending on locations of inlet and outlet locations for reactants and products) are shown in Figure 2.2. For heat transfer, two methods can be considered: one is transferring heat through the tube wall and the other is transferring heat through heat exchanger tubes into or out of the reactor (this method is used when relatively large diameters are used).

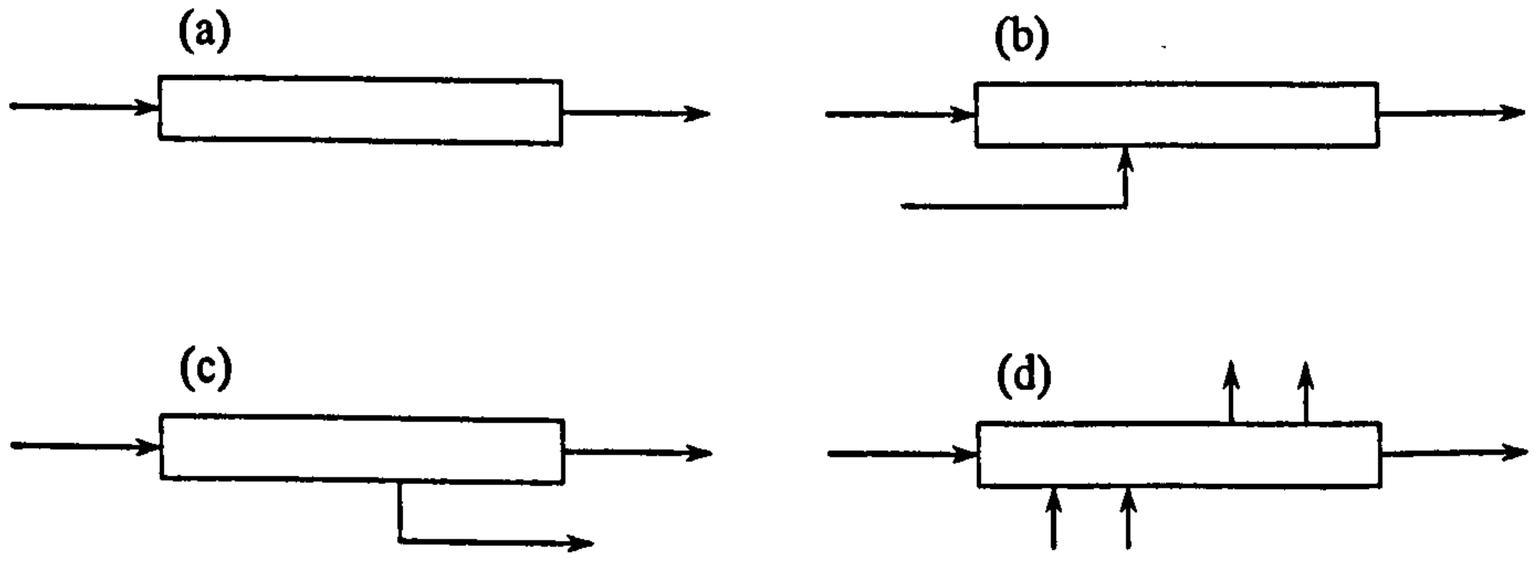


**Figure 2.2. Operational modes of tubular reactors: (a) single inlet and outlet; (b) multi-inlets and single outlet; (c) single inlet and multi-outlets; (c) multi-inlets and multi-outlets**

The larger the aspect ratio (length/diameter), the closer the flow turns to piston flow, which promotes ideal reactions and normally better selectivity. Small

tube diameters offer good heat transfer and are easy to control, however, if the diameter is too small, resistance to flow increases, which results in a large pressure drop between inlet and outlet.

Tubular reactors are used for continuous homogeneous reactions such as thermal cracking in a gas phase [31], neutralisation in a liquid phase [32], esterification with an acid catalyst, saponification and acid hydrolysis.

### *2.1.1.2 Stirred tank reactors (STR)*

Stirred tank reactor (as previously mentioned) is a mixing tank with perfectly mixed flow. The liquid phase is usually used in this type of reactor which can be operated with a batch, semi-continuous or continuous mode.

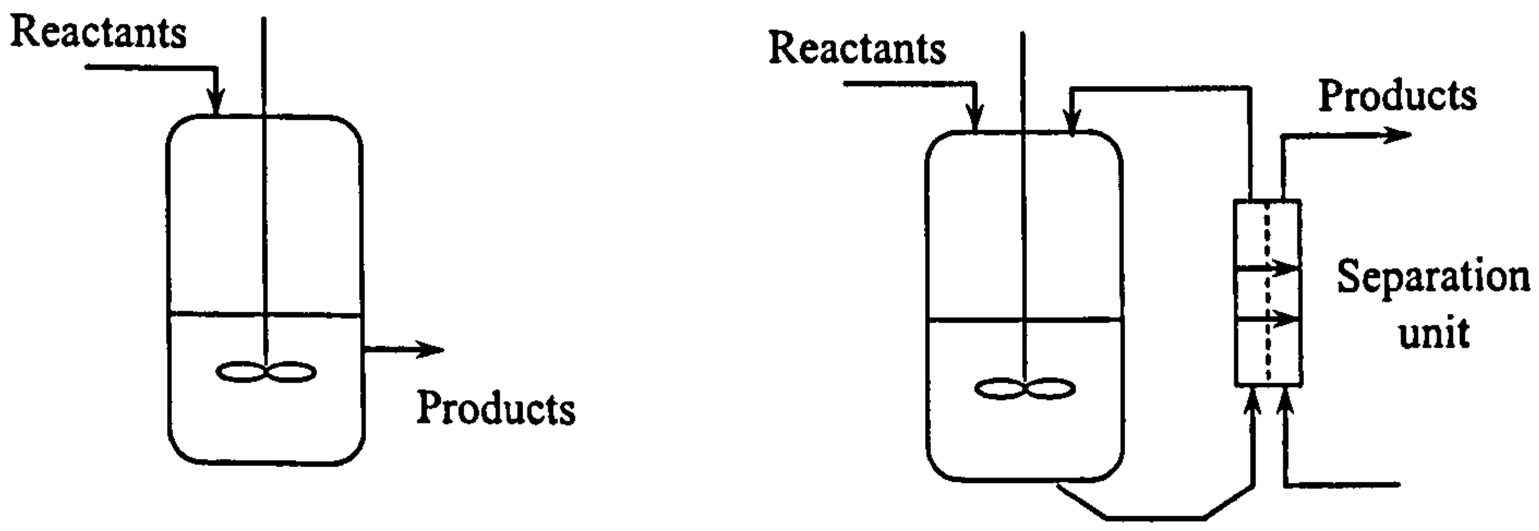


**Figure 2.3. Typical types of systems using stirred tank reactors (a) continuous stirred tank reactor (b) stirred tank reactor combined with separation unit**

Typical types of systems using stirred tank reactors are shown in Figure 2.3. Due to its good mixing performance and high capacity, this reactor is suited to regulate reactions which might succumb to runaway, or for the careful control of reacting conditions. Depending on the heat exchange method, stirring method and size of the reactor, there are slight differences in stirred tank structures. A mixing blade ought to be designed carefully when the reactants contain solid particles, when solids are formed by reaction, or when the viscosity of the materials is increased.

Stirred tank reactors are used for neutralisation, hydrolysis, esterification [33], amide formation, chelate formation as well as polymerisation [34].

#### *2.1.1.3 Other homogeneous reactors*

Reactors with an aspect ratio of about 3–20 (between tubular and STR) can be classified as column reactors. This reactor can be positioned vertically or horizontally (in which case it is called a lateral reactor). Circulation in this type of reactors is sometimes preferred to control reacting conditions (e.g. temperature and pH).

### 2.1.2 HETEROGENEOUS REACTORS

If more than one phase is present, reactor can be described as heterogeneous. These can be used for both non-catalytic and catalytic reactions. Further sub-division can be made within this group of reactors, as some of them are mainly used in laboratories, whilst some are more suitable for industrial exploitation.

#### *2.1.2.1 Laboratory scale reactors*

##### 2.1.2.1.1 Fixed bed reactor

Fixed beds are formed by packing solid particles in a reactor. Although catalysts are usually applied, there may be cases in which solids react with fluids, i.e., not the catalyst bed. Typical types of this reactor are shown in Figure 2.4. In a reactor of this type, fluid flow behaves similarly to plug flow, offering high conversion and good reaction selectivity. The reaction feed should be well designed in a fixed bed to disperse the feed of reactant uniformly over the cross-section. In addition to mass flow, temperature control is also crucial. Radial heat transfer is realised by radial fluid flow (convection) and by heat conduction through solids. Rate of heat transfer is relatively low in fixed beds therefore full attention must be devoted to temperature control.

Fixed bed microreactor is typically used for testing of 0.1 – 1 g of the catalyst and for catalyst screening. It works isothermally, but it is not ideal for kinetic studies.

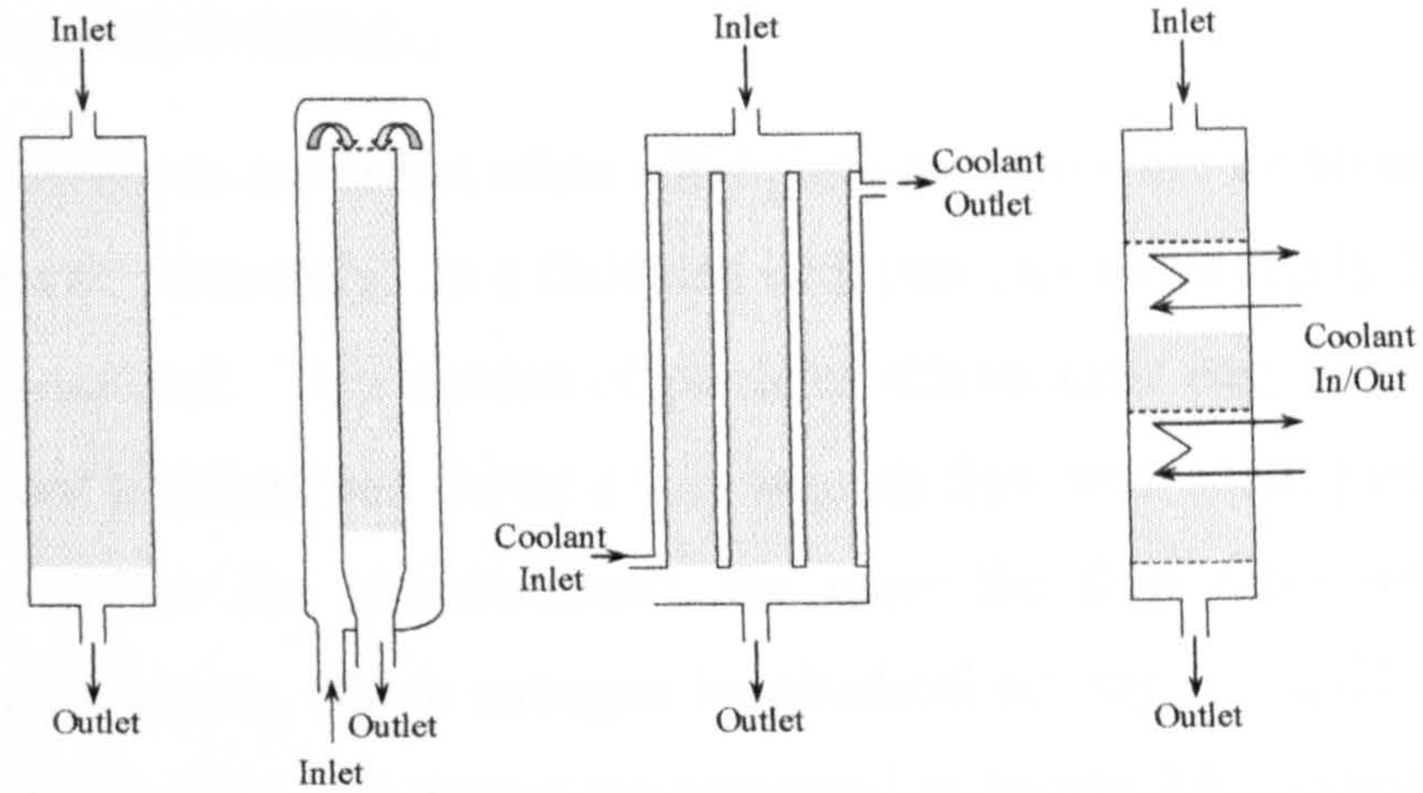


(a) (b) (c) (d)

**Figure 2.4. Several types of fixed bed reactor: (a) Down flow type, (b) Self-thermal-exchange type, (c) Cooling type, (d) Intermediate cooling type**

2.1.2.1.2 Moving bed reactor

Fixed beds offer fluid mixing close to that of piston flow with good reactor performance; however, solid particles can not be removed from the reactor. If the catalyst deteriorates or solid-gas reactions are performed, particles ought to be supplied and removed continuously (or semi-continuously) in order to perform steady state operations. Solid particles then move slowly in the reactor towards outlet. This is a moving bed (Figure 2.5).

The fluid property of the moving bed is almost identical to those of the fixed bed.

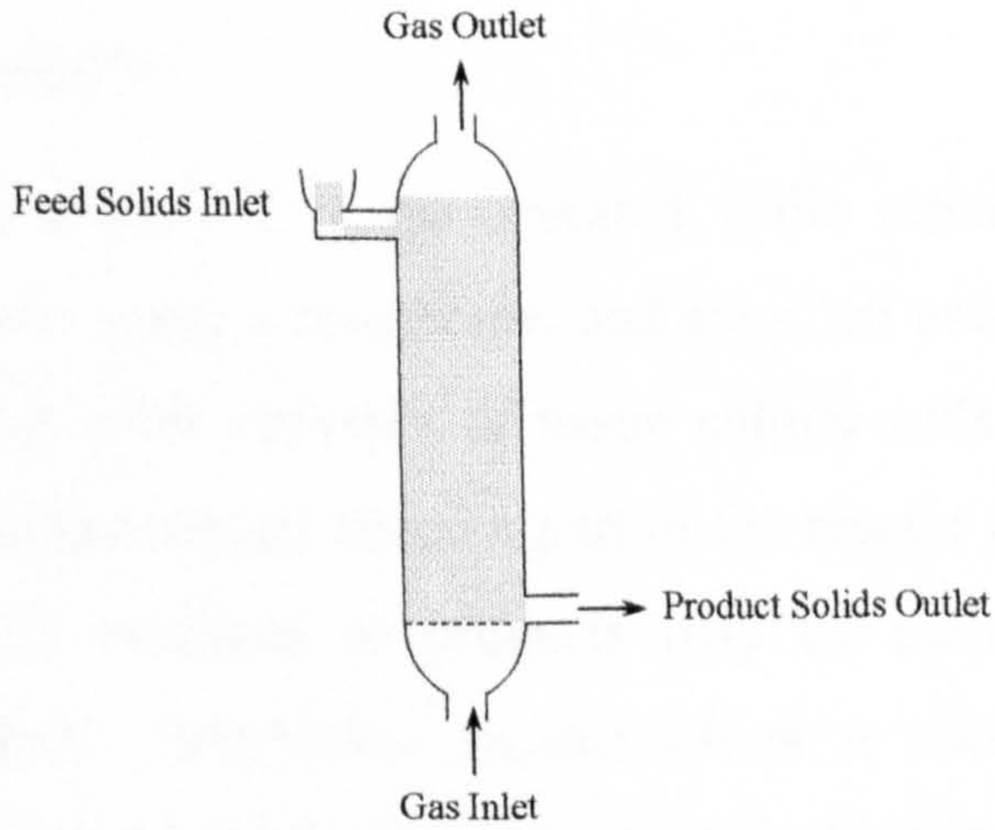


**Figure 2.5. Moving bed**

2.1.2.1.3 Fluidised bed reactor

Fluidised beds are useful when solid particles which are involved in reactions must be removed frequently. In a fluidised bed, particles move freely floated by the fluid flowing upward. This motion of particles allows their easy removal from the bed. The liquid fluidised bed shows a very smooth flow with small particles. Larger the particle size (or the bed diameter), the more the flow turns into circulation because of channelling, which enlarges longitudinal mixing of liquid and particles. Some types of fluidised bed reactor are presented in Figure 2.6. Typically, fluidised bed is used in fluidised catalytic cracking (FCC) [35] as well as synthesis of acrylonitrile [36], as an example.

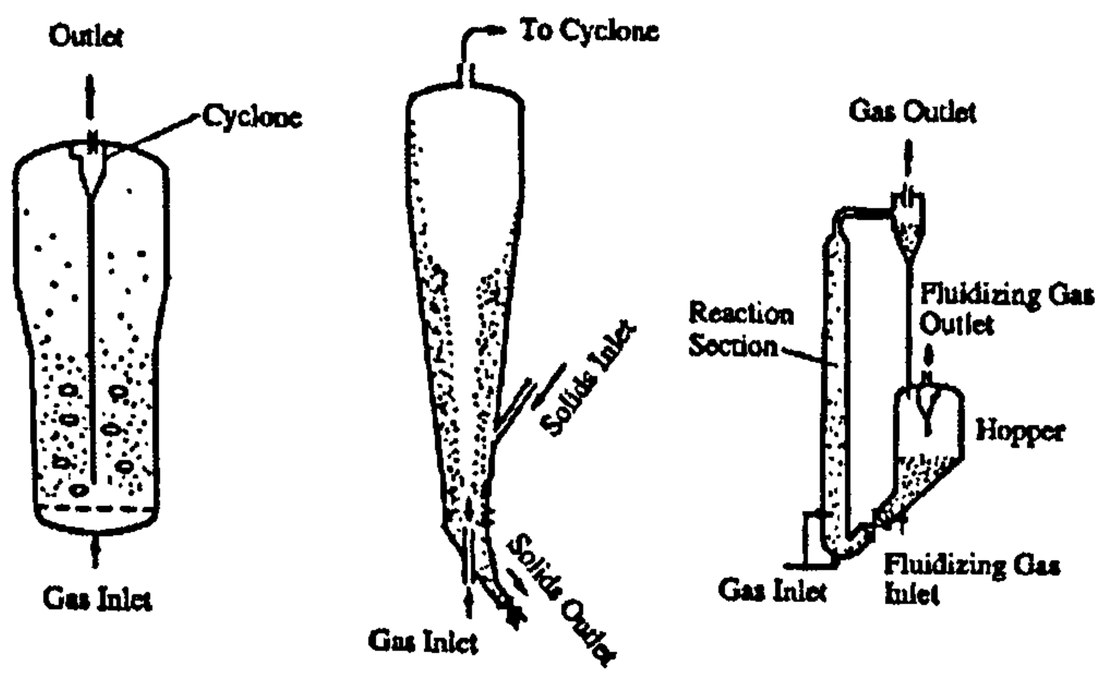


(a) (b) (c)

**Figure 2.6. Several types of fluidised bed reactor: (a) Bubbling fluidised bed, (b) Spouted bed, (c) Circulating fluidised bed**

2.1.2.1.4 Membrane reactor

These reactors (Figure 2.7) are operated while separating catalysts from reactants and/or products using a membrane, and are often used as bioreactors. For example, a system that holds enzymes or tissue culture cells of micro-organisms, animal or plant cells (biocatalysts) inside a part of the reactor divided by membrane to separate them from reactants or products may be considered as a kind of immobilised biocatalyst. Membrane reactor offers a variety of immobilising methods: mixing biocatalysts with reactants or products; contacting reactants with biocatalysts through a membrane; and reacting by biocatalysts immobilised inside a membrane.

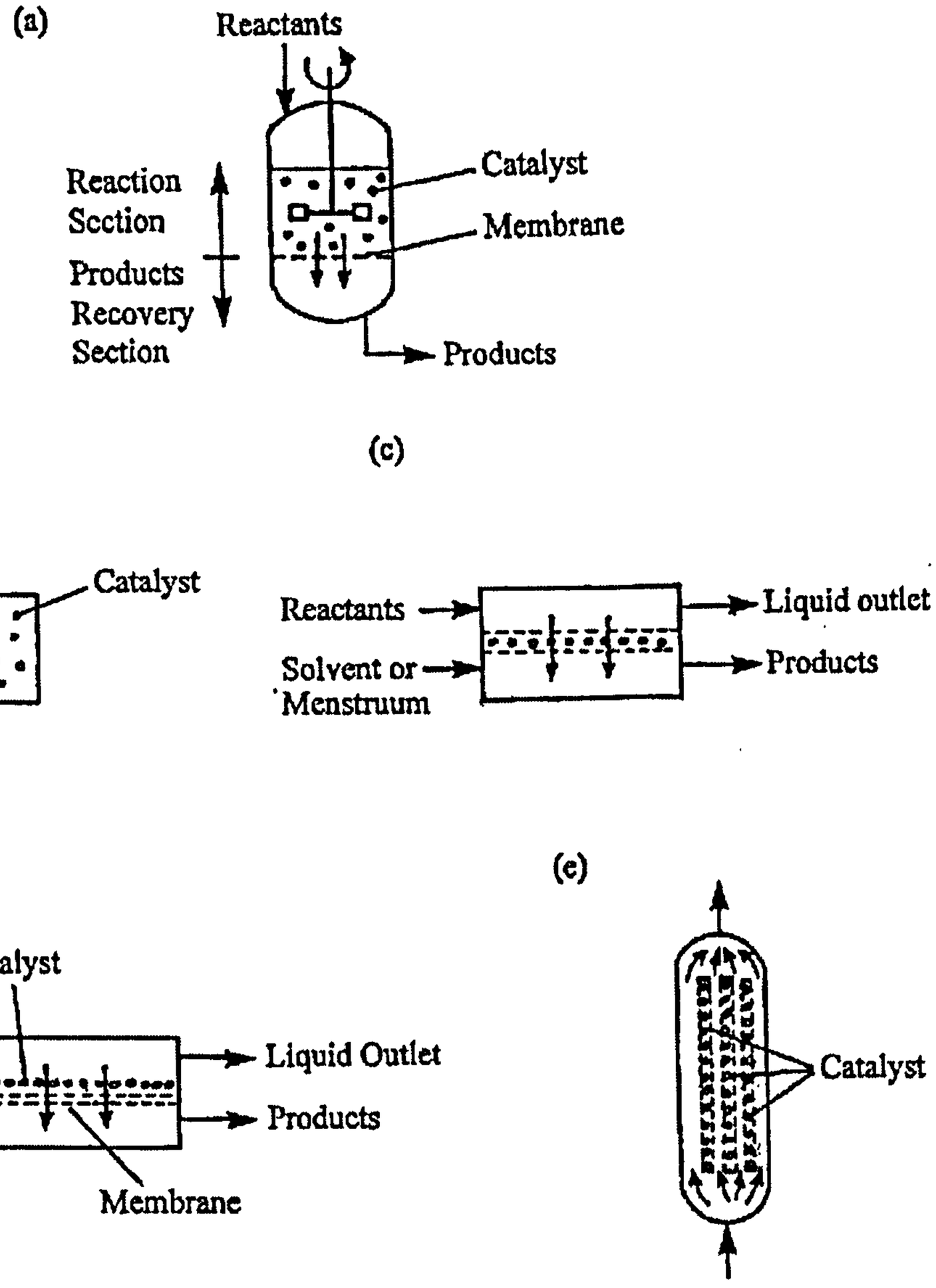


**Figure 2.7. Membrane reactors: (a) Products filtration (suspended catalysts), (b) Diffusion through membrane, (c) The catalyst is immobilised inside the membrane, (d) The catalyst accumulates and is attached on the membrane, (e) The membrane serves as the carrier of the catalyst**

Additionally, other type of reactors, such as spinning basket reactor, can also be used to perform the catalytic reactions in order to minimise diffusion limitations/concentration effects and to obtain low conversion kinetic data.

### *2.1.2.2 Industrial reactors*

Industrial catalytic reactors exhibit a great variety of shapes, types and sizes. A survey of the most important reactor types is given by Ullmann [37]. In general, heterogeneous catalytic reactors can be divided in two categories, depending on the size of the catalyst particles, large and small.

2.1.2.2.1 Large Particle Catalyst Reactors

Large particle catalysts can be kept stationary, so that packed in a bed they can be kept in the reactor and the reaction mixture passes through the bed of particles. The aim is to keep the catalyst charge as long as possible in the reactor, say for many years. This method avoids all the trouble of eliminating the catalyst from the product stream coming out of the reactor. Whatever the shape of the particles, their size in industrial reactors is usually larger than 2 mm. Some examples of reactors with catalyst beds are given in Figure 2.8. Figure 2.8 (a) shows the common adiabatic packed bed reactor. This reactor is used for single-phase reaction mixtures, either gases or liquids with moderate heat effects [38-41]. Systems with multiple beds with cooling in between the beds are frequently used, such as for $NH_3$ and $CH_3OH$ production. The cooled tubular reactor is used for reactions with high heat effects (Figure 2.8 (b)) [42-45]. This reactor consists of a large number of parallel tubes, which are cooled with a coolant flowing around the outside of the tubes. To maintain the catalyst bed in the tubes as isothermal as possible, only a small number of particles across a tube diameter is permitted, say between 3 and 20 particles. Depending on the required reactor capacity the number of tubes varies between 30 to 30,000 [46]. Both adiabatic packed bed and cooled tubular reactors can be used for gaseous and liquid reactor feeds.

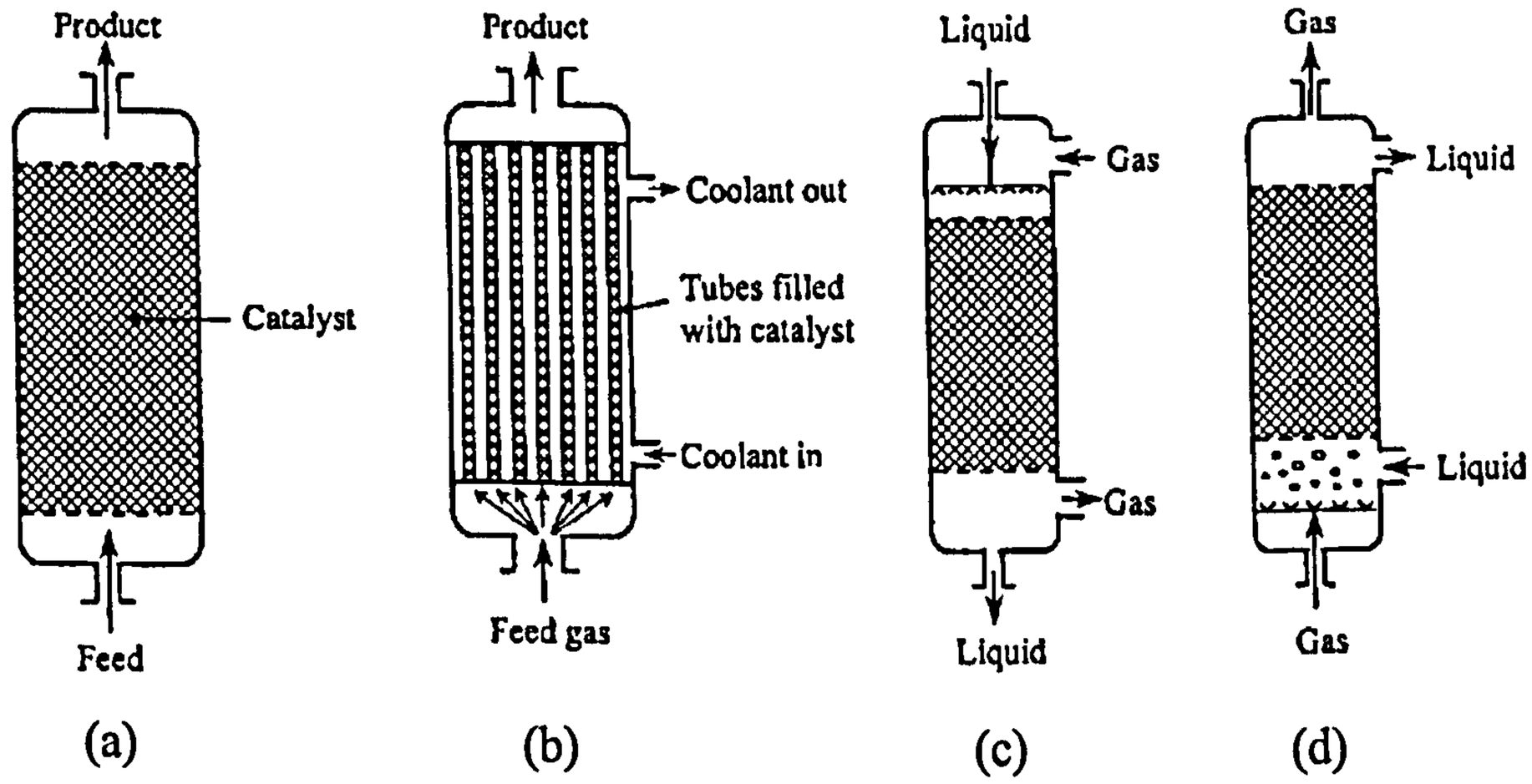


**Figure 2.8. Examples of reactors with fixed catalyst beds: (a) Adiabatic Packed Bed; (b) Cooled Tubular Reactor, (c) Cocurrent Trickle Bed Reactor; (d) Packed Bubble Column**

When a mixture of gas and liquid is to be fed to a packed bed reactor then,

depending on the required residence times in the reactor, two reactor types are commonly used. In Figure 2.8 (c) the trickle flow reactor is shown, in which the gas and the liquid streams are fed cocurrently at the top of the reactor [47-49]. The liquid wets the catalyst particles and slowly trickles to the bottom through the bed. The gas dissolves in the liquid and is transported to the catalyst surface, where reaction takes place with reactants coming from the liquid phase. A counter current flow of gas and liquid can also be applied. Residence times for the liquid phase in industrial trickle flow reactors can be as high as 10–15 min. If much larger residence times are required for the liquid phase, the packed bed bubble column reactor in Figure 2.8 (d) is often used [50-54]. Here gas and liquid are both fed to the bottom of the reactor. The reactor is filled with liquid through which the gas bubbles slowly upwards. In these reactors liquid residence times of the order of hours can easily be achieved; the catalyst is fully wetted with the liquid phase.

#### 2.1.2.2.2 Small Particle Catalyst Reactors

For small catalyst particles completely different reactor types are used. The catalyst is now suspended in the flowing reaction mixture and has to be separated at the reactor exit or is carried along with the fluid. Particle sizes are now from 10 μm up to 1 mm. In Figure 2.9 some of the common reactor types are shown. Figure 2.9 (a) shows the fluid bed reactor [55-59], where the gaseous feed keeps the small catalyst particle in suspension. Catalyst carried over in the exit stream is separated, for example, in cyclones. For even shorter contact times, riser reactors are used in which the solid catalyst is transported in the gas stream. Fluid bed reactors are also used for feed mixtures of a liquid and a gas.

In cases when the feed stream is a liquid, which requires rather long residence times, the suspension bubble column [60, 61] or an agitated tank reactor [62-64] is used (Figures 2.9 (b) and 2.9 (c)). Here, in the reactor exit, quite elaborate filtering systems are required to remove the catalyst from the liquid stream. In these reactors a gas is generally supplied, because these suspension reactors are mostly used for hydrogenations and oxidations.

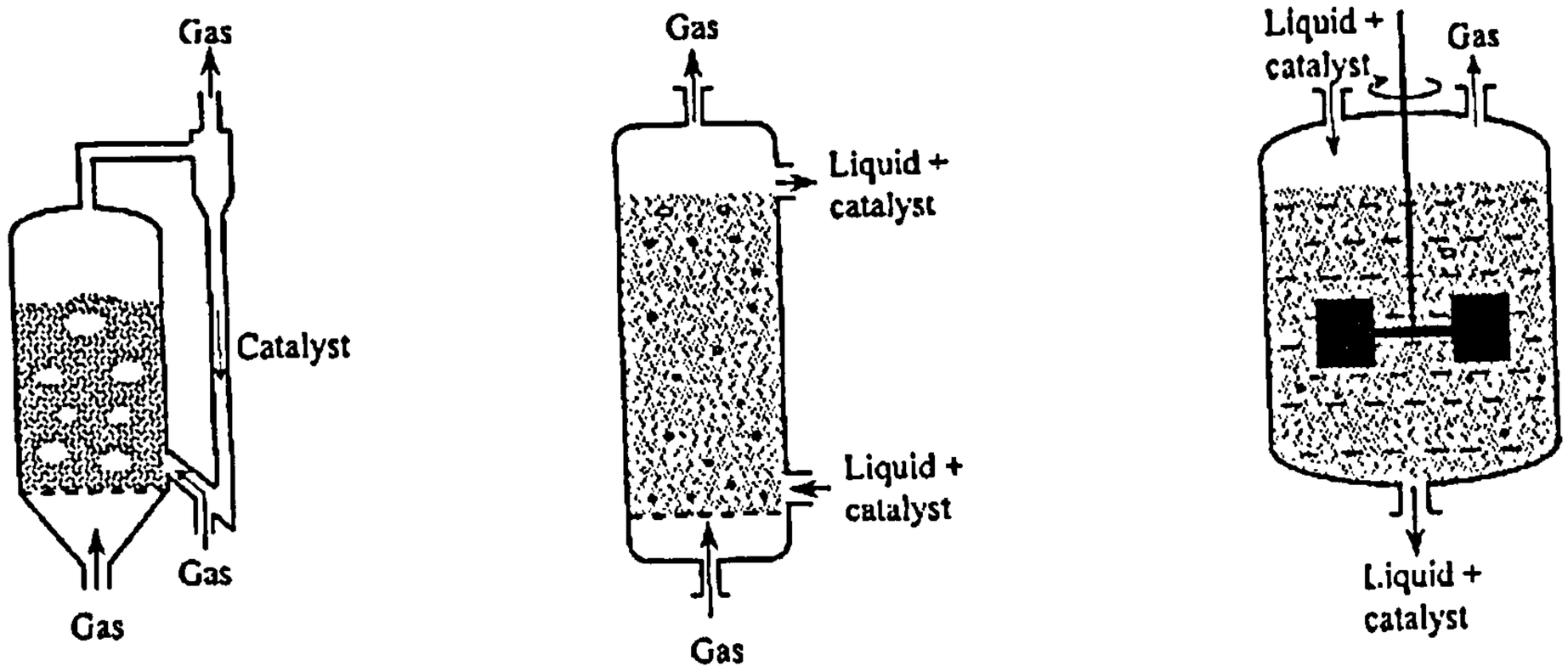


(a) (b) (c)

**Figure 2.9. Example of reactors with moving catalyst beds: (a) Fluid-bed Reactor; (b) Bubble Column with suspended catalyst; (c) Sparged Stirred Tank with suspended catalyst**

## 2.2 PROCESS INTENSIFYING EQUIPMENT

### 2.2.1 SPINNING CONE REACTORS

Intensified mixing devices, which have tight control not only on the intensity of mixing, but also on the flow pattern, may be used to produce nano to larger size particles by addressing the appropriate process parameters. Producing in situ nano particle slurry with narrow crystal size distribution can transform the chemical mechanical polishing (CMP) process for the electronic industry. A typical example for the continuous production of tailored particles is the spinning cone reactor, shown in Figure 2.10, where precipitates of barium sulphate have been formed by using equimolar concentrations of sodium sulphate and barium chloride solutions having initial supersaturation ratios of 500 and 5000 [65]. It was shown that at high supersaturation conditions, the particle size formed with the spinning cone is much smaller than in the batch reaction.

### 2.2.2 ROTATING PACKED BEDS

Rotating packed beds (RPBs) [66, 67] utilise centrifugal acceleration to intensify mass transfer processes previously conducted in packed columns. The RPBs were used for separation processes (absorption, extraction, distillation), but can be used for reacting systems. One of the main applications of RPBs is counter-current gas/liquid mass transfer [68].

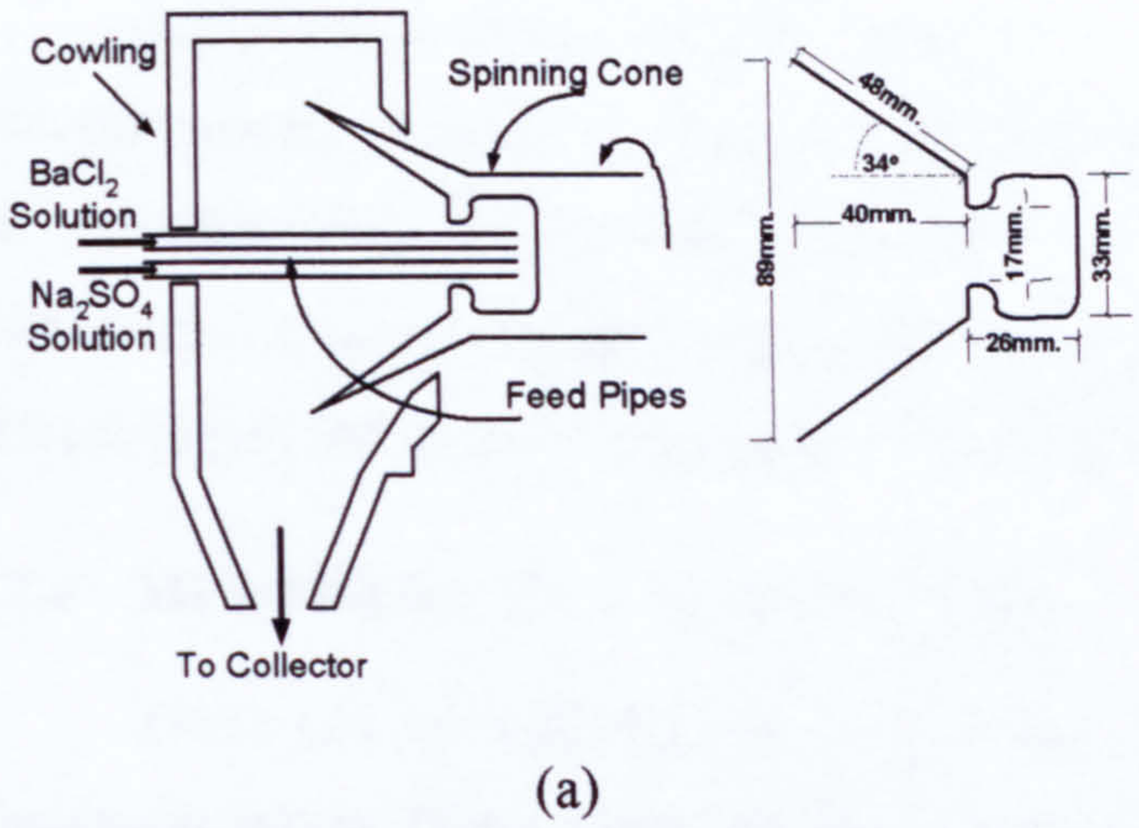


(a) (b)

**Figure 2.10. Spinning cone reactor (a) Schematic of the $BaSO_4$ precipitation process; (b) View on the spinning cone reactor**

### 2.2.3 MICRO-REACTORS

Improved methods of manufacturing at the micro scale are opening up new avenues for development of compact devices for functions ranging from reactions to separation. Much of the initial work in this field has concentrated on the development of systems using single phase flow with diffusive transfer between parallel reacting fluid streams. Work within Newcastle University has however focused on the more complex system of multiphase flow in narrow channels and in particular immiscible liquid-liquid processes [69]. The main method adopted to perform multiphase reactions is the use of slug flow to allow both convective and diffusive processes to operate within the reactor channel. An illustration of the mechanisms involved is presented in Figure 2.11. A titration process involving acetic acid transfer from kerosene into an aqueous solution of NaOH and KOH was used to visualise the mass transfer.

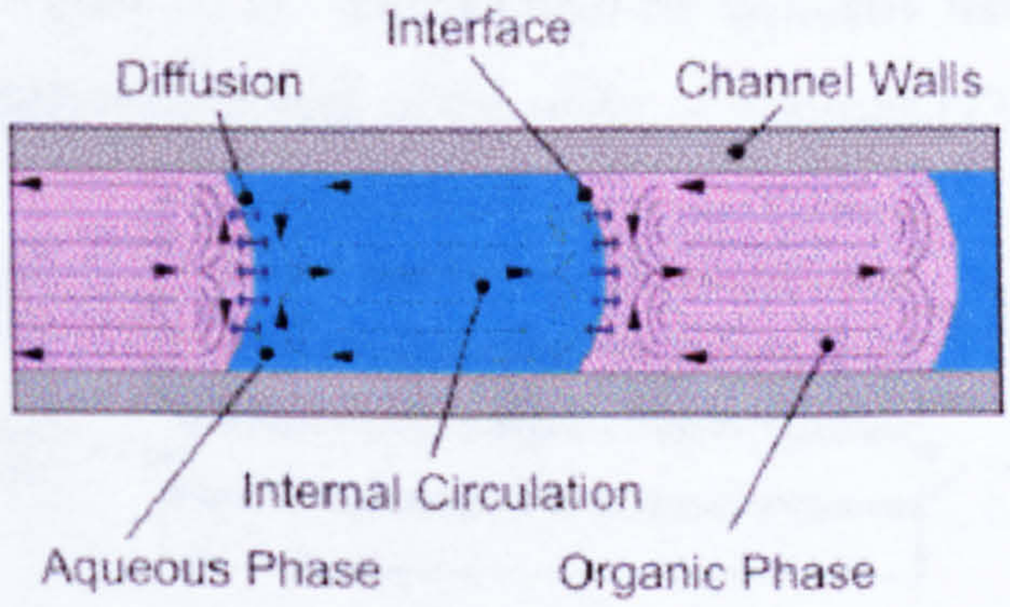


**Figure 2.11. Circulation patterns within slug flow provide high mass transfer performance between phases**

Experiments using slug flow reactors were performed for the industrially relevant process of organic nitration. Results from benzene and toluene nitration showed that slug flow could be used to provide significant conversion to nitrobenzene and nitrotoluene in seconds using coiled PTFE reactors of 30 cm to 180 cm length and compared favourably with industrial processes [70].

### 2.2.4 MULTIFUNCTIONAL REACTORS

These can be described as reactors that, in order to enhance the chemical conversion taking place and to achieve a higher degree of integration, combine at least one more function that conventionally would be performed in a separate piece of equipment [71, 72]. Example of this type of a reactor is reverse-flow reactor which integrates reaction and heat transfer in a multifunctional unit. This is of importance for exothermic processes, where heat of reaction is utilised by keeping it within catalyst bed and after reversion of the flow direction, using it to preheat the cold reactant gases. Catalytic Plate Reactors can be described as multifunctional as well. Other applications include reactive distillation and reactive extraction (integrating reaction and separation), to name but a few.

#### *2.2.4.1 Catalytic plate reactors*

Supplying heat directly into an endothermic reaction, rather than via inter-stage heaters or by radiation to a packed tube is a vital key to intensifying many important chemical processes. The catalytic plate reactor (CPR) offers an attractive route for achieving this. In a CPR, metal plates coated with a suitable catalyst are arranged in such a manner that exothermic and endothermic reactions take place in alternate channels (Figure 2.12). These channels typically have a height of order of millimetres and a catalyst thickness of the order of microns [73, 74].

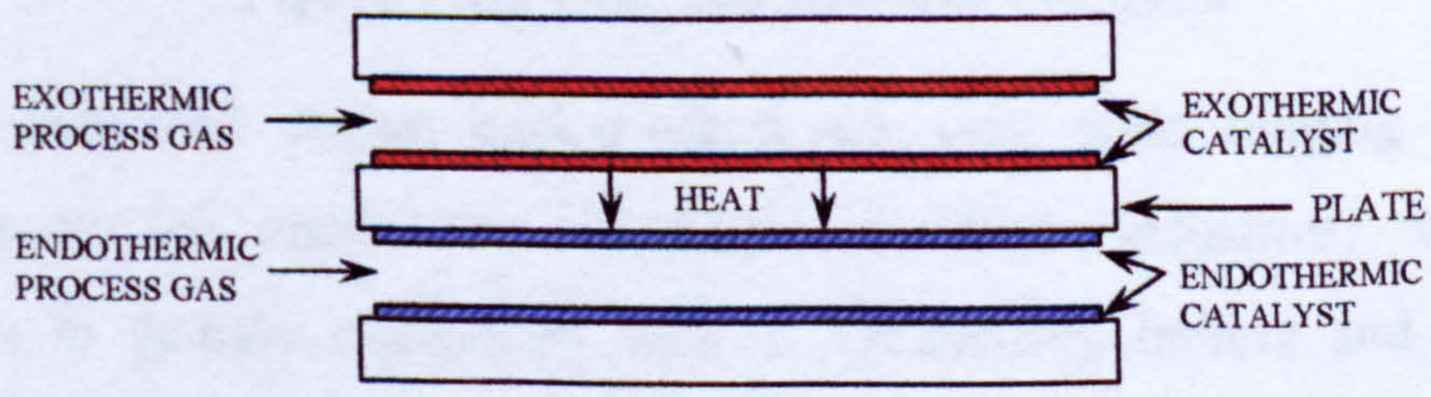


**Figure 2.12. A pair of adjacent channels in the catalytic plate reactor**

The advantages of CPR designs over conventional reactors arise due to excellent heat transfer characteristics and minimal intra-catalyst diffusion resistance.

The heat transfer mechanism within a CPR is via conduction through the plates separating alternate process channels and as such is largely independent of the process gas superficial velocity. The catalyst layers within a CPR are thin which results in minimal diffusion limitations and thus high catalyst utilisation. These advantages result in reactors which are smaller, lighter and with a small associated pressure drop than conventional alternatives.

### 2.2.5 POLYMER FILM COMPACT HEAT EXCHANGERS (PFCHE)

A novel concept of thin film polymer heat exchangers has been developed [75], which offers high thermal efficiency, reduced fouling, significant reduction in weight and cost, resistance to chemically aggressive fluids and the ability to handle both liquids and gases [76]. The units are of compact construction and can be of square or spiral configuration (Figure 2.13). An important feature of these heat exchangers that sets them apart from those on the current market is the use in some variants, of a high temperature resistant polymer, poly ether ether ketone (PEEK). PEEK has a continuous use temperature of up to 220$^0$C. Although the thermal conductivity of the polymer is not as high as metals, the PFCHE made of 100 μ thick PEEK films offers negligible thermal resistance when the heat transfer coefficient is less than 4000 W/(m$^2$K).

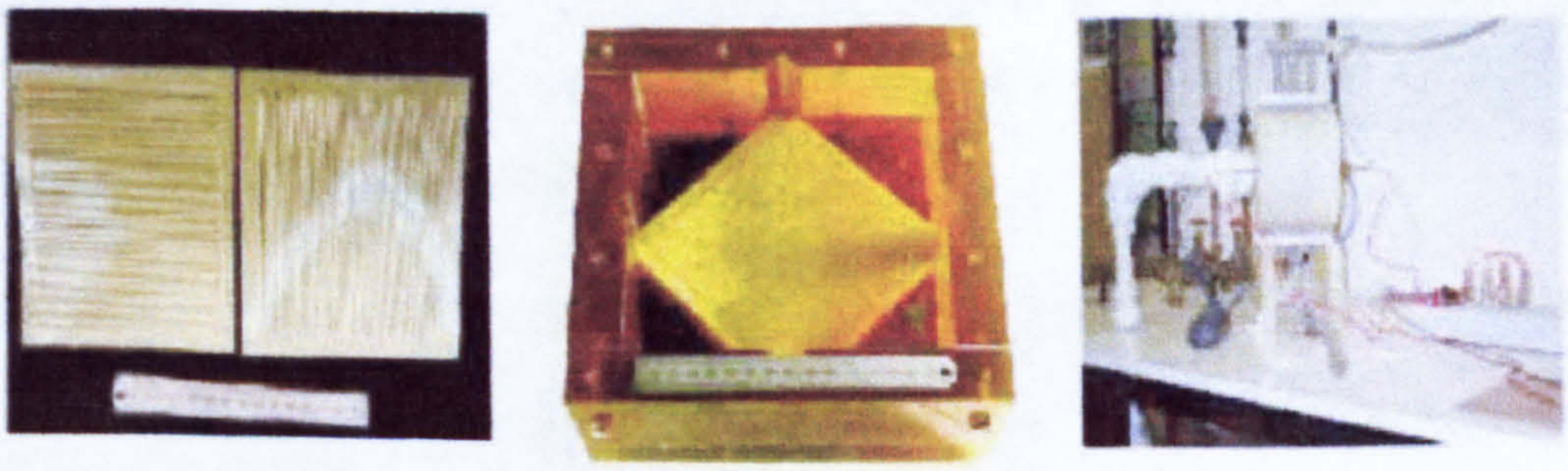

**Corrugated** **Square** **Spiral**

**Figure 2.13. Configurations of PFCHEs**

The potential market opportunities are very wide ranging and include applications in the chemicals and food and drink industries, with possible applications in generic equipment such as condensing boilers and refrigeration plants. There are also opportunities in the aviation, fuel cell and automobile industries in the form of cabin air coolers, filter coolers and radiators. Case studies on the PFCHEs as a metal alternative in the aviation and fuel cell industries have

been carried out using heat transfer and pressure drop correlations developed from different fluid systems. The fluid systems investigated are air/air, water/water and glycerol-water mixtures/water for the square PFCHE whilst a water/air system was studied for the spiral PFCHE. The results are very positive as huge cost and energy savings can be achieved [77].

### 2.2.6 SCFs REACTORS

Supercritical fluids (SCFs) are used industrially for the processing of natural products; because of their unique properties, SCFs are attractive media for mass-transfer operations (e.g. extraction and chemical reaction) [78]. Many of the physical and transport properties of SCFs are intermediate between those of a liquid and a gas. For example, diffusivity in a SCF falls between a liquid and a gas, therefore reactions which are diffusion limited in the liquid phase could become faster in a SCF phase. Because of their unique solubility properties, compounds that are largely insoluble in a fluid at ambient conditions can become soluble in the fluid at supercritical conditions. SCFs have been investigated for number of systems including polymerisations, enzyme reactions and heterogeneously catalysed reactions.

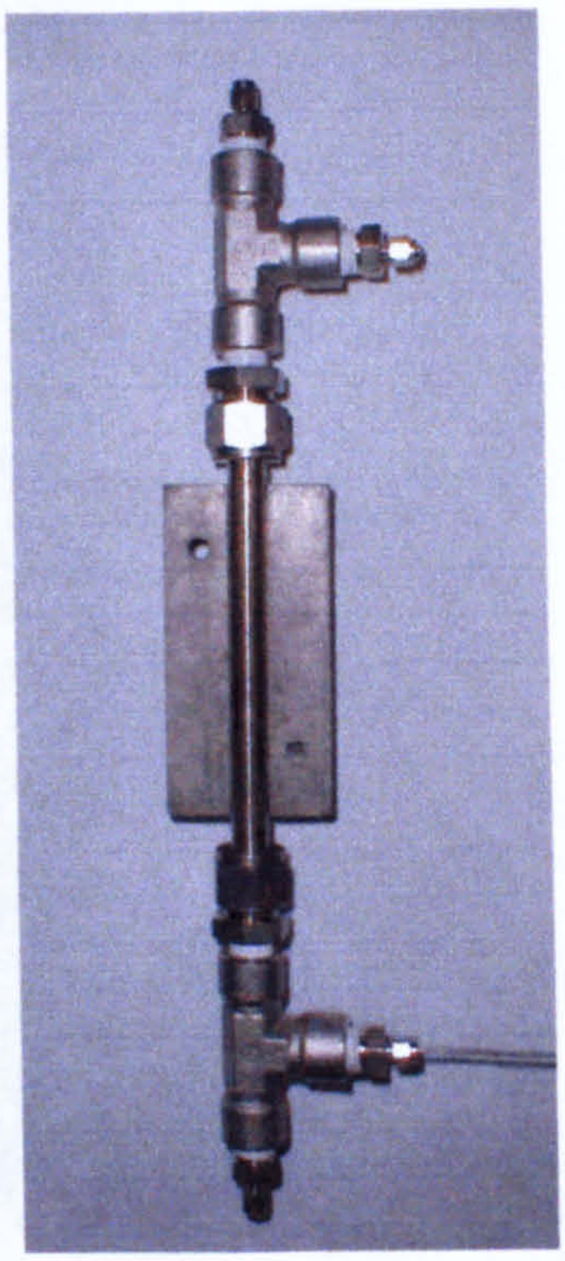

**Figure 2.14. SCF reactor [79][1]**

A photograph of the continuous flow reactor used in Nottingham to study heterogeneous catalysed reactions [80] is shown in Figure 2.14.

### 2.2.7 OSCILLATORY BAFFLED REACTORS (OBRs)

The OBR offers enhanced fluids mixing at very low and uniform shear rate in comparison with traditional stirred vessels and this is advantageous especially for biochemical, biomedical and pharmaceutical applications where shear sensitive

[1] Photo reproduced from The Clean Technology Research Group web site with permission from Professor Poliakoff

cultures are involved. Some research at Heriot-Watt University, for example, includes studies into continuous crystallisation, fermentation of biopolymer and cell cultures, continuous production of nano-particles and defouling [81].

OBR used in the Centre for Oscillatory Baffled Reactor Applications (Edinburgh) is shown in Figure 2.15 below.

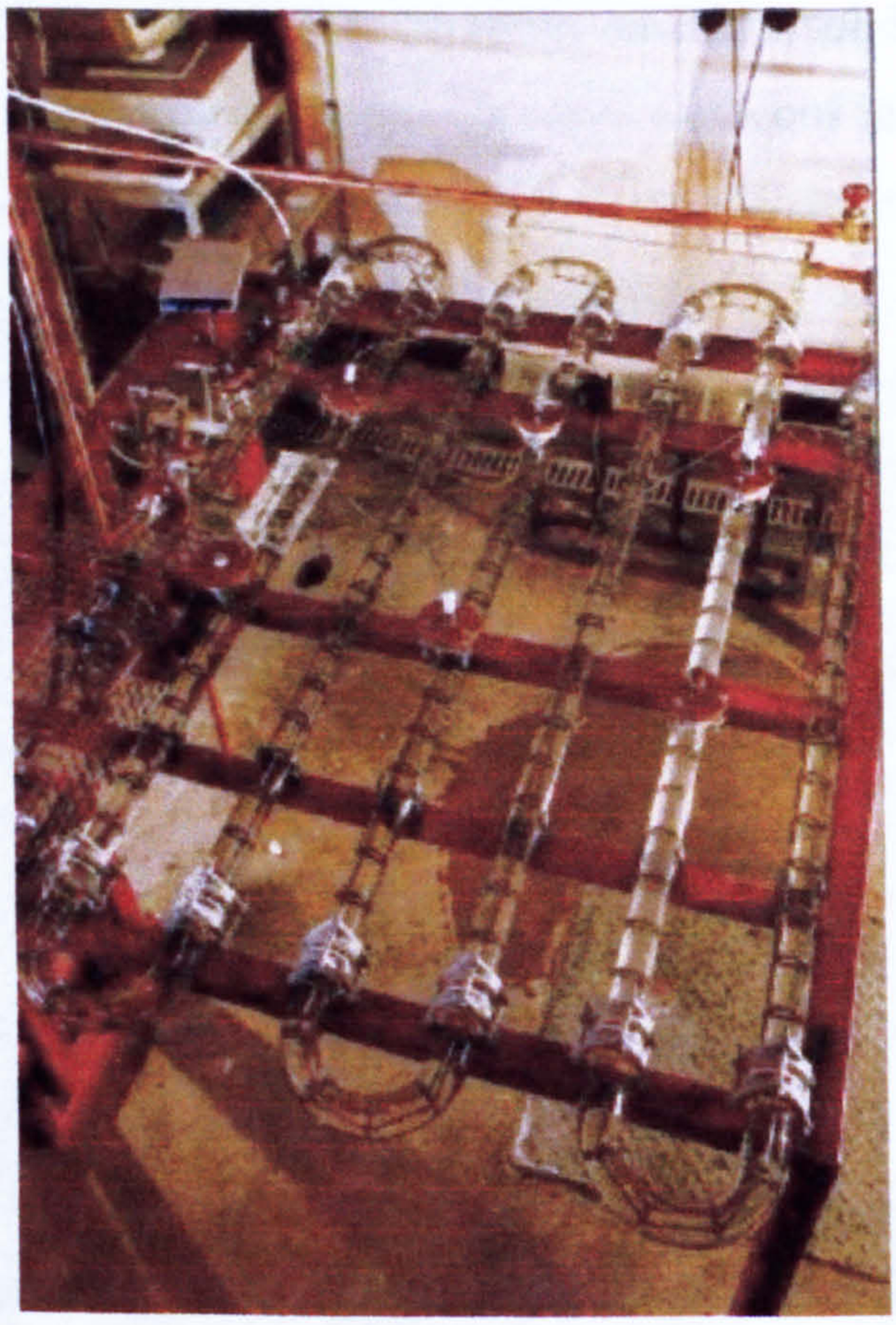

**Figure 2.15. Oscillatory baffled reactor [82][2]**

The Spinning Disc Reactor technology will be described in details in Chapter 3. All of these new technologies (not all of them mentioned above) may result in the extinction of some traditional types of equipment, if not whole unit operations [83].

## 2.3 HETEROGENEOUS CATALYSIS

A catalyst is a substance that increases the rate at which a chemical reaction approaches equilibrium without, itself, becoming permanently involved in the reaction. The key word in this definition is *permanently* since there is ample

[2] Photo reproduced from The COBRA web site with permission from Professor Ni

evidence showing that the catalyst and the reactants interact before a reaction can take place. The product of this interaction is a reactive intermediate from which the products are formed. This substrate-catalyst interaction can take place homogeneously with both the reactants and the catalyst in the same phase, usually the liquid, or it can occur at the interface between two phases. These heterogeneously catalysed reactions generally utilise a solid catalyst with the interaction taking place at either the gas/solid or liquid/solid interface [84, 85]. Additional phase transport problems can arise when a gaseous reactant is also present in the liquid/solid system. Since a catalyst merely accelerates the rate of reaction it can not be used to initiate a reaction that is thermodynamically unfavourable. The enthalpy of the reaction as well as other thermodynamic factors (see Appendix A) are a function of a nature of the reactants and the products only and, thus, can not be modified by the presence of a catalyst. Kinetic factors, such as the reaction rate, activation energy (Figure 2.16), nature of the transition state, and so on, are the reaction characteristic that can be affected by a catalyst.

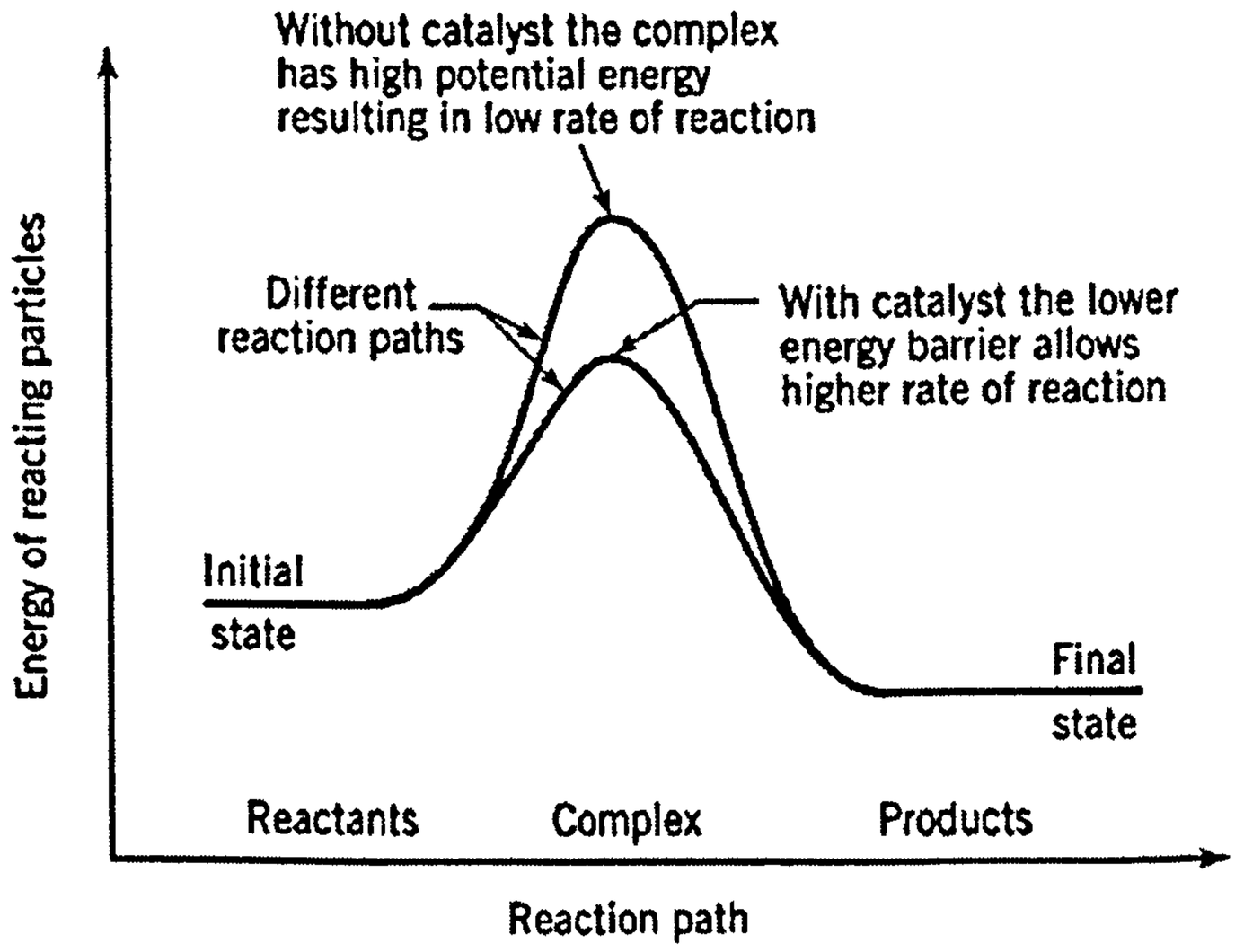


**Figure 2.16. Catalyst Effect on Activation Energy**

In heterogeneous catalysis reactants have to be transported to the catalyst through the pores of the particle to the active material. In this case all kinds of transport resistances may play a role, which prevent the catalyst from being fully effective in its industrial application. Furthermore, because appreciable heat effects accompany most reactions, heat has to be removed from the particle or supplied to it

in order to keep it in the appropriate temperature range, where the catalyst is really fully effective. Heterogeneous catalysis is one of the most complex branches of chemical kinetics. Rarely do we know the compositions, properties or concentrations of the reaction intermediates that exist on the surfaces covered with the catalytically effective material. The chemical factors that govern reaction rates under these conditions are less well known than in homogeneous catalysis. Yet solid catalysts display specificities for particular reactions, and selectivities for desired products, that in most practical cases can not be equalled in other ways. Thus use of solid catalysts is essential.

### 2.3.1 THE CATALYST CYCLE

Unlike in a homogeneously catalysed reaction where the determination of the kinetic factors for the process is usually straightforward, a heterogeneously catalysed process is more complex because the catalyst is not uniformly distributed throughout the reaction medium. In a two-phase system, either vapour/solid or liquid/solid, with the solid phase the catalyst, several steps are needed to complete the catalyst cycle:

1. Transport of reactants to the catalyst;
2. Interaction of the reactants with the catalyst (adsorption);
3. Reaction of adsorbed species to give the product(s);
4. Desorption of the product(s) from the catalyst;
5. Transport of the product(s) away from the catalyst.

Reaction only takes place in Step 3, but Steps 2 and 4 also involve chemical changes and that is why any rate data obtained from such reactions includes all three steps. Steps 1 and 5 merely involve a physical transport and either one can be the rate limiting step for the overall reaction process [86].

### 2.3.2 ADSORPTION

Adsorption on a catalyst surface must be energetically favourable, have relatively low activation energy and lead to the formation of reactive surface species. While the adsorption of the reactants on the catalyst surface is a necessary feature in

catalytic processes, adsorption, of itself, does not necessarily lead to a catalysed reaction. For a reaction between adsorbed species to take place the adsorption of the reactants can not be too strong nor too weak. When the adsorption is too weak the amount of adsorbed species is too low to sustain the reaction. When strong adsorption occurs the substrate can not leave the surface and the catalyst becomes poisoned for further reaction. For instance, hydrogen can be adsorbed on almost all metals and ethylene on most of them [85] yet only a few are capable of promoting the hydrogenation of ethylene. On metals such as Ti, V, Cr, Mo or W, ethylene adsorbs so strongly that the hydrogenation can not be promoted. On other metals such as Mn, Au, or Ag hydrogen chemisorption is too weak so the formation of the active surface hydride can not take place.

For practical purposes all adsorptions can be classified as one of two types. It can involve merely the van der Waals interaction between the substrate and the catalyst, a process that is termed physical adsorption or physisorption. Alternately, it can involve the formation of catalyst-substrate bonds. This is termed chemical adsorption or chemisorption. While the latter is the basis for the chemistry of catalysts, physisorption is the basis for the Brunauer, Emmett and Teller (BET) procedure which is commonly used to measure the surface area of solids [87, 88].

### 2.3.3 CHEMISORPTION

Physisorption involves only a weak attraction between the substrate and the adsorbent but in chemisorption a chemical reaction takes place between the adsorbent and atoms on the catalyst surface [89]. As a result, chemisorbed species are attached to the surface with chemical bonds and are more difficult to remove. If the adsorption of hydrogen on nickel is considered as an example, the reaction involves the breaking of an H-H bond and the formation of two Ni-H bonds on the surface.

The activation energies of most chemisorptions are very low, sometimes even zero [85]. The reason for this low activation energy is shown in Figure 2.17 which illustrates the potential energy curves for both the physisorption (curve P) and chemisorption (curve C) of hydrogen on a nickel surface. The reaction involves the physisorption of the hydrogen on the nickel with the energy minimum of curve P corresponding to the sum of the van der Waals radii of hydrogen and nickel (z). This

physisorption process brings the hydrogen molecule close enough to the nickel so the electron orbitals of the atoms on the surface can begin to interact with the molecular orbitals of the hydrogen. As this interaction strengthens, the hydrogen molecule is attracted closer to the nickel surface and the potential energy for the interaction increases slightly following the physisorption energy curve (P) until it intersects with the chemisorption curve (C). At this point attractive forces predominate resulting in a shortening of the Ni-H distance along with the weakening and ultimate breaking of the H-H bond [86].

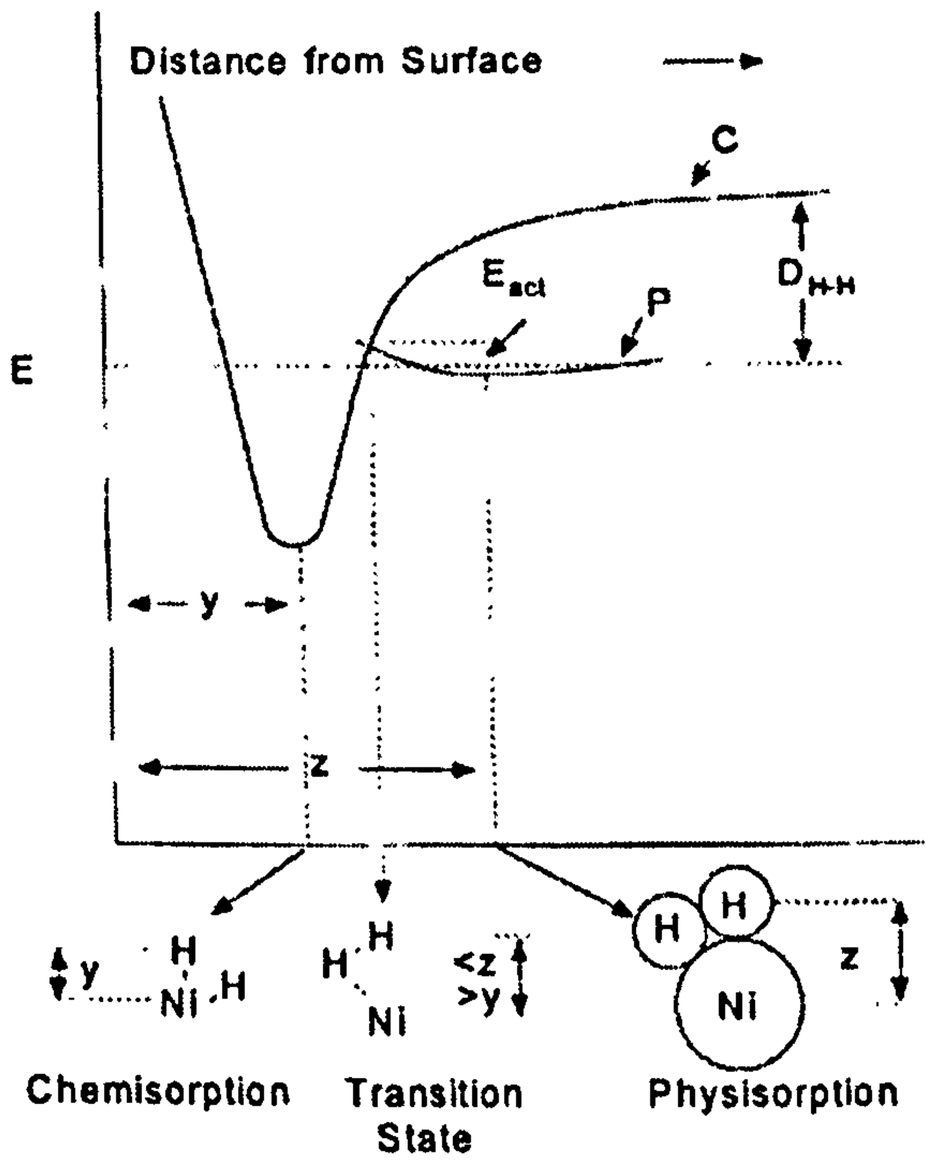


**Figure 2.17. Potential energy curves for adsorption**

The minimum of the chemisorption potential energy curve (C corresponds to the sum of the Ni and H atomic radii (y)) is a result of the formation of the Ni-H bonds. Figure 2.17 also shows the atomic arrangements at the various stages of this interaction as related to the appropriate positions on the potential energy curves.

### 2.3.4 DIFFUSION

If we consider a long, slender cylinder filled with catalyst pellets and a flow of reactants entering at one end where the reactant stream may be a gas, a liquid or a gas/liquid mixture, the flow occurs in the interstices between the catalyst granules. The rate of flow, relative to the catalyst particle, is the prime factor, together with temperature and catalyst properties, in determining the amount of conversion. The

velocity and turbulence of the flow determine how rapidly molecules are carried from the fluid phase to the exterior surfaces of catalyst pellets. Rapid transfer from fluid to solid outer surface is obtained with highly turbulent flow, which means a highly irregular flow pattern with momentary velocities strongly deviating from the main flow direction. High turbulence is obtained with high flow velocities, large particles and low viscosities. The amount of turbulence also has a strong influence on the rate of heat transfer between the catalyst pellet and the fluid, and also to the wall of the cylinder.

If diffusion is fast relative to the rate of reaction, then all the interior surfaces of a catalyst pellet are bathed in fluid of the same composition. This composition will depend on the position of the pellet in the reactor, that is, on the distance from the inlet. But if the diffusion rate is of the same order of magnitude as the reaction rate, or slower, the concentration of the reactants and product will vary within the pores: we then speak of a diffusion limitation of the transport of reactants, generally resulting in a lower conversion rate. Diffusion limitation can have quite profound effects. Some of these are listed below [85].

- The apparent activity of the catalyst is generally lowered;
- The apparent order of the reaction may be changed;
- The selectivity may be altered markedly;
- The temperature gradient within a pellet may become large;
- Inner portions of pellets may be more or less rapidly deactivated than outer portions, or vice versa.

Temperature differences between catalyst and fluid will exist even without a diffusion limitation. For an exothermic reaction the entire catalyst pellet must be somewhat hotter than the surrounding, flowing fluid, as only this temperature difference serves as the driving force for removal of the heat of reaction. This excess temperature is usually only some tenths of a degree to a few degrees centigrade. When reaction rates are extremely high compared to the heat removal capabilities, the temperature difference between pellet and fluid may become very large and can be around the local adiabatic temperature rise of the reaction. This adiabatic

temperature rise $\Delta T_{ad}$ is an extremely important property of a reaction and is given by [46]:

$$\Delta T_{ad} = \frac{(-\Delta H)_A C_A}{\rho c_P} \qquad (2.1)$$

where $(-\Delta H)_A$ – is the heat of reaction evolved (kJ/mol),

$C_A$ – the inlet concentration of the reactant in the fluid (kmol/m$^3$) and

$\rho c_p$ – the sensible heat per unit of volume of the reaction mixture.

When $\Delta T_{ad}$ is low, heat effects are relatively unimportant, for high values heat removal is a must in catalyst utilisation.

## 2.4 CATALYST PERFORMANCE

The two most important performance properties of a catalyst are deactivation behaviour and its selectivity.

### 2.4.1 DEACTIVATION

Deactivation of the catalyst is caused mostly by fouling (e.g. coke formation) or by poisoning. In most organic reactions a decomposition may occur, which leads to fine carbonaceous deposits, which are generally called coke. When these coke deposits occur at the inlet of the pores of a porous catalyst, deactivation may occur rather rapidly [90]. Deactivation also may occur due to extremely small amounts of contaminants in the feed to the reactor. Sulphur is a well-known poison, as are traces of many metals.

To reactivate a coked catalyst, the coke can usually be removed by burning off the deposits at a controlled temperature with a mixture of air and an inert diluent, such as nitrogen or steam. The temperature level at which the coke deposits ignite has to be determined experimentally. The allowable content of $O_2$ in the air-diluent mixture can be premeditated [91].

### 2.4.2 SELECTIVITY

The selectivity of a catalyst plays a role as soon as multiple reactions occur. The following main types of multiple reactions can be distinguished:

- parallel reactions;
- consecutive reactions;
- combination reactions, consisting of a combination of parallel and consecutive reactions

For the reaction:

$$\nu_A A+\nu_B B \rightarrow \nu_P P+\nu_Q Q$$

The selectivity, $\sigma_P$, is the ratio between the amount of desired product P obtained and the amount of key reactant A converted; both quantities are usually expressed such that $\sigma_P$ ranges between 0 (no P formed) and 1 (all A converted to P). This definition leads to:

$$\sigma_P = \frac{\left(\omega_P - \omega_{P,0}\right) M_A}{\left(\omega_{A,0} - \omega_A\right) M_P \nu_P} \tag{2.2}$$

where:

$\omega_X$ – is the mass fraction of component X (X = A, B, P, Q);

$\omega_{X,0}$ – the mass fraction of component X at time t = 0;

$\nu_X$ – the stoichiometric coefficient for component X.

For constant density of the reaction mixture, this can be written as:

$$\sigma_P = \frac{\left(C_P - C_{P,0}\right)}{\left(C_{A,0} - C_A\right) \nu_P} \tag{2.3}$$

The yield, $Y_P$, is the ratio between the amount of desired product P obtained and the amount that could be obtained if all of key reactant A was converted to P with 100% selectivity. Therefore, $Y_P$ can be calculated from:

$$Y_P = \sigma_P \frac{\omega_{A,0} - \omega_A}{\omega_{A,0}} \tag{2.4}$$

Like $\sigma_P$, the yield $Y_P$ usually varies between 0 and 1. It is high when both the

selectivity and the relative degree of conversion are high; it is low when either of them is low.

If in the product separation section of the reactor, the key reactant A can be removed and recycled to the reactor, selectivity is the key factor in economical operation of the plant. However, if A cannot be recycled, then yield is the key factor.

## 2.5 FINE CHEMICALS PRODUCTION AND NOVEL CATALYSTS

Conventional homogeneously catalysed processes utilised by the fine and speciality chemicals industries produce vast amounts of waste on removal of the catalyst from the reaction. Tightening environmental legislation has led to a drive to develop new heterogeneous systems that offer ease of catalyst separation combined with high activities and selectivity, thus reducing the production of waste [92-94].

The manufacture of fine chemicals and especially of pharmaceuticals can be characterised as follows:

- Rather complex molecules (isomers, stereochemistry, several functional groups) with limited thermal stability;
- Production via multistep synthesis, with short product lives;
- Production usually in solution, at ambient pressure and low to medium temperature in relatively small (500 l – 10 $m^3$) multipurpose batch equipment;
- Relatively small-scale products (1 – 1000 t per year);
- High purity requirements (usually >98%);
- High value added and therefore tolerant to higher product costs (particularly for very effective, small-scale products);
- Short development time for the production process (few months to 1–2 years) since time to market affects the profitability of the product;
- Typically relatively high E-factor with large amounts of unwanted products (solvents, salts, by-products, etc., that must be eventually recycled or discarded).

Catalysis can contribute on two levels to the clean production of chemicals; firstly, by providing improved production processes and secondly, by helping to remove or transform unwanted, or even toxic by-products. Lately, impressively large number of highly selective catalytic transformations is recorded in the literature that in principle can be applied to the synthesis of fine chemicals. When heterogeneous catalysis is applied to manufacture of fine chemicals, a few key problems might occur, such as:

- Insufficient performance (selectivity, activity, productivity, stability) of catalysts developed in academic research;
- Substrate specificity of highly selective catalysts leading to lack of predictability and making synthesis planning very difficult;
- Lack of time (and money) to find suitable, commercially available catalyst;
- High demands on the purity of starting materials and control or reaction conditions.

Many prerequisites must be fulfilled in order to render a catalytic process technically viable. Once applied, novel catalytic methods could lead to a better, more environmentally friendly and often cheaper production.

The use of solid heterogeneous catalysts in the chemical industry is very important, especially in cracking and isomerisation reactions. Nevertheless, application of such catalysts in liquid phase reactions has been limited to the field of hydrogenation and it is only in the last decade that solid catalysts become important in liquid phase applications. One of the reasons for rapid expansion of such catalysts has been the development of supported reagents. Early ones consisted mainly of stoichiometric reagents adsorbed onto a high surface area solid such as alumina, silica or clay, following the idea that the dispersion of the reagent over the large surface areas typical of these supports would allow more rapid reaction through greater accessibility of the reagents and substrates. Furthermore, inorganic supported reagent and spent reagent can be easily filtered or centrifuged from the reaction system, contrary to their unsupported equivalent. Main disadvantage of stoichiometric supported reagents remains the large amount of solid required in the

reaction mixture. New supported reagents are catalytically active, therefore they retain all the advantages of stoichiometric supported reagents, without the drawback of requiring excessive quantities of solid. Not only are the catalytic supported reagents easy to separate and recycle, but it has often been shown that they display enhanced selectivity compared to their solution phase counterparts. Solid acid catalysts have found application in Friedel–Crafts reactions, nitrations and halogenations of aromatics, to name but a few [95]. Review of preparation techniques for some of the novel catalysts can be found in [92].

A second group of materials which have contributed in the expansion of solid catalysts are zeolites [96], used for many years in gas phase reactions, but only recently exploited in liquid phase systems. This was due to the microporous nature of the original zeolites, which limits their application to small molecules. More recently the field of zeolites has expanded with significant variety of structures and types of zeolitic materials, including mesoporous materials prepared in similar way to zeolites, but having pores with tightly defined dimensions which can be controllably varied from 1.8 – 10 nm (e.g. MCM – Mobil Composite Materials) and the fact that porosity is in mesoporous range is very important in the field of fine chemicals. Areas in which zeolites show strong environmental potential, by minimising the output of pollutants and by secondary treatment of effluents produced are:

- reduction of atmospheric oxides of nitrogen ($NO_x$);
- cutting emissions of volatile organic compounds (VOCs), including from cold starting of automobiles and
- process improvements in the chemical process industries.

Narrow pore sized hexagonal mesoporous silica ($HMS_x$, where x denotes the pore size in $\mathring{A}$), as a support to immobilised $AlCl_3$, have been shown to improve selectivity towards monoalkylation in the reaction of alkylation of aromatics with alkenes [97, 98], whereas zeolites, such as HZSM-4, have very poor activity, especially in the reactions involving large alkene molecules. Increased selectivity of the catalyst was related to the alkylation taking place within the pores of the catalyst.

### 2.5.1 REACTIONS CATALYSED BY SOLID ACIDS

There are many reactions which fall into this category. The ones which will be mentioned have been selected because of their commercial importance, the environmental unacceptability of current manufacturing processes, the range of the chemistry and the catalysis required, and the opportunities for exploiting the new chemistry in novel or original ways. These are:

(a) Friedel–Crafts acylations [99] based on the use of carboxylic acids, acid chlorides and anhydrides and including the preparation of acetophenones (important pharmaceutical and agrochemical) [100]:

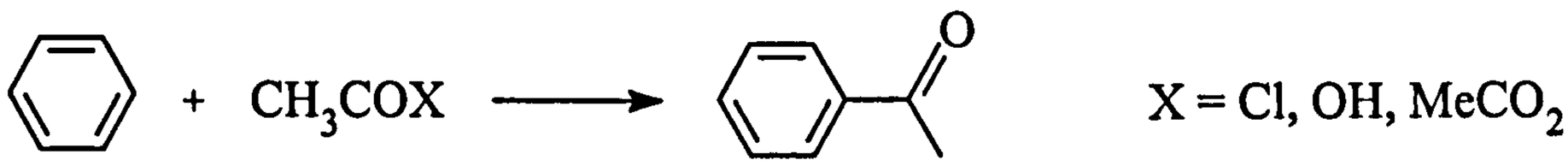


(b) Rearrangements including the highly sensitive acid-catalysed rearrangement of α–pinene oxide to campholenic aldehyde, an important intermediate in the manufacture of several fragrances:

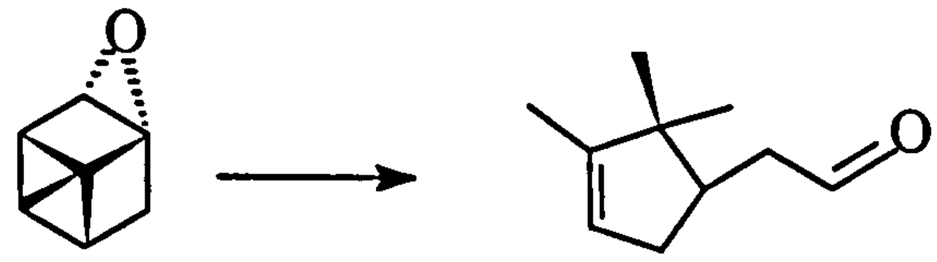


This reaction will be discussed later in more detail. Another important traditionally acid-catalysed rearrangement is that of cyclohexanone oxime to the nylon-6 intermediate caprolactam [101]:

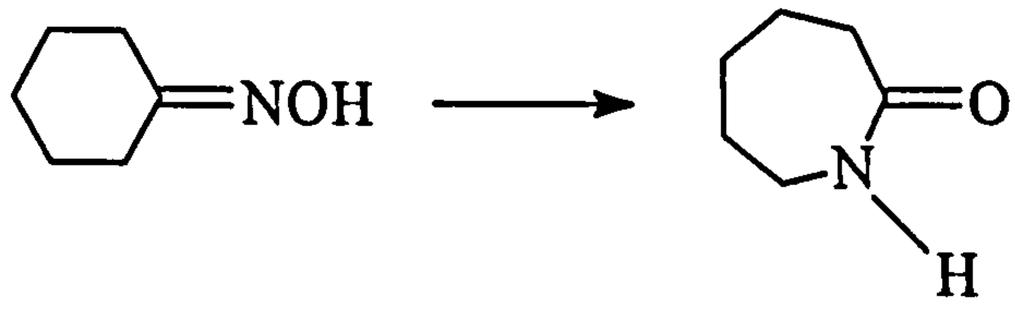


The above reaction is carried out in industry using concentrated sulphuric acid with serious problems resulting from corrosion and waste salts. It is believed that the rate-limiting step in solid-acid catalysed reactions is diffusion of the product from the catalyst and control of the steric and electronic properties of solid acid

catalytic sites as well as an understanding of adsorption-desorption are essential if an effective alternative to the liquid acid route is to be developed.

(c) Aromatic halogenations including the bromination of the deactivated compounds benzaldehyde and benzotrifluoride:

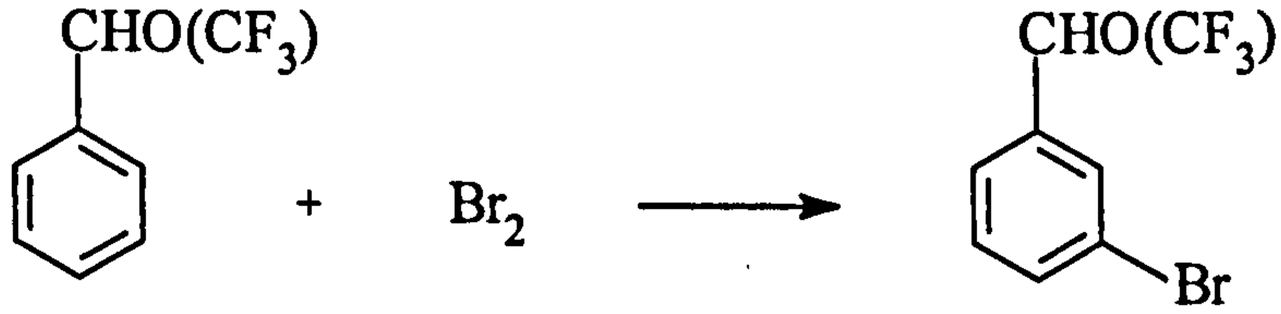


The meta-bromoproducts are important pharmaceutical intermediates. 3-bromobenzaldehyde is normally produced using large quantities of $AlC1_3$ whereas 3-bromobenzotrifluoride requires the use of highly corrosive HF since HCl (almost inevitably present in $AlC1_3$ systems) causes loss of the valuable fluorine through acid-catalysed halogen exchange.

(d) Alkene oligomerisations [102] leading to hydrocarbon resins of value in adhesives and other applications. The reactions of interest are based on the use of cationic catalysis to promote the oligomerisation of cracked petroleum distillates made up of mixtures of low molecular weight aromatics and alkenes to give resins based on a degree of polymerisation of ca. 10 monomer units. Current manufacturing processes are typically carried out in continuous stirred tank reactors at up to 10 t $h^{-1}$ with $AlCl_3$-based catalysts and suffer from contaminated products and large volumes of hazardous waste resulting from the need for continuous water quenching of the product/$AlCl_3$ mixtures.

(e) Lewis acid catalysed peroxide reactions where the ability to prepare strong solid acids that are largely or entirely Lewis acid in character would be very important in preventing side-reactions that lead to explosive peroxy products. A good example of this is the oxidation of cyclohexanone to caprolactone using hydrogen peroxide [103], which is known to be subject to Lewis acid catalysis:

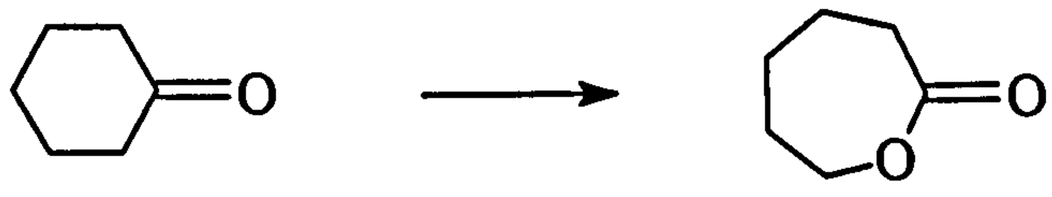

The reaction chosen for the study is that of rearrangement of α–pinene oxide to campholenic aldehyde.

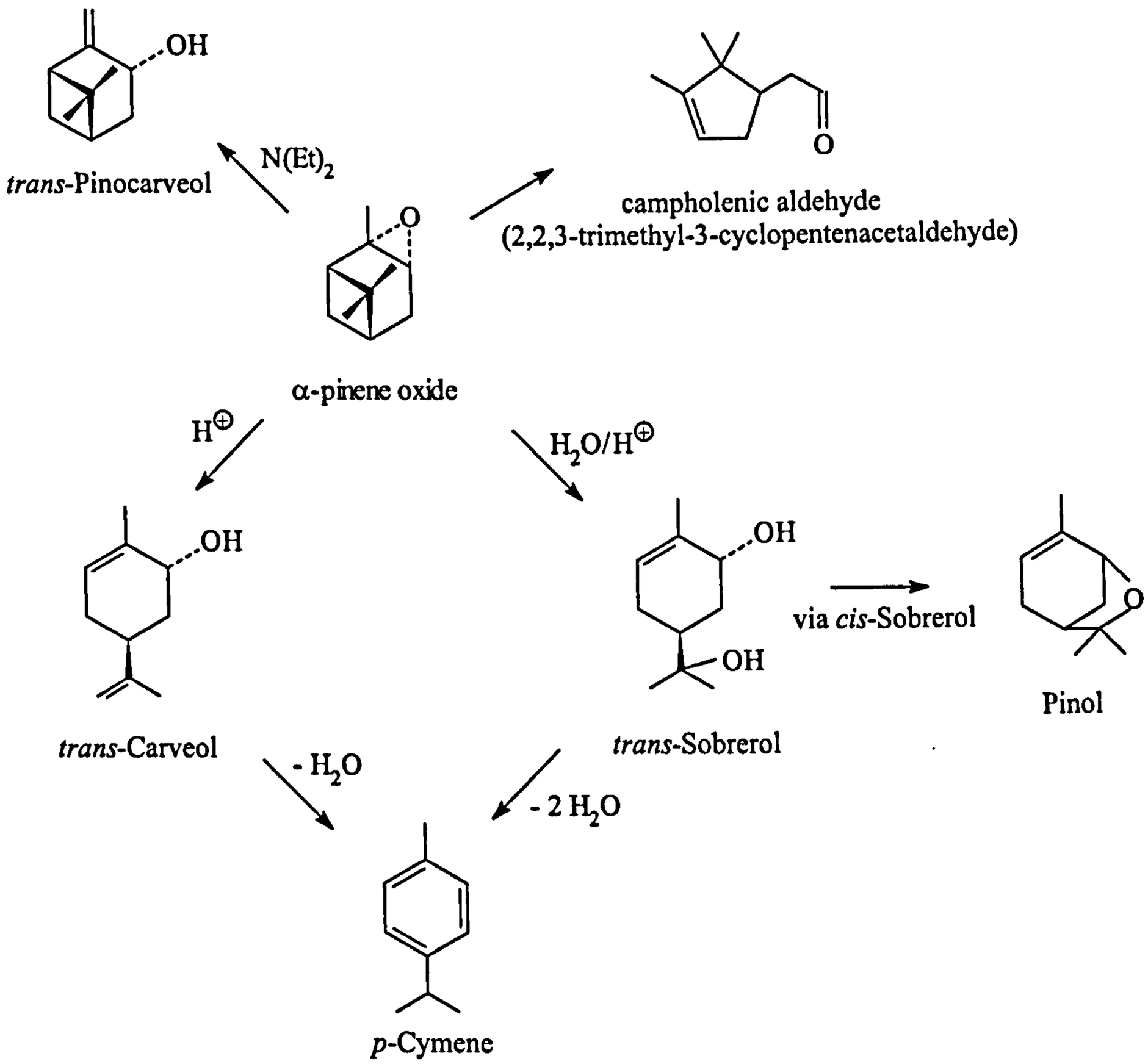


**Figure 2.18. Main products from the rearrangement of the α–pinene oxide**

## 2.5.2 REARRANGEMENT OF α–PINENE OXIDE

One of the conventionally homogeneously catalysed processes is the rearrangement of the α–pinene oxide to campholenic aldehyde, which is an important intermediate used by the fragrance industry in the synthesis of several sandalwood fragnances, and is currently prepared by Lewis acid catalysed rearrangement of α-pinene oxide [104]. The reaction can lead to production of over 100 products that have been reported, under different reaction conditions. Only the

major products formed during acid catalysed rearrangement are summarised in Figure 2.18, however a more detailed overview is available elsewhere [101, 105]. The use of mild Lewis acids favours the production of campholenic aldehyde, while Brönsted acid sites will result in the formation of trans-carveol, trans-sobrerol and p-cymene. In general, Brönsted acids give maximum selectivities of 55%, while solid Lewis acids, especially the zinc halides, can give selectivities of up to 85%. The most active and selective homogenous systems used in this reaction are $ZnCl_2$ and $ZnBr_2$, but the problem is that aqueous extraction of these catalysts from the reaction results in the formation of huge quantities of zinc contaminated water which is environmentally unacceptable. That is why there is an urgent need for the alternative heterogeneous catalysts.

One of the attempts to develop heterogeneous catalysts for this reaction have involved the use of mixed oxide solid acids [106], and US-Y zeolites [101, 107]. Depending on reaction conditions, selectivities towards campholenic aldehyde of 55-80% have been reported. In the recent reports authors have used zeolite titanium Beta to rearrange α–pinene oxide in both the liquid and vapour phase, with the later conditions forming campholenic aldehyde with an initial selectivity of up to 94% (at conversions of above 95%), dropping to 80% after 6 hours [108]. Maximum achieved selectivity in liquid phase was 89%. Ravasio et al. [109] reported maximum of 72% selectivity at full conversion using mixed cogels in the presence and in the absence of copper. They concluded that the presence of copper lowers the support activity and modifies the product distribution in a significant way. Vialemaringe et al. [110] recently reported 90% selectivity when reaction is performed in benzene with Lewis acid catalyst ($ZnBr_2$).

Possible isomerisation pathway is shown in Figure 2.19. Protonation of the oxygen induces epoxy ring opening with a subsequent alkyl shift. At several points in this mechanism, the intermediates can react with other components, solvent molecules or undergo isomerisation to form different products [111].

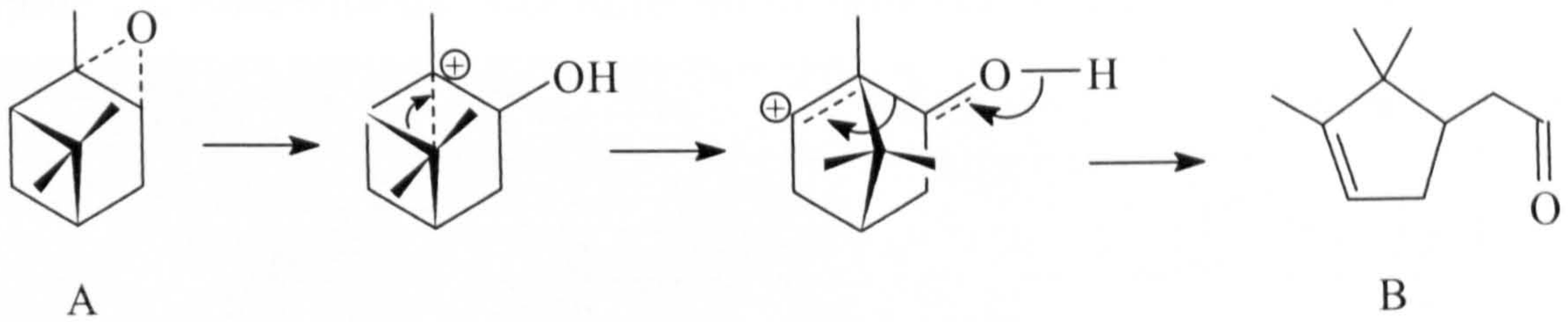


**Figure 2.19. Reaction pathway for the acid catalysed isomerisation of α–pinene oxide (A) to campholenic aldehyde (B)**

Different solvents, as well as catalysts, affect conversion and selectivity; hence it is very important to choose an appropriate solvent. Generally, activity and selectivity were found to decrease with increasing polarity of the solvent. Effect of some solvents on catalysed isomerisation of α-pinene oxide at $20^0$C with $ZnCl_2$ as a catalyst is shown in Table 2.2 [105].

**Table 2.2. Solvent effects on Brönsted acid catalysed isomerisation**

| Solvent | Time (h) | Conversion (%) | Selectivity (%) |
|---|---|---|---|
| Benzene | 1 | 100 | 87 |
| Dichloroethane (DCE) | 1 | 100 | 85 |
| Diethyl ether | 2 | 50 | 82 |
| Dioxanee | 1 | 61 | 66 |
| THF | 2 | 7 | 37 |

When operating with high activity catalysts, high substrate/catalyst ratios are needed to control the exothermic reaction (for heat of reaction calculations see Appendix A). The reaction can become violent at higher catalyst concentrations even at room temperature.

Comparison between Brönsted and Lewis acids catalysed reactions is shown in Tables 2.3 and 2.4. It can be seen that some Lewis acids are very active and selective towards campholenic aldehyde.

**Table 2.3. Isomerisation with different Brönsted catalysts in DCE ($20^0$C)**

| Catalyst | Time (h) | Conversion (%) | Selectivity (%) |
|---|---|---|---|
| HCOOH | 2 | 19 | 58 |
| HCOOH/NaA | 5 | 100 | 50 |
| DOWEX | 6 | 78 | 54 |
| $H_3BO_4$ | 1 | 27 | 49 |
| $La(CF_3SO_3)_3$ | 1 | 100 | 31 |
| $Zn_2SiW_{12}O_{40}$ | 5 | 84 | 49 |
| $Al_4(SiW_{12}O_{40})_3$ | 20 | 100 | 51 |
| $H_4SiW_{12}O_{40}$ | 2 | 86 | 48 |
| $H_3PW_{12}O_{40}$/Carbon | 3 | 51 | 50 |

**Table 2.4. Isomerisation with different Lewis acids catalysts in DCE ($84^0$C)**

| Catalyst | Time (h) | Conversion (%) | Selectivity (%) |
|---|---|---|---|
| $ZnF_2$ | 1 | 14 | 41 |
| $ZnCl_2$ | 1 | 100 | 85 |
| $ZnBr_2$ | 1 | 100 | 72 |
| $CuCl_2$ | 4 | 100 | 52 |
| $CoCl_2$ | 4 | 17 | 45 |
| $NiCl_2$ | 1 | 40 | 42 |
| $CdCl_2$ | 1 | 11 | 37 |
| $AlCl_3$ | 0.5 | 100 | 45 |
| $TiCl_4$ | 1 | 90 | 28 |

New solid acid catalysts based on silica supported zinc triflate have been prepared in the University of York for use in the rearrangement of α–pinene oxide to campholenic aldehyde [112]. These catalysts have considerable activity and can be recycled without loss of selectivity towards the aldehyde. The selectivity towards the aldehyde can be increased to 80% (at 50% conversion) when the reaction is performed at $25^0$C using Hexagonal Mesoporous Silica ($HMS_{24}$) as the catalyst support.

The main problem of having such an active catalyst for this rearrangement reaction is that the products formed are themselves highly reactive, and consecutive reactions will decrease the observed selectivity towards campholenic aldehyde. In other words, reaction is not as simple as presented in Figure 2.20.


**Figure 2.20. Schematic of the reaction (A – α–pinene oxide, B – Campholenic aldehyde)**

Simplified reaction paths look like those presented in Figure 2.21, where at the same time a lot of parallel and consecutive reactions are taking place.

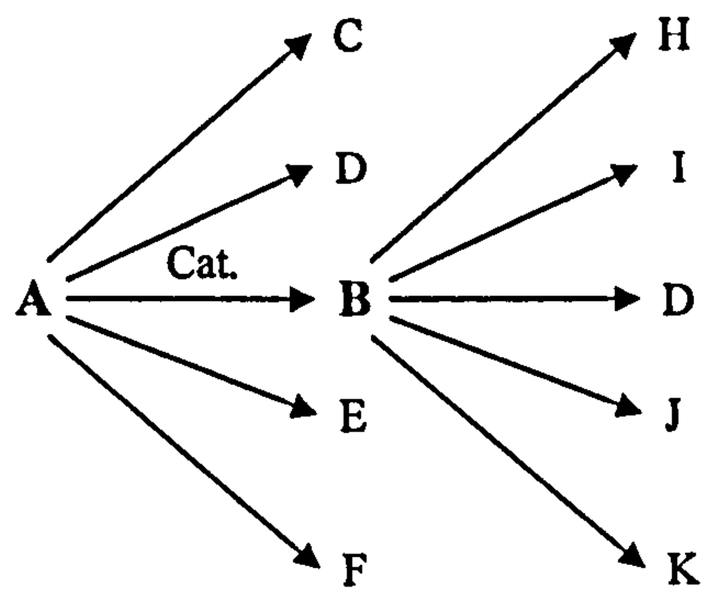


**Figure 2.21. Schematic of simplified reaction paths**

Therefore, it is very important not only to "direct" reaction towards forming campholenic aldehyde (B), but to stop the reaction at that point. It is hoped that this can be achieved by use of novel catalysts. Furthermore, it is also expected that by use of alternative intensifying reactors "greener" process with improved selectivity will be accomplished.

# CHAPTER 3

## SPINNING DISC REACTOR TECHNOLOGY

The Spinning Disc Reactor (SDR) has already been introduced in Chapter 1. To provide more insight into this technology, in this Chapter a detailed review of the hydrodynamics (including flow visualisation) and heat and mass transfer characteristics of the thin films is given.

### 3.1 HYDRODYNAMICS OF THIN FILM FLOW

First studies of thin film flow were conducted in the early XX century, instigated from realisation that thin film flows on the plane surfaces due to gravity have great practical importance in chemical engineering operations [113-117]. It was clear back then that such films enhanced heat and mass transfer as well as mixing action due to the creation of surface waves subjected to the gravitational field [118-122]. However, there is a limit to a force that can be applied to a system in order to form thinner films and increase mass transfer, since the force along the vertical axis is that of terrestrial gravity. More recently it was discovered that the centrifugal force generated on a horizontally rotating disc is much greater than the force acting on films flowing under gravity and films produced in this way have been shown to have improved characteristics. Extensive research into the flow over rotating disc has been done by Bassom and Seddougui [123].

#### 3.1.1 FLOW MODELS

On rotating surfaces, the centrifugal acceleration provides a known driving force for liquid flow across these surfaces, making this a convenient system for achieving sustainable and controllable flow of very thin films.

The modified Navier-Stokes equations for the conservation of momentum and the equation of continuity can fully describe the flow of thin liquid films on a smooth horizontal rotating disc [124]. The full nonlinear equations of motions can be seen in work by Baddour and Zu [125]. Simplified versions of the Navier-Stokes equation are treated in several models from which expressions for velocity

distribution, film thickness and residence times on the rotating surface can be obtained. The equations derived from these models are applicable to smooth, fully developed laminar flow which is only obtained for a very restricted range of conditions.

Several models developed to describe the flow in the spinning disc, were conveniently summarised and analysed by Boodhoo [124]. The following review will show the equations for flow on a horizontal smooth disc rotating about a vertical axis (Figure 3.1) which can be represented by considering vertical cylindrical coordinates (r, θ, z). The modified Navier-Stokes equation is given by the following expressions:

In the radial direction, r:

$$\rho\frac{dv_r}{dt}-\rho\frac{v_\theta^2}{r}=\mu\left(\nabla^2 v_r-\frac{v_r}{r^2}-\frac{2}{r^2}\frac{\partial v_\theta}{\partial\theta}\right)-\frac{\partial p}{\partial r}+\rho g_r \qquad (3.1)$$

In the angular direction, θ:

$$\rho\frac{dv_\theta}{dt}-\rho\frac{v_\theta v_r}{r}=\mu\left(\nabla^2 v_\theta-\frac{v_\theta}{r^2}+\frac{2}{r^2}\frac{\partial v_r}{\partial\theta}\right)-\frac{1}{r}\frac{\partial p}{\partial\theta}+\rho g_\theta \qquad (3.2)$$

In the vertical z- direction:

$$\rho\frac{dv_z}{dt}=\mu\nabla^2 v_z-\frac{\partial p}{\partial z}-\rho g_z \qquad (3.3)$$

where:

$$\frac{d}{dt}=\frac{\partial}{\partial t}+v_r\frac{\partial}{\partial r}+v_\theta\frac{\partial}{\partial\theta}+v_z\frac{\partial}{\partial z}$$

$$\nabla^2=\frac{\partial^2}{\partial r^2}+\frac{1}{r}\frac{\partial}{\partial r}+\frac{1}{r^2}\frac{\partial^2}{\partial\theta^2}+\frac{\partial^2}{\partial z^2}$$

The following equation must be fulfilled (governing the conservation of mass):

$$\frac{\partial \rho}{\partial t}+\nabla(\rho v)=0 \qquad (3.4)$$

If a horizontal rotating disc is concerned, equation (3.4) can be expressed as:

$$\frac{\partial \rho}{\partial t}+\frac{1}{r}\frac{\partial}{\partial r}(\rho r v_r)+\frac{1}{r}\frac{\partial}{\partial \theta}(\rho v_\theta)+\frac{\partial}{\partial z}(\rho v_z)=0 \qquad (3.5)$$

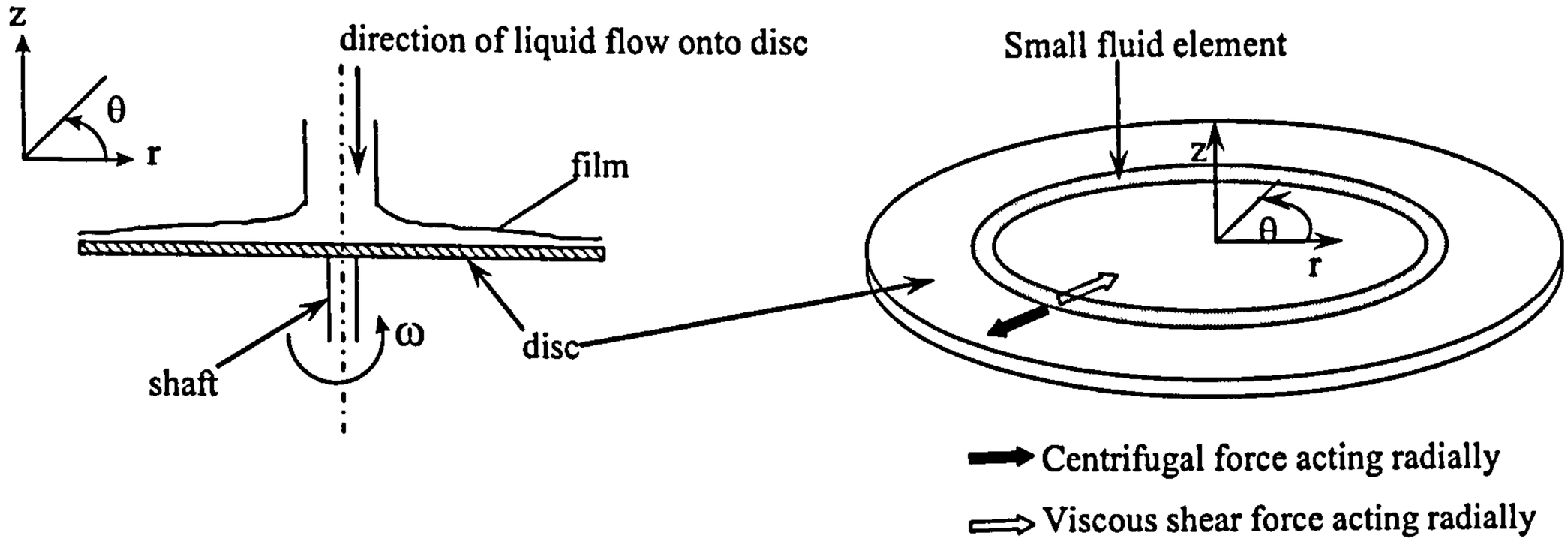


(a) Side view of film flow (b) Top view of film flow

**Figure 3.1. Thin film flow on a rotating disc**

For an incompressible fluid (where the density ρ is constant), equation (3.5) can be simplified:

$$\frac{1}{r}\frac{\partial}{\partial r}(r v_r)+\frac{1}{r}\frac{\partial v_\theta}{\partial \theta}+\frac{\partial v_z}{\partial z}=0 \qquad (3.6)$$

or, on expansion,

$$\frac{\partial v_r}{\partial r}+\frac{v_r}{r}+\frac{1}{r}\frac{\partial v_\theta}{\partial \theta}+\frac{\partial v_z}{\partial z}=0 \qquad (3.7)$$

Fluid flow in a rotating system is fully defined by equations (3.1), (3.2), (3.3) and (3.7).

The general Navier-Stokes equations (3.1), (3.2), (3.3) can be simplified, as it has been done by a number of workers, to obtain an adequate model describing the flow on the rotating disc [126, 127].

### *3.1.1.1 Centrifugal model*

Emslie et al. [127] have described the hydrodynamics of thin film flow on a smooth disc by means of a simple balance between the centrifugal force and the opposing viscous forces in the radial direction. They made following assumptions to simplify the Navier-Stokes equations:

1. *Liquid.* The liquid is a continuum incompressible fluid and has a viscosity that is independent of the rate of shear (i.e. a Newtonian fluid).

2. *Disc.* The surface of the rotating disc is smooth.

3. *Symmetry.* The system is axisymmetric. The thickness of the liquid is a function of the distance to the rotation axis, r, and time, t. The radial velocity at the height z from the surface is also a function of r, and δ: $v_r(r, z, \delta)$.

4. *Forces.* Forces due to the following are negligible: gravity, Coriolis acceleration (since $v_r << v_\theta = r\omega$ where $\omega$ is the angular velocity) and disjoining and capillary pressure gradients (since the slope $(\partial\delta/\partial r)$ and curvature $(\partial^2\delta/\partial^2 r)$ are both very small). Only centrifugal and viscous forces are relevant to the flow.

5. *Inertia terms.* Inertia terms in the Navier-Stokes equation are negligible in comparison with the viscous and centrifugal terms.

6. *Lubrication approximation.* This approximation states that both shear resistance and flow are only appreciable in horizontal directions (in this axisymmetrical system, only in the radial direction).

With these assumptions, the Navier-Stokes equation becomes:

$$-\frac{v_\theta^{\,2}}{r} = \nu \frac{\partial^2 v_r}{\partial z^2} \tag{3.8}$$

Substituting $v_\theta = r\omega$, equation (3.8) becomes:

$$-\omega^2 r = \nu \frac{\partial^2 v_r}{\partial z^2} \tag{3.9}$$

where $\nu$ is the kinematic viscosity.

### *3.1.1.2 Velocity profile*

The radial velocity profile across the thin film on the rotating disc can be obtained by integration of equation (3.9) with following boundary conditions:

$$\text{at } z = 0 \qquad v_r = 0 \qquad \text{('no slip' at the disc surface)}$$

$$\text{at } z = \delta \qquad \frac{\partial v_r}{\partial z} = 0 \qquad \text{(zero shear at the free surface of the film)}$$

Therefore,

$$v_r = \frac{\omega^2 r}{\nu}\left(\delta z - \frac{z^2}{2}\right) \tag{3.10}$$

where $\delta$ is the thickness of the film.

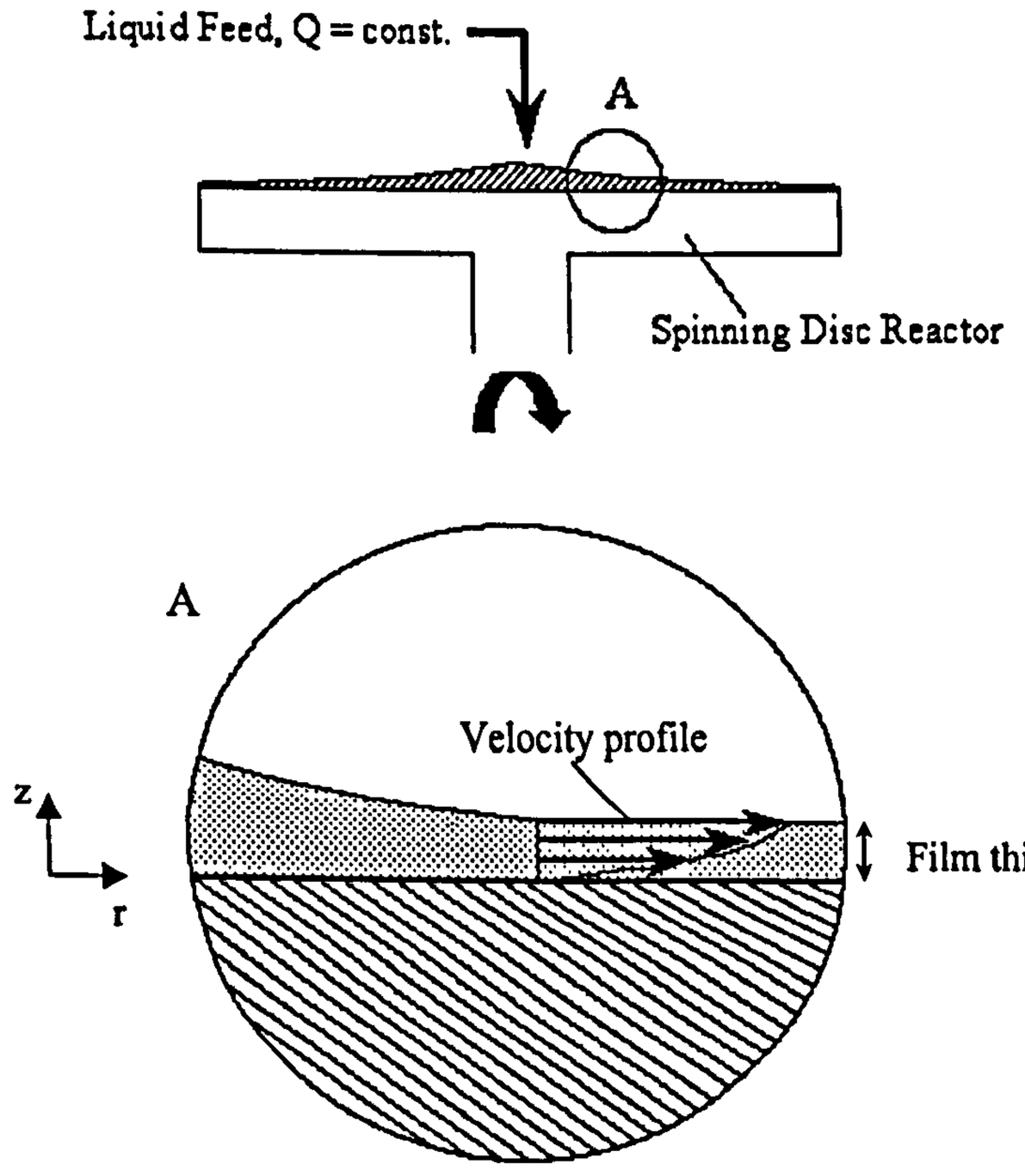


**Figure 3.2. Thin liquid film flow (velocity profile) in the SDR**

It was shown experimentally [128] that once a fluid spreads on the disc it quickly adjusts to the rotation rate of the disc in an entrance region of small radii. The flow is dominated to the first order by a balance of centrifugal and viscous

forces. Shear stress at the free surface of the thin film at low gas pressures is negligible therefore a semi-parabolic velocity profile develops in the radial direction (Figure 3.2).

First approximation is that circumferential velocity component v of the film is equal to that of the disc $v = 2\pi f r = \omega r$ over the full height of the film, so that no shear stress occurs in circumferential direction (where f is the rotation rate in Hz). The radial velocity field v(r, z) (3.10) can be also expressed as:

$$v(r, z) = \frac{r\,\omega^2\,\delta^2}{\nu} \cdot \left( \frac{z}{\delta} - \frac{1}{2}\left(\frac{z}{\delta}\right)^2 \right) \tag{3.11}$$

The shear rate in radial direction $\dot{\gamma}$ is formed by the two velocity gradients:

$$\dot{\gamma}(r, z) = \frac{\partial v}{\partial z} + \frac{\partial \varpi}{\partial z} \tag{3.12}$$

but since the axial velocity component $\varpi$ is very small, $\dot{\gamma}$ can be expressed as:

$$\dot{\gamma}(r, z) \approx \frac{\partial v}{\partial z} = \left( \frac{3\,Q\,\omega^4\,r}{2\pi\nu^2} \right)^{1/3} \left( 1 - \left( \frac{z}{\delta} \right) \right) \tag{3.13}$$

It can be seen that the shear rate is zero when $z = \delta$, linearly increases with decreasing axial co-ordinate z and has a maximum value at the surface of the rotating disc. Furthermore, it increases in radial direction from the centre to the rim of the rotating disc (applied to spinning disc experiments, see Appendix B). The shear rates across the disc are higher than in a conventional batch reactor, in order of at least one magnitude.

### *3.1.1.3 Film thickness*

From the equation for the velocity distribution in the film, the average radial film velocity can be presented as:

$$\bar{v}_r = \frac{1}{\delta} \int_0^{\delta} v_r \, dz = \frac{\omega^2\,r\,\delta^2}{3\nu} \tag{3.14}$$

where $\nu$ is the kinematic viscosity; or in terms of the volumetric flow rate Q per unit area of cross-section available for flow:

$$\bar{v}_r = \frac{Q}{2\pi r \delta} \tag{3.15}$$

An expression for the film thickness as a function of the system parameters is then formulated by combining equations (3.14) and (3.15):

$$\frac{Q}{2\pi r \delta} = \frac{\omega^2 r \delta^2}{3\nu}$$

which, on rearrangement, yields:

$$\delta = \left( \frac{3}{2\pi} \frac{\nu Q}{\omega^2 r^2} \right)^{1/3} \tag{3.16}$$

### *3.1.1.4 Mean residence time*

The mean residence time of the film between two radial positions on the disc can be calculated from equation (3.14), substituting for $\delta$ from equation (3.16). Following can be obtained:

$$\frac{dr}{dt} = \left( \frac{\omega^2 Q^2}{12\pi^2 \nu} \right)^{1/3} r^{-1/3} \tag{3.17}$$

After integration within the limits given below:

$t = 0, \qquad r = r_i$

$t = t_{res}, \qquad r = r_o$

where: $r_i$ – is the radial distance of the inlet from the centre of the disc,

$r_o$ – is the radius at exit;

expression for the residence time $t_{res}$ can be presented as:

$$t_{res} = \left(\frac{81\pi^2 \nu}{16\omega^2 Q^2}\right)^{1/3} \left(r_0^{4/3} - r_i^{4/3}\right) \tag{3.18}$$

As the simplest formulation of the Navier-Stokes equation, centrifugal model validity is strongly dependent on many assumptions which for some systems do not hold true. In such cases, alternative models have to be applied.

### *3.1.1.5 Other models*

In many models, such as centrifugal, the Coriolis acceleration, $a_{Cor} = 2\, v_r\, \omega$, can be disregarded since radial velocity, $v_r$, is negligible. Therefore if the radial velocity component has to be taken into account the Coriolis model has been formulated to give a more rigorous description of film flow. Coriolis force acts on the film in an azimuthal direction opposite to the direction of disc rotation and as a result, the fluid velocity in the angular direction is lower than that for the disc. Bell [22] took the Coriolis effect into consideration and used equations (3.19) and (3.20) in the analysis:

$$-\frac{v_\theta^2}{r} = \nu \frac{\partial^2 v_r}{\partial z^2} \tag{3.19}$$

$$\frac{v_\theta v_r}{r} + v_r \frac{\partial v_\theta}{\partial r} = \nu \frac{\partial^2 v_\theta}{\partial z^2} \tag{3.20}$$

In the above equations $v_\theta$ can be replaced by $r\omega^2$ giving equations (3.21) and (3.22) which have been solved by Bell [22] and Lim [24] to obtain a velocity profile for $v_\theta$ in terms of the radial position r and the upward vertical distance z:

$$-\omega^2 r = \nu \frac{\partial^2 v_r}{\partial z^2} \tag{3.21}$$

$$2 v_r \omega = \nu \frac{\partial^2 v_\theta}{\partial z^2} \tag{3.22}$$

Emslie et al. [127] have specified that the Coriolis effect can be ignored if $\nu >> \omega\delta^2$, therefore the applicability of the much simplified centrifugal model is limited to relatively thin films of high viscosity fluids at a given angular velocity.

Several other models have also been developed to include inertial and gravitational effects on the film flowing on a rotating disc. Momoniat and Mason [129] have neglected inertia terms but retained Coriolis force terms and derived an equation which determines the evolution of the free surface of the thin film due to effect of viscous, centrifugal and Coriolis forces. They observed that the correction due to Coriolis force to the height of the free surface is of the same order of magnitude as the inertia terms neglected in Navier-Stokes equation. If $\delta/E$ (where $\delta$ is film thickness and E is Ekman's boundary layer thickness) is small, they found that Emslie et al. have derived extremely accurate equation. Myers and Charpin [130] have shown that in the absence of surface tension and gravity (axisymetric flow) the Coriolis term in the radial velocity equation is negligible, which again led to equation derived by Emslie et al. [127].

Simple centrifugal model was found adequate to describe the flow on a fairly large disc since inertia, gravity and Coriolis acceleration were found to have any significant effect on the thin film flow behaviour only at relatively small distances from the discharge point of the fluid on the disc [131].

### 3.1.2 FLOW REGIMES

#### *3.1.2.1 Reynolds number*

Reynolds number (Re) directly affects the rate of mixing, heat and mass transfer in the fluid. As the velocity varies with r, Re is radius-dependent, but not rotation rate-dependant. The Reynolds number of the thin film is evaluated using the average velocity:

$$Re = \frac{\bar{v}\delta}{\nu} = \frac{2Q_v}{\pi r \nu} \qquad (3.23)$$

where $\bar{v}$ – average velocity (m/s)

$\nu$ – kinematic viscosity ($m^2/s$)

$Q_v$ – volumetric flow rate ($m^3/s$)

r – radius at point of measurement on disc (m)

The criteria governing the type of flow (smooth laminar, wavy laminar and turbulent) obtained on a plane vertical surface have been measured experimentally by various researchers [114, 115, 118, 122]. These criteria are:

Re < 16: smooth laminar flow (no surface waves)

16≤ Re < 40: Undulations across the film (small amplitude waves)

40 ≤ Re < 80: Sinusoidal waves gradually replaced by regular waves

80 ≤ Re < 1000 – 2000: Random surface waves (wavy laminar flow)

Re ≥ 1000 – 2000: Turbulent regime

Although the above criteria have been defined on the basis of film flow under gravity, they are also applicable to films formed by the action of high centrifugal fields.

Shear instabilities in thin film flow arise at very large Re (>950). On the other hand, thin liquid flows are unstable with respect to surface waves even at the lowest Re.

### 3.1.3 FLOW VISUALISATION

The direct visual observation of the generated flow pattern can also help to determine the operating flow regime on the rotating surface. Small waves appear initially on a liquid film falling down a smooth surface and quickly develop into large waves further downstream (lumps of liquid moving on a thin film) [132]. If the feed rate is kept constant along horizontal entrance, two-dimensional waves, with horizontal wavefronts, appear at low Reynolds numbers and are very sensitive to disturbances. Within a short distance from the wave inception line waves tend to become three-dimensional and therefore more chaotic.

Most of the flow visualisation experiments were performed using smooth surfaces [21-24, 133]. A separate study involving tailored rotating surfaces [27]

showed a difference in the flow regimes obtained on such mechanically treated surfaces. Three different surface configurations were tested and compared to the flow on a smooth disc: metal sprayed, re-entry grooved (Figure 3.3 (a)) and normal grooved discs (Figure 3.3 (b)). Results showed that for a given flow rate and rotational speed, tailored surfaces (grooved types in particular), created more waves of small amplitude and short wavelength at the film surface than the smooth disc. More waves were observed for the re-entry grooves at low rotational speeds compared to those on the normal grooved disc. At high rotational speeds the normal grooved disc generated more waves, hence more instabilities and thus was more efficient.

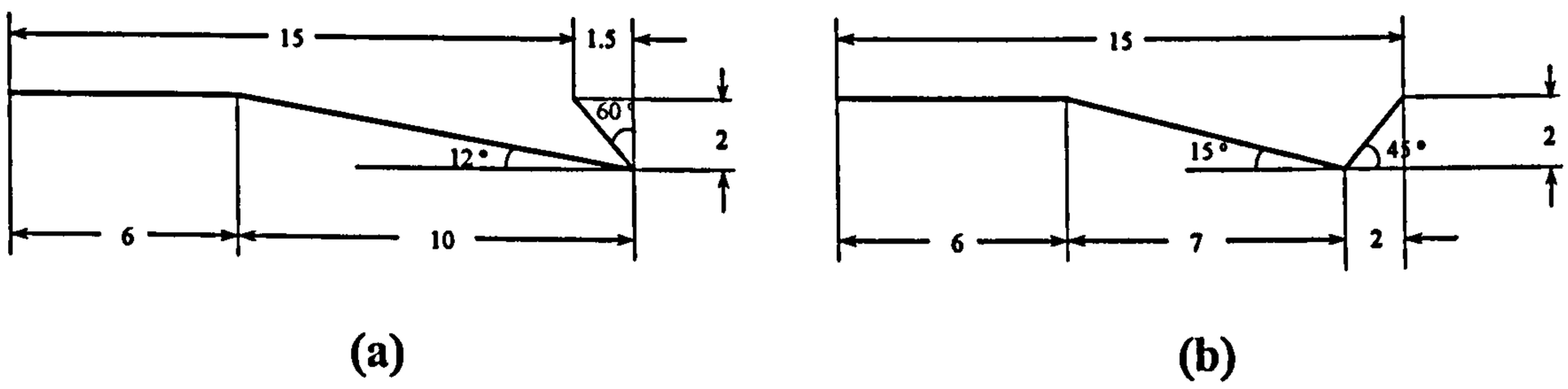


(a) (b)

**Figure 3.3. Grove geometry [27] (a) re-entry grove; (b) normal grove**

Tzeng et al. [134] have developed a scheme for visualisation which utilises the strong adhesion forces between micrometer-sized particles and solid surfaces to register surface streaklines or streamlines for steady flows. They used fluorescent particles to allow the spectral separation of particle fluorescence emission from morphology-related elastic light scattering from the surface. The surface streaklines provided information about the boundary layers on the disc while the spreading angle of the jets in the self-pumped through-flow revealed details about the bulk flow outside the boundary layer. The spreading of the streaklines (Figure 3.4) was found to increase linearly with radius and the spiral angle of the streaklines ($\alpha$) over a major portion of the disc surface and was found to be in good agreement with the theory for laminar Ekman boundary layers.

Dhanak [135] has estimated the wave angle of the spiral vortices that precede turbulent flow from critical conditions under suction (which was found to have stabilising effect on the flow, whereas blowing is destabilising). Wave angle was shown to decrease with increase in suction rate.

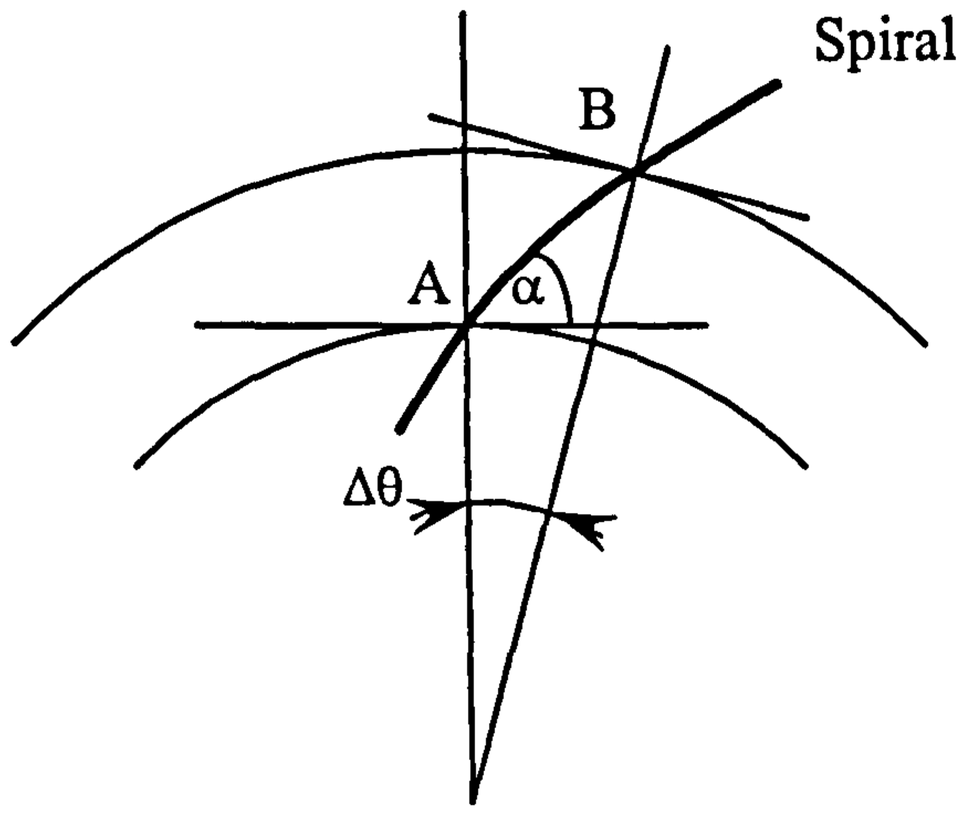


**Figure 3.4. Trajectory of the surface streaklines**

The stability of the rotating disc flows has been the subject of many studies, one reason for this being that the basic boundary layer flow given by Von Karman's [136] exact solution is fully three dimensional. Interest also stems from the observed similarities in the type of instability occurring in rotating disc work [137]. This instability, known as cross-flow instability, is due to inflectional character of the basic velocity profile and was first extensively studied by Gregory et al. [137]. The authors suggested, using inviscid theory, that the instability could be associated with a particular inflectional profile in which inflection point coincided with a point of zero velocity somewhere in the flow.

Several attempts have been made to explain the observed spiral patterns by means of a linear stability theory [138-140]. Malik et al. [139] showed that Coriolis force and streamline curvature can not be neglected. This point was first made by Faller and Kaylor [141] and Lilly [142] in the context of the Ekman boundary layer. The theoretical results of Mack [140] strongly suggest that a spiral streaks observed in flow visualisation experiments are the constant phase lines of the merged wave patterns produced by several random sources on the disc. This was first found by the experiments of Wilkinson and Malik [143] who revealed that the wave patterns from each point source spread out circumferentially downstream of the cover of the entire circumference of the disc.

Fedorov et al. [144] showed that for various rotational rates of the disc an instability occurred which also appeared as a pattern of spiral vortices. Malik [138] calculated the neutral stability curve for stationary disturbances and demonstrated

that two types of mode could exist. The first, the upper branch of the neutral curve, corresponds to the inviscid mode described by Stewart [137]. The second, the lower branch mode, is an essentially viscous disturbance which corresponds to zero wall stress of the crossflow velocity profile.

Charwat et al. [145] had identified stability boundaries for different types of flow pattern generated on rotating disc. Smooth film flow was typically characterised by low flow rates and low rotational speeds. At many other conditions of disc rotational speeds, flow rates, surface tension and viscosity of the fluid studied, different types of waves were observed. When the flow rate increased at low rotational speeds concentric waves were noticed and they remained close to the centre of the disc due to the outflow from the nozzle distributor and not because of surface instabilities in the film. Tendency of those waves was to move radially outwards and inevitably decay at a certain radial distance from the centre of the disc leaving a smooth film surface on the outer part. At higher rotational speeds and relatively low flow rates spiral waves appeared, originating from some radius away from the centre, and then decayed close to the edge of the disc. A combination of very high flows and rotational speeds led to the highly unstable film and the spiral wave fronts were seen to break up into numerous individual three-dimensional wavelets decaying at large radii.

Wave-associated flow regimes on rotating discs were also considered by Woods [21]. He carried out study on the formation and propagation of waves at the free surface of films of water mixed with a coloured dye flowing on a rotating disc. Three distinct flow regions were observed at different radial locations on the disc: an inner region with a smooth flow, middle section with a single tightly wound spiral having a longer wavelength as the rate of rotation was stepped up and an outer region up to the boundary of the disc with a multitude of spirals with irregularities along the wavefronts eventually disintegrated into random three-dimensional wavelets on propagation across the disc.

Lim [24] observed that at the highest flows and rotational speeds the whole surface of the disc was covered with three-dimensional wavelets or ripples. He introduced correlations for the 'wave inception' wave amplitude and wavelength in terms of the non-dimensional Reynolds number Re and Taylor number Ta.

Makarytchev et al. [146] have studied wavy liquid films in the spinning cone and developed models for film thickness and velocity, since thickness of the film significantly influences the mass transfer characteristics and capacity of gas-liquid contacting devices. They also gave comparison to rotating discs as a limiting case of a cone.

A method of rapid measurement of liquid film thickness on a spinning disc surface is currently under development by Burns et al. [147]. The concepts used are based on the analysis of the electrical resistance of the liquid film and its relationship to film thickness when high frequency voltages are applied.

### 3.1.4 HEAT AND MASS TRANSFER

As mentioned before, the first studied thin films were those falling under gravity and it has been known for a long time that the heat transfer in such thin films is enhanced. The phenomenon is greatly exploited in condensers or evaporators, the commonly encountered falling film equipment. First centrifugal evaporator used in sea-water desalination, developed by Hickman [148] illustrated the successful application of the spinning surface technology in the field of heat transfer. Ever since, a number of researchers have investigated use of the high centrifugal fields created by rotating surfaces for enhancement of the heat and mass transfer. It has been shown [16] that the heat transfer coefficient during boiling/evaporation or condensation under those acceleration fields, has been incredibly increased by 1000%. Wood and Watts [133] tested the heat transfer properties of a small disc rotating about a horizontal axis and the results showed that high heat transfer rates could be achieved by increasing the liquid flow rate and rotational speed.

Heat transfer coefficients on rotating disc can be calculated using correlations such as (3.24) for turbulent flow in tubes [149]:

$$\frac{\alpha d_e}{\lambda_{fluid}} = j_h \, Re \, Pr^{0.33} \left( \frac{\mu_{bulk}}{\mu_{wall}} \right)^{0.14} \qquad (3.24)$$

where:

$\alpha$ – heat transfer coefficient ($Wm^{-2}K^{-1}$)

$d_e$ – equivalent hydraulic diameter (m)

$\lambda$ – thermal conductivity ($Wm^{-1}K^{-1}$)

$j_h$ – heat transfer factor

$\mu$ – dynamic viscosity (Pa s)

For the calculation of $d_e$ in (3.24), the channel width and film thickness can be used to obtain values of heat transfer coefficient for heat transfer fluid, $\alpha_{HTF}$ and coefficient for process fluid, $\alpha_{PF}$ respectively. Overall heat transfer coefficient, U, can be computed as a function of the radial distance from the disc centre, r:

$$\frac{1}{U(r)} = \frac{1}{\alpha_{HTF}(r)} + \frac{x}{\lambda_{disc}} + \frac{1}{\alpha_{PF}} \qquad (3.25)$$

where x is the disc thickness (m).

Oxley et al. [150] have used various heat transfer fluids and disc types (with n-heptane as a process fluid) to determine the profile of overall heat transfer coefficient on the disc. It was shown that disc material did not have much influence on overall heat transfer coefficient when the thermal conductivity of a heat transfer fluid was low. To promote effective heat transfer, a heat transfer fluid with high thermal conductivity and a narrow channel underneath the disc is essential.

Yanniotis and Kolokotsa [151, 152] explored the heat transfer characteristics of boiling liquid films and condensing vapours on both smooth and grooved spinning disc surfaces. The results indicated large enhancements in heat transfer with heat coefficients of up to 16 $kW/(m^2K)$ for boiling and 30 $kW/(m^2K)$ for condensation for a rotational speed of 1000 rpm. They also showed that the local heat transfer coefficient does not change with radius.

Evaporation on the surface of a horizontal rotating disc heated by condensing steam on the underside was studied by Bell [22]. He tried to correlate the measured evaporation film coefficient with Reynolds number and Taylor number. Khan [25] investigated heat transfer on a rotating disc with and without phase change. And recently, Jachuck and Ramshaw [27] studied the effect of different types of grooves in the disc surface on the convective heat transfer characteristics of the disc. As the test fluid authors used water. Results demonstrated that surface instabilities and heat

transfer coefficients were significantly increased in the presence of grooves to an average value of 18 kW/($m^2$K) in comparison to the smooth surface.

Rahman et al. [153-155] have done a computational analysis of the heat transfer characteristics using an iterative procedure applied to a three-dimensional co-ordinate system. Their results showed that heat transfer coefficients became much larger with increases in radial distance, rotational speed and liquid flow rate. Improvements in the theoretical model and computational procedure for the prediction of film height and heat transfer coefficient are presented in the latest work of the same authors [156].

Lim [24] investigated the mass transfer rates during the absorption of oxygen in thin liquid films on a rotating disc. Mass transfer coefficients reported in this work were much larger than can be predicted on the basis of molecular diffusion in a smooth laminar liquid film alone. This was attributed to vigorous bulk mixing action of the many ripples formed on the film surface. The effect of rotation on mass transfer processes using various perforated and smooth plates as the active mass transfer surfaces was investigated by Moore [26]. He observed that mass transfer coefficients for the perforated surfaces were much higher than those on the smooth disc due to excessive random turbulent waves.

Many researchers tried to model the mass transfer processes inside the thin wavy liquid films flowing on rotating surfaces [157-160], but as with heat transfer models, there is not a universally accepted model to predict the mass transport phenomenon in the presence of surface waves on thin liquid films. Many developments have been patented as a result of the success of the intensified processes, such as Higee contactor [161] for intensified mass transfer operations. For more insight into heat and mass transfer equations, see Appendix C.

# CHAPTER 4

## AIMS OF THE PRESENT INVESTIGATION

### 4.1 INTRODUCTION

The fine and speciality chemical industries are among the most successful in the UK but their future growth will heavily depend on the development and application of new more environmentally friendly technologies aimed at the reduction of waste at source. The manufacture of fine and speciality chemicals in batch processes has commonly been associated with the production of large quantities of hazardous waste. Many of these processes employ large quantities of traditional mineral acids or Lewis acids as catalysts leading to serious operational and environmental hazards including:

- handling difficulties (e.g. with corrosive acids and water-sensitive reagents leading to health and safety as well as engineering difficulties);
- inorganic contamination of the organic products (requiring additional separation/purification stages leading to loss of product and additional waste);
- the formation of large quantities of inorganic waste which is often contaminated with organics making treatment and disposal especially difficult (e.g. ca. 7,500T of $AlCl_3$ is currently imported into the UK per annum leading to 6,000T of HCl produced and 26,000T of aqueous acidic effluent containing aluminium salts and organic residue which must be removed prior to discharge [162]);
- poor reaction selectivity leading to the formation of unwanted isomers and high molecular weight side-products.

There is definitely much scope for applying new reactor technologies and catalysts for improved control, selectivity, product quality and intrinsic safety.

## 4.2 AIMS AND OBJECTIVES

The suitability of the spinning disc reactor for performing organic catalytic reaction involving the rearrangement of α-pinene oxide will be investigated. Novel supported catalysts, prepared at the University of York, will be tested. In order to carry out a systematic investigation, the following objectives were established:

- Performance studies using a batch reactor for obtaining reaction rate data for characterisation and bench marking the performance of a SDR;
- Design and fabrication of the SDR;
- Performance studies of the SDR for carrying out the α-pinene oxide rearrangement reaction and studying the influence of the disc rotational speed, feed flow rate and disc temperature on conversion/selectivity;
- Study of a range of catalysts (e.g. 0.05 mmol/g $Zn(OTf)_2/SiO_2$, 0.01 mmol/g $Zn(OTf)_2$/K100 and 0.05 mmol/g $Zn(OTf)_2/HMS_{24}$) for the model reaction in the SDR;
- Reaction rate kinetics investigation and establishment of performance models;
- Scale up/scale out investigation and methods for improving selectivity and conversion.

## 4.3 OUTLINE OF THE APPROACH

In order to make a realistic evaluation of the implementation of the spinning disc reactor for catalytic reaction of α-pinene oxide isomerisation, performance data from the SDR will be benchmarked against data obtained using a laboratory batch reactor. Data containing the reaction rate, conversion and selectivity will be compared as a function of temperature and residence time. The above data will be obtained by using liquid/gas chromatography (LC/GC) analysis.

Spinning Disc runs will be tried initially at different temperatures (ranging from 25–85°C) for evaluation of the optimum temperature, whilst other parameters such as rotational speed and flow rate will be varied subsequently. A range of

catalysts will be investigated and optimum conditions for each of them will be determined with regards to selectivity towards campholenic aldehyde. The product from each run will be analysed for conversion and selectivity using LC/GC.

The concept of using the SDR in a cascade fashion will also be theoretically investigated for achieving longer residence time.

Using the batch data, activation energies will be determined for each catalyst.

# CHAPTER 5

## APPARATUS AND EXPERIMENTAL PROCEDURES

### 5.1 INTRODUCTION

This section describes the experimental facility, analytical equipment and experimental procedures used in this study. The apparatus used in this investigation can be divided into two main parts. The first part is the batch reactor used for kinetics and benchmarking purposes and the second part is the SDR. Each of them have been used to study the influence of three catalyst systems, namely 0.05 mmol/g $Zn(OTf)_2$ supported on $SiO_2$, 0.01 mmol/g $Zn(OTf)_2$ supported on K100 and 0.05 mmol/g $Zn(OTf)_2$ supported on $HMS_{24}$ for performing the α-pinene oxide rearrangement reaction. The analytical technique used has been consistent for all the three catalysts that were used.

In order to compare the performance of the catalytic SDR with that of a batch reactor, a range of experiments were performed. Details of these experiments along with the details of experiments carried out to investigate the reaction kinetics have been presented in this Chapter in section 5.3.

Analytical techniques employed in this investigation have been detailed in section 5.4.

### 5.2 CATALYTIC EXPERIMENTS

#### 5.2.1 BATCH APPARATUS

A batch reactor, shown in Figure 5.1 and schematically in Figure 5.2, was used to obtain the data needed to benchmark the performance of the SDR using comparable reaction temperatures. It consisted of a 250 ml capacity volume 'Pyrex' glass vessel surrounded by a water circulator system. The circulating water was pumped from a constant temperature bath which was provided with a digital controller unit for temperature control. The reactor was placed in the centre of a

magnetic plate which, together with a magnetic stirrer in the reaction mixture, was used to provide uniform temperature and adequate mixing. The speed of mixing in the batch mixture was manually controlled by a knob on the magnetic plate. Access to the glass vessel was provided by two stopped arms and a thermocouple was inserted through one of them and connected to the data logger to record the temperature of the mixture. The other arm was used for feeding reactant, solvent and catalyst into the reactor and for taking samples from the reaction mixture as required. The top end of the vessel was fitted with a vertical condenser system to prevent loss of volatile material.

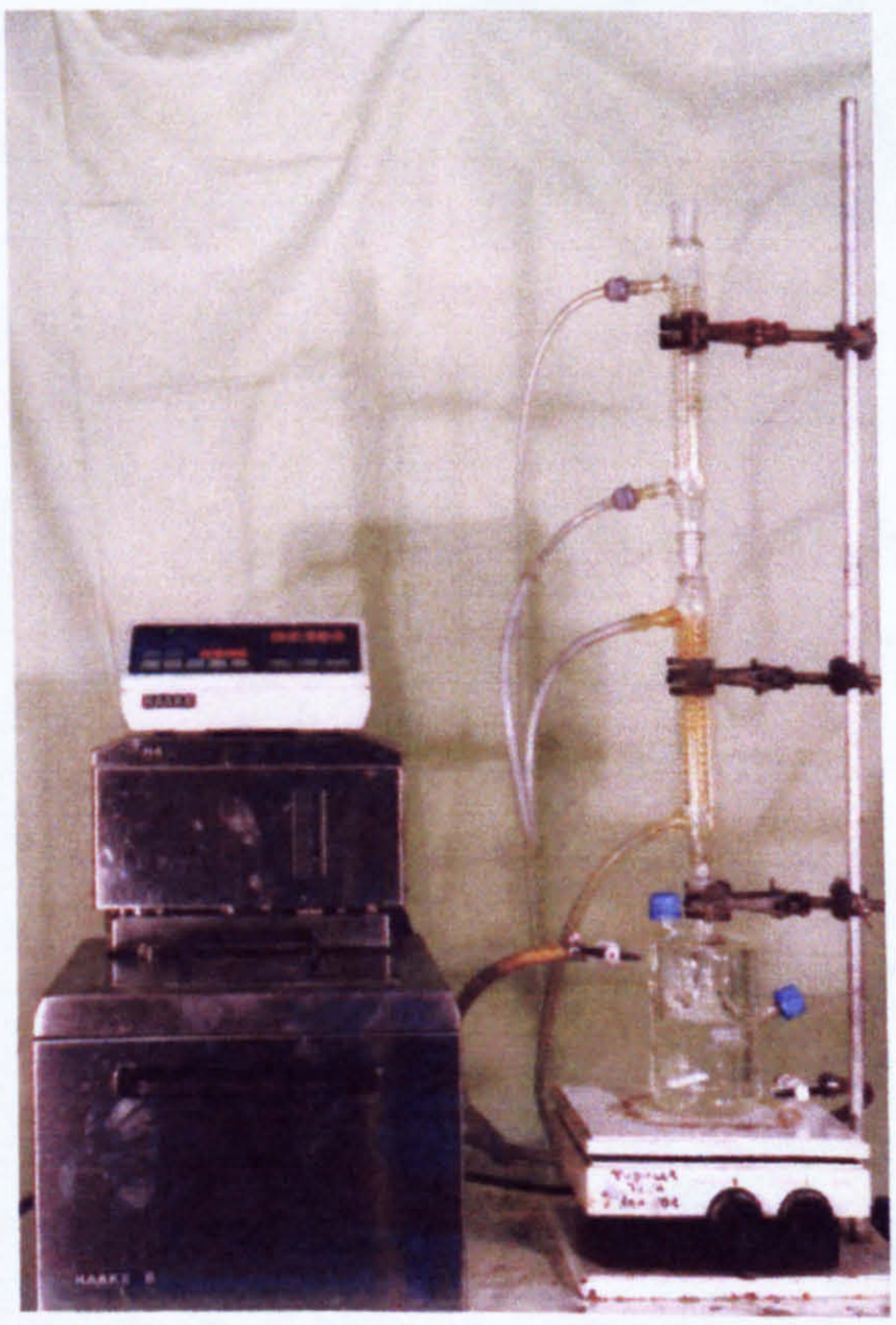

**Figure 5.1. Batch Reactor**

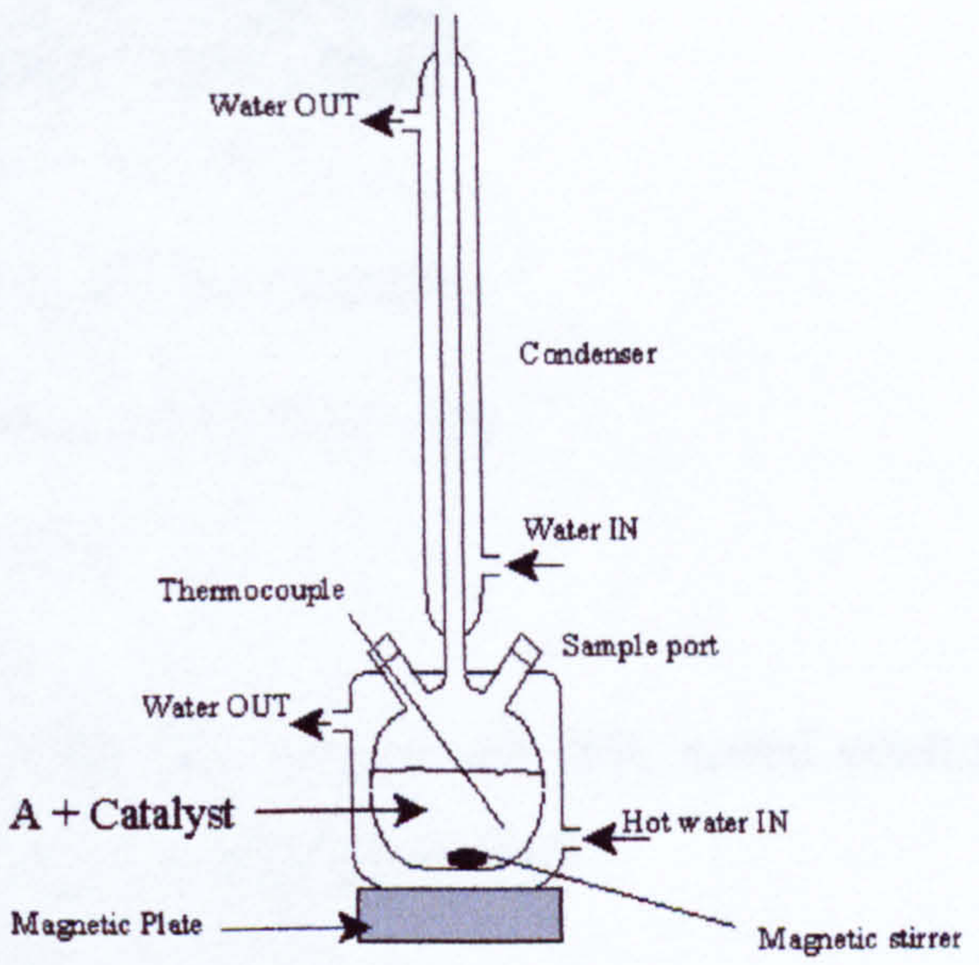


**Figure 5.2. Schematic of Batch Reactor**

### 5.2.2 SPINNING DISC APPARATUS

As a part of the project, a new SDR was designed and constructed. Delay of fabrication meant that slightly modified existing SDR, as shown in Figure 5.3, was used for this investigation. Nevertheless, as an evidence of expertise and knowledge about SDR design, the detailed drawings of the new SDR, which has now been constructed and used extensively in the Centre, is presented in Appendix D.

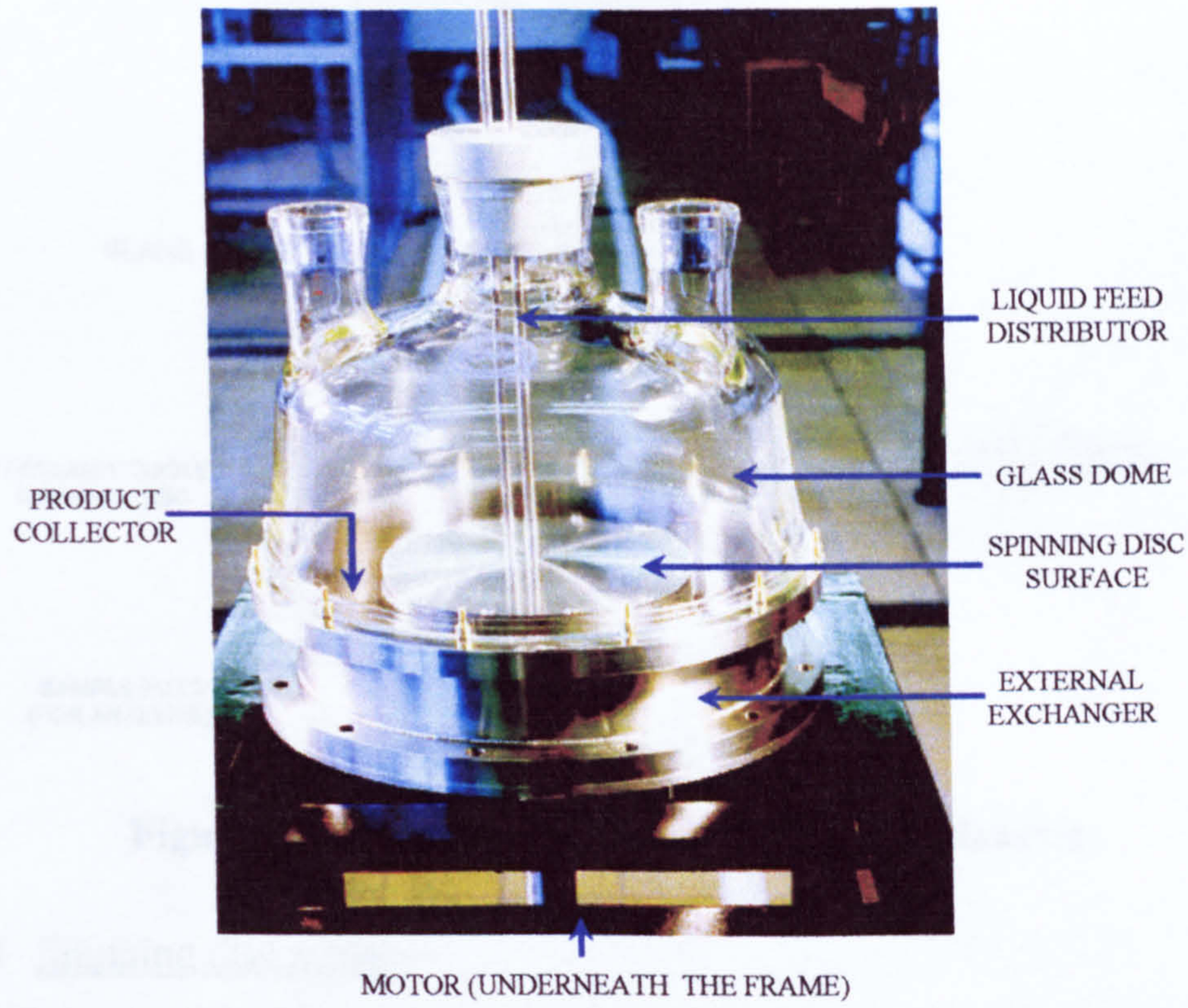


**Figure 5.3. Outside view on the SDR**

The spinning disc test facility consisted of the following:

1. Spinning Disc Reactor (SDR)
2. External temperature bath
3. Instrumentation (temperature data acquisition unit, speed control regulator and rotational speed measuring device)

*5.2.2.1 Spinning Disc Reactor*

A view of the SDR is presented in Figure 5.3. Most of the main parts of the reactor can be seen schematically in Figure 5.4, which consist of the following: spinning disc surface, thermocouples and motor, liquid feed distributor, product collector and reactor housing with external exchanger and glass dome.

Most of the design features of the spinning disc reactor which has been described in this section were adopted from the previous work [163], where the disc was designed and used for exothermic reactions studies. A few modifications with regard to the feed distributor and the disc surface coating have been made for this study. Details of the modifications are given in sections 5.2.2.1.3 and 5.3.2 respectively.

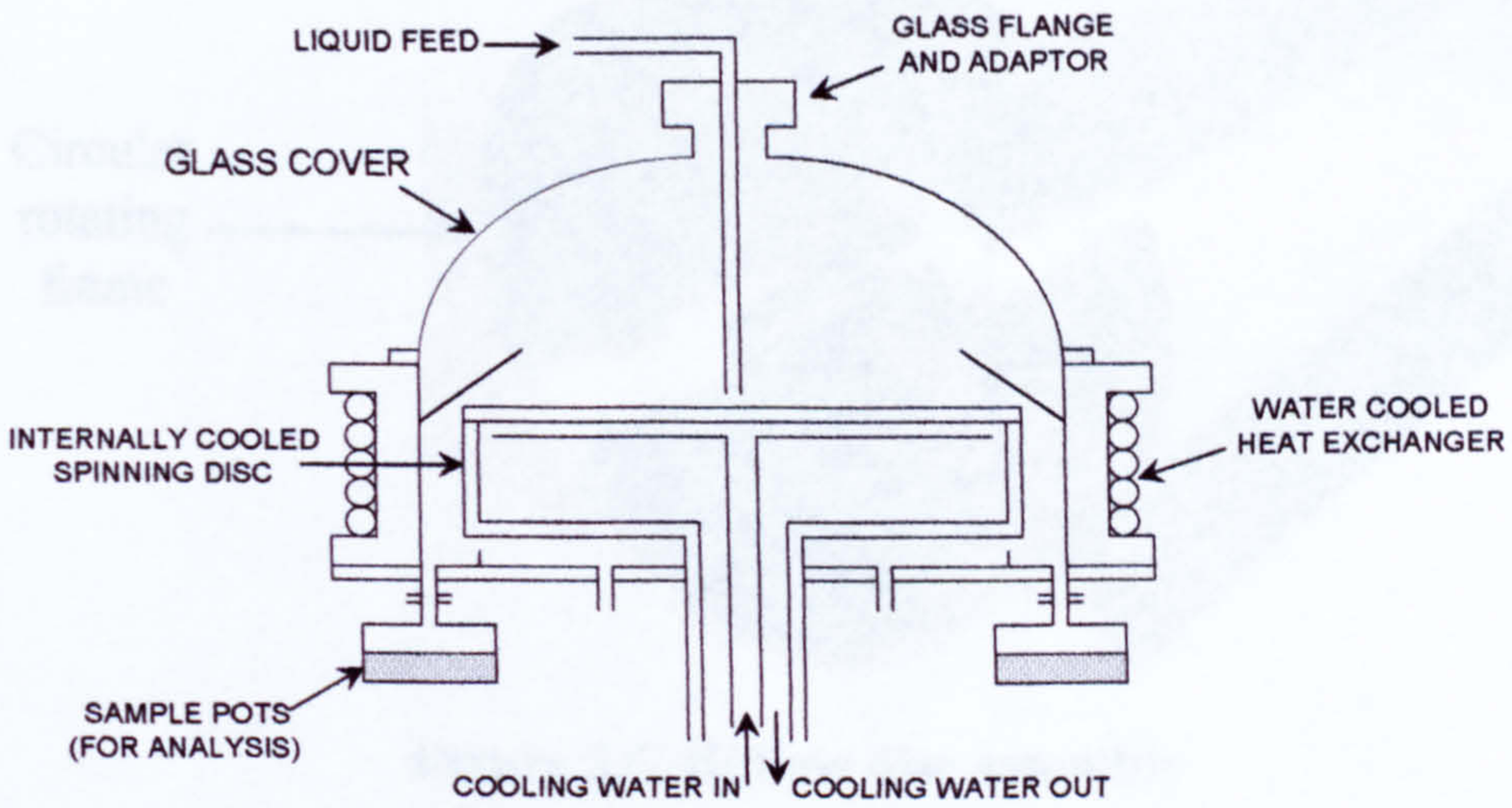


**Figure 5.4. Schematic of the Spinning Disc Reactor**

5.2.2.1.1 Spinning disc surface

The disc itself was constructed of stainless steel and is 200 mm in diameter (Figure 5.5), giving a heat transfer area of 0.03 $m^2$ for the exchange of heat between the liquid film and the disc. Two smooth discs of thickness 3 mm and 5 mm were constructed, but only a 3 mm disc was used in this investigation.

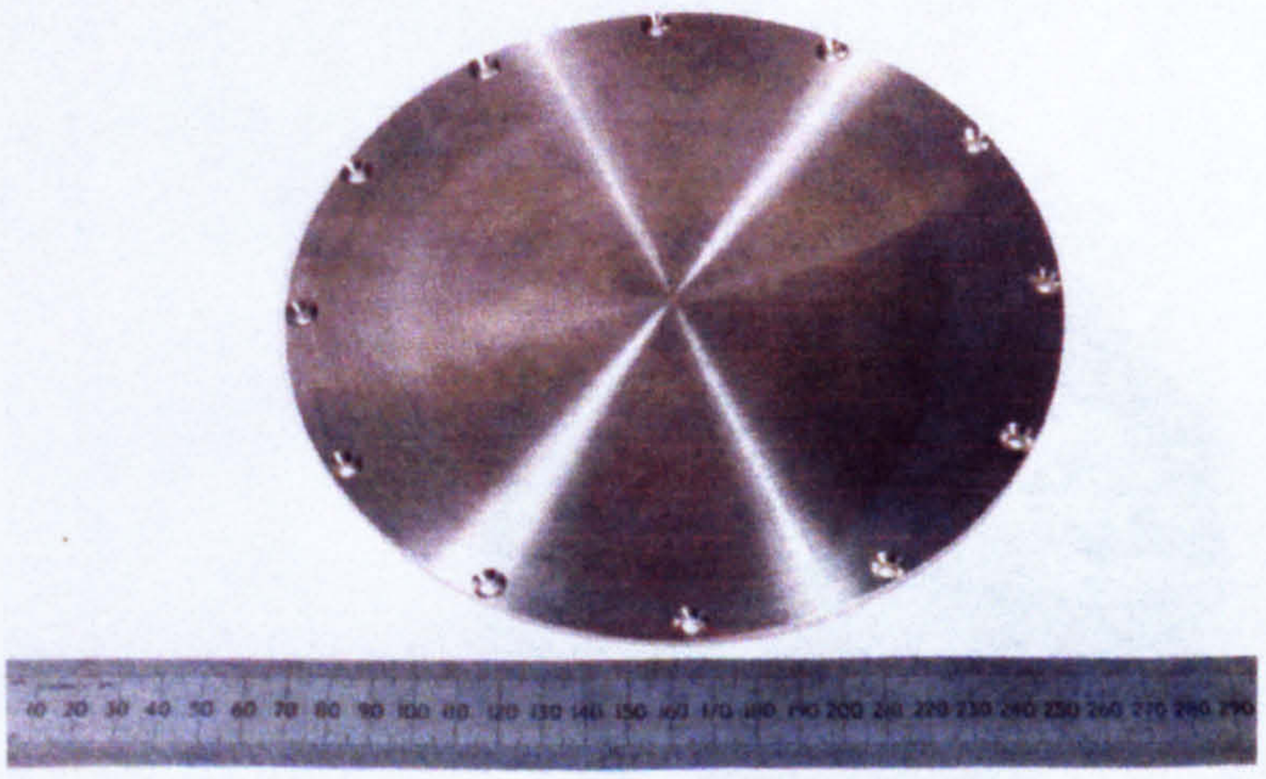

**Figure 5.5. Disc surface**

The disc was bolted onto a circular stainless steel frame, 65 mm in depth, to form an effectively hollow disc. This frame was then attached to the drive shaft which had an external diameter of 35 mm and an internal of 25 mm. Fitted inside the drive shaft was a thin tube (approx.17 mm diameter) which formed the inlet channel for the heat transfer fluid (water in this case) to flow (Figure 5.6).

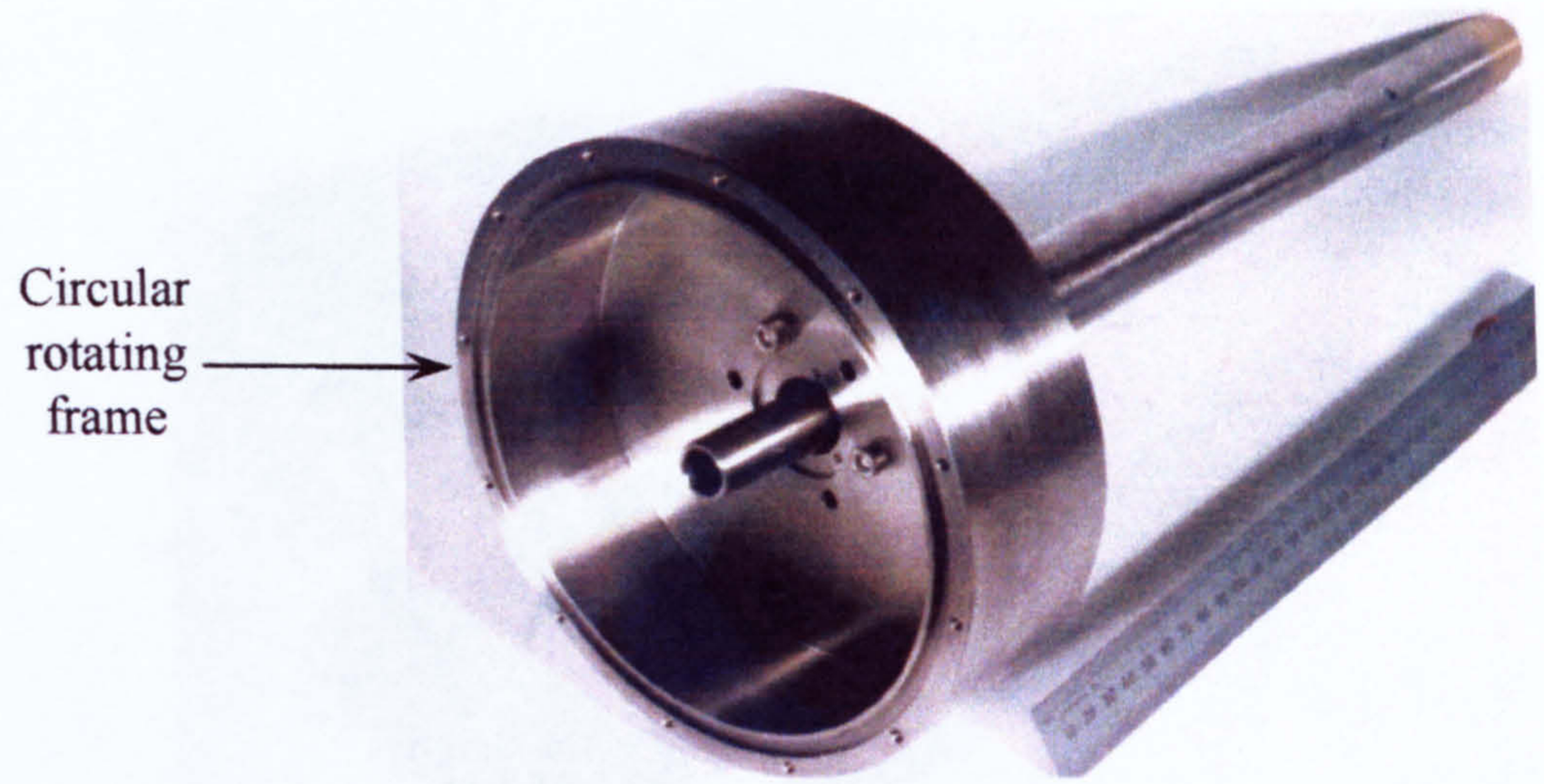


**Figure 5.6. Hollow disc assembly**

At the top of this tube was a thin circular plate, presented in Figure 5.7, which was located inside the frame and was positioned several millimetres below the underside of the top disc. The disc assembly can be seen in Figure 5.8. The drive shaft had several holes located towards the lower end to allow the cooling water to be removed from the shaft. A rotary union (Deublin 57-000-094) was attached to the lower end of the drive shaft.

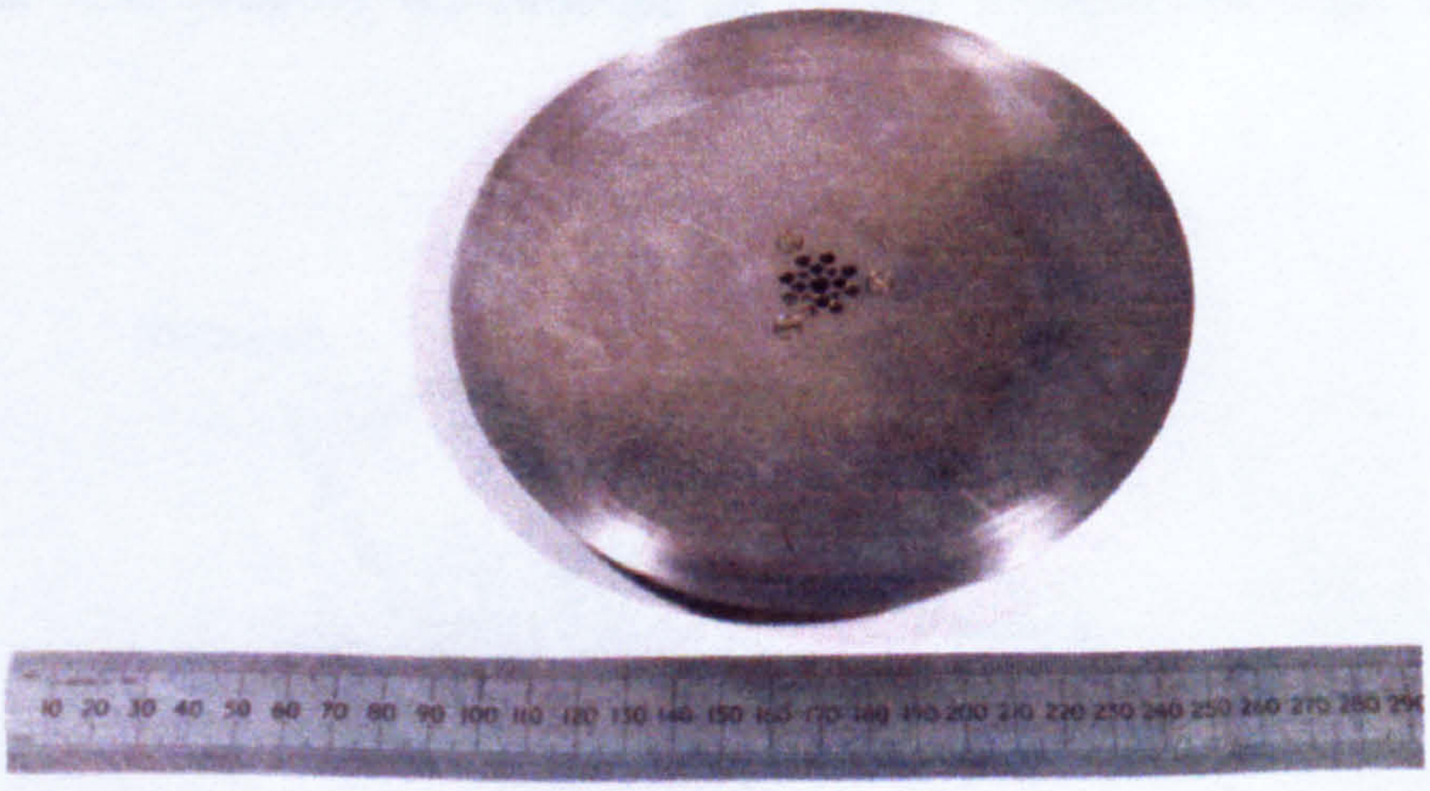

**Figure 5.7. Internal plate**

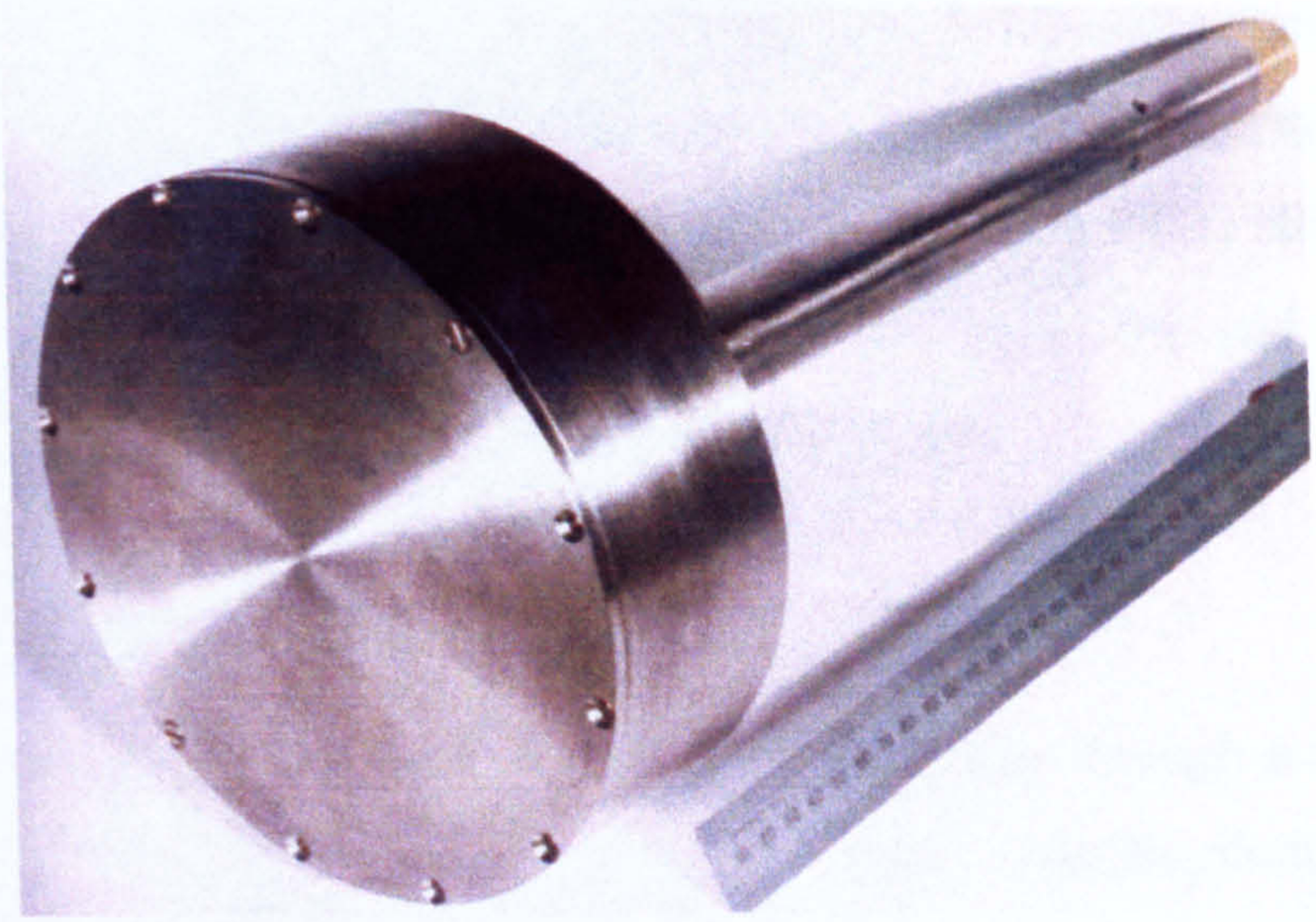

**Figure 5.8. Assembled disc system**

5.2.2.1.2 Thermocouples and motor

Five thermocouples have been used to measure the temperature of the disc, feed inlet and outlet and the temperatures of the heat transfer fluid. The locations of these thermocouples have been shown in Figure 5.9.

Thermocouples in Positions 1 and 3 were utilised to obtain the temperature of the heating/cooling fluid on the inlet and outlet positions. Thermocouple in Position 2 was used to detect the fluid temperature on the contact with disc surface. Remaining two (Positions 4 and 5) were used to measure the feed temperature before it hits the disc and product temperature as it has been thrown off the disc respectively.

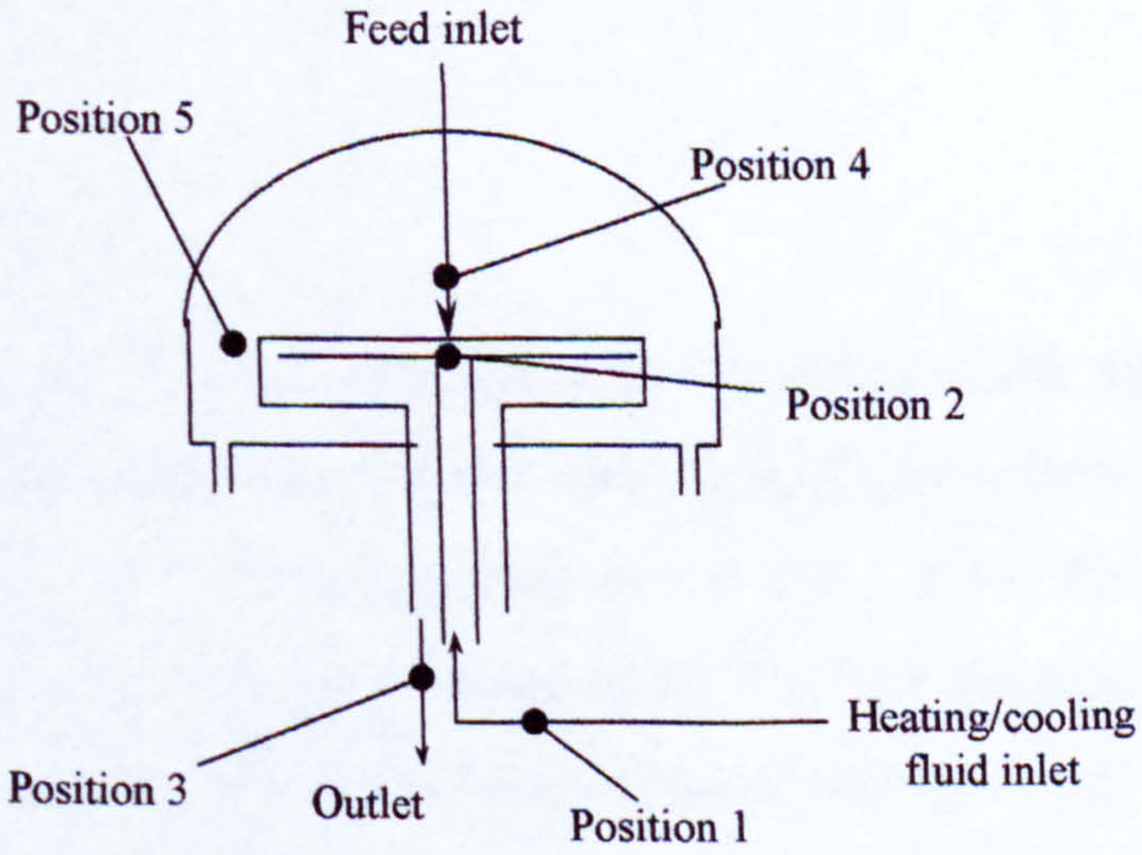


**Figure 5.9. Position of thermocouples**

The disc was driven by a variable ¾ kW motor allowing rotational speeds in the horizontal plane of up to 2000 rpm. For almost the whole duration of the study the ratio between the motor speed and disc speed was 1.454 : 1, allowing the disc speeds of up to 1375. This ratio was changed towards the end of the studies therefore higher speeds (up to 1600 rpm) were obtained.

#### 5.2.2.1.3 Liquid feed distributor

Liquid feed was transferred onto the disc surface through a feed distributor (Figure 5.10) incorporating a 2 mm in diameter tube. The distributor was fixed on top of the glass dome, as seen in Figure 5.3, located at the centre of the disc surface and was placed 2–5 mm above the surface. This height could be easily adjusted by using a shim. Liquid was delivered from the batch by means of peristaltic pump using suitable tubing connected to distributor. Pulsing was minimised by adjusting the tube and feed distributor diameters.

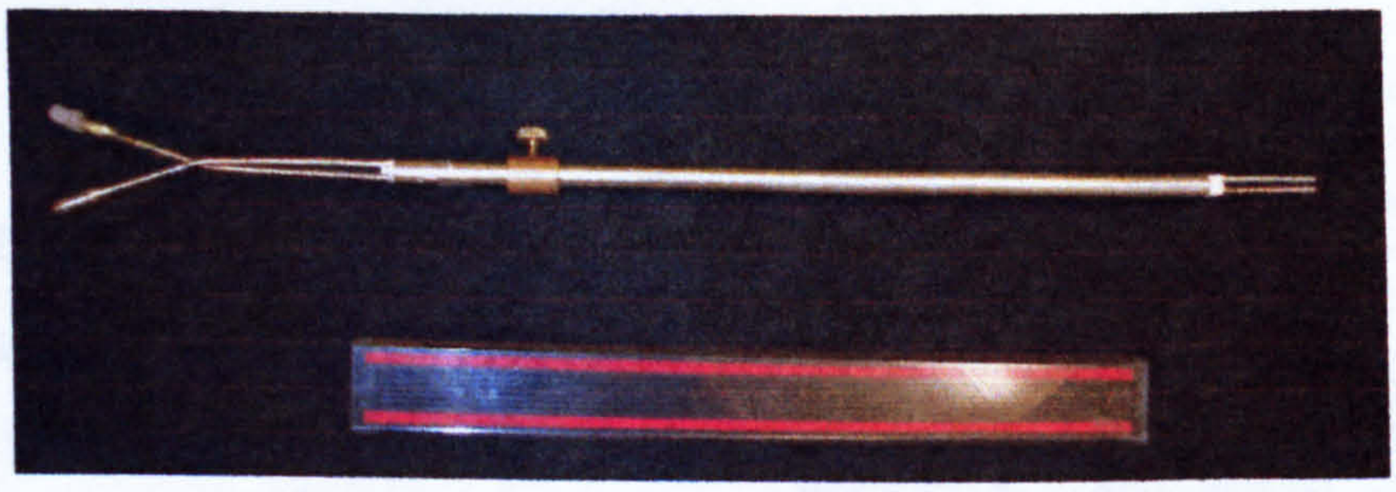

**Figure 5.10. Feed distributor**

#### 5.2.2.1.4 Product collector

When the liquid feed was introduced to the centre of the rotating disc, a thin film was formed. This film, upon contact with the catalyst on the surface, formed the product which was thrown off at the edge of the disc. It hit the inner wall of the housing and flowed down on the housing base. For the purpose of collecting the samples, there were four holes on the base as shown in Figure 5.11; only two can be seen on the schematic, through which product continued to flow down and could be collected for analysis and storage.

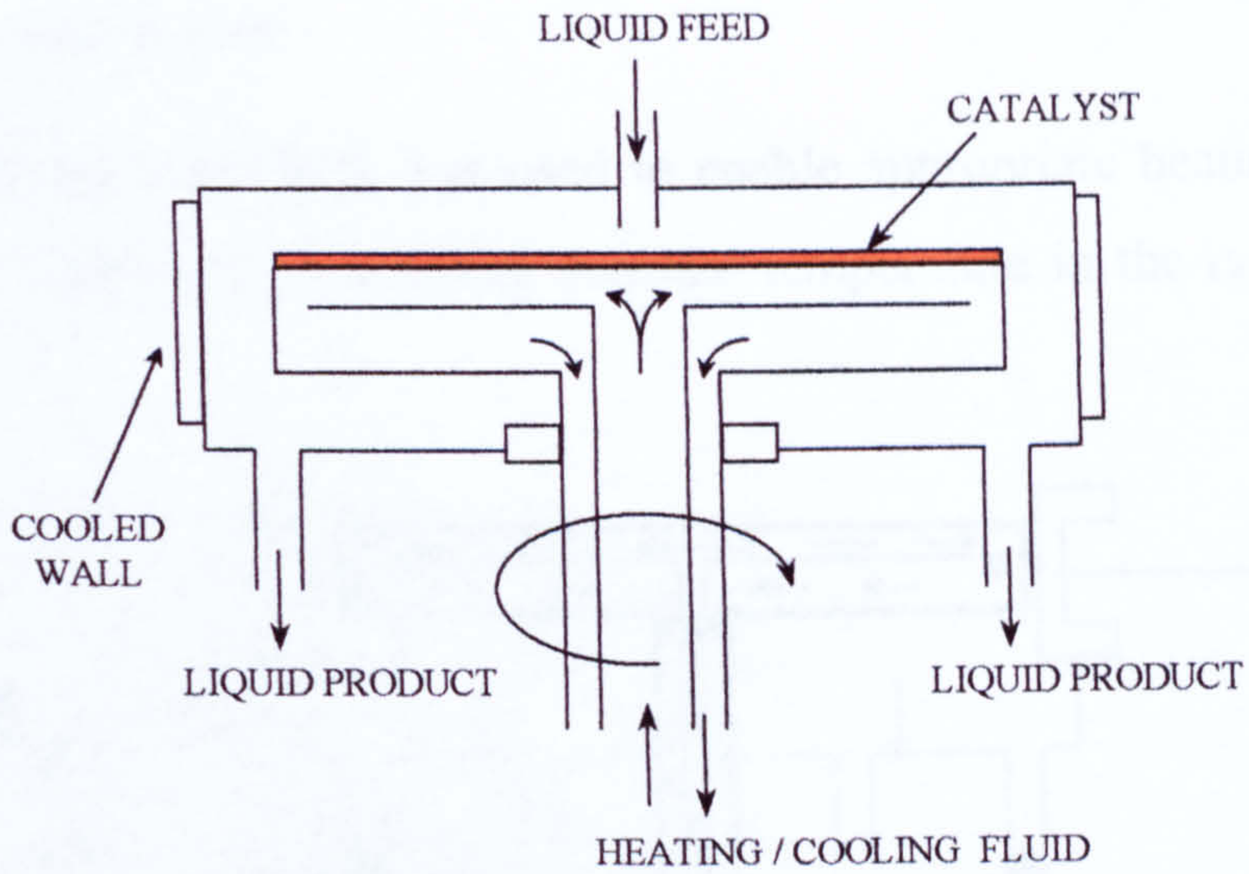


**Figure 5.11. Schematic of the Spinning Disc Reactor (SDR)**

5.2.2.1.5 Reactor housing with external exchanger and glass dome

The spinning disc surface together with associated parts described above were housed in an enclosure which consisted of a removable, but securely bolted, top glass dome (as shown in Figure 5.3) and stainless steel bottom section fixed to the framework support, as shown in Figure 5.12. To make sure that the top and bottom sections were completely sealed, PTFE joint sealant was used. Glass top had three ports, of which central one was used for distributor and thermocouple, second one for thermocouple only while the third one was kept closed. Direct visual observation of the flow over the disc was possible due to transparency of a glass dome at the top of the reactor. On the bottom section, several copper coils were wound around the outside, as a cooling jacket and padded.

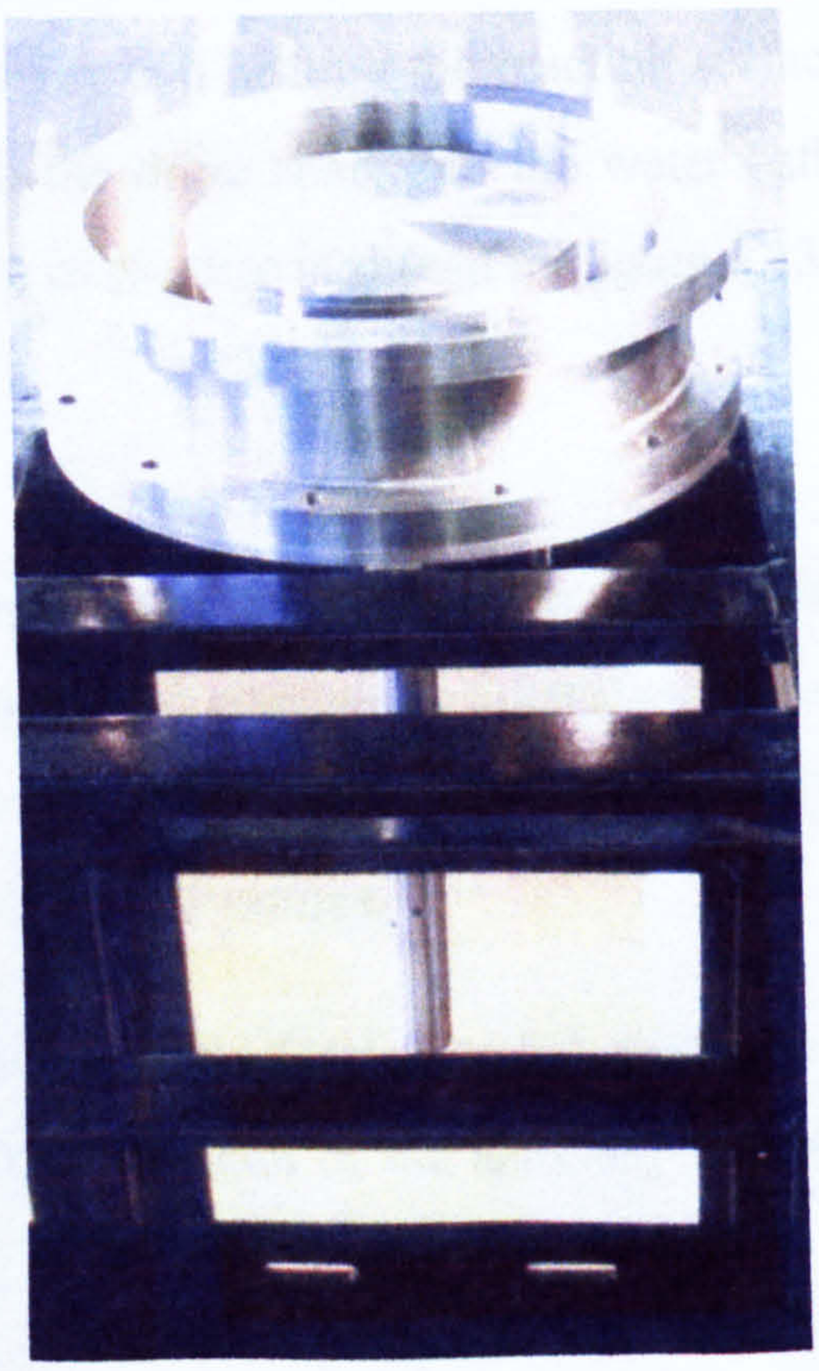

**Figure 5.12. View on the SDR (without the glass top and cooling coils)**

### *5.2.2.2 Temperature bath*

An external water bath was used to enable appropriate heating of the disc. The bath was capable of maintaining constant temperature in the range of 20°C to about 90°C.

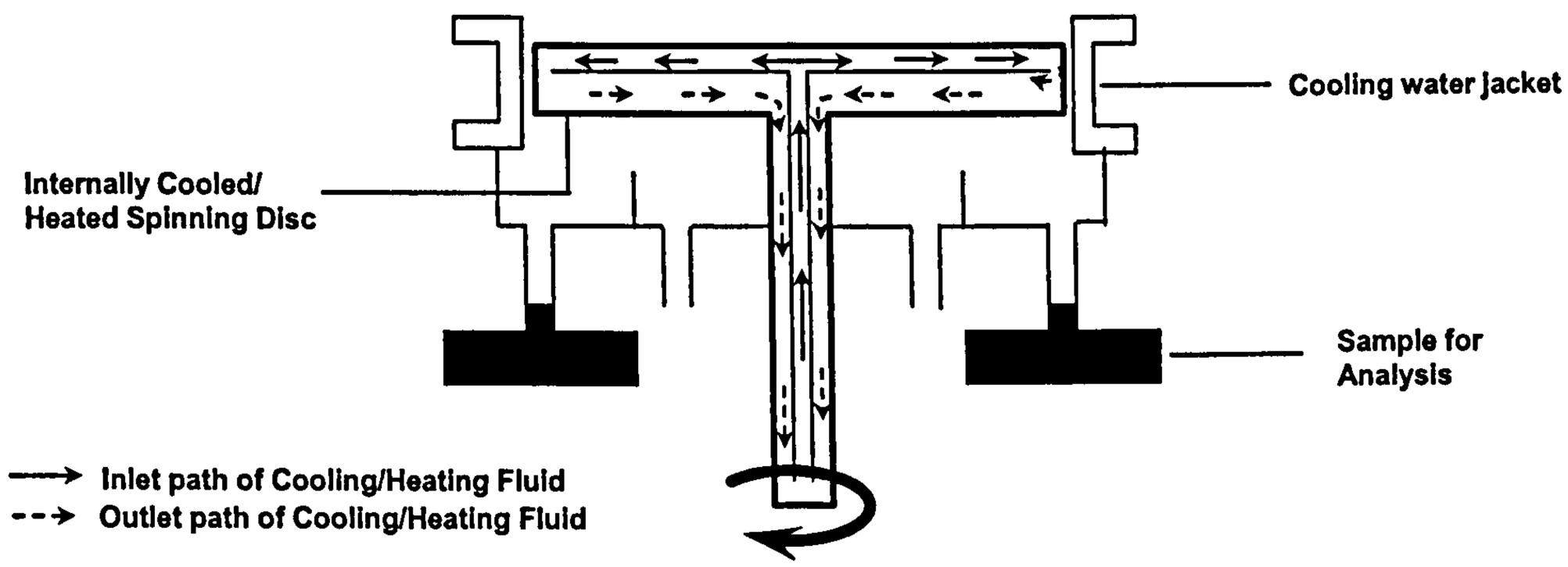


**Figure 5.13. Arrangement of heating**

Water was pumped through the inner tube in the drive shaft, then in between the plate and the disc surface, giving the heat away and heating the reacting surface to desired temperature, and finally out through the drive shaft into the water bath. Schematic of the arrangement of internal heating of the disc is shown in Figure 5.13.

### *5.2.2.3 Instrumentation*

Temperature of the disc was regulated by a digital controller unit on the external water bath. All the thermocouples could be connected to a data acquisition unit and a full profile of temperature could be obtained. Handheld digital thermometer was also used to measure and record temperatures.

Speed control regulator system was used to vary the disc speed in the range of 150 up to a maximum 1600 rpm. The rotational speed of the spinning disc was measured on a digital device with an accuracy of ± 1 rpm.

Experimental set up of the rig is presented in Figure 5.14.

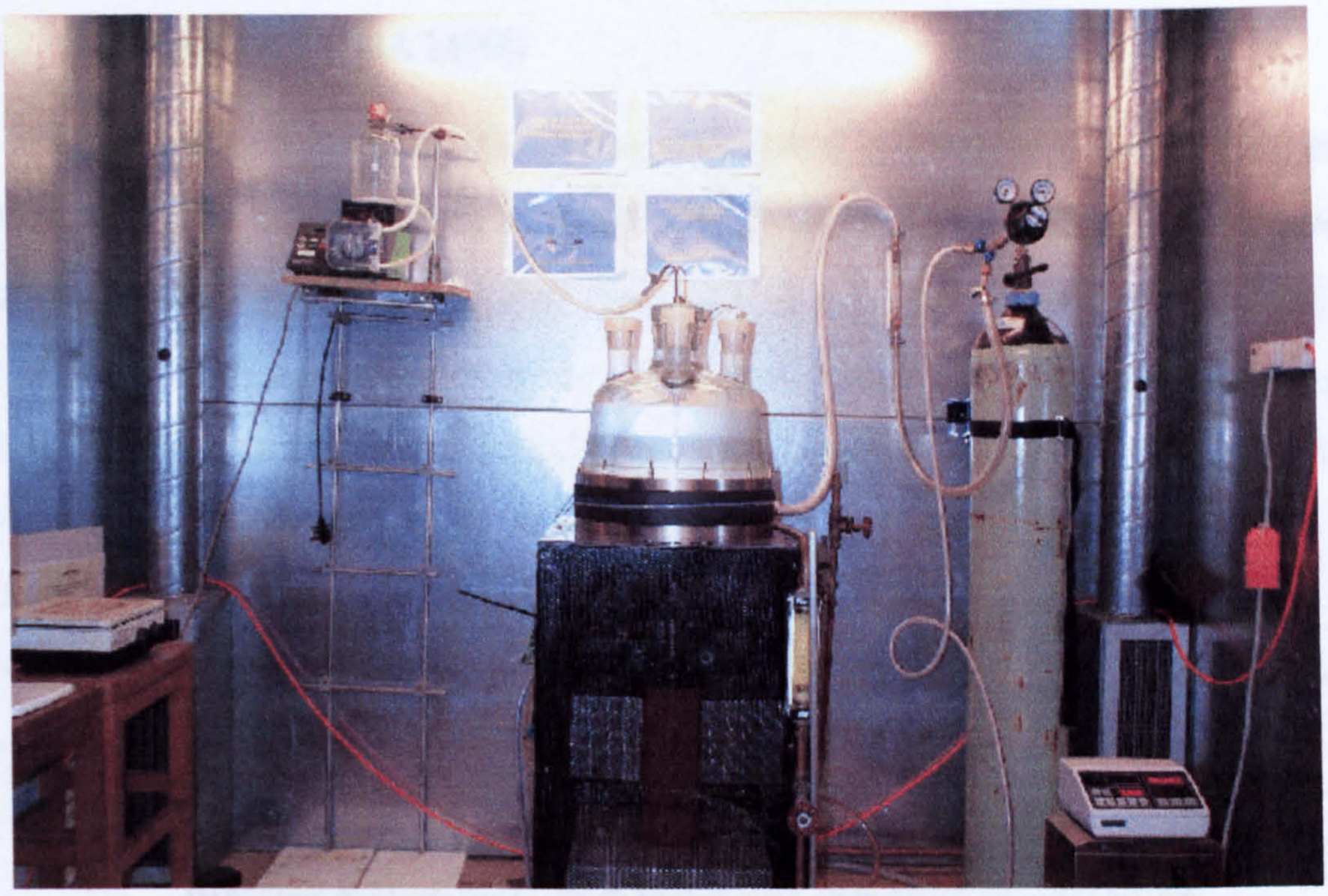

**Figure 5.14. Experimental set up**

## 5.3 PROCEDURES

### 5.3.1 BATCH CALIBRATION RUNS

In order to compare the results achieved in the spinning disc reactor, preliminary batch reactor experiments were performed for each catalyst. Conversion and selectivity data were gathered and plotted against time of reaction. Afterwards they were compared to SDR results at given temperature.

Previously described glass batch vessel was used for calibration runs. 1 g of α–pinene oxide (reactant, Aldrich 99%), 100 ml of 1, 2-dichloroethane (solvent, Aldrich 98%) and 0.5 g decane (Aldrich 99%, used as internal standard) were put in a reactor which was preheated to an operating temperature. Magnetic stirrer (15 mm in diameter) was used to provide uniform temperature control in a batch reactor. The catalyst was added to the mixture (0.15 – 0.2 g, depending on catalyst loading), samples were taken by pipette through one of the arms every 10 minutes at the first stage of the reaction and analysed straight away. If a full conversion was achieved in a shorter time, reaction was performed again and samples taken more often in an interval of interest (from the beginning to a point when a full conversion was accomplished). If 100% conversion was not achieved, reaction was performed again for a longer period until full conversion was attained. Results in terms of conversion and selectivity were plotted as a function of time.

### 5.3.2 CATALYST COATING

For the purpose of this study, the disc had to be coated with catalyst (provided by the collaborators from the University of York) before the experiments were performed. Epoxy based glue (two component UHU plus®) was applied to the disc surface with a spatula, in a very thin layer, as uniform as possible (to ensure uniform coating and reproducibility, catalyst and glue quantities were measured after each coating, as presented in Appendix G), and catalyst sprinkled on the glued surface straight after. The disc was then left for 24 hours to allow the glue to dry completely. Disc coated with the catalyst is shown in Figures 5.15 and 5.16, ready to be assembled back to the SDR.

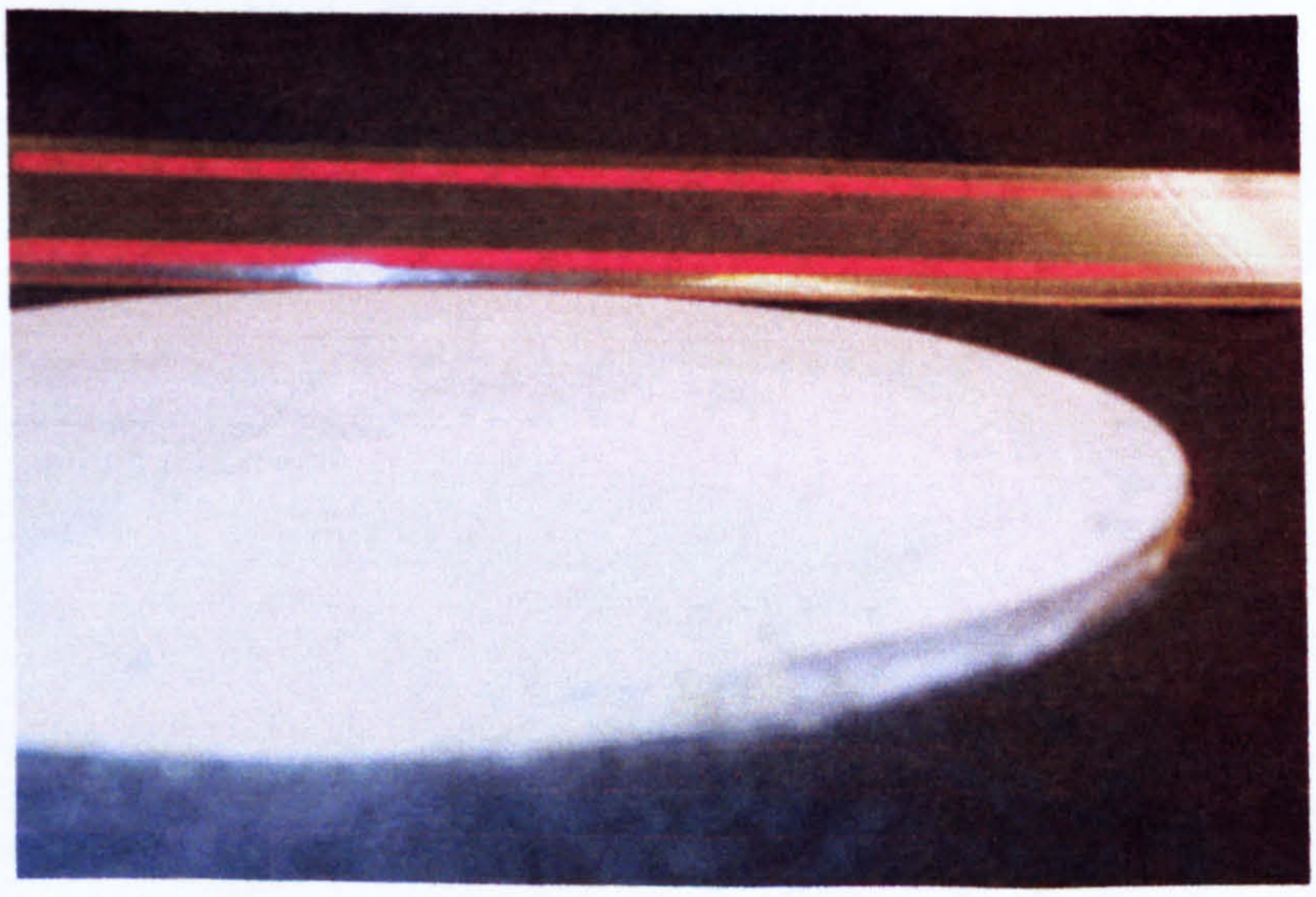

**Figure 5.15. Catalyst coated on the disc surface**

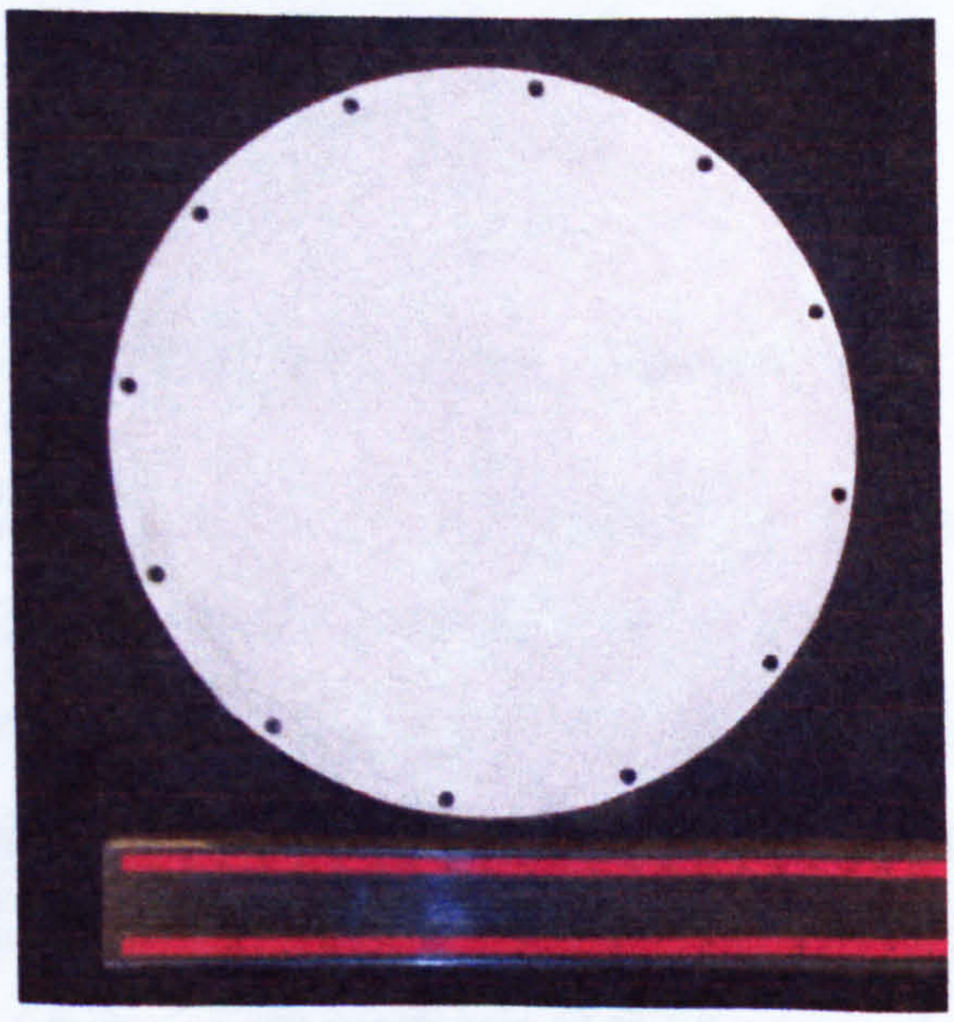

**Figure 5.16. Top view on the catalyst coated disc**

### 5.3.3 SPINNING DISC RUNS

Before the reactant mixture was transferred on to a spinning disc reactor, all the 'ingredients' without catalyst were put in a glass feed vessel (same amounts as in a batch reactor, 1 g of α–pinene oxide, 100 ml of 1, 2-dichloroethane and 0.5 g of decane). From the pot to a feed distributor mixture was delivered through Tygon tubing by a peristaltic pump (see Figure 5.14).

Peristaltic pump was calibrated with 1, 2-dichloroethane (DCE) for determination of flow rates (instead of flow marks). Pump was set to a mark and the time required to achieve a given flow volume was recorded. Linear plot of flow rates versus flow marks on the pump is presented in Figure 5.17.

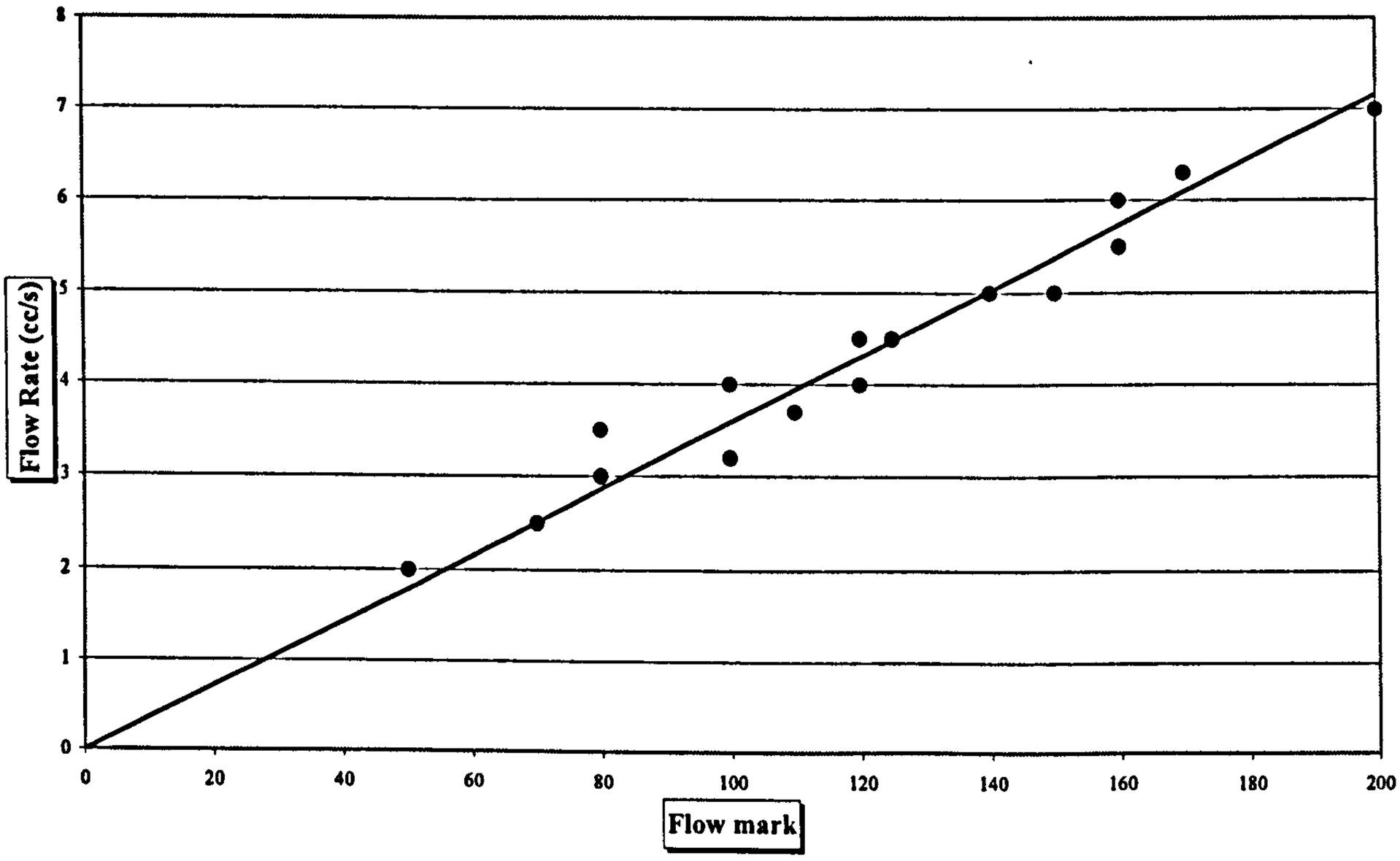


**Figure 5.17. Pump calibration**

Preparing the disc for a run involved heating the disc surface up to a desired temperature, which was achieved by rotating the disc at a low speed. When the disc reached the required temperature, the speed was set on a control panel and cooling water to skirt jacket turned on. The reactant mixture was then delivered to the disc surface using the feed distributor system (as described earlier) onto a disc. As the reactant contacted the rotating disc surface it flowed across the disc and was thrown off the edge into the collector pipe, being cooled on the way from the disc by the

water jacket wall. Samples were collected immediately and analysed. One sample from each run was taken from a glass pot to ensure that reaction did not take place before the disc stage.

### 5.3.4 KINETIC EXPERIMENTS

For the purpose of acquiring information about reaction kinetics in a batch reactor and evaluating activation energies of the catalysts, series of experiments were performed. α–pinene oxide, 1, 2-dichloroethane, decane and 0.15 or 0.2 g of the catalyst (for 0.05 mmol/g and 0.01 mmol/g respectively) were used in each run with the temperature of the batch varied. Temperatures in the range of 25-85$^0$C were used for each catalyst, samples were taken at appropriate interval (depending on reaction time; one experiment was performed several times if reaction time was long in order get more data points at different intervals) and conversion and selectivity data obtained and plotted versus time.

## 5.4 ANALYTICAL PROCEDURES

### 5.4.1 LIQUID/GAS CHROMATOGRAPHY

All the samples were analysed using FID UNICAM Series 610 LC-GC system, shown in Figure 5.18. This GC had a HP1 packed (100% dimethylpolysiloxane) column. An internal standard method as explained in Appendix E was used. Concentration data obtained from the GC analysis were used to calculate the overall conversion and selectivity of the process. Calibration was performed using several prepared solutions of α–pinene oxide in 1, 2-dichloroethane as well as known concentration solutions of campholenic aldehyde.

Additionally, several samples were re–analysed at the University of York using a HP5890 Gas Chromatograph fitted with a 25 m HP1 capillary column for confirmation and reproducibility of results. Tests carried out at both Universities showed identical results. Samples of chromatographs can be seen in the Appendix E.

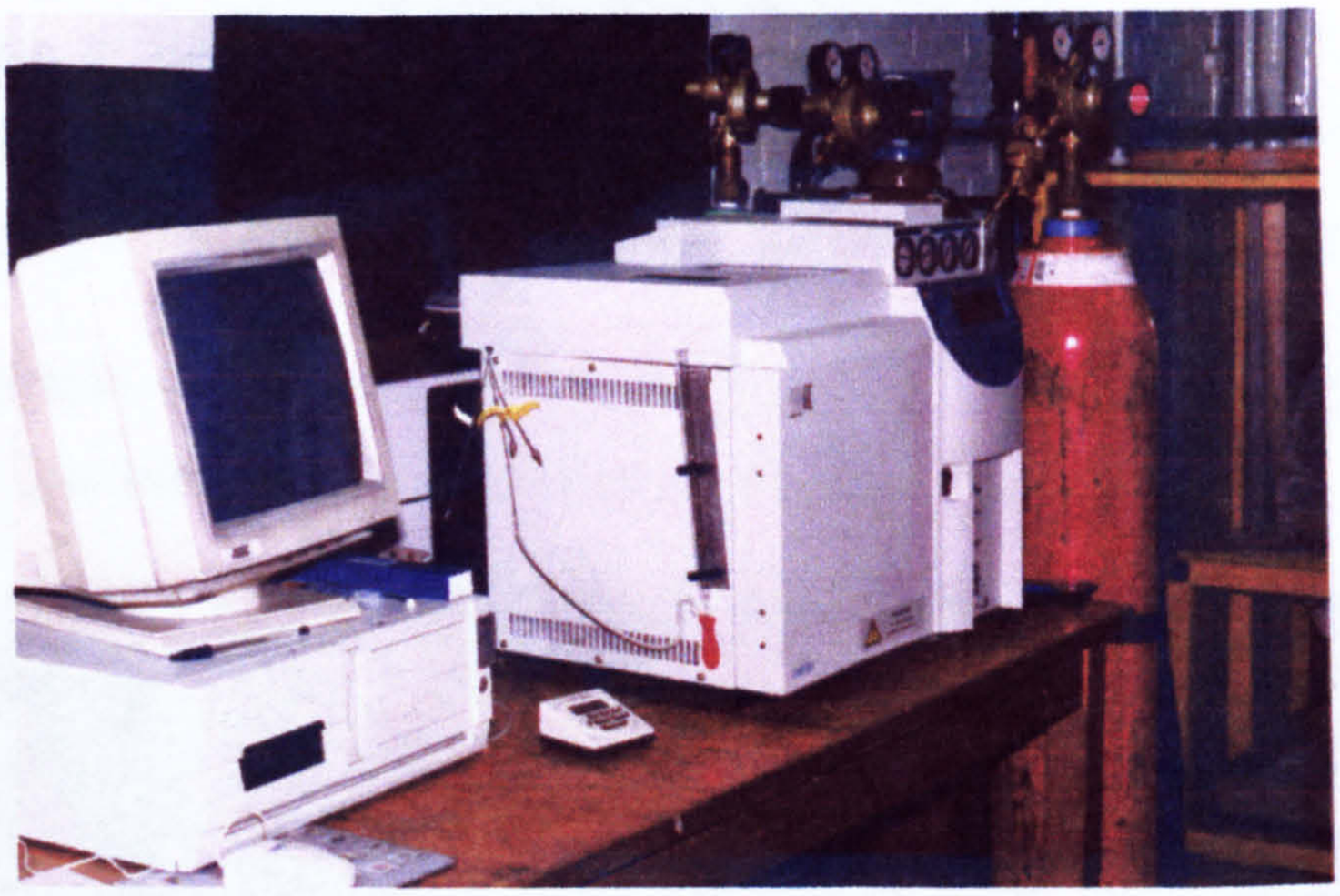

**Figure 5.18. Liquid/gas chromatograph**

*5.4.1.1 Sample analysis*

Before injection, LC/GC software was started with an appropriate method which has been described below. The sample was injected when the set temperature was reached. Every sample was filtered prior to analysis, making sure that there was no residue of catalyst in it.

Operating conditions for the GC were as follows:

**Ramp one:**

Injector temperature: 60°C

Injection time: 0

Rate: 10°C/min

Final temperature: 150°C

**Ramp two:**

Rate: 25°C/min

Final temperature: 280°C

## 5.4.2 VISCOMETRY

Viscosity of the feed as well as the product samples were measured by using a Bohlin Visco 88 BV viscometer. This set up can be seen in Figure 5.19. Hot water from a temperature controlled water bath was used to maintain the temperature of the base plate of the viscometer.

Three different cone and plate geometries namely CP5/30, CP2.5/15, CP2.5/30 (where CP5/30 refers to a cone angle of $5^0$ and a cone diameter of 30 mm etc.) were used to measure shear stress, shear rate and viscosity of samples.

Viscosity measurements were carried out in order to calculate the film thickness, residence time and shear rates of the liquid on the disc reactor.

**(a) (b) (c)**

**Figure 5.19. Viscometer set-up (a) Viscometer, (b) Temperature controlled water bath, (c) Data logger**

*5.4.2.1 Sample analysis*

The gap between the truncated cone and the plate was first set using the appropriate shims provided, that is 70 μm for $2.5^0$ cone and 150 μm for the $5^0$ cone. The temperature of the water bath was set to operating temperature (according to equivalent temperatures on the disc). A small amount of the test sample was placed on the plate and the cone was lowered to the preset position determined by the gap setting procedure described above. The excess sample after compression was removed, leaving only a slight bulge around the edge of the cone. Measurements were immediately started using the software "Viscometry" (supplied by Bohlin Instruments Ltd.) installed on the external computer system. The data was collected and processed by the software together with an associated file converter used to save

the data in ANSI format in order to enable direct transfer into Microsoft Excel for producing the required rheological plots.

### 5.4.3 DENSITY MEASUREMENTS

Density of samples was calculated using equation (5.1):

$$\rho\left(\frac{kg}{m^3}\right)=\frac{m(kg)}{V(m^3)} \tag{5.1}$$

Therefore simple measurement of mass for a given volume was used to obtain density values. Results from viscosity and density measurements can be found in the Appendix F.

## 5.5 TREATMENT OF MEASURED DATA

Concentration data (in terms of molarity) obtained by GC were used to calculate conversion and selectivity.

Conversion of α-pinene oxide ($x_A$) was calculated using the following equation:

$$x_A(\%)=\frac{C_{A0}-C_A}{C_{A0}}\cdot 100 \tag{5.2}$$

where $C_{A0}$ is the concentration of α-pinene oxide at the beginning of the experiment (starting concentration, at time t = 0), while $C_A$ is the concentration of α-pinene oxide at any given time (the time when the sample was taken).

Selectivity ($\sigma_P$) of the catalyst for the α-pinene oxide rearrangement reaction towards campholenic aldehyde can be calculated using the equation (2.3), knowing that in all the experiments $\nu_P$ is 1 (equimolar reaction) and the starting concentration of campholenic aldehyde ($C_{P0}$) is zero.

$$\sigma_P(\%)=\frac{(C_P-C_{P,0})}{(C_{A,0}-C_A)\nu_P}\cdot 100=\frac{C_P}{C_{A,0}-C_A}\cdot 100 \tag{5.3}$$

In the above equation, $C_P$ is the concentration of campholenic aldehyde at any given time.

Example: In a batch process for Catalyst 1 at $85^0$C (section 6.4.1; data from Table G.2 in the Appendix G) after 4 minutes of reaction collected sample is shown to have a concentration of α-pinene oxide of 0.0045 mol/dm$^3$ and concentration of campholenic aldehyde of 0.0389 mol/dm$^3$.

Initial concentration of α-pinene oxide can be calculated since the initial amount of α-pinene oxide (1 g) and volume of solvent (100 ml) are known and constant in experiments using the following expression:

$$C_{A0} = \frac{\text{number of moles of the reactant (kmol)}}{\text{volume}(m^3)} \tag{5.4}$$

Number of moles ($n_A$) of reactant (α-pinene oxide) can be calculated as:

$$n_A = \frac{m_A}{M_A} = \frac{1\,g}{152\,\frac{g}{mol}} = 0.006578\,mol = 6.578\,mmol \tag{5.5}$$

where: $m_A$ – Mass of the reactant (α–pinene oxide) [g] = 1 g

$M_A$ – Molecular mass of α–pinene oxide [g/mol] = 152 g/mol

$$C_{A0} = \frac{6.578 \cdot 10^{-6}}{10^{-4}} = 6.578 \cdot 10^{-2}\,\frac{kmol}{m^3} \tag{5.6}$$

Conversion of α-pinene oxide can be calculated using equation (5.2) as:

$$x_A\,(\%) = \frac{0.06578 - 0.0045}{0.06578} \cdot 100 = 93.16$$

$$x_A = 93\%$$

Selectivity of the Catalyst 1 for the α-pinene oxide rearrangement reaction towards campholenic aldehyde is calculated using the equation (5.3) as:

$$\sigma_P\,(\%) = \frac{0.0389}{0.06578 - 0.0045} \cdot 100 = 0.6352 \cdot 100$$

$$\sigma_P = 63\%$$

All the data collected are treated in this manner. If not stated otherwise, conversion always means conversion of the reactant (α-pinene oxide) in the rearrangement reaction and selectivity always means selectivity of the catalyst for the α-pinene oxide rearrangement reaction towards the desired product (campholenic aldehyde).

# CHAPTER 6

# EXPERIMENTAL RESULTS

## 6.1 OVERVIEW OF EXPERIMENTS

Using the experimental facility described in Chapter 5, tests were carried out to investigate the performance of a catalytic SDR. Three different catalysts, namely 0.05 mmol/g $Zn(OTf)_2$ supported on $SiO_2$, 0.01 mmol/g $Zn(OTf)_2$ supported on K100 (silica) and 0.05 mmol/g $Zn(OTf)_2$ supported on $HMS_{24}$ (silica) were used and their influence on the α–pinene oxide rearrangement reaction has been presented in three separate sections. Each of the sections has experimental findings in terms of reaction conversion and selectivity as a function of temperature, feed flow rate and disc rotational speed.

Details of preliminary experiments carried out to demonstrate the reaction took place only in the presence of the catalyst have also been presented.

## 6.2 TREATMENT OF DATA (SAMPLE CALCULATIONS)

As described in section 5.5, all the collected data were used to calculate the conversion and selectivity for the performed runs (both the SDR and batch) in the same manner as already illustrated.

For each SDR experiment, the independent variables included: disc rotational speed (the speed was set-up before the experiment and recorded), feed flow rate (also set-up and recorded), disc temperature (heated to required temperature and recorded) and the dynamic viscosity of the feed (obtained as described in section 5.4.2.1). The parameters needed for this study (residence time, film thickness, shear rate, Reynolds number, Fourier number) were then calculated using the independent variables. The sample calculations for each dependant variable will be presented in the following sections.

### 6.2.1 RESIDENCE TIME CALCULATION

Residence times in the SDR were estimated for each run using the equation (3.18). In all calculations, values for outer and inner radius were constant as the disc size had a constant diameter of 200 mm (therefore outer radius had a value of 100 mm) and the feed was always introduced to the centre of the disc, hence the inner radius had a value of zero.

Kinematic viscosity, $\nu$, was calculated using the following equation:

$$\nu = \frac{\mu}{\rho} \tag{6.1}$$

where $\mu$ is dynamic viscosity (independent variable) and $\rho$ is density of the sample.

Angular velocity, $\omega$, was determined from the rotational speed of the disc, N, using the following formula:

$$\omega = \frac{2\,\pi\,N}{60} \tag{6.2}$$

Example: For the run performed in the SDR at T = 85$^0$C, with the feed flow rate of 4 cm$^3$/s and with the disc rotating at N = 1000 rpm (Run 17 from the Table G.5 in the Appendix G), kinematic viscosity and angular velocity can be determined by using equations (6.1) and (6.2) respectively.

$$\nu = \frac{\mu}{\rho} = \frac{6.109 \cdot 10^{-4}\ \text{Pa s}}{964\ \frac{\text{kg}}{\text{m}^3}} = 6.32 \cdot 10^{-7}\ \frac{\text{m}^2}{\text{s}} \tag{6.3}$$

$$\omega = \frac{2\,\pi\,N}{60} = \frac{2\,\pi \cdot 1000}{60} = 33.33\,\pi = 104.72\ \frac{\text{rad}}{\text{s}} \tag{6.4}$$

Equation (3.18) can now be re-written and residence time for Run 17 computed as:

$$t_{res} = \left( \frac{81\,\pi^2\; 6.32 \cdot 10^{-7} \left[\frac{m^2}{s}\right]}{16 \left(104.72 \left[\frac{rad}{s}\right]\right)^2 \left(4 \cdot 10^{-6} \left[\frac{m^3}{s}\right]\right)^2} \right)^{1/3} \left( 0.1\,[m]^{4/3} \right)$$

$$t_{res} = 0.2615 \text{ s} \tag{6.5}$$

### 6.2.2 FILM THICKNESS CALCULATION

Film thickness at any radial position for each run was approximated by using the equation (3.16).

Example: For the same run as in section 6.2.1 (Run 17 from Table G.5 in the Appendix G), film thickness at the edge of the disc (r = 0.1 m) can be calculated using the values for kinematic viscosity and angular velocity given by equations (6.3) and (6.4).

$$\delta = \left( \frac{3}{2\,\pi} \frac{6.32 \cdot 10^{-7} \left[\frac{m^2}{s}\right] 4 \cdot 10^{-6} \left[\frac{m^3}{s}\right]}{\left(104.72 \left[\frac{rad}{s}\right]\right)^2 (0.1\,[m])^2} \right)^{1/3}$$

$$\delta = 2.22444 \cdot 10^{-5} \text{ m} = 2.22444 \cdot 10^{-2} \text{ mm} \tag{6.6}$$

### 6.2.3 SHEAR RATE CALCULATION

Shear rate at any radial point (r direction in the Figure 3.2 in Chapter 3) and very close to the surface of the disc (z direction in the Figure 3.2) can be calculated by using the equation (3.13).

Example: Considering Run 17 in this example as well, using the independent variable of feed flow rate of 4 $cm^3/s$, already determined values of kinematic viscosity, given by equation (6.3), angular velocity, given by equation (6.4), average film thickness, calculated in previous section and having z very close to zero, equation (3.13) becomes:

$$\dot{\gamma} = \left( \frac{3 \cdot 4 \cdot 10^{-6} \left[ \frac{m^3}{s} \right] \left( 104.72 \left[ \frac{rad}{s} \right] \right)^4 0.1 \lceil m \rceil}{2 \pi \left( 6.32 \cdot 10^{-7} \left\lceil \frac{m^2}{s} \right\rceil \right)^2} \right)^{1/3} \left( 1 - \left( \frac{10^{-15}}{2.224 \cdot 10^{-5} \lceil m \rceil} \right) \right)$$

$$\dot{\gamma} = 3.8597 \cdot 10^4 \frac{1}{s} \qquad (6.7)$$

### 6.2.4 REYNOLDS NUMBER CALCULATION

Reynolds number is calculated from the equation (3.23).

Example: For the above used Run 17, knowing the flow rate (4 $cm^3/s$) and using the already determined value of kinematic viscosity (equation (6.3)), Reynolds number can be calculated as:

$$Re = \frac{2 \cdot 4 \cdot 10^{-6} \left[ \frac{m^3}{s} \right]}{\pi \cdot 0.1 \lceil m \rceil \cdot 6.32 \cdot 10^{-7} \left\lceil \frac{m^2}{s} \right\rceil}$$

$$Re = 40 \qquad (6.8)$$

### 6.2.5 FOURIER NUMBER CALCULATION

Fourier number is determined using the equation (8.2). Diffusion coefficient, D, is estimated by Hayduk & Laudie's method [164] (as the properties of DCE and water are similar), as well as using a web software [165].

Example: For Run 17, knowing the residence time (calculated in section 6.2.1) and the film thickness (calculated in section 6.2.2), Fourier number can be calculated as:

$$Fo = \frac{3.49 \cdot 10^{-7} \left[ \frac{m^2}{s} \right] \cdot 0.2615 \, [s]}{\left( 2.22444 \cdot 10^{-5} \, [m] \right)^2} .$$

$$Fo = 184.87 \qquad (6.9)$$

## 6.3 TEST RUNS

### 6.3.1 TEST RUN 1 – UNCOATED DISC

In order to check the performance of the SDR, a 'blank' test was performed on an uncoated spinning disc. The disc was heated to 85°C and rotated at 500 rpm before the reactant was fed to it. The collected product was analysed by GC and showed no traces of campholenic aldehyde. It was therefore concluded that no reaction had occurred on the uncoated disc surface.

### 6.3.2 TEST RUN 2 – GLUE TEST

Tests were also carried out using a disc coated with epoxy based glue. The reason for this test was to check if there is any component in the glue which may react with α–pinene oxide. The disc was coated with a very thin coat of glue. No catalyst was sprinkled on and such coated disc was left to dry out. Test runs similar to the conditions in Test run 1 were carried out and the result showed that no isomerisation had occured.

### 6.3.3 TEST RUN 3 – SUPPORT REACTIVITY TEST

Tests were also carried out by using a silica coated disc. Silica, which is used as a support for the catalysts, was used in order to check for support reactivity. These tests again showed no conversion of α-pinene oxide confirming that neither the stainless steel disc, not the glue or the silica had any chemical reactivity in the isomerisation reaction.

### 6.3.4 CATALYST QUANTITY

In order to determine the actual mass of the catalyst used for coating, the disc was weighed before the coating, after the glue coating and after the sprinkling of the catalyst every time the coating was performed.

For the purpose of accuracy, the disc coated with the glue and catalyst was weighed before and after the glue dried on the surface. No difference was observed. The results for measuring the amount of catalyst can be seen in Appendix G (Table G1).

## 6.4 CATALYST 1

The first catalyst used in this investigation was 0.05 mmol/g $Zn(OTf)_2$ supported on $SiO_2$.

### 6.4.1 BATCH REACTION

Batch reactor used for benchmarking the SDR performance consisted of a glass vessel with water jacket around for temperature control, as described in the previous Chapter. The batch temperature was additionally controlled by a thermocouple immersed in the reactant/product mixture. Samples were taken every minute during the reaction, and every five minutes after the reaction was finished. The reason for taking samples after the reaction had achieved completion was to check the stability of the campholenic aldehyde. Samples were immediately analysed on the GC. Test results obtained at the temperature of 85°C are shown in Figure 6.1 and also presented in Appendix G.

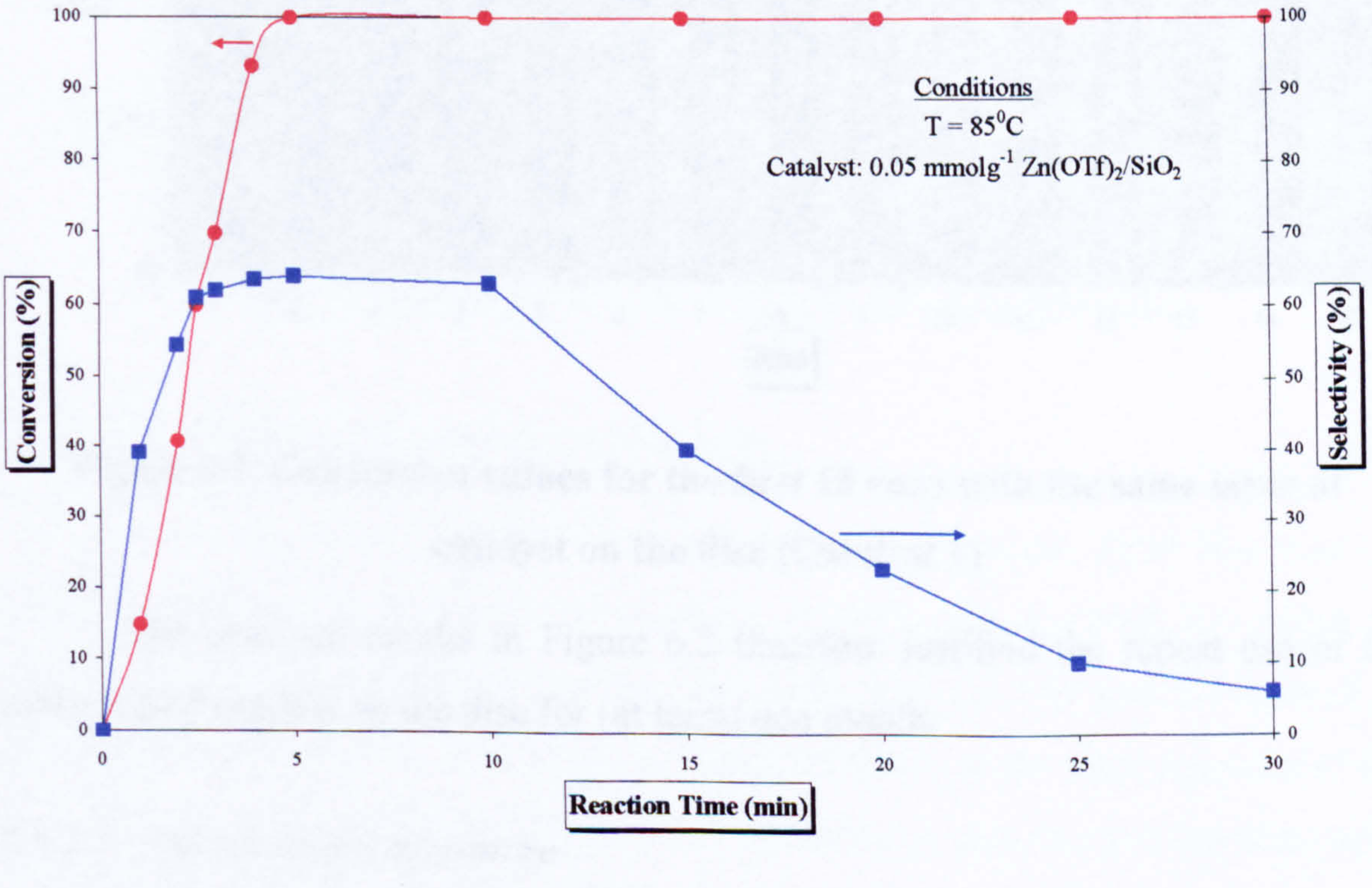


**Figure 6.1. Batch reaction data (Catalyst 1)**

### 6.4.2 CATALYST ACTIVITY INVESTIGATION

A series of experiments were performed to investigate how the supported catalyst will perform in the spinning disc reactor. The objective of the study was also to investigate the long-term performance and re-usability of the catalyst as well as to compare batch and SDR processes.

Therefore first 15 runs were completed at chosen temperature of 25$^0$C, flow rate of 4 cm$^3$/s and fixed disc speed of 150 rpm. As said, the aim of this investigation was to determine if the catalyst activity remained unchanged over time. The gap between any two experiments was 2–3 days (the results are shown in Figure 6.2). No traces of the desired product (campholenic aldehyde) were observed whatsoever, but the conversion of the α–pinene oxide remained constant at approximately 20% during the time.

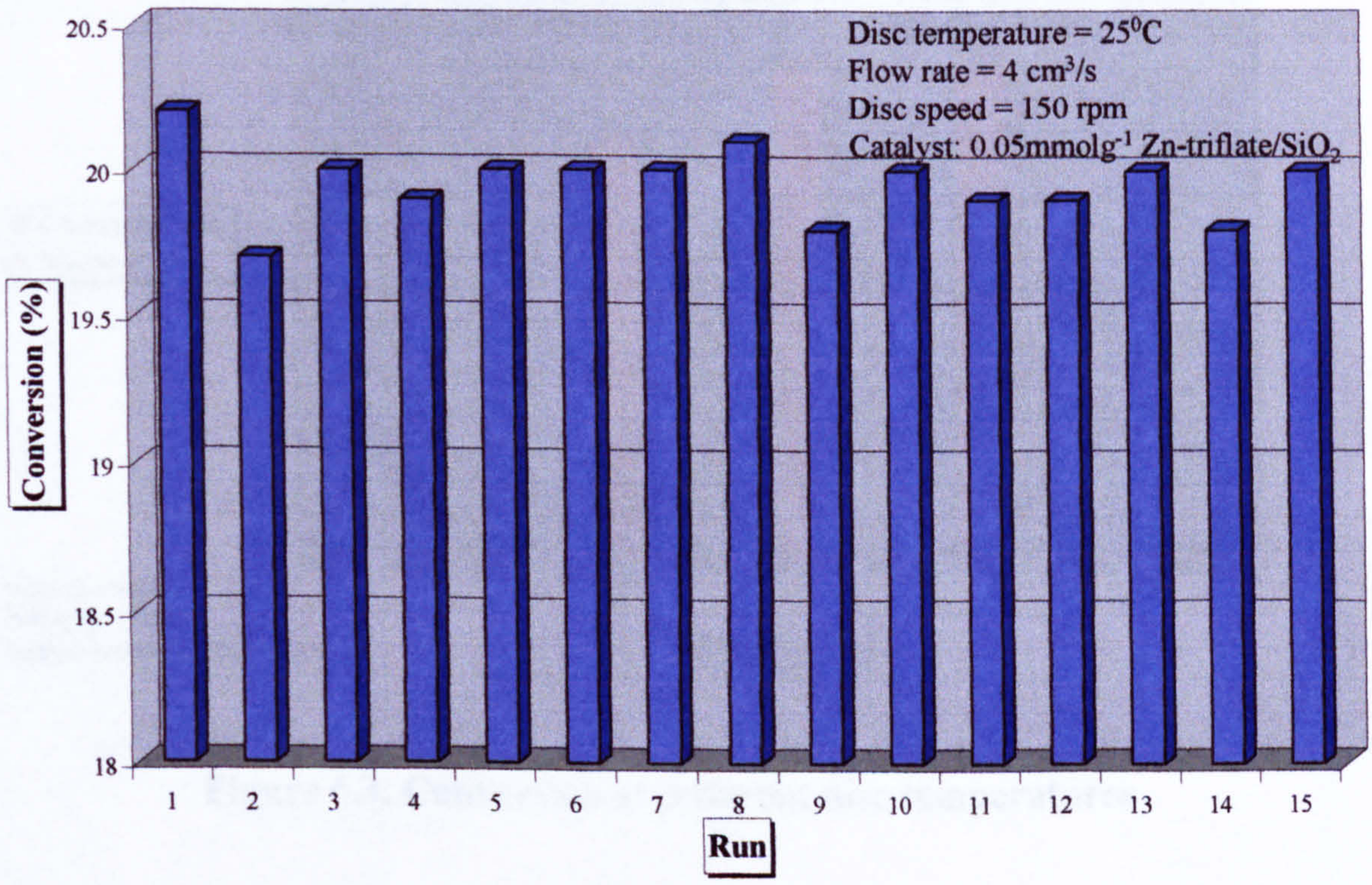


**Figure 6.2. Conversion values for the first 15 runs with the same layer of catalyst on the disc (Catalyst 1)**

The obtained results in Figure 6.2 therefore justified the repeat use of the same coated catalyst on the disc for (at least) one month.

### *6.4.2.1 Influence of temperature*

It was very important to find the optimum temperature for given catalyst before all other conditions were varied (e.g. disc speed, flow rate). Figure 6.3 shows the performance of the SDR (in terms of conversion of α–pinene oxide) at different temperatures, ranging from 25 to 85$^0$C. For the purpose of determining the optimum temperature, all the other conditions were kept constant: disc speed at 500 rpm and flow rate at 4 cm$^3$/s. It was already established before (Figure 6.2) that conversion at

25°C was not high enough; as the temperature got higher, the conversion increased from ~27% to a 100%. A temperature of 85°C was chosen as the optimal temperature for this catalyst; this temperature was also the highest that could be achieved on the disc, since water bath was used to heat the disc. For achieving higher temperatures, heating fluid would have to be changed.

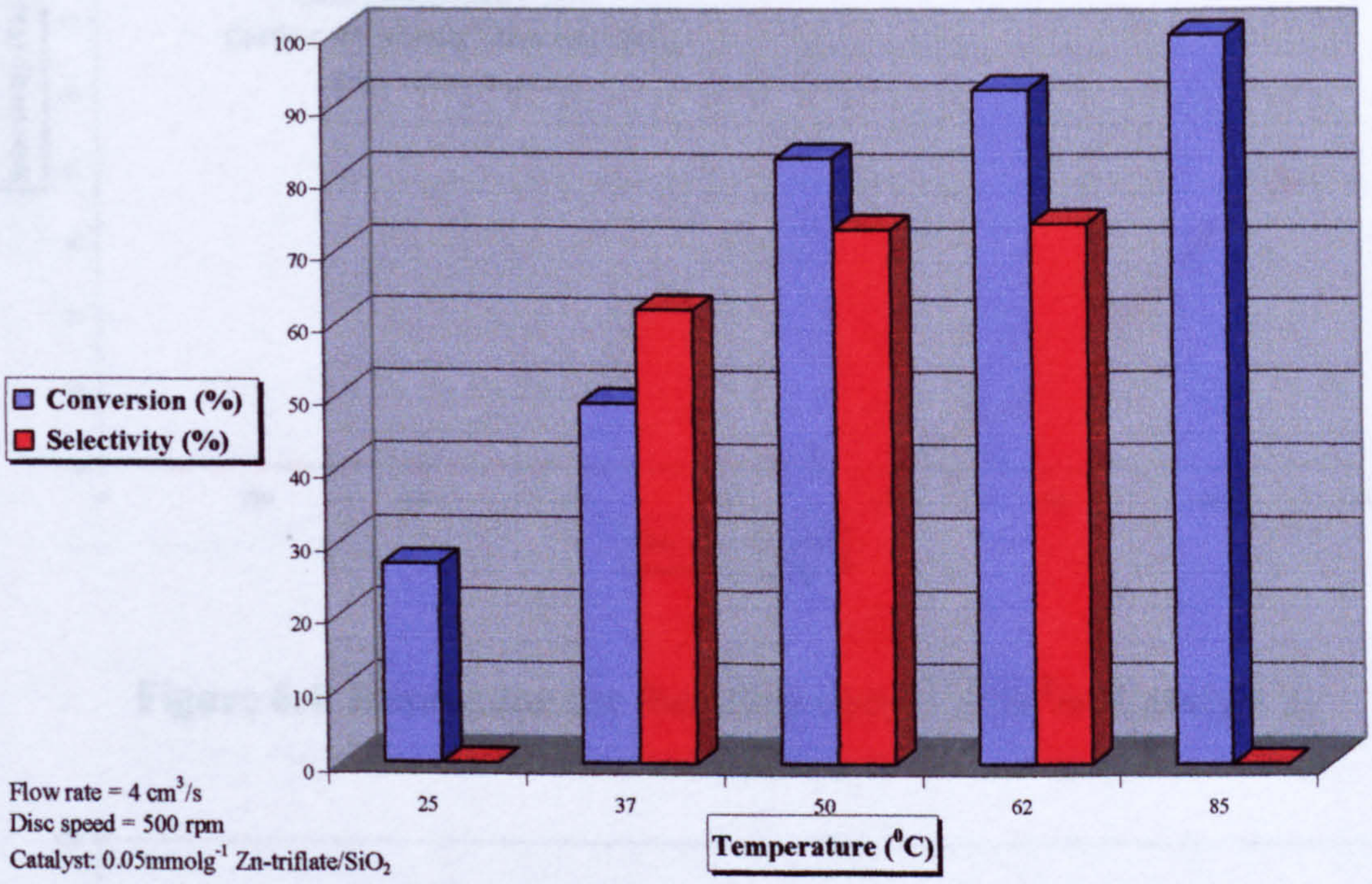


**Figure 6.3. Conversion at different disc temperatures**

*6.4.2.2 Influence of disc speed and flow rate*

Next runs were tried at 85°C, with various disc speeds. Feed flow rate was constant at this stage (4 $cm^3/s$). Conversion of 100% was achieved, but selectivity towards campholenic aldehyde was very low, even zero at lower speeds (Figure 6.4). This can be explained by the extremely sensitive nature of the rearrangement of this particular reaction. Not only is the reactant itself highly reactive and can form many products, but the desired product is even more reactive and the high performance of the spinning disc enhanced consecutive rearrangement. This could be investigated if all the products coming of the disc were known and from appropriate mechanisms of the consecutive reactions. The maximum observed selectivity towards aldehyde at this point was ~40%. As the selectivity increases on higher rotational speeds, residence time is a decisive factor in the reaction.

The conditions and results of these runs are also presented in the Appendix G.

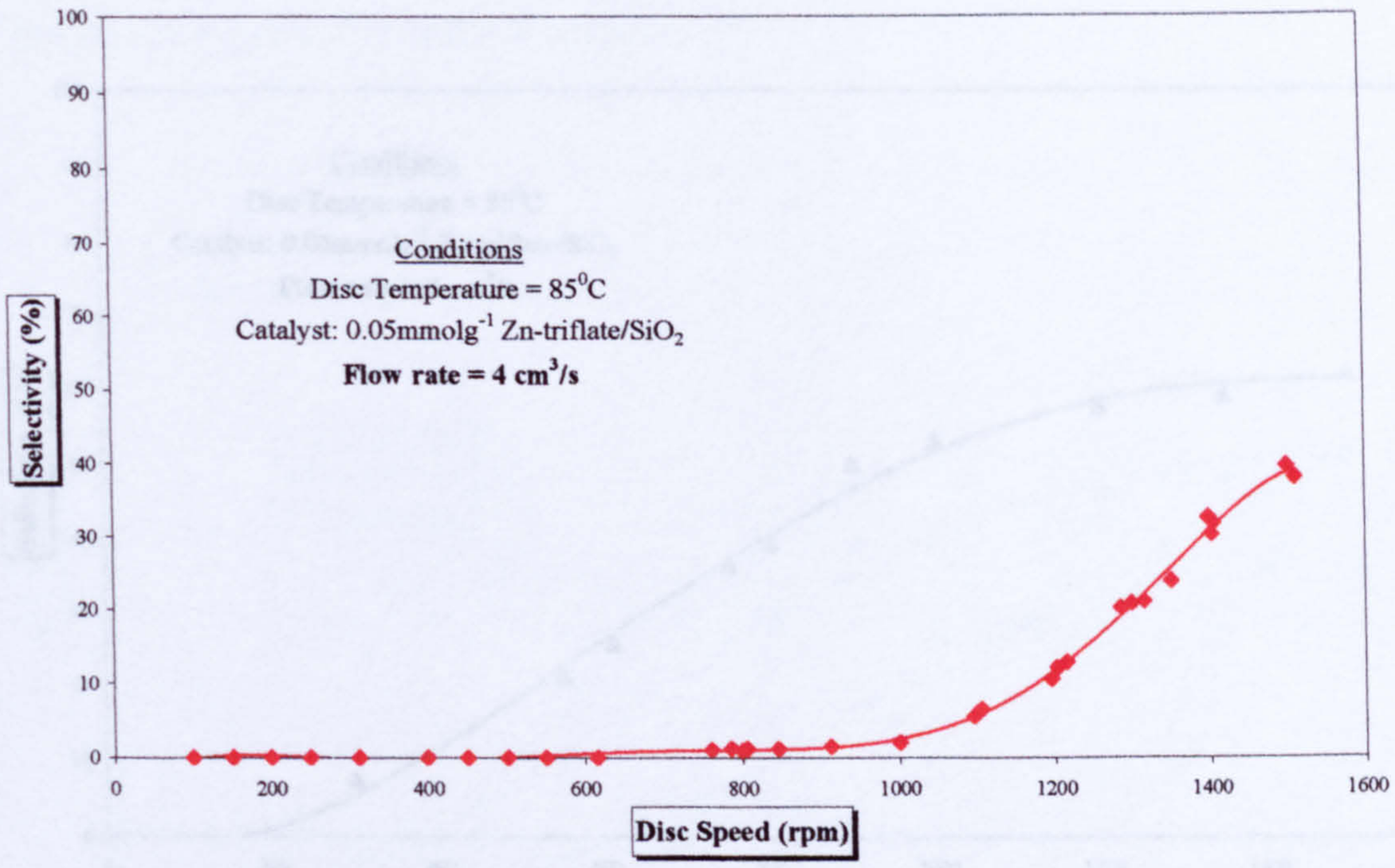


**Figure 6.4. Results for the feed flow rate of 4 $cm^3/s$ (Catalyst 1)**

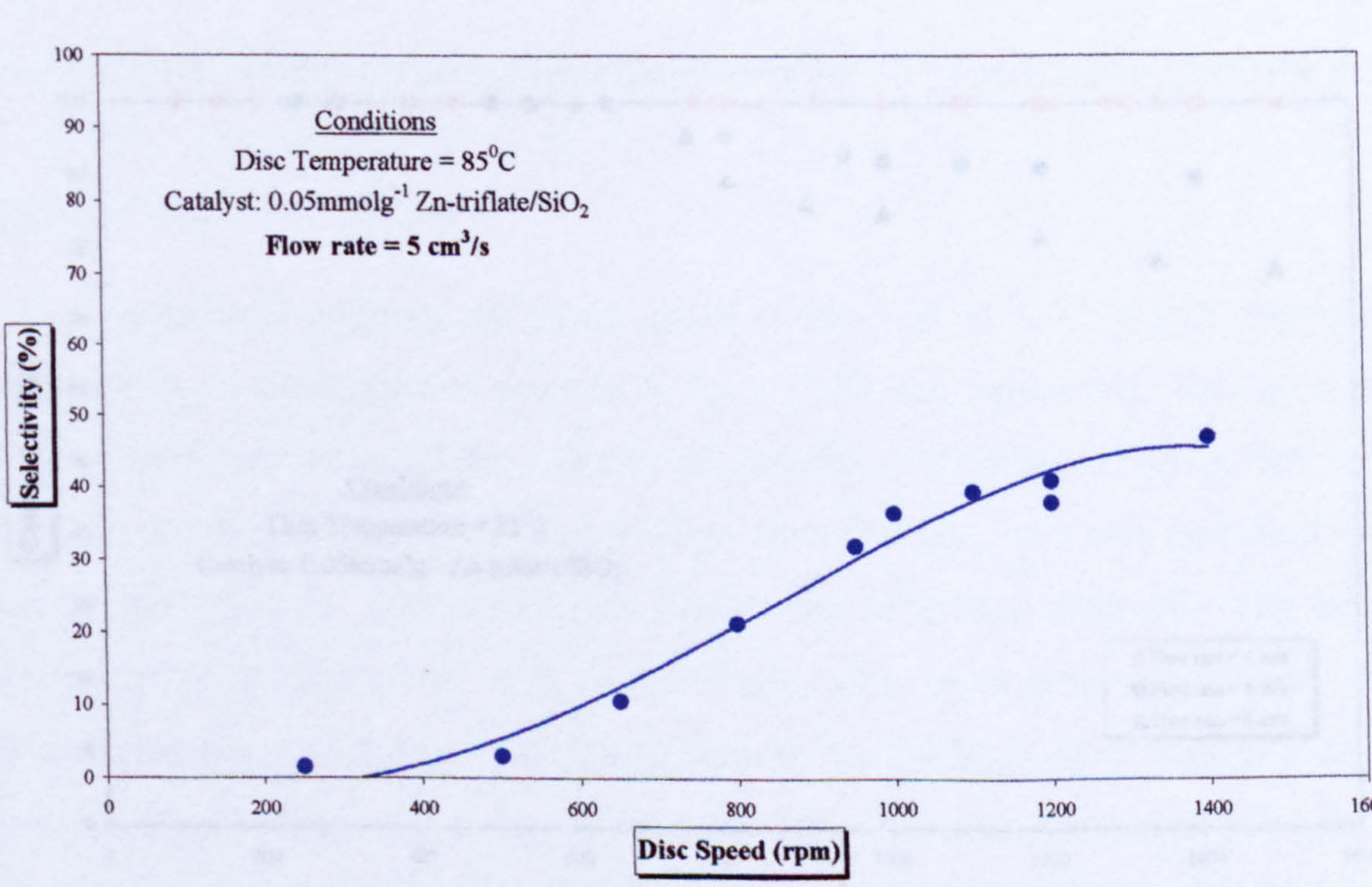


**Figure 6.5. Results for the feed flow rate of 5 $cm^3/s$ (Catalyst 1)**

Instead of pushing the disc speeds up to the limit (1500 rpm was the maximum) residence time was reduced by increasing the flow rate. The observed

selectivities for flow rates of 5 and 6 $cm^3/s$ are shown in Figures 6.5 and 6.6 respectively.

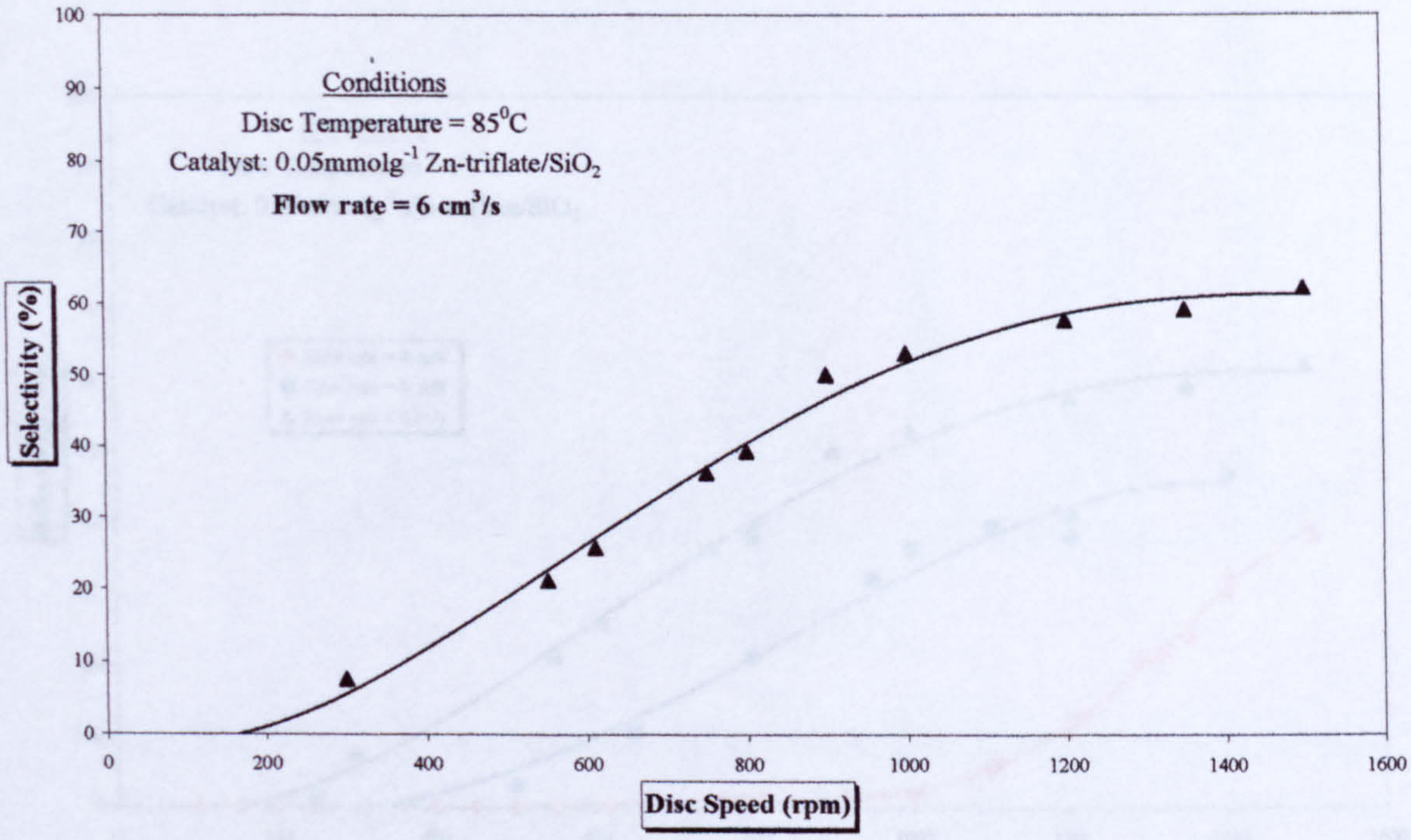


**Figure 6.6. Results for the feed flow rate of 6 $cm^3/s$ (Catalyst 1)**

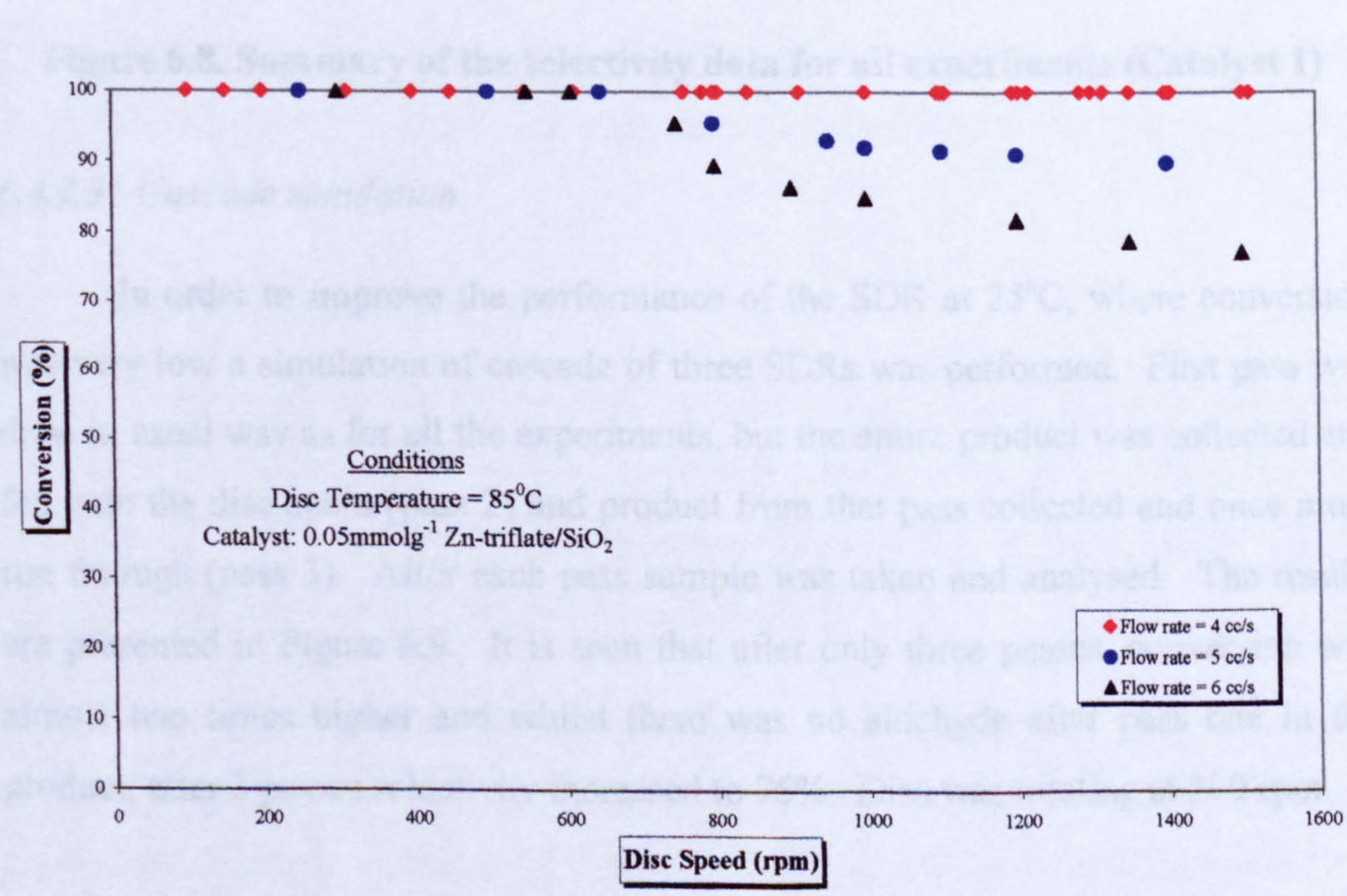


**Figure 6.7. Summary of the conversion data for all experiments (Catalyst 1)**

High conversions in excess of 78% of α–pinene oxide were achieved in all the runs. Summary of conversion and selectivity data collected for all conditions are presented in Figures 6.7 and 6.8 respectively.

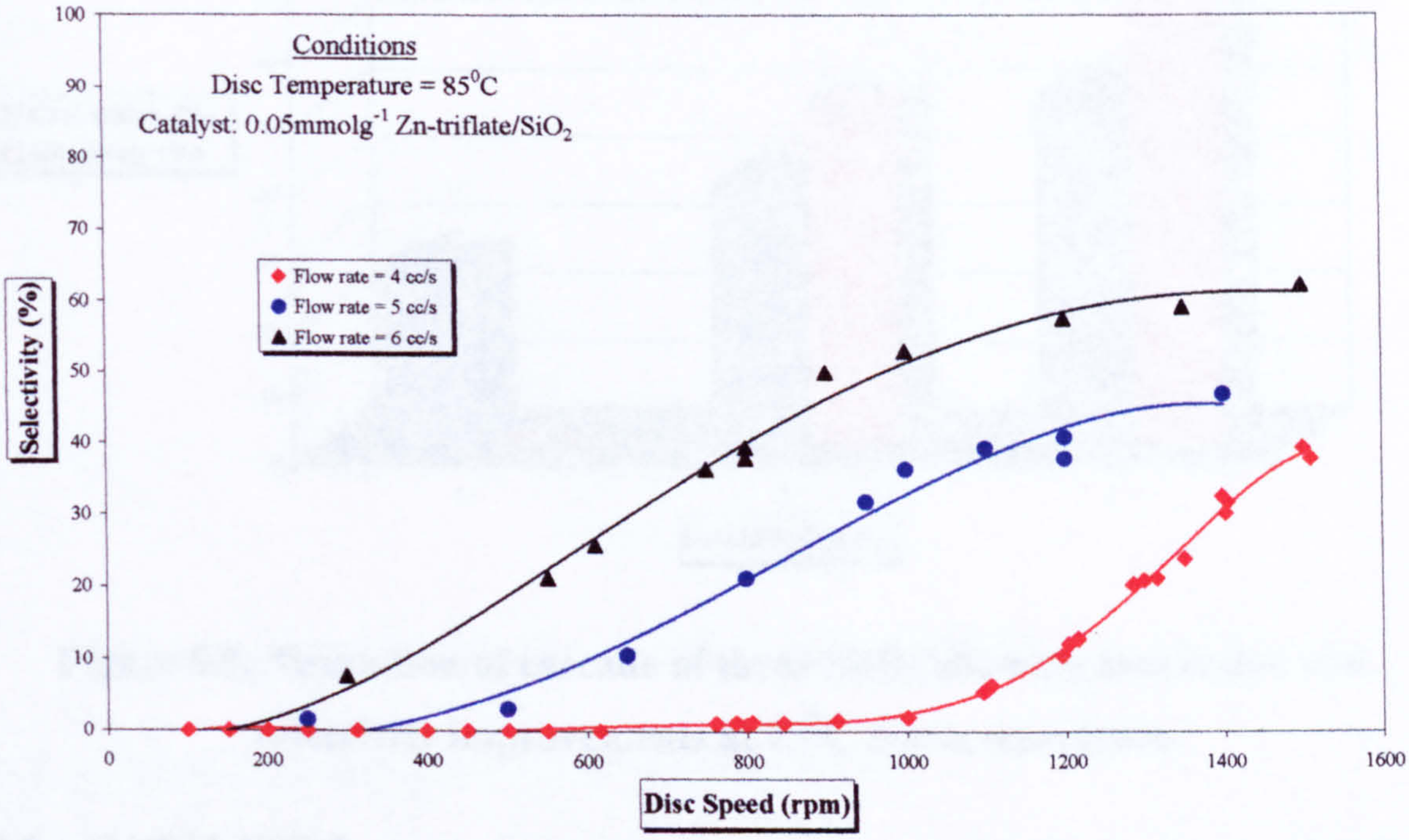


**Figure 6.8. Summary of the selectivity data for all experiments (Catalyst 1)**

*6.4.2.3 Cascade simulation*

In order to improve the performance of the SDR at 25°C, where conversion was very low a simulation of cascade of three SDRs was performed. First pass was done in usual way as for all the experiments, but the entire product was collected and fed onto the disc again (pass 2) and product from that pass collected and once more run through (pass 3). After each pass sample was taken and analysed. The results are presented in Figure 6.9. It is seen that after only three passes, conversion was almost two times higher and whilst there was no aldehyde after pass one in the product, after 3 passes selectivity increased to 76%. Disc was rotating at 500 rpm.

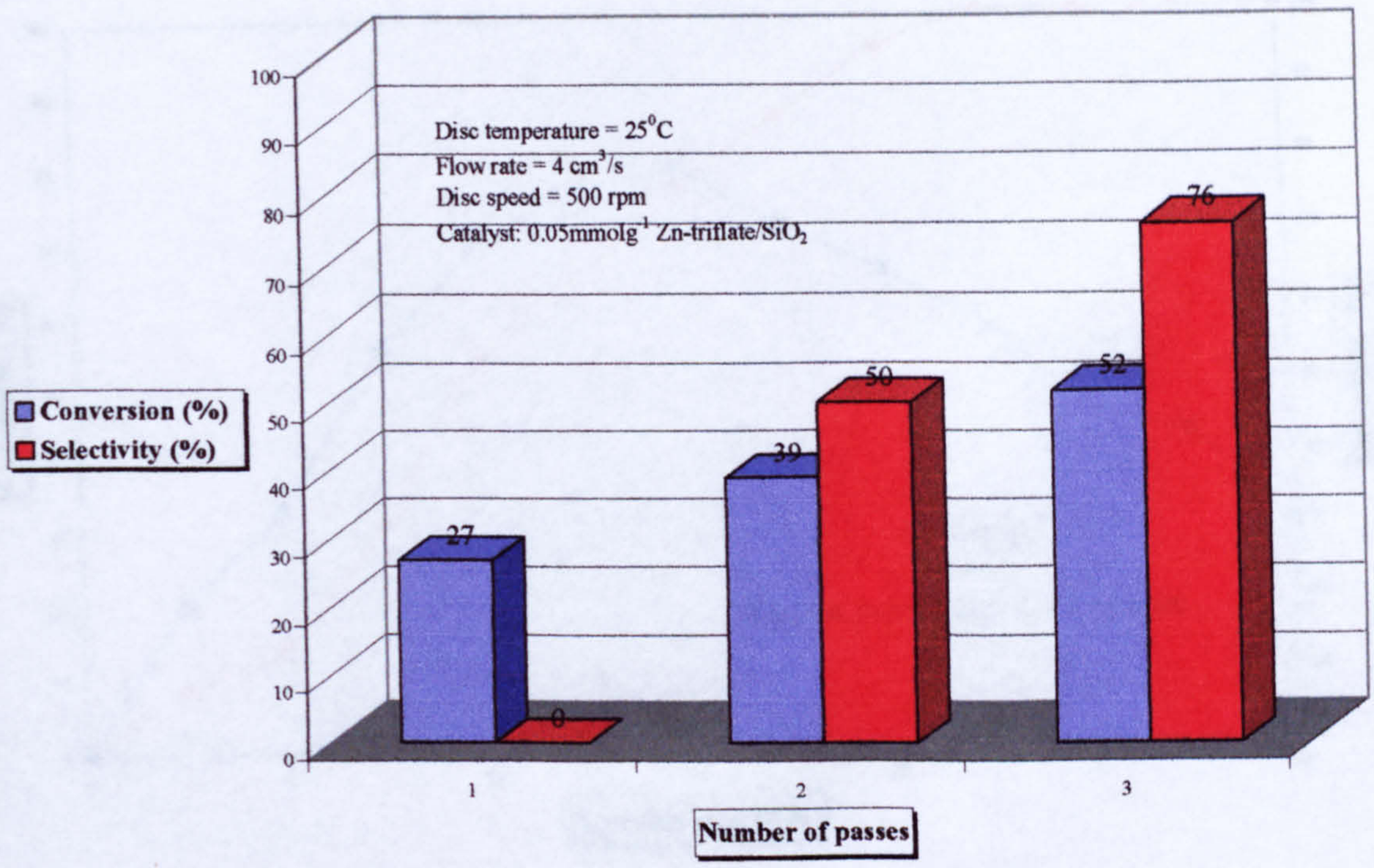


**Figure 6.9. Simulation of cascade of three SDRs showing conversion and selectivity improvements at 25$^0$C disc temperature**

## 6.5 CATALYST 2

Second catalyst used for the isomerisation reaction was 0.01 mmol/g $Zn(OTf)_2$ supported on K100. Similar set of experiments as for the first catalyst were performed.

### 6.5.1 BATCH REACTION

Batch reaction for the second catalyst was performed at 85$^0$C, with same procedures as for the previous catalyst. Since the reaction was slower this time, there was no need to take samples more frequently than once in every 2.5 minutes. All the samples were immediately analysed after collection.

The conversion and selectivity as the reaction progress are shown in Figure 6.10. It can be seen that conversion steadily increases during the course of reaction up until all reactant is used (~22 minutes), while selectivity initially increases to a maximum of 80% after which point it gradually drops. Latest recorded selectivity after the point of 30 minutes is 30%.

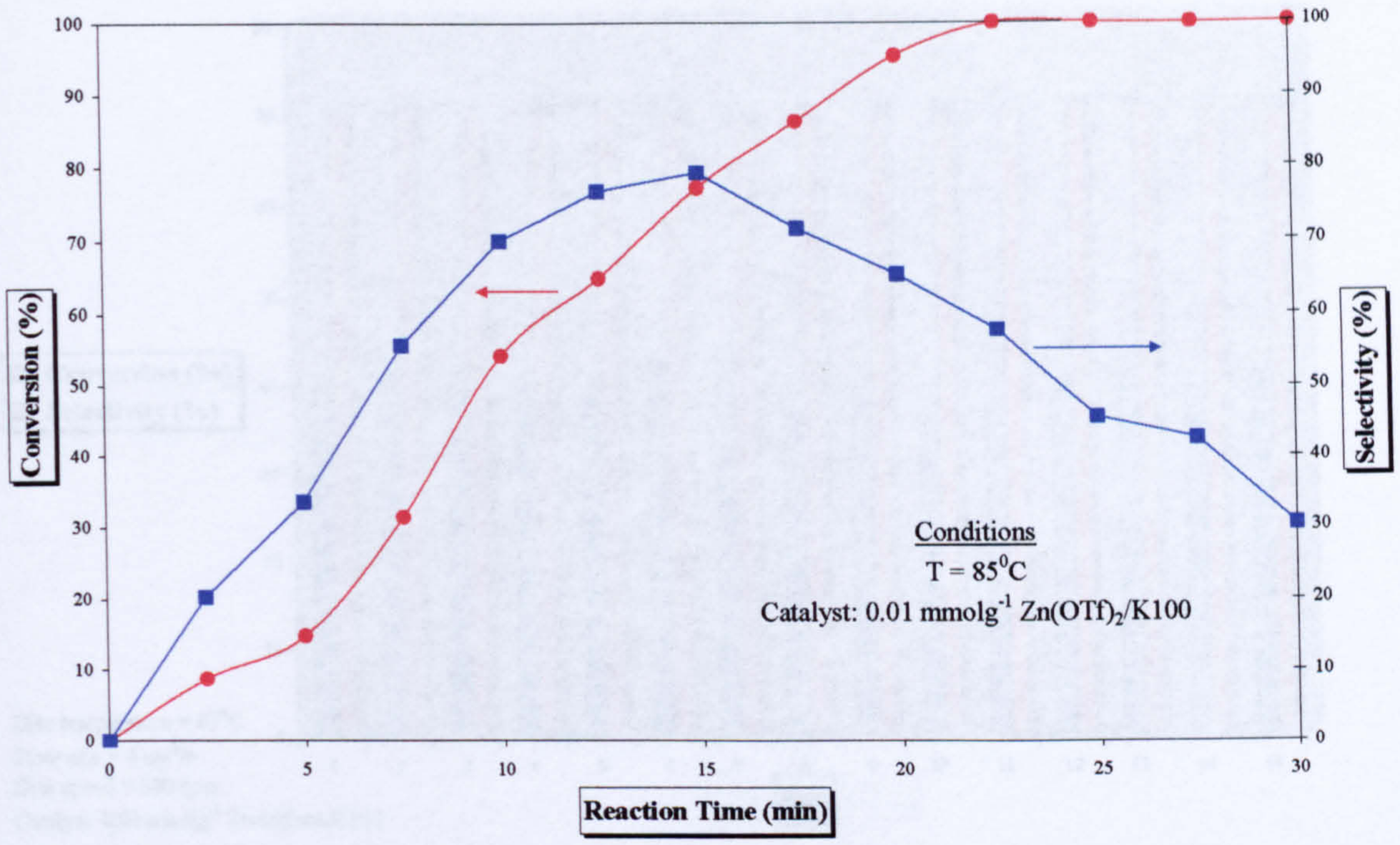


**Figure 6.10. Batch reaction data (Catalyst 2)**

## 6.5.2 CATALYST ACTIVITY INVESTIGATION

First part of the study of proposed reaction in the spinning disc reactor was performance of the catalyst under the same disc conditions and same catalyst coating over period of time to test re-usability and reproducibility of data. Again, one run was performed every 2–3 days, with fixed conditions as follows:

- Disc speed: 500 rpm
- Disc temperature: 45°C
- Flow rate: 4 $cm^3/s$

Results can be seen in Figure 6.11. Conversion values were observed to be consistent run after run at ca. 40%, but more importantly this catalyst was more selective at low conversions towards campholenic aldehyde. A selectivity of 70% was observed at this initial stage.

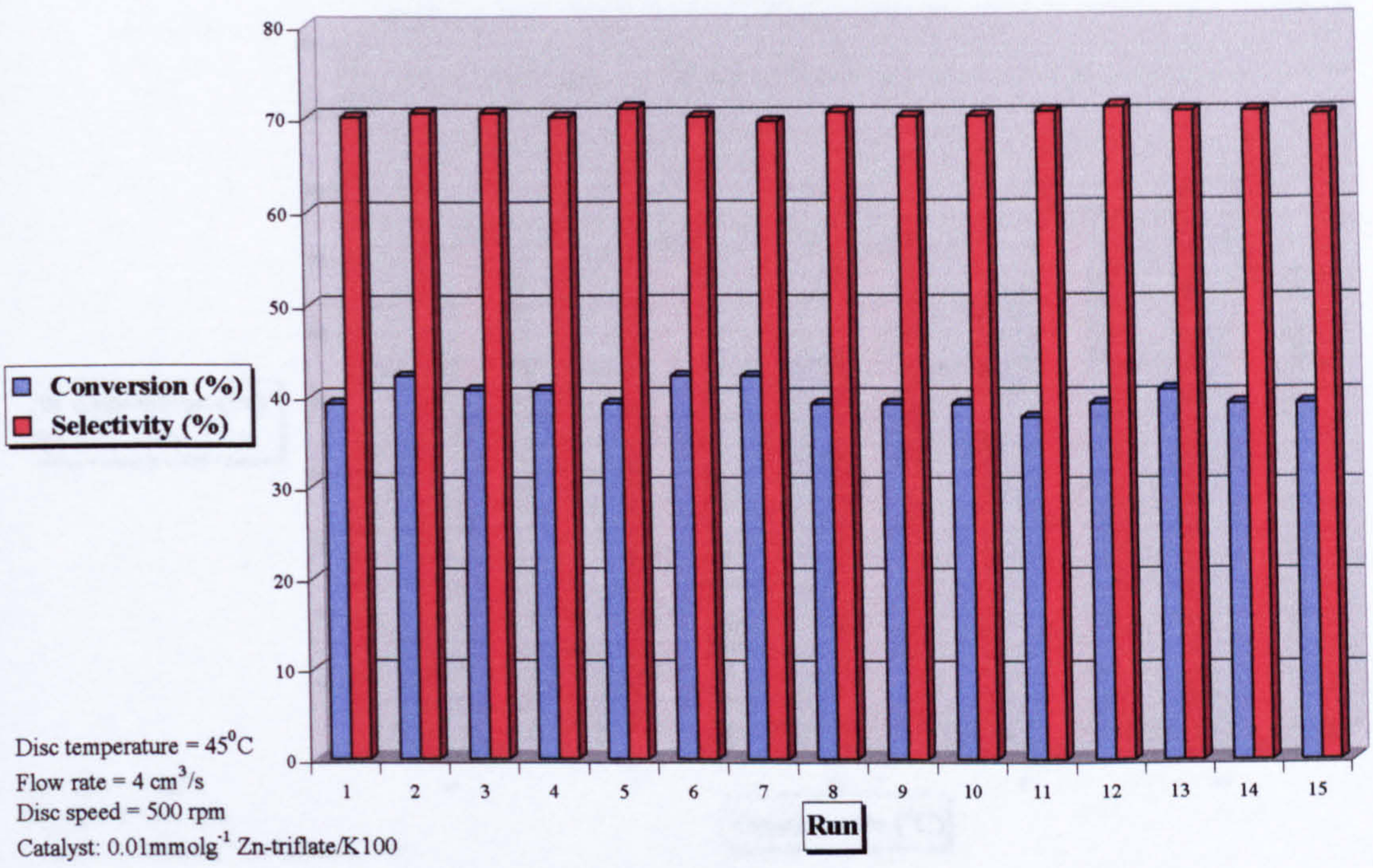


**Figure 6.11. Conversion values for the first 15 runs (Catalyst 2)**

### *6.5.2.1 Influence of temperature*

Again, first optimum factor to be found for the reaction was the temperature of the disc. Temperatures in the range of 25°C to 85°C were tested with rotational speed of the disc kept at 500 rpm and feed flow rate at 4 $cm^3/s$. Results are presented in Figure 6.12.

Conversion of α-pinene oxide increased with temperature, with 70% achieved at 85°C. Change in temperature did not have as significant influence on the observed selectivities, nevertheless much higher selectivity values were observed using this catalyst (65–74%);

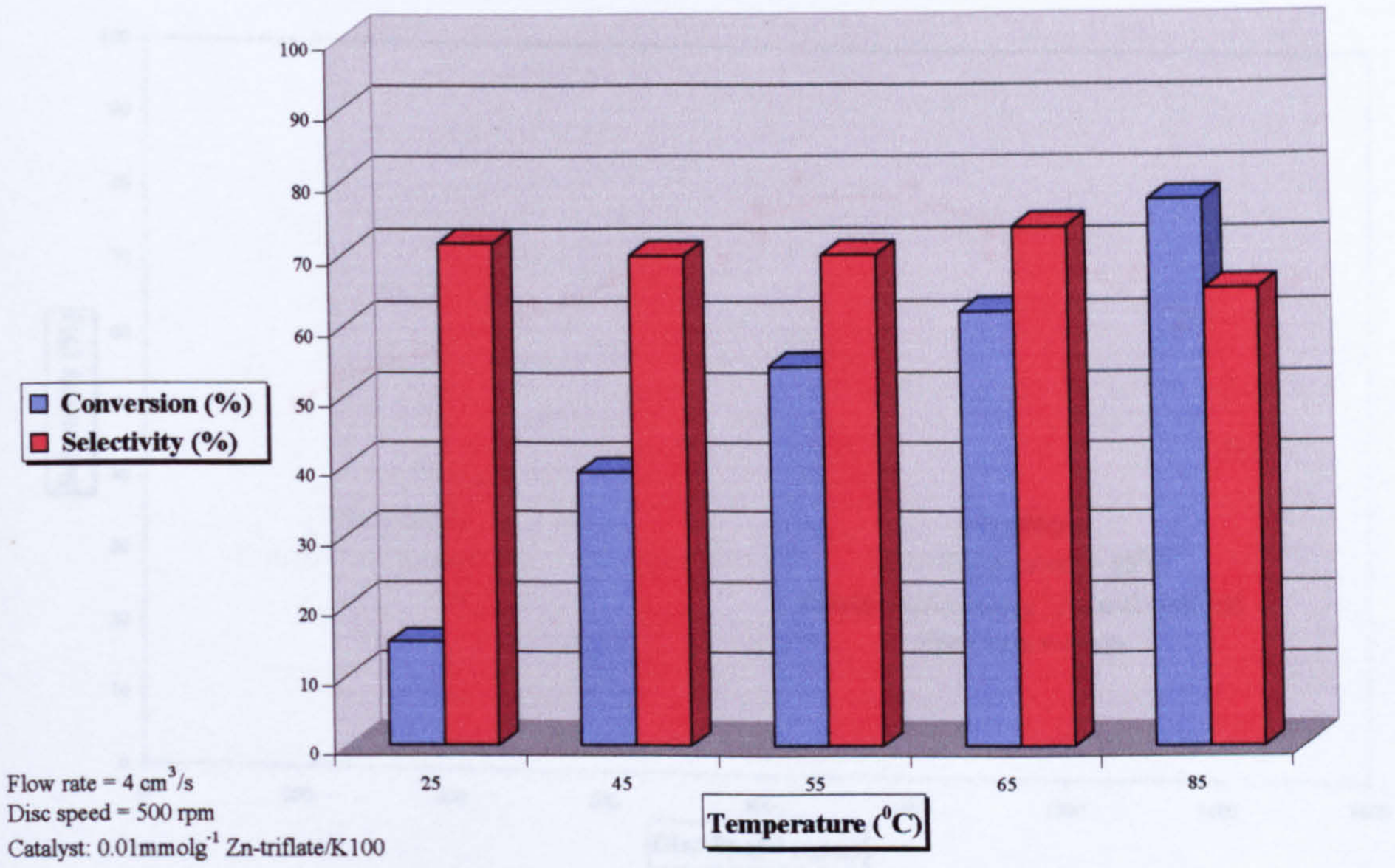


**Figure 6.12. Conversion and selectivity at different disc temperatures**

### *6.5.2.2 Influence of disc speed and flow rate*

As the highest conversion/selectivity were observed at 85°C, this was the temperature chosen for the SDR experiments. Various disc speeds, ranging from 200 to 1500 rpm, were tested as well as different flow rates in the range from 3 to 6 $cm^3/s$. Influence of disc speed on selectivity towards campholenic aldehyde for flow rates of 4, 5 and 6 $cm^3/s$ can be seen in Figures 6.13, 6.14 and 6.15 respectively. Overall, selectivity was higher than for the previous catalyst even at the low flow rates, which was not the case before. If we compare the batch reactions for the two catalysts used so far, it can be seen that the first catalyst was about 4 times more active than the second one, therefore increased selectivity achieved in the SDR using second catalyst was due to lack of time for the consecutive reactions to take place. This is to be confirmed later when conversion results are analysed. Maximum selectivity achieved was 83% (at 850 rpm and 4 $cm^3/s$) with a general trend of lower selectivities at higher flow rates, with peaks going towards lower speeds as the flow rate increases.

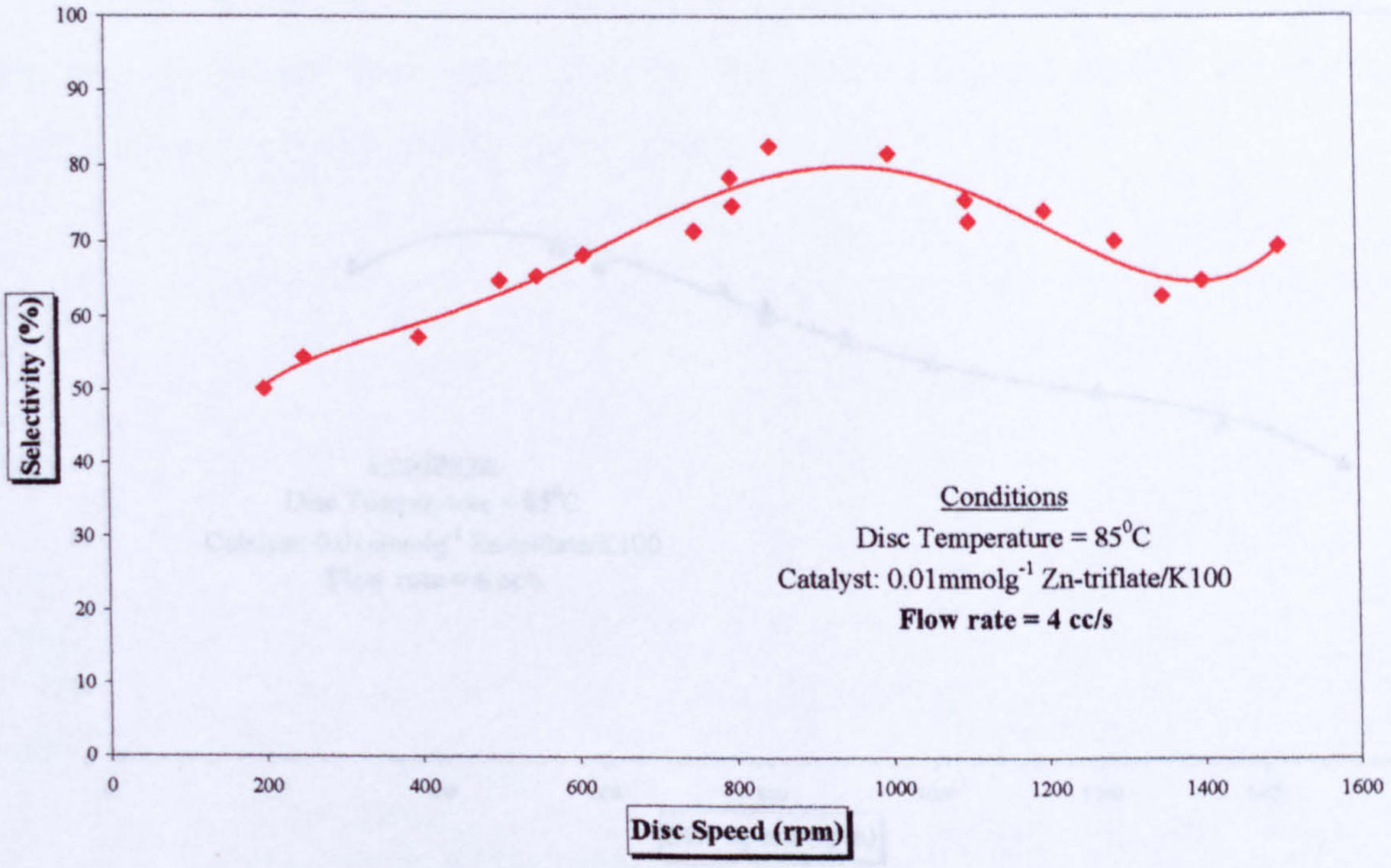


**Figure 6.13. Results for the feed flow rate of 4 $cm^3/s$ (Catalyst 2)**

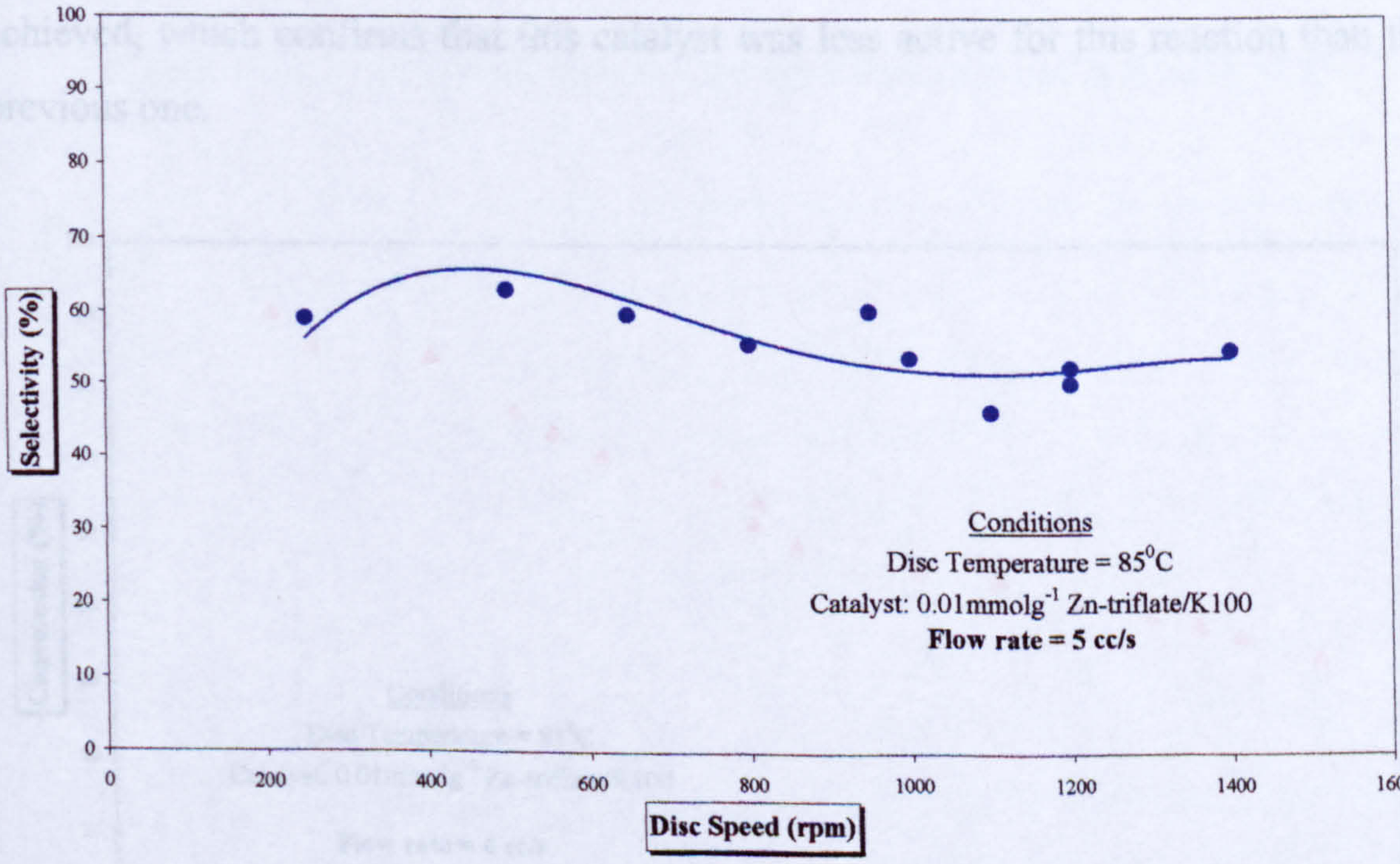


**Figure 6.14. Results for the feed flow rate of 5 $cm^3/s$ (Catalyst 2)**

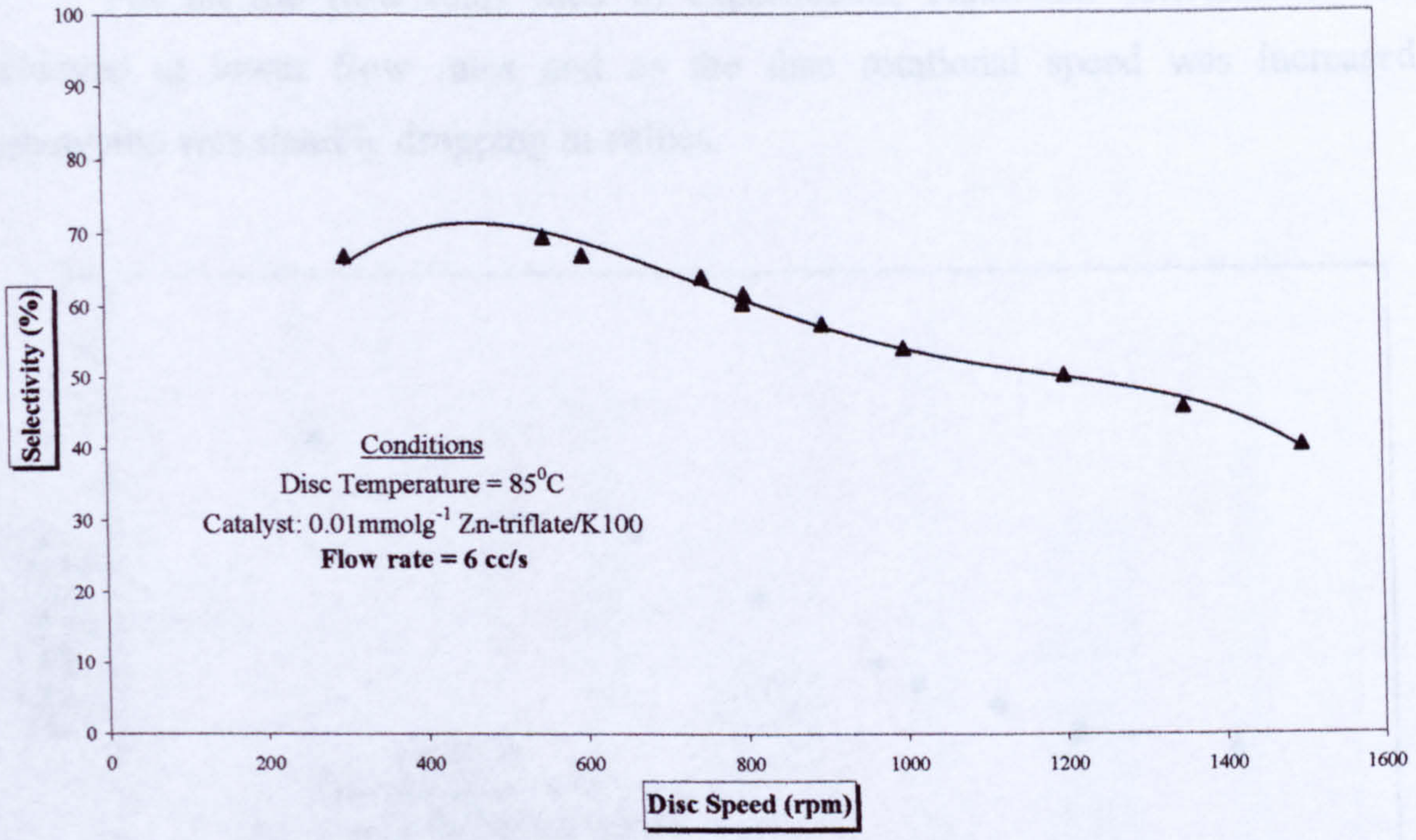


**Figure 6.15. Results for the feed flow rate of 6 $cm^3/s$ (Catalyst 2)**

Conversion results for flow rates of 4, 5 and 6 $cm^3/s$ are presented in Figures 6.16, 6.17 and 6.18 respectively. Full conversion of α–pinene oxide was never achieved, which confirms that this catalyst was less active for this reaction than the previous one.

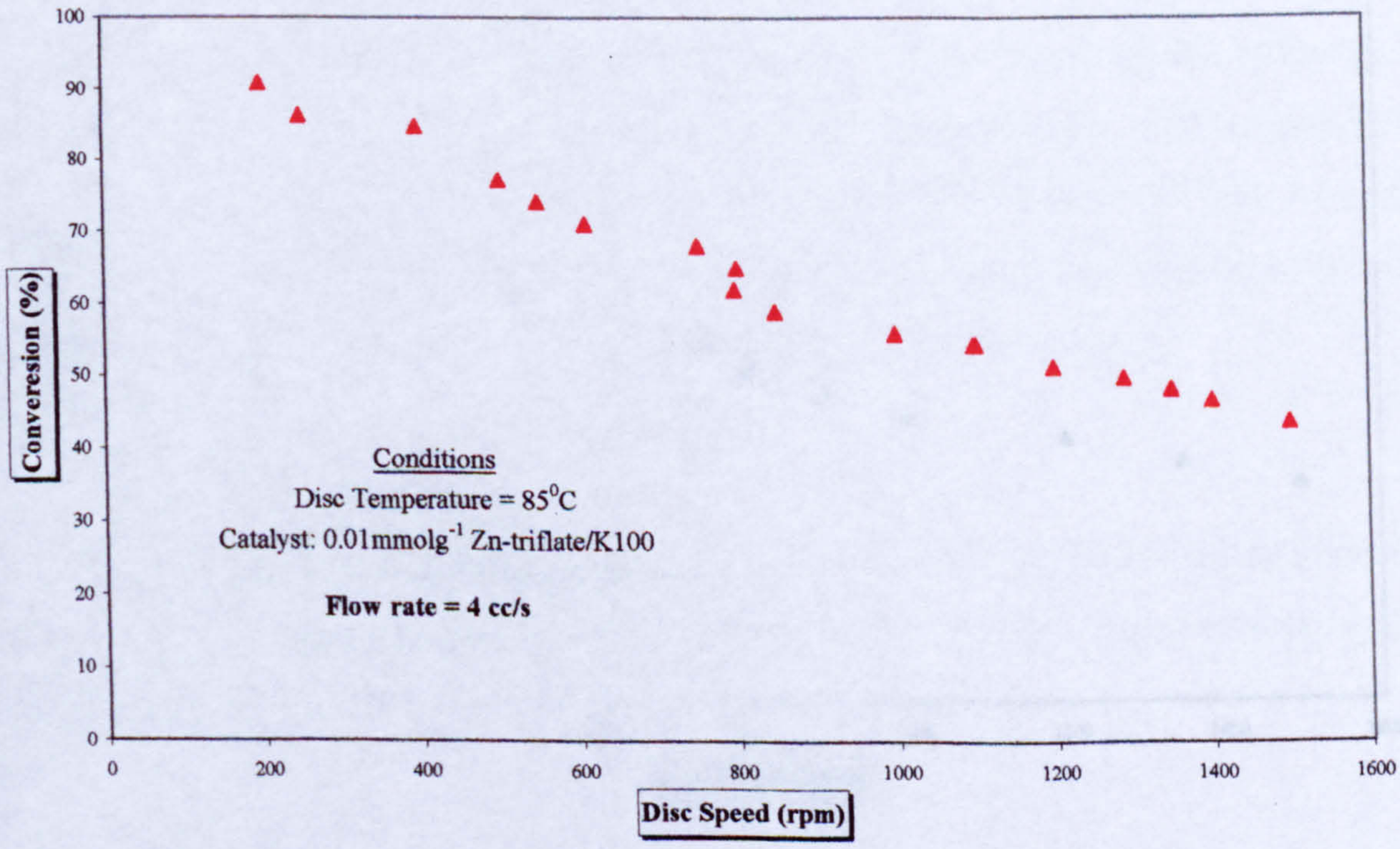


**Figure 6.16. Conversion for the feed flow rate of 4 $cm^3/s$ (Catalyst 2)**

For all the flow rates used in experiments, maximum conversions were achieved at lower flow rates and as the disc rotational speed was increased, conversion was steadily dropping in values.

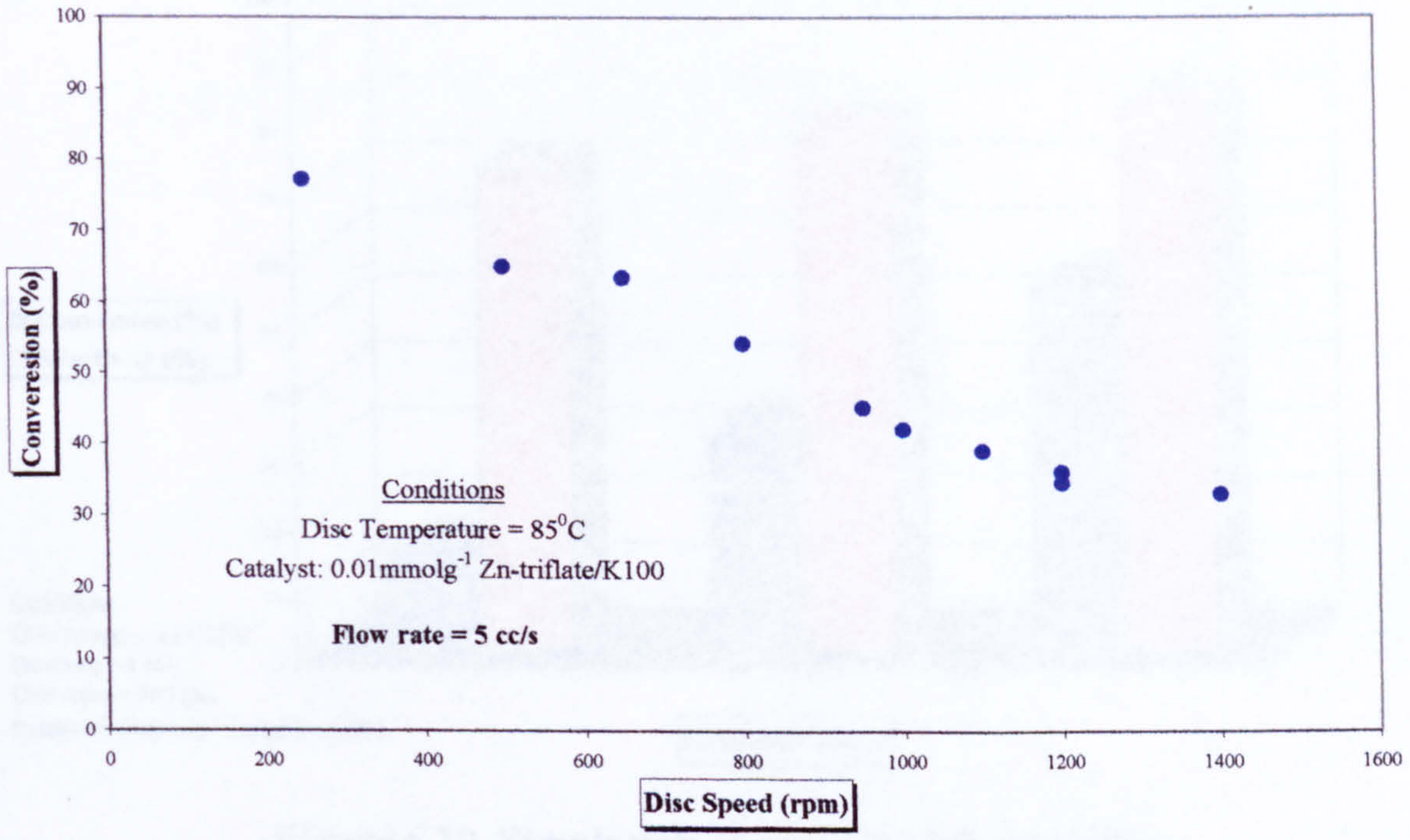


**Figure 6.17. Conversion for the feed flow rate of 5 $cm^3/s$ (Catalyst 2)**

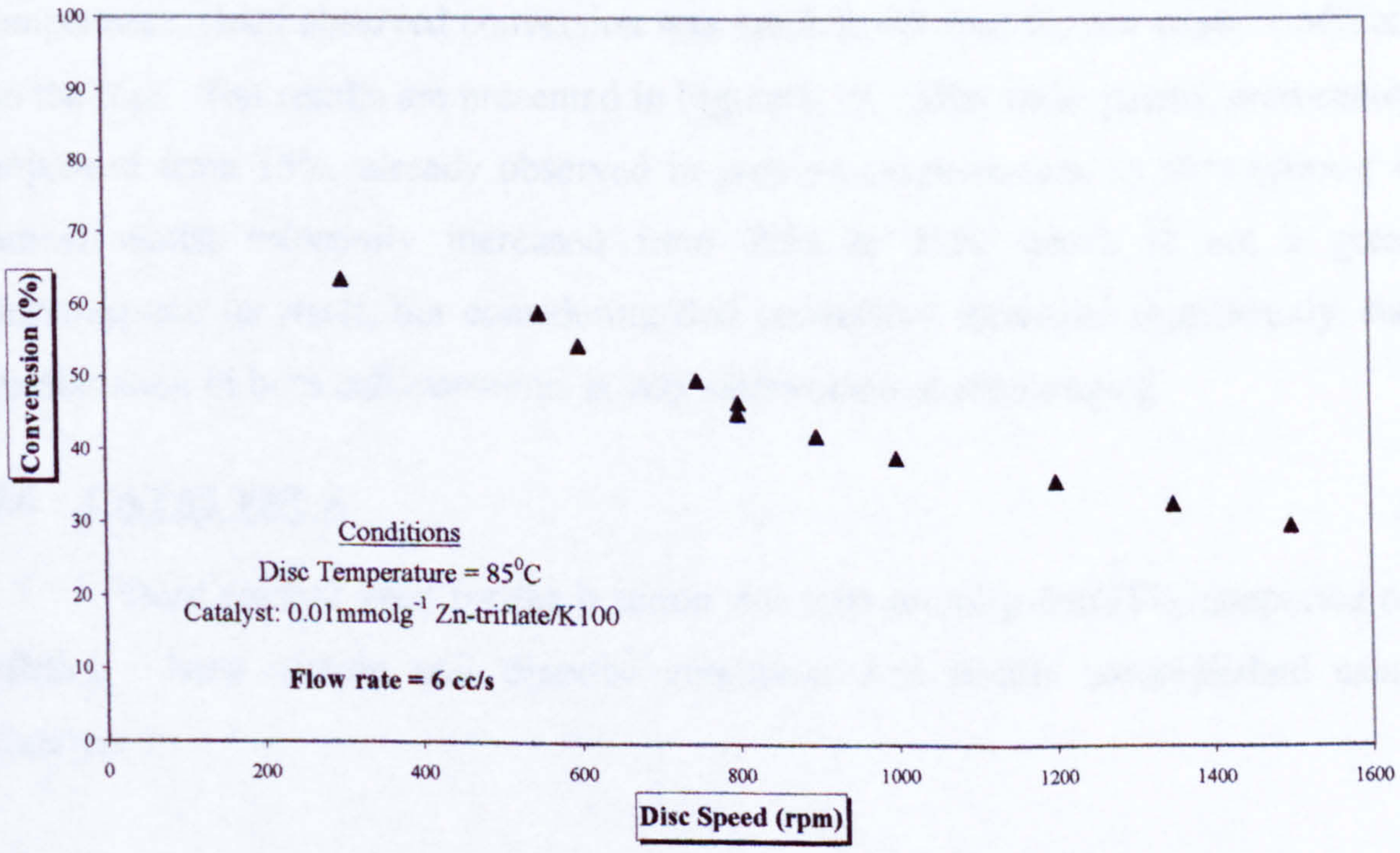


**Figure 6.18. Conversion for the feed flow rate of 6 $cm^3/s$ (Catalyst 2)**

### *6.5.2.3 Cascade simulation*

Cascade simulation was performed the same way as for the previous catalyst.

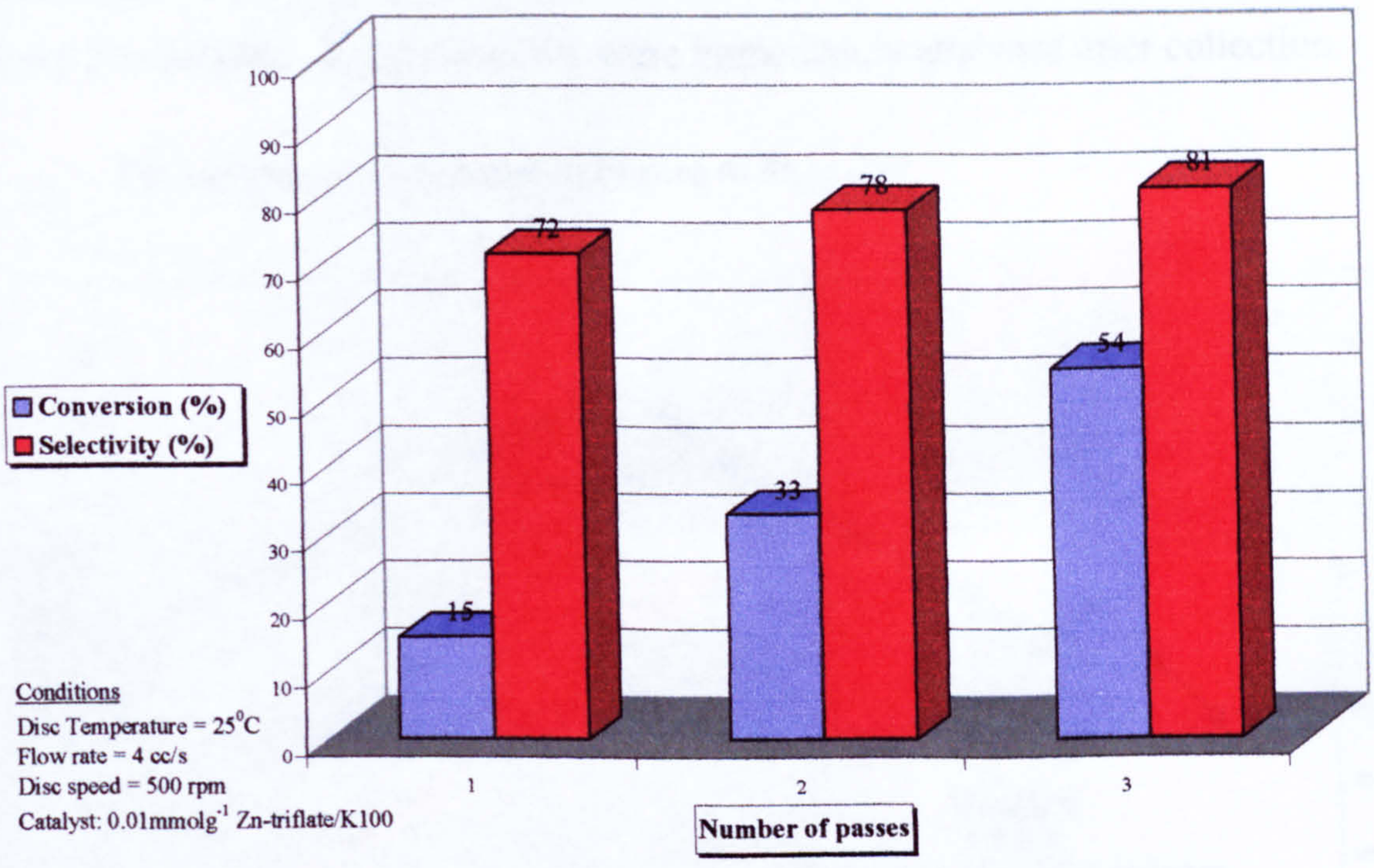


**Figure 6.19. Simulation of cascade of three SDRs**

Three passes on the disc were performed and after each pass a sample was taken and analysed. Temperature of 25°C was selected again as an operating temperature, since observed conversion was much lower than for any other condition on the disc. The results are presented in Figure 6.19. After three passes, conversion improved from 15%, already observed in previous experiments, to 54% (almost 4 times) whilst selectivity increased from 72% to 81% which is not a great improvement on itself, but considering that conversion increased significantly, the combination of both enhancements is very important and encouraging.

## 6.6 CATALYST 3

Third catalyst used for the reaction was 0.05 mmol/g $Zn(OTf)_2$ supported on $HMS_{24}$. Next section will describe conditions and results accomplished using Catalyst 3.

### 6.6.1 BATCH REACTION

Batch reaction for the third catalyst was performed at 45°C, with the same procedures employed as for the previous two catalysts. Samples were taken once in every 2.5 minutes. All the samples were immediately analysed after collection.

The results are presented in Figure 6.20.

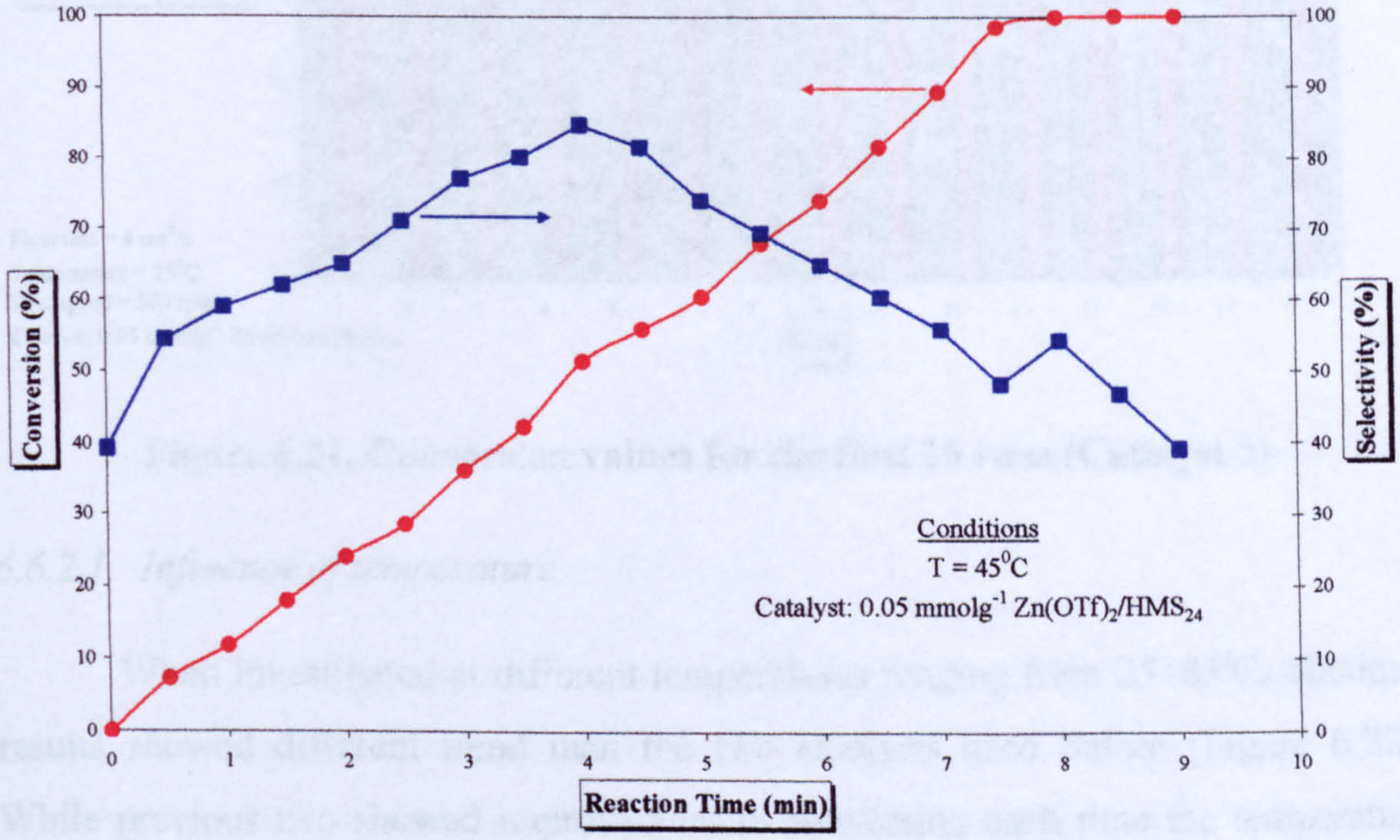


**Figure 6.20. Batch reaction data (Catalyst 3)**

### 6.6.2 CATALYST ACTIVITY INVESTIGATION

As practiced before, the catalyst was checked for activity and stability. 15 runs performed on 25°C with disc rotating at 500 rpm and with feed flow rate of 4 $cm^3/s$, showed great reproducibility; therefore coated catalyst could be repeatedly used without concern of lost activity over time (Figure 6.21). Furthermore, initial results at temperature this low were very encouraging since 70% conversion was achieved (with ~66% selectivity).

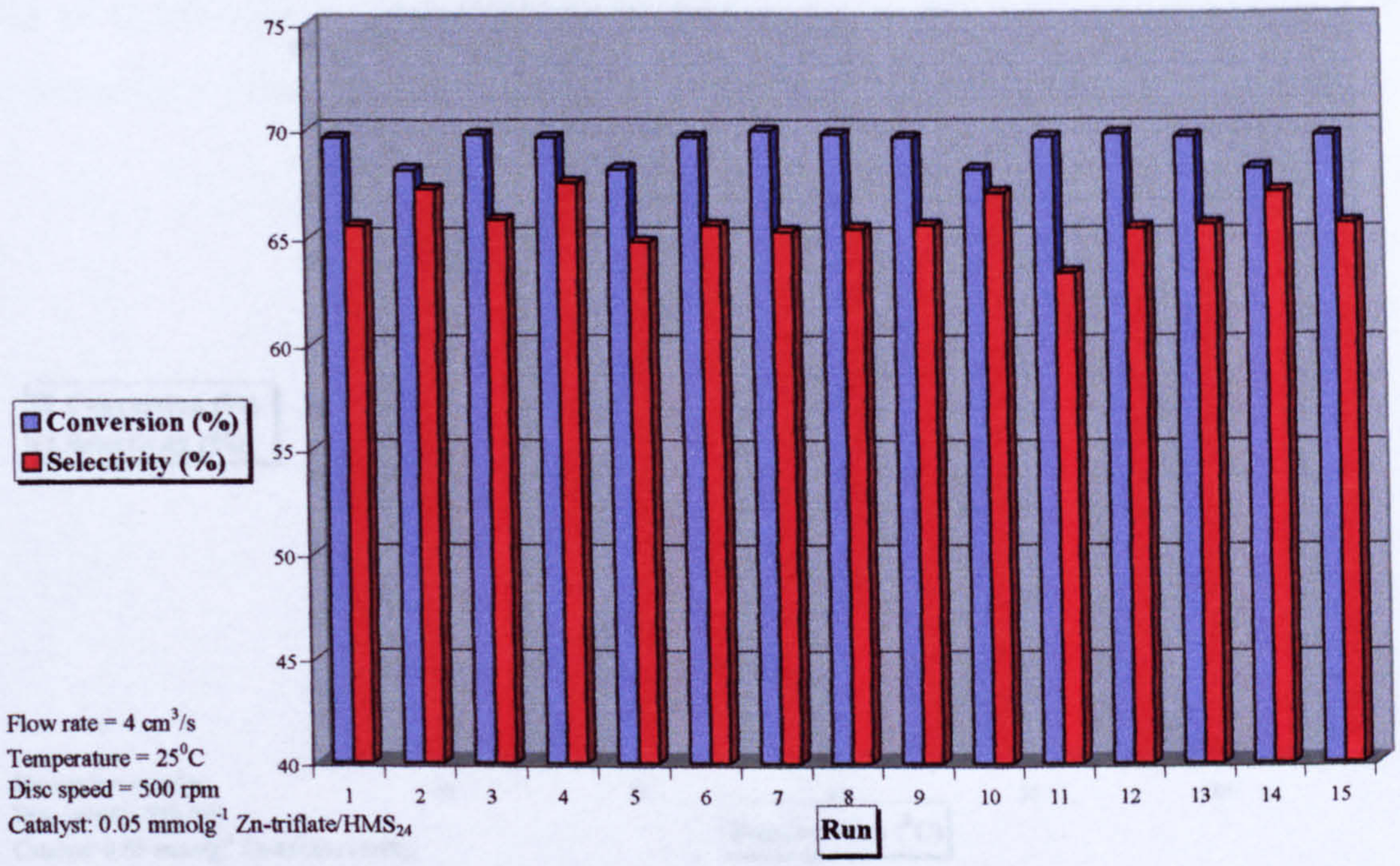


**Figure 6.21. Conversion values for the first 15 runs (Catalyst 3)**

### *6.6.2.1 Influence of temperature*

When investigated at different temperatures ranging from 25–85°C, obtained results showed different trend than the two catalysts used before (Figure 6.22). While previous two showed improvement in conversion each time the temperature was increased, this catalyst followed similar trend from 25–45°C, when full conversion was accomplished. If all the catalysts had the same behaviour, it would be expected that from 45°C above conversion would remain full. But instead there was a slight drop after 45°C, and at 85°C, where the results were the best for the other two catalysts, conversion was 60%. For that reason 45°C was selected as the optimum temperature for the third catalyst and was kept as a fixed condition in order to investigate the influence of other parameters.

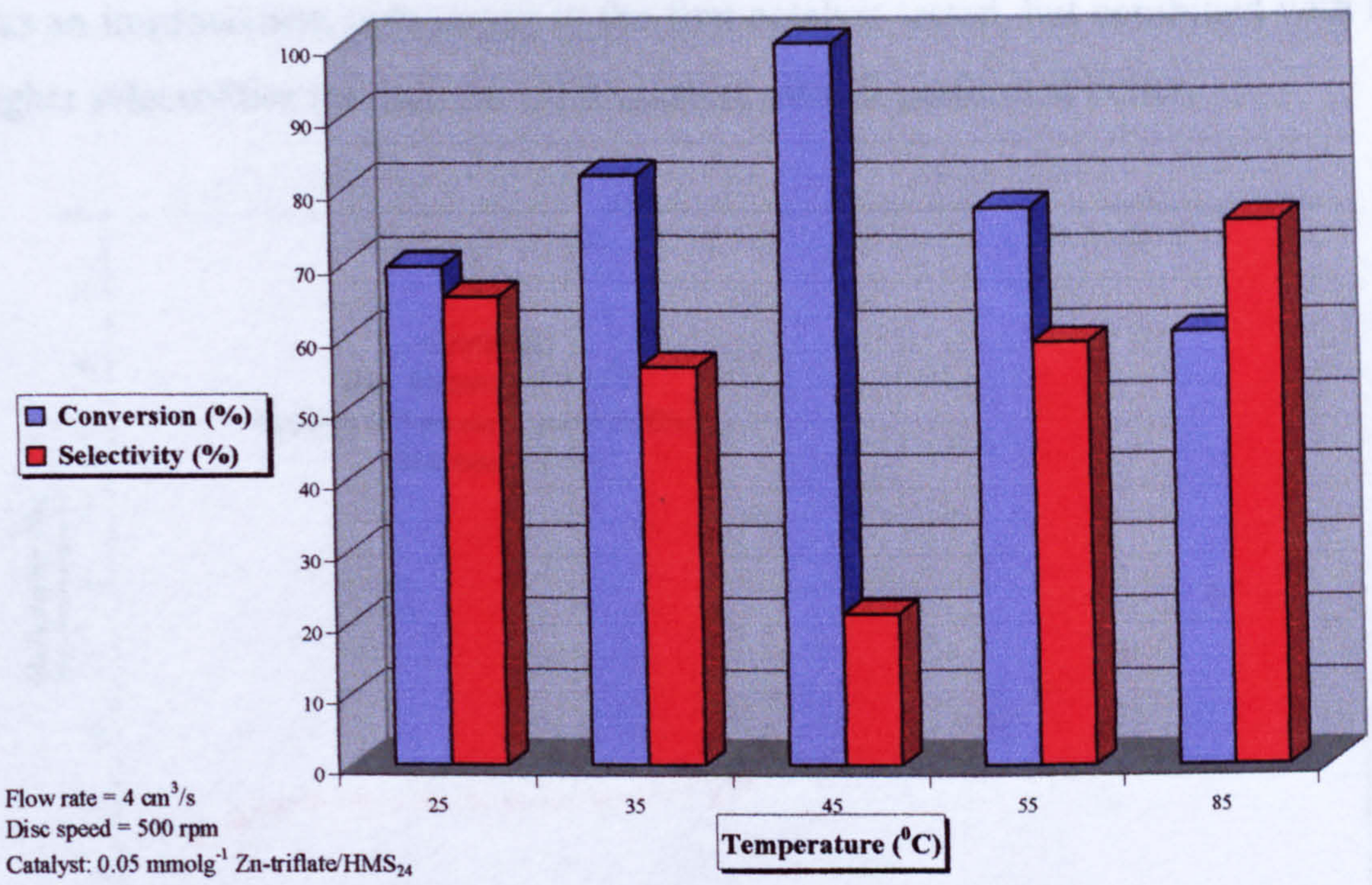


**Figure 6.22. Conversion and selectivity at different disc temperatures**

### *6.6.2.2 Influence of disc speed and flow rate*

As previously stated, next runs were undertaken at 45°C, with various disc speeds. Feed flow rate was constant at this stage (4 $cm^3/s$). Selectivity results for this flow rate can be seen in Figure 6.23. The trend is similar as that of the first catalyst, but selectivities were much higher (by 20%). Conversion at this stage was full at all conditions (see Figure 6.26).

The maximum observed selectivity towards aldehyde was 52%. As for the first catalyst, as selectivity increases on higher rotational speeds, residence time was a critical factor in the reaction.

Experimental results for the feed flow rates of 5 $cm^3/s$ and 6 $cm^3/s$ are shown in Figures 6.24 and 6.25 respectively. Similar pattern can be observed as for the flow rate of 4 $cm^3/s$, but the selectivity at higher flow rates was greater. At 45°C with disc spinning at 1500 rpm and for the feed flow rate of 6 $cm^3/s$, 75% selectivity was achieved, which was the maximum selectivity observed.

As far as conversion of α–pinene oxide is concerned for these two flow rates (Figure 6.26), for the disc speeds up to a 1000 rpm conversion was 100%; at rotational speeds higher than 1000 rpm conversion was in between 80–95% which

was an improvement comparing to the first catalyst tested, but combined with much higher selectivities reached the third catalyst overall performed better.

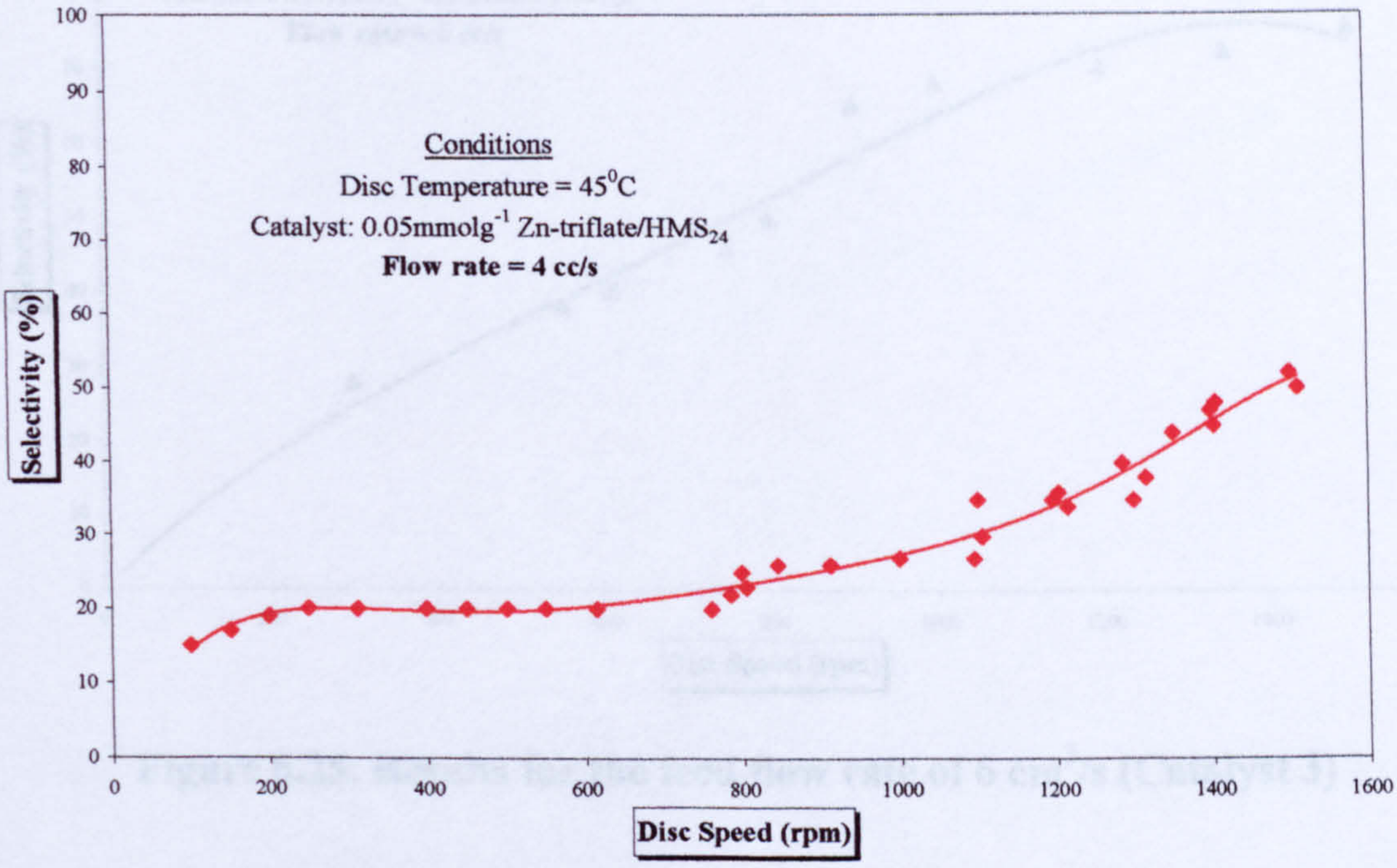


**Figure 6.23. Results for the feed flow rate of 4 $cm^3/s$ (Catalyst 3)**

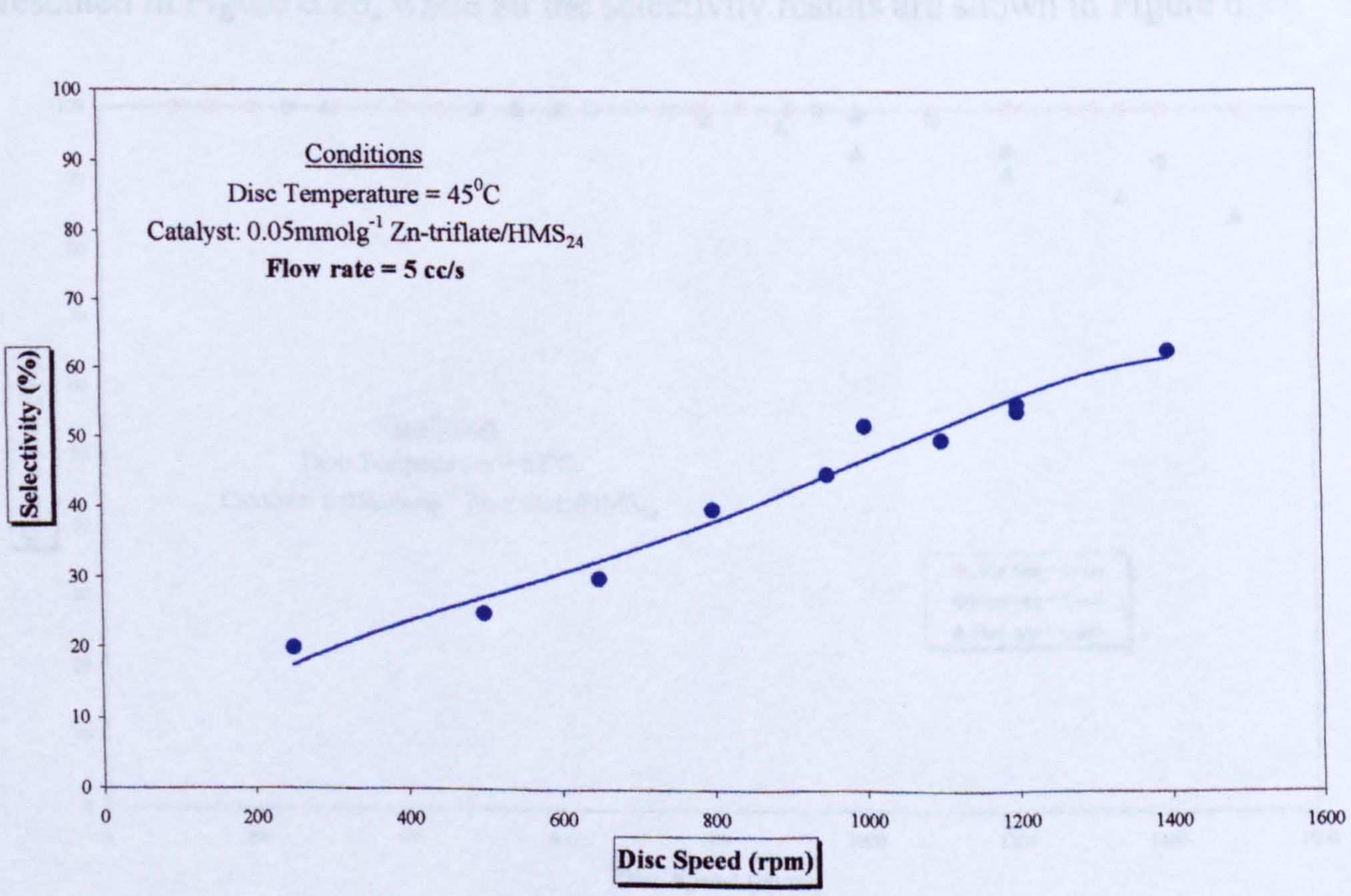


**Figure 6.24. Results for the feed flow rate of 5 $cm^3/s$ (Catalyst 3)**

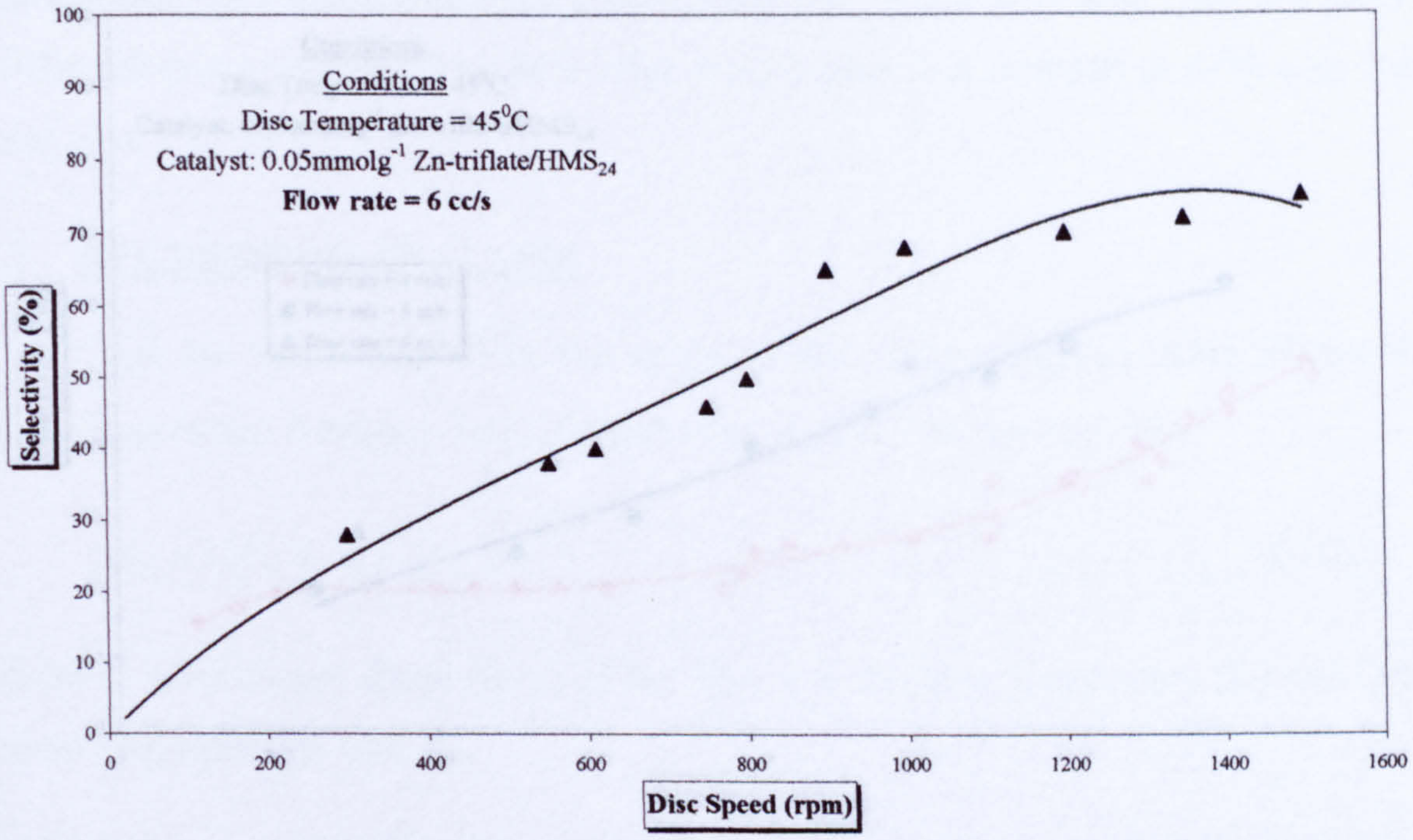


**Figure 6.25. Results for the feed flow rate of 6 $cm^3/s$ (Catalyst 3)**

Conversion results for all the conditions used for performing experiments are presented in Figure 6.26, while all the selectivity results are shown in Figure 6.27.

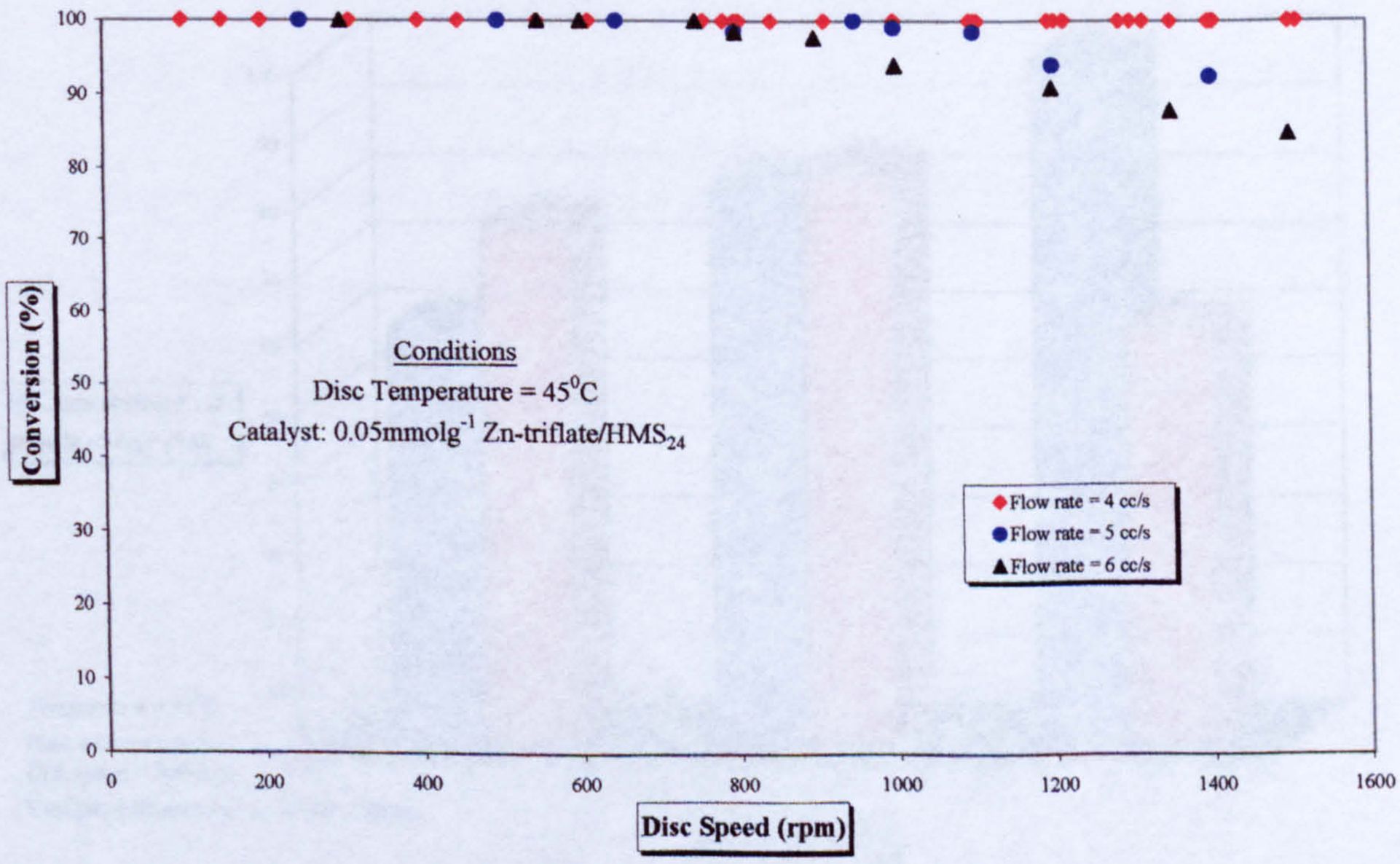


**Figure 6.26. Summary of the conversion data for all experiments (Catalyst 3)**

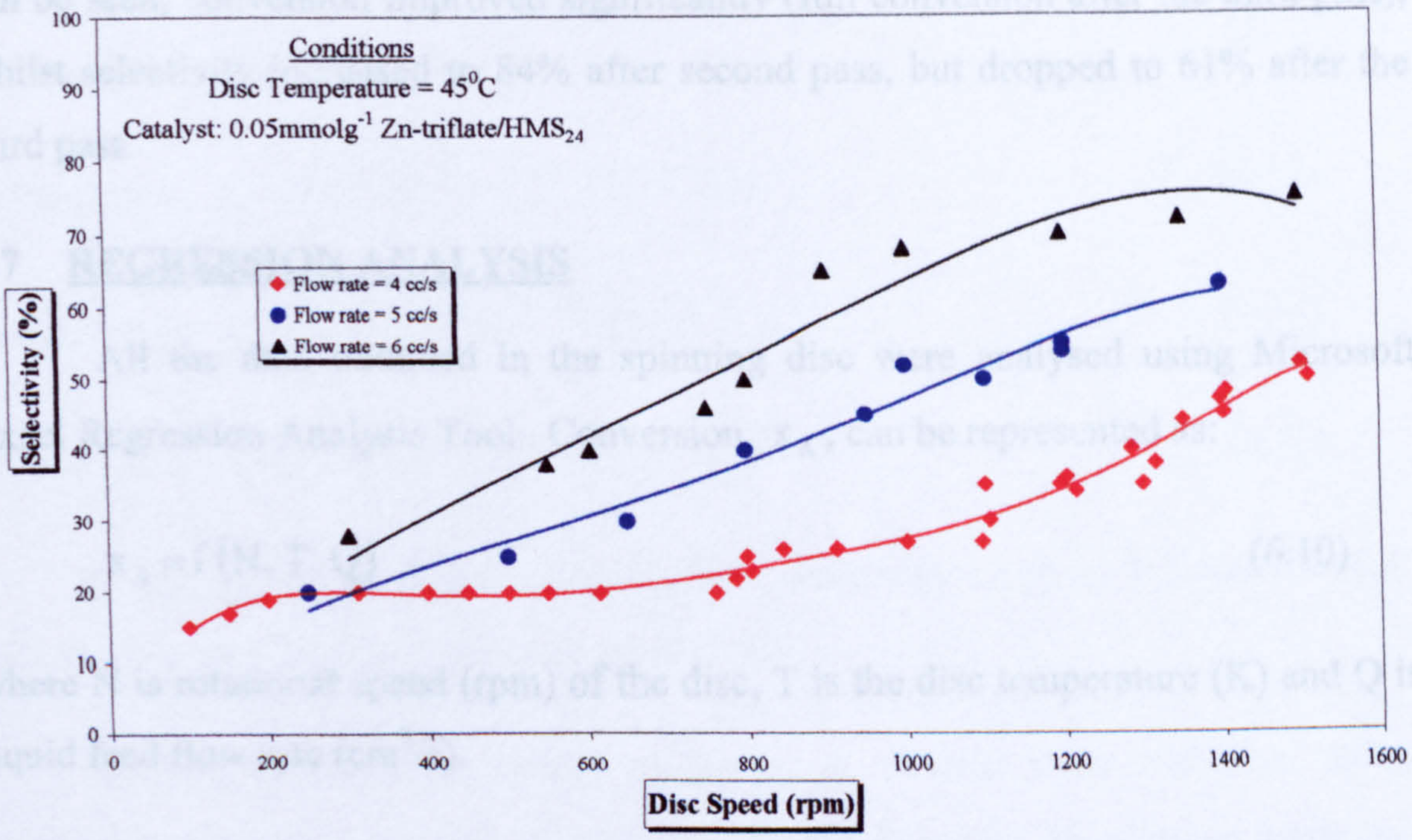


**Figure 6.27. Summary of the selectivity data for all experiments (Catalyst 3)**

### *6.6.2.3 Cascade simulation*

As for the other two catalysts, another simulation of cascade of three reactors was tried. Experimental procedure was the same as before.

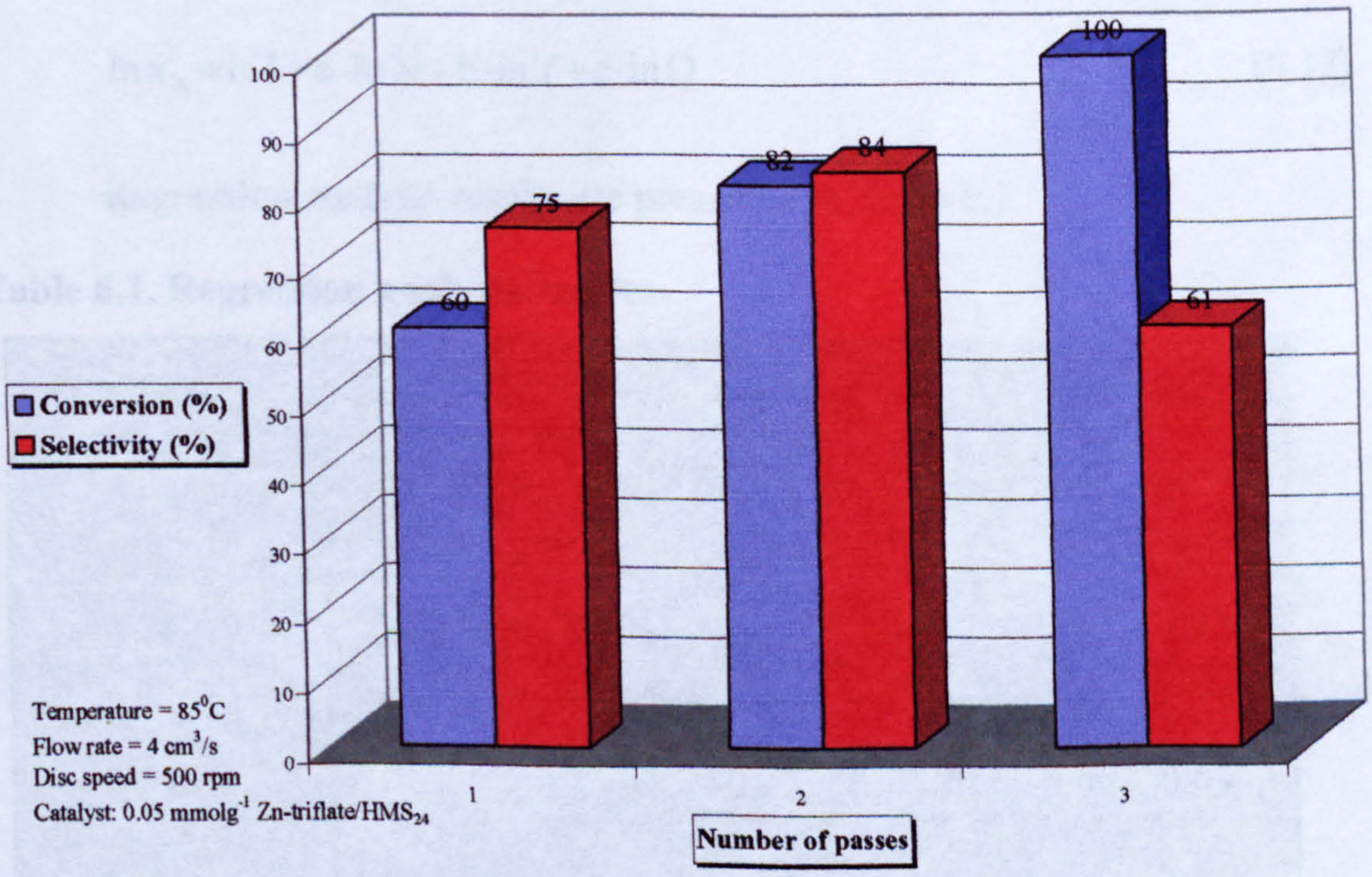


**Figure 6.28. Simulation of cascade of three reactors**

Obtained results are presented in the Figure 6.28. Temperature of 85°C was selected as this was the temperature with the lowest conversion (Figure 6.22). As it

can be seen, conversion improved significantly (full conversion after the third pass), whilst selectivity increased to 84% after second pass, but dropped to 61% after the third pass.

## 6.7 REGRESSION ANALYSIS

All the data obtained in the spinning disc were analysed using Microsoft Excel Regression Analysis Tool. Conversion, $x_A$, can be represented as:

$$x_A = f(N, T, Q) \tag{6.10}$$

where N is rotational speed (rpm) of the disc, T is the disc temperature (K) and Q is liquid feed flow rate ($cm^3/s$).

Or:

$$x_A = I(N)^a\ (T)^b\ (Q)^c \tag{6.11}$$

where I, a, b and c are regression parameters in the equation.

Equation (6.11) can be written in a more suitable form:

$$\ln x_A = \ln I + a \cdot \ln N + b \cdot \ln T + c \cdot \ln Q \tag{6.12}$$

Regression analysis results are presented in Table 6.1.

**Table 6.1. Regression analysis results**

| | Catalyst 1 | Catalyst 2 | Catalyst 3 |
|---|---|---|---|
| **ln I** | -48.32 ± 1.6 | -30.19 ± 1.69 | -17.35 ± 2.66 |
| **I** | $1.03 \cdot 10^{-21}$ | $7.71 \cdot 10^{-14}$ | $2.90 \cdot 10^{-8}$ |
| **a** | 0.02 ± 0.02 | -0.46 ± 0.03 | 0.04 ± 0.02 |
| **b** | 8.26 ± 0.3 | 5.76 ± 0.31 | 2.94 ± 0.47 |
| **c** | -0.30 ± 0.1 | -0.82 ± 0.09 | 0.06 ± 0.09 |
| **$R^2$** | 0.96 | 0.87 | 0.42 |
| **Standard error** | 0.13 | 0.11 | 0.12 |

Therefore following model equations which describe conversion in the spinning disc reactor can be written:

For Catalyst 1: $x_A = 1.03 \cdot 10^{-21} (N)^{0.02} (T)^{8.26} (Q)^{-0.30}$ (6.13)

For Catalyst 2: $x_A = 7.71 \cdot 10^{-14} (N)^{-0.46} (T)^{5.76} (Q)^{-0.82}$ (6.14)

For Catalyst 3: $x_A = 2.90 \cdot 10^{-8} (N)^{0.04} (T)^{2.94} (Q)^{0.06}$ (6.15)

$R^2$ values for the first two correlations were very close to 1 (ideal fitting); while the third correlation was not as good (0.42).

In order to check the model equations, $x_A$ values were calculated using (6.13) to (6.15) and compared to real (experimental) values by plotting predicted values against experimental. If the two were in good agreement, the best linear fit would be y = x. It would be more realistic to expect y = Kx, where coefficient K would be close to 1. These graphs are presented in Figures 6.29 (Catalyst One) to 6.31.

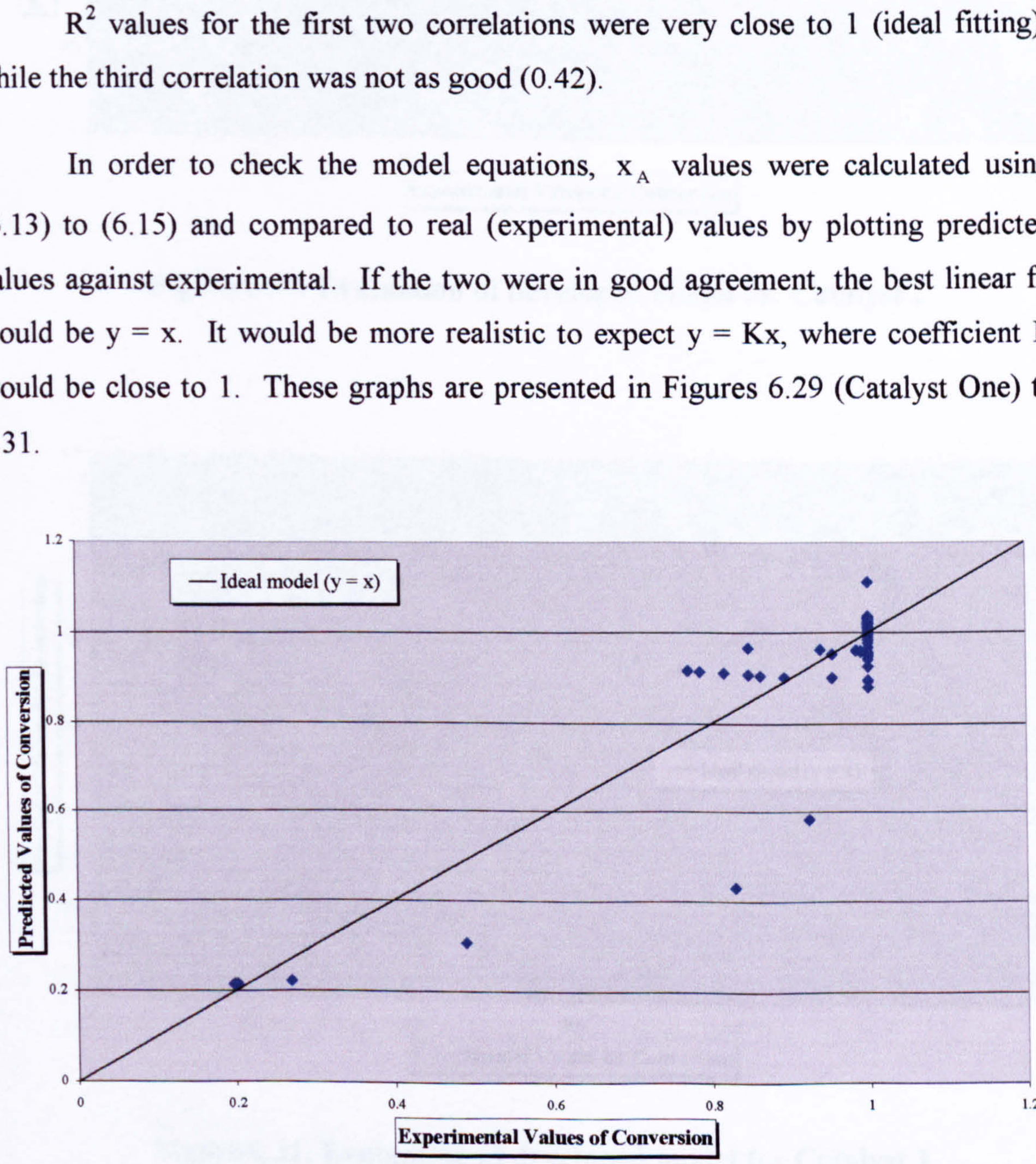


**Figure 6.29. Evaluation of developed model for Catalyst 1**

Model equation for Catalyst One is in very good agreement with obtained values and well describes conversion on the disc.

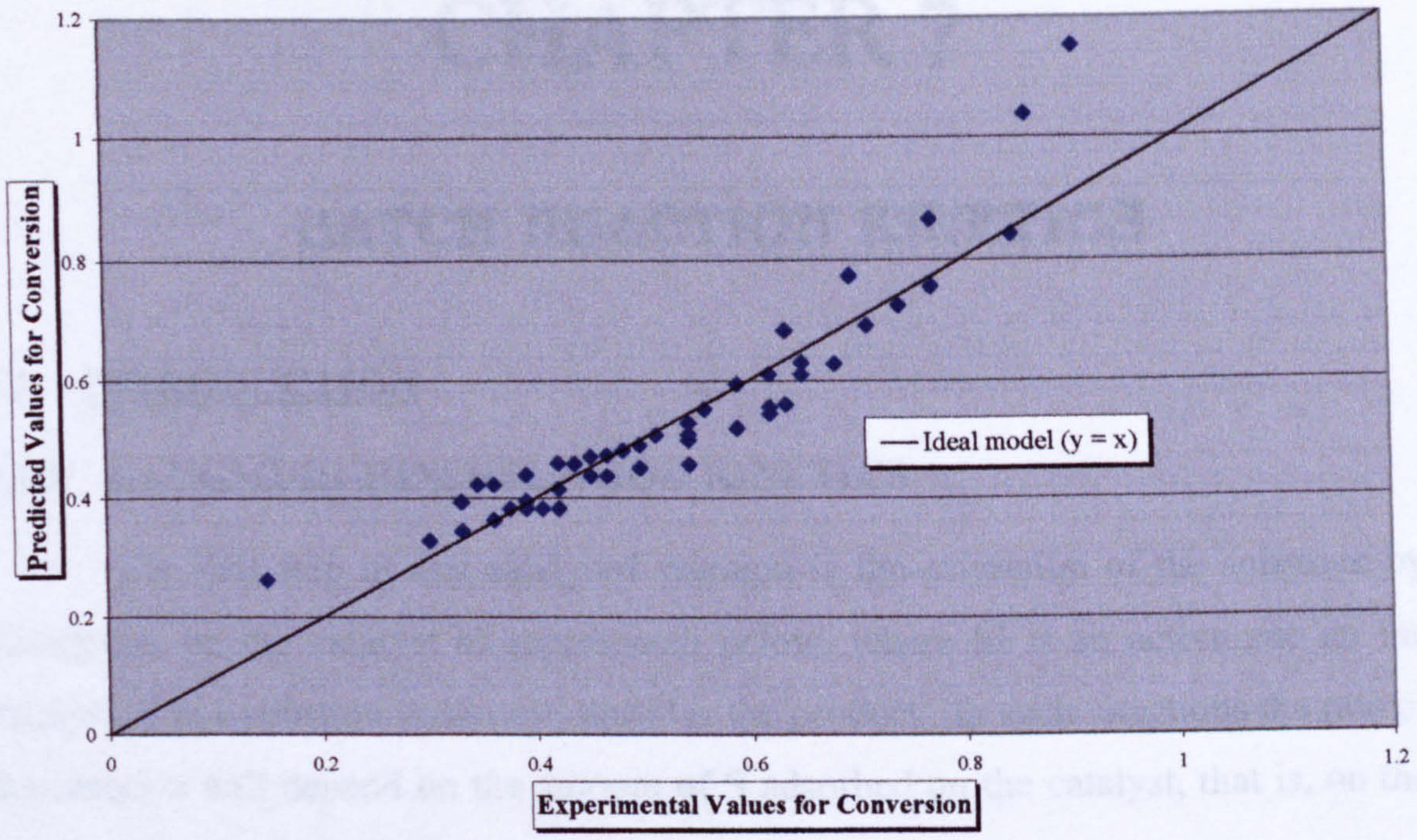


**Figure 6.30. Evaluation of developed model for Catalyst 2**

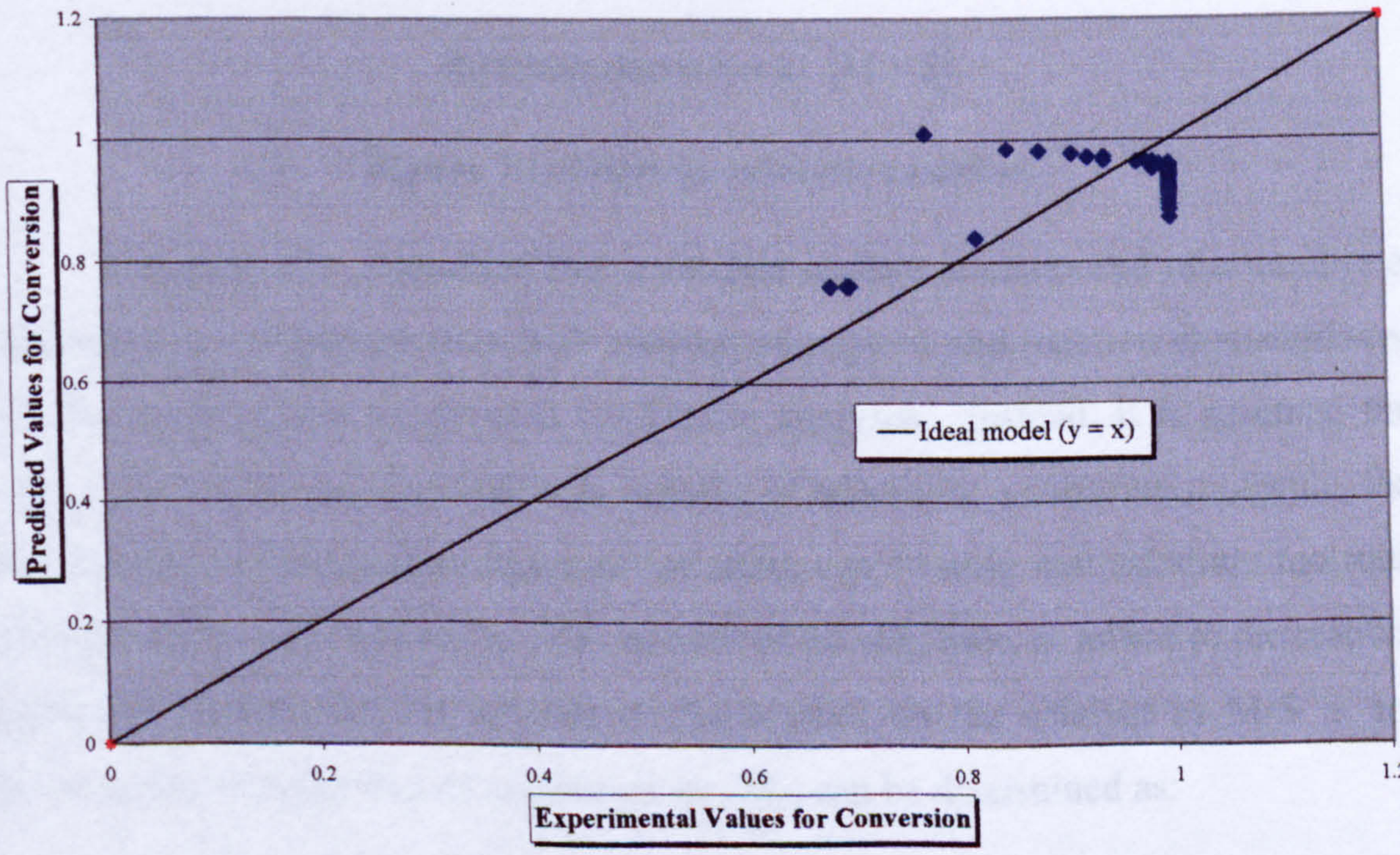


**Figure 6.31. Evaluation of developed model for Catalyst 3**

The other two fittings are also as good as the first one implying that predicted values of conversion are very much in agreement with the obtained experimental data.

# CHAPTER 7

## BATCH REACTION KINETICS

### 7.1 INTRODUCTION

#### 7.1.1 LANGMUIR-HINSHELWOOD KINETICS

The first step in any catalysed reaction is the activation of the substrate by adsorption on the catalyst as represented below, where M is an active site on the catalyst, S is a substrate molecule, and P is the product. In such situations the rate of the reaction will depend on the amount of S adsorbed on the catalyst, that is, on the concentration of M-S [84].

$$M + S \underset{k_{-1}}{\overset{k_1}{\rightleftharpoons}} M{-}S \xrightarrow{k_2} M + P$$

$$\text{Reaction rate} = r = k_2\,[M-S]$$

**Figure 7.1. Steps in catalytic reaction**

It is generally recognised that a catalyst surface is composed of a number of different types of surface sites with varying adsorption and reaction characteristics, but this model is not easily used for kinetic analyses. Instead, it is assumed that every surface atom on the catalyst is capable of adsorbing a substrate molecule, that they all do so with equal energy and that there can be only one substrate molecule adsorbed on each surface atom. The amount of the substrate, S, added to the reaction mixture is known, but the amount of S adsorbed on the catalyst as M-S is not. However the total number of surface atoms, $M_0$, can be determined as:

$$[M_0]=[M]+[M-S] \qquad (7.1)$$

Then the equilibrium constant for the adsorption equilibrium, K, can be written as:

$$K=\frac{k_1}{k_{-1}}=\frac{[M-S]}{[M][S]} \tag{7.2}$$

If we combine last two reactions following equation can be derived:

$$K=\frac{[M-S]}{[M][S]}=\frac{[M-S]}{([M_0]-[M-S])[S]}=\frac{[M-S]}{[M_0][S]-[M-S][S]} \tag{7.3}$$

Or, after rearrangement:

$$[M-S]=\frac{K[M_0][S]}{1+K[S]} \tag{7.4}$$

With $[M_0]=1$ and having [M-S] defined as θ, previous equation becomes:

$$\Theta=\frac{K[S]}{1+K[S]} \tag{7.5}$$

So, therefore, reaction rate can be expressed as:

$$r=k_2\Theta=\frac{k_2 K[S]}{1+K[S]} \tag{7.6}$$

In this case r is generally expressed as an areal turnover frequency (TOF), the number of molecules reacted per unit time per unit surface area. If the catalytic process follows this model, the rate r will be related to [S] as shown in Figure 7.1. The rate is first order at low values of [S] and decreases to zero order as [S] increases. By analogy [M-S] is expected to be small when S is weakly adsorbed and the reaction should be first order. When S is strongly adsorbed a larger value for [M-S] should result and the reaction will be zero order.

In order to explore the kinetics of the reaction as well as the value of the activation energies of the catalysts as a part of the kinetics, data from the batch reaction performed at York University for Catalyst 1 at 25°C [112] and data from the batch experimental work performed as a part of the study at other temperatures, as well as other catalysts (at different temperatures) were analysed using an integral method for determining reaction order [30, 166].

Considering a very complex nature of the chosen reaction and many unknown product (and mechanisms) to which a reaction could lead, following assumptions had to be made:

1. There were no products formed from campholenic aldehyde

2. The reaction can be summarised simply by $A \rightarrow B + C$

## 7.2 RATE EQUATIONS

### 7.2.1 DERIVATION FOR ZERO ORDER REACTIONS

Rate expression for zero order reaction can be written as:

$$r = k; \quad \frac{dC_A}{dt} = -k \tag{7.7}$$

Or after integration:

$$C_A - C_{A0} = -kt, \tag{7.8}$$

where:

$C_A$ – concentration of the reactant at time t;

$C_{A0}$ – concentration of the reactant at t = 0;

k – rate coefficient

t – time (s)

$R^2$ value from linear fit $C_A \div$ time defines how well results can be correctly determined as those corresponding to a zero order reaction.

### 7.2.2 DERIVATION FOR FIRST ORDER REACTIONS

In the case of first order reaction, rate of reaction is expressed as:

$$r = kC_A = -\frac{dC_A}{dt} \tag{7.9}$$

After integration, equation (7.9) becomes:

$$\frac{1}{k}\int_{C_{A0}}^{C_{A,t}}\frac{dC_A}{C_A}=-\int_0^t dt \tag{7.10}$$

$$\ln\left(\frac{C_A}{C_{A0}}\right)=-kt \tag{7.11}$$

Fitting experimental data into the equation (7.11) relates $\ln\left(\frac{C_A}{C_{A0}}\right)$ and time, where negative value of the slope in the linear fit is k.

### 7.2.3 DERIVATION FOR SECOND ORDER REACTIONS

Equation for the second order reaction is:

$$r=kC_A^{\,2}=-\frac{dC_A}{dt} \tag{7.12}$$

$$\frac{1}{C_A}-\frac{1}{C_{A0}}=kt \tag{7.13}$$

If we plot $\frac{1}{C_A}$ versus time, slope is k and the intercept is $\frac{1}{C_{A0}}$.

## 7.3 EXPERIMENTAL RESULTS

### 7.3.1 CATALYST 1

All the acquired data from the batch reaction for Catalyst 1 can be seen in Figure 7.2. Thereafter data for each temperature were used in equations (7.8), (7.11) and (7.13) for evaluation of the reaction order. Results at 25°C are presented in Figures 7.3 (for zero order), 7.4 (first order) and 7.5 (second order).

The fittings for all other temperatures can be found in Appendix H.

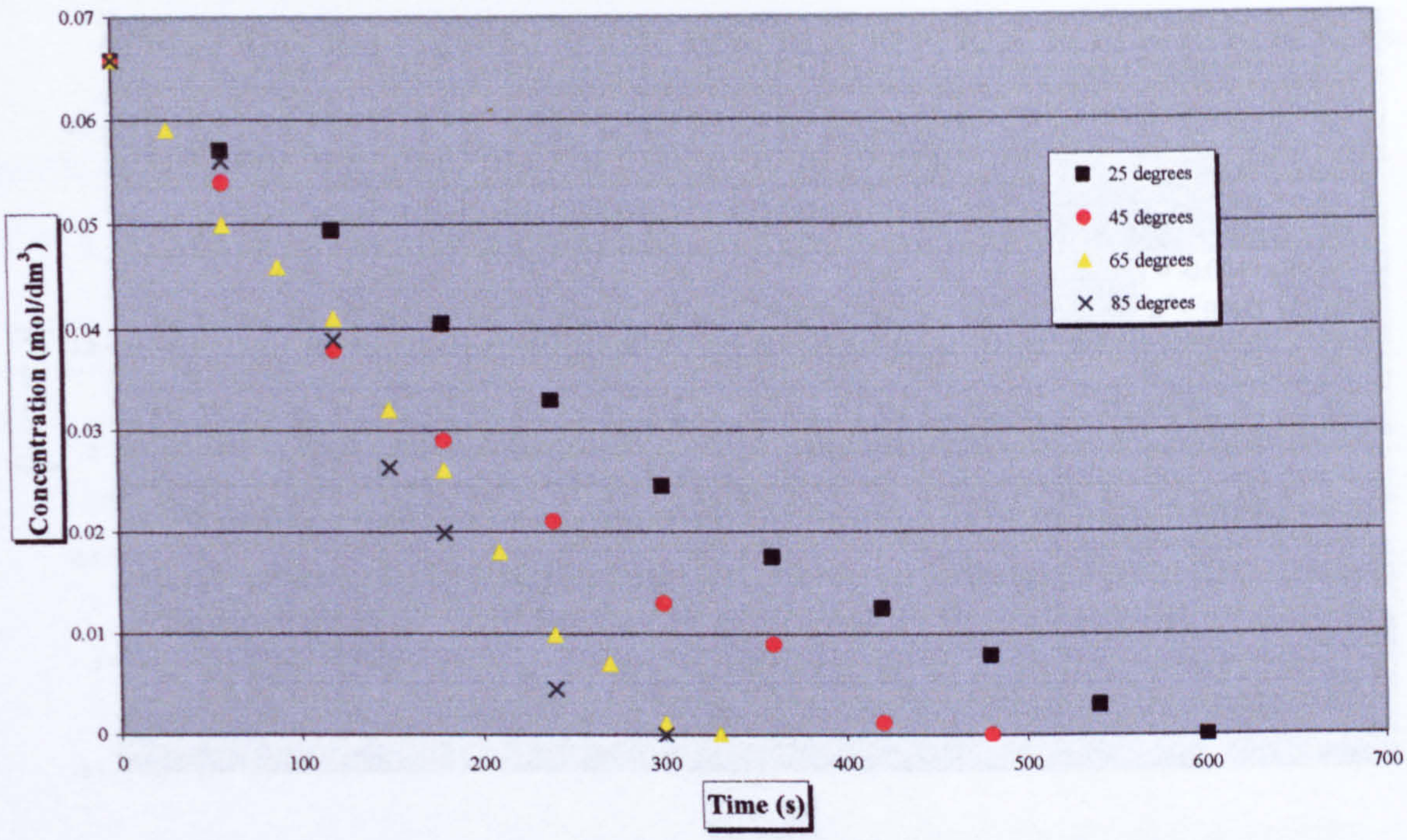


**Figure 7.2. Concentration at different temperatures for Catalyst 1**

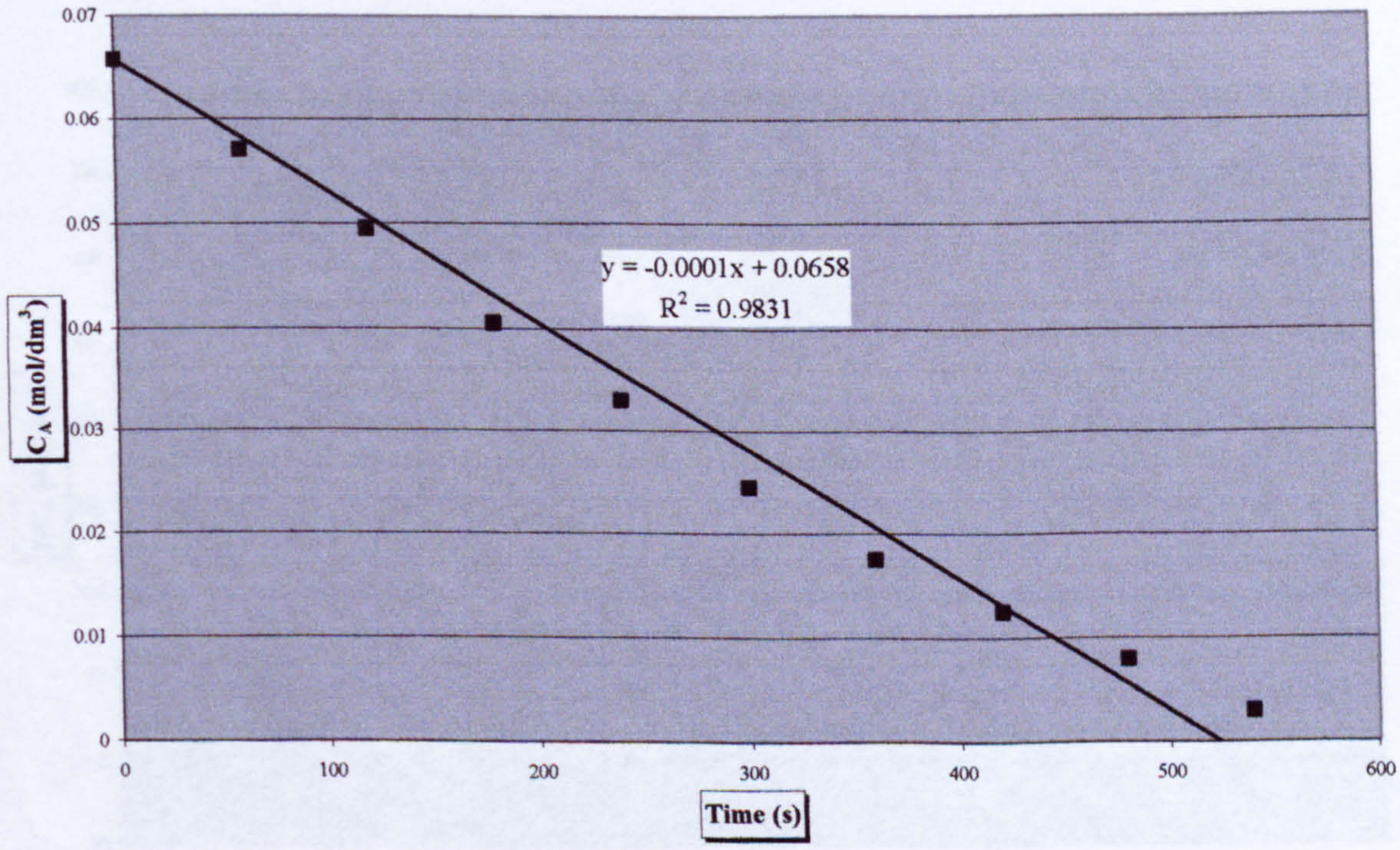


**Figure 7.3. Fitting of experimental data into zero order equation (Catalyst 1, 25$^0$C)**

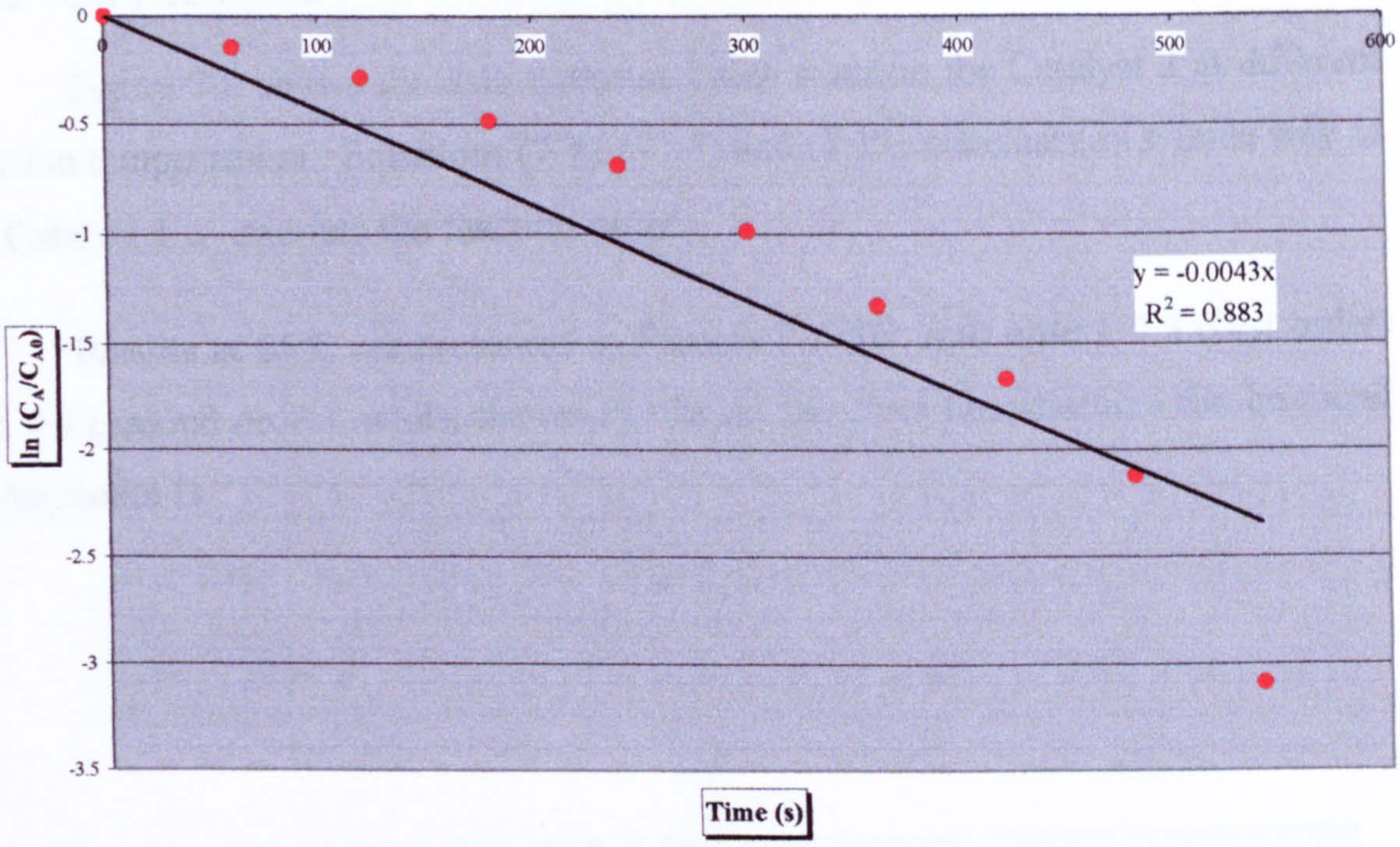


**Figure 7.4. Fitting of experimental data into first order equation (Catalyst 1, 25$^0$C)**

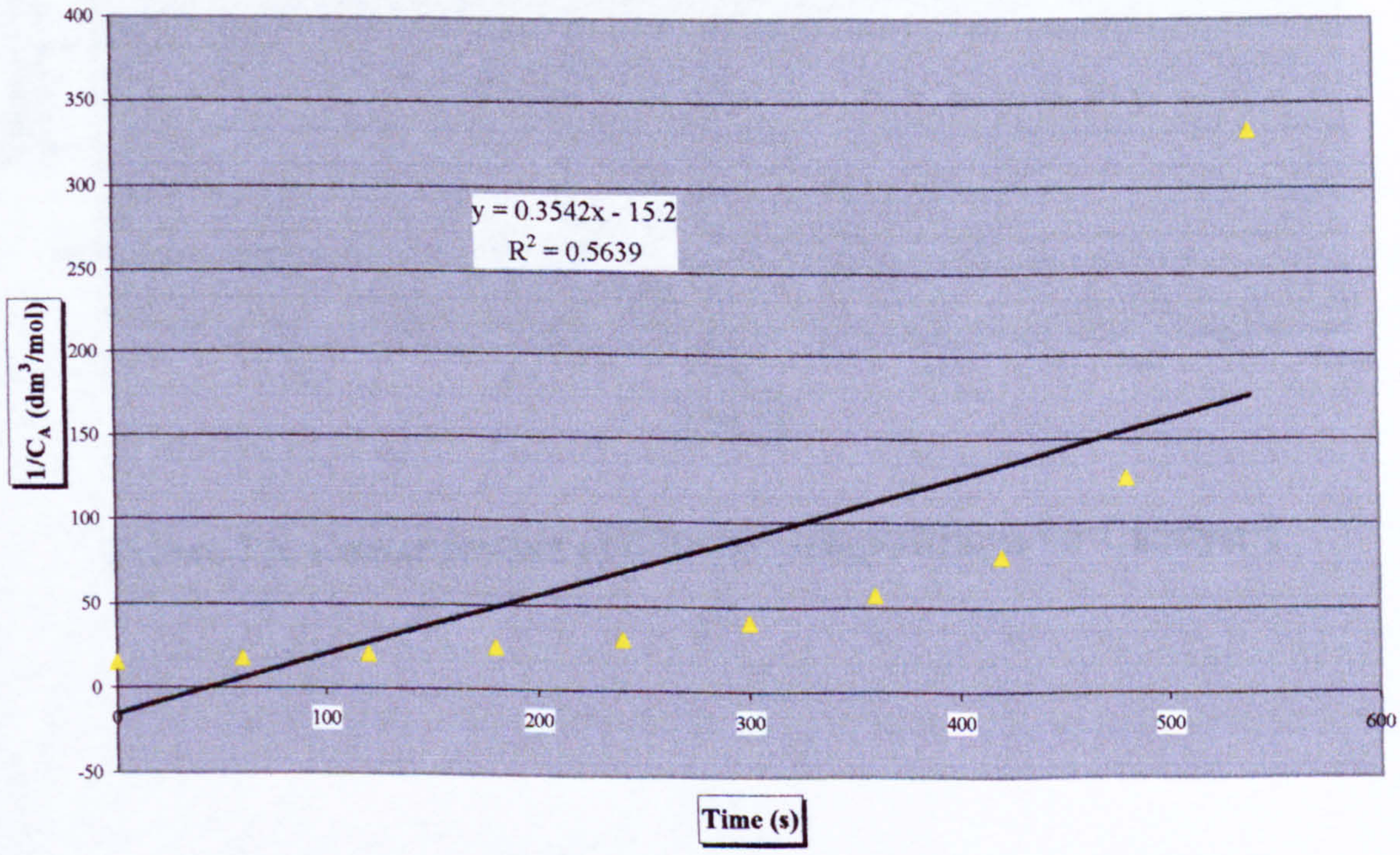


**Figure 7.5. Fitting of experimental data into second order equation (Catalyst 1, 25$^0$C)**

### 7.3.2 CATALYST 2

Figure 7.6 shows the data from the batch reaction for Catalyst 2 at different reaction temperatures. Equations (7.8), (7.11) and (7.13) were used in a same way as for Catalyst 1 to evaluate the reaction order.

Results at 25°C are presented in Figures 7.7 (for zero order), 7.8 (first order) and 7.9 (second order), whilst the results for all the other temperatures can be found in Appendix H.

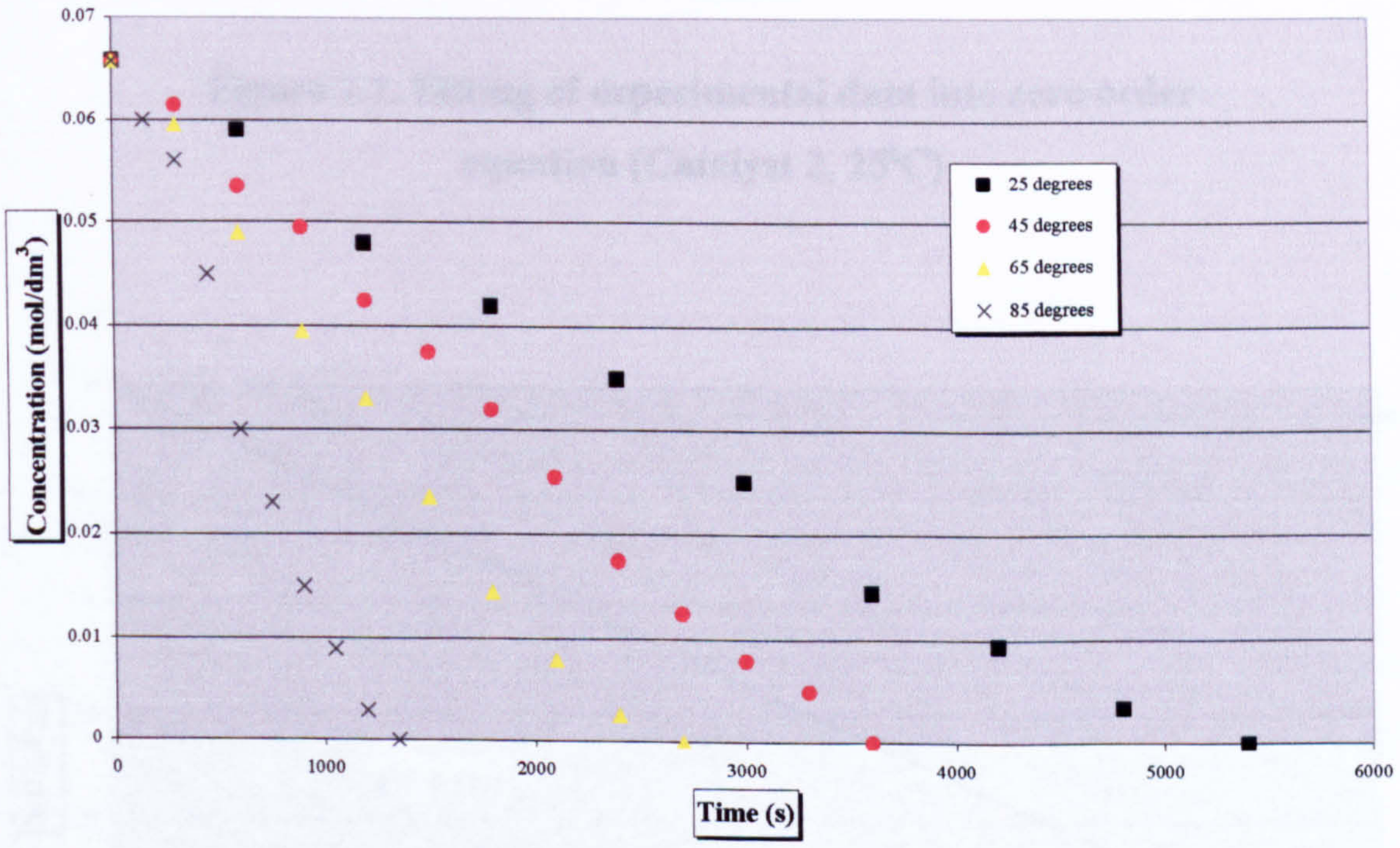


**Figure 7.6. Concentration at different temperatures for Catalyst 2**

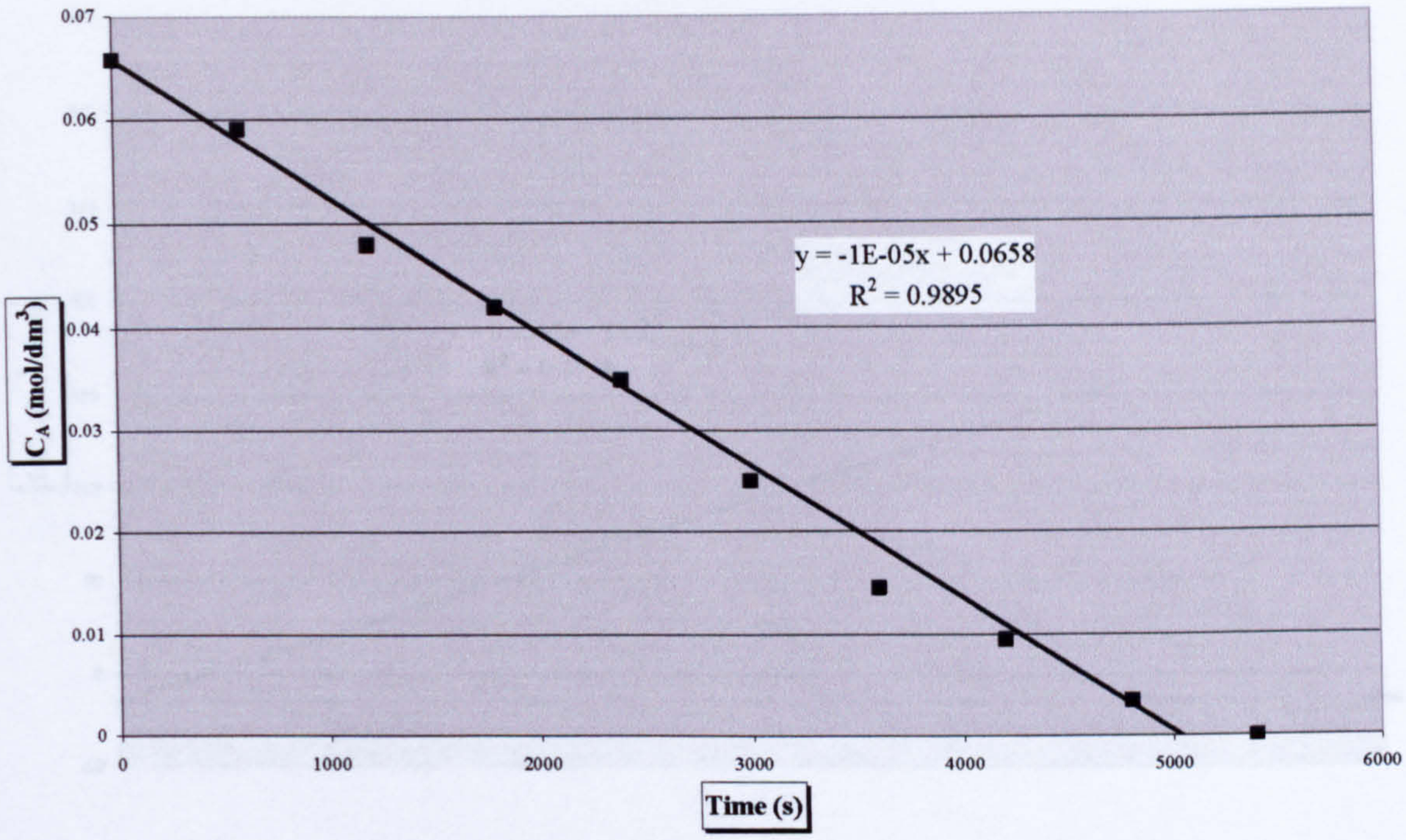


**Figure 7.7. Fitting of experimental data into zero order equation (Catalyst 2, 25$^0$C)**

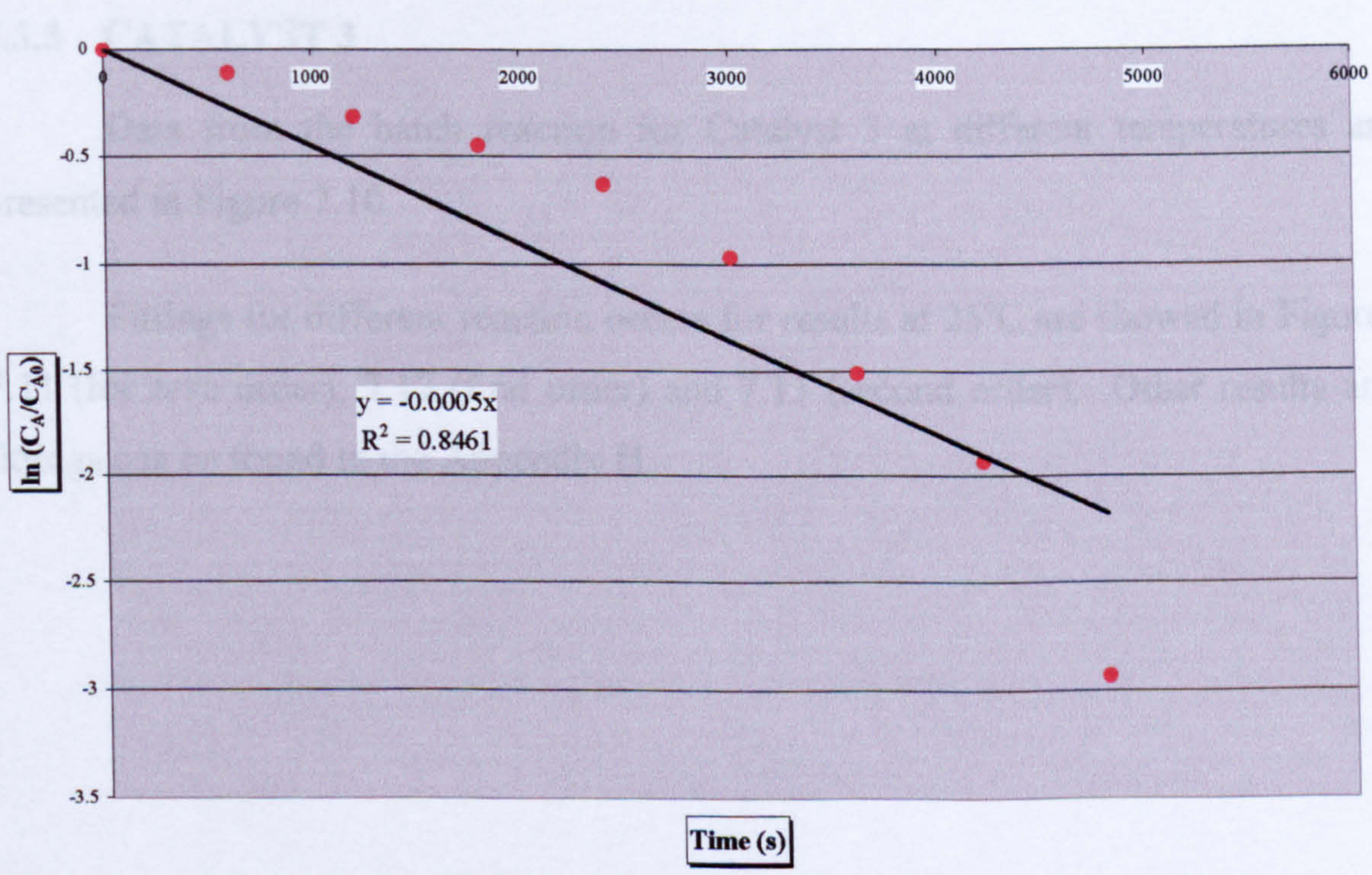


**Figure 7.8. Fitting of experimental data into first order equation (Catalyst 2, 25$^0$C)**

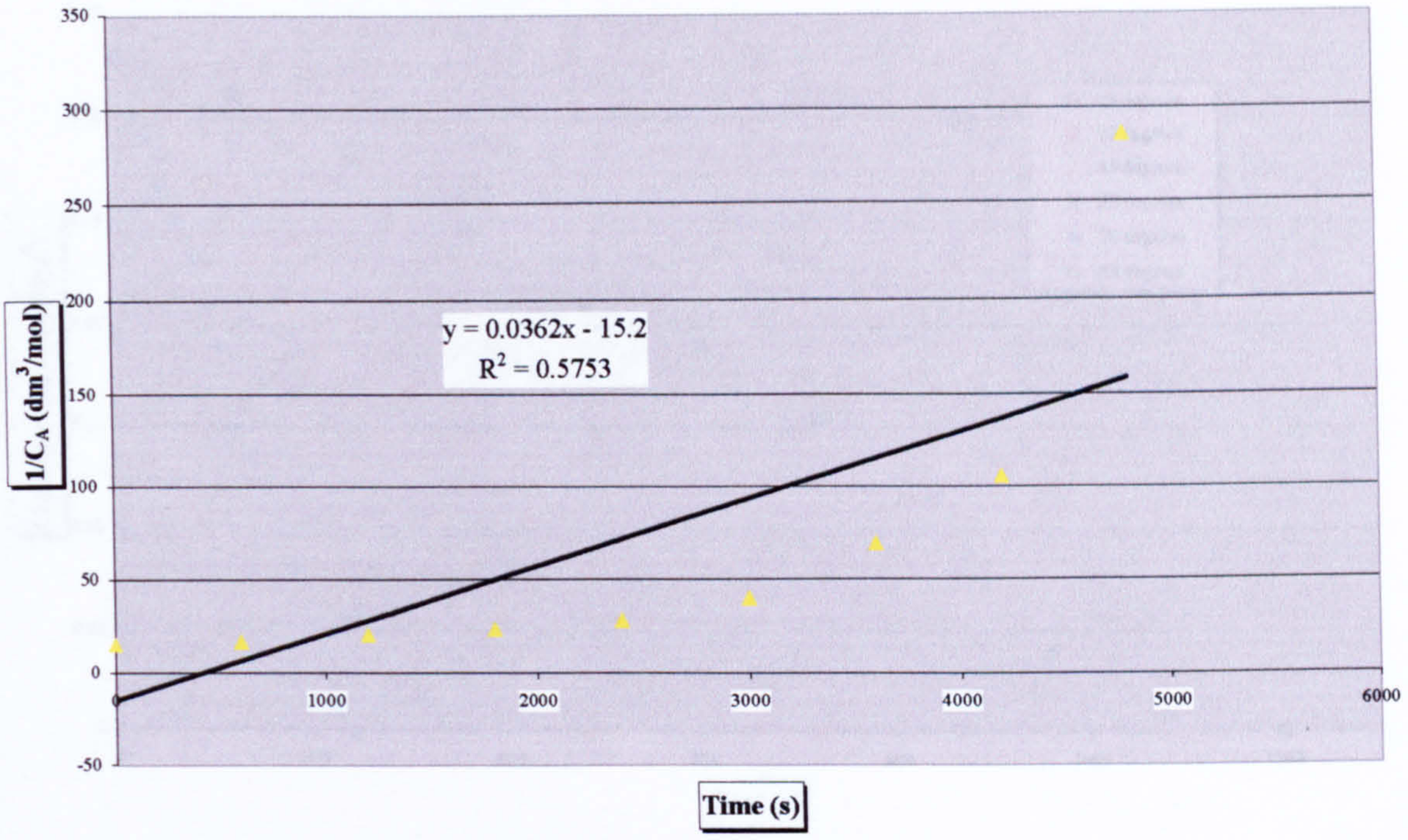


**Figure 7.9. Fitting of experimental data into second order equation (Catalyst 2, 25$^0$C)**

### 7.3.3 CATALYST 3

Data from the batch reaction for Catalyst 3 at different temperatures are presented in Figure 7.10.

Fittings for different reaction orders for results at 25$^0$C are showed in Figures 7.11 (for zero order), 7.12 (first order) and 7.13 (second order). Other results and fittings can be found in the Appendix H.

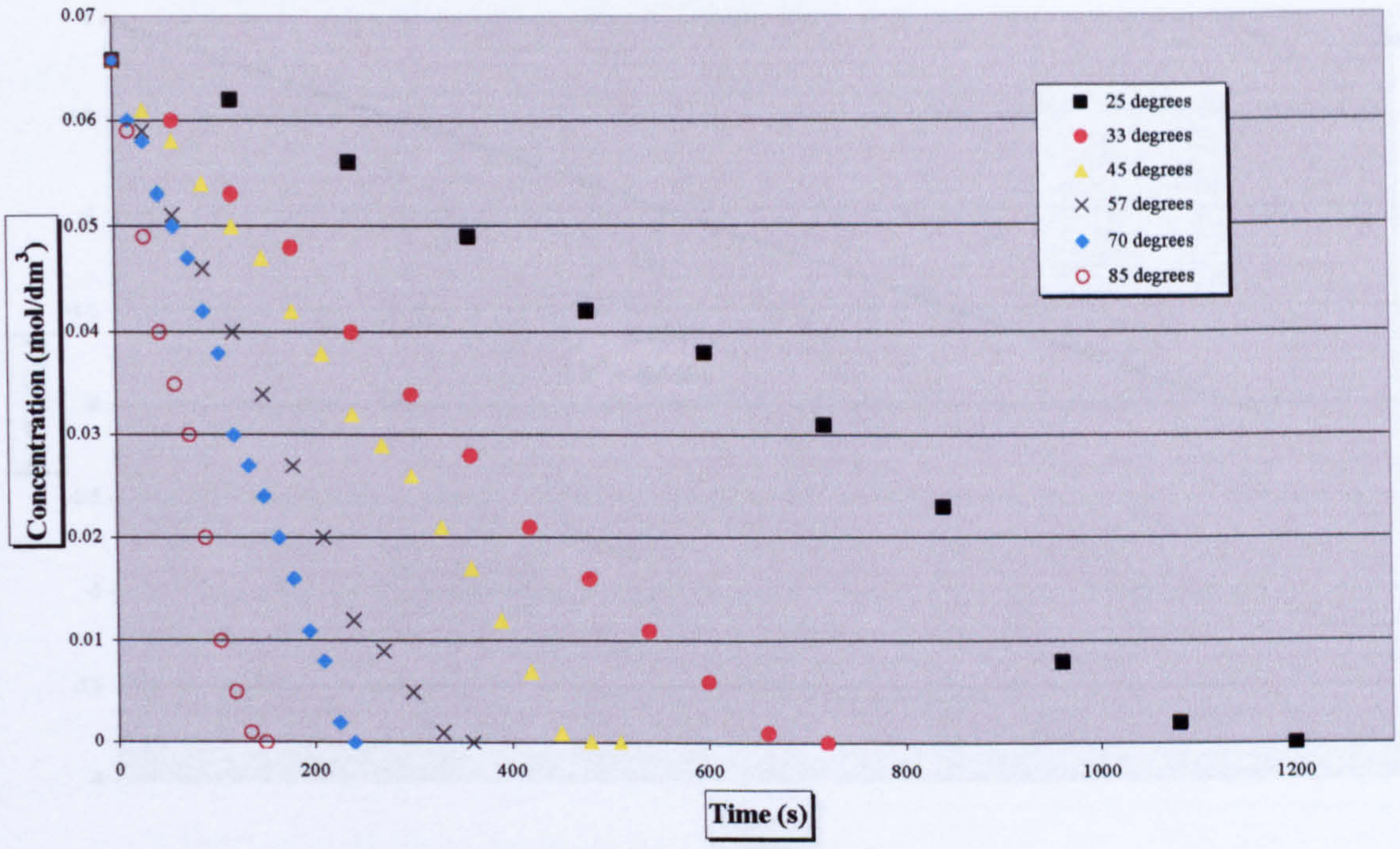


**Figure 7.10. Concentration at different temperatures for Catalyst 3**

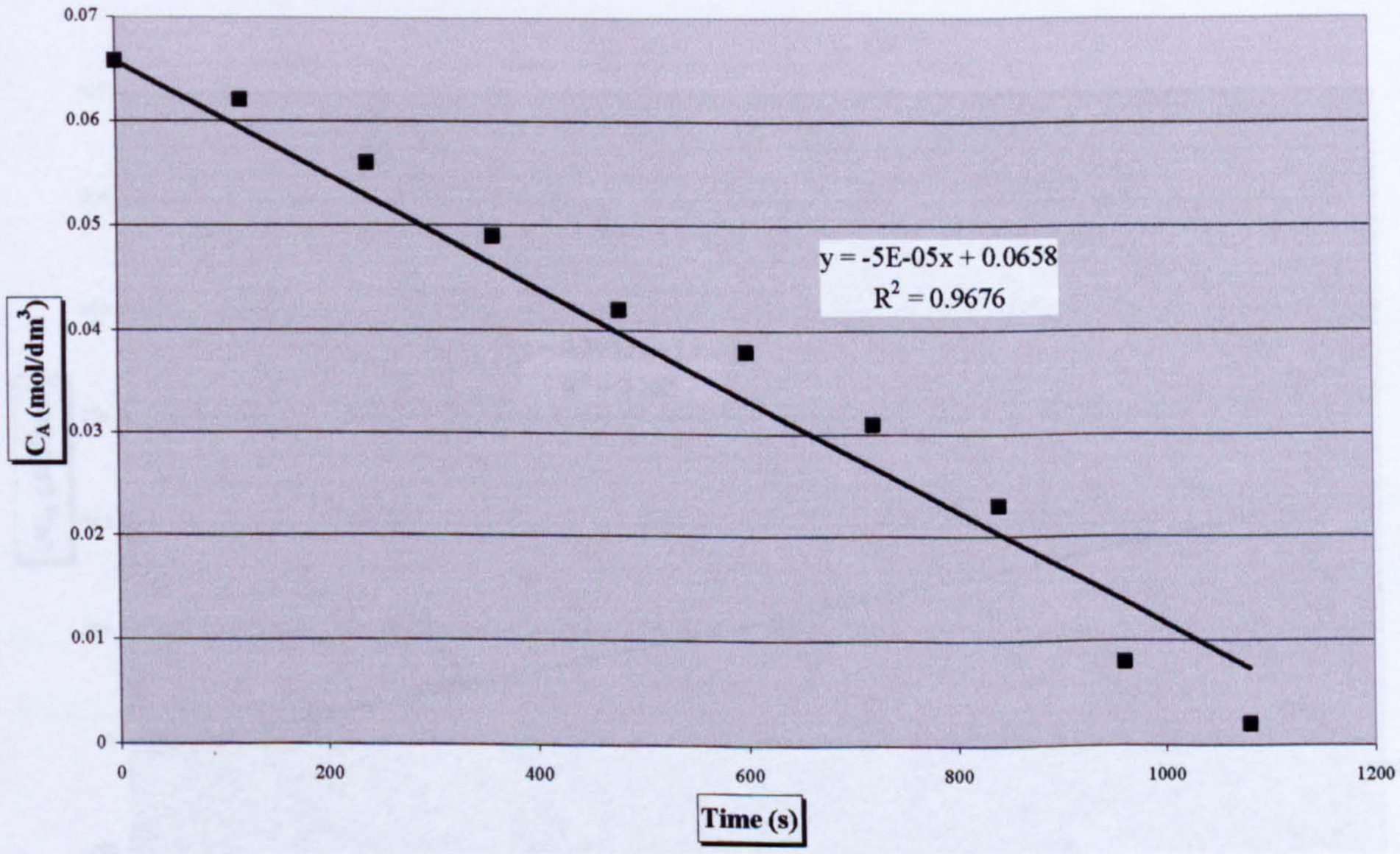


**Figure 7.11. Fitting of experimental data into zero order equation (Catalyst 3, 25$^0$C)**

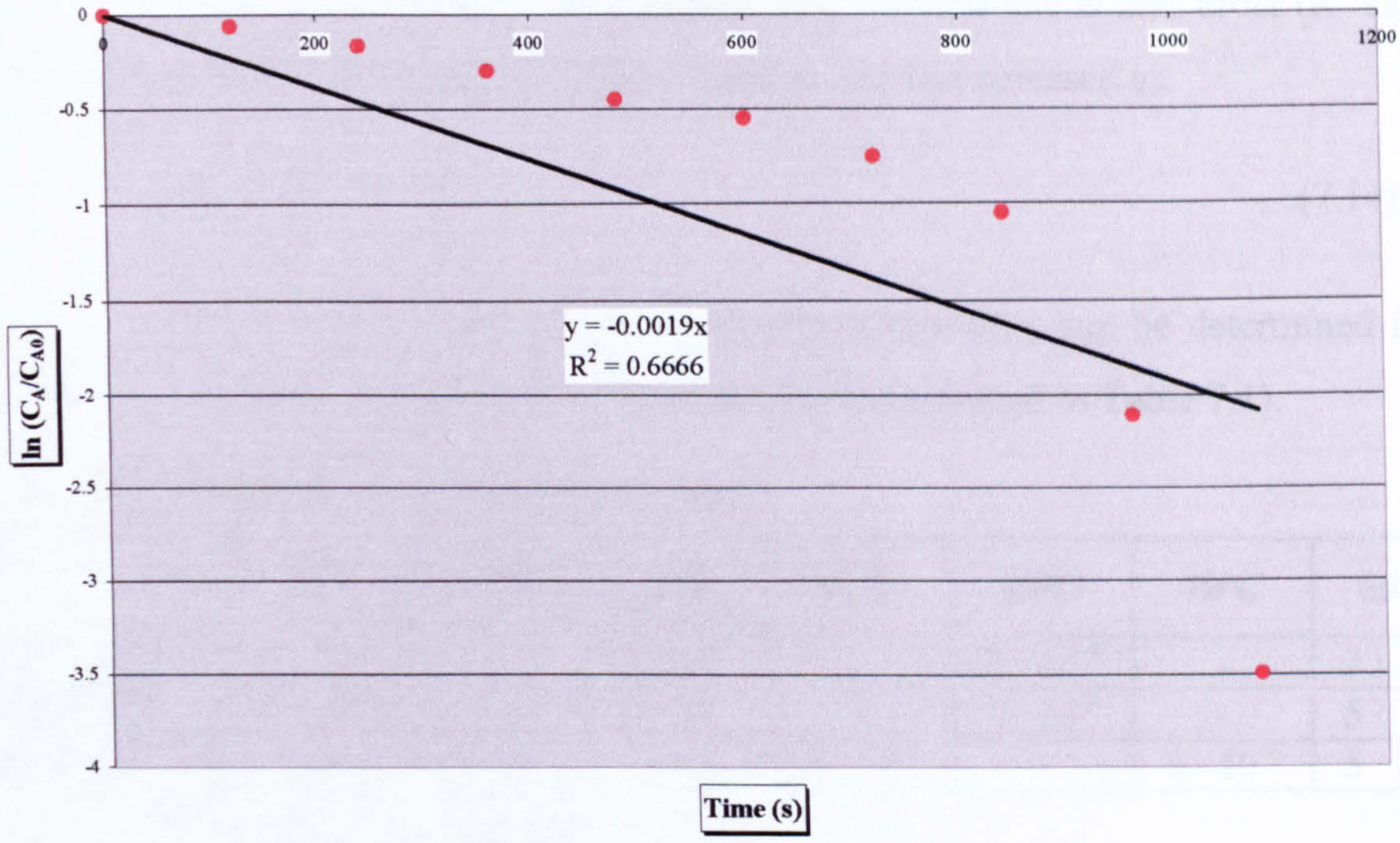


**Figure 7.12. Fitting of experimental data into first order equation (Catalyst 3, 25$^0$C)**

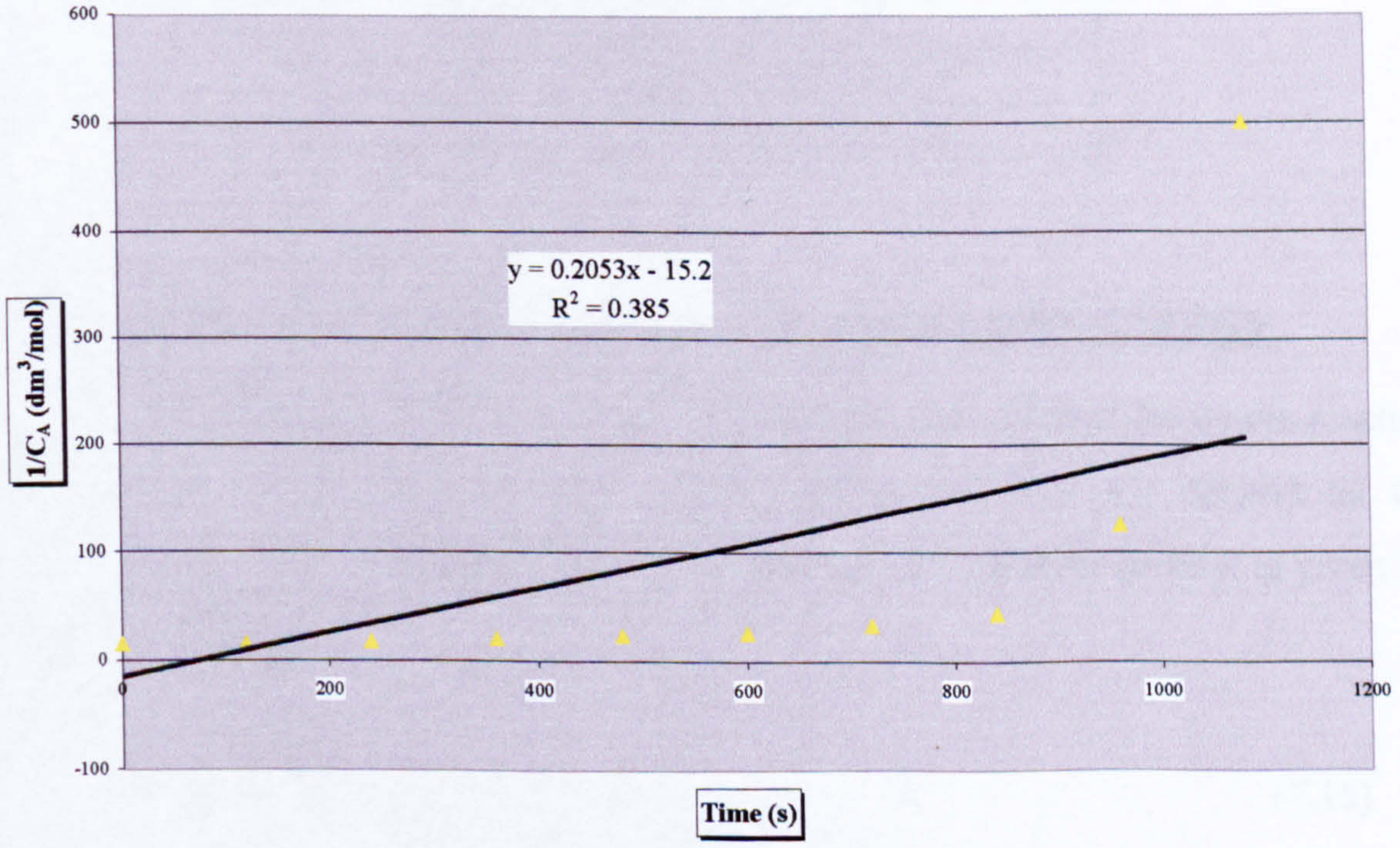


**Figure 7.13. Fitting of experimental data into second order equation (Catalyst 3, 25$^0$C)**

Collected and analysed data suggest that reaction rate is zero order ($R^2$ values of 0.9 and above) and therefore rate of reaction can be expressed as:

$$(-r_A)=k \tag{7.14}$$

Values of rate constants (at different temperatures) can be determined from (zero order) plots as a negative value of the slope (presented in Table 7.1).

**Table 7.1. Reaction rate constant values***

| | 25°C | 33°C | 45°C | 57°C | 65°C | 70°C | 85°C |
|---|---|---|---|---|---|---|---|
| Catalyst 1 | $1 \cdot 10^{-4}$ | - | $2 \cdot 10^{-4}$ | - | $2 \cdot 10^{-4}$ | - | $3 \cdot 10^{-3}$ |
| Catalyst 2 | $1 \cdot 10^{-5}$ | - | $2 \cdot 10^{-5}$ | - | $3 \cdot 10^{-5}$ | - | $5 \cdot 10^{-5}$ |
| Catalyst 3 | $5 \cdot 10^{-5}$ | $1 \cdot 10^{-4}$ | $1 \cdot 10^{-4}$ | $2 \cdot 10^{-4}$ | - | $3 \cdot 10^{-4}$ | $5 \cdot 10^{-4}$ |

* For units of rate constant see Table 7.2.

**Table 7.2. Units of rate constant, k, based on volume of voids in the reactor (see section 8.9.1)**

| Reaction order | Units of k |
|---|---|
| 0 | $mol\ m^{-3}\ s^{-1}$ |
| 1 | $s^{-1}$ |
| 2 | $m^3\ mol^{-1}\ s^{-1}$ |
| 3 | $m^6\ mol^{-2}\ s^{-1}$ |

## 7.4 PRE-EXPONENTIAL FACTOR AND ACTIVATION ENERGY

The influence of temperature on the reaction is accounted for by the reaction rate constant k, referred to as a constant because it does not depend on the composition of the reaction mixture. The temperature dependence of k is given by Arrhenius equation:

$$k=A\cdot\exp\left(-\frac{E_a}{R\cdot T}\right) \tag{7.15}$$

where $E_a$ is called the activation energy of the reaction, whilst R is the universal gas constant ($R = 8.314\ Jmol^{-1}K^{-1}$). The term $E_a/R$ is sometimes referred to as the activation temperature.

For most reactions the activation energy lays in the range 40-300 kJ/mol; hence the activation temperature $E_a/R$ ranges from 5000 K to 35000 K. For industrial purposes, only the range $RT/E_a < 1$ is of interest [85].

For the analysis of batch experimental data, equation (7.15) is used in a more suitable form:

$$\ln k = \ln A - \left(\frac{E_a}{R \cdot T}\right) \tag{7.16}$$

By plotting ln k against $\left(-\frac{1}{T}\right)$, intercept will subsequently give value of pre-exponential factor A, whilst value of the slope will be $\left(\frac{E_a}{R}\right)$. For each catalyst used, activation energy can be determined in this way. This is presented in Figures 7.14 - 7.16 for Catalyst 1, 2 and 3 respectively.

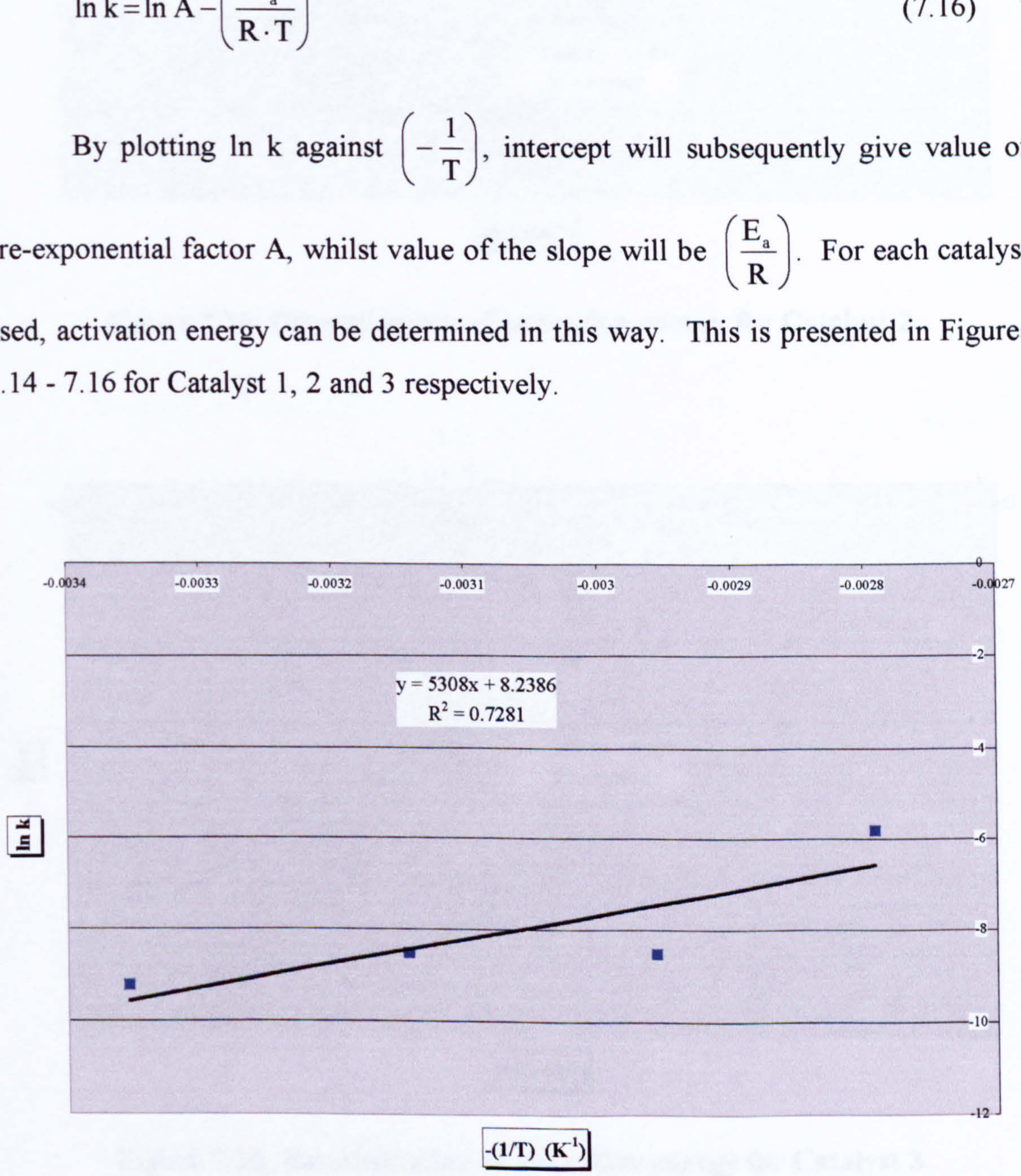


**Figure 7.14. Determination of activation energy for Catalyst 1**

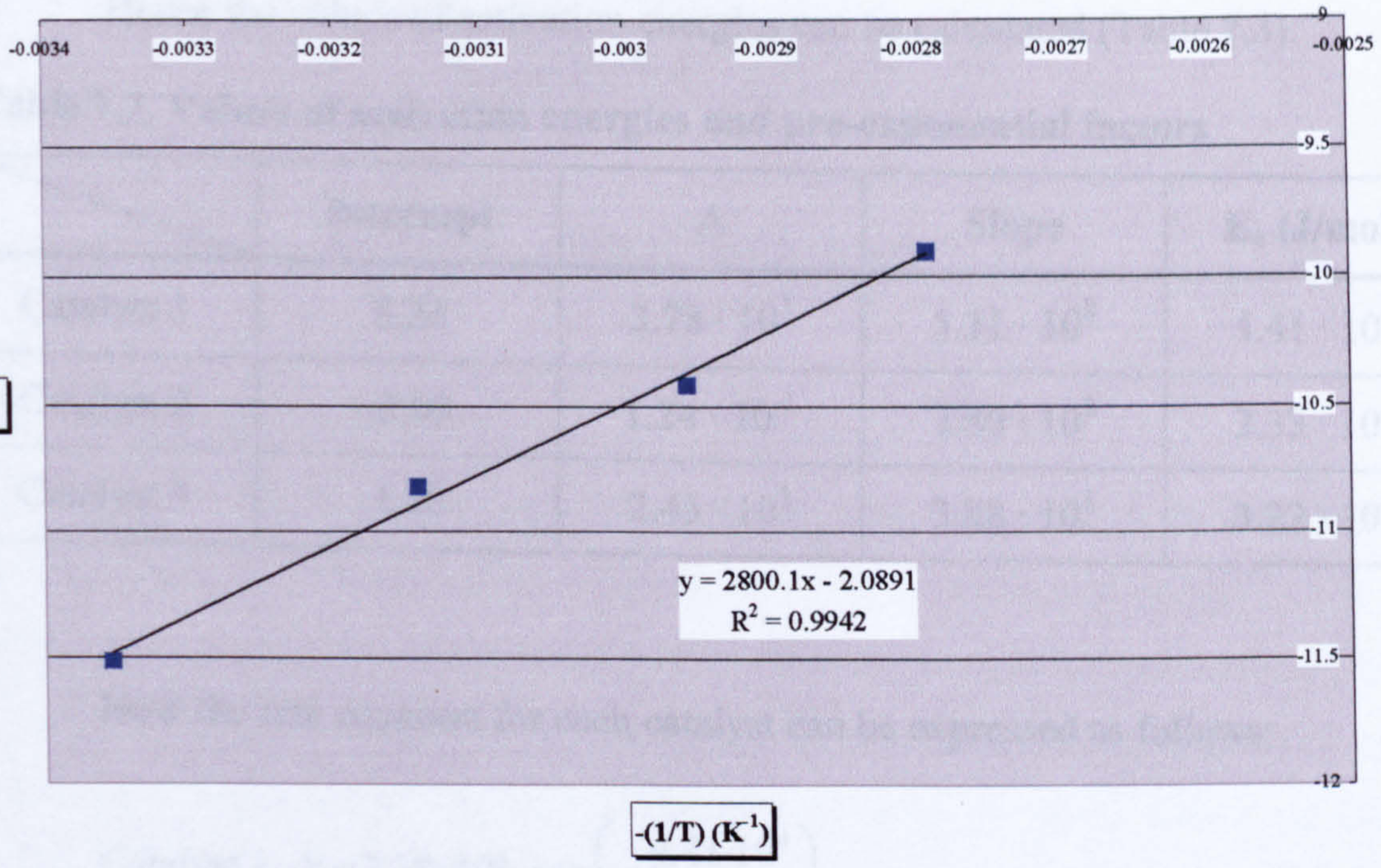


**Figure 7.15. Determination of activation energy for Catalyst 2**

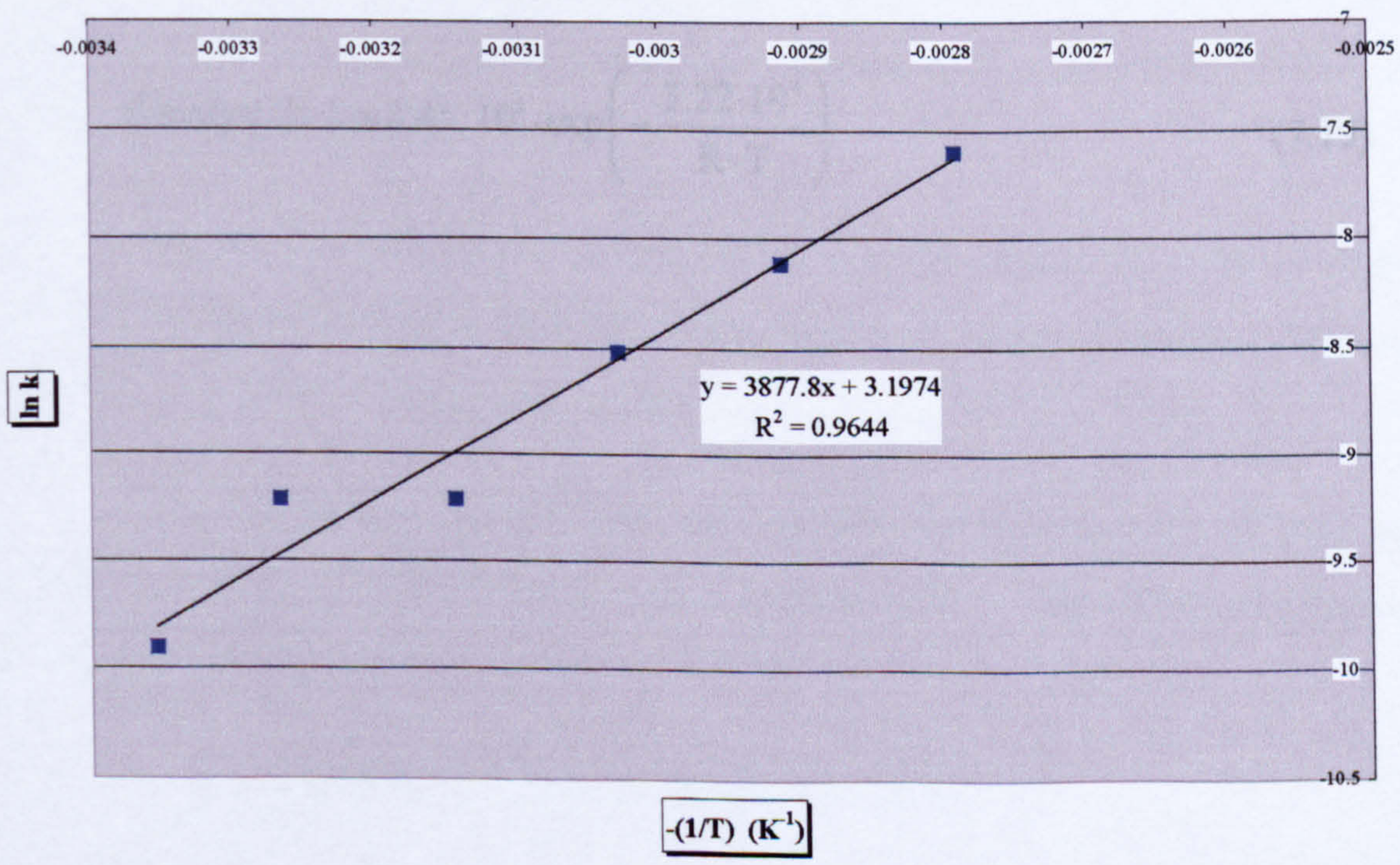


**Figure 7.16. Determination of activation energy for Catalyst 3**

Hence the values of activation energies can be calculated (Table 7.3).

**Table 7.3. Values of activation energies and pre-exponential factors**

| | Intercept | A | Slope | $E_a$ (J/mol) |
|---|---|---|---|---|
| Catalyst 1 | 8.24 | $3.78 \cdot 10^3$ | $5.31 \cdot 10^3$ | $4.41 \cdot 10^4$ |
| Catalyst 2 | -2.09 | $1.24 \cdot 10^{-1}$ | $2.80 \cdot 10^3$ | $2.33 \cdot 10^4$ |
| Catalyst 3 | 3.20 | $2.45 \cdot 10^1$ | $3.88 \cdot 10^3$ | $3.22 \cdot 10^4$ |

Now the rate equation for each catalyst can be expressed as follows:

$$\text{Catalyst 1: } k=3.78\cdot10^3\cdot\exp\left(-\frac{4.41\cdot10^4}{R\cdot T}\right) \tag{7.17}$$

$$\text{Catalyst 2: } k=1.24\cdot10^{-1}\cdot\exp\left(-\frac{2.33\cdot10^4}{R\cdot T}\right) \tag{7.18}$$

$$\text{Catalyst 3: } k=2.45\cdot10^1\cdot\exp\left(-\frac{3.22\cdot10^4}{R\cdot T}\right) \tag{7.19}$$

# CHAPTER 8

## DISCUSSION

### 8.1 INTRODUCTION

In this Chapter the results from the experimental studies in the SDR and kinetic studies in a batch reactor (Chapters 6 and 7) are discussed in detail. Not only that catalytic processes were never before tried on a spinning disc reactor, but a process as a whole (even when performed in a conventional equipment) offers innovative approach to the old-fashioned and ever so often not-so-clean-and-environmentally-friendly catalytic chemistry.

Spinning disc results for all three catalysts are analysed, compared and discussed and optimal conditions given for accomplishing best conversion/selectivity. An experimental model is presented to describe the catalytic reaction kinetics in the SDR. These results are compared to a reaction performed in a laboratory batch reactor.

Results of experiments carried out in a batch reactor in order to explore reaction kinetics in more detail are also discussed in this Chapter. Activation energies for each catalyst are also given.

Three catalysts developed and characterised at the University of York were tried for the rearrangement reaction of α–pinene oxide. The differences between these three catalysts were:

1. Loading of $Zn(OTf)_2$ (0.05 and 0.01 mmol/g);

2. Type of catalyst support ($SiO_2$, K100 and $HMS_{24}$).

These characteristics are used to explain some of the results obtained in the SDR.

## 8.2 SDR RUNS

### 8.2.1 PURPOSE OF THE TEST RUNS IN THE SDR

For the reasons mentioned in Chapter 6, three test runs were performed in the SDR before any actual experimental work was commenced. These runs proved that reaction did not happen without the presence of the catalyst and both silica support and glue had no influence on the rearrangement reaction. Since the results of the test runs showed that reaction did not take place it was concluded that the data obtained on the catalyst coated disc were due to the catalyst activity in the spinning disc reactor only.

Actual mass of the catalyst used for coating was measured each time the coating was performed (Appendix G) and it was a constant value of 0.8 g each time.

Before each catalyst was tested, a set of 15 runs was performed to evaluate the activity/life of each catalyst, suitability of the catalyst coating in the long run, as well as reproducibility of the experiments. The experimental conditions were kept the same during each individual run (fixed feed flow rate, predetermined disc speed and disc temperature). Over one month period (for each tested catalyst) the trials were performed with the following conditions:

- Feed flow rate = 4 $cm^3/s$;
- Disc speed = 500 rpm (for Catalysts 2 & 3); 150 rpm (for Catalyst 1);
- Disc temperature = 25°C (for Catalysts 1 & 3); 45°C (for Catalyst 2).

Summary of results can be observed in Figure 8.1.

Over the trial period the catalysts performance remained the same, therefore proving that one coat of catalyst could be used over and over again for at least a month (or 15 runs) without loosing its activity.

If the performances of the catalysts at these conditions are compared, it is clear that the most active was Catalyst 3, with 70% conversion at 25°C. However, not much difference was seen in the long-term performance of the other two catalysts

at this stage, Catalyst 2 being more active than Catalyst 1 (due to the higher temperature used for experiment with Catalyst 2).

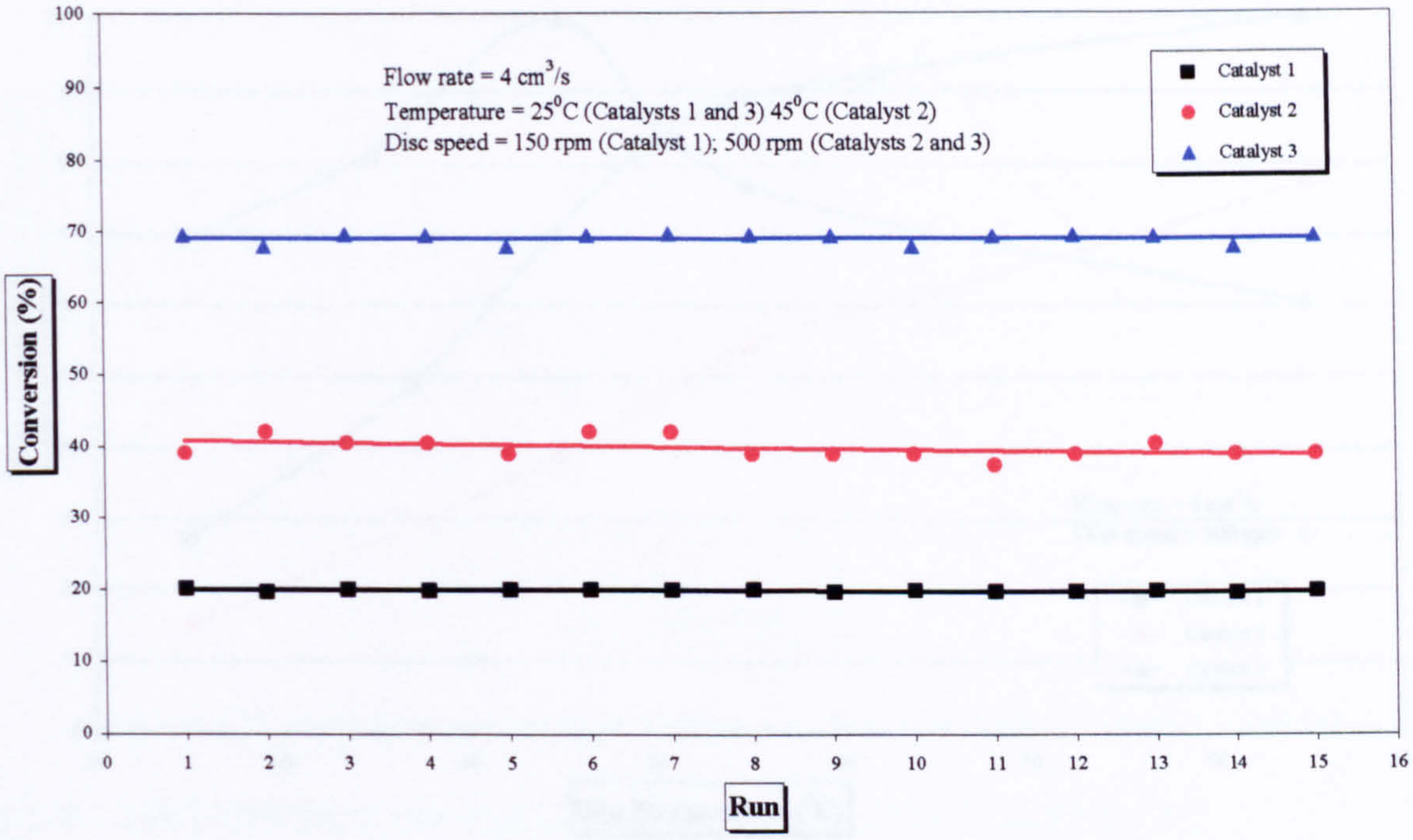


**Figure 8.1. Reproducibility and re-usability of catalysts**

### 8.2.2 THE EFFECT OF DISC TEMPERATURE

First parameter to be tested for each catalyst was the disc temperature. At this point, in order to assess the influence of the disc temperature on the results, feed flow rate was kept constant at 4 $cm^3/s$, and the disc rotational speed was fixed at 500 rpm. Disc temperature was varied, ranging from 25 to 85°C. Results from these runs are given in Chapter 6 for each individual catalyst and summarised in Figure 8.2 below. Increased activity at higher disc temperatures was observed for both Catalysts 1 and 2. Although similar trend was observed for these two catalysts, Catalyst 1 was 10–20% more active at each tried temperature. Since the best conversion was obtained at 85°C for both catalysts, this temperature was chosen as an optimal temperature for the spinning disc runs. As for Catalyst 3, increase of temperature to 50°C increased the conversion to 100%, but after this point it started to drop. It peaked at the interval of 45° – 50°C, hence 45° was the chosen (optimal) temperature for the rest of the spinning disc experiments. The rate of reaction is highly influenced by temperature, in cases of the first two catalysts by the power of 8 and 6, whilst in case of Catalyst 3 the influence of temperature is lower by almost 3

orders of magnitude, as the model equations suggest. This will be discussed in more detail in section 8.6.

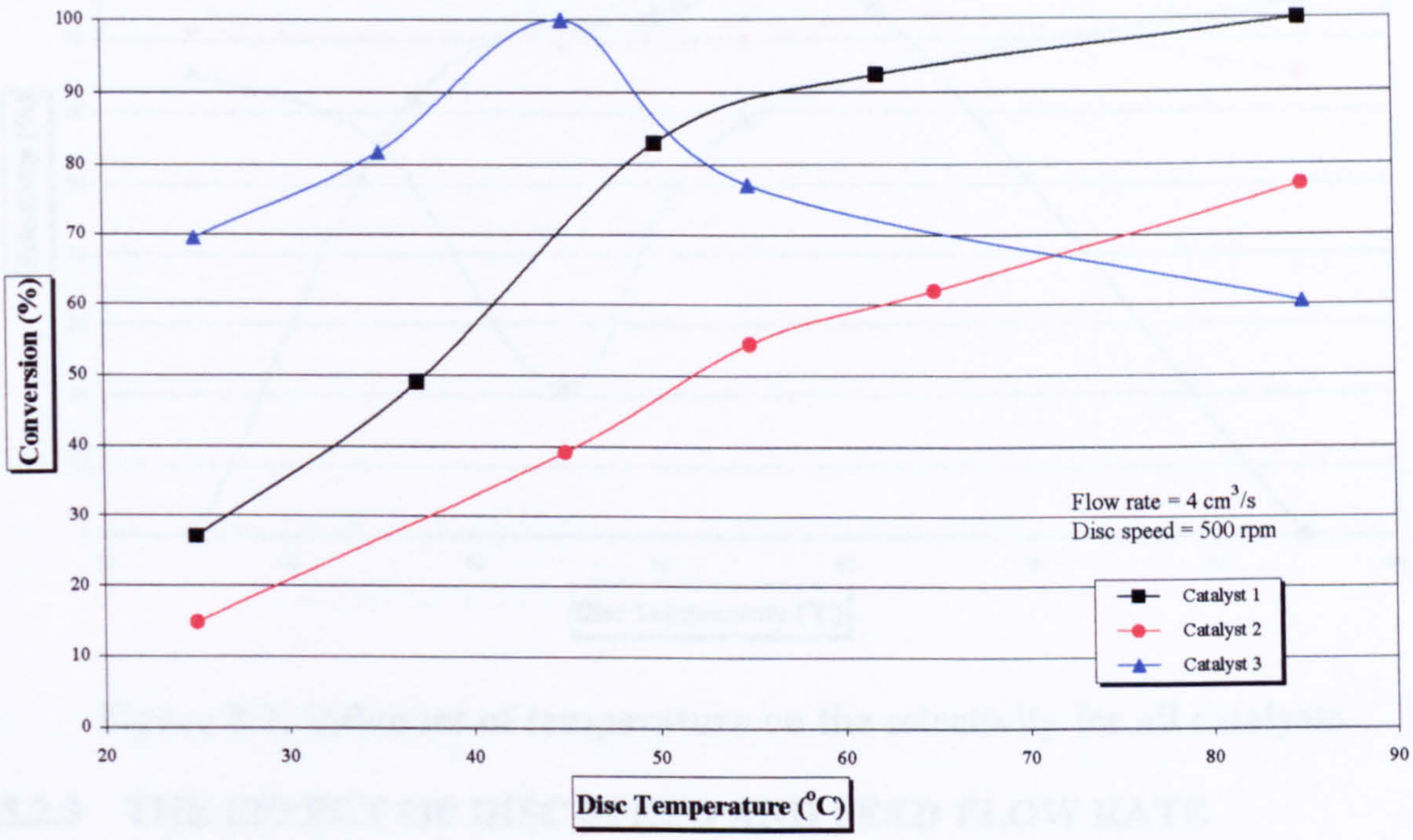


**Figure 8.2. Influence of temperature on the conversion for all catalysts**

The effect of temperature on selectivity for each of the three catalysts is summarised in Figure 8.3. At lower temperature reaction only just started and initially the rate of formation of other products (apart from campholenic aldehyde) was much higher resulting in 0% selectivity when using Catalyst 1. In other words, parallel reactions were promoted much more than formation of campholenic aldehyde. However, at higher temperatures consecutive reactions occurred which again resulted in 0% selectivity.

The most selective was Catalyst 2 (around 70%) but it needs to be mentioned again that this catalyst had the lowest conversion of the three. Catalyst 3 had very reasonable selectivity – around 70%, except at temperatures around 45°C where it was ~20%, which again made this temperature worth exploring further.

After the effect of disc temperature was assessed, the effects of disc rotational speed and feed flow rate on conversion and selectivity were considered.

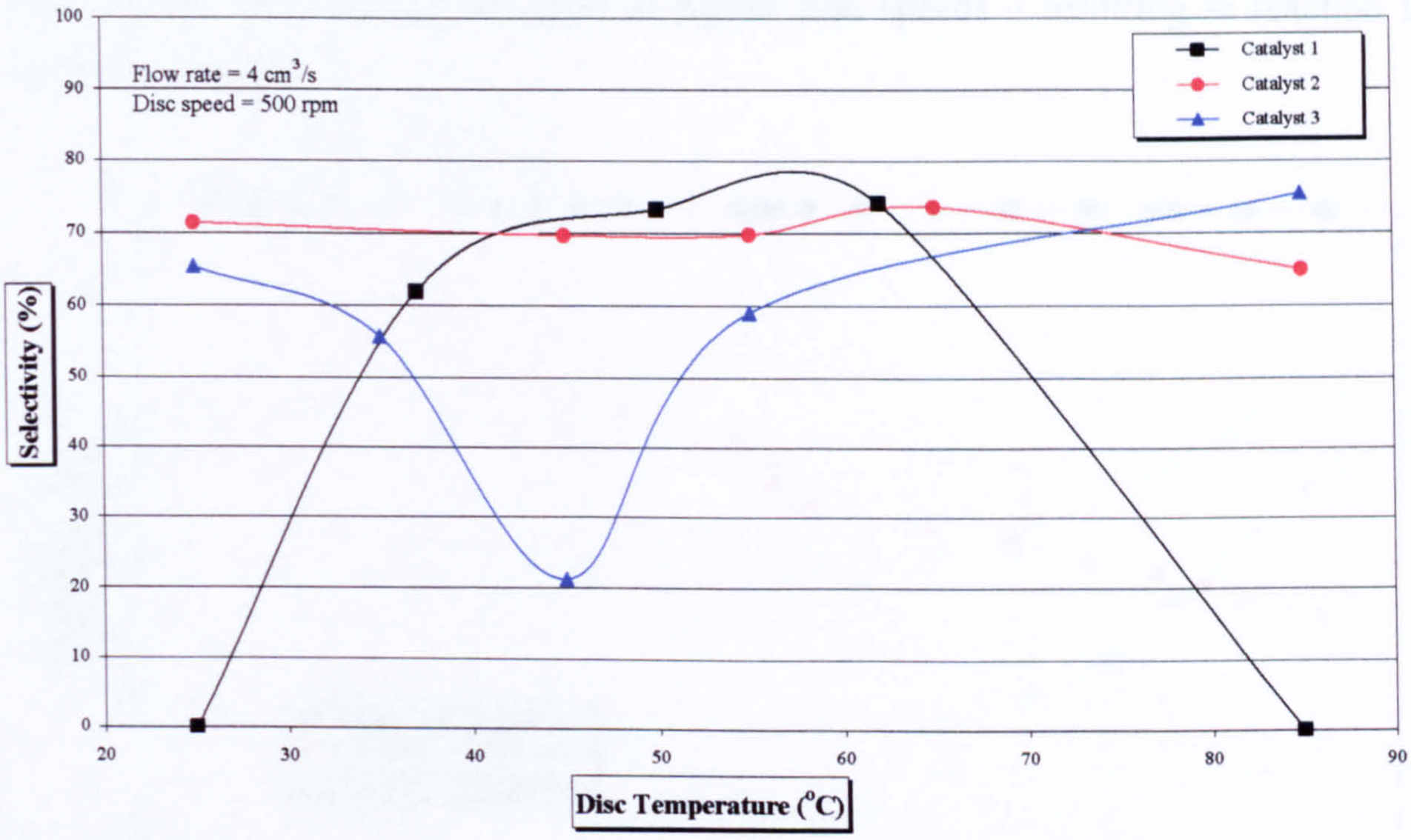


**Figure 8.3. Influence of temperature on the selectivity for all catalysts**

## 8.2.3 THE EFFECT OF DISC SPEED AND FEED FLOW RATE

As reported in Chapter 6, all catalysts were tested (at chosen temperatures) at various disc speeds ranging from 100 to 1500 rpm. Feed flow rate was constant at each stage, varying from 3 to 6 $cm^3/s$. This section will provide comparison between the three catalysts used for this reaction as well as give overview of the individual catalyst's performance.

### *8.2.3.1 Comparison of all catalysts*

Conversion and selectivity results for all three catalysts at 4 $cm^3/s$ are summarised in Figures 8.4 and 8.5 respectively.

These trends may be explained by connecting the catalyst activities and residence times achieved. As shown in Figure 8.4, with catalysts 1 and 3 full conversion of α–pinene oxide was achieved no matter what disc speed was used because of the fast reaction, with 100% conversion obtained within the minimum residence time provided. Catalyst 2 did not have the same activity and the reaction involving Catalyst 2 was not as fast as when using the other two catalysts. Lower disc speeds (and therefore higher residence times) resulted in 90% conversion being accomplished, steeply dropping to as low as 40% when the residence time of the

material on the disc was too short at higher disc speeds – resulting in reaction not being completed.

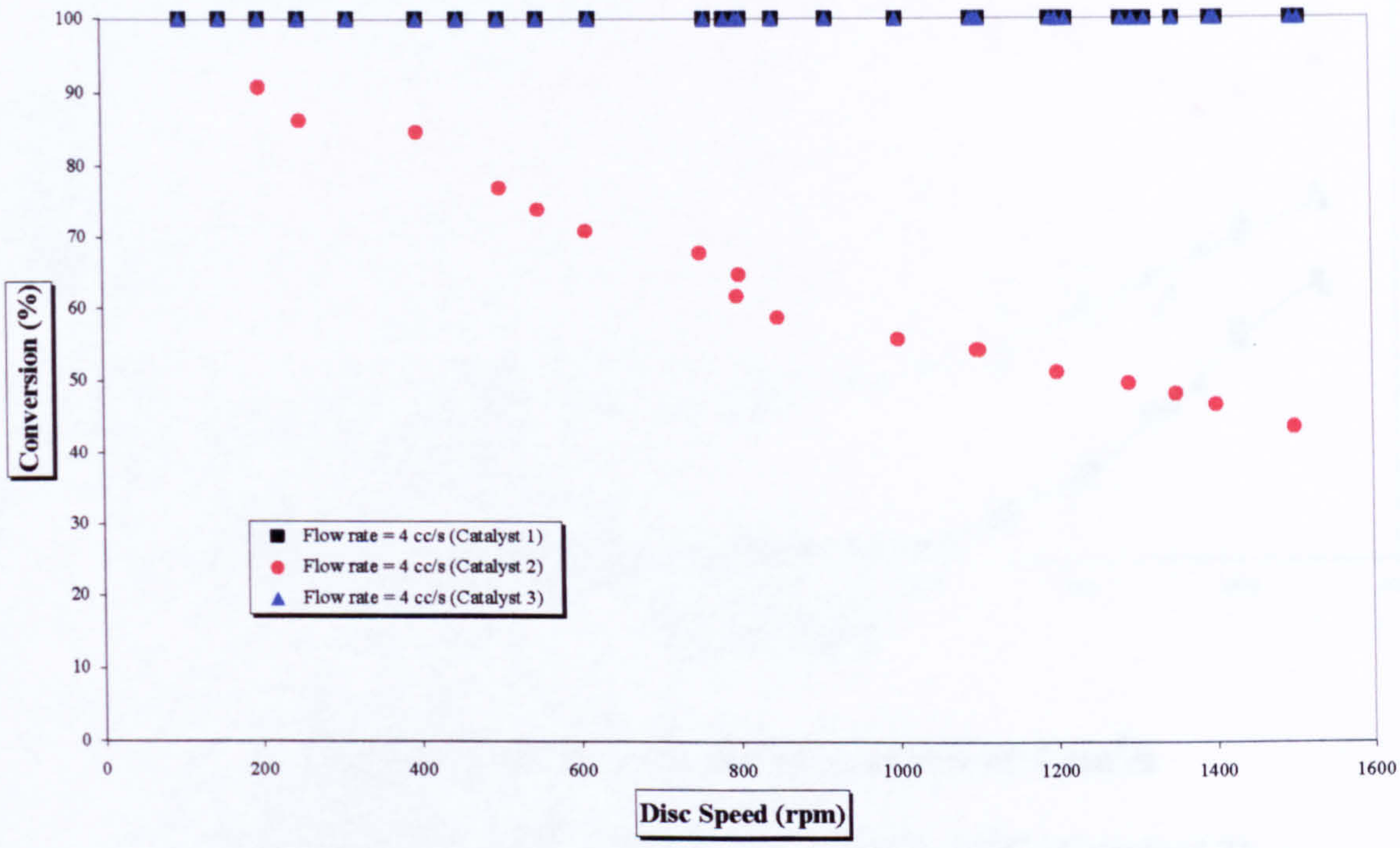


**Figure 8.4. Conversion for all catalysts at 4 $cm^3/s$**

**Temperatures: $85^0C$ (Catalysts 1 and 2); $45^0C$ (Catalyst 3)**

When trends for selectivity results are compared (Figure 8.5) it is noticeable that both "fast" catalysts (1 and 3) have very low selectivity towards campholenic aldehyde comparing to less active Catalyst 2; in fact when residence time was long, none of the aldehyde was observed when using Catalyst 1. This could be explained in two ways: either the catalysts 1 and 3 were promoting other reactions, or the aldehyde is being formed, but due to its high reactivity, rearranged itself which resulted in not as much aldehyde being seen at the end of the reaction on the disc. Knowing that aldehyde that is formed in a batch reaction is easily consumed after its formation, second explanation looks more likely, but needed further exploration.

All conversion and selectivity results for the flow rate of 5 $cm^3/s$ are summarised in Figures 8.6 and 8.7 respectively. By increasing the flow rate, residence time is reduced and therefore higher selectivity is expected (to confirm consecutive reactions theory).

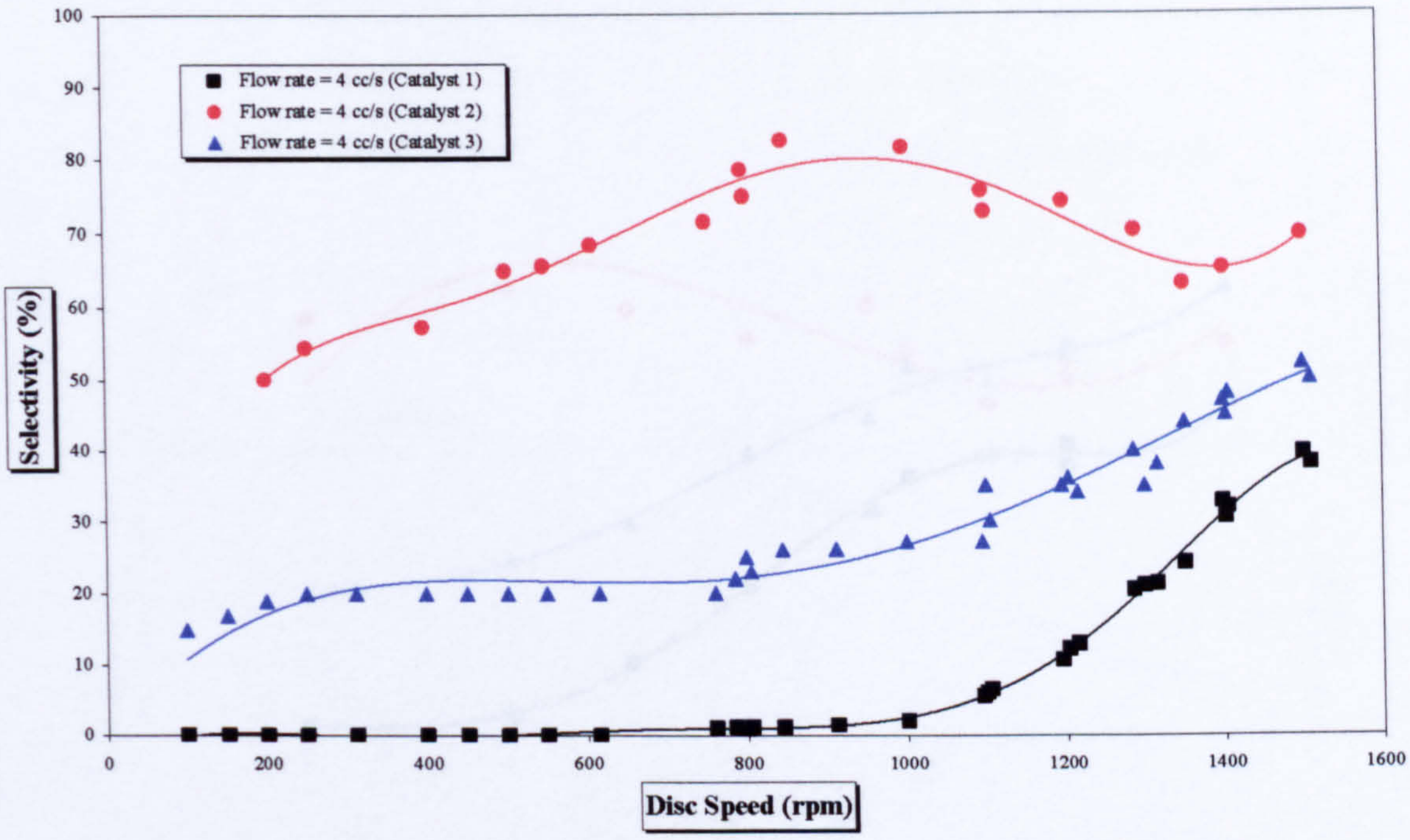


**Figure 8.5. Selectivity for all catalysts at 4 $cm^3/s$**

**Temperatures: $85^0C$ (Catalysts 1 and 2); $45^0C$ (Catalyst 3)**

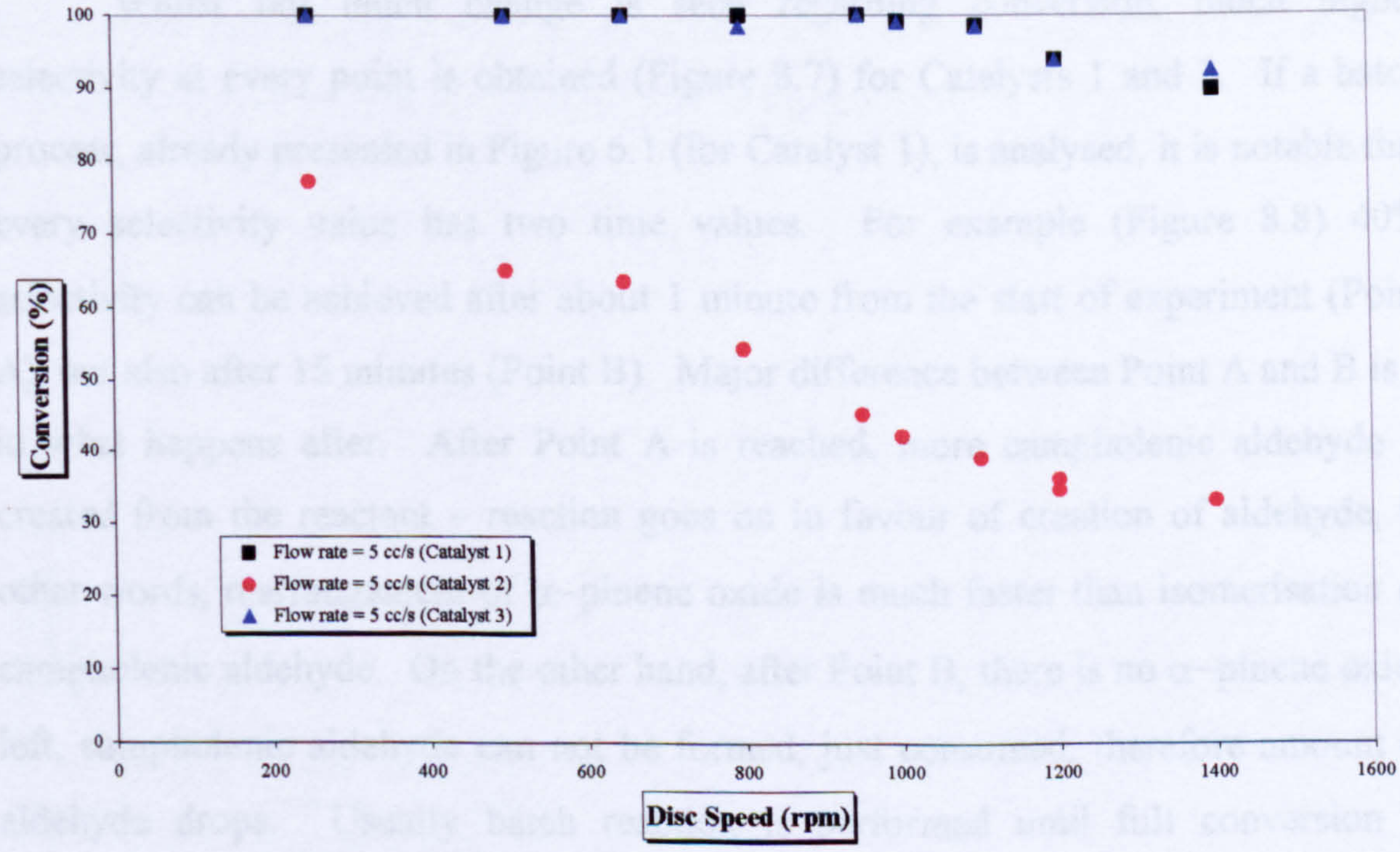


**Figure 8.6. Conversion for all catalysts at 5 $cm^3/s$**

**Temperatures: $85^0C$ (Catalysts 1 and 2); $45^0C$ (Catalyst 3)**

Very similar conversion results are obtained as for the flow rate of 4 $cm^3/s$, it is only at higher speeds that a small drop in reaction rates is observed.

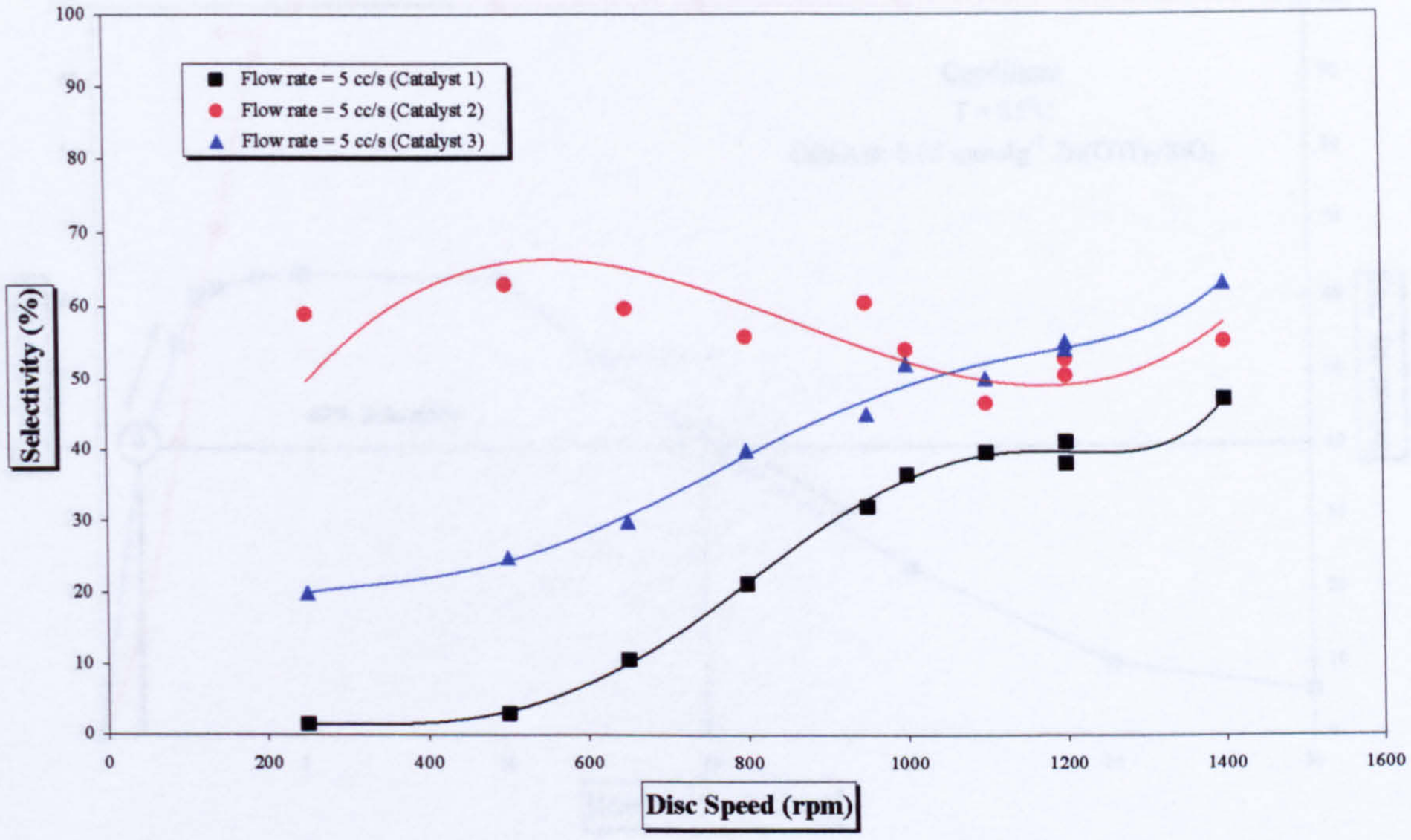


**Figure 8.7. Selectivity for all catalysts at 5 $cm^3/s$**

**Temperatures: $85^0C$ (Catalysts 1 and 2); $45^0C$ (Catalyst 3)**

Whilst not much change is seen regarding conversion, much higher selectivity at every point is obtained (Figure 8.7) for Catalysts 1 and 3. If a batch process, already presented in Figure 6.1 (for Catalyst 1), is analysed, it is notable that every selectivity value has two time values. For example (Figure 8.8) 40% selectivity can be achieved after about 1 minute from the start of experiment (Point A), but also after 15 minutes (Point B). Major difference between Point A and B is – in what happens after. After Point A is reached, more campholenic aldehyde is created from the reactant – reaction goes on in favour of creation of aldehyde, in other words, rearrangement of α–pinene oxide is much faster than isomerisation of campholenic aldehyde. On the other hand, after Point B, there is no α–pinene oxide left, campholenic aldehyde can not be formed, just consumed, therefore amount of aldehyde drops. Usually batch reaction is performed until full conversion is achieved, and selectivity values taken at, say, 50% and 100% conversion. In this case it was important to see what is happening to reaction after all of the reactant is consumed. In most of the cases when very high conversion is obtained on the disc, not much aldehyde in the product was observed, as it would be expected, due to all the reactant being consumed. Final product analysed from the disc is equivalent as taken somewhere around Point B (or after Point B) in a batch process.

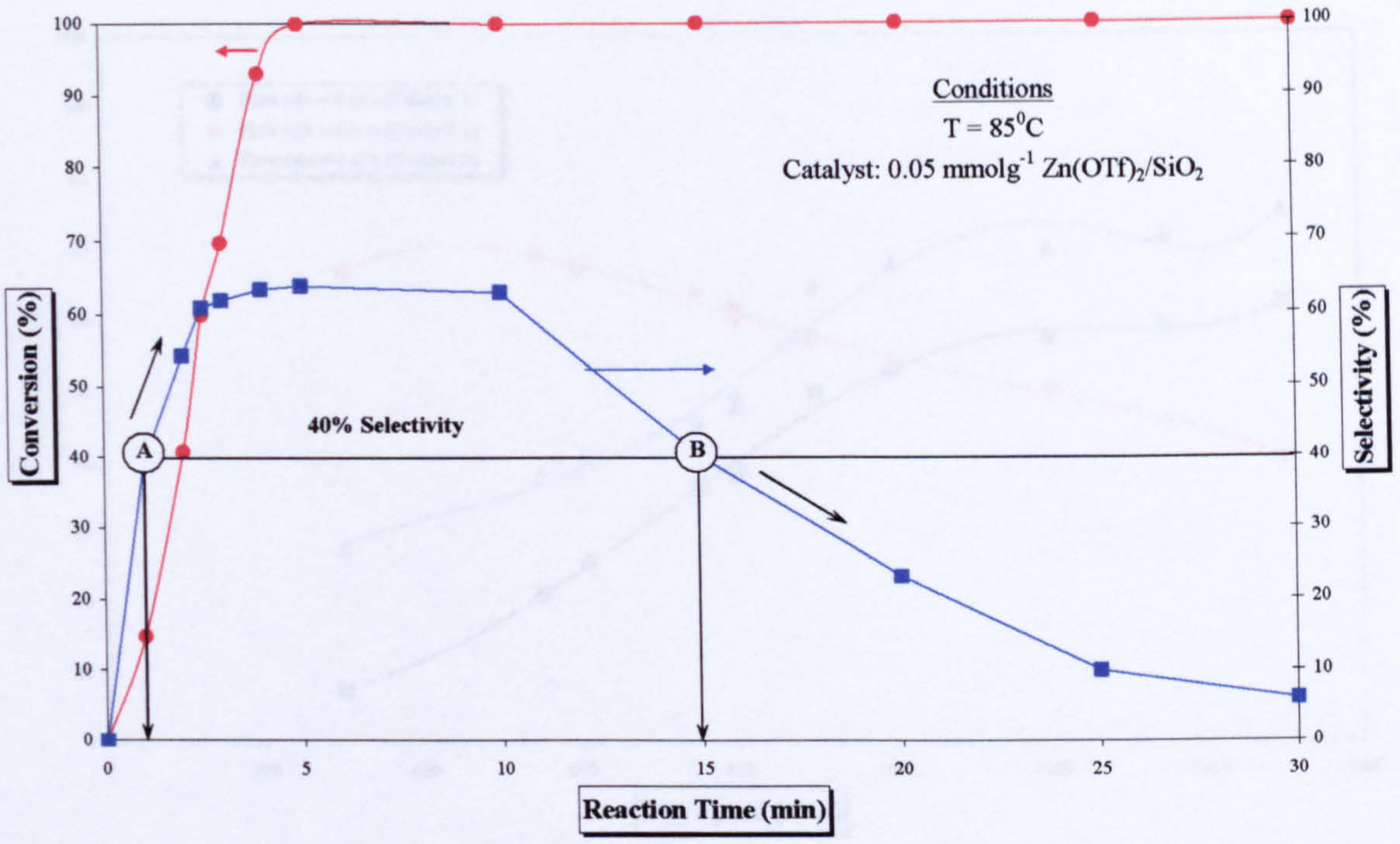


**Figure 8.8. Batch process analysis (example)**

Hence the increase in selectivity values is observed at higher flow rates, approximately 20% more at 6 $cm^3/s$ as showed in Figure 8.10. Conversion results for all three catalysts with the feed flow rate of 6 $cm^3/s$ are presented in Figure 8.9, whereas selectivity results are summarised in Figure 8.10.

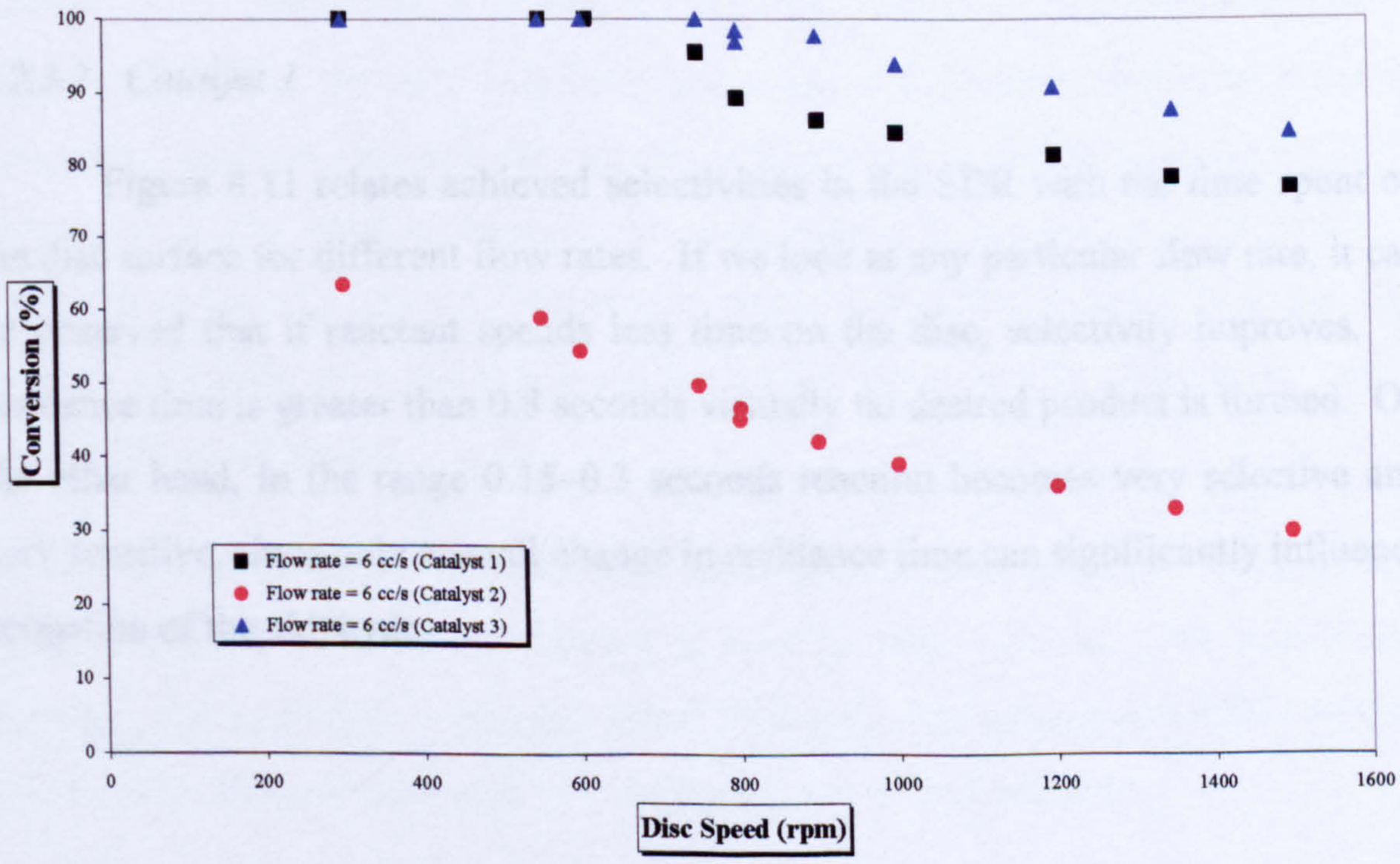


**Figure 8.9. Conversion for all catalysts at 6 $cm^3/s$**

**Temperatures: $85^0$C (Catalysts 1 and 2); $45^0$C (Catalyst 3)**

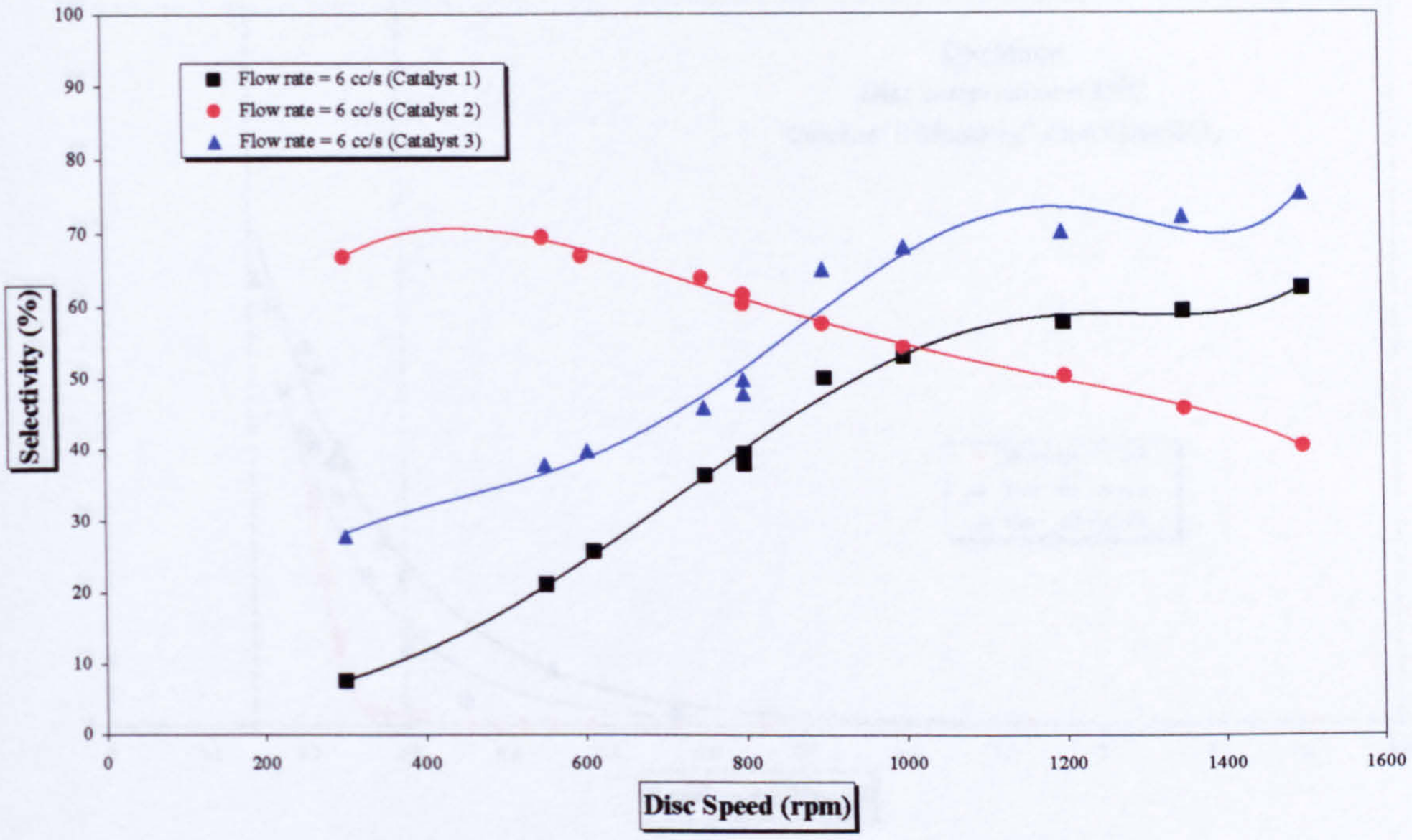


**Figure 8.10. Selectivity for all catalysts at 6 $cm^3/s$**

**Temperatures: $85^0C$ (Catalysts 1 and 2); $45^0C$ (Catalyst 3)**

Effect of residence time on conversion and selectivity results will be presented in some detail in sections 8.2.3.2 (Catalyst 1), 8.2.3.3 (Catalyst 2) and 8.2.3.4 (Catalyst 3).

### *8.2.3.2 Catalyst 1*

Figure 8.11 relates achieved selectivities in the SDR with the time spent on the disc surface for different flow rates. If we look at any particular flow rate, it can be observed that if reactant spends less time on the disc, selectivity improves. If residence time is greater than 0.8 seconds virtually no desired product is formed. On the other hand, in the range 0.15–0.3 seconds reaction becomes very selective and very sensitive, since only a small change in residence time can significantly influence formation of the aldehyde.

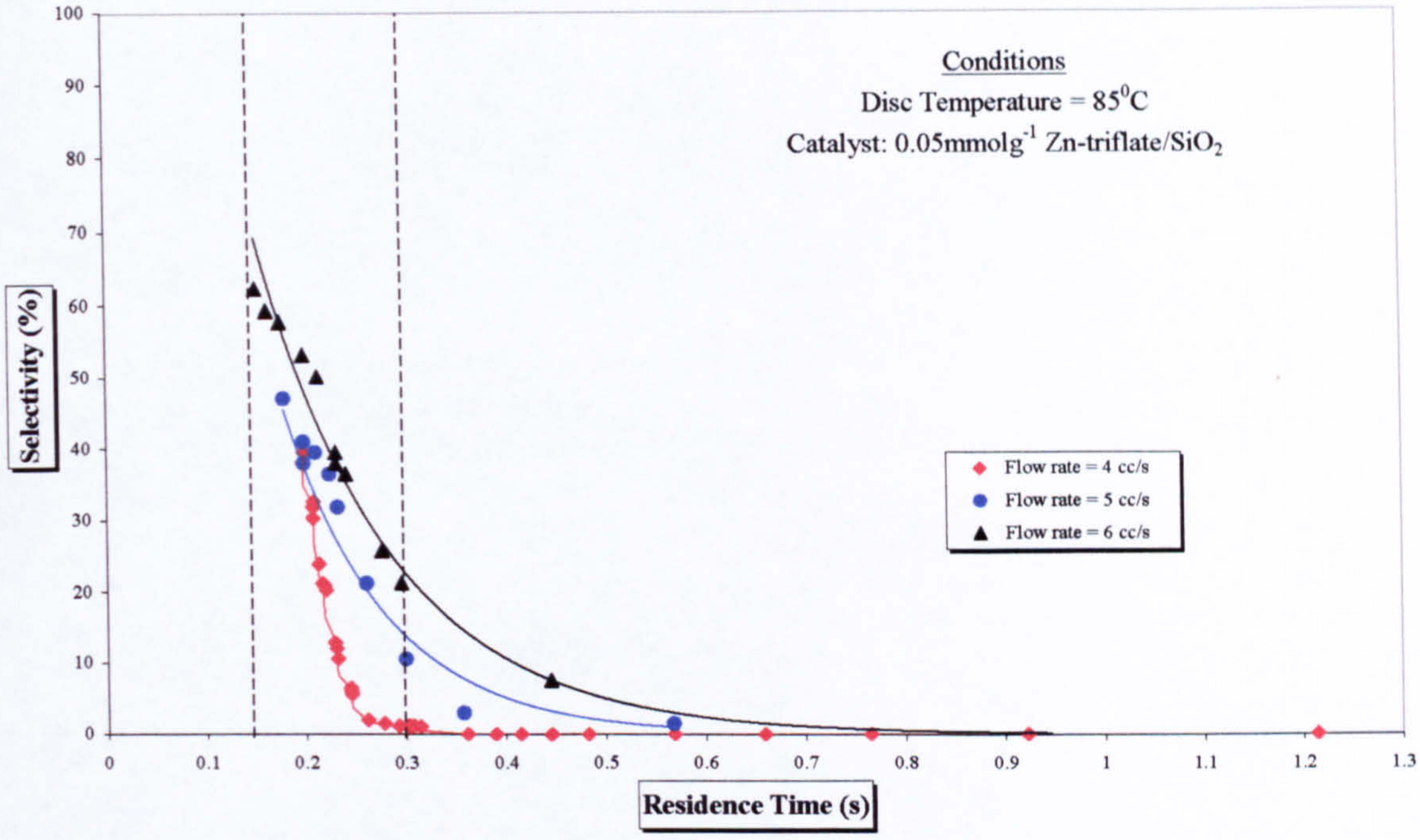


**Figure 8.11. Selectivity change with residence time**

At the same time, when the selectivity rises as a result of increased flow rate, a drop in conversion can be seen (Figures 8.12 and 8.13 for different disc speeds). A profile of conversion with residence time is shown in Figure 8.14. Again, the same interval (0.15–0.3 seconds) of residence time is of interest. The residence time needed for full conversion is around 0.3 seconds. But if reactant spends too much time on the disc, the side reactions begin and campholenic aldehyde starts to disappear; therefore although the reaction is completed in full, there is no aldehyde remaining in the product mixture; in other words selectivity is very low. A compromise had to be found – either conversion to be lower than 100% to get high yield of aldehyde, or a reaction could have been performed to completion, with a lower yield of aldehyde.

This investigation however was concerned about campholenic aldehyde as a product, therefore the best achieved selectivity was 62% at 77% conversion; optimum disc conditions were: disc speed 1500 rpm, disc temperature 85°C and flow rate 6 $cm^3/s$, all combining to give a residence time of 0.15 seconds.

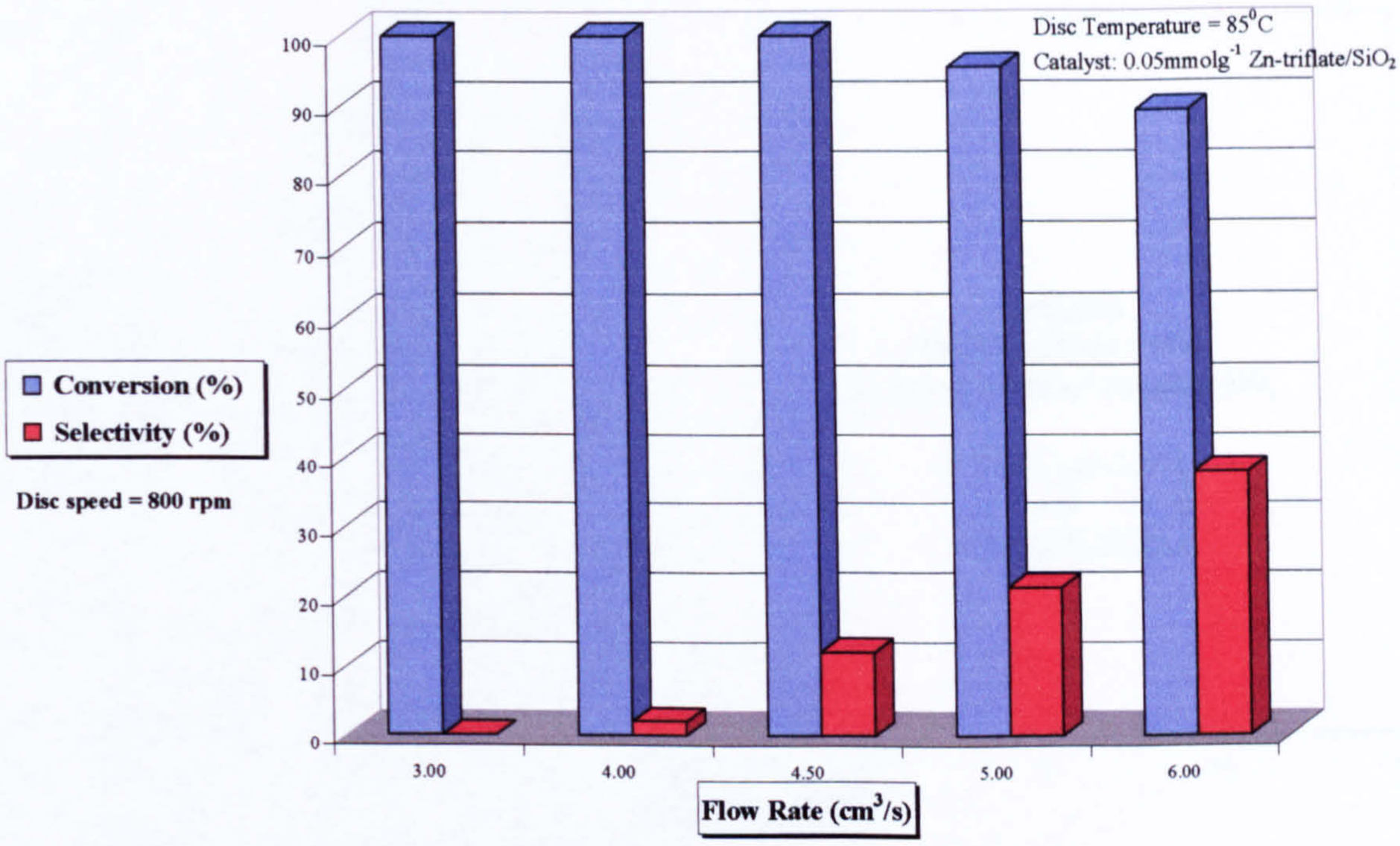


**Figure 8.12. Selectivity and conversion change with flow rate at 800 rpm**

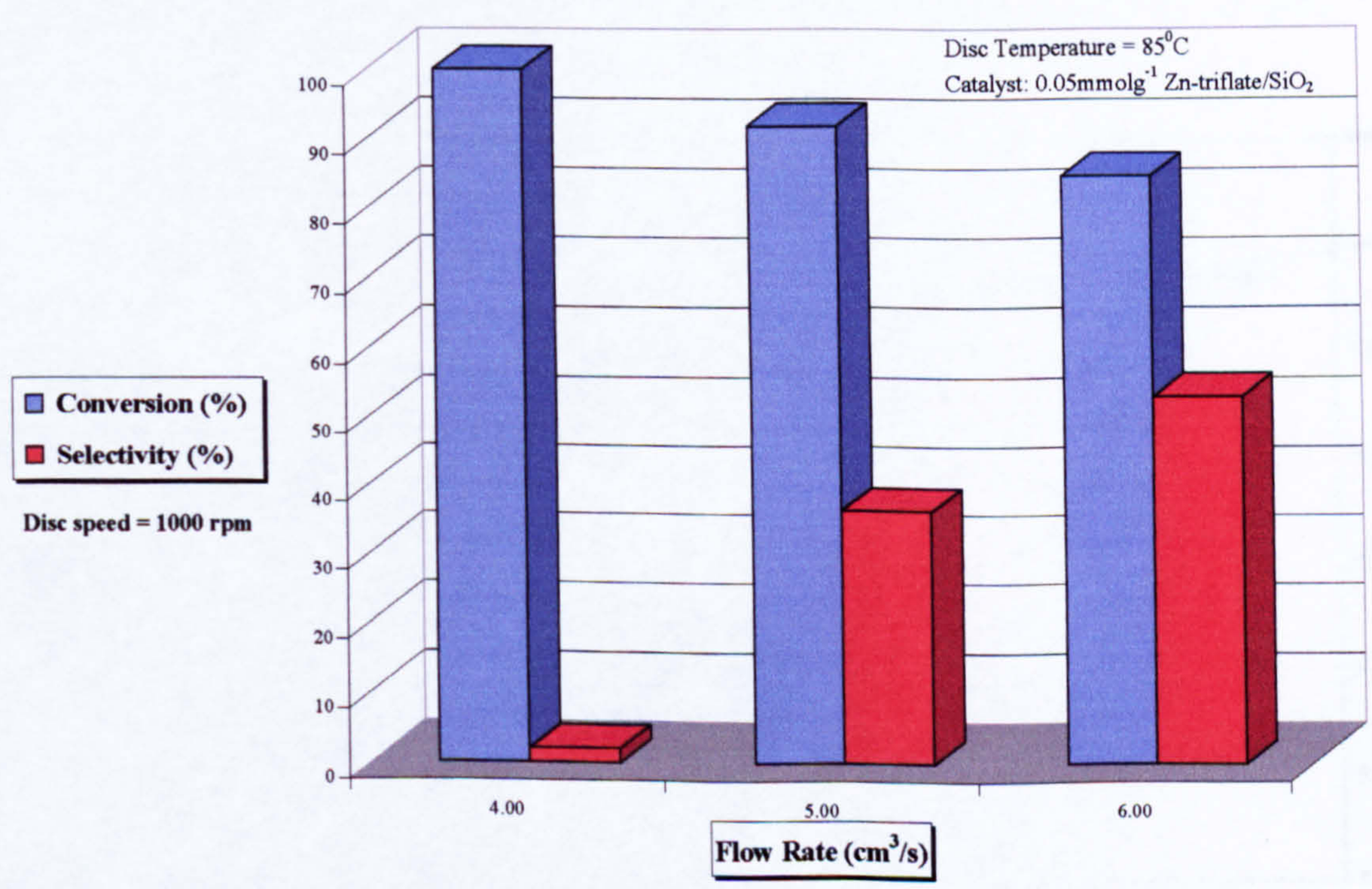


**Figure 8.13. Selectivity and conversion change with flow rate at 1000 rpm**

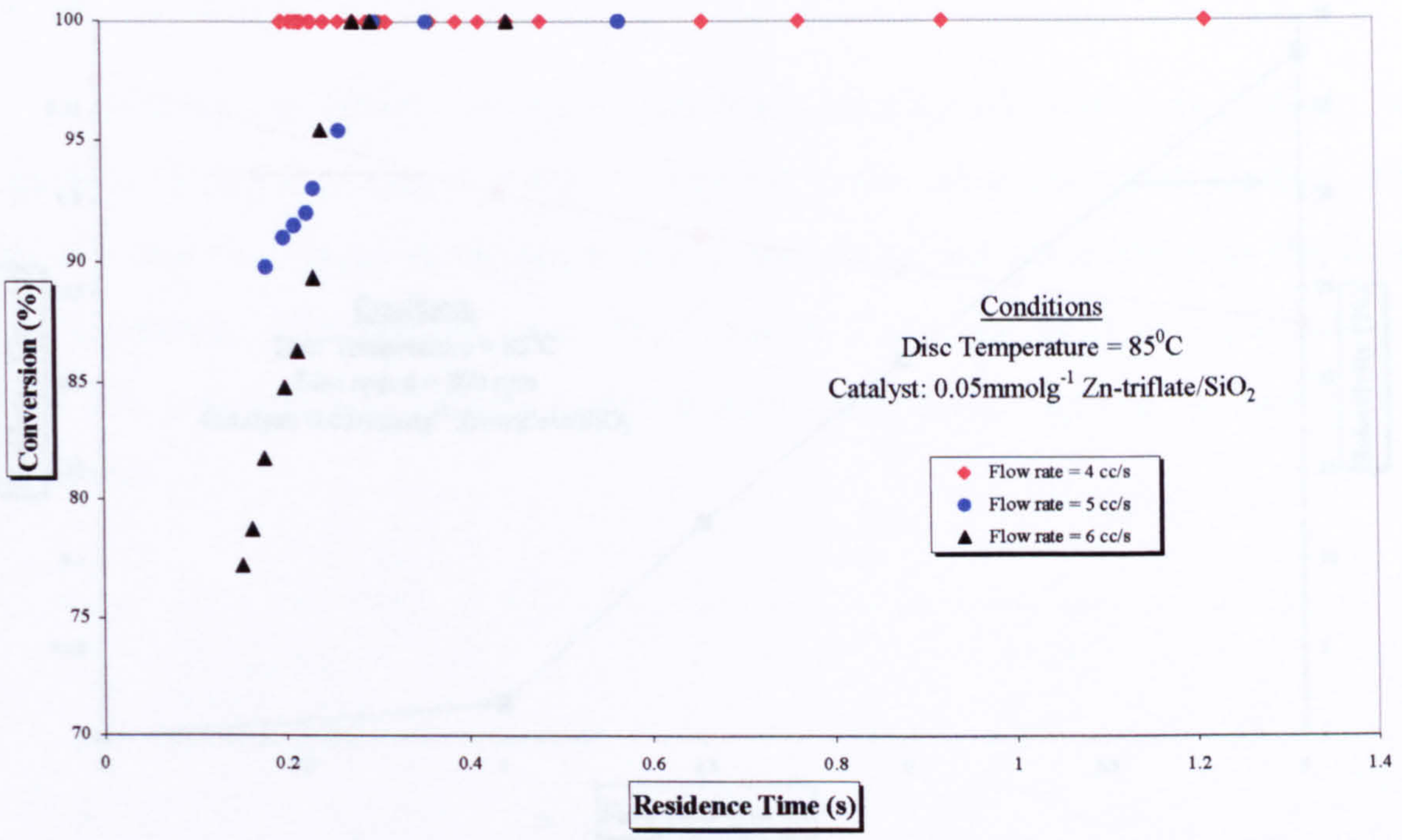


**Figure 8.14. Conversion change with residence time**

Change of residence time and film thickness with flow rates (ranging from 3 to 6 $cm^3/s$) is demonstrated in Figure 8.15. Disc speed was kept constant at 800 rpm and the disc heated to $85^0C$.

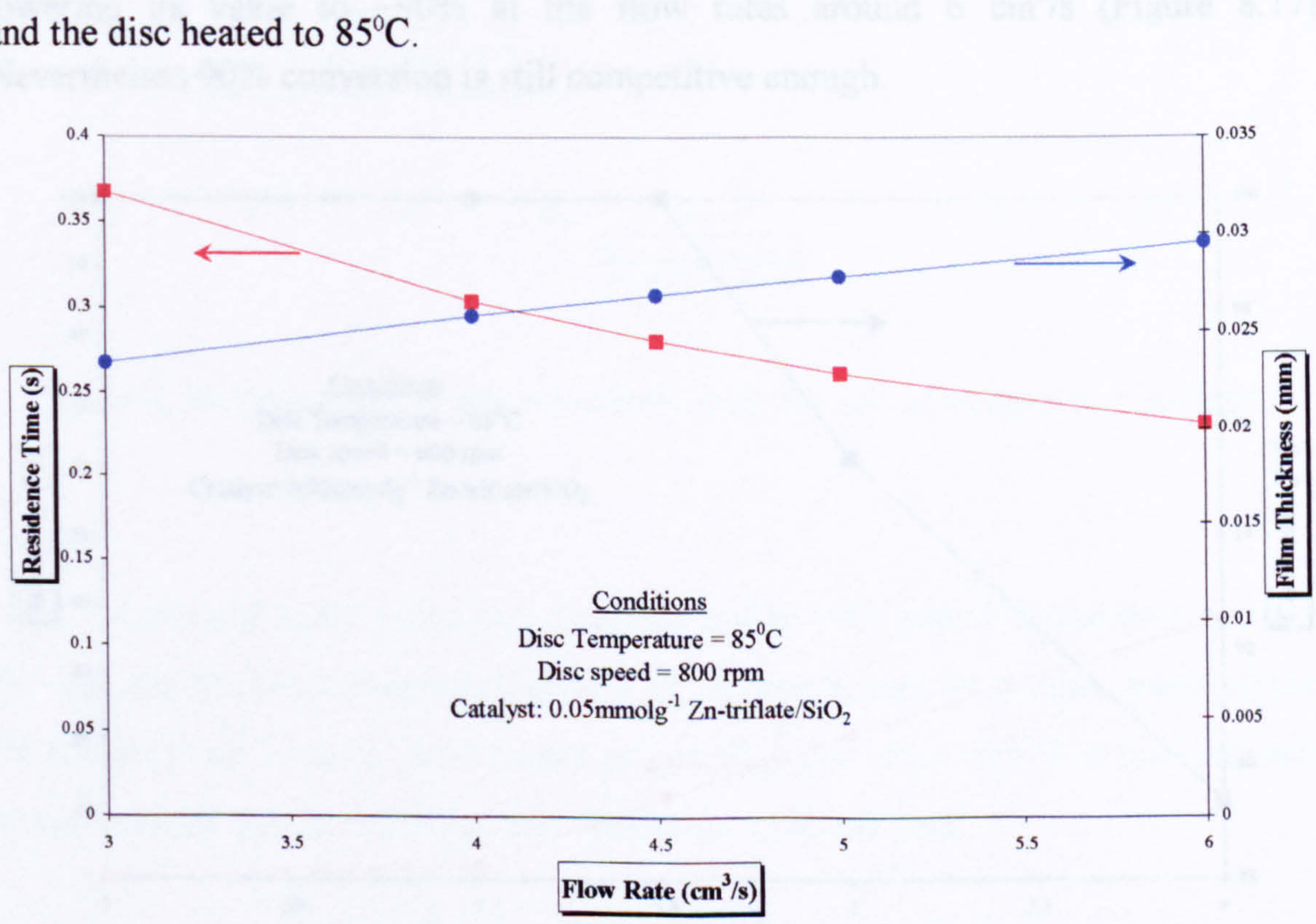


**Figure 8.15. Change in residence time and film thickness with flow rate**

As the flow rate increases, reactant spends less time on the disc increasing the amount of campholenic aldehyde in the product, since campholenic aldehyde does not have enough time to react itself (Figure 8.16).

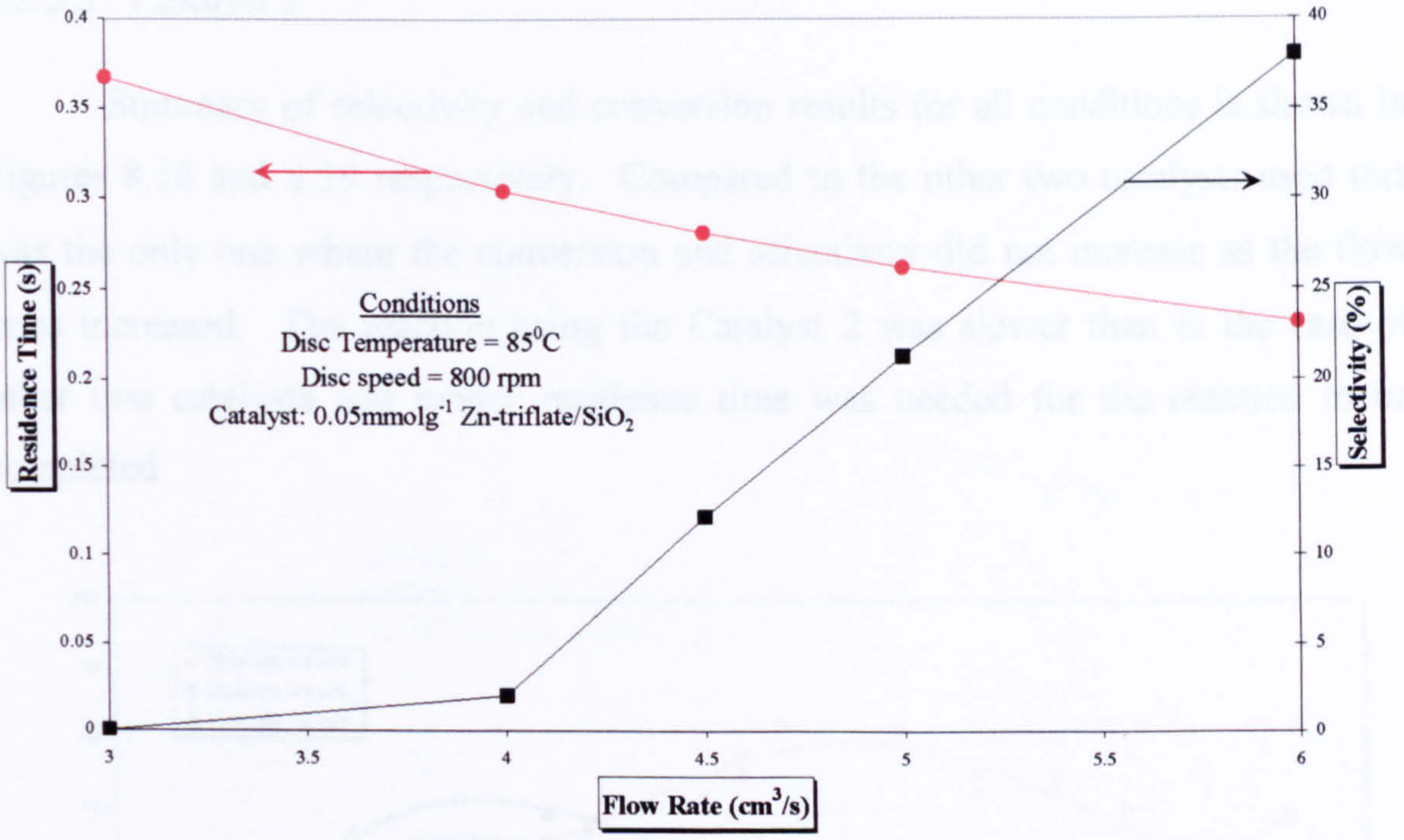


**Figure 8.16. Residence time and selectivity change with flow rates**

Again the critical point time of less than 0.3 seconds influenced conversion, lowering its value to ~90% at the flow rates around 6 $cm^3/s$ (Figure 8.17). Nevertheless 90% conversion is still competitive enough.

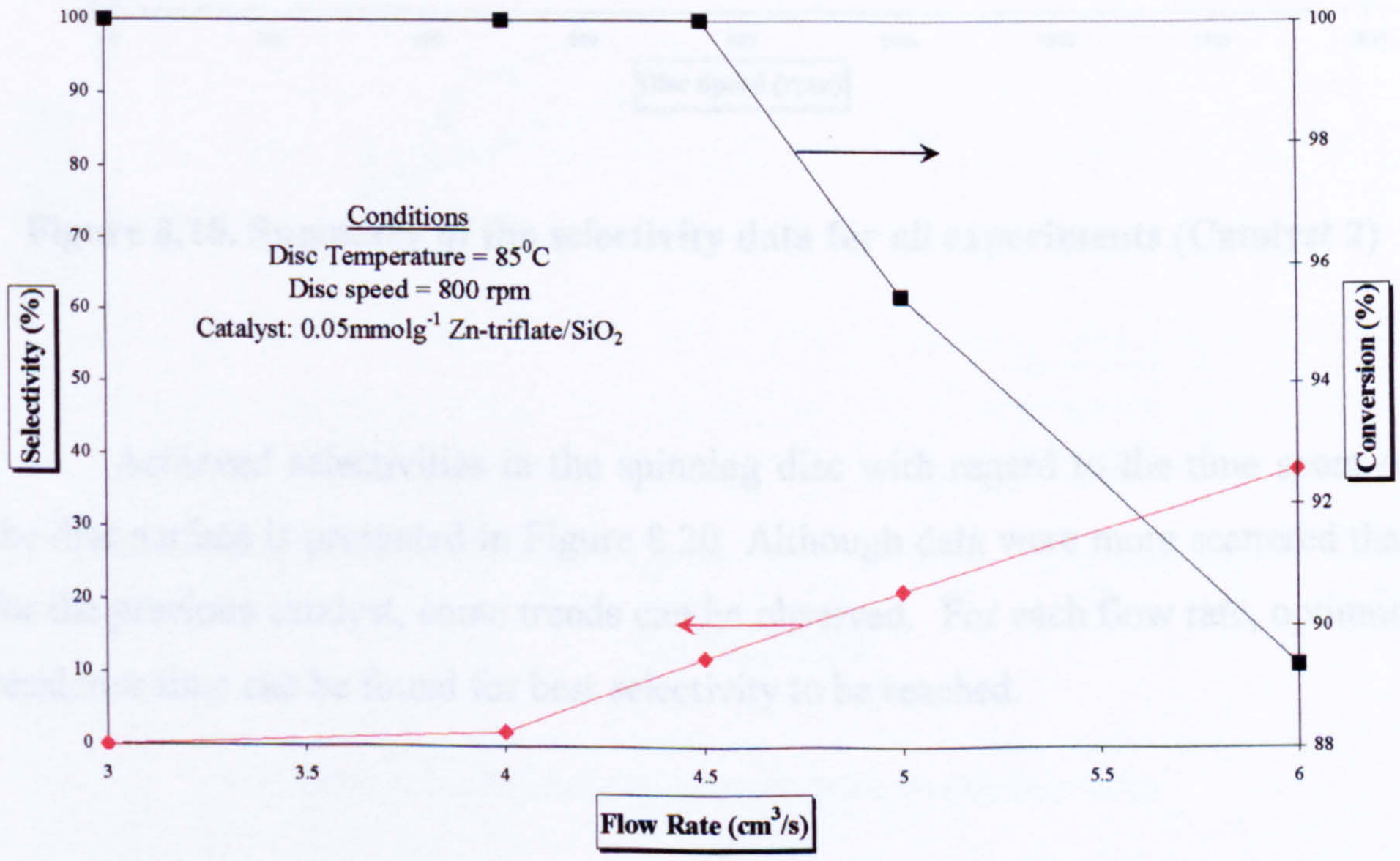


**Figure 8.17. Selectivity and conversion change with flow rates**

### *8.2.3.3 Catalyst 2*

Summary of selectivity and conversion results for all conditions is shown in Figures 8.18 and 8.19 respectively. Compared to the other two catalysts used this was the only one where the conversion and selectivity did not increase as the flow rates increased. The reaction using the Catalyst 2 was slower than in the case of other two catalysts and longer residence time was needed for the reaction to be completed.

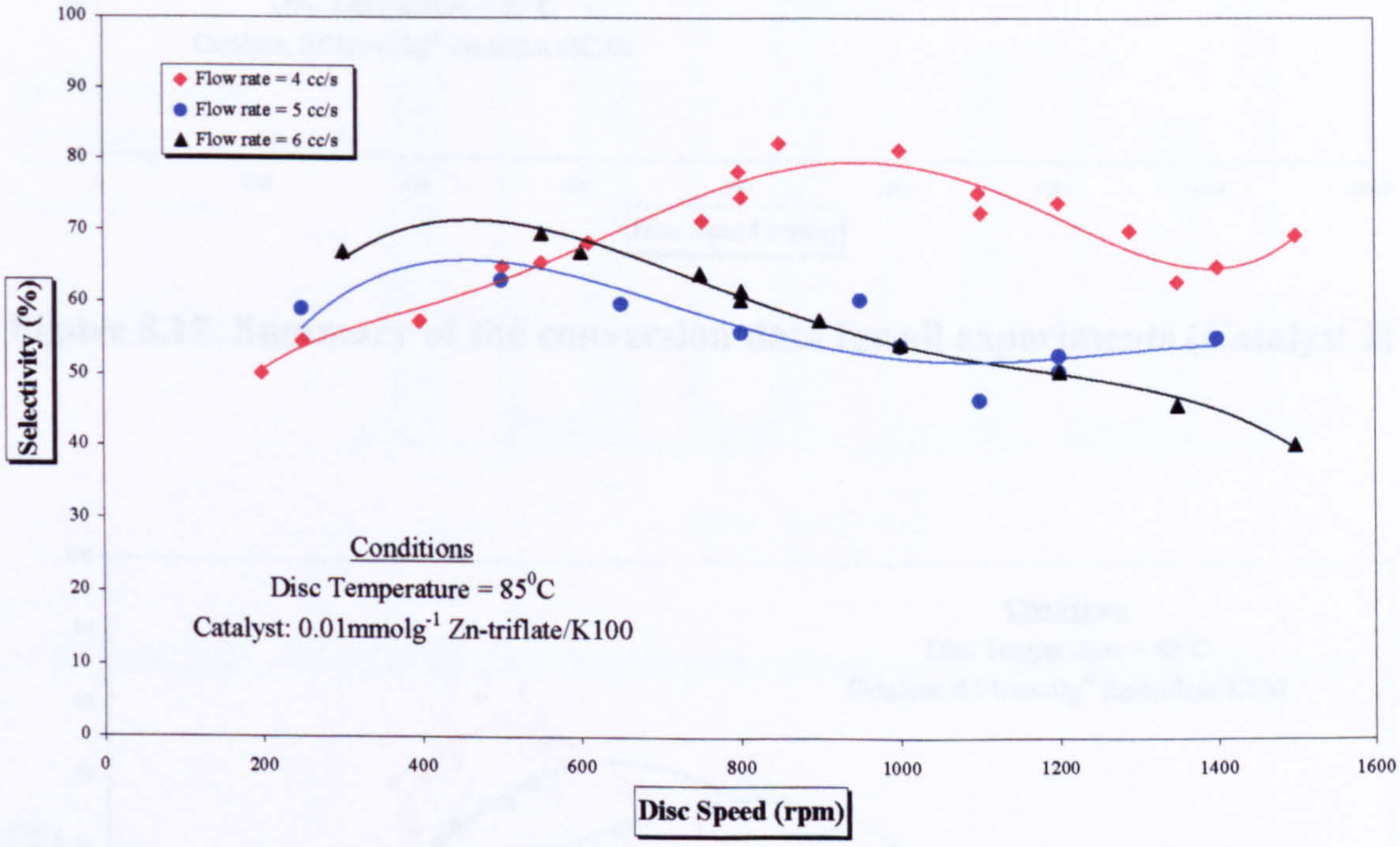


**Figure 8.18. Summary of the selectivity data for all experiments (Catalyst 2)**

Achieved selectivities in the spinning disc with regard to the time spent on the disc surface is presented in Figure 8.20 Although data were more scattered than for the previous catalyst, some trends can be observed. For each flow rate, optimum residence time can be found for best selectivity to be reached.

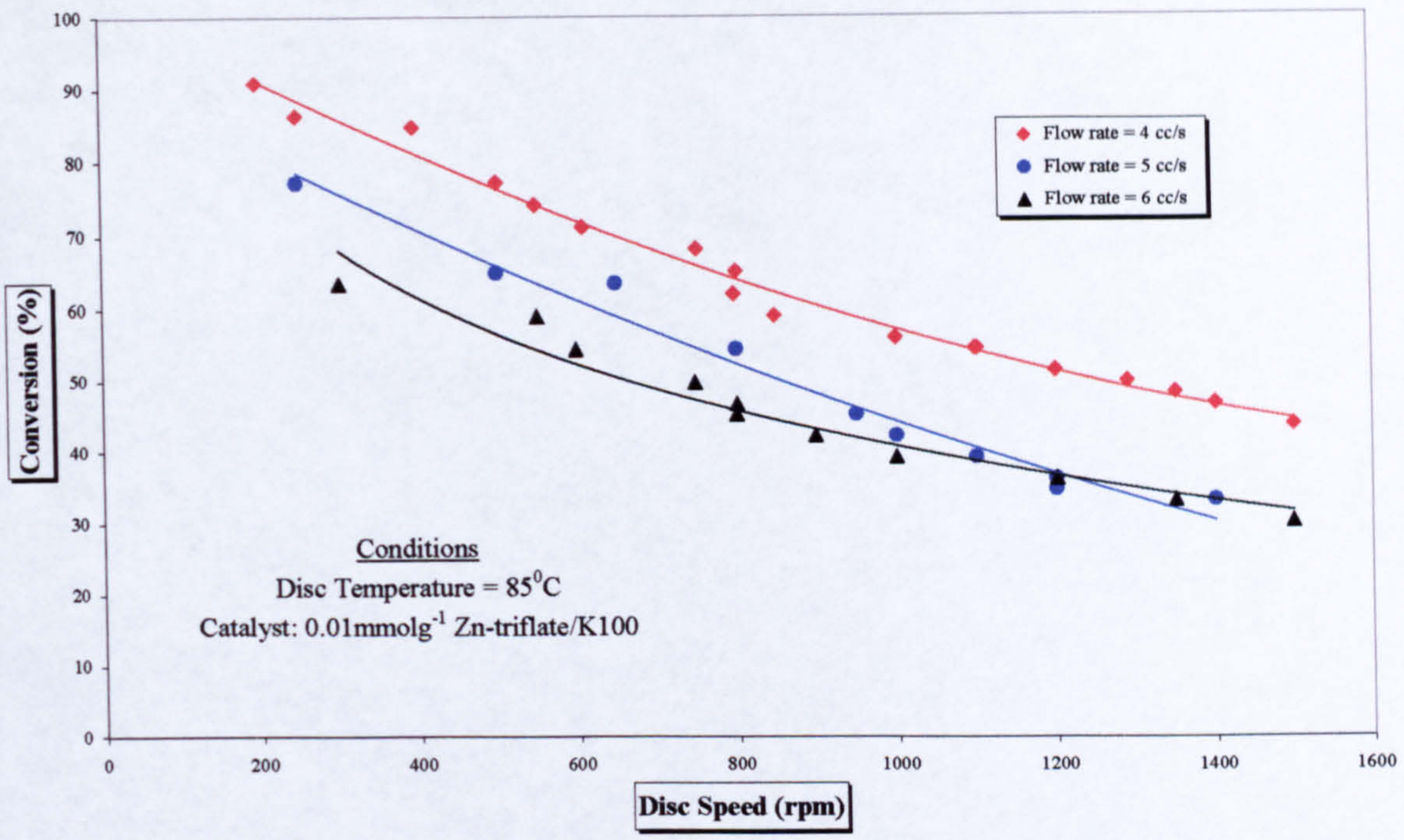


**Figure 8.19. Summary of the conversion data for all experiments (Catalyst 2)**

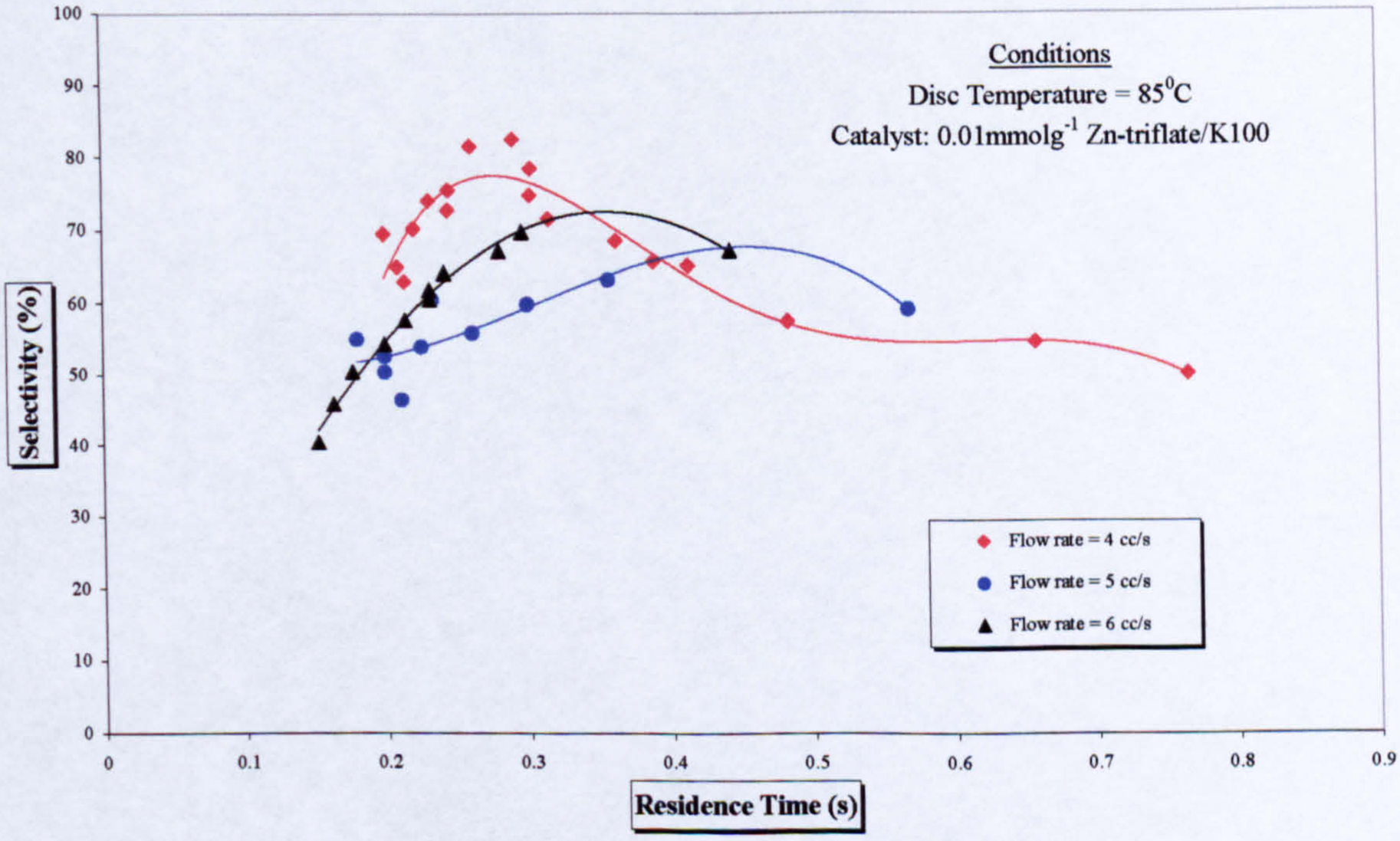


**Figure 8.20. Selectivity change with residence time**

If various flow rates are considered for the fixed rotational speed (and the disc temperature) it can be observed that conversion decreases with the increase of flow rate, which is not the case for selectivity results. The best agreement can be

accomplished with a flow rate of 4 $cm^3/s$, where conversion is not much lower than for the flow rate of 3 $cm^3/s$, but selectivity is the highest (75%), as in Figure 6.21.

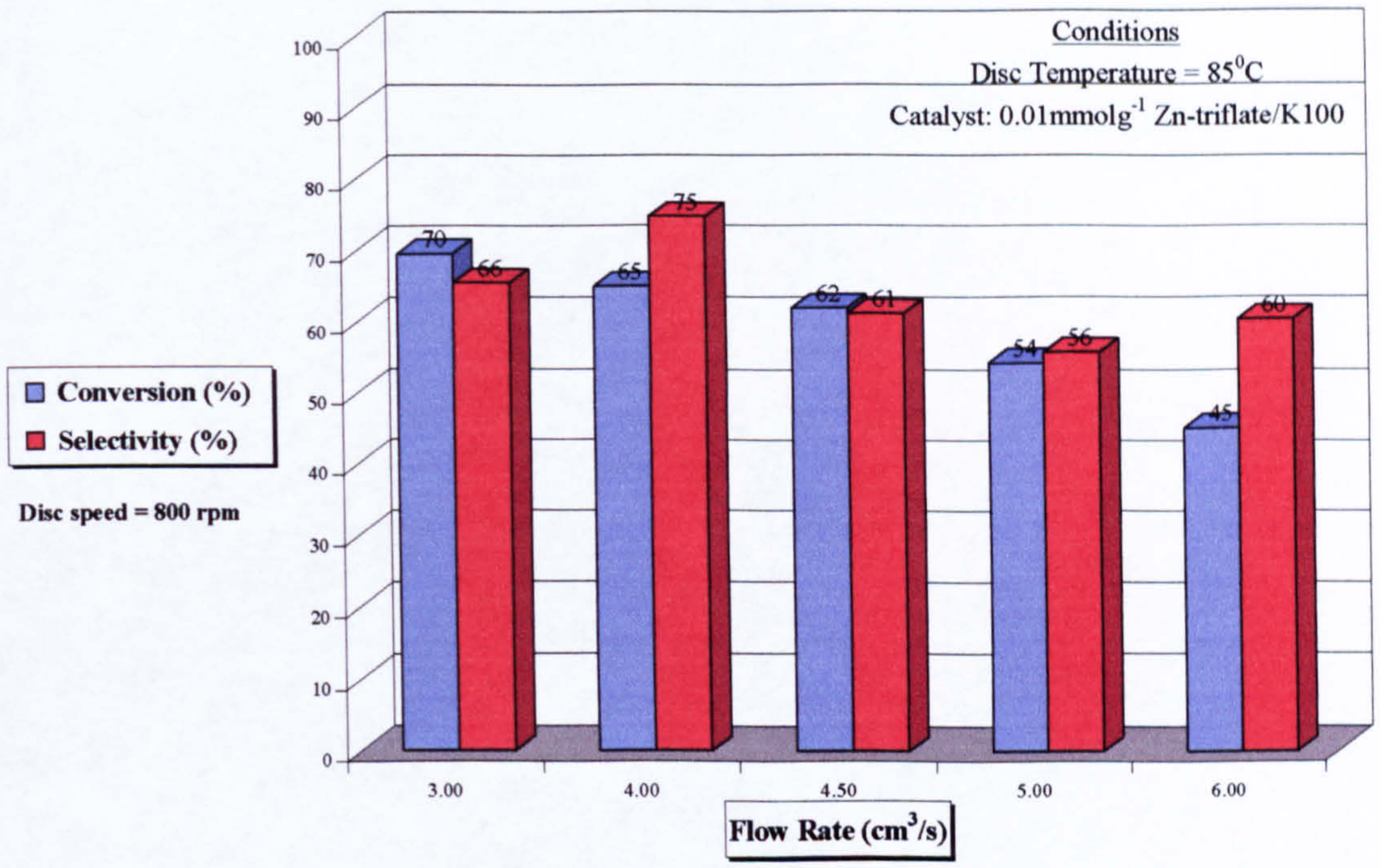


**Figure 8.21. Selectivity and conversion change with flow rate at 800 rpm**

For the disc speed of 1000 rpm, optimum flow rate was 4 $cm^3/s$ again, as shown in Figure 6.22.

For higher conversions in the spinning disc, residence time had to be much longer (for full conversion, residence time around 1 second would be needed) (Figure 6.23). This is where a compromise has to be made, either to have high conversion, with reasonable selectivity, or a reasonable conversion with high selectivity.

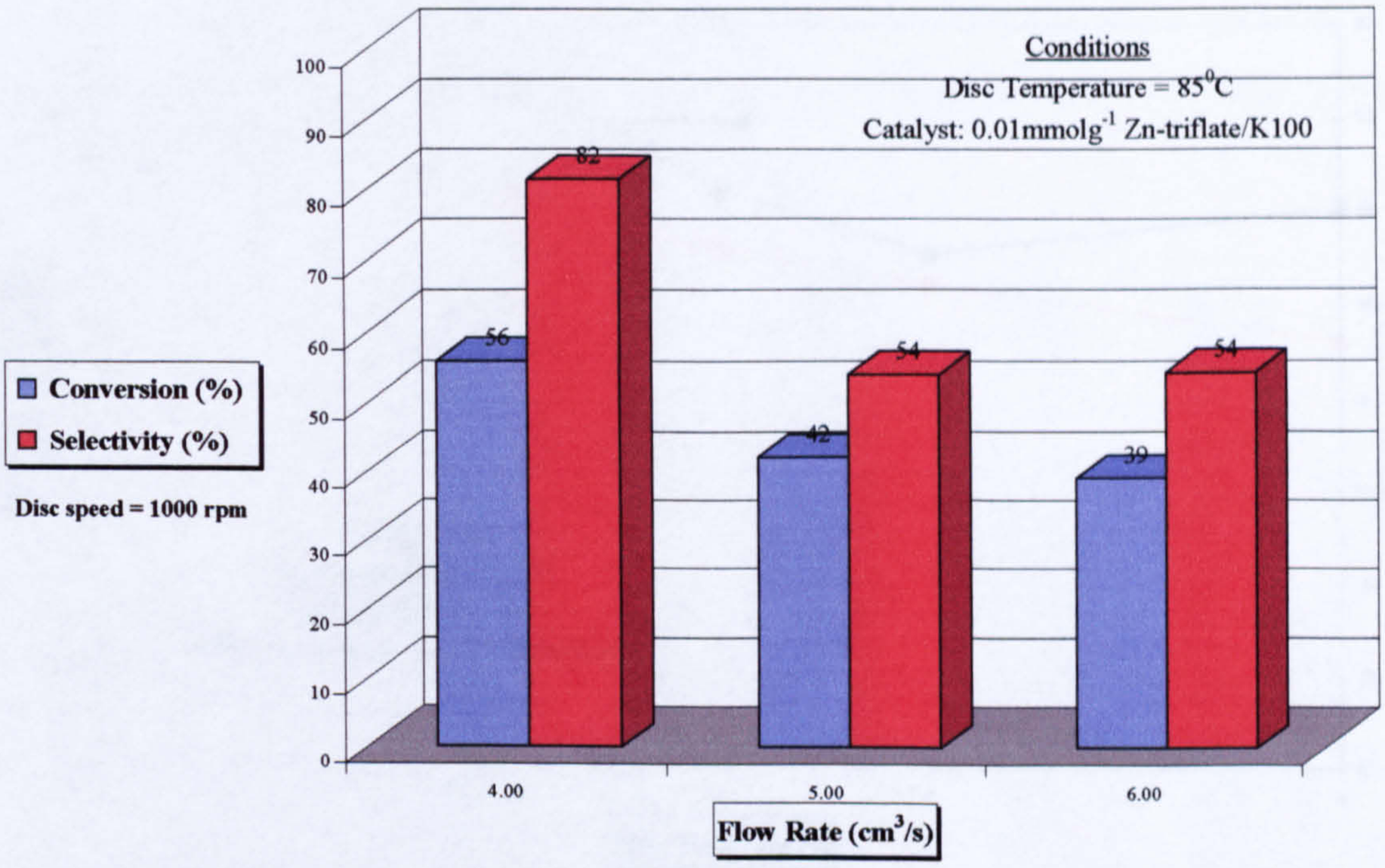


**Figure 8.22. Selectivity and conversion change with flow rate at 1000 rpm**

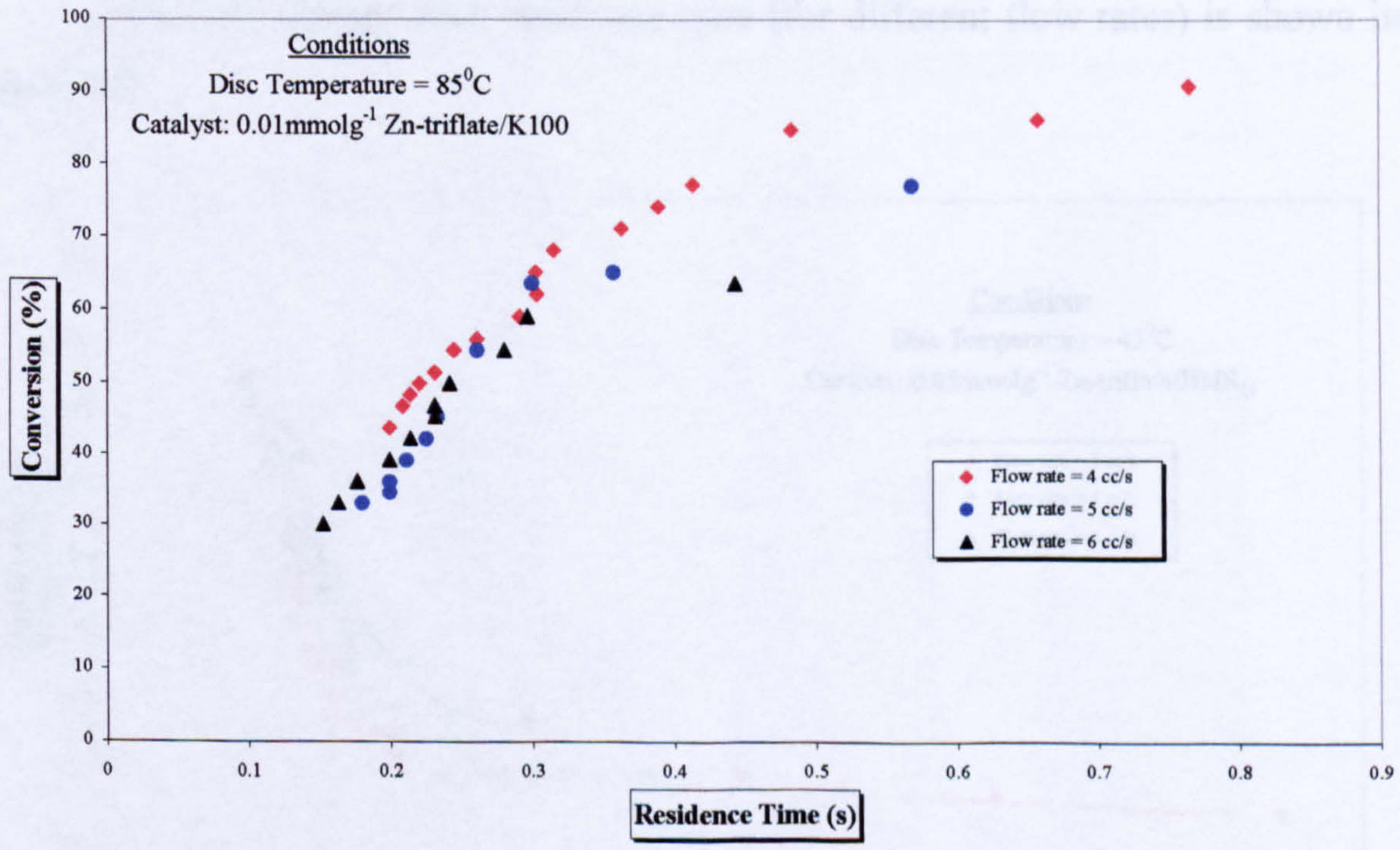


**Figure 8.23. Conversion change with residence time**

Residence time and film thickness changes with flow rates do not depend on the catalyst utilised; therefore Figure 8.15 can be used for each of the three catalysts. Residence time and selectivity changes with flow rates are presented in Figure 8.24.

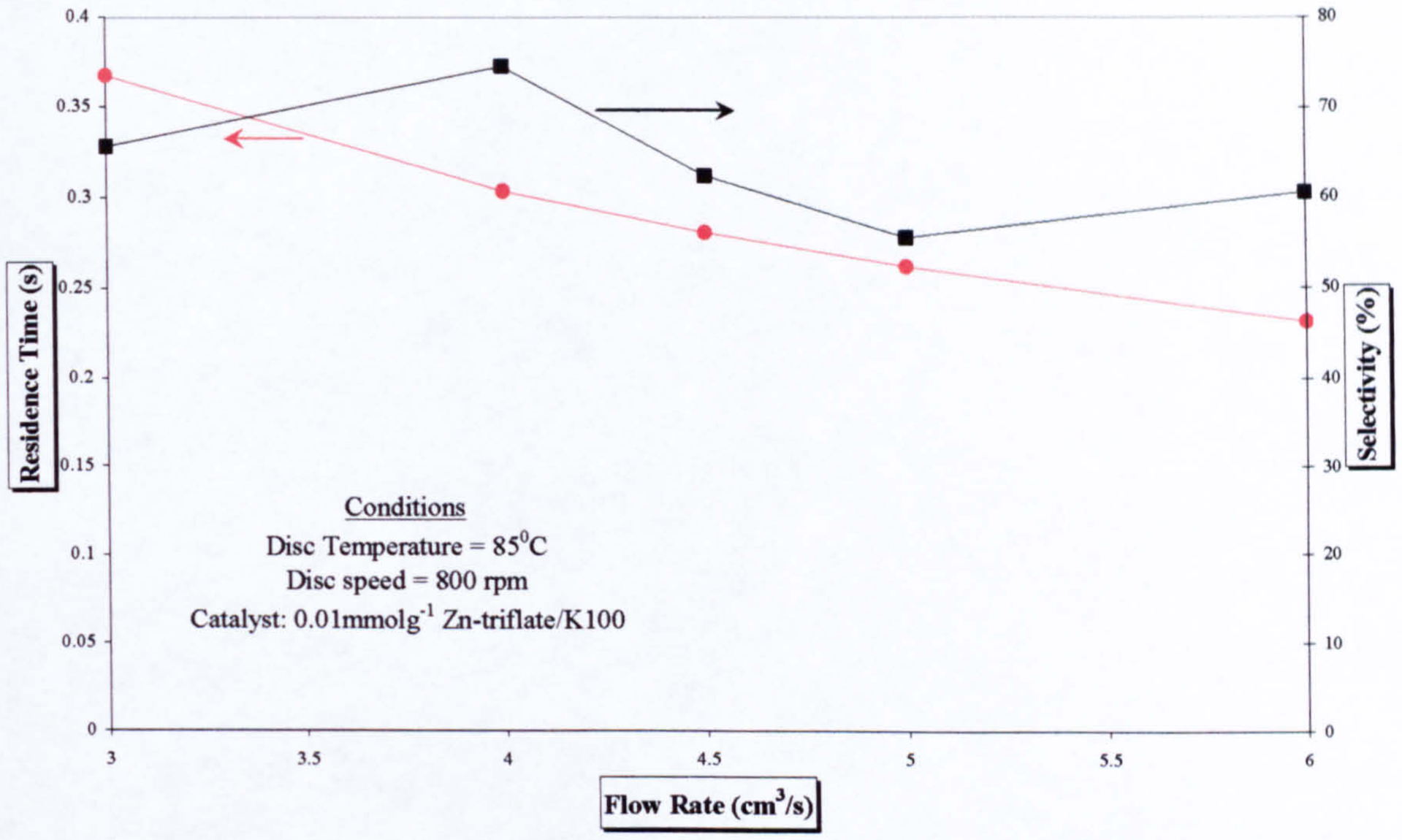


**Figure 8.24. Residence time and selectivity change with flow rates**

### *8.2.3.4 Catalyst 3*

Selectivity change with residence time (for different flow rates) is shown in Figure 8.25.

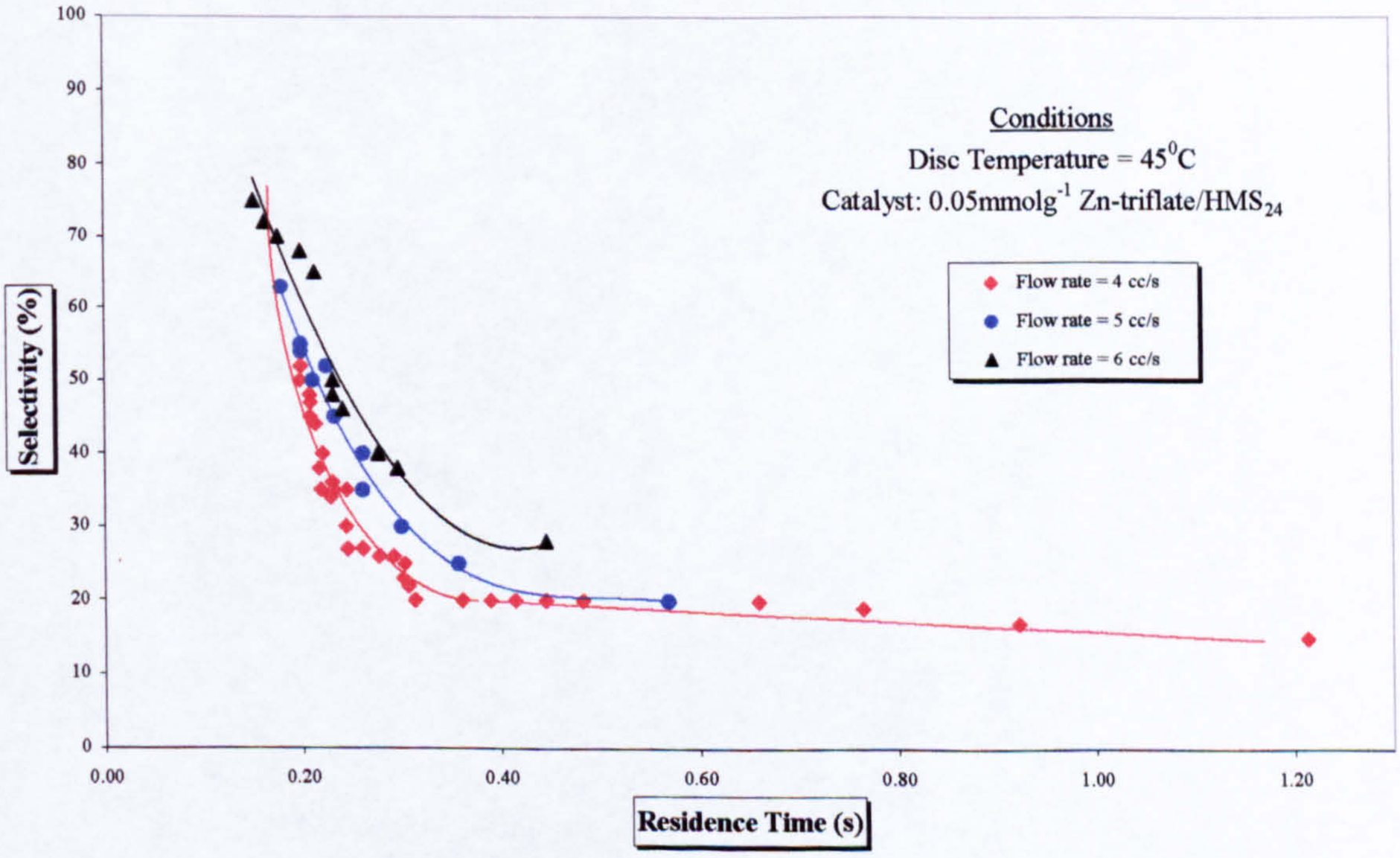


**Figure 8.25. Selectivity change with residence time**

For the fixed disc speed, changing the flow rates (for 800 rpm see Figure 8.26; for 1000 rpm see Figure 8.27) not much change in conversion was observed, but apparent selectivity increase can be noticed.

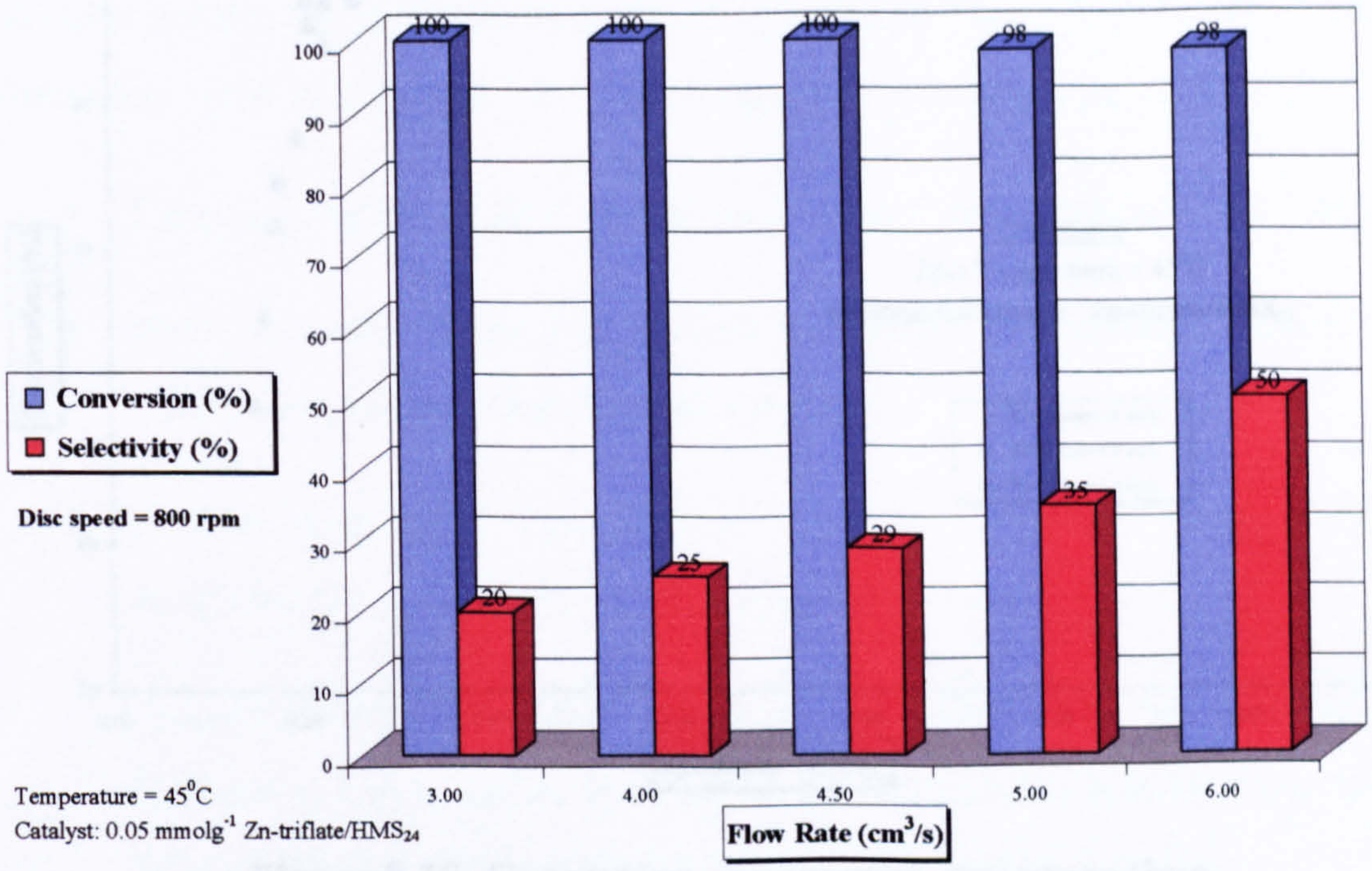


**Figure 8.26. Selectivity and conversion change with flow rate at 800 rpm**

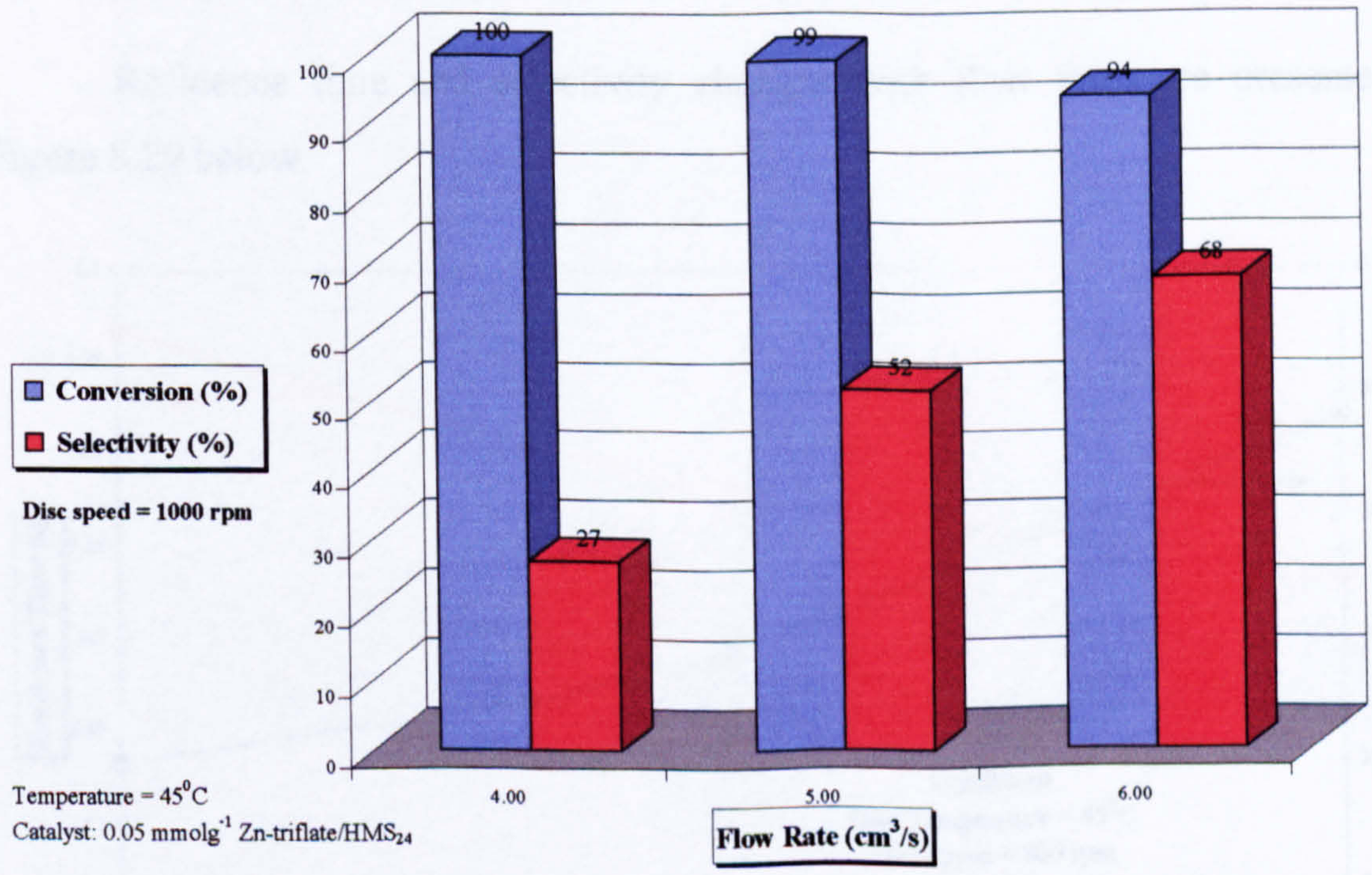


**Figure 8.27. Selectivity and conversion change with flow rate at 1000 rpm**

Therefore optimum flow rate for the third catalyst was the same as for the first one, 6 $cm^3/s$.

Figure 8.28 is showing conversion change with residence time for various flow rates.

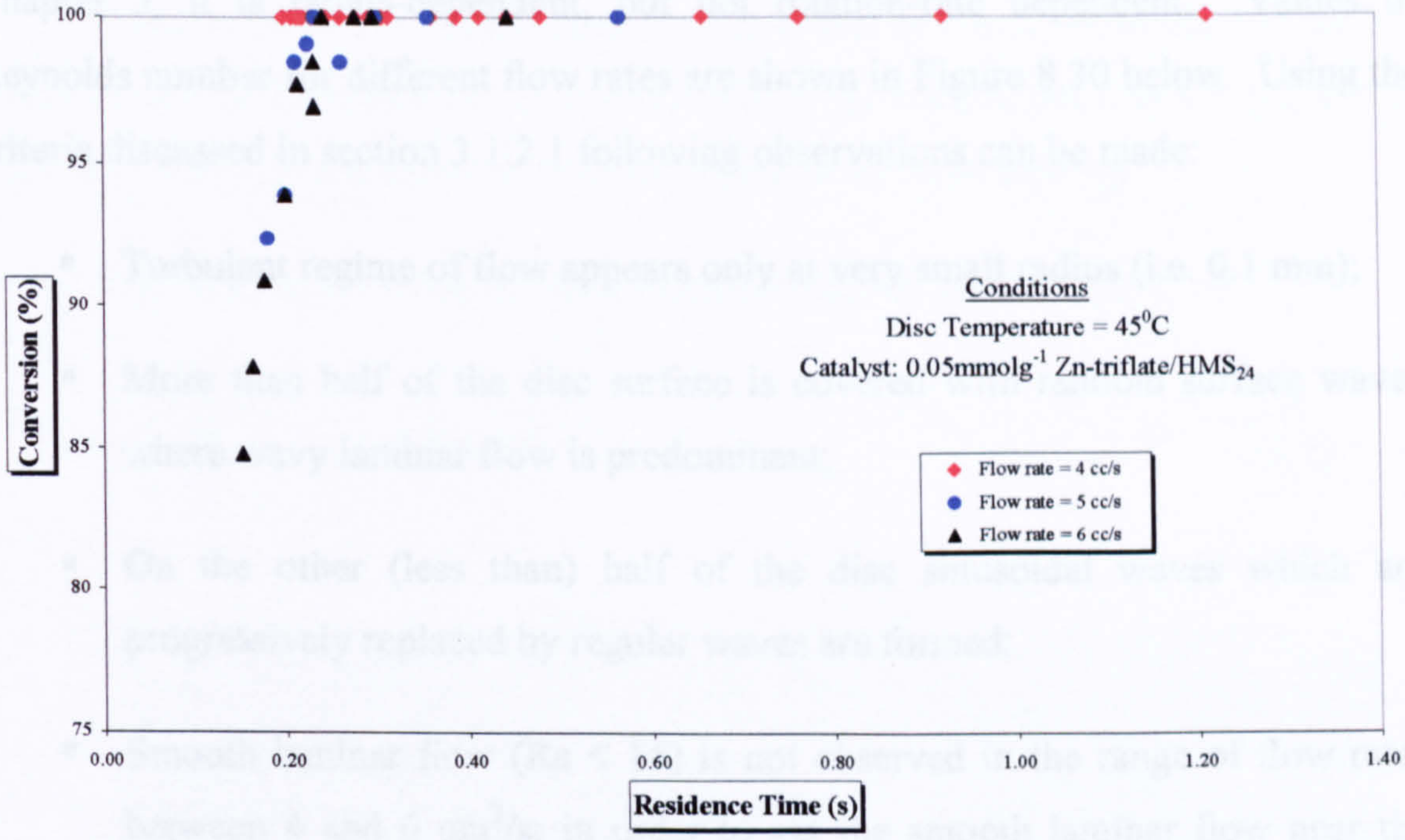


**Figure 8.28. Conversion change with residence time**

Residence time and selectivity changes with flow rates are presented in Figure 8.29 below.

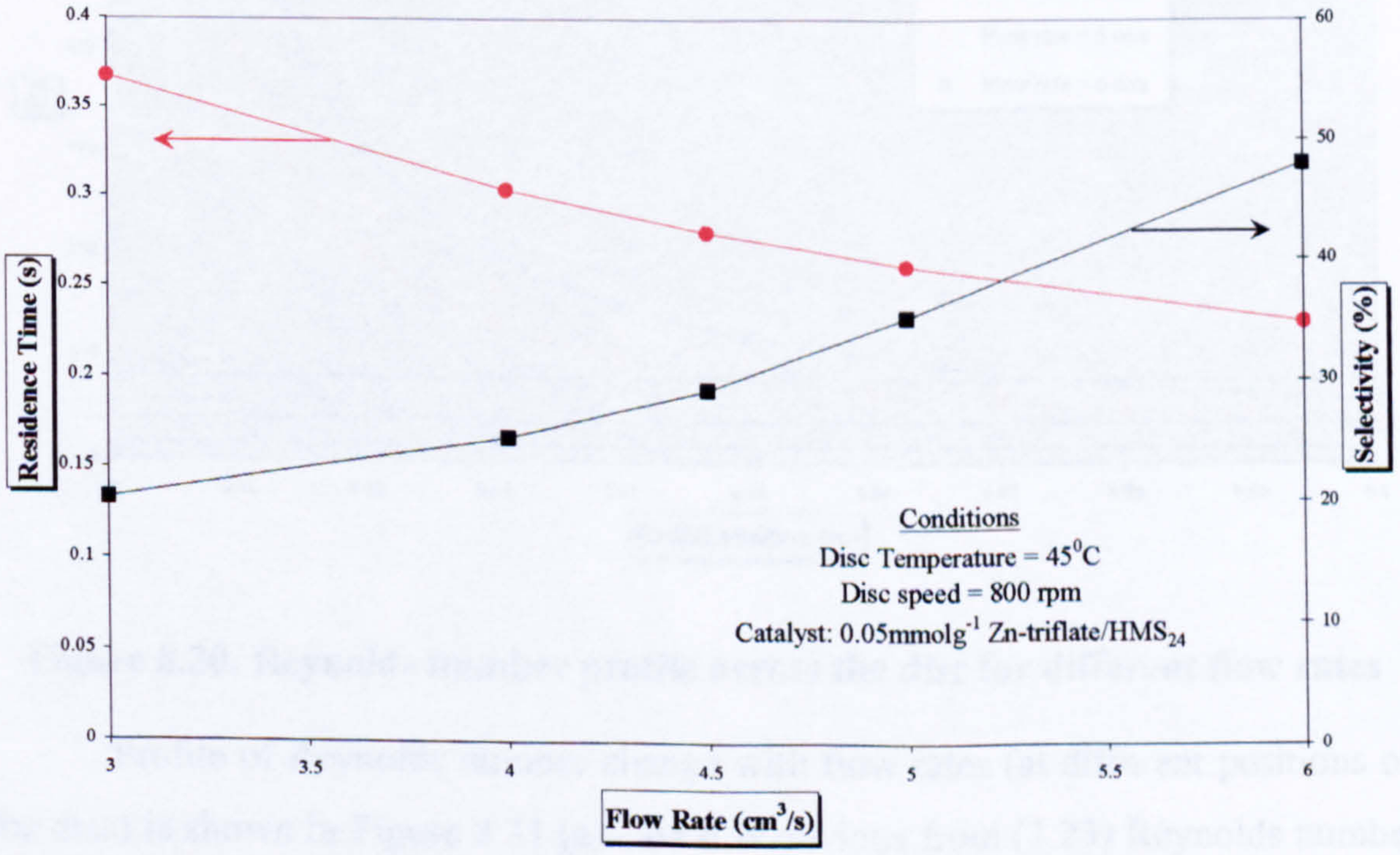


**Figure 8.29. Residence time and selectivity change with flow rates**

## 8.3 REYNOLDS NUMBER AND FLOW REGIMES

Reynolds number can be determined from the Equation (3.23). As said in Chapter 3, it is radius-dependent, but not rotation-rate dependent. Values of Reynolds number for different flow rates are shown in Figure 8.30 below. Using the criteria discussed in section 3.1.2.1 following observations can be made:

- Turbulent regime of flow appears only at very small radius (i.e. 0.1 mm);
- More than half of the disc surface is covered with random surface waves where wavy laminar flow is predominant;
- On the other (less than) half of the disc sinusoidal waves which are progressively replaced by regular waves are formed;
- Smooth laminar flow (Re < 16) is not observed in the range of flow rates between 4 and 6 $cm^3/s$; in order to get the smooth laminar flow near the edge of the disc, flow rate has to be in the region of 1.5 $cm^3/s$.

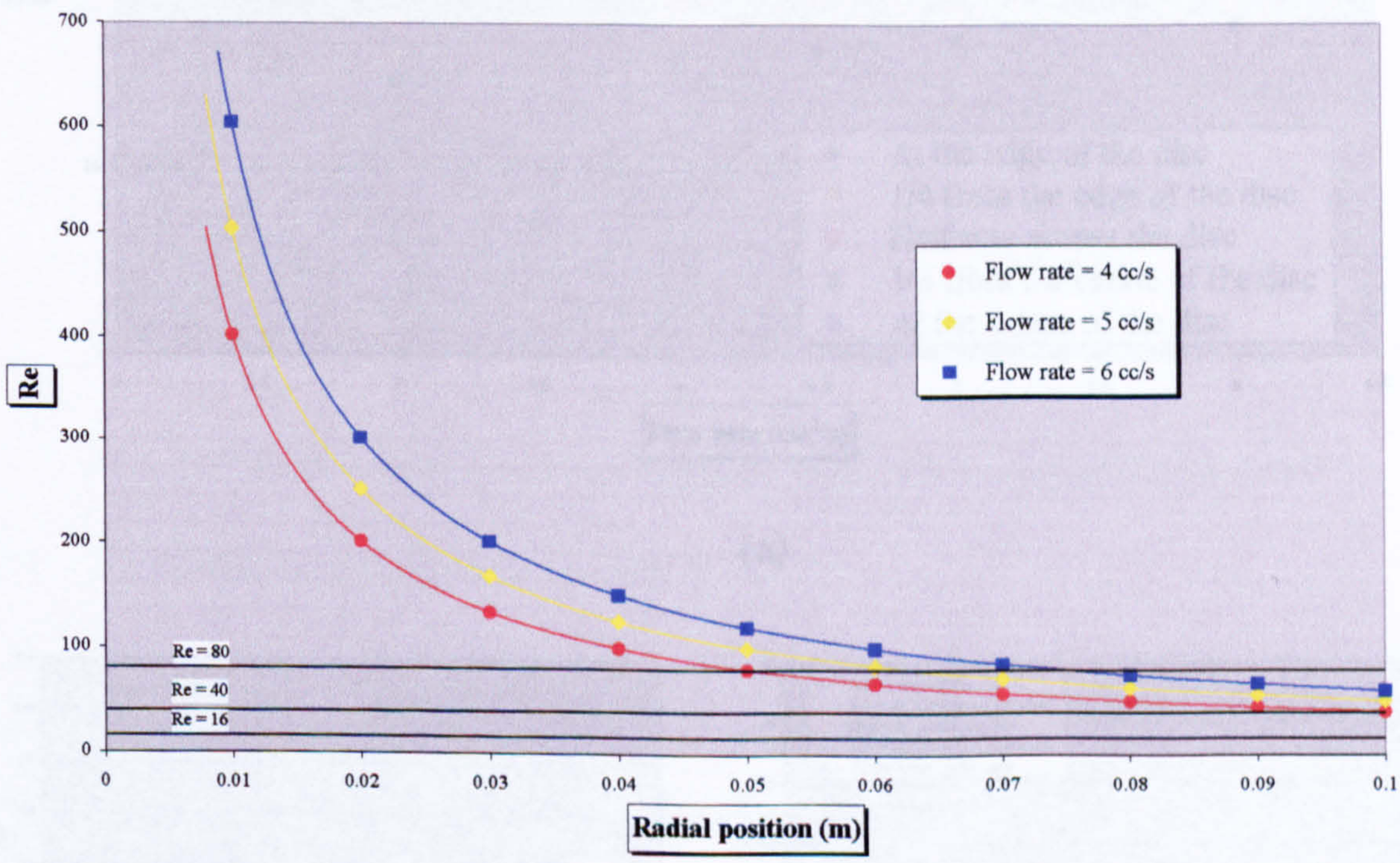


**Figure 8.30. Reynolds number profile across the disc for different flow rates**

Profile of Reynolds number change with flow rates (at different positions on the disc) is shown in Figure 8.31 (a). As it is obvious from (3.23) Reynolds number

is proportional with Q, therefore increase of Re is distinguished with the increase of the flow rate.

Reynolds number values increase more nearer to the centre of the disc, as it is evident from the Figures 8.31 (b) and (c) (where the scale is not logarithmic) and in the Figure 8.31 (c) (cut-scale, in order to see the trend more clearly).

Film thickness can be expressed using Reynolds number [167]:

$$\delta \left( \frac{r \omega^2}{\nu^2} \right)^{1/3} = 0.909 \, \mathrm{Re}^{1/3} \qquad (8.1)$$

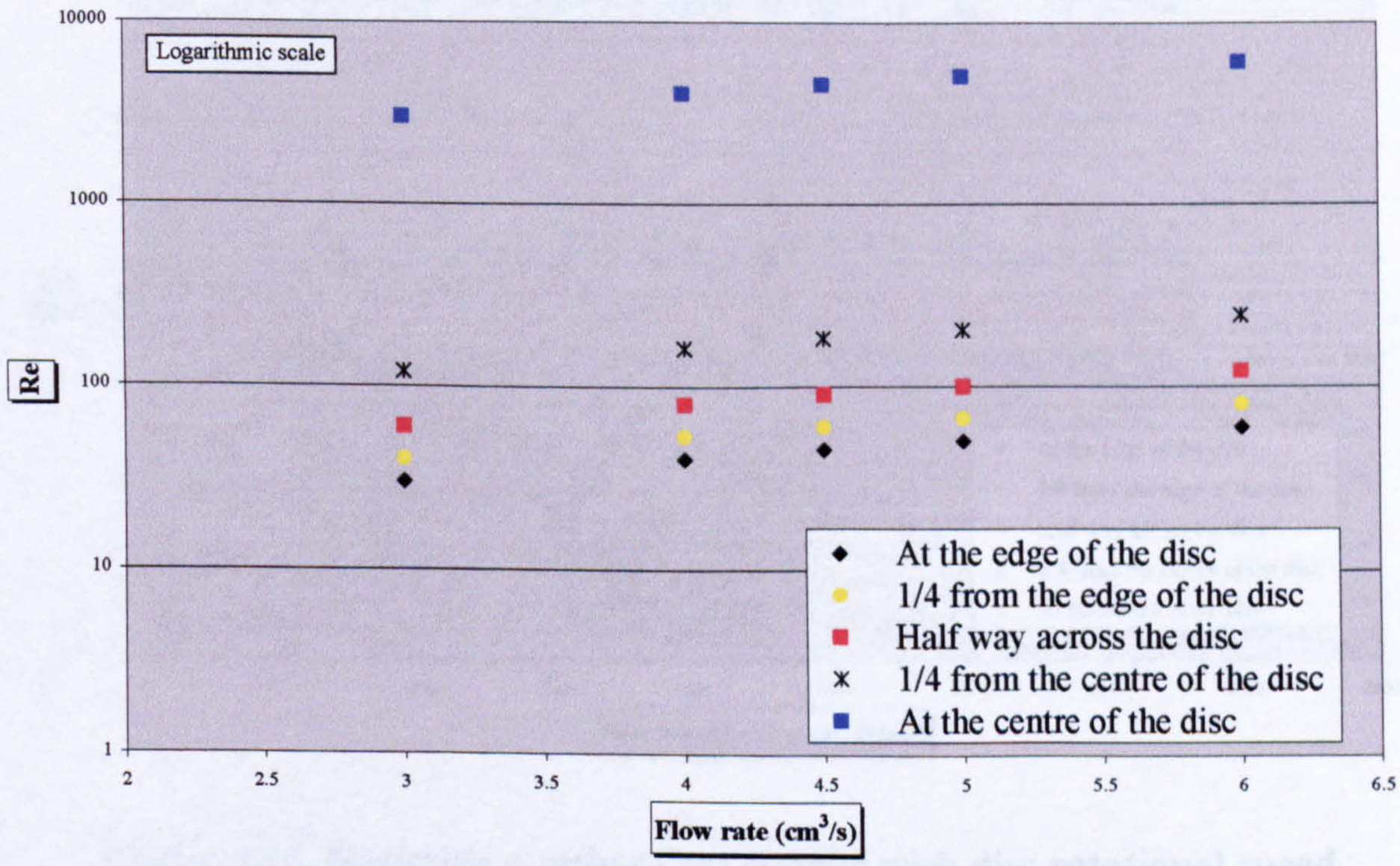


(a)

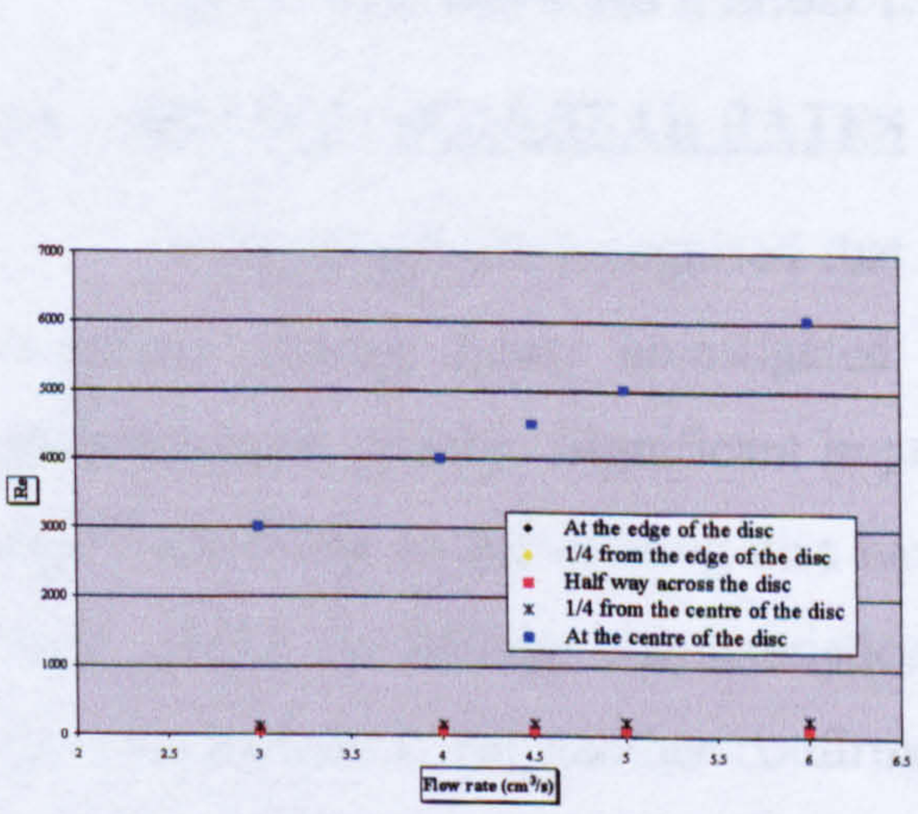


(b)

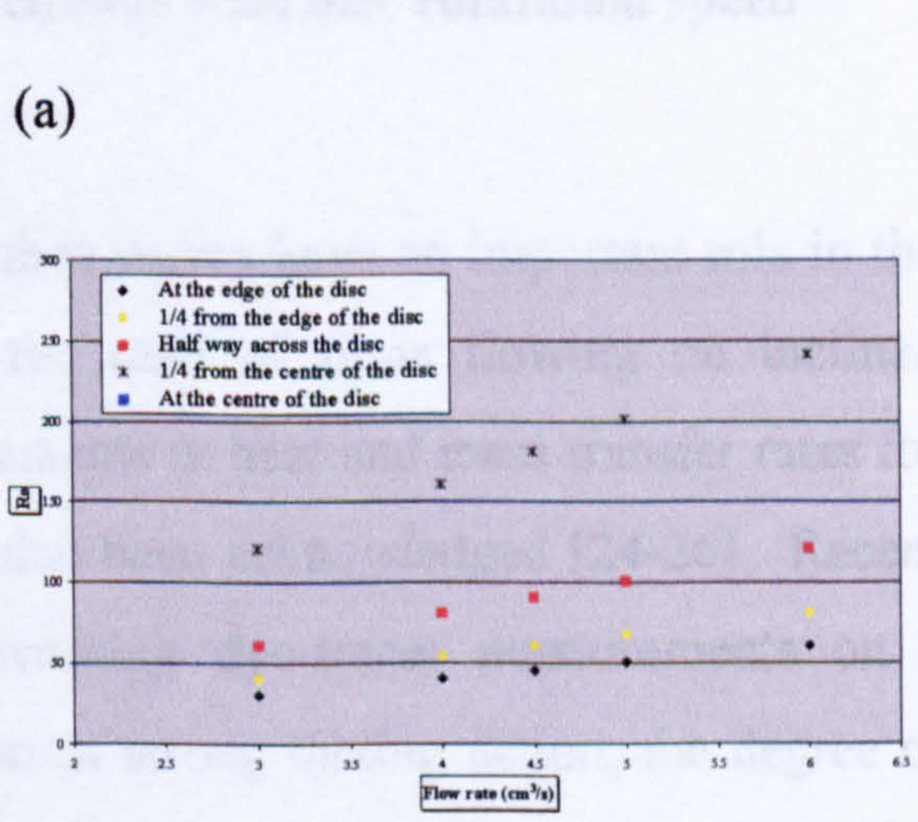


(c)

**Figure 8.31. Reynolds number change with flow rate at different positions**

As said, Reynolds number, hence wave formation, is independent of the disc rotational speed. Nevertheless, many researchers have found that the rate of rotation influenced the type of wave pattern (concentric, spiral or irregular waves) on the film surface, whilst Epsig and Hoyle [167] observed that a decline in the speed of rotation causes the amplitude of the wave to rise and vice versa. Woods [21] detected that increase of the rotational speed results in the surface waves appearing closer to the centre of the disc, hence occupying a larger area of the disc. However, using data from this study, no influence of rotational speed on Reynolds number is observed (Figure 8.32), since the viscosity of processed material did not vary noticeably.

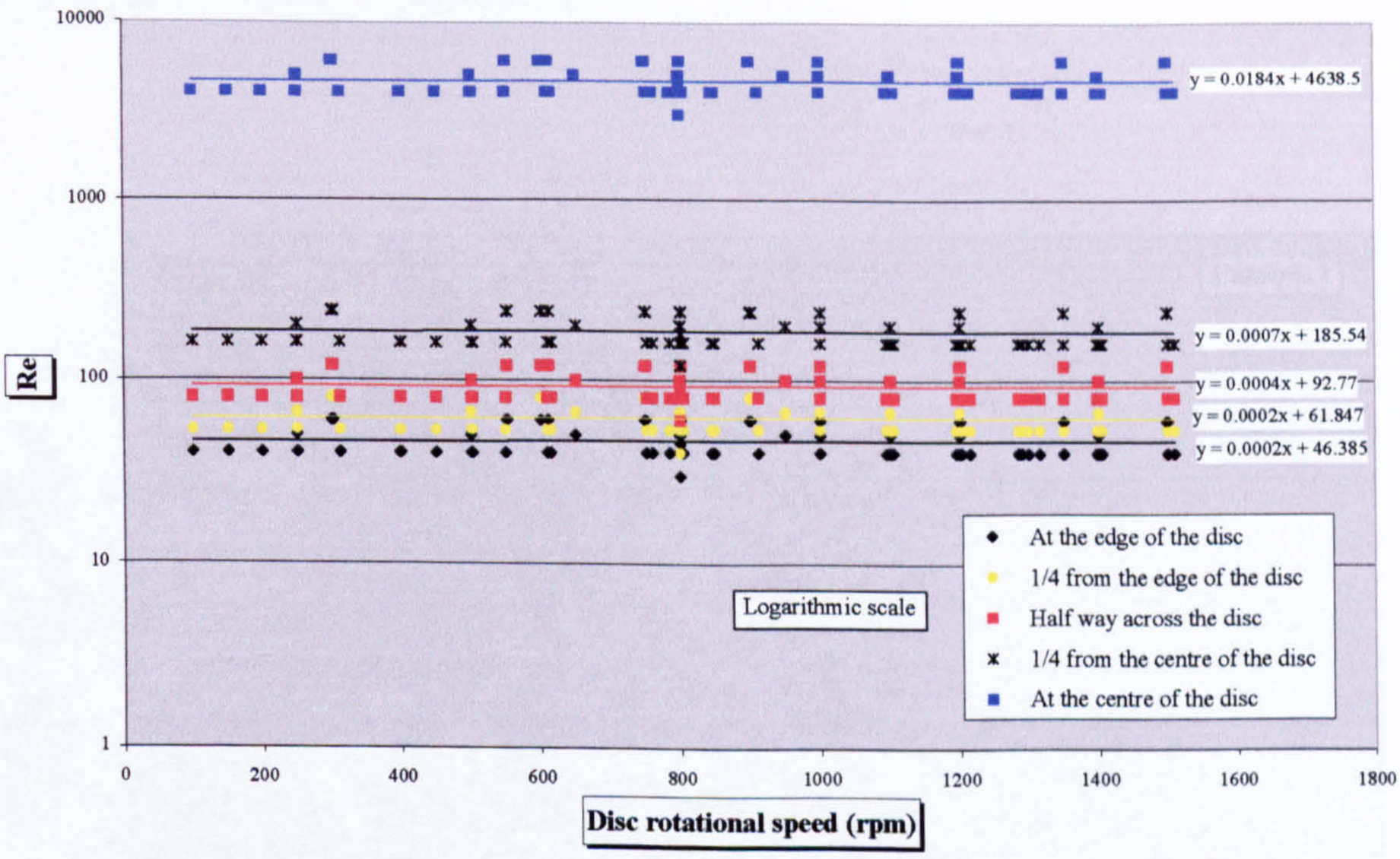


**Figure 8.32. Reynolds number (no) change with disc rotational speed**

## 8.4 MIXING AND SHEAR RATES

It has long been recognised that surface waves have an important role in the enhanced mixing, firstly investigated in the case of films flowing on inclined surfaces under gravity. Significant improvements in heat and mass transfer rates for thin liquid films on the rotating disc have also been acknowledged [24-26]. Recent study [168] on mixing characteristics involving dye-tracer measurements on a grooved surface is yet another confirmation of strong mixing action, the degree of which is predisposed by disc rotational speed, volumetric flow rate and radial position.

In the Appendix B shear rate profile across the disc for different rotation speeds (for the system used in this study) can be seen. In some cases shear rates as high as $7.5 \cdot 10^5$ $s^{-1}$ are calculated and it is noted that with current systems available in the Centre it would be very easy to increase the shear rate by one more order of magnitude.

Applied to the results achieved in the SDR for conversion and selectivity, it can be observed that there is an opposite effect of the observed shear rate on these parameters. Overall, higher conversion can be expected with decreasing shear rate. The effect of the shear rates on conversion can be seen in Figures 8.33, 8.35 and 8.37 for Catalysts 1, 2 and 3 respectively.

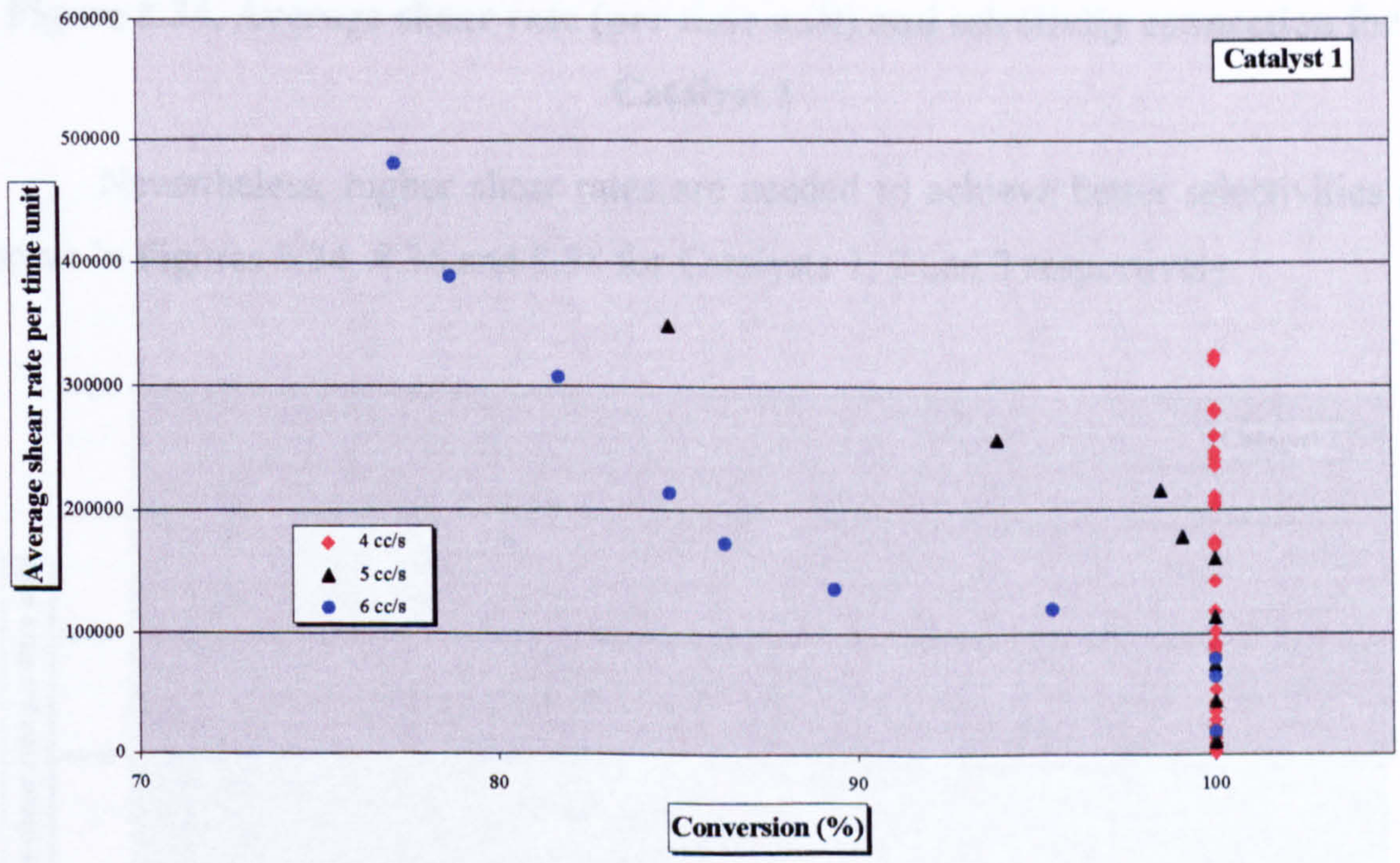


**Figure 8.33. Average shear rate (per time unit) and conversion connection for Catalyst 1**

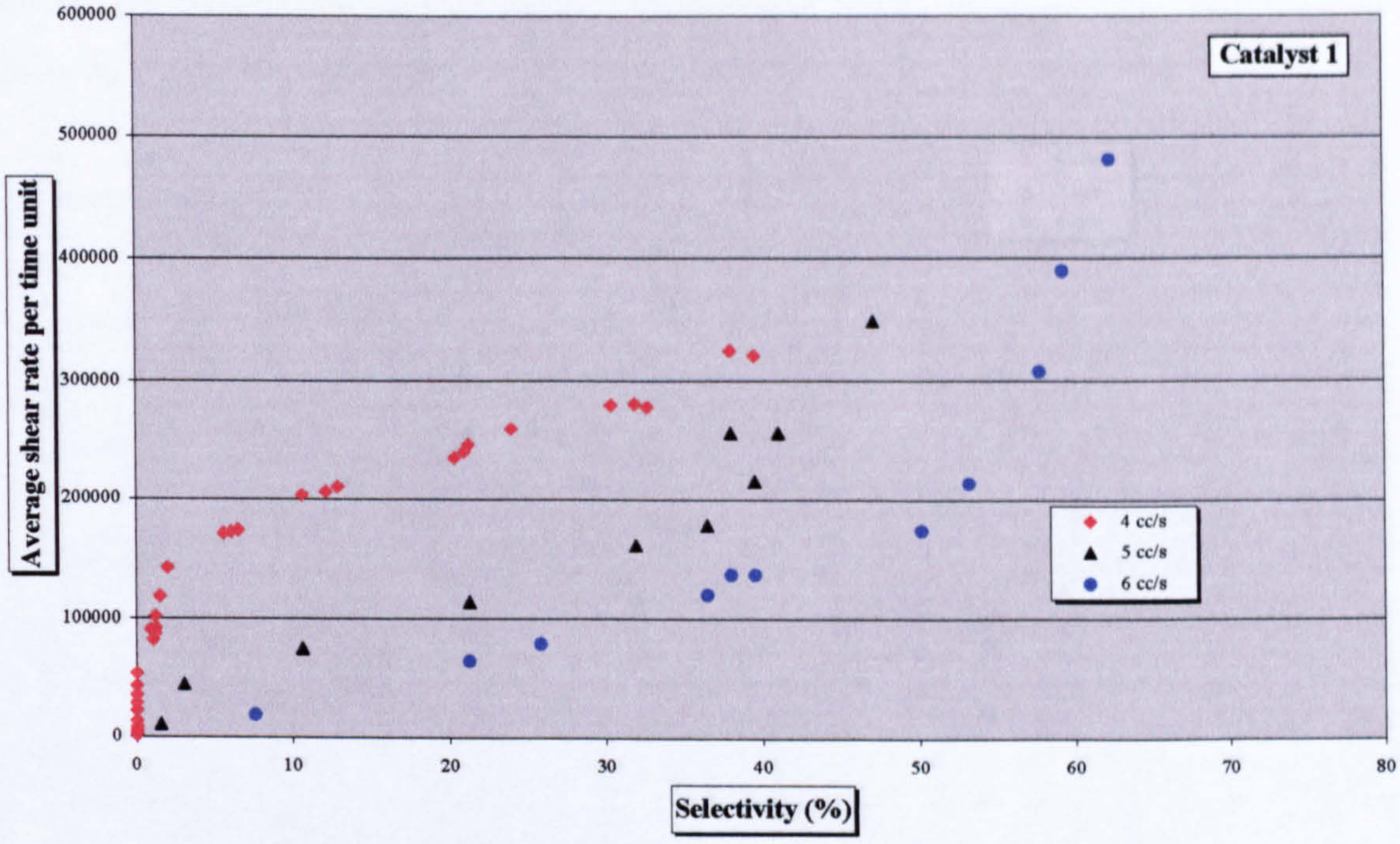


**Figure 8.34. Average shear rate (per time unit) and selectivity connection for Catalyst 1**

Nevertheless, higher shear rates are needed to achieve better selectivities as shown in Figures 8.34, 8.36 and 8.38 for Catalysts 1, 2 and 3 respectively.

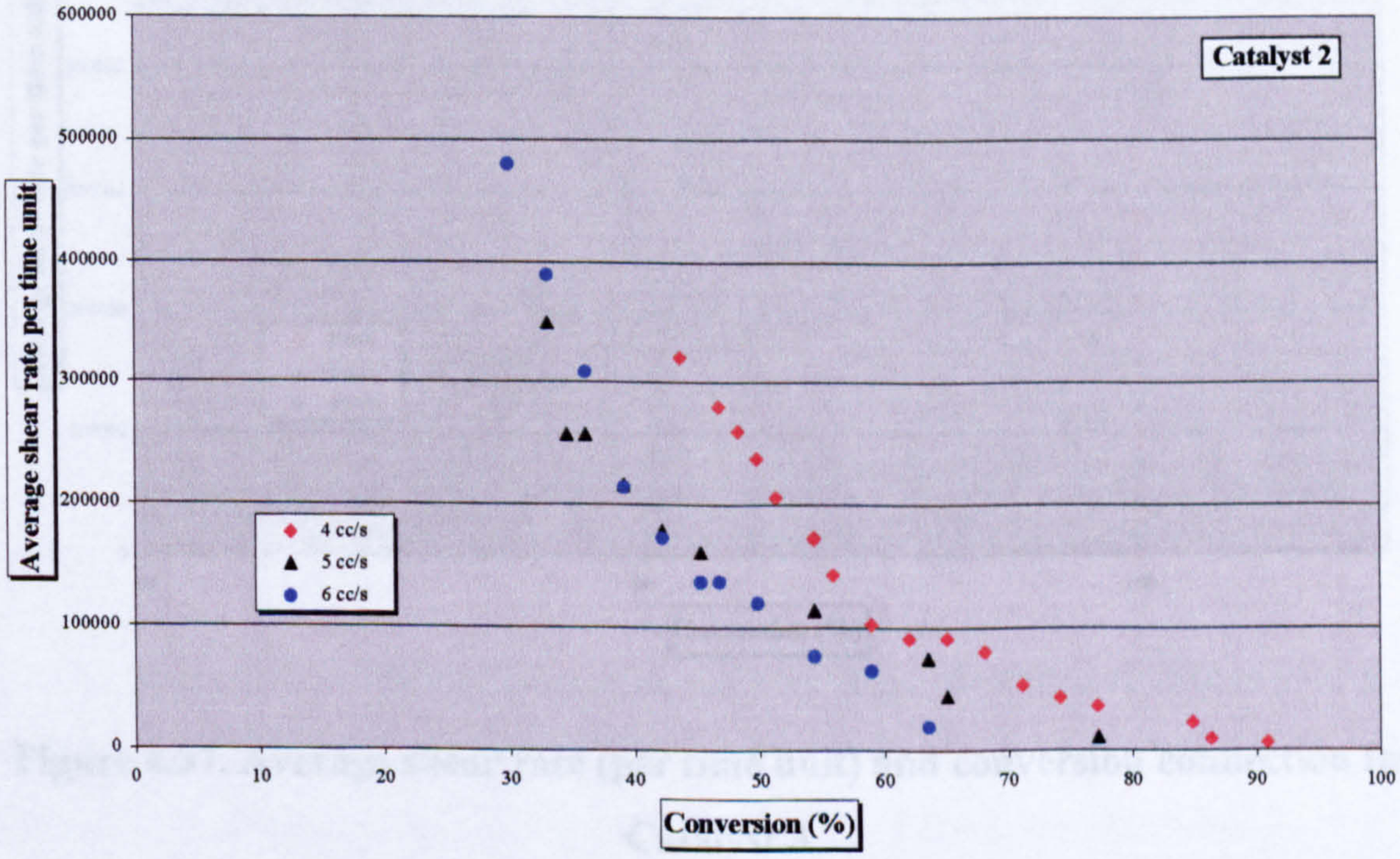


**Figure 8.35. Average shear rate (per time unit) and conversion connection for Catalyst 2**

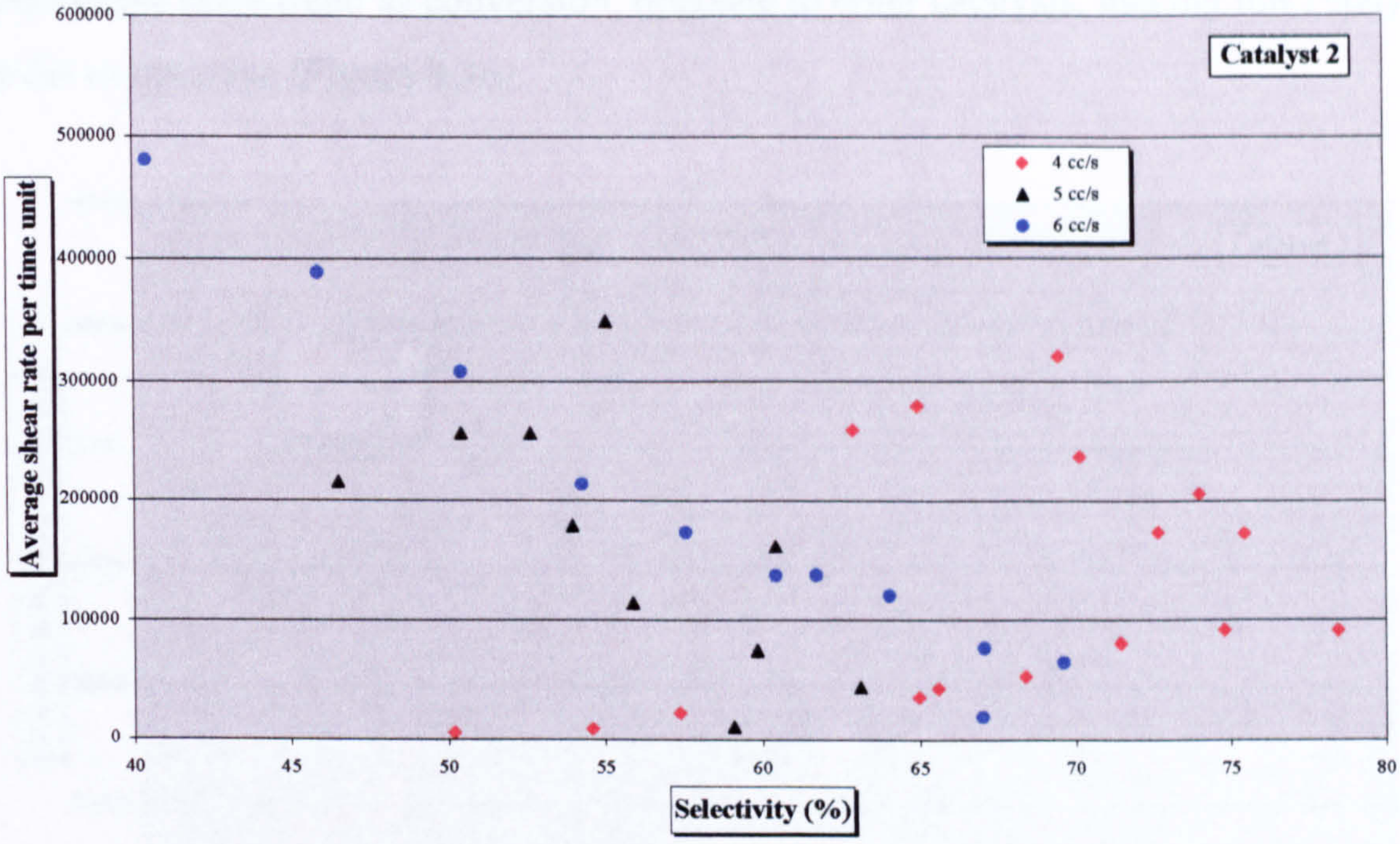


**Figure 8.36. Average shear rate (per time unit) and selectivity connection for Catalyst 2**

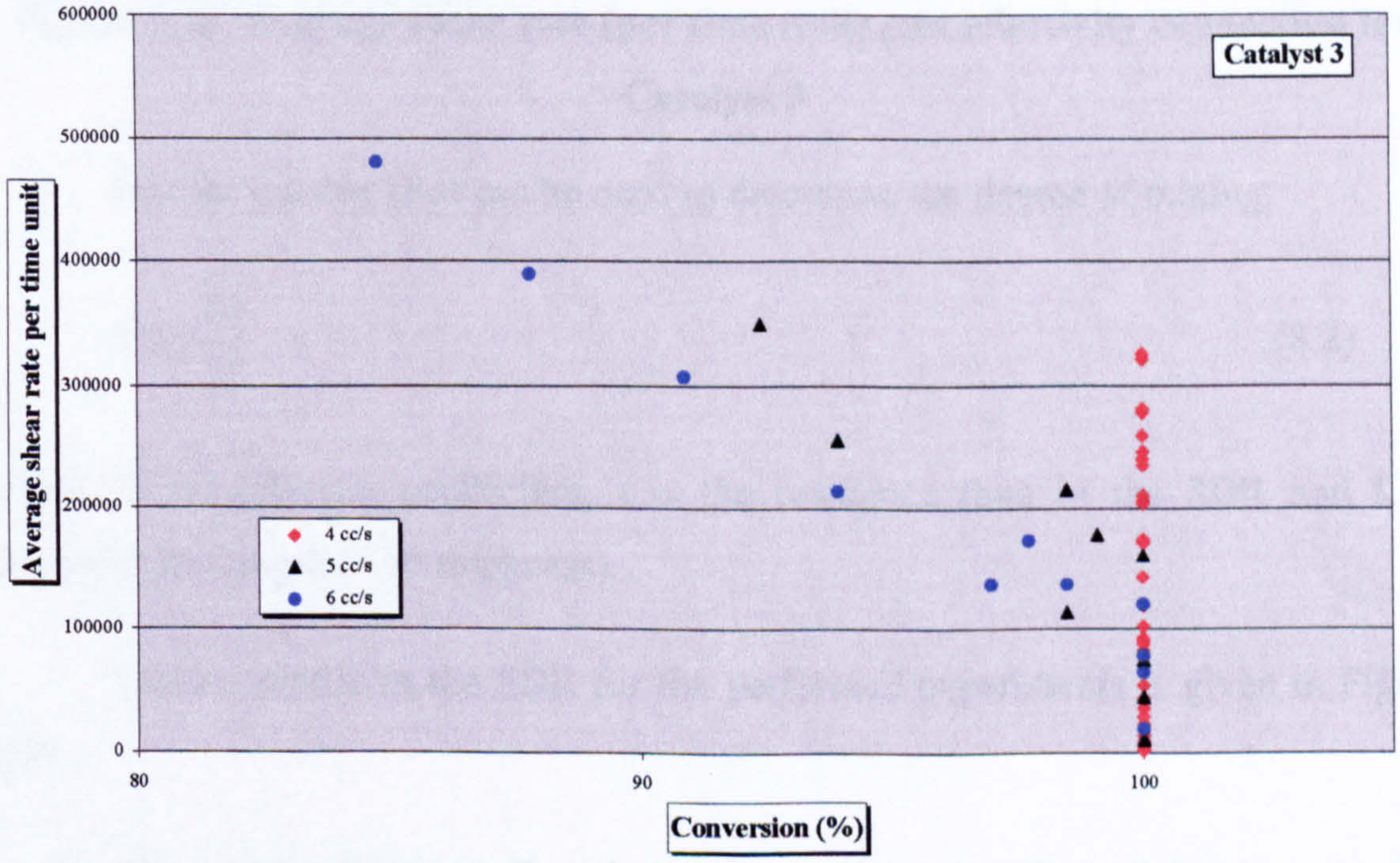


**Figure 8.37. Average shear rate (per time unit) and conversion connection for Catalyst 3**

This is partly true for Catalyst 2, as the conversion trend follows the above guidelines (Figure 8.35). Selectivity trend however, especially at higher flow rates,

follows the same trend as conversion, opposite to other catalysts, making this catalyst easier to optimise (Figure 8.36).

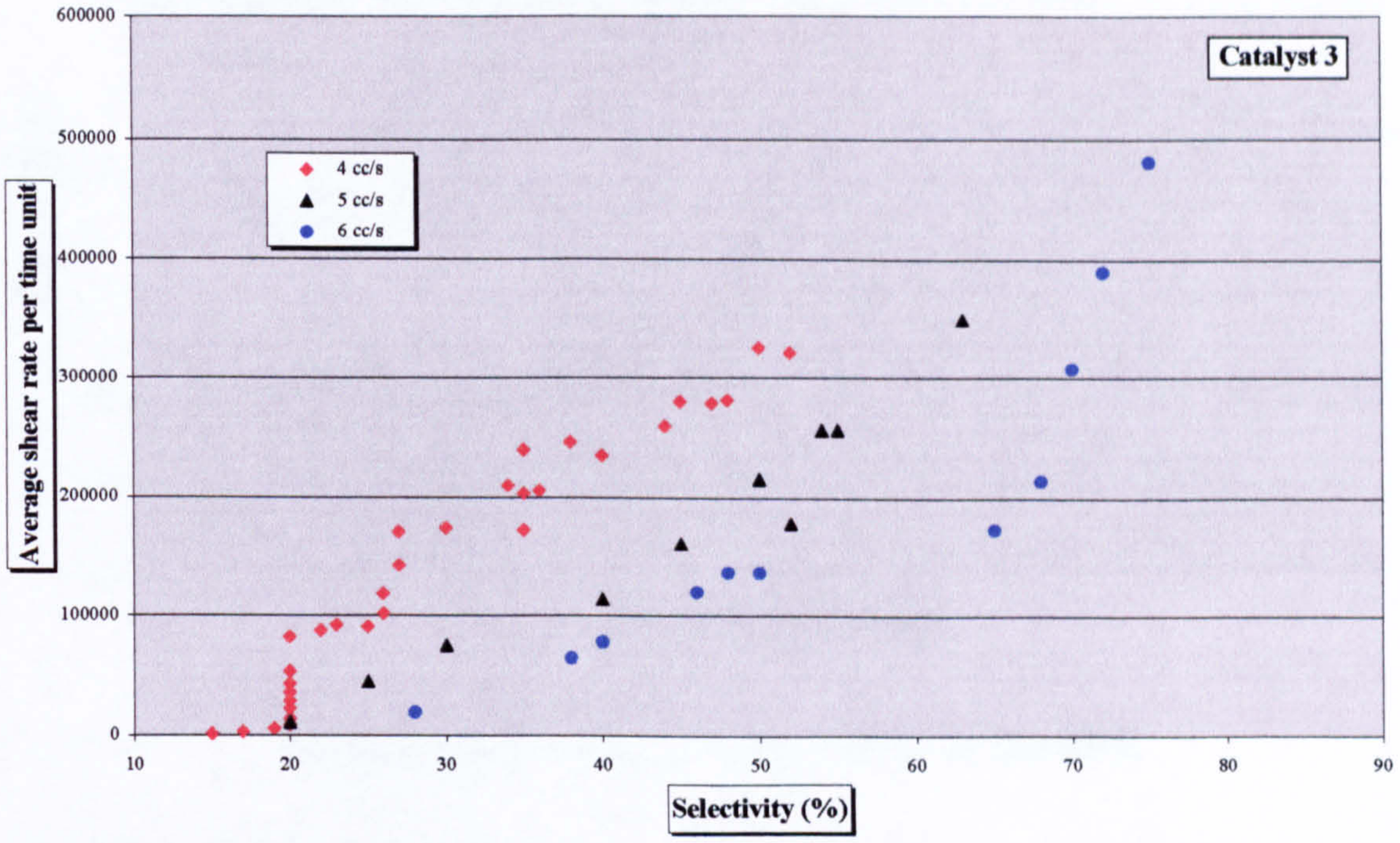


**Figure 8.38. Average shear rate (per time unit) and selectivity connection for Catalyst 3**

Fourier number (Fo) can be used to determine the degree of mixing:

$$Fo = \frac{Dt}{L^2} \tag{8.2}$$

where: D is diffusion coefficient, t is the residence time in the SDR and L is characteristic length (film thickness).

The Fo profile in the SDR for the performed experiments is given in Figure 8.39.

As it can be observed, Fo values are very high, therefore mixing is very good through the thin film – practically there is no gradient in a vertical direction. Minimum residence times on the disc can be found from the condition Fo = 1, in order to achieve good degree of mixing, but not to overdo it, as in this case of rearrangement reaction.

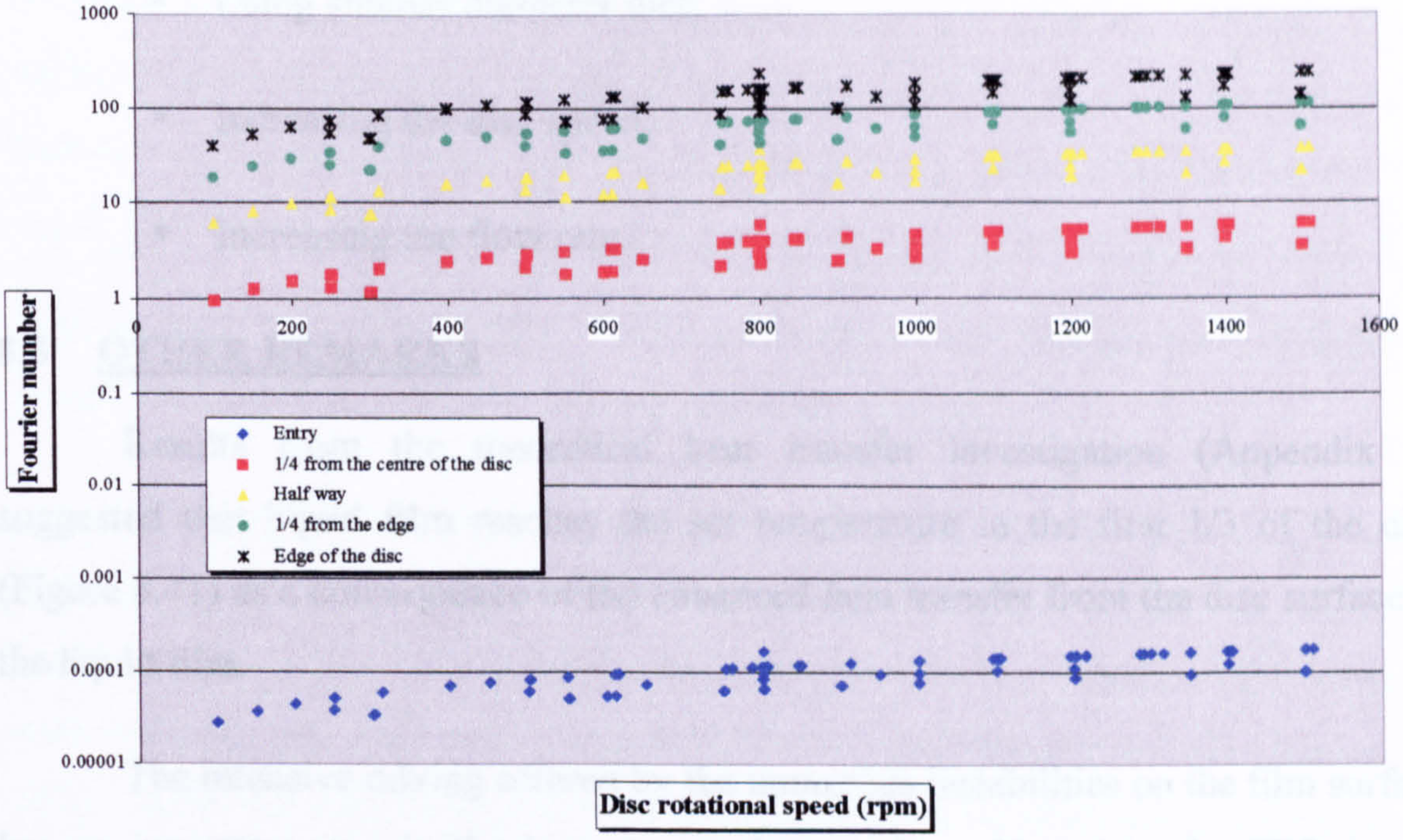


**Figure 8.39. Fourier number profile in the SDR**

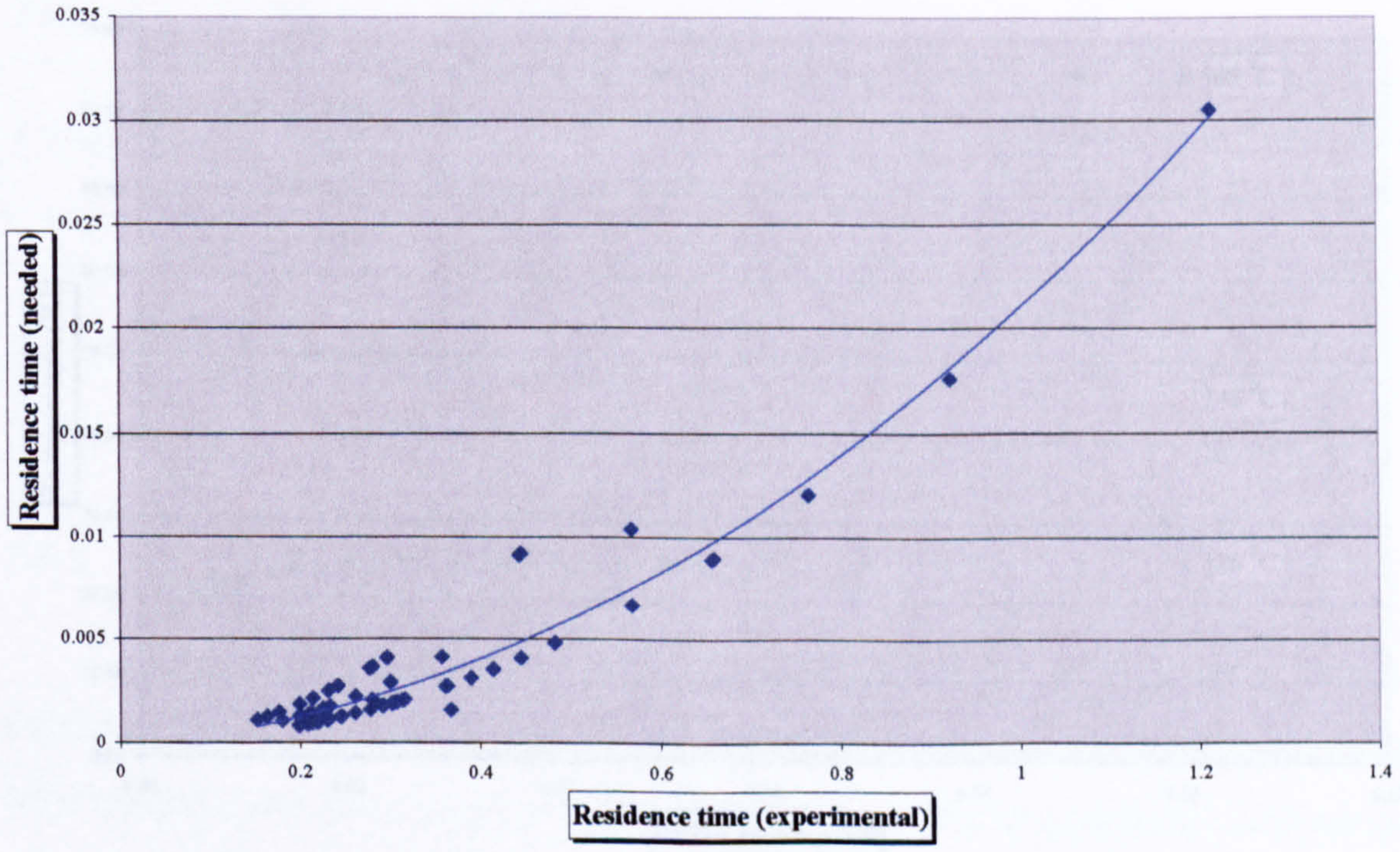


**Figure 8.40. Relation between residence times achieved in experiments and needed for better selectivity**

Relation between residence time achieved in experiments and residence time that would be needed for the above condition are given in Figure 8.40. It can be concluded that residence time needed to be much less than it was in order to stop the reaction. This can be done in many ways:

- Using smaller diameter disc;
- Increasing the disc speed;
- Increasing the flow rate.

## 8.5 OTHER REMARKS

Results from the theoretical heat transfer investigation (Appendix C) suggested that liquid film reaches the set temperature in the first 1/3 of the disc (Figure 8.41) as a consequence of the enhanced heat transfer from the disc surface to the liquid film.

The intensive mixing offered by the numerous instabilities on the film surface has an important part in the high conversion results achieved in the SDR in the rearrangement reaction of α-pinene oxide.

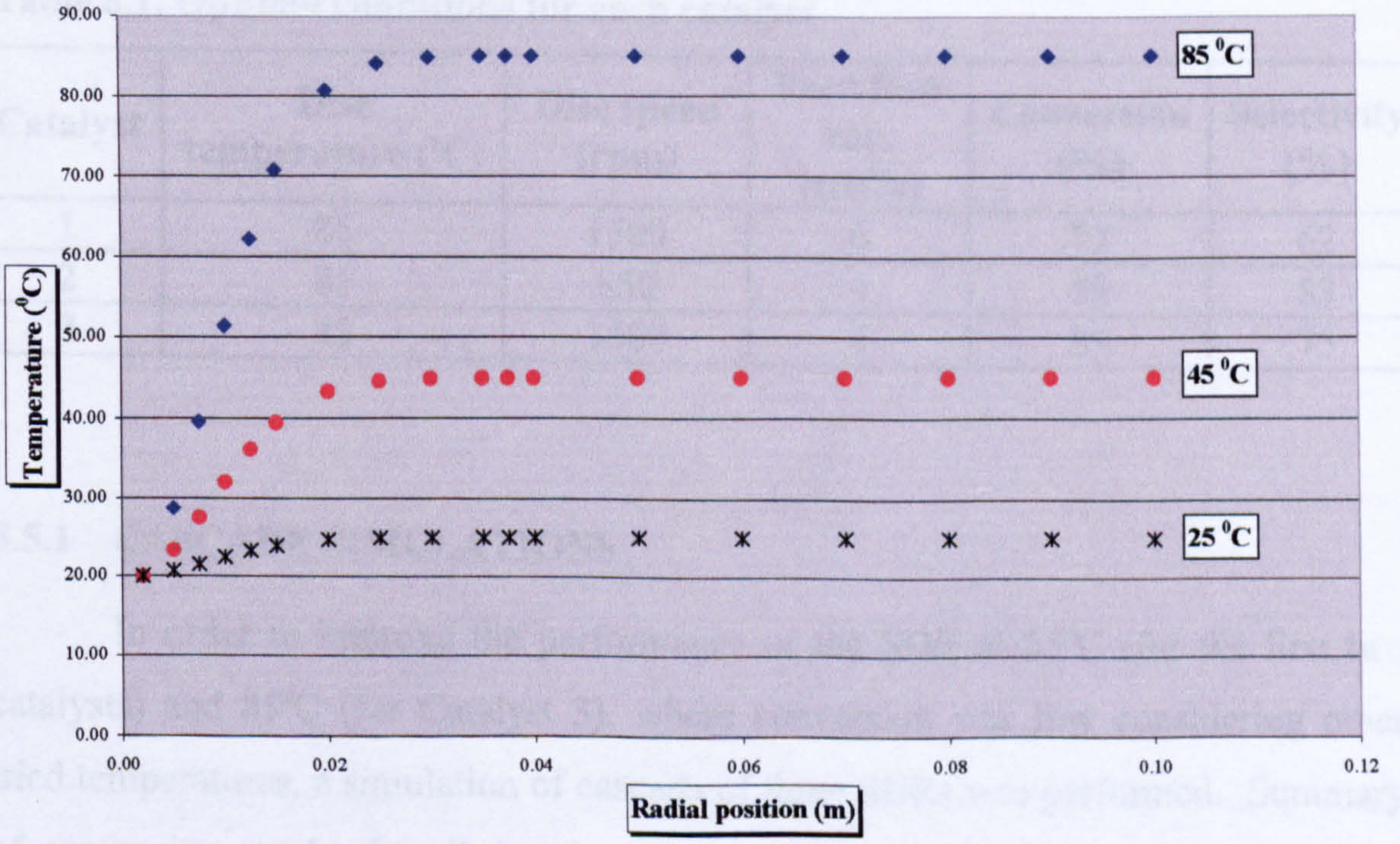


**Figure 8.41. Temperature profile on the disc surface (from Table C.1 in the Appendix C)**

An increase in temperature is used to speed up chemical reactions, but it can have an undesired effect when the reaction is reversible and exothermic, in which case equilibrium is reached quicker but with a reduced yield because the increased temperature moves the equilibrium to the left. Instead reaction rate can be increased

(without decreasing the yield) by using catalyst. In the Appendix A some valuable thermodynamic data were calculated in order to obtain the value for the heat of reaction, most importantly. It was shown that the reaction is exothermic with $\Delta H^0_{r,298}$ = -73.17 kJ/mol. Consequently equilibrium constant was calculated; the high value of it confirmed that reaction is *not* reversible (only the product is present at equilibrium) therefore only proceeds from left to right.

When compared to results achieved in the batch reactor, it was concluded that good mixing and excellent heat/mass transfer characteristics of the SDR [27] promoted the isomerisation much further than expected, initialising consecutive isomerisations and that was the only reason why selectivity was not even higher than 75%. Since this study was concerned about campholenic aldehyde as a product, the optimum SDR conditions to achieve maximum selectivity are presented in Table 8.1 below.

**Table 8.1. Optimal conditions for each catalyst**

| Catalyst | Disc temperature ($^0$C) | Disc speed (rpm) | Feed flow rate ($cm^3/s$) | Conversion (%) | Selectivity (%) |
|---|---|---|---|---|---|
| 1 | 85 | 1500 | 6 | 77 | 62 |
| 2 | 85 | 850 | 4 | 59 | 83 |
| 3 | 45 | 1500 | 6 | 85 | 75 |

### 8.5.1 CASCADE SIMULATIONS

In order to improve the performance of the SDR at 25$^0$C (for the first two catalysts) and 85$^0$C (for Catalyst 3), where conversion was low considering other tried temperatures, a simulation of cascade of three SDRs was performed. Summary of conversion results for all three catalysts can be seen in Figure 8.42. It can be observed that in all cases conversion improved 10–20% after each pass.

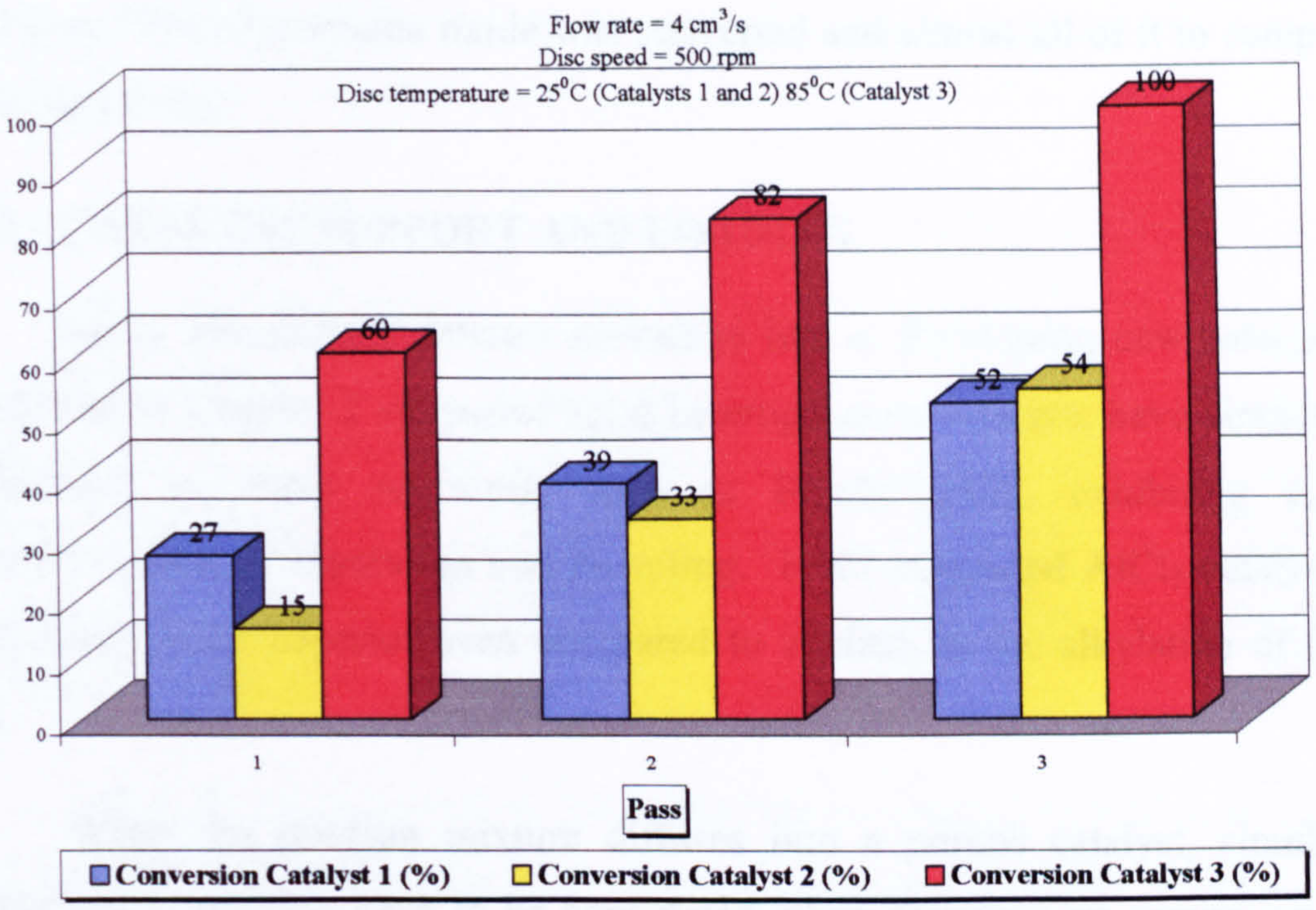


**Figure 8.42. Conversion change for all catalysts after three passes**

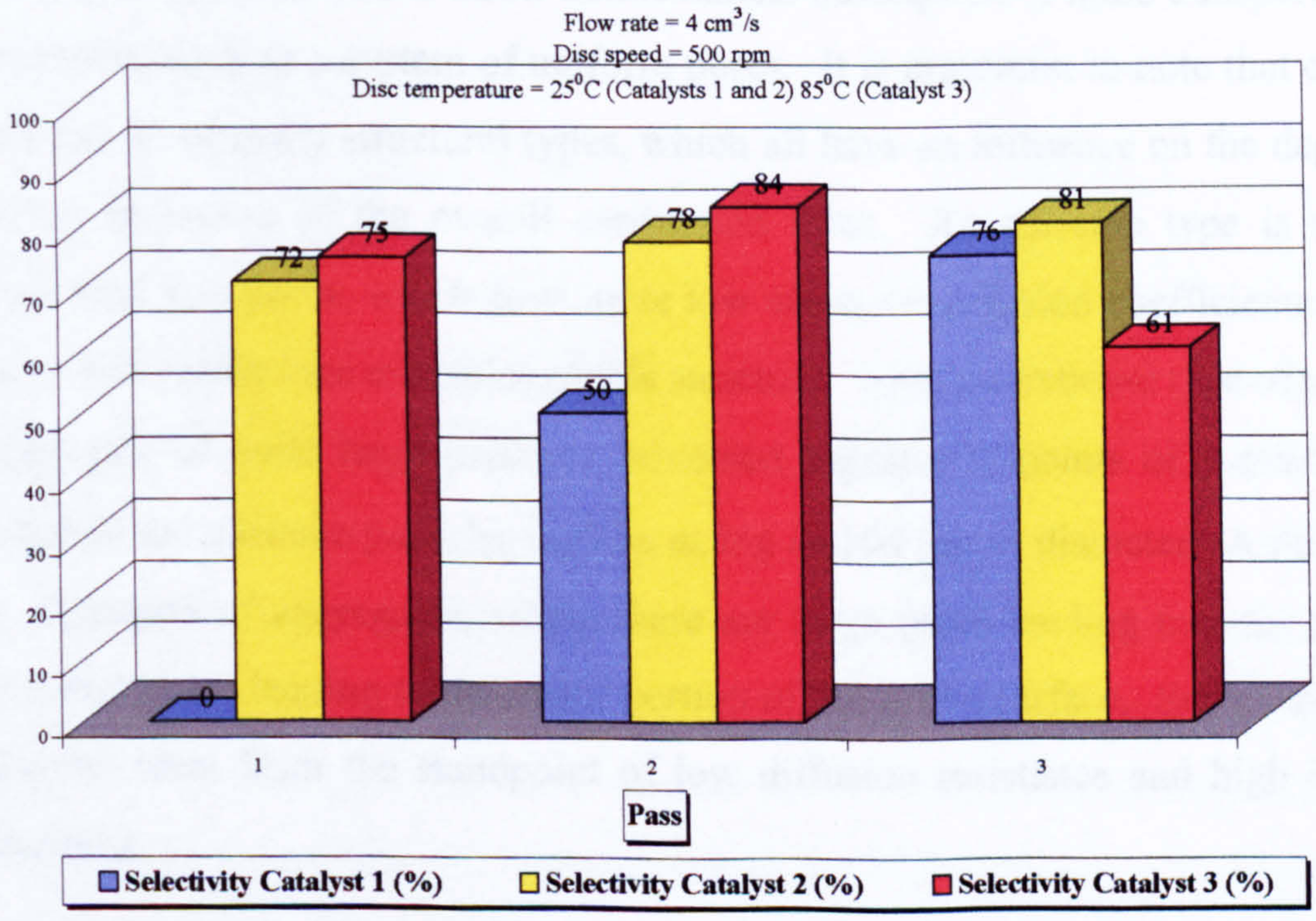


**Figure 8.43. Selectivity change for all catalysts after three passes**

Considering that residence time, if using a cascade of several discs, would not change dramatically (it would still be in order of seconds), improvements in both conversion and selectivity (Figure 8.43), are very significant. Especially in the cases where conversion was very low to begin with (e.g. for Catalyst 1, after first pass conversion was only 27% with no campholenic aldehyde in the product, but after the

third pass 52% of α-pinene oxide was converted and almost all of it to campholenic aldehyde (76%).

### 8.5.2 CATALYST SUPPORT AND LOADING

Many researchers' interest nowadays lies in developing new catalysts. As mentioned in Chapter 2 supported solid heterogeneous catalysts have already found application in many reactions, such as Friedel-Crafts, exhibiting enhanced selectivity, ease of separation and recycling. HMS supported $AlCl_3$ catalysts have been found to be superior even compared to zeolites in the alkylation of benzene [98].

When the reaction mixture diffuses into a porous catalyst, simultaneous reaction and diffusion have to be considered when obtaining an expression for the overall conversion rate. The pore system is normally some kind of complex maze and must be approximated to allow mathematical description of mass transport inside the particles, such as a system of uniform pores. It is important to note that catalyst pellets can be of many structural types, which all have an influence on the degree of diffusion limitation of the overall conversion rates. An extreme type is the gel catalyst with tiny pores, which have quite low effective diffusion coefficients: silica, alumina and zeolites are examples of this structure. Another extreme type of pellet is an aggregate of quite large particles cemented together at points of contact. The channels in the ultimate particles may be as big as 100 μm in diameter. A third type is an aggregate of aggregates, where there are large pores leading into the interior and smaller pores leading to the major portion of the active surface. Such a structure is close to ideal from the standpoint of low diffusion resistance and high internal surface area.

Characterisation of all catalysts used in this study has been performed by the collaborators at the University of York and the results can be seen in [112]. SEM images of all the supported catalysts used in this investigation are presented in Figure I.1 in the Appendix I. Different types of silica were used as a catalyst support, the main difference between them being the size of the pores. $HMS_{24}$ (Figure I.1 e and f) has the more regular pore structure, therefore diffusion rates of the reactants and

products is enhanced. This was confirmed in the SDR as well, since the catalyst with this support (Catalyst 3) performed the best.

It was also noticed that the loading of the catalyst has significant influence on the reaction. Higher loadings of the catalyst (e.g. 2 mmol/g – 7.5 wt% Zn) result in a very fast (batch) reaction, finished in less than 30 seconds [112]. Lower loadings however (e.g. 0.05 or 0.01 mmol/g) result in reaction times of around 60 minutes. For this study, lower catalyst loadings were chosen in order to completely see advantages and potential of the SDR technology as well as for better understanding of the time savings and improvements in the SDR.

Catalysts 1 and 3 used in this study had the loading of 0.05 mmol/g, whilst Catalyst 2 had the loading of 0.01 mmol/g. This could explain slightly different behaviour of Catalyst 2 in the SDR and somewhat inferior performance compared to other two catalysts.

## 8.6 SDR MODEL EQUATIONS

All the data obtained in the spinning disc were converted into a model equation which connects achieved conversion, $x_A$, with the disc parameters (rotational speed, disc temperature and feed flow rate). For each catalyst, parameters I, a, b and c were found (equation 6.11) and the model equations obtained (Equations 6.13-6.15 in Chapter 6).

It is notable for all three catalysts that conversion is highly dependent on temperature, more significantly for catalysts 1 and 2 where small temperature change can increase conversion much more than in case of reactions involving Catalyst 3. The reactant flow rate has the opposite effect; the higher throughput reduces final conversion, apart from Catalyst 3 where flow rate does not have as significant effect. The effect of disc rotational speed is the least significant factor and it does not influence reaction as much as the other two variables, especially for Catalysts 1 and 3. For Catalyst 2 disc rotational speed is a significant factor and it can be expected to obtain higher conversions at lower speeds.

When the model equations (6.13) - (6.15) were tested using experimental data it was seen that all three empirical models can be used to predict conversion very

well (all theoretical values were almost the same values as experimental, see Chapter 6).

The model equations were developed under the following conditions:

$$150 \leq N \leq 1500$$

$$25^{o}C \leq T \leq 85^{o}C$$

$$3\ cm^3/s \leq Q \leq 6\ cm^3/s.$$

## 8.7 PROCESS ADVANTAGES

In this section a comparison between batch and SDR processes will be made and advantages of using new technology pointed out.

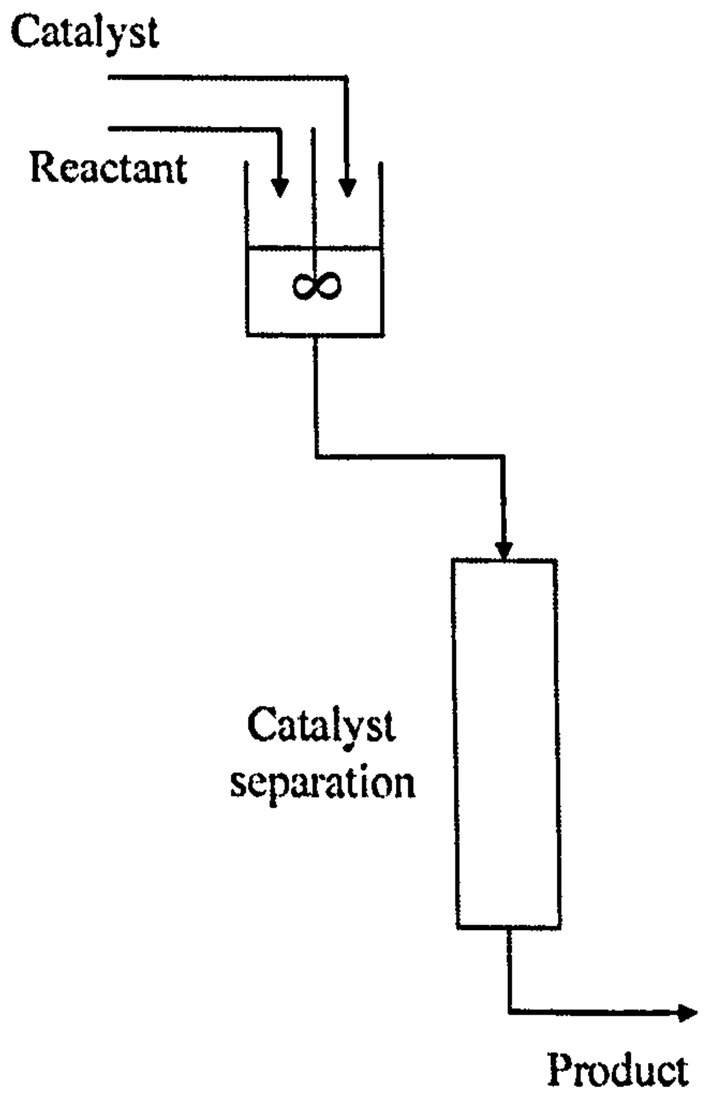


**Figure 8.44. Schematic of the Batch Process**

In a batch reactor, both catalyst and reactant are mixed and processed. Times may vary, depending on conditions, but are usually in order of 30-60 minutes for this particular reaction. After the reaction is finished, the catalyst and solvent have to be removed from the mixture in order to get clean product (Figure 8.44). This is not the case for the process carried out in the spinning disc. Not only that reaction times are very low (in order of seconds, rather than hours), but there is no need for the separation process to be completed, since there is no catalyst in the product mixture

(Schematic in Figure 8.45) and the process is fully continuous which is a huge advantage of its own.

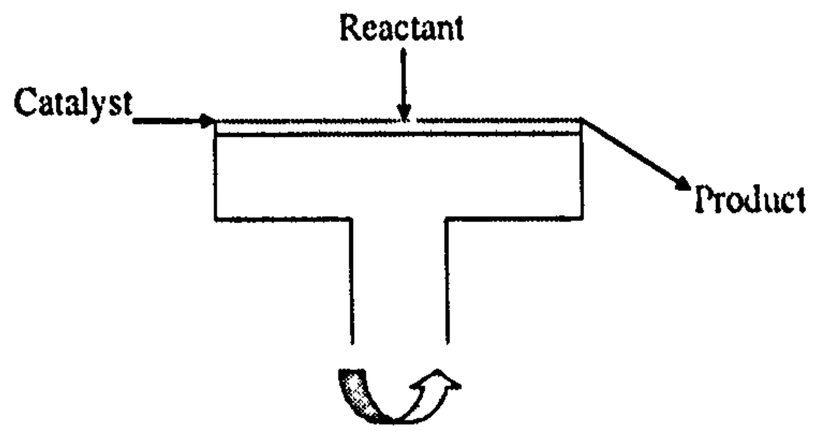


**Figure 8.45. Schematic of the Spinning Disc Process**

Comparison Table 8.2 demonstrates the advantages of using Spinning Disc Technology. There is an apparent difference between processed feed per hour in a batch and SDR (by order of magnitude). SDR had competitive conversion and selectivity, not as high as in a batch reactor in every experiment, but together with all the other benefits the process is just too good to be dismissed.

**Table 8.2. Comparison between Batch and Spinning Disc Reactor**

| | **Batch Process[3]** | **SDR Process[4]** |
|---|---|---|
| **Processed Feed (g/h)** | 12 | $2.16 \cdot 10^2$ |
| **Conversion (%)** | 56 | 85 |
| **Selectivity (%)** | 82 | 75 |
| **Additional Notes** | Catalyst separation | No loss of catalyst<br>Continuous process |

[3] Based on a process at 45°C with 0.05 mmol/g Zn-triflate/$HMS_{24}$

[4] Based on a process at 45°C, feed flow rate of 6 $cm^3/s$ and disc rotational speed of 1500 rpm with 0.05 mmol/g Zn-triflate/$HMS_{24}$ as a catalyst

The use of spinning disc surfaces at a commercial level may be associated with several other important benefits. It is envisaged that exceptionally good heat transfer characteristics that can be achieved on the rotating disc will allow the use of much smaller discs, hence in case of isomerisation reaction described here it will be possible to achieve even better selectivities. Furthermore, as the process described will be operated under continuous mode with reaction times drastically reduced, the amount of inventory in the reactor at any given time will be small and as a result the intrinsic safety of the process will be improved. This applies to all processes carried out in the spinning disc reactors.

## 8.8 PROCESS ECONOMICS

It is important to consider the economic viability of a catalyst and catalytic process early in the selection process. The economics of using a supported catalyst depend on catalyst turnover number, i.e. the amount of product produced per amount of catalyst used, and on catalytic activity or turnovers per unit time. For supported catalysts it is often convenient to calculate costs in terms of the weight of product produced per weight of catalyst used, or catalyst productivity. Catalyst productivity, *P*, is defined as:

$$P=\frac{n\sigma_P}{W} \tag{8.3}$$

where $n$ is the number of times a catalyst is used, $\sigma_P$ is reaction selectivity as a weight percent (weight of desired product produced per weight of feedstock), and W is catalyst loading as a weight percent (weight of catalyst used per weight of feedstock). The cost of the catalyst per unit weight of product can be determined by dividing the total cost of the catalyst by the catalyst productivity.

Catalysts used in this study are highly active, exhibiting turnover numbers (TON) of 3000 or more.

## 8.9 BATCH KINETIC RESULTS

The rate of reaction of reactant (A) on a porous catalyst particle may depend on:

(1) Surface kinetics, or what happens at the surfaces, interior or exterior of the particle. This may involve the adsorption of reactant A onto the surface, reaction on the surface, or desorption of product.

(2) Pore diffusion resistance which may cause the interior of the particle to be starved for reactant.

(3) Particle $\Delta T$ or temperature gradients within the particle. This is caused by large heat release or absorption during reaction.

(4) Film ΔT between the outer surface of the particle and the main stream. For example, the particle may be uniform in temperature throughout but hotter than surrounding.

(5) Film diffusion resistance or concentration gradients across the film surrounding the particle.

For gas/porous catalyst systems slow reactions are influenced by (1) alone, in faster reactions (2) intrudes to slow the rate, then (3) and/or (4), but (5) unlikely limits the overall rate. In liquid systems the order in which these effects intrude is (1), (2), (5), and very rarely (3) and/or (4). Different combinations of these five factors can be seen in Table 8.3 for different applications.

**Table 8.3. Factors which influence the rate of reaction of particles [85]**

| Rate influencing factor | Porous catalyst particle | Catalyst coated surface | Burning of a droplet of fluid | Cells and simple living creatures |
|---|---|---|---|---|
| Surface reaction | Yes | Yes | No | Yes |
| Pore diffusion | Yes | No | No | Maybe |
| Particle ΔT | Not too likely | No | No | No |
| Film ΔT | Sometimes | Rare | All important | No |
| Film mass transfer | No | Yes | All important | Could be |

These are all the possible factors which can affect the rate, however in majority of situations with porous catalyst particles only factors (1) and (2) are considered.

### 8.9.1 THE RATE EQUATION FOR SURFACE KINETICS

Since catalytic reactions have great importance in the industrial application, considerable effort has been spent in developing theories from which kinetic equations can be realistically developed [89]. The most useful supposes that the reaction takes place on an active site on the surface of the catalyst. Thus three steps are viewed to occur successively at the surface:

1. A molecule is adsorbed onto the surface and is attached to an active site.

2. It then reacts either with another molecule on an adjacent site (dual-site mechanism), with one coming from the main stream (single-site mechanism), or it simply decomposes while on the site (single-site mechanism).

3. Products are desorbed from the surface, which then frees the site.

Rate expressions derived from various postulated mechanisms are all of the form:

$$\text{rate of reaction} = \frac{(\text{kinetic term})(\text{driving force or displacement from equilibrium})}{(\text{resistance term})}$$

In catalytic systems the rate of reaction can be expressed in one of many equivalent ways. For example, for first order kinetics:

| | | |
|---|---|---|
| Based on volume of voids in the reactor | $(-r_A) = -\frac{1}{V}\frac{dN_A}{dt} = kC_A,$ | $\left[\frac{\text{mols reacted}}{\text{m}^3\text{ voids}\cdot\text{s}}\right]$ |
| Based on weight of catalyst pellets | $(-r_A)' = -\frac{1}{W}\frac{dN_A}{dt} = k'C_A,$ | $\left[\frac{\text{mol reacted}}{\text{kg cat}\cdot\text{s}}\right]$ |

Three steps mentioned above are all chemical in nature and may be regarded as jointly constituting the catalytic reaction. Two additional steps, as noted in section 2.3.1 (Chapter 2), involve transport of reactant(s) to the catalyst (before it is adsorbed) and transport of product(s) away from the catalyst (after being desorbed) and are physical processes, whereby the reactant(s) are brought through the gaseous or liquid phase surrounding the solid catalyst to the active site. This is a diffusion process and the phenomenon is called mass transport or mass transfer. Diffusion limitation at the external surface of catalyst is recognised by the following characteristics [85]:

1. The rate is proportional to the catalyst weight (or to the concentration of the active component) raised to a power less than unity, which in the limit may be zero.

2. The rate is increased by improving the movement of the gas or liquid with respect to catalyst.

3. The temperature coefficient is low and the apparent activation energy may be as low as 10 – 15 kJ/mol: gaseous diffusion processes do not in fact obey the Arrhenius equation, their rates being proportional to $T^{1/2}$.

On the other hand, reactions whose rate is truly governed by a chemical step show the following characteristics:

1. The rate is accurately proportional to catalyst weight or the concentration of the active component.

2. The rate is unaffected by better agitation.

3. The apparent activation energy is usually in excess of 25 kJ/mol.

Since diffusion coefficients are much lower in liquids than in gases, reactions where a liquid phase is present are more likely to become diffusion limited than those where only gaseous reactants participate. Diffusion can only occur in the presence of a concentration gradient and the diffusion coefficient D is defined by Fick's first law of diffusion:

$$-\frac{1}{A}\frac{dn_A}{dt}=D\frac{dc}{dx} \qquad (8.4)$$

where $-\frac{dn_A}{dt}$ is the flux of molecules across an area $A$ at which there is a concentration gradient of $\frac{dc}{dx}$.

Diffusion limitation can also occur within porous catalyst particles and the indicators are similar to those listed above for diffusion limitation outside the particles, however, significant difference is that improved motion of the fluid phase with respect of the catalyst has no effect on the rate of diffusion within the catalyst pores. To avoid the problem, catalysts have to be prepared in such way that pore size distribution is appropriate to the particular application.

In the design of catalysts, every care is taken that internal diffusion would not be a limiting step in the reaction; external diffusion was also carefully considered,

using different stirrer speeds as well as different catalyst concentrations. Activation energies obtained are also an indicator weather a reaction is a mass transfer limited.

A set of experiments for each catalyst at different temperatures was performed in order to get concentration profile with time and as a result reaction rate order, using an integral method. Integral method for determining reaction order involves developing rate expressions in a suitable form (integration) to get linear terms in which x value should include time and y value concentration of reactant. These terms can be seen in sections 7.2.1 – 7.2.3.

After the data for any particular experiment have been plotted for different rate order terms (zero, first and second order), it was then evaluated which line fits the experimental data best (using $R^2$ values).

In all experiments the best fitting was obtained using zero order expression, implying that reaction rate is zero order with respect to reactant concentration. $R^2$ values were very high, 0.9 or more and thus it was concluded that reaction rate can be expressed as:

$$(-r_A)=k \qquad (8.5)$$

Since an assumption was made at the beginning that a simple path can describe this reaction (valid assumption since reaction rate equation was determined as rate of disappearance of α-pinene oxide), it is very probable that rate expression is more complicated than Equation (8.5) shows. Usually heterogeneous catalytic systems are well described by Langmuir–Hinshelwood's equation (7.6); if we assume that reaction actually obeys Langmuir–Hinshelwood kinetics, case of zero order means that substrate molecule for this reaction (α-pinene oxide) is strongly adsorbed to a catalyst's active site, causing the values of concentration of the adsorbed molecule to be greatly enhanced. As a result, $\frac{K[S]}{1+K[S]} = 1$ (see section 7.1.1) and thus reaction is zero order as it is confirmed by experimental data. There is currently an ongoing discussion regarding the kinetics of isomerisation of α-pinene to camphene, which is a very similar reaction [169]. Latest claim is that it

follows the first order kinetics, but there are also a lot of claims that it is a zero order reaction [170].

Rate constant (k) values at different temperatures were then determined from the slope values and are given in Table 7.1 in Chapter 7. Whilst k does not depend on the composition of the reaction mixture, it does depend on the temperature, which is taken into account in the Arrhenius equation (7.15).

Once a rate constant dependence on temperature is known (for several temperatures, not less than three, but the more experiments the better), values of activation energy ($E_a$) and pre-exponential factor (A) can be easily gained for each catalyst (Table 8.3).

**Table 8.4. Activation energy and pre-exponential factor values**

| | A | $E_a$ (J/mol) $\cdot 10^{-4}$ |
|---|---|---|
| **Catalyst 1** | $3.78 \cdot 10^{3}$ | 4.41 |
| **Catalyst 2** | $1.24 \cdot 10^{-1}$ | 2.33 |
| **Catalyst 3** | $2.45 \cdot 10^{1}$ | 3.22 |

The expressions to include temperature dependence for rate constant (therefore reaction rate since rate is equal to k) for each catalyst can be seen in section 7.4 (equations 7.17-7.19).

Values of pre-exponential factors clearly show that Catalyst 2 is the least active of the three ($A = 1.24 \cdot 10^{-1}$) whilst Catalyst 1 is the most active of the tried catalysts ($A = 3.78 \cdot 10^{3}$). This factor (often called frequency factor) is a constant that indicates how many collisions have the correct orientation to lead to products [171].

As mentioned in Chapter 7, the activation energy for most reactions is in the range 25–300 kJ/mol and consequently the activation temperature $E_a/R$ ranges from 5000 K to 35000 K. $E_a/R$ values for all the catalysts utilised for the study are given in the Table 8.4 below.

**Table 8.5. Activation energy evaluation[3]**

| | $E_a$ (J/mol) | $E_a/R$ (K) |
|---|---|---|
| **Catalyst 1** | 44130.7 | 5308 |
| **Catalyst 2** | 23280.0 | 2800 |
| **Catalyst 3** | 32240.0 | 3878 |

It can be seen that activation energies are higher than 25 kJ/mol, which indicates that reaction is not mass transfer limited and that obtained kinetic expressions are accurate.

[3] For the temperature range 25 – 85$^0$C

# CHAPTER 9

## CONCLUSIONS AND RECOMMENDATIONS

In this Chapter the key scientific findings which may be drawn as a result of the current investigation are pointed out. In addition, the next section of the Chapter is dedicated to potential followers and contains some recommendations for future work to be carried out in this field.

### 9.1 CONCLUSIONS

It has been shown that the Spinning Disc Reactor (SDR) can be used to perform organic catalytic reactions, such as that of isomerisation of α-pinene oxide. Overall, approximately 500 experiments were performed in both SDR and batch reactor for this investigation. SDR proved to be capable of enhancing the overall rate of reaction at 85°C by as much as 60-100 times in comparison to reaction in a batch reactor, due to an intense mixing mechanism within the thin film in a SDR. Additionally, the selectivity towards campholenic aldehyde is not only as high as in batch processes (as reported in literature), but also easily controlled (i.e. by disc diameter and disc speed).

High conversions (full conversions) achieved in a SDR compromised even better selectivity towards campholenic aldehyde; however, campholenic aldehyde is not the only valuable product of this reaction. Almost every product is an important component in pharmaceutical industry.

Novel heterogeneous catalysts developed at the University of York proved to be very successful for this type of reaction and depending on the catalyst loading reaction times in a batch reaction could be in order of minutes. To investigate the performance in a catalytic SDR, lower catalyst loadings were used to explore the time savings and reaction rates properly.

For each catalyst, an investigation of catalyst activity was performed and it was proved that there was no catalyst poisoning or reduced activity over time.

Primary parameters studied for each catalyst used were disc rotational speed and feed flow rate with the aim of fully assessing the influence of residence time on conversion and selectivity. A rise in selectivity values from 0 to 75% was observed by changing the rotational speed from 200 to 1500 rpm, while influence on conversion was not as significant since the conversion values were high for most of the conditions, varying from 80 to 100% (this is valid for Catalysts 1 and 3; for Catalyst 2 conversion varied from 40 to 90%). It was also observed that increase of the flow rate by 1 $cm^3/s$ resulted in the increase of selectivity of at least 10% in cases of more active catalysts 1 and 3. However, different disc temperatures were also studied, as it was one of the main factors that influence the rate of reaction. From the results it can be concluded that higher disc temperatures increased the conversion of α-pinene oxide in cases of the first two catalysts, whilst optimum temperature for accomplishing highest conversion for third catalyst was seen at 45°C.

From the performed batch processes it was clear that reaction does not stop after all the α-pinene oxide was used, a range of consecutive reactions take place and campholenic aldehyde disappears as well, therefore even when conversion is 100% on the SDR, reaction has gone much further and for this reason selectivity towards campholenic aldehyde is reduced. It is expected that more campholenic aldehyde can be obtained at full conversion if smaller discs are used.

Investigation of flow rates showed that better selectivity was obtained when higher flow rate was used. Conversion values were not compromised as much, as a drop of 10% (conversion) was seen when selectivity value increased from 0 to 40%.

Optimal SDR conditions were determined (Table 8.1) for all the catalysts for accomplishing highest conversion/selectivity. These conditions are as follows:

- Catalyst 1: disc temperature of 85°C, disc rotational speed of 1500 rpm and feed flow rate of 6 $cm^3/s$ for achieving 62% selectivity at conversion of 77%;
- Catalyst 2: disc temperature of 85°C, disc rotational speed of 850 rpm and feed flow rate of 4 $cm^3/s$ for achieving 83% selectivity at conversion of 59%;
- Catalyst 3: disc temperature of 45°C, disc rotational speed of 1500 rpm and feed flow rate of 6 $cm^3/s$ for achieving 75% selectivity at conversion of 85%.

By using a simulation of cascade of three reactors it was shown that reaction can be carried out further even when the rate of reaction was lower (e.g. at lower temperature)

- Catalyst 1: conversion from 27 (first pass) to 52% (third pass), selectivity from 0 to 76%;

- Catalyst 2: conversion from 15 to 54%, selectivity from 72 to 81%;

- Catalyst 3: conversion from 60 to 100%, selectivity from 75 to 61%.

Regression analysis was used to obtain SDR models which can describe dependency of conversion of α-pinene oxide upon the SDR variables (disc rotational speed, feed flow rate and disc temperature):

$$\text{Catalyst 1:}\quad x_A = 1.03\cdot 10^{-21}\,\frac{N^{0.02}\,T^{8.26}}{Q^{0.30}}; \qquad R^2 = 0.96$$

$$\text{Catalyst 2:}\quad x_A = 7.71\cdot 10^{-14}\,\frac{T^{5.76}}{N^{0.46}\,Q^{0.82}}; \qquad R^2 = 0.87$$

$$\text{Catalyst 3:}\quad x_A = 2.90\cdot 10^{-8}\,T^{2.94}\,N^{0.04}\,Q^{0.06}; \qquad R^2 = 0.42$$

Batch experiments were performed in order to study the kinetics of reaction and order of reaction was determined using the integral method as zero. Assumptions made in Section 7.1 can be considered as fully valid as the campholenic aldehyde reacts to form further products more rapidly only after the oxide was used. Also the kinetic equation is in the form of disappearance of α-pinene oxide from the reaction mixture and not formation of campholenic aldehyde. Activation energy for each catalyst was also determined and Arrhenius equations given in Section 7.4.

Other potential benefits apart from enhanced reaction rate to be gained from the proposed process may include an improvement in its intrinsic safety as a result of reduced inventory in the system at any given time and minimal risk of thermal runaways at high operating temperatures due to short residence times and enhanced heat removal rates.

## 9.2 RECOMMENDATIONS FOR FUTURE WORK

The present investigation has shown that SDR can be successfully employed to perform organic catalytic reactions. It was also revealed that problems of using a heterogeneous catalyst with regards to catalyst separation can be avoided by supporting the catalyst on to the reaction surface. However, a number of possibilities still remain to be explored before a complete and thorough understanding of the principles behind the spinning disc technology as applied to catalytic systems in general can be acquired. It is hoped that the following section will give a useful suggestions in the future exploration of Spinning Disc Reactors for performing organic catalytic reactions.

Rearrangement of α-pinene oxide was chosen as a model reaction for this investigation for its high commercial potential. However the complicated and unpredictable reaction paths (e.g. parallel/consecutive reactions) make this reaction very difficult to study. It is expected that much more understanding into the catalytic systems can be gained by using simpler model reactions, such as benzoylation of anisole.

Variables such as disc rotational speed and feed flow rate are well explored in this investigation. However, it is recommended that the disc temperature variable be explored in greater detail, especially for conditions already presented in this study where both conversion and selectivity were low. Simulation of cascade of SDRs has shown that both conversion and selectivity can be improved greatly with longer residence times without much compromise in the overall reaction time. This also leads to exploration into the use of different size discs, as the residence time is the most important variable. Depending on reaction conditions smaller disc can be used at higher temperatures to quench the reaction sooner; it is also expected that larger discs can be used at lower temperatures to obtain high conversion/selectivity. The construction of an empirical relationship which will predict the effect of all the spinning disc variables on the product conversion/selectivity would therefore be possible and not limited to certain disc size and restricted conditions.

A detailed kinetic study into α-pinene oxide isomerisation (or similar catalytic reaction) should be carried out in the spinning disc to determine the

elements responsible for the rate enhancements observed in the present investigation. In order to do this, the concentration profile across the disc should be determined. The method used in this investigation for kinetic studies in the batch can also be employed for spinning disc (concentration) results.

Additionally, to achieve the full Green Chemistry process, the amount of solvent used in the reaction should be reduced, or the reaction should be even tried without any solvent on the SDR.

Ultimately, the development of a pilot plant scale spinning disc reactor operating in continuous mode would allow relevant industrial processes to be practically evaluated in the Spinning Disc Reactor.

# REFERENCES


1. Charpentier, J.C., *Four Main Objectives for the Future of Chemical and Process Engineering.* Ingineria Qiumica, 2003(Achema 2003 Special): p. 69-87.
2. Ramshaw, C., *A game for n-players.* The Chemical Engineer, 1985.
3. *Process intensification moves on site.* Professional Engineering, 1998. **11**(7): p. 48.
4. Whiting, M.J.L., *The Benefits Of Process Intensification For Caro Acid Production.* Chemical Engineering Research & Design, 1992. **70**(2): p. 195-196.
5. Etchells, J., *Runaway.* The Chemical Engineer, 1996: p. 17-21.
6. Kletz, T., *Lessons From Disaster.* 1993: IChemE.
7. Kletz, T., *What Went Wrong?* 3rd ed. 1994, Houston, Texas: Gulf Publishing Company.
8. Kletz, T., *Process Plants: A Handbook for Inherently Safer Design.* 1998: Taylor & Francis.
9. Kletz, T., *What you don't have, can't leak.* Chemistry and Industry, 6 May 1978: p. 287-292.
10. Hendershot, D.C., *Process Minimisation: Making Plants Safer.* Chemical Engineering Progress, January 2000: p. 35-40.
11. Fell, N., *Innovation offers a new spin on drug production.* The Chemical Engineer, 1998: p. 23-25.
12. Jachuck, R.J., et al., *Process intensification for energy saving.* Applied Thermal Engineering, 1997. **17**(8-10): p. 861-867.
13. Caruana, C.M., *ChEs seek big gains from process miniaturisation.* Chem. Eng. Prog., April 1996. **92**: p. 12-19.
14. Fell, N., *Bespoke Reactions.* The Chemical Engineer, 1997: p. 17-18.
15. Green, A., *Process intensification: the key to survival in global markets?* Chemistry & Industry, 1998(5): p. 168-172.
16. Reay, D.A., *Heat transfer enhancement- A review of techniques and their possible impact on energy efficiency in the UK.* Heat Recovery Systems & CHP, 1991. **11**(1): p. 1-40.
17. Ramshaw, C., *The Opportunities For Exploiting Centrifugal Fields.* Heat Recovery Systems & CHP, 1993. **13**(6): p. 493-513.
18. Stankiewicz, A.I. and J.A. Moulijn, *Process Intensification.* Ind. Eng. Chem. Res., 2002. **41**: p. 1920-1924.
19. Jachuck, R.J. and C. Ramshaw, *Process Intensification: Spinning Disc Polymeriser.* IChemE Research Event/1st European Conference, 1995: p. 556-558.

20. Boodhoo, K.V.K. and R.J. Jachuck. *Application of the Spinning-Disc Technology for Process Intensification in the Chemical Process Industry.* in *Centrifugal Materials Processing IV Conference.* 29 May-2 June 2000. Potsdam, New York, USA: Kluwer Academic.

21. Woods, W., *The hydrodynamics of thin liquid films flowing over a rotating disc*, in *Chemical and Process Engineering.* 1995, Newcastle upon Tyne: Newcastle.

22. Bell, C., *The hydrodynamics and heat transfer characteristics of liquid films on a rotating disc*, in *Chemical and Process Engineering.* 1975, Newcastle Upon Tyne: Newcastle Upon Tyne.

23. Jazayeri, A., *The hydrodynamics of Newtonian and non-Newtonian liquid films flowing across a rotating disc*, in *Chemical and Process Engineering.* 1980, Newcastle Upon Tyne: Newcastle Upon Tyne.

24. Lim, S.T., *Hydrodynamics and mass transfer processes associated with the absorption of oxygen in liquid films flowing across a rotating disc*, in *Chemical and Process Engineering.* 1980, Newcastle Upon Tyne: Newcastle Upon Tyne.

25. Khan, J.R., *Heat transfer on a rotating disc with and without phase change*, in *Chemical and Process Engineering.* 1986, Newcastle Upon Tyne: Newcastle Upon Tyne.

26. Moore, S.R., *Mass Transfer to Thin Liquid Films On Rotating Surfaces, With and Without Chemical Reaction*, in *Chemical and Process Engineering.* 1986, Newcastle upon Tyne: Newcastle upon Tyne.

27. Jachuck, R.J.J. and C. Ramshaw, *Process Intensification - Heat-Transfer Characteristics Of Tailored Rotating Surfaces.* Heat Recovery Systems & Chp, 1994. **14**(5): p. 475-491.

28. Boodhoo, K.V.K. and R.J. Jachuck, *Process Intensification: Spinning Disk Reactor for Styrene Polymerisation.* Applied Thermal Engineering, 2000. **20**(12): p. 1127-1146.

29. Waldram, S., *Batch Runaway Rethink.* The Chemical Engineer, 1998: p. 15-16.

30. Fogler, H.S., *Elements of Chemical Reaction Engineering.* 3rd ed. 1999: Prentice Hall PTR.

31. Sundaram, K.M. and G.F. Froment, *Two dimensional model for the simulation of tubular reactors for thermal cracking.* Chem. Eng. Sci., 1980. **35**(1-2): p. 364-371.

32. Hjertager, L.K., B.H. Hjertager, and T. Solberg, *CFD modelling of fast chemical reactions in turbulent liquid flows.* Computers & Chemical Engineering, 2002. **26**(4-5): p. 507-515.

33. Garcia, T., et al., *Kinetic model for the esterification of oleic acid and cetyl alcohol using an immobilized lipase as catalyst.* Chem. Eng. Sci., 2000. **55**(8): p. 1411-1423.

34. Zeaiter, J., et al., *Inferential conversion monitoring and control in emulsion polymerisation through calorimetric measurements.* Chem. Eng. Journal, 2002. 89(1-3): p. 37-45.

35. Gupta, A. and D. Subba Rao, *Effect of feed atomization on FCC performance: simulation of entire unit.* Chem. Eng. Sci., 2003. 58(20): p. 4567-4579.

36. Masetti, S., F. Trifirò, and G. Blanchard, *Fluid-bed tin-based catalyst for propane ammoxidation.* Applied Catalysis A: General, 2001. 217(1-2): p. 119-129.

37. Westerterp, K.R. and R.J. Wijngaarden, *Principles of Chemical Reaction Engineering and Plant Design*. 5th ed. Ullmann's Encyclopedia of Industrial Chemistry. Vol. B4. 1992: Weinheim: VCH.

38. Bhatia, Q.S. and V. Hlavacek, *Modeling Of Tubular Non-Isothermal Non-Adiabatic Packed-Bed Reactors With Catalyst Poisoning.* Acs Symposium Series, 1983. 237: p. 393-413.

39. Bos, A.N.R., et al., *Behavior Of an Adiabatic Packed-Bed Reactor .1. Experimental-Study.* Chemical Engineering Communications, 1993. 121: p. 27-53.

40. Bos, A.N.R., et al., *Behavior Of an Adiabatic Packed-Bed Reactor .2. Modeling.* Chemical Engineering Communications, 1993. 121: p. 55-80.

41. Chocron, M., N.E. Amadeo, and M.A. Laborde, *Heterogeneous modeling of an adiabatic packed bed reactor with catalyst decay. Intraparticle diffusion effects.* Abstracts Of Papers Of the American Chemical Society, 1998. 216(Pt1): p. 124-FUEL.

42. Hartig, F. and F.J. Keil, *Large-Scale Spherical Fixed-Bed Reactors - Modeling and Optimization.* Industrial & Engineering Chemistry Research, 1993. 32(3): p. 424-437.

43. Koning, G.W. and K.R. Westerterp, *Modeling of heat transfer in wall-cooled tubular reactors.* Chemical Engineering Science, 1999. 54(13-14): p. 2527-2533.

44. Westerink, E.J., N. Koster, and K.R. Westerterp, *The Choice Between Cooled Tubular Reactor Models - Analysis Of the Hot-Spot.* Chemical Engineering Science, 1990. 45(12): p. 3443-3455.

45. Wijngaarden, R.J. and K.R. Westerterp, *Incorporation Of Statistical Distributions Of Particle Properties In Chemical Reactor Design and Operation - the Cooled Tubular Reactor.* Chemical Engineering Science, 1992. 47(8): p. 1881-1895.

46. Wijngaarden, R.J., A. Kronberg, and K.R. Westerterp, *Industrial Catalysis - Optimizing Catalysts and Processes*. 1998: WILEY-VCH.

47. Popken, T., et al., *Reaction kinetics and reactive distillation - On the transfer of kinetic data from a batch reactor to a trickle-bed reactor.* Chemical Engineering & Technology, 1999. 22(5): p. 401-404.

48. Latifi, M.A., A. Naderifar, and N. Miidoux, *Energetic analysis of the liquid-to-wall mass transfer in a trickle bed reactor.* Chemical Engineering Research & Design, 1999. **77**(A1): p. 69-73.

49. Attou, A., C. Boyer, and G. Ferschneider, *Modelling of the hydrodynamics of the cocurrent gas-liquid trickle flow through a trickle-bed reactor.* Chemical Engineering Science, 1999. **54**(6): p. 785-802.

50. Oukaci, R., A.H. Singleton, and J.G. Goodwin, *Comparison of patented CoF-T catalysts using fixed-bed and slurry bubble column reactors.* Applied Catalysis a-General, 1999. **186**(1-2): p. 129-144.

51. vanderLaan, G.P., A. Beenackers, and R. Krishna, *Multicomponent reaction engineering model for Fe-catalyzed Fischer- Tropsch synthesis in commercial scale slurry bubble column reactors.* Chemical Engineering Science, 1999. **54**(21): p. 5013-5019.

52. Orejas, J.A., *Modelling and simulation of a bubble-column reactor with external loop: Application to the direct chlorination of ethylene.* Chemical Engineering Science, 1999. **54**(21): p. 5299-5309.

53. Inga, J.R. and B.I. Morsi, *Effect of operating variables on the gas holdup in a large-scale slurry bubble column reactor operating with an organic liquid mixture.* Industrial & Engineering Chemistry Research, 1999. **38**(3): p. 928-937.

54. Winterbottom, J.M., et al., *Catalytic hydrogenation in a packed bed bubble column reactor.* Catalysis Today, 1999. **48**(1-4): p. 221-228.

55. Shimizu, T., et al., *A twin fluid-bed reactor for removal of CO2 from combustion processes.* Chemical Engineering Research & Design, 1999. **77**(A1): p. 62-68.

56. Cai, G.Y., et al., *Light Alkenes From Syngas Via Dimethyl Ether.* Applied Catalysis a-General, 1995. **125**(1): p. 29-38.

57. Bolthrunis, C.O., *An Industrial Perspective On Fluid Bed Reactor Models.* Chemical Engineering Progress, 1989. **85**(5): p. 51-54.

58. Krambeck, F.J., et al., *Predicting Fluid-Bed Reactor Efficiency Using Adsorbing Gas Tracers.* Aiche Journal, 1987. **33**(10): p. 1727-1734.

59. Grace, J.R. and R.L. Varma, *Recent Advances In Fluid Bed Reactor Modeling.* Abstracts Of Papers Of the American Chemical Society, 1980. **180**(AUG): p. 23-INDE.

60. Adewuyi, Y.G., et al., *Simultaneous absorption and oxidation of NO and SO2 by aqueous solutions of sodium chlorite.* Chemical Engineering Communications, 1999. **174**: p. 21-51.

61. Soong, Y., et al., *Ultrasonic characterizations of slurries in a bubble column reactor.* Industrial & Engineering Chemistry Research, 1999. **38**(5): p. 2137-2143.

62. Meszena, Z.G., et al., *Towards tailored molecular weight distributions through controlled living polymerisation reactors: A simple predictive algorithm.* Polymer Reaction Engineering, 1999. **7**(1): p. 71-95.

63. Dohi, N., et al., *Mixing characteristics in slurry stirred tank reactors with multiple impellers.* Chemical Engineering Communications, 1999. **171**: p. 211-229.

64. Yao, Z., et al., *Continuous thermal bulk copolymerization of styrene and maleic anhydride.* Journal Of Applied Polymer Science, 1999. **73**(5): p. 615-622.

65. Hetherington, P., R.J.J. Jachuck, and M.J. Scalley. *Process Intensification: Continuous Production of Barium Sulphate using a Spinning Cone Precipitator.* in *4th International Conference on Process Intensification for the Chemical Industry.* 10-12 September 2001. Brugge, Belgium.

66. Burns, J.R., *Liquid distribution in a rotating packed bed*, in *Chemical and Process Engineering*. 1996, Newcastle upon Tyne: Newcastle.

67. Hassan-Beck, H.M., *Process intensification: Mass transfer and pressure drop for counter-current rotating packed beds*, in *Department of Chemical and Process Engineering*. 1997, Newcastle upon Tyne: Newcastle.

68. Burns, J.R. and C. Ramshaw, *Process intensification: Visual study of liquid maldistribution in rotating packed beds.* Chemical Engineering Science, 1996. **51**(8): p. 1347-1352.

69. Burns, J.R. and C. Ramshaw, *Development of a Microreactor for Chemical Production.* Trans IChemE, May 1999. **77**(A): p. 206-211.

70. Burns, J. and C. Ramshaw. *A Multiphase Microreactor for Organic Nitration.* in *4th International Conference on Process Intensification for the Chemical Industry: Better Processes for Better Products.* 10-12 September 2001. Brugge, Belgium.

71. Dautzenberg, F.M. and M. Mukherjee, *Process Intensification Using Multifunctional Reactors.* Chemical Engineering Science, 2001(56): p. 251-267.

72. Bandelier, P., *Improvement of multifunctional heat exchangers applied in industrial processes.* Applied Thermal Engineering, 1997. **17**(8-10): p. 777-788.

73. Babovic, M., et al. *Catalytic Plate Reactors for Endo- and Exothermic Reactions.* in *4th International Conference on Process Intensification for the Chemical Industry.* 10-12 September 2001. Brugge, Belgium.

74. Charlesworth, R.J., *Steam reforming and combustion of methane on a micro-thin catalyst for use in a catalytic plate reactor,*, in *Department of Chemical and Process Engineering*. 1996, Newcastle upon Tyne: Newcastle.

75. Jachuck, R.J.J. and C. Ramshaw, *Process Intensification - Polymer Film Compact Heat-Exchanger (Pfche).* Chemical Engineering Research & Design, 1994. **72**(A2): p. 255-262.

76. Zaheed, L. and R. Jachuck, *Review of Polymer Compact heat Exchangers.* 2002.

77. Zaheed-Maheswaran, L., *Process intensification : cross-corrugated polymer film compact heat exchanger (PFCHE)*, in *School of Chemical Engineering and Advanced Materials*. 2003, University of Newcastle upon Tyne.

78. McHugh, M.A. and V.J. Krukonis, *Supercritical Fluid Extraction: Principles & Practice.* 1994, Boston: Butterworth-Heinemann.

79. Poliakoff, M., Supercritical Etherification Reactions, www.nottingham.ac.uk/supercritical/scether.html, (accessed: November 2003).

80. Gray, W.K., et al., *The Continuous Acid Catalysed Dehydration of Alcohols in Supercritical Fluids: A New Approach to the Cleaner Synthesis of Acetals, Ketals and Ethers with High Selectivity.* J. Am. Chem. Soc, 1999. **121**: p. 10711-18.

81. Ni, X.-W.V., Andrew; Liao, Anting; Sermage, Sylvie B. C.; Thomson, Gillian B.; Roberts, Kevin J.. *On the Crystal Polymorphic Forms of L-Glutamic Acid Following Temperature Programmed Crystallization in a Batch Oscillatory Baffled Crystallizer.* Crystal Growth & Design, 2004. 4(6): p. 1129-1135.

82. Centre for Oscillatory Baffled Reactor Applications, http://www.cobra.hw.ac.uk/, (accessed: November 2003).

83. Stankiewicz, A.I. and J.A. Moulijn, *Process Intensification: Transforming Chemical Engineering.* Chemical Engineering Progress, January 2000: p. 22-33.

84. Satterfield, C.N., *Heterogeneous Catalysis in Practice.* 1980, New York: McGraw Hill.

85. Bond, G.C., *Heterogeneous Catalysis, Principles and Applications.* 2nd ed. Oxford Chemistry Series. 1987, Oxford: Oxford University Press.

86. Augustine, R.L., *Heterogeneous catalysis for the synthetic chemist.* 1996: Marcel Dekker, inc.

87. Emmett, P.H., Adv. Catal., 1948. **1**(65).

88. Innes, W.B., *Experimental Methods in Catalysis Research*, ed. E. R.B. Anderson. Vol. I. 1968, New York: Academic Press.

89. Thomas, J.M. and W.J. Thomas, *Introduction to the Principles of Heterogeneous Catalysis*. 1967, London/New York: Academic Press.

90. Bartholomew, C.H., Chem. Eng., 1986(12): p. 96.

91. Westerterp, K.R., H.J. Fontein, and F.P.H. Van Bekkum, Chem. Eng. Technol., 1988. **11**: p. 367.

92. Clark, J.H. and D.J. Macquarrie, *Catalysis of liquid phase organic reactions using chemically modified mesoporous inorganic solids.* Chemical Communications, 1998(8): p. 853-860.

93. Sheldon, R.A., *Catalysis and pollution prevention.* Chemistry & Industry, 1997(1): p. 12-15.

94. Holderich, W.F., *New Reactions In Various Fields and Production Of Specialty Chemicals.* Studies In Surface Science and Catalysis, 1993. **75**(PtA): p. 127-163.

95. Clark, J.H. and D.J. Macquarrie, *Heterogeneous catalysis in liquid phase transformations of importance in the industrial preparation of fine chemicals.* Organic Process Research & Development, 1997. 1(2): p. 149-162.

96. Marcus, B.K. and W.E. Cormier, *Going Green With Zeolites.* Chemical Engineering Progress, June 1999.

97. Clark, J.H., et al., *Environmentally friendly catalysis using supported reagents: Enhanced selectivity without loss in activity in the alkylation of benzene using hexagonal mesoporous silica (HMS)-supported aluminium chloride.* Journal Of Chemical Research-S, 1997(11): p. 430-431.

98. Price, P.M., et al., *Enhanced selectivity in the preparation of linear alkylbenzenes using hexagonal mesoporous silica supported aluminium chloride.* Organic Process Research & Development, 1998. 2(4): p. 221-225.

99. Kawamura, M., et al., *Lewis acid-catalyzed Friedel–Crafts acylation reaction using carboxylic acids as acylating agents.* Tetrahedron Letters, 2003. 44(42): p. 7715-7717.

100. Deutsch, J., et al., *Acetylation and benzoylation of various aromatics on sulfated zirconia.* Journal of Molecular Catalysis A: Chemical, 2003. **In Press**.

101. Holderich, W.F., et al., *The use of zeolites in the synthesis of fine and intermediate chemicals.* Catalysis Today, 1997. 37(4): p. 353-366.

102. Connelly, N.G., P.T. Draggett, and M. Green, *The catalysis of alkene isomerisation, oligomerisation, and polymerisation by cationic nitrosylrhodium complexes.* Journal of Organometallic Chemistry, 1977. 140(1): p. C10-C11.

103. Berkessel, A. and M.R.M. Andreae, *Efficient catalytic methods for the Baeyer–Villiger oxidation and epoxidation with hydrogen peroxide.* Tetrahedron Letters, 2001. 42(12): p. 2293-2295.

104. Lewis, J.B. and G.W. Hedrick, *Reaction of alpha-pinene oxide with zinc bromide and rearrangement of 2,2,3-trimethyl-3-cyclopentene products derived thereform.* 1965.

105. Kaminska, J., et al., *The Isomerization Of Alpha-Pinene Oxide With Bronsted and Lewis-Acids.* Recueil Des Travaux Chimiques Des Pays-Bas-Journal Of the Royal Netherlands Chemical Society, 1992. 111(10): p. 432-437.

106. Arata, K. and K. Tanabe, Chemistry Letters, 1979: p. 1017.

107. Liebens, A.T., C. Mahaim, and W.F. Holderich, *Selective isomerization of alpha-pinene oxide with heterogeneous catalysts.* Studies In Surface Science and Catalysis, 1997. **108**: p. 587-594.

108. Kunkeler, P.J., et al., *Application of zeolite titanium Beta in the rearrangement of alpha- pinene oxide to campholenic aldehyde.* Catalysis Letters, 1998. 53(1-2): p. 135-138.

109. Ravasio, N., M. Finiguerra, and M. Gargano. *α-pinene isomerisation promoted by mixed solids*. in *Third International Symposium on Supported Reagents and Catalysis in Chemistry*. 1997. University of Limerick: The Royal Society of Chemistry.

110. Vialemaringe, M., et al., *Pinene oxide and Lewis acids: an update.* Comptes Rendus De L Academie Des Sciences Serie II Fascicule C-Chimie, 1999. **2**(7-8): p. 449-454.

111. Vialemaringe, M., et al., *Isomerisation d'epoxypinenes fonctionnels en milieu basique.* Tetrahedron Letters, 2000. **41**: p. 4901-4904.

112. Wilson, K., A. Renson, and J.H. Clark, *Novel heterogeneous zinc triflate catalysts for the rearrangement of alpha-pinene oxide.* Catalysis Letters, 1999. **61**(1-2): p. 51-55.

113. Nusselt, Ver. Deut. Ingr. Z., 1916. **60**: p. 549.

114. Friedman, S.J. and C.O. Miller, *Liquid Films in the viscous flow region.* Ind. Eng. Chem., 1941. **33 (7)**: p. 885-891.

115. Binnie, A.M., *Experiments on the onset of wave formation on a film of water flowing down a vertical plane.* J. Fluid Mech., 1957. **2**: p. 551-553.

116. Wilkes, J.O. and R.M. Nedderman, *The Measurement of Velocities in Thin Films of Liquid.* Chem. Eng. Sci., 1962. **17**: p. 177-187.

117. Andreev, A.F., *Stability of the laminar flow of the thin liquid layers.* J. Exp.Theo. Phys., 1964. **18 (2)**: p. 519-521.

118. Kirkbride, C.G., *Heat transfer by condensing vapour on vertical tubes.* Ind. Eng. Chem., 1934. **26 (4)**: p. 425-428.

119. Jackson, M.L., *Liquid films in viscous flow.* AIChE J., 1955. **1**(231).

120. Emmert, R.E. and R.L. Pigford, *A study of gas absorption in falling liquid films.* Chem. Eng. Progr., 1964. **50 (2)**: p. 87-93.

121. Davies, J.T. and K.V. Warner, *The Effect of Large Scale Roughness in Promoting Gas Absorption.* Chem. Eng. Sci., 1969. **24**: p. 231-240.

122. Fulford, G.D., *The flow of liquids in thin films.* Advances in Chemical Engineering. Vol. 5. 1964: Academic Press, New York. 151-236.

123. Bassom, A.P. and S.O. Seddougui, *The Effects Of Suction On the Nonlinear Stability Of the 3- Dimensional Boundary-Layer Above a Rotating-Disk.* Proceedings Of the Royal Society Of London Series a-Mathematical Physical and Engineering Sciences, 1992. **436**(1897): p. 405-415.

124. Boodhoo, K.V.K., *Spinning Disc Polymeriser for Production of Polystirene*, in *Chemical and Process Engineering*. 1999, Newcastle upon Tyne: Newcastle.

125. Baddour, N. and J.W. Zu, *A Revisit of Spinning Disk Models. Part I: Derivation of Equations of Motions.* Applied Mathematical Modelling, 2001. **25**: p. 541-559.

126. Rahman, M. and A. Faghri, *Analysis of Heating and Evaporation from a Liquid Film Adjacent to a Horizontal Rotating Disc.* Int. J. Heat Mass Transfer, 1992. **35**(10): p. 2655-2664.

127. Emslie, A.G., F.T. Booner, and L.G. Peck, *Flow of a viscous liquid on a rotating disk.* J. Appl. Phys., 1958. **29**(5): p. 858-862.

128. Leneweit, G., et al., *Shear Degradation and Deformation of Polysaccharides in Thin Liquid Film Flow on a Rotating Disk.* Polymer Degradation and Stability, 2000(70): p. 283-297.

129. Momoniat, E. and D.P. Mason, *Investigation of the Effect of the Coriolis Force on a Thin Fluid Film on a Rotating Disk.* Int. J. Non-Linear Mechanics, 1998. **33**(6): p. 1069-1088.

130. Myers, T.G. and J.P.F. Charpin, *The Effect of the Coriolis Force on Axisymmetric Rotating Thin Film Flows.* International Journal of Non-Linear Mechanics, 2001. **36**: p. 629-635.

131. Rauscher, J.W.e.a., *An Asymptotic Solution for the Laminar Flow of a Thin Liquid Film on a Rotating Disc.* ASME J. Appl. Mechanics, 1975. **40**: p. 43-47.

132. Nosoko, T., et al., *Characteristics of Two-Dimensional Waves on a Falling Liquid Film.* Chemical Engineering Science, 1996. **51**(5): p. 725-732.

133. Wood, R.M. and B.E. Watts, *The Flow, Heat and Mass Transfer Characteristics of Liquid Films on Rotating Discs.* Trans. Instn Chem. Engrs, 1973. **51**: p. 315-322.

134. Tzeng, H.M., A.C. Munce, and L. Crawforth, *Quantitative Visualisation of Surface Flows on Rotating Disks.* Journal of Fluids Engineering, 1994. **116**: p. 494-498.

135. Dhanak, M.R., *Effects Of Uniform Suction On the Stability Of Flow On a Rotating- Disk.* Proceedings Of the Royal Society Of London Series a-Mathematical Physical and Engineering Sciences, 1992. **439**(1906): p. 431-440.

136. Karman, T.v., *Uber Laminare und Turbulente Reibung.* Z. angrew. Math. Mech., 1921. **1**: p. 233-252.

137. Gregory, N., J.T. Stuart, and W.S. Walker, *On the stability of three dimensional boundary layers with application to the flow due to a rotating disc.* Phil. Trans. R. Soc. Lond., 1995(A248): p. 155-199.

138. Malik, M.R., *The neutral curve for stationary disturbances in rotating disc flow.* J. Fluid Mech., 1986. **164**: p. 275-287.

139. Malik, M.R., S.P. Wilkinson, and S.A. Orszag, *Instability and transition in rotating disc flow.* AIAA J., 1981. **19**: p. 1131-1138.

140. Mack, L.M., *The wave pattern produced by a point source on a rotating disc.* AIAA Paper no. 85-0490, 1985.

141. Faller, A.J. and R.E. Kaylor, *A numerical study of the instability of the laminar Ekman boundary layer.* J. atmos. Sci., 1966. **23**: p. 466-480.

142. Lilly, D.K., *On the instability of Ekman boundary layer flow.* J. atmos. Sci., 1966. **24**: p. 481-494.

143. Wilkinson, S.P. and M.R. Malik, *Stability experiment in rotating disc flow.* AIAA J., 1985. **23**: p. 588-595.

144. Fedorov, B.I., et al., *Transitional flow conditions on a rotatin disc.* J. Eng. Phys., 1976. **31**: p. 1448-1453.

145. Charwat, A.F.e.a., *The flow and stability of thin liquid films on a rotating disk.* J. Fluid Mech., 1972. **53 (2)**: p. 227-255.

146. Makarytchev, S.V., T.A.G. Langrish, and R.G.H. Prince, *Thickness and Velocity of Wavy Liquid Films on Rotating Conical Surfaces.* Chemical Engineering Science, 2001. **56**: p. 77-87.

147. Burns, J.R., C. Ramshaw, and R.J. Jachuck, *Measurement of liquid film thickness and the determination of spin-up radius on a rotating disc using an electrical resistance technique.* 2002.

148. Hickman, K.C.D., *Centrifugal boiler compression still.* Ing. Eng. Chem., 1957. **48 (5)**: p. 786-789.

149. Coulson, J.M. and J.F. Richardson, *Chemical Engineering, Vol. 1.* 1995, Oxford: Butterworth-Heinemann.

150. Oxley, P., et al., *Evaluation of Spinning Disk Reactor Technology for the Manufacture of Pharmaceuticals.* Ind. Eng. Chem. Res., 2000. **39**: p. 2135-2182.

151. Yanniotis, S. and D. Kolokotsa, *Boiling on the surface of a rotating disc.* Journal Of Food Engineering, 1996. **30**(3-4): p. 313-325.

152. Yanniotis, S. and D. Kolokotsa, *Experimental study of water vapour condensation on a rotating disc.* International Communications In Heat and Mass Transfer, 1996. **23**(5): p. 721-729.

153. Rahman, M.M., et al., *Prediction Of Heat-Transfer to a Thin Liquid-Film In Plane and Radially Spreading Flows.* Journal Of Heat Transfer-Transactions Of the Asme, 1990. **112**(3): p. 822-825.

154. Rahman, M.M., W.L. Hankey, and A. Faghri, *Analysis Of the Fluid-Flow and Heat-Transfer In a Thin Liquid-Film In the Presence and Absence Of Gravity.* International Journal Of Heat and Mass Transfer, 1991. **34**(1): p. 103-114.

155. Rahman, M.M. and A. Faghri, *Numerical-Simulation Of Fluid-Flow and Heat-Transfer In a Thin Liquid-Film Over a Rotating-Disk.* International Journal Of Heat and Mass Transfer, 1992. **35**(6): p. 1441-1453.

156. Rahman, M.M., A. Faghri, and W.L. Hankey, *Fluid-Flow and Heat-Transfer In a Radially Spreading Thin Liquid-Film.* Numerical Heat Transfer Part a-Applications, 1992. **21**(1): p. 71-90.

157. Javdani, K., *Mass Transfer in Wavy Liquid Films.* Chem. Eng. Sci., 1974. **29**: p. 61-69.

158. Long, R. and T. Pattni, *Mass Transfer in a Laminar Rippling Film in a Conical Centrifugal Film Reactor. Part I: Film Thickness Profile and Velocity Profile*, in *Industrial Mixing Fundamentals with Applications*. 1995. p. 61-69.

159. Long, R. and T. Pattni, *Mass Transfer in a Laminar Rippling Film in a Conical Centrifugal Film Reactor. Part II: Stability Analysis for the Film Flow*, in *Industrial Mixing Fundamentals with Applications*. 1995. p. 70-79.

160. Long, R. and T. Pattni, *Mass Transfer in a Laminar Rippling Film in a Conical Centrifugal Film Reactor. Part III: Enhanced Mass Transfer in*

*Ripple Flow*, in *Industrial Mixing Fundamentals with Applications*. 1995. p. 80-87.

161. Malinson, R. and C. Ramshaw, *European Pat. 2568B*. 1979.

162. Tafreen, S., Y. Anjaneyulu, and A.V.S. Prabhakara Rao. *Aluminium Removal from Friedel Crafts' Reaction Reagents Waste*. in *ICIPACT*. 2001.

163. Johnstone, J.C., *Process intensification : thin film spinning disc reactor for controlled continuous photo-polymerisation of acrylates*. 2000, University of Newcastle upon Tyne.

164. Hayduk, W. and H. Laudie, *Prediction of diffusion coefficients for nonelectrolytes in dilute aqueous solutions*. AIChE Journal, 1974. **20**(3): p. 611-615.

165. http://www.epa.gov/athens/learn2model/part-two/onsite/estdiffusion.htm, (accessed: 2003).

166. Levenspiel, O., *Chemical Reaction Engineering*. 3rd ed. 1999: John Wiley & Sons. Inc.

167. Epsig, H. and R. Hoyle, *Waves in a thin liquid layer on a rotating disc*. J. Fluid Mech., 1965. **22**(4): p. 671-677.

168. Turnbull, J., *Mixing characteristics on a rotating disc*. 1997, MEng. Report, University of Newcastle Upon Tyne.

169. Akpolat, O., et al., *Isomerization of α–pinene over calcined natural zeolites*. Applied Catalysis A: General, 30 June 2004. **265**(1): p. 11-22.

170. Rudakov, G.A., et al., Lesokhim, Gidroliz Prom. 4, 1975. 7.

171. http://www.chem.purdue.edu/gchelp/gloss/freqfac.html, (accessed: July 2004).

# PUBLICATIONS

1. M. Vicevic, R.J.J. Jachuck and K. Scott, PROCESS INTENSIFICATION: ORGANIC CATALYTIC REACTIONS ON THE SPINNING DISC REACTOR, Younger Chemists' Meeting – The Royal Society, SET for Britain and Chemistry 2000, 21 November 2000.

2. M. Vicevic, R.J.J. Jachuck and K. Scott, OPPORTUNITIES OFFERED BY CATALYTIC SPINNING DISC REACTORS, AIChe Conference, April 2001, USA.

3. M. Vicevic, R.J.J. Jachuck and K. Scott, PROCESS INTENSIFICATION FOR GREEN CHEMISTRY: REARRANGEMENT OF ALPHA-PINENE OXIDE ON THE SPINNING DISC REACTOR, 4th International Conference on Process Intensification for the Chemical Industry, Brugge – Belgium, 10-12 September 2001, p.201-213

4. M. Vicevic, R.J.J. Jachuck and K. Scott, APPLICATION OF SDR FOR GREEN CHEMISTRY PROCESS, Green Chemistry Network Symposium, 4th April 2002, University of York http://www.chemsoc.org/pdf/gcn/York.pdf.

5. M. Vicevic, R.J.J. Jachuck, K. Scott, J. H. Clark and K. Wilson, REARRANGEMENT OF ALPHA-PINENE OXIDE USING SUPPORTED CATALYST IN A SPINNING DISC REACTOR, Green Chem., 2004, 6(10), p.533-537.

# APPENDIX A

## THERMODYNAMIC PROPERTIES

### A.1 THERMOCHEMICAL DATA ESTIMATIONS

Accurate thermodynamic data are available for relatively few compounds. A chemical reaction: A → B (which corresponds to the rearrangement of α–pinene oxide), if proceeded to a state of dynamic equilibrium, is completely described by specification of temperature (T), pressure (P) and chemical composition. Equilibrium constant, $K_{eq}$, is defined by:

$$K_{eq} = \frac{C_A}{C_B} \qquad (a.1)$$

where $C_A$ – concentration of α-pinene oxide;

$C_B$ – concentration of campholenic aldehyde.

Standard Gibbs free-energy change ($\Delta G^0$) for the reaction can be written as:

$$\Delta G_T^0 = -RT\ln K_P = \Delta G_{fT}^0(B) - \Delta G_{fT}^0(A), \qquad (a.2)$$

where: $\Delta G_{fT}^0(A)$ and $\Delta G_{fT}^0(B)$ are standard Gibbs free energies of formation for reactant (A) and product (B) and R is universal gas constant. Relation between Gibbs free energy, standard enthalpy $\Delta H_T^0$ and standard entropy change $\Delta S_T^0$ for the reaction is defined by the following equation:

$$\Delta G_T^0 = \Delta H_T^0 - T\Delta S_T^0. \qquad (a.3)$$

$\Delta H_T^0$ and $\Delta S_T^0$ connection with standard absolute enthalpies/entropies of the species is specified by equations a.4 and a.5:

$$\Delta H_T^0 = \Delta H_{fT}^0(B) - \Delta H_{fT}^0(A) \qquad (a.4)$$

$$\Delta S_T^0 = \Delta S_T^0(B) - \Delta S_T^0(A). \qquad (a.5)$$

Standard entropies and standard heats of formation of reactant and product give the value of the equilibrium constant and thus they represent our basic thermochemical data. Their variation with temperature is given by:

$$\left[\frac{\partial(\Delta H^0)}{\partial T}\right]_P = \Delta C_P^0 \qquad \left[\frac{\partial(\Delta S^0)}{\partial T}\right]_P = \frac{\Delta C_P^0}{T} \tag{a.6}$$

where $\Delta C_P^0$ is the standard molar heat capacity for the reaction and can be calculated as:

$$\Delta C_P^0 = C_P^0(B) - C_P^0(A). \tag{a.7}$$

$\Delta C_P^0(A)$ and $\Delta C_P^0(B)$ are standard molar heat capacities of reactant and product respectively.

To obtain the values for $\Delta H_T^0$ and $\Delta S_T^0$, if the values for $\Delta H_{T_0}^0$ and $\Delta S_{T_0}^0$ are known, functional dependence of $\Delta C_P^0$ between temperatures T and $T_0$ is needed. Integration of equation (a.6) gives next relations:

$$\Delta H_T^0 = \Delta H_{T_0}^0 + \int_{T_0}^{T} (\Delta C_p^0)\,dT\,; \tag{a.8}$$

$$\Delta S_T^0 = \Delta S_{T_0}^0 + \int_{T_0}^{T} \left(\frac{\Delta C_P^0}{T}\right) dT\,. \tag{a.9}$$

Since $\Delta C_P^0$ for reactions tend to be very small and change very little over intervals of temperature, it seems adequate to take an average value $\Delta C_P^0$ over the $(T - T_0)$ interval and therefore previous formula becomes:

$$\Delta H_T^0 = \Delta H_{T_0}^0 + \Delta C_{pT_m}^0 (T - T_0) \tag{a.10}$$

$$\Delta S_T^0 = \Delta S_{T_0}^0 + \Delta C_{pT_m}^0 \ln\frac{T}{T_0}\,. \tag{a.11}$$

$\Delta C_P^0$ is commonly represented by polynomial expression:

$$\Delta C_p^0 = a + bT + cT^2 \qquad (a.12)$$

where a, b, c are polynomial constants.

Several groups of authors have proposed empirical methods of correlation that allow us to estimate the thermodynamic properties of compounds. All of these methods are based on the assumption that a given thermodynamic property, such as entropy, of an organic substance can be resolved into contributions from each of the constituent groups in the molecule. With tables of such group contributions assembled from available experimental data, we can estimate the thermodynamic properties of any molecule by adding the contributions of the constituent groups. Additional corrections can be made for the effect of neighbouring groups.

### A.1.1 BENSON'S METHOD

One of the principles of this method [A1] is to calculate the data by adding partial bond contributions that the molecule consists of. For example, $CHCl_3$ consists of one C–H and three C–Cl bonds, so $\Delta C_p^0$ and $\Delta S_T^0$ can be represented as:

$$\Delta C_P^0(CHCl_3) = \Delta C_P^0(C-H) + 3\Delta C_P^0(C-Cl) \qquad (a.13)$$

$$\Delta S_T^0(CHCl_3) = \Delta S_T^0(C-H) + 3\Delta S_T^0(C-Cl) - R\ln 3. \qquad (a.14)$$

The (–R ln3) is added for a symmetry correction (–R lnσ, where σ is the symmetry number). There are other types of corrections for molecules in this method, such as various ring corrections; cis-, ortho- and gauche corrections.

Other more useful principle is calculation of data by treating the molecule as composure of groups and again adding the data values of those constituent groups (a group being a polyvalent atom with ligancy ≥ 2 in a molecule with all his ligands). First step is to identify the polyvalent atom and then its ligands. In the Tables given by Benson [A1], C–$(H)_3$(C) represents a C atom connected to three H atoms and one C atom, therefore it is a primary methyl group. One group molecules, such as $CHCl_3$ or $CH_4$ have only one such atom and are irreducible entities; therefore can not be treated by group contribution method.

### *A.1.1.1 Data for α–pinene oxide*

Using the data from Benson's Tables (Tables A.3–A.10), thermochemical properties for α–pinene oxide can be calculated. Table A.1 shows extracted data which are used for this estimation method.

**Table A.1. Estimation of thermochemical properties of α-pinene oxide**

| Group | $\Delta H^0_{f,298}$ (kcal/mol) | $\Delta S^0_{int,298}$ (cal/molK) | $\Delta C^0_{P\ 300}$ (cal/molK) | $\Delta C^0_{P\ 400}$ (cal/molK) | Number of groups |
|---|---|---|---|---|---|
| C–(C)(H)$_3$ | -10.2 | 30.41 | 6.19 | 7.84 | 3 |
| C–(C)$_2$(H)$_2$ | -4.93 | 9.42 | 5.5 | 6.95 | 2 |
| C–(C)$_3$(H) | -1.9 | -12.07 | 4.54 | 6 | 2 |
| C–(C)$_4$ | 0.5 | -35.1 | 4.37 | 6.13 | 1 |
| O–(C)$_2$ | -23.2 | 8.68 | 3.4 | 3.7 | 1 |
| C–(C)$_2$(H)(O) | -7.2 | -11 | 4.8 | 6.64 | 1 |
| C–(O)(C)$_3$ | -6.6 | -33.56 | 4.33 | 6.19 | 1 |
| C–O–C ring correction | 26.9 | 30.5 | -2 | -2.8 | 1 |
| Cyclobutane ring correction | 26.2 | 29.8 | -4.61 | -3.89 | 1 |
| Cyclohexane ring correction | 0 | 18.8 | -5.8 | -4.1 | 1 |

As described previously, **C**–(C)(H)$_3$ groups are three methyl groups in the molecule (C atoms 1, 2 and 3 in Figure A.1), **C**–(C)$_2$(H)$_2$ are two C atoms connected to two another C atoms and two H atoms (2 groups C–**C**H$_2$–C, C atom (bold) the one forming the group; atoms 4 and 5 in Figure A.1), **C**–(C)$_3$(H) are two groups formed by atoms 6 and 7; **C**–(C)$_4$ are C atoms without any bonds to H atoms, connected to four other C atoms (C atom 9); **C**–(C)$_2$(H)(O) represents atom 8 connected to two carbons, H and O while **C**–(C)$_3$(O) is carbon numbered 10 in the Figure A.1.

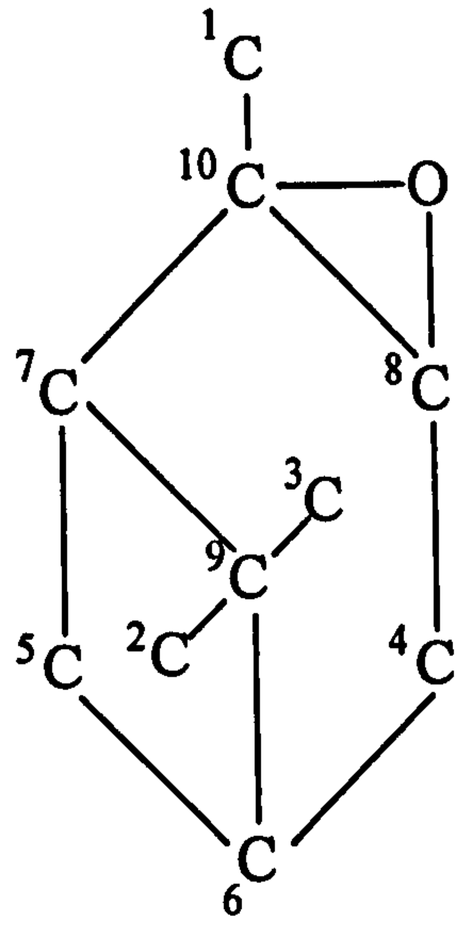


**Figure A.1. Constituent atoms of α–pinene oxide**

In the interest of better presentation, H atoms are not presented in Figure A.1. There is also contribution of O atom connected to two carbons, **O**–(C)$_2$.

There are three ring corrections that need to be added, one is for the cyclohexane ring (between C atoms 4, 6, 5, 7, 10 and 8), one for cyclobutane ring (atoms 5, 6, 9 and 7) and one for C atoms 8 and 10 which are forming the 3-membered ring with O atom.

After the structure was determined, estimated (added) values of $\Delta H^0_{f,298}$, $\Delta S^0_{int,298}$ and $\Delta C^0_{P\ 300}$ are as follows:

$\Delta H^0_{f,298}$ = -27.66 kcal/mol = **-115.73 kJ/mol**
$\Delta S^0_{int,298}$ = 94.05 cal/molK = **393.50 J/molK**
$\Delta C^0_{P\ 300}$ = 43.14 cal/molK = **180.50 J/molK**

### *A.1.1.2 Data for campholenic aldehyde*

Same principle was used for obtaining data for campholenic aldehyde. Table A.2 represents the group values used from Tables A.3–10.

**Table A.2. Estimation of thermochemical properties of campholenic aldehyde**

| Group | $\Delta H^0_{f,298}$ (kcal/mol) | $\Delta S^0_{int,298}$ (cal/molK) | $\Delta C^0_{P,300}$ (cal/molK) | $\Delta C^0_{P,400}$ (cal/molK) | Number of groups |
|---|---|---|---|---|---|
| C–(C or $C_{dbl}$[a])$(H)_3$ | -10.2 | 30.41 | 6.19 | 7.84 | 3 |
| C–$(C)_3$(H) | -1.9 | -12.07 | 4.54 | 6 | 1 |
| Cyclopentene ring correction | 5.9 | 25.8 | -5.98 | -5.35 | 1 |
| CO–(H)(C) | -29.1 | 34.9 | 7 | 7.8 | 1 |
| C–$(C_{dbl})(C)_3$ | 1.68 | -34.72 | 3.99 | 6.04 | 1 |
| $C_{dbl}$–$(C)_2$ | 10.34 | -12.7 | 4.1 | 4.61 | 1 |
| $C_{dbl}$–(C)(H) | 8.59 | 7.97 | 4.16 | 5.03 | 1 |
| C–$(C_{dbl})(C)(H)_2$ | -4.76 | 9.8 | 5.12 | 6.86 | 1 |
| C–$(CO)(C)(H)_2$ | -5.2 | 9.6 | 6.2 | 7.7 | 1 |

(a) By convention group contribution of C–$(X)(H)_3$ is equal to that of C–$(C)(H)_3$ when X is $C_{dbl}$, $C_{tpl}$, $C_B$, O or S.

Again the same theory is applied. Campholenic aldehyde molecule consists of three groups **C**–$(C)(H)_3$ (methyl groups, atoms 1, 2 and 3 on Figure A.2), one **C**-$(C)_3$(H) group (atom 4), one **CO**–(H)(C) group (C atom 5), one **C**–$(C_{dbl})(C)_3$ (atom 6 in Figure A.2), one $\mathbf{C_{dbl}}$–$(C)_2$ (atom 7), one $\mathbf{C_{dbl}}$–(C)(H) group (atom 8), one group **C**–$(C_{dbl})(C)(H)_2$ (C atom 9) and one group **C**–$(CO)(C)(H)_2$ (atom 10).

There is also a 5-ring correction to be added.

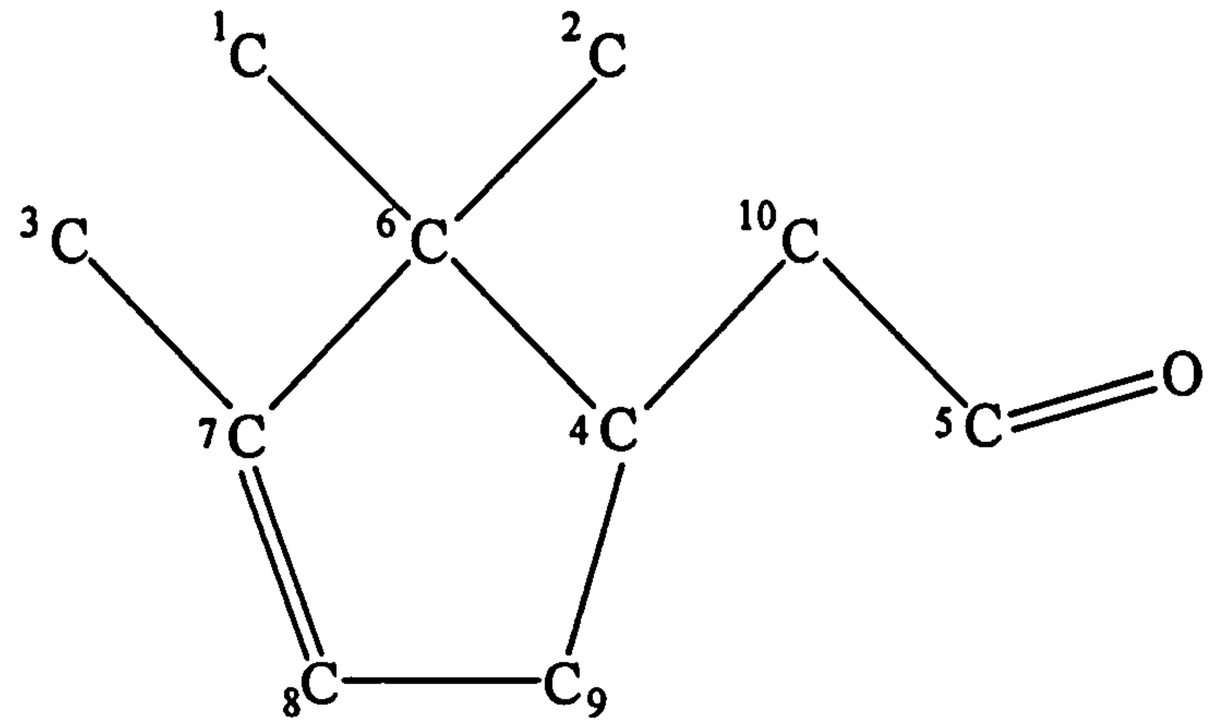


**Figure A.2. Constituent atoms of campholenic aldehyde**

Following data were therefore calculated:

$\Delta H^0_{f,298}$ = -45.05 kcal/mol = **-188.49 kJ/mol**

$\Delta S^0_{int,298}$ = 119.81 cal/molK = **501.29 J/molK**

$\Delta C^0_{P\ 300}$ = 47.7 cal/molK = **199.58 J/molK**

Hence the heat of the rearrangement reaction can be estimated by this method.

$\Delta H^0_{r,298}$ = -17.39 kcal/mol = **-72.76 kJ/mol**

The following Tables contain data for calculation of thermochemical characteristics of compounds used in this study. Group values can be found in Tables 3 and 4 (only for compounds containing C, H and O as appropriate for the case of α-pinene oxide rearrangement), while Tables 5–10 contain various corrections that can be applied.

## Table A.3. Group values (Hydrocarbons) (Reprinted from [A1])

| Group | $\Delta H_f^\circ$ 298 | $S_{int}^\circ$ 298 | $C_p^\circ$ 300 | 400 | 500 | 600 | 800 | 1000 | 1500 |
|---|---|---|---|---|---|---|---|---|---|
| C—(H)$_3$(C) | −10.20 | 30.41 | 6.19 | 7.84 | 9.40 | 10.79 | 13.02 | 14.77 | 17.58 |
| C—(H)$_2$(C)$_2$ | −4.93 | 9.42 | 5.50 | 6.95 | 8.25 | 9.35 | 11.07 | 12.34 | 14.25 |
| C—(H)(C)$_3$ | −1.90 | −12.07 | 4.54 | 6.00 | 7.17 | 8.05 | 9.31 | 10.05 | 11.17 |
| C—(C)$_4$ | 0.50 | −35.10 | 4.37 | 6.13 | 7.36 | 8.12 | 8.77 | 8.76 | 8.12 |
| | | | | | | | | | |
| C$_d$—(H)$_2$ | 6.26 | 27.61 | 5.10 | 6.36 | 7.51 | 8.50 | 10.07 | 11.27 | 13.19 |
| C$_d$—(H)(C) | 8.59 | 7.97 | 4.16 | 5.03 | 5.81 | 6.50 | 7.65 | 8.45 | 9.62 |
| C$_d$—(C)$_2$ | 10.34 | −12.70 | 4.10 | 4.61 | 4.99 | 5.26 | 5.80 | 6.08 | 6.36 |
| C$_d$—(C$_b$)(H) | 6.78 | 6.38 | 4.46 | 5.79 | 6.75 | 7.42 | 8.35 | 8.99 | 9.98 |
| C$_d$—(C$_b$)(C) | 8.88 | −14.6 | (4.40) | (5.37) | (5.93) | (6.18) | (6.50) | (6.62) | (6.72) |
| [C$_d$—(C$_b$)(H)] | 6.78 | 6.38 | 4.46 | 5.79 | 6.75 | 7.42 | 8.35 | 8.99 | 9.98 |
| C$_d$—(C$_b$)(C) | 8.64 | (−14.6) | (4.40) | (5.37) | (5.93) | (6.18) | (6.50) | (6.62) | (6.72) |
| [C$_d$—(C$_b$)(H)] | 6.78 | 6.38 | 4.46 | 5.79 | 6.75 | 7.42 | 8.35 | 8.99 | 9.98 |
| C$_d$—(C$_b$)$_2$ | 8.0 | | | | | | | | |
| C$_d$—(C$_b$)$_2$ | 4.6 | | | | | | | | |
| | | | | | | | | | |
| C—(C$_b$)(C)(H)$_2$ | −4.76 | 9.80 | 5.12 | 6.86 | 8.32 | 9.49 | 11.22 | 12.48 | 14.36 |
| C—(C$_b$)$_2$(H)$_2$ | −4.29 | (10.2) | (4.7) | (6.8) | (8.4) | (9.6) | (11.3) | (12.6) | (14.4) |
| C—(C$_d$)(C$_b$)(H)$_2$ | −4.29 | (10.2) | (4.7) | (6.8) | (8.4) | (9.6) | (11.3) | (12.6) | (14.4) |
| C—(C$_b$)(C)(H)$_2$ | −4.73 | 10.30 | 4.95 | 6.56 | 7.93 | 9.08 | 10.86 | 12.19 | 14.20 |
| C—(C$_b$)(C)(H)$_2$ | −4.86 | 9.34 | 5.84 | 7.61 | 8.98 | 10.01 | 11.49 | 12.54 | 13.76 |
| C—(C$_d$)(C)$_2$(H) | −1.48 | (−11.69) | (4.16) | (5.91) | (7.34) | (8.19) | (9.46) | (10.19) | (11.28) |
| C—(C$_b$)(C)$_2$(H) | −1.72 | (−11.19) | (3.99) | (5.61) | (6.85) | (7.78) | (9.10) | (9.90) | (11.12) |
| C—(C$_b$)(C)$_2$(H) | −0.98 | (−12.15) | (4.88) | (6.66) | (7.90) | (8.75) | (9.73) | (10.25) | (10.68) |
| | | | | | | | | | |
| C—(C$_d$)(C)$_3$ | 1.68 | (−34.72) | (3.99) | (6.04) | (7.43) | (8.26) | (8.92) | (8.96) | (8.23) |
| C—(C$_b$)(C)$_3$ | 2.81 | (−35.18) | (4.37) | (6.79) | (8.09) | (8.78) | (9.19) | (8.96) | (7.63) |
| | | | | | | | | | |
| C$_t$—(H) | 26.93 | 24.7 | 5.27 | 5.99 | 6.49 | 6.87 | 7.47 | 7.96 | 8.85) |
| C$_t$—(C) | 27.55 | 6.35 | 3.13 | 3.48 | 3.81 | 4.09 | 4.60 | 4.92 | 6.35) |
| C$_t$—(C$_d$) | 29.20 | (6.43) | (2.57) | (3.54) | (3.50) | (4.92) | (5.34) | (5.50) | (5.80) |
| C$_t$—(C$_b$) | (29.20) | 6.43 | 2.57 | 3.54 | 3.50 | 4.92 | 5.34 | 5.50 | 5.80 |
| | | | | | | | | | |
| C$_b$—(H) | 3.30 | 11.53 | 3.24 | 4.44 | 5.46 | 6.30 | 7.54 | 8.41 | 9.73 |
| C$_b$—(C) | 5.51 | −7.69 | 2.67 | 3.14 | 3.68 | 4.15 | 4.96 | 5.44 | 5.98 |
| C$_b$—(C$_d$) | 5.68 | −7.80 | 3.59 | 3.97 | 4.38 | 4.72 | 5.28 | 5.61 | 5.75 |
| [C$_b$—(C$_b$)] | 5.68 | −7.80 | 3.59 | 3.97 | 4.38 | 4.72 | 5.28 | 5.61 | 5.75 |
| C$_b$—(C$_b$) | 4.96 | −8.64 | 3.33 | 4.22 | 4.89 | 5.27 | 5.76 | 5.95 | (6.05) |
| | | | | | | | | | |
| C$_b$ | 34.20 | 6.0 | 3.9 | 4.4 | 4.7 | 5.0 | 5.3 | 5.5 | 5.7 |
| | | | | | | | | | |
| C$_{br}$—(C$_b$)$_2$(C$_{br}$) | 4.8 | −5.0 | 3.0 | 3.7 | 4.2 | 4.6 | 5.2 | 5.5 | — |
| C$_{br}$—(C$_b$)(C$_{br}$)$_2$ | 3.7 | −5.0 | 3.0 | 3.7 | 4.2 | 4.6 | 5.2 | 5.5 | — |
| C$_{br}$—(C$_{br}$)$_3$ | 1.5 | 1.4 | 2.0 | 2.9 | 3.5 | 4.0 | 4.7 | 5.1 | — |

# Table A.4. Oxygen containing compounds (Reprinted from [A1])

| Group | $\Delta H^\circ_{f\,298}$ | $S^\circ_{m\,298}$ | $C^\circ_p$ 300 | 400 | 500 | 600 | 800 | 1000 | 1500 |
|---|---|---|---|---|---|---|---|---|---|
| $O(H_2)$ | −57.8 | 45.1 | 8.0 | 8.4 | 9.2 | 9.9 | 11.2 | | |
| O(H)(C) | −37.9 | 29.07 | 4.3 | 4.4 | 4.8 | 5.2 | 6.0 | 6.6 | |
| $O(H)(C_B)$ | −37.9 | 29.1 | 4.3 | 4.5 | 4.8 | 5.2 | 6.0 | 6.6 | |
| O(H)(O) | −16.3 | 27.85 | 5.2 | 5.8 | 6.3 | 6.7 | 7.2 | 7.5 | 8.2 |
| O(H)(CO) | −58.1 | 24.5 | 3.8 | 5.0 | 5.8 | 6.3 | 7.2 | 7.8 | |
| $O(C)_2$ | −23.2 | 8.68 | 3.4 | 3.7 | 3.7 | 3.8 | 4.4 | 4.6 | |
| $O(C)(C_m)$ | −30.5 | 9.7 | | | | | | | |
| $O(C)(C_B)$[a] | −23.0 | | | | | | | | |
| O(C)(O) | −4.5 | [9.4] | 3.7 | 3.7 | 3.7 | 3.7 | 4.2 | 4.2 | 4.8 |
| O(C)(CO) | −43.1 | 8.4 | | | | | | | |
| $O(C_d)_2$ | −33.0 | 10.1 | | | | | | | |
| $O(C_m)_2$ | −21.1 | | | | | | | | |
| $O(C_d)(CO)$ | −45.2 | | | | | | | | |
| $O(C_B)(CO)$ | −36.7 | | | | | | | | |
| O(O)(CO) | −19.0 | | | | | | | | |
| $O(CO)_2$ | −46.5 | | | | | | | | |
| $O(O)_2$ | [19.0] | [9.4] | [3.7] | [3.7] | [3.7] | [3.7] | [4.2] | [4.2] | [4.8] |
| $CO(H)_2$ | −26.0 | 52.3 | 8.5 | 10.5 | 13.4 | 14.8 | 17.0 | | |
| CO(H)(C) | −29.1 | 34.9 | 7.0 | 7.8 | 8.8 | 9.7 | 11.2 | 12.2 | |
| $CO(H)(C_m)$[b] | −29.1 | | | | | | | | |
| $CO(H)(C_d)$ | −29.1 | | | | | | | | |
| $CO(H)(C_t)$ | −29.1 | | | | | | | | |
| CO(H)(CO) | −25.3 | | | | | | | | |
| CO(H)(O) | −32.1 | 34.9 | 7.0 | 7.9 | 8.8 | 9.7 | 11.2 | 12.2 | |
| $CO(C)_2$ | −31.4 | 15.0 | 5.6 | 6.3 | 7.1 | 7.8 | 8.9 | 9.6 | |
| $CO(C)(C_B)$ | −30.9 | | | | | | | | |
| $CO(C_m)_2$ | −25.8 | | | | | | | | |
| CO(C)(O) | −35.1 | 14.8 | 6.0 | 6.7 | 7.3 | 8.0 | 8.9 | 9.4 | |
| CO(C)(CO) | −29.2 | | | | | | | | |
| $CO(C_d)(O)$[c] | −32.0 | | | | | | | | |
| $CO(C_B)(O)$ | −36.6 | | | | | | | | |
| $CO(C_m)(CO)$ | −26.8 | | | | | | | | |
| $CO(O_2)$ | −29.9 | | | | | | | | |
| CO(O)(CO) | −29.3 | | | | | | | | |
| $C(H)_3(O)$[d] | −10.08 | 30.41 | 6.19 | 7.84 | 9.40 | 10.79 | 13.03 | 14.77 | 17.58 |
| $C(H)_2(O)(C)$ | −8.1 | 9.8 | 4.99 | 6.85 | 8.30 | 9.43 | 11.11 | 12.33 | |
| $C(H)_2(O)(C_d)$ | −6.5 | | | | | | | | |
| $C(H)_2(O)(C_B)$ | −8.1 | 9.7 | | | | | | | |
| $C(H)_2(O)(C_t)$ | −6.5 | | | | | | | | |
| $C(H)_2(O)(CO)$ | | | | | | | | | |
| $C(H)_2(O)_2$ | −16.1 | | | | | | | | |
| $C(H)(O)(C)_2$ | −7.2 | −11.0 | 4.80 | 6.64 | 8.10 | 8.73 | 9.81 | 10.40 | |
| $C(H)(O)_2(C)$ | −16.3 | | | | | | | | |
| $C(O)(C)_3$ | −6.6 | −33.56 | 4.33 | 6.19 | 7.25 | 7.70 | 8.20 | 8.24 | |
| $C(O)_2(C)_2$ | −18.6 | | | | | | | | |
| $C(H)_3(CO)$[e] | −10.08 | 30.41 | 6.19 | 7.84 | 9.40 | 10.79 | 13.02 | 14.77 | 17.58 |
| $C(H)_2(CO)(C)$ | −5.2 | 9.6 | 6.2 | 7.7 | 8.7 | 9.5 | 11.1 | 12.2 | |
| $C(H)_2(CO)(C_d)$ | −3.8 | | | | | | | | |
| $C(H)_2(CO)(C_B)$ | −5.4 | | | | | | | | |
| $C(H)_2(CO)(C_t)$ | −5.4 | | | | | | | | |
| $C(H)_2(CO)_2$ | −7.6 | | | | | | | | |
| $C(H)(CO)(C)_2$[f] | −1.7 | −12.0 | | | | | | | |
| $C(CO)(C)_3$ | 1.4 | | | | | | | | |
| $C_d(O)(H)$[g] | 8.6 | 8.0 | 4.2 | 5.0 | 5.8 | 6.5 | 7.6 | 8.4 | 9.6 |
| $C_d(O)(C)$[h] | 10.3 | | | | | | | | |
| $C_d(O)(C_d)$[i] | 8.9 | | | | | | | | |
| $C_d(O)(CO)$ | 11.6 | | | | | | | | |
| $C_d(H)(CO)$ | 5.0 | | | | | | | | |
| $C_d(CO)(C)$ | 7.5 | | | | | | | | |
| $C_B(O)$ | −0.9 | −10.2 | 3.9 | 5.3 | 6.2 | 6.6 | 6.9 | 6.9 | |
| $C_B(CO)$ | 3.7 | | | | | | | | |

**Table A.5. Ring corrections for oxygen containing compounds (Reprinted from [A1])**

| Strain | $\Delta H^\circ_{f\,298}$ | $S^\circ_{int\,298}$ | $C_p^\circ$ 300 | 400 | 500 | 600 | 800 | 1000 | 1500 |
|---|---|---|---|---|---|---|---|---|---|
| Ether–oxygen *gauche* | 0.5 | | | | | | | | |
| Di-tertiary ethers | 7.8 | | | | | | | | |
| Oxygen *gauche* | 0 | | | | | | | | |
| Oxygen *ortho* | 0 | | | | | | | | |
|  | 26.9 | 30.5 | −2.0 | −2.8 | −3.0 | −2.6 | −2.3 | −2.3 | |
|  | 25.7 | 27.7 | −4.6 | −5.0 | −4.2 | −3.5 | −2.6 | +0.2 | |
|  | 5.9 | | | | | | | | |
| 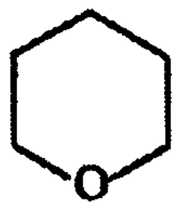 | 0.5 | | | | | | | | |

**Table A.6. Corrections to be applied to ring-compound estimates (Reprinted from [A1])**

| Ring ($\sigma$) | $\Delta H^\circ_f$ 298 | $S^\circ_{int}$ 298 | $C_p^\circ$ 300 | 400 | 500 | 600 | 800 | 1000 | 1500 |
|---|---|---|---|---|---|---|---|---|---|
| Cyclopropane (6) | 27.6 | 32.1 | −3.05 | −2.53 | −2.10 | −1.90 | −1.77 | −1.62 | (−1.52) |
| Cyclopropene (2) | 53.7 | 33.6 | | | | | | | |
| Cyclobutane (8) | 26.2 | 29.8 | −4.61 | −3.89 | −3.14 | −2.64 | −1.88 | −1.38 | −0.67 |
| Cyclobutene (2) | 29.8 | 29.0 | −2.53 | −2.19 | −1.89 | −1.68 | −1.48 | −1.33 | −1.22 |
| Cyclopentane (10) | 6.3 | 27.3 | −6.50 | −5.5 | −4.5 | −3.8 | −2.8 | −1.93 | −0.37 |
| Cyclopentene (2) | 5.9 | 25.8 | −5.98 | −5.35 | −4.89 | −4.14 | −2.93 | −2.26 | −1.08 |
| Cyclopentadiene (2) | 6.0 | 28.0 | −4.3 | | | | | | |
| Cyclohexane (6) | 0 | 18.8 | −5.8 | −4.1 | −2.9 | −1.3 | 1.1 | 2.2 | 3.3 |
| Cyclohexene (2) | 1.4 | 21.5 | −4.28 | −3.04 | −1.98 | −1.43 | −0.29 | 0.08 | 0.81 |
| Cyclohexadiene 1,3 | 4.8 | | | | | | | | |
| Cyclohexadiene 1,4 | 0.5 | | | | | | | | |
| Cycloheptane (1) | 6.4 | 15.9 | | | | | | | |
| Cycloheptene | 5.4 | | | | | | | | |
| Cycloheptadiene, 1,3 | 6.6 | | | | | | | | |
| Cycloheptatriene 1,3,5 (1) | 4.7 | 23.7 | | | | | | | |
| Cyclooctane (8) | 9.9 | 16.5 | | | | | | | |
| *cis*-Cyclooctene | 6.0 | | | | | | | | |
| *trans*-Cyclooctene | 15.3 | | | | | | | | |
| Cyclooctatriene 1,3,5 | 8.9 | | | | | | | | |
| Cyclooctatetraene | 17.1 | | | | | | | | |
| Cyclononane | 12.8 | | | | | | | | |
| *cis*-Cyclononene | 9.9 | | | | | | | | |
| *trans*-Cyclononene | 12.8 | | | | | | | | |
| Cyclodecane | 12.6 | | | | | | | | |
| Cyclododecane | 4.4 | | | | | | | | |
| Spiropentane (4) | 63.5 | 67.6 | | | | | | | |
| Bicycloheptadiene | 31.6 | | | | | | | | |
| Biphenylene | 58.8 | | | | | | | | |

**Table A.7. Comparison of the entropies of some ring compounds with open chain compounds (Reprinted from [A1])**

| Ring ($\sigma$) | | $S_{int}$[a] | Open-Chain Compound ($\sigma$) | | $S_{int}$[a] | $\Delta S_{int\ rot}$[b] | Residual[c] Ring Entropy |
|---|---|---|---|---|---|---|---|
| $C_3H_6$ | (4) | 55.3 | $C_2H_6$ | (18) | 60.7 | 5.4 | |
| $CH_3CH{=}CH_2$ | (3) | 66.1 | $C_3H_8$ | (18) | 70.3 | 4.2 | |
| *Trans*-Butene-2 | (18) | 76.7 | $n$-$C_4H_{10}$ | (18) | 79.7 | 3.0 | |
| $C_3H_6$ | (6) | 60.4 | $C_3H_8$ | (18) | 70.3 | 4.9 | 0 |
| $\overline{CH_2CH_2O}$ | (2) | 59.5 | $C_2H_5OH$ | (3) | 69.7 | 5.1 | |
| | | | $CH_3OCH_3$ | (18) | 69.5 | 5.0 | |
| $\overline{CH_2CH_2NH}$ | (1) | | $C_2H_5NH_2$ | (3) | (69.9 | | |
| | | | $(CH_3)_2NH$ | (9) | 69.8 | | |
| $\overline{CH_2CH_2S}$ | (2) | 62.5 | $(CH_3)_2S$ | (18) | 74.1 | 5.8 | |
| | | | $C_2H_5SH$ | (18) | 73.0 | 5.3 | |
| $C_4H_8$ | (8) | 67.6 | $n$-$C_4H_{10}$ | (18) | 79.7 | 4.0 | 2.7 |
| $C_5H_{10}$ | (10) | 74.6 | $n$-$C_5H_{12}$ | (18) | 89.1 | 3.6 | 5.2 |
| $C_6H_{12}$ | (6) | 74.9 | $n$-$C_6H_{14}$ | (18) | 98.5 | 4.7 | 1.0 |
| $C_7H_{14}$ | (1) | 81.8 | $n$-$C_7H_{16}$ | (18) | 107.9 | 4.4 | 3.0 |
| $C_8H_{16}$[d] | (8) | 91.9 | $n$-$C_8H_{18}$ | (18) | 117.3 | 3.6 | 9.1 |

[a] $S^{\circ}_{int} = S^{\circ} + R \ln \sigma$.

[b] $\Delta S_{int\ rot} = [S^{\circ}_{int\ (open\ chain)} - S^{\circ}_{int\ (ring)}]/(n-1)$, where $n$ is the number of atoms in the ring.

[c] Defined with reference to cyclopropane as $(n-1)[4.9 - \Delta S^{\circ}_{int\ rot}]$.

[d] Crown form.

**Table A.8. Entropies of some saturated and unsaturated rings (Reprinted from [A1])**

| Ring | ($\sigma$) | $S^{\circ}_{int}$ | Ring-($H_2$) | ($\sigma$) | $S^{\circ}_{int}$ | $\Delta S^{\circ}_{int}$ |
|---|---|---|---|---|---|---|
| $C_3H_6$ | (6) | 60.4 | $C_3H_4$ | (2) | 59.8 | −0.6 |
| $C_4H_8$ | (8) | 67.6 | $C_4H_6$ | (2) | 64.4 | −3.2 |
| $C_5H_{10}$ | (10) | 74.6 | $C_5H_8$ | (2) | 70.6 | −4.0 |
| $C_5H_8$ | (2) | 70.6 | $C_5H_6$ | (2) | 67.0 | −3.6 |
| $C_6H_{12}$ | (6) | 74.9 | $C_6H_{10}$ | (2)($n=2$) | 74.3 | −0.6 |
| $C_6H_{10}$ | (2) | 74.3 | [benzene][a] | (12) | 69.3 | −5.0 |

[a] Here we have lost $2H_2$.

**Table A.9. Tightness ring corrections on cyclisation changes (Reprinted from [A1])**

| Ring System | Double Bonds | $\Delta S^{\circ}_{3(a)}$ | $\Delta C^{\circ}_{p}$ ($T$°K) | | | | |
|---|---|---|---|---|---|---|---|
| | | | 300 | 500 | 800 | 1000 | 1500 |
| $C_3$ | 0 | 0 | 0 | 0 | 0 | 0 | 0 |
| | 1 | 0 | 0 | 0 | 0 | 0 | 0 |
| $C_4$ | 0 | 1.9 | 0.2 | 0.1 | 0 | 0 | 0 |
| | 1 | −1.9 | −0.2 | −0.1 | 0 | 0 | 0 |
| | 2 | −1.4 | −0.7 | −0.3 | −0.1 | −0.1 | 0 |
| $C_5$ | 0 | 3.9 | −0.8 | −0.9 | −1.0 | −1.0 | −1.0 |
| | 1 | −3.9 | 0.8 | 0.9 | 1.0 | 1.0 | 1.0 |
| | 2 | −2.8 | −1.4 | −0.6 | −0.2 | −0.2 | 0 |
| $C_6$ | 0 | 0 | 0 | 0 | 0 | 0 | 0 |
| | 1 | 0 | −1.0 | −1.0 | −1.0 | −1.0 | −1.0 |
| | 2 | 0(−1.4)[c] | 0(−0.7)[c] | 0(−0.3) | 0(−0.1) | 0 (0) | 0 (0) |
| | 3 | −2.8 | −1.4 | −0.6 | −0.3 | −0.2 | −0.1 |
| $C_7$ | 0 | 2.5 | 0.3 | 0.1 | −0.2 | −0.5 | −0.7 |
| | 1 | −2.5 | −0.3 | −0.1 | 0.2 | 0.5 | 0.7 |
| | 2 | 0(−1.4)[c] | 0(−0.7)[c] | 0(−0.3) | 0(−0.1) | 0 (0) | 0 (0) |
| | 3 | −1.4 | −0.7 | −0.3 | −0.1 | −0.1 | 0 |
| $C_8$ | 0 | 8.4 | 0.8 | 0.5 | −0.4 | −0.8 | −1.4 |
| | 1 | −3.2 | −0.3 | −0.1 | 0.2 | 0.4 | 0.7 |
| | 2[d] | | | | | | |
| | (1, 3) | −4.2 | −0.4 | −0.3 | 0.1 | 0.3 | 0.6 |
| | (1, 4) | −1.0 | −0.1 | −0.1 | 0.1 | 0.1 | 0.1 |
| | (1, 5) | 0 | 0 | 0 | 0 | 0 | 0 |
| | 3 | −3.8 | −1.3 | −0.6 | −0.2 | 0 | 0 |
| | | (−1.0)[d] | (−0.1) | (−0.1) | (0) | (0) | (0) |
| | 4 | −3.4 | −1.5 | −0.7 | −0.2 | 0 | 0 |
| Spirane[b] | | 1.4 | 0.7 | 0.3 | 0.1 | 0.1 | 0 |

[a] These corrections are standardized on the tightest rings, cyclopropane and cyclohexane, which thus have zero corrections. Double bond corrections are cummulative, that is, for two double bonds, we add the corrections for the first, second, and so on.

[b] These corrections apply only when both rings are $C_4$ or smaller.

[c] Values in parentheses are for conjugated double bonds.

[d] Index numbers show position of double bonds in ring.

**Table A.10. Entropy and heat capacity changes in cyclisation (Reprinted from [A1])**

| Groups | $\Delta S^{\circ}_{300}$ | $\Delta C^{\circ}_p$ ($T$°K) | | | | |
|---|---|---|---|---|---|---|
| | | 300 | 500 | 800 | 1000 | 1500 |
| One-end $CH_3$ | −5.2 | −3.3 | −4.5 | −6.1 | −7.1 | −8.5 |
| Internal group | −4.9 | −0.8 | −0.6 | 0.0 | 0.1 | 0.7 |
| Two-end $CH_3$ | −9.3 | −4.6 | −5.0 | −6.0 | −6.6 | −7.9 |
| Introduction of double bond in ring | −0.4 | −1.4 | −3.8 | −6.3 | −7.5 | −9.3 |

### A.1.2 ANDERSON-BEYER-WATSON-YONEDA METHOD (ABWY)

In this approach the thermodynamic properties in the ideal gaseous state are estimated by considering a given compound as built up from a base group which has been modified by appropriate substitutions to yield the desired molecule [A2]. Table A.11 shows the base group properties by this method.

**Table A.11. Base group contributions**

| Base Group | $\Delta_f H^0_{m298.15K}$ (kJ/mol) | $S^0_{m298.15K}$ (kJ/(mol K)) | Heat Capacity Constants | | |
|---|---|---|---|---|---|
| | | | a | b | c |
| Methane | -74.85 | 186.19 | 16.69 | 65.61 | -9.96 |
| Cyclopentane | -77.24 | 292.88 | -41.92 | 473.71 | -182.59 |
| Cyclohexane | -123.14 | 298.24 | -52.22 | 599.78 | -230.91 |
| Benzene | 82.93 | 269.20 | -22.51 | 402.54 | -171.42 |
| Naphtalene | 150.96 | 335.64 | -28.41 | 623.25 | -268.91 |

After the base group is determined, in case of more complex molecules thermodynamic properties are obtained by adding the contributions of the appropriate substitution group(s) to the value for the base group. Table A.12 gives the values for the primary substitution of $CH_3$ group on a single C atom in each of base groups. It is worth mentioning that for the cyclic base group several carbon atoms are available for successive primary substitutions (there can be no more than one primary substitution on each C atom; that is only first replacement of H atom with $CH_3$ group is counted as a primary substitution). Second substitution of a methyl group on a single C atom is called secondary substitution and it depends on the nature of C atom on which the replacement is being made (Atom A) and on the

nature of the adjacent carbon atoms (Atom B). All the carbon atoms are described by "type", showed in Table A.13. Types are determined as such **before** the substitution is being made.

**Table A.12. Contributions of primary $CH_3$ substitution (Reprinted from [A2])**

| | | | Heat Capacity Constants | | |
|---|---|---|---|---|---|
| Base Group | $\Delta(\Delta H_m)$ | $\Delta S_m$ | $\Delta a$ | $\Delta b$ | $\Delta c$ |
| Methane | −9.83 | 43.30 | 9.92 | 103.81 | −43.51 |
| Cyclopentane | | | | | |
| First primary substitution | −34.43 | 49.25 | 8.74 | 68.24 | −23.18 |
| Second primary substitution to form | | | | | |
| 1,1- | −26.61 | 17.15 | −6.02 | 116.36 | −55.56 |
| 1,2(*cis*)- | −17.87 | 24.02 | −3.64 | 110.46 | −53.22 |
| 1,2(*trans*)- | −25.02 | 24.69 | −2.47 | 107.57 | −52.13 |
| 1,3(*cis*)- | −24.18 | 24.69 | −2.47 | 107.57 | −52.13 |
| 1,3(*trans*)- | −21.92 | 24.69 | −2.47 | 107.57 | −52.13 |
| Cyclohexane | | | | | |
| First primary substitution | −33.64 | 46.32 | 11.59 | 81.21 | −39.58 |
| Second primary substitution to form | | | | | |
| 1,1- | −24.23 | 20.46 | −13.51 | 111.42 | −41.00 |
| 1,2(*cis*)- | −15.40 | 29.96 | −7.99 | 100.00 | −38.70 |
| 1,2(*trans*)- | −23.22 | 26.36 | −5.82 | 103.30 | −43.22 |
| 1,3(*cis*)- | −27.99 | 25.90 | −6.32 | 95.14 | −33.01 |
| 1,3(*trans*)- | −19.79 | 31.67 | −4.31 | 88.41 | −32.17 |
| 1,4(*cis*)- | −19.87 | 25.90 | −4.31 | 88.41 | −32.17 |
| 1,4(*trans*)- | −27.82 | 20.25 | −8.41 | 107.61 | −44.02 |
| Benzene | | | | | |
| First primary substitution | −35.48 | 47.91 | 5.77 | 64.43 | −19.50 |
| Second primary substitution to form | | | | | |
| 1,2- | −27.78 | 36.40 | 12.47 | 50.00 | −11.97 |
| 1,3- | −29.12 | 41.63 | 5.02 | 64.77 | −19.62 |
| 1,4- | −28.70 | 36.19 | 5.48 | 60.29 | −16.15 |
| 1,2,3- | −30.38 | 42.84 | 14.14 | 29.25 | 9.67 |
| 1,2,4- | −33.47 | 43.60 | 16.40 | 18.62 | 16.23 |
| 1,3,5- | −34.39 | 26.82 | 6.19 | 58.37 | −14.73 |
| Naphthalene | | | | | |
| First primary substitution to form | | | | | |
| 1- | −34.10 | 41.80 | 6.36 | 37.36 | −32.09 |
| 2- | −34.85 | 44.39 | 10.67 | 61.76 | −20.17 |
| Second primary substitution to form | | | | | |
| 1,2- | −26.40 | 30.29 | 13.05 | 64.77 | −24.56 |
| 1,3- | −27.74 | 35.56 | 5.61 | 79.54 | −32.22 |
| 1,4- | −27.32 | 30.08 | 6.07 | 75.06 | −28.74 |
| 2,3- | −26.40 | 30.29 | 13.10 | 64.77 | −24.56 |

**Table A.13. Type numbers of carbon atoms [A2]**

| Type number | Nature |
|---|---|
| 1 | $-CH_3$ |
| 2 | $-CH_2-$ |
| 3 | >CH– |
| 4 | >C< |
| 9 | C in aromatic ring |

Once we know the types of Atoms A (on which a secondary substitution is being made) and B (highest type of adjacent C atom), appropriate corrections can be made using the data from Table A.14. Corrections for introducing multiple bonds are tabulated in Table A.15.

Every time a pair of conjugated double bonds is formed by any preceding substitution, an additional contribution must be added.

**Table A.14. Contribution of secondary methyl substitution (Reprinted from [A2])**

| Type Number | | | | Heat Capacity Constants | | |
|---|---|---|---|---|---|---|
| A | B | $\Delta(\Delta H_m)$ | $\Delta S_m$ | $\Delta a$ | $\Delta b$ | $\Delta c$ |
| 1 | 1 | −21.09 | 43.68 | −3.68 | 98.16 | −42.26 |
| 1 | 2 | −20.59 | 38.87 | 1.46 | 81.42 | −31.46 |
| 1 | 3 | −15.36 | 36.61 | −0.96 | 91.63 | −38.95 |
| 1 | 4 | −15.36 | 36.61 | −0.96 | 91.63 | −38.95 |
| 1 | 9 | −19.66 | 45.31 | 1.55 | 88.53 | −37.66 |
| 2 | 1 | −28.74 | 21.46 | −2.09 | 95.69 | −41.67 |
| 2 | 2 | −26.57 | 27.32 | −0.63 | 90.67 | −37.53 |
| 2 | 3 | −22.22 | 27.36 | −4.90 | 97.61 | −41.63 |
| 2 | 4 | −20.67 | 27.49 | −1.21 | 92.05 | −37.99 |
| 2 | 9 | −24.35 | 28.07 | −3.18 | 90.37 | −36.32 |
| 3 | 1 | −31.46 | 11.76 | −2.76 | 107.70 | −49.25 |
| 3 | 2 | −28.62 | 17.99 | −6.90 | 111.71 | −51.67 |
| 3 | 3 | −20.75 | 25.94 | −6.90 | 111.71 | −51.71 |
| 3 | 4 | −23.68 | 4.56 | −4.18 | 129.54 | −66.32 |
| 3 | 9 | −26.11 | 28.07 | −3.18 | 90.37 | −36.32 |

**Table A.15. Multiple bond contributions replacing single bonds (Reprinted from [A2])**

| Type of Bond or Correction | $\Delta(\Delta H_m)$ | $\Delta S_m$ | Heat Capacity Constants | | |
|---|---|---|---|---|---|
| | | | $\Delta a$ | $\Delta b$ | $\Delta c$ |
| 1=1 | 136.98 | −10.04 | 0.50 | −32.76 | 3.72 |
| 1=2 | 126.15 | −5.98 | 3.81 | −50.92 | 16.32 |
| 1=3 | 116.90 | 0.71 | 12.80 | −71.38 | 27.91 |
| 2=2(cis) | 118.41 | −6.32 | −6.40 | −37.57 | 11.30 |
| 2=2(trans) | 114.43 | −11.38 | 9.16 | −67.53 | 26.78 |
| 2=3 | 114.64 | 0.59 | −1.05 | −54.06 | 21.21 |
| 3=3 | 115.90 | −2.09 | 5.90 | −95.86 | 57.53 |
| 1≡1 | 311.42 | −28.66 | 19.16 | −98.74 | 22.97 |
| 1≡2 | 290.79 | −20.79 | 16.53 | −117.07 | 40.71 |
| 2≡2 | 274.22 | −23.93 | 12.84 | −127.03 | 51.67 |
| Adjacent double bonds | 41.38 | −13.26 | 9.75 | −7.78 | 2.13 |
| Conjugated double bonds | −15.31 | −16.99 | −6.69 | 37.28 | −27.49 |
| Double bond conjugated with aromatic ring | −7.20 | −9.50 | 5.36 | −9.08 | 5.19 |
| Triple bond conjugated with aromatic ring | 8.8 | −20.1 | −3.8 | 4.6 | 0.4 |
| Conjugated triple bonds | 17.6 | −20.5 | 3.3 | 14.6 | −14.6 |
| Conjugated double and triple bonds | 13.8 | −5.9 | 12.6 | 22.2 | 9.6 |

Introduction of various functional groups instead of one or two of the methyl groups on a given C atom is shown in Table A.16. Introduction of =O structure requires replacement of two methyl groups (which must be substituted **before** they are replaced by =O); all the other groups replace one methyl group. After substitution and corrections were made, additional correction has to be done for the type of C atom to which the functional group is attached; the type is determined **after** the substitution was made. Correction entry in Table A.17 is then multiplied by type number (e.g. if a group is attached to carbon type 3, appropriate entry from Table A.17 has to be multiplied by 3).

**Table A.16. Contributions of functional groups (Reprinted from [A2])**

| Functional Group[a] | $\Delta(\Delta H_m)$ | $\Delta S_m$ | Heat Capacity Constants $\Delta a$ | $\Delta b$ | $\Delta c$ |
|---|---|---|---|---|---|
| Oxygen | | | | | |
| =O(aldo) | −10.13 | −54.39 | 17.11 | −214.05 | 84.27 |
| =O(keto) | −29.66 | −84.47 | 6.32 | −148.49 | 36.65 |
| -OH | −118.99 | 8.62 | 7.28 | −65.69 | 24.43 |
| @OH | −146.48 | −1.26 | 12.01 | −49.79 | 24.27 |
| -O- | −85.48 | −5.27 | 13.26 | −85.31 | 38.58 |
| @O- | −97.78 | −15.1 | 18.0 | −69.5 | 38.1 |
| -OOH | −103.3 | | | | |
| -OO- | −21.84 | | | | |
| -COOH | −350.16 | 53.01 | 7.91 | 29.20 | −26.65 |
| @COOH | −337.65 | 51.88 | −8.03 | 25.19 | −4.56 |
| -COO- | −305.93 | 54.8 | −17.6 | 1.3 | 7.9 |
| @COO- | −317.69 | 54.8 | −17.6 | 1.3 | 7.9 |
| @OOC- | −310.12 | | | | |
| -COOCO- | −469.95 | 116.86 | −5.27 | 124.64 | −69.25 |
| -$COO_2CO$- | −392.0 | | | | |
| HCOO- | −275.85 | 71.76 | 7.91 | 29.20 | −26.65 |
| -$CO_3$- | −490.24 | | | | |

**Table A.17. Corrections for type number and multiple substitutions of functional groups (Reprinted from [A2])**

| Functional Group[a] | $\Delta(\Delta H_m)$ | $\Delta S_m$ | Heat Capacity Constants $\Delta a$ | $\Delta b$ | $\Delta c$ |
|---|---|---|---|---|---|
| Oxygen | | | | | |
| =O(aldo) | −22.68 | 18.83 | −3.60 | 6.74 | −4.81 |
| =O(keto) | −13.81 | 30.92 | 6.65 | −47.28 | 34.35 |
| -OH | −11.09 | 0.84 | 0.42 | 0.00 | −0.42 |
| -O- | −9.54 | −2.30 | 2.13 | −5.02 | 3.31 |
| @O- | −11.76 | −2.5 | 2.1 | −5.0 | 3.3 |
| -OOH | 8.4 | | | | |
| -OO- | −10.46 | | | | |
| -COOH | 6.44 | 35.90 | 0.0 | 0.0 | 0.0 |
| %COO- | −11.72 | −2.5 | 2.1 | −5.0 | 3.3 |
| @COO- | 7.49 | −2.5 | 2.1 | −5.0 | 3.3 |
| -COOCO- | −5.06 | 36.0 | 0.0 | 0.0 | 0.0 |
| -$COO_2CO$- | −21.3 | | | | |
| HCOO- | 33.43 | −2.5 | 2.1 | −5.0 | 3.3 |
| -$CO_3$- | −1.21 | | | | |

### *A.1.2.1 Data for α–pinene oxide*

Applied to α–pinene oxide, step one is to determine base group, which is cyclohexane (C atoms 4, 5, 6, 7, 8 and 10 showed in Figure A.1). There are four primary substitutions (on $C_6$, $C_7$, $C_8$ and $C_{10}$), but the primary substitution on $C_6$ (or $C_7$) can be treated as closing of a four-member ring, for which ABWY method does not give data. This problem will be discussed later. For now, we will assume that there are only three primary substitutions and add contributions for them. Note that there are no contributions for more than two primary substitutions, therefore it is not a big mistake not to count substitution on $C_6$. Next step is to add contributions for secondary methyl substitutions (and to define the type of C atoms). There are two secondary substitutions on $C_9$; first one is type 1 ($CH_3$ is the group on which substitution was made) – 3 (highest type of adjacent group is CH), and second one on same atom $C_9$ is type 2 – 1 (on $C_9$ there are two H atoms after previous substitution, therefore it is type 2 and $CH_3$ group is now adjacent, hence type 1). Now that we have a structure, two rings need to be closed. As said, appropriate contributions for ring closings can not be found in ABWY method, so $\Delta H^0_{f,298}$ is calculated for various cycloparaffins and their linear counterparts, where the difference between the two would give a contribution for ring closing. As it can be seen in Table A.19, contributions are very similar to Benson's (Table A.6), so therefore can be used in approximation. Figure A.3 gives correlation between difference in energies and members in ring.

Added contributions now include 4-member ring closing ($C_5$, $C_6$, $C_7$, $C_9$) and 3-member ring closing ($C_8$, $C_{10}$ and C which is still in place of O atom). Last step is to replace the added $CH_3$ group (which became $CH_2$ after the last ring closing) on $C_8$ with O and add contributions for O group (Table A.16) and correction for type 3 carbon atom to which O is attached (3 times entry in Table A.17).

All the data needed to calculate $\Delta H^0_{f,298}$ of α–pinene oxide are presented in Table A.18.

**Table A.18. Estimation of thermochemical properties of α–pinene oxide**

| α–pinene oxide | | | | | |
|---|---|---|---|---|---|
| **Contribution type** | $\Delta H^0_{f,298}$ **kJ/mol** | $\Delta S^0_{int,298}$ **kJ/(molK)** | **a** | **b** | **c** |
| Base group: Cyclohexane | -123.14 | 298.24 | -52.22 | 599.78 | -230.9 |
| First Primary $C^1H_3$ (on C10) | -33.64 | 46.32 | 11.59 | 81.21 | -39.58 |
| Second Primary $C^9H_3$ (1,2 trans-) (on C7) | -23.22 | 26.36 | -5.82 | 103.3 | -43.22 |
| Third Primary $CH_3$ (on C8) | - | - | - | - | - |
| Fourth Primary $CH_3$ (on C6) | - | - | - | - | - |
| Secondary $CH_3$ (1–3) (on C9 creating C2) | -15.36 | 36.61 | -0.96 | 91.63 | -38.95 |
| Secondary $CH_3$ (2–1) (on C9 creating C3) | -28.74 | 21.46 | -2.09 | 95.69 | -41.67 |
| 4 C ring closing (C5, C6, C7, C9) | 109.62 | 124.68* | N/A | N/A | N/A |
| 3 C ring closing (C8, C10, O) | 146.94* | 134.31* | N/A | N/A | N/A |
| –O–substitution | -85.48 | -5.27 | 13.26 | -85.31 | 38.58 |
| –O– substitution correction (Type 3) | -9.54 | -2.3 | 2.13 | -5.02 | 3.31 |

We now have complete data to estimate $\Delta H^0_{f,298}$ and $\Delta S^0_{int,298}$:

$$\Delta H^0_{f,298} = \mathbf{-81.64\ kJ/mol}$$

$$\Delta S^0_{int,298} = \mathbf{673.51\ kJ/(mol\ K)}$$

**Table A.19. Ring closing estimates (calculated as difference between cycloparaffin and paraffin analogues)**

| **Molecule** | $\Delta H^0_{f,298}$**, kJ/mol** | **Difference, kJ/mol** |
|---|---|---|
| Cyclohexane | -123.14 | **44.4** |
| n-hexane | -167.54 | |
| Cyclopentane | -77.24 | **69.71** |
| n-pentane | -146.95 | |
| Cyclobutane | - | **109.62** (from Figure A.3) |
| n-butane | -126.36 | |
| Cyclopropane | 41.17 | **146.94** |
| Propane | -105.77 | |

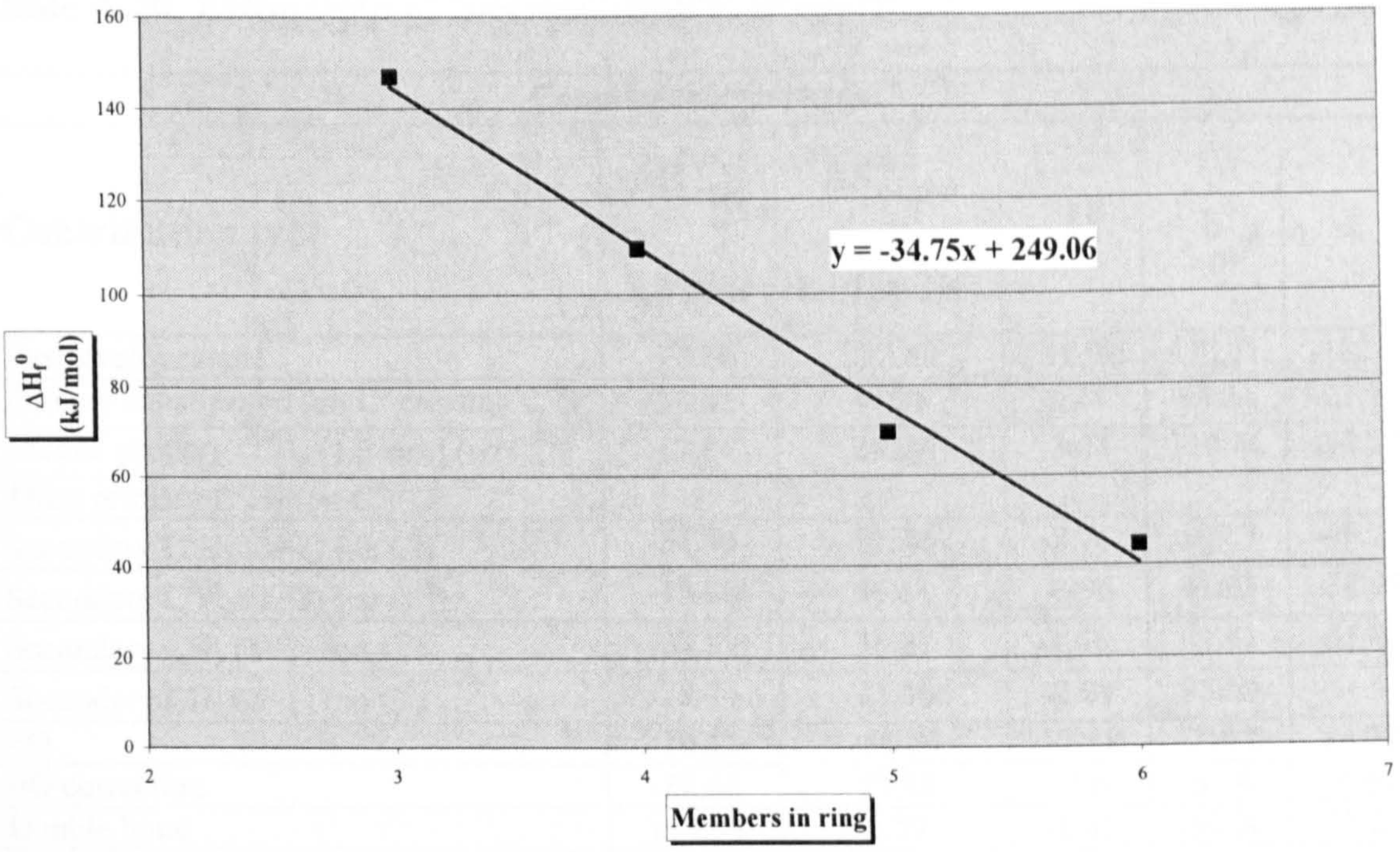


**Figure A.3. Correlation for ring closing calculation**

### *A.1.2.2 Data for campholenic aldehyde*

Following the same procedure, the base structure for campholenic aldehyde is cyclopentane. There are three primary substitutions (on $C_4$, $C_6$ and $C_7$ presented in Figure A.2 creating $C_1$, $C_3$ and $C_{10}$). First secondary substitution is on $C_6$ (type 3–1) creating $C_2$; second is on $C_{10}$ (type 1–3), creating $C_5$. Now we need to add two more methyl groups into the structure (both on $C_5$), since =O group requires replacement of two methyl groups. Therefore there are two additional secondary substitutions; first one is type 1–2 and second is type 2–1. A correction for double bond between carbon atoms type 2 and 3 in cyclopentane must be added as well. Last step is to replace two added methyl groups with =O. Again, corrections for functional group as well as correction for the type of carbon to which =O is attached have to be considered.

Data for estimating properties of campholenic aldehyde are presented in Table A.20.

**Table A.20. Estimation of thermochemical properties of campholenic aldehyde**

| Campholenic aldehyde | | | | | |
|---|---|---|---|---|---|
| **Contribution type** | $\Delta H^0_{f,298}$ **kJ/mol** | $\Delta S^0_{int,298}$ **kJ/(molK)** | **a** | **b** | **c** |
| Base cyclopentane | -77.24 | 292.88 | -41.92 | 473.71 | -182.6 |
| Primary substitution (on $C^4$ creating $C^{10}$) | -34.43 | 49.25 | 8.74 | 68.24 | -23.18 |
| Second primary $C^1H_3$ (1,2 cis-) (on $C^6$) | -17.87 | 24.02 | -3.64 | 110.46 | -53.22 |
| Third primary $C^3H_3$ (on $C^7$) | - | - | - | - | - |
| Secondary $C^2H_3$ (3–1) (on $C^6$) | -31.46 | 11.76 | -2.76 | 107.7 | -49.25 |
| Secondary $C^5H_3$ (1–3) (on $C^{10}$) | -15.36 | 36.61 | -0.96 | 91.63 | -38.95 |
| Secondary $CH_3$ (1–2) (on $C^5$) | -20.59 | 38.87 | 1.46 | 81.42 | -31.46 |
| Secondary $CH_3$ (2–1) (on $C^5$) | -28.74 | 21.46 | -2.09 | 95.69 | -41.67 |
| =O | -10.13 | -54.39 | 17.11 | -214.0 | 84.27 |
| =O correction | -22.68 | 18.83 | -3.6 | 6.74 | -4.81 |
| Double bond | 114.64 | 0.59 | -1.05 | -54.06 | 21.21 |

Thermodynamic properties can be approximated as:

$\Delta H^0_{f,298}$ **= -143.86 kJ/mol**

$\Delta S^0_{int,298}$ **= 439.88 kJ/molK**

### A.1.3 VERMA – DORAISWAMY METHOD

This method [A3] is similar to Benson's, constituent groups have to be identified and corrections for the rings (together with group contributions) added to get the values of a and b, which determine $\Delta H^0_{f,298}$ as:

$$\Delta H^0_{f,T} = a + bT \qquad (a.15)$$

Appropriate group contributions for α–pinene oxide are summarised in Table A.21.

**Table A.21. Estimation of $\Delta H^0_{f,298}$ for α-pinene oxide**

| Group | a | $b \cdot 10^2$ | Number of groups |
|---|---|---|---|
| $-CH_3$ | -8.948 | -0.436 | 3 |
| $>CH_2$ | -4.24 | -0.235 | 2 |
| >CH- | -1.57 | 0.095 | 3 |
| >C< | -0.65 | 0.425 | 2 |
| –O– | -30.5 | 0 | 1 |
| 3 member ring | 24.85 | -0.24 | 1 |
| 4 member ring | 19.76 | -0.44 | 1 |
| Hexane ring | 0.378 | -0.382 | 1 |

a = -26.846

b = -0.00465

$\Delta H^0_{f,298}$ = -28.24 kcal/mol = **-117.73 kJ/mol**

The same path is used for approximation of $\Delta H^0_{f,298}$ for campholenic aldehyde, presented in Table A.22.

**Table A.22. Estimation of $\Delta H^0_{f,298}$ for campholenic aldehyde**

| Group | a | $b \cdot 10^2$ | Number of groups |
|---|---|---|---|
| $-CH_3$ | -8.948 | -0.436 | 3 |
| $>CH_2$ | -4.24 | -0.235 | 2 |
| >CH– | -1.57 | 0.095 | 1 |
| >C< | -0.65 | 0.425 | 1 |
| CHO | -29.167 | -0.183 | 1 |
| >C=CH- | 20.1 | 0 | 1 |
| Double cis 1,2 branching | -1.1 | 0 | 1 |
| Double trans 1,2 branching | 0.7 | 0 | 1 |
| Double 1,1 branching | 0.3 | 0 | 1 |
| 5 member ring | 7.084 | -0.552 | 1 |

a = -39.627

b = -0.00993

$\Delta H^0_{f,298}$ = -42.61 kcal/mol = **-177.35 kJ/mol**

## A.1.4 COMBINED METHOD (THINH/PERRY)

A method developed by Thinh [A4, A5] proved to be the most accurate, but is for hydrocarbons only. Perry's handbook also gives data for group contributions

method [A6]. Apart from values for functional groups (for which Thinh gives no data), the two are very similar and combined can give approximate values for properties of molecules of interest. Tables A.23 and A.24 give data for α–pinene oxide and campholenic aldehyde respectively.

**Table A.23. Group contributions for α–pinene oxide**

| Group | a | $b \cdot 10^2$ | $c \cdot 10^4$ | $d \cdot 10^8$ | $\Delta H^0_{f,298}$ | Number of groups |
|---|---|---|---|---|---|---|
| –$CH_3$ | 0.6087 | 2.1433 | -0.0852 | 0.1135 | -10.118 | 3 |
| >$CH_2$ | 0.3945 | 2.1363 | -0.1197 | 0.2596 | -4.93 | 2 |
| >CH– | -3.5232 | 3.4158 | -0.2816 | 0.8015 | -1.796 | 3 |
| >C< | -5.8307 | 4.4541 | -0.4208 | 1.263 | 0.802 | 2 |
| –O– | 2.8461 | -0.01 | 0.0454 | -0.2728 | -24.2 | 1 |
| C(3) ring | -3.532 | -0.03 | 0.0747 | -0.5514 | 24.629 | 1 |
| C(4) ring | -8.655 | 1.078 | 0.0425 | 0.025 | 18.45 | 1 |
| C(6) ring | -13.3923 | 2.1392 | -0.0429 | -0.1865 | 0.15 | 1 |

$\Delta H^0_{f,298}$ **= -104.47 kJ/mol**

**Table A.24. Group contributions for campholenic aldehyde**

| Group | a | $b \cdot 10^2$ | $c \cdot 10^4$ | $d \cdot 10^8$ | $\Delta H^0_{f,298}$ | Number of groups |
|---|---|---|---|---|---|---|
| –CH3 | 0.6087 | 2.1433 | -0.0852 | 0.1135 | -10.118 | 3 |
| >CH2 | 0.3945 | 2.1363 | -0.1197 | 0.2596 | -4.93 | 2 |
| >CH– | -3.5232 | 3.4158 | -0.2816 | 0.8015 | -1.796 | 1 |
| >C< | -5.8307 | 4.4541 | -0.4208 | 1.263 | 0.802 | 1 |
| >C=O | 1.0016 | 2.0763 | -0.1636 | 0.4494 | -31.48 | 1 |
| >C=CH– | -1.4714 | 3.3842 | -0.2371 | 0.6063 | 20.184 | 1 |
| C(5) ring | -6.8813 | 0.7818 | -0.0345 | 0.0591 | 4.094 | 1 |

$\Delta H^0_{f,298}$ **= -202.55 kJ/mol**

## A.2 SUMMARY

### A.2.1 ENTHALPIES

$\Delta H^0_{f,298}$ values calculated by the four methods used are presented in Table A.25. It can be observed that estimated results by different methods are very much in agreement with each other. In the case of campholenic aldehyde, standard deviation of results is 25.02 and for α-pinene oxide 16.56. These variations are due

to extremely difficult structure of the molecules (branching, forming of rings). Approximation of thermodynamic data is very close to reality if fewer contributions are added; in the case of complicated molecules, there is a possibility of making a greater mistake.

**Table A.25. Comparison of all methods of estimation for approximation of $\Delta H^0_{f,298}$**

| Method ($\Delta H^0_{f,298}$, kJ/mol) | α–pinene oxide | Campholenic aldehyde |
|---|---|---|
| Benson | -115.73 | -188.49 |
| ABWY | -81.64 | -143.86 |
| Verma – Doraiswamy | -117.73 | -177.35 |
| Thinh/Perry | -104.47 | -202.55 |
| **Average** | **-104.89** | **-178.06** |

Therefore it can be approximated that the heats of formation have these values:

$$\Delta H^0_{f,298\text{, α–pinene oxide}} = \mathbf{-104.89\ kJ/mol}$$

$$\Delta H^0_{f,298\text{, campholenic aldehyde}} = \mathbf{-178.06\ kJ/mol}$$

Heat of reaction can be calculated as:

$$\Delta H^0_{r,298} = \Delta H^0_{f,298\text{, campholenic aldehyde}} - \Delta H^0_{f,298\text{, α-pinene oxide}}$$

Table A.26 represents the heat of reaction calculated by four methods, as well as the average value.

**Table A.26. Comparison of all methods of estimation of heat of reaction**

| Method | Heat of Reaction (kJ/mol) |
|---|---|
| Benson | -72.76 |
| ABWY | -62.22 |
| Verma – Doraiswamy | -59.62 |
| Thinh/Perry | -98.09 |
| **Average** | **-73.17** |

$$\Delta H^0_{r,298} = \mathbf{-73.17\ kJ/mol}$$

It can be concluded that isomerisation of α–pinene oxide is an exothermic reaction with the released heat of 73.17 kJ/mol. If the obtained values for ABYW method are excluded from consideration as off-values, heat of reaction value changes to -76.82 kJ/mol. It can also be concluded that Benson's method alone gives the most accurate approximations.

### A.2.2 ENTROPIES

As estimated by Benson's method:

$$\Delta S^0_{r,298} = \Delta S^0_{f,298\text{, campholenic aldehyde}} - \Delta S^0_{f,298\text{, α-pinene oxide}}$$

$$\Delta S^0_{r,298} = 501.29 - 393.5 = 107.79 \text{ J/(molK)} = \mathbf{0.11 \text{ kJ/(molK)}}$$

### A.2.3 HEAT CAPACITIES

Heat capacities are estimated as:

$$\Delta C^0_{P\ 300\text{, α-pinene oxide}} = 179.58 \text{ J/molK}$$

$$\Delta C^0_{P\ 300\text{, campholenic aldehyde}} = 195.06 \text{ J/molK}$$

$$\Delta C^0_{P,r\ 300} = \Delta C^0_{P\ 300\text{, campholenic aldehyde}} - \Delta C^0_{P\ 300\text{, α-pinene oxide}}$$

$$\Delta C^0_{P,r\ 300} = 199.58 \text{ J/molK} - 180.5 \text{ J/molK} = 19.08 \text{ J/molK} =$$

$$= \mathbf{1.91\ 10^{-2} \text{ kJ/molK}}$$

### A.2.4 GIBBS FREE ENERGY CHANGE AND EQUILIBRIUM CONSTANT

Gibbs free energy change for this reaction can be calculated from equation (a.3):

$$\Delta G^0_{298} = \Delta H^0_{r,298} - T\,\Delta S^0_{r,298} = -73.17 \text{ kJ/mol} - 298 \text{ K} \cdot 0.11 \text{ kJ/(molK)}$$

$$\mathbf{\Delta G^0_{298} = -109.35 \text{ kJ/mol}}$$

Using equation (a.2), $K_{eq}$ can be calculated as:

$$K_{eq} = e^{-\frac{\Delta G_T^0}{RT}} = e^{\frac{109350\ J/mol}{8.314\ J/mol\,K \cdot 298\,K}}$$

$$K_{eq} = 1.47 \cdot 10^{19}$$

### A.2.5 ADIABATIC TEMPERATURE RISE

Using equation (2.1) and the data from Appendix A, adiabatic temperature rise for the reaction can be calculated as:

$$\Delta T_{ad} = \frac{(-\Delta H)_A C_A}{\rho \frac{C_P}{M_r}} = \frac{73.17 \cdot 10^3 \frac{J}{mol} \cdot 65.78 \frac{mol}{m^3}}{964 \cdot 10^3 \frac{g}{m^3} \cdot \frac{179.58 \frac{J}{molK}}{152 \frac{g}{mol}}} = 4.22K \qquad (a.16)$$

## A.3 REFERENCES


A1. Benson, S.W., *Thermochemical Kinetics*. 2 ed. 1976: John Wiley and Sons, Inc.

A2. Klotz, I.M. and R.M. Rosenberg, *Chemical Thermodynamics: Basic Theory and Methods*. 6 ed. 2000: John Wiley & Sons, Inc.

A3. Verma, K.K. and L.K. Doraiswamy, *Estimation of Heats of Formation of Organic Compounds*. I & EC Fundamentals, November 1965. 4(4): p. 389-396.

A4. Thinh, T.P., J.L. Duran, and S. Ramalho, *Estimation of Ideal Gas Heat Capacities of Hydrocarbons from Group Contribution Techniques*. Ind. Eng. Chem. Process Des. Develop., 1971. **10**(4): p. 576-582.

A5. Thinh, T.P., *Estimation of Standard Heats of Formation $\Delta H^*_{fT}$, Standard Entropies of Formation $\Delta S^*_{fT}$,Standard Free Energies of Formation $\Delta F^*_{fT}$ and Absolute Entropies $S^*_T$ of Hydrocarbons from Group Contributions: An Accurate Approach*. The Canadian Journal of Chemical Engineering, August 1976. **54**: p. 344-357.

A6. Perry, *Perry's Chemical Engineer's Handbook*. p. Table 3-335.

# APPENDIX B

## SHEAR RATES IN THE SDR

Using the Equation (3.13), shear rates on the SDR can be calculated at various positions (different radial position and/or different film height). Tables B.1 to B.3 give values of shear rates across the disc surface as close as possible to the surface (where z is virtually zero).

**Table B.1. Shear rates in the SDR (for the disc speed of 500 rpm)**

| Radial Position | $\dot{\gamma} \cdot 10^{-5}$ ($s^{-1}$) |
|---|---|
| r = 25 mm | 1.08 |
| r = 50 mm | 1.36 |
| r = 75 mm | 1.56 |
| r = 100 mm | 1.71 |

**Table B.2. Shear rates in the SDR (for the disc speed of 1000 rpm)**

| Radial Position | $\dot{\gamma} \cdot 10^{-5}$ ($s^{-1}$) |
|---|---|
| r = 25 mm | 2.72 |
| r = 50 mm | 3.42 |
| r = 75 mm | 3.92 |
| r = 100 mm | 4.31 |

**Table B.3. Shear rates in the SDR (for the disc speed of 1500 rpm)**

| Radial Position | $\dot{\gamma} \cdot 10^{-5}$ ($s^{-1}$) |
|---|---|
| r = 25 mm | 4.67 |
| r = 50 mm | 5.88 |
| r = 75 mm | 6.73 |
| r = 100 mm | 7.41 |

Profile of shear rates can also be seen on Figure B.1.

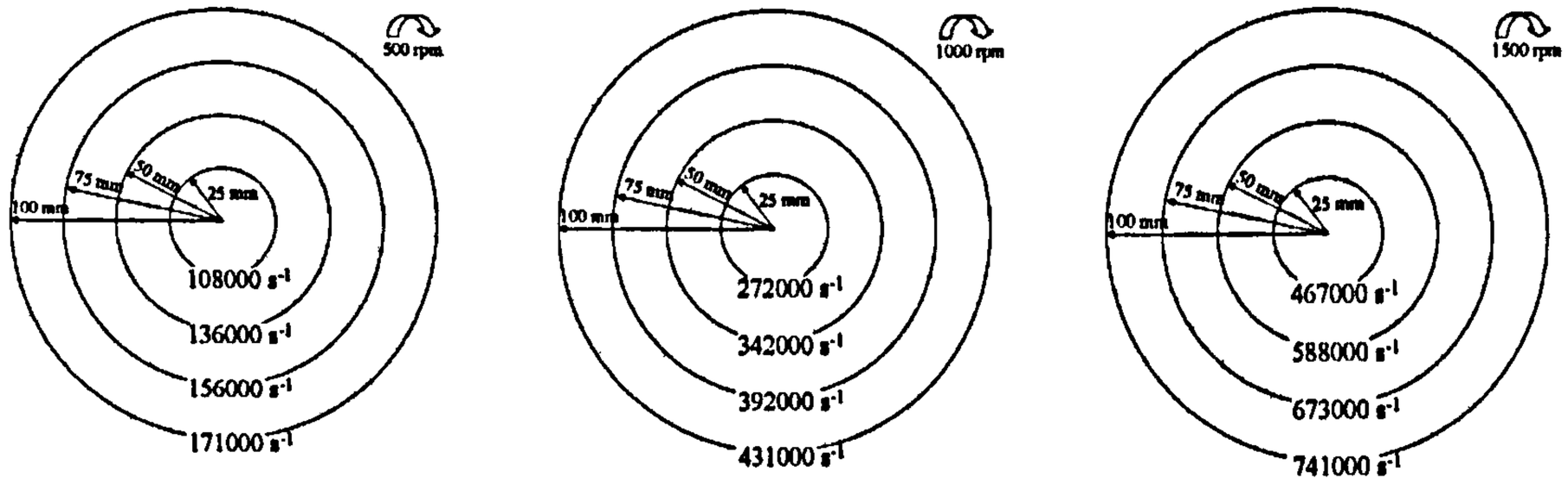


(a) (b) (c)

**Figure B.1. Shear rates profile across the disc surface**
**(a) 500 rpm; (b) 1000 rpm and (c) 1500 rpm**

It can be observed that shear rate increases form the centre to the outer edge of the disc. The values are calculated for z (axial distance from the surface, $z \leq \delta$) very close to zero ($10^{-12}$), as the shear has the highest values close to the surface. Shear rate decreases through the film and when $z = \delta$, shear rate is zero.

As the disc speed increases, shear is increasing as well and it can be seen that by increasing the speed from 500 rpm to 1500 rpm, shear rate is higher by almost an order of magnitude. If we consider the disc that can achieve speed of only 4000 rpm, the shear rate at the outer edge of the disc of the same diameter would be $2.74 \cdot 10^6$.

This is why it is adequate to say that SDR really is high shear mixer.

# APPENDIX C

## HEAT AND MASS TRANSFER

### C.1 HEAT TRANSFER

#### C.1.1 INTRODUCTION

As the heat flows across temperature differences (the second low of thermodynamics), heat can be transferred in three ways: conduction, radiation and convection. While conduction and radiation are fundamental physical mechanisms, convection is really a conduction as affected by fluid flow [C1].

*Conduction* can be defined as exchange of energy by direct interaction between molecules of a substance containing temperature differences and can occur in gases, liquids or solids.

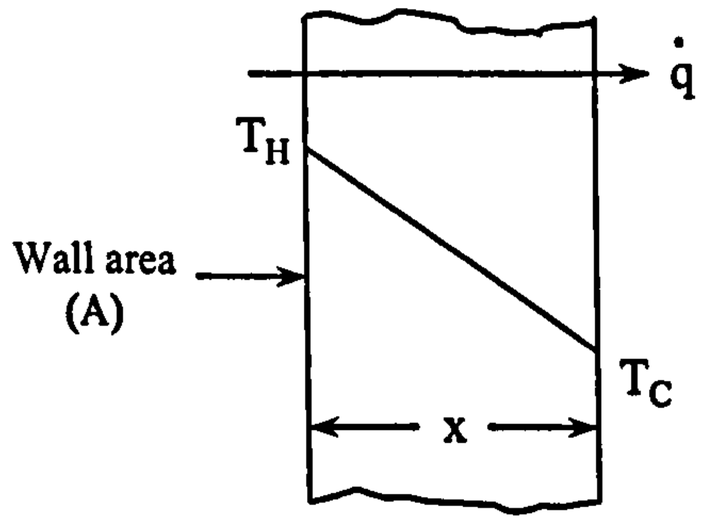


**Figure C.1. Conduction schematic**

The rate of heat flow $\dot{q}$ over the area $A$ and small distance dx may be written as (Fourier's law) [C2]:

$$\dot{q} = -\lambda A \left( \frac{dT}{dx} \right) \qquad \text{(c.1)}$$

where: $\left( \frac{dT}{dx} \right)$ – the temperature gradient in the direction normal to the area $A$;

$\lambda$ – thermal conductivity of the material.

If the temperature profile within the material is linear (such in a homogeneous medium of fixed thermal conductivity during steady state heat transfer), it is acceptable to replace the temperature gradient with:

$$\frac{\Delta T}{\Delta x}=\frac{T_C-T_H}{x_C-x_H} \qquad (c.2)$$

The thermal conductivity of the material, $\lambda$ ($Wm^{-1}K^{-1}$) is a constant which depend on temperature and pressure.

*Radiation* is a transfer of thermal energy in the form of electro-magnetic waves emitted by atomic and subatomic agitation at the surface of a body. The radiant heat transfer is proportional to the fourth power of the absolute temperature, as presented in the Stefan-Boltzmann law:

$$\dot{q}=\sigma A T^4 \qquad (c.3)$$

The Stefan-Boltzmann constant, $\sigma$, is independent of surface, medium and temperature and has a value of $5.67x10^{-8}$ $W/(m^2K^4)$.

*Convection* can be described as conduction in a fluid as enhanced by the motion of the fluid. Convection is the most difficult subject of all heat transfer modes and as such most heavily studied, since it is being strongly influenced by geometry, turbulence and fluid properties.

Heat transfer by convection arises from the mixing of elements of fluid and takes place as consequence of relative motion between the elements of fluid or fluid and solid. Whenever a solid body is exposed to a moving fluid having a temperature different from that of the body, energy is carried or convected from or to the body by the fluid. Convective heat transfer is quantified by Newton's law of cooling, which is for temperature of the fluid $T_f$, wall temperature $T_w$ and area for heat transfer $A$ given as [C1]:

$$\dot{q}=\alpha A (T_f-T_w), \text{ where } \alpha - \text{heat transfer coefficient } (W/m^2K) \qquad (c.4)$$

If the motions of the elements of fluid occur as a result of density differences (different temperature in different regions of fluid), the process is known as natural convection; if mixing in the fluid is caused by eddy movement in the fluid (produced by a pump, a stirrer, or some other outside means), process is called forced convection.

Different applications involve one or more heat transfer mechanisms. Therefore overall heat transfer coefficient, U ($W/m^2K$), defines the efficiency of the overall heat transfer processes in a heat exchanger.

$$\dot{q} = U A \Delta T \qquad (c.5)$$

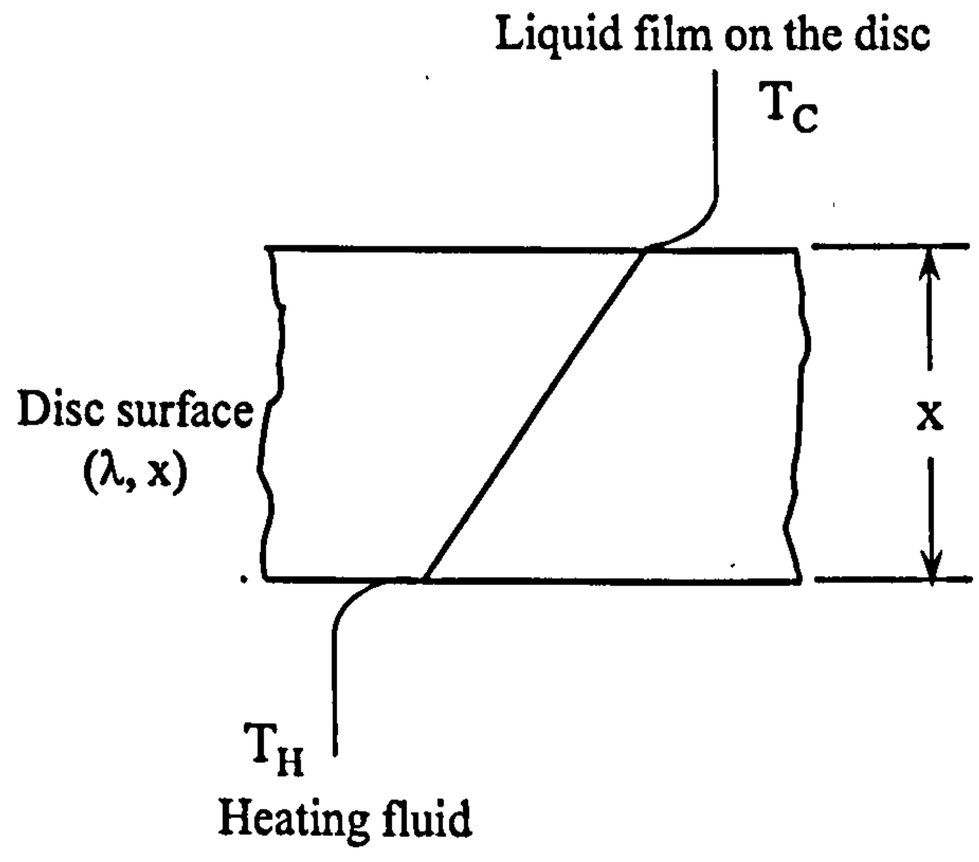


**Figure C.2. SDR as a heat exchanger**

Typically, U will be a combination of convection, conduction and fouling (scaling) on the exchanger surface. If a SDR is presented as a heat exchanger as in Figure C.2, the overall heat transfer coefficient can be calculated from the two local convective heat transfer coefficients on either side of the wall and the conduction resistance of the wall (SDR material with thermal conductivity $\lambda_{disc}$ and thickness x):

$$\frac{1}{U} = \frac{1}{\alpha_{HTF}} + \frac{x}{\lambda_{disc}} + \frac{1}{\alpha_{PF}} \qquad (c.6)$$

For a disc coated with catalyst, additional resistance has to be added:

$$\frac{1}{U_{CAT}} = \frac{1}{U} + \frac{y}{\lambda_{CAT}} \qquad (c.7)$$

where:

$U_{CAT}$ – Overall heat transfer coefficient (disc and catalyst) (W $K^{-1}m^{-2}$);

y – Thickness of the catalyst coat (m);

$\lambda_{CAT}$ – Thermal conductivity of the catalyst; $\lambda_{cat} = 1.4$ W $m^{-1}$ $K^{-1}$.

Thickness of the catalyst coat can be calculated from the catalyst weight used for coating (Appendix G), catalyst density (2.2 g/$cm^3$ for silica) and the disc diameter; since 2.2 g are in 1 $cm^3$, 0.8 g (used for coating) have a volume of 0.36 $cm^3$. Therefore disc area multiplied by catalyst coat thickness should be equal to 0.36 $cm^3$. From here, the coat thickness can be estimated as $1.16 \cdot 10^{-5}$ m.

## C.1.2 HEAT TRANSFER COEFFICIENT

Heat transfer coefficients can be calculated by means of dimensionless groups that can be derived by dimensional analysis. These groups are:

$$Nu = \frac{\alpha d_e}{\lambda} = \text{Nusselt number} \qquad (c.8)$$

$$Pr = \frac{C_P \mu}{\lambda} = \text{Prandtl number} \qquad (c.9)$$

$$Re = \frac{\rho d_e v}{\mu} = \text{Reynolds number} \qquad (c.10)$$

$$Gr = \rho^2 d_e^{\,3} \left( \frac{(\beta \Delta T) g}{\mu^2} \right) = \text{Grashof number} \qquad (c.11)$$

where:

$C_P$ – heat capacity (kJ/(kg K);

$\mu$ – viscosity (Pa s);

$\rho$ – density (kg/m$^3$);

$d_e$ – characteristic length (m);

v – velocity (m/s);

$\beta$ – coefficient of expansion (1/K);

g – gravitational acceleration (m/(s$^2$)).

The general equations derived by dimensional analysis are [C3]:

- For natural convection: $Nu = f(Gr, Pr)$ (c.12)

- For forced convection: $Nu = f(Re, Pr)$ (c.13)

Applied to spinning disc, the internal heat transfer coefficient ($\alpha_{HTF}$) can be estimated from the correlations for Nu given in following equations [C1]:

$$Nu = 1.62\left(Re\,Pr\frac{d}{l}\right)^{1/3} \quad (c.14)$$

$$Nu = \frac{\alpha_{HTF}\,l}{\lambda_{HTF}} \quad (c.15)$$

where:

$d$ – channel width (m);

l – distance from the disc centre (m);

$\lambda$ – thermal conductivity (W m$^{-1}$ K$^{-1}$).

Both internal ($\alpha_{HTF}$) and external ($\alpha_{PF}$) heat transfer coefficients can be calculated using equation (3.24), for example, using the channel width in the calculation of $d_e$ in case of internal and film thickness in the case of external coefficient. Heat transfer factor (from the equation 3.24) can be found, and is dependent on the value of Reynolds number:

$$j_h = \frac{0.641}{Re^{0.54}}, \quad 10 \le Re \le 200$$

$$j_h = \frac{0.491}{Re^{0.49}}, \quad 200 < Re < 5000 \qquad \text{(c.16)}$$

$$j_h = \frac{0.351}{Re^{0.45}}, \quad 5000 \le Re \le 10^6.$$

## C.1.3 DETERMINATION OF U VALUE

### *C.1.3.1 NTU method*

One of the ways to determine the U value is by using Number of Transfer Units (NTU) Method. The number of transfer units (N) is defined by:

$$N = \frac{UA}{\left(\dot{m}c_p\right)_{min}} \qquad \text{(c.17)}$$

where $\left(\dot{m}c_p\right)_{min}$ is the lower of the two values $\dot{m}_1 c_{p,1}$ (Stream 1) and $\dot{m}_2 c_{p,2}$ (Stream 2).

The thermal performance of the system can be expressed with heat–transfer effectiveness, $\eta$, which is the ratio of the actual rate of heat transfer in the exchanger, $\dot{q}$, to the thermodynamically maximum possible rate of heat transfer, $\dot{q}_{max}$:

$$\eta = \frac{\dot{q}}{\dot{q}_{max}} \qquad \text{(c.18)}$$

$$\dot{q} = \dot{m}_1 c_{p,1} (T_{12} - T_{11}) \qquad \text{(c.19)}$$

$\dot{q}_{max}$ is the heat transfer rate which would be achieved if it were possible to bring the outlet temperature of the stream with lower heat capacity to the inlet

temperature of the other stream. Using the nomenclature in Figures C.3 and C.4, and taking stream 1 as having the lower value of $\left(\dot{m}\, c_p\right)$:

$$\dot{q}_{max} = \dot{m}_1\, c_{p,\,min}\left(T_{11} - T_{21}\right) \qquad \text{(c.20)}$$

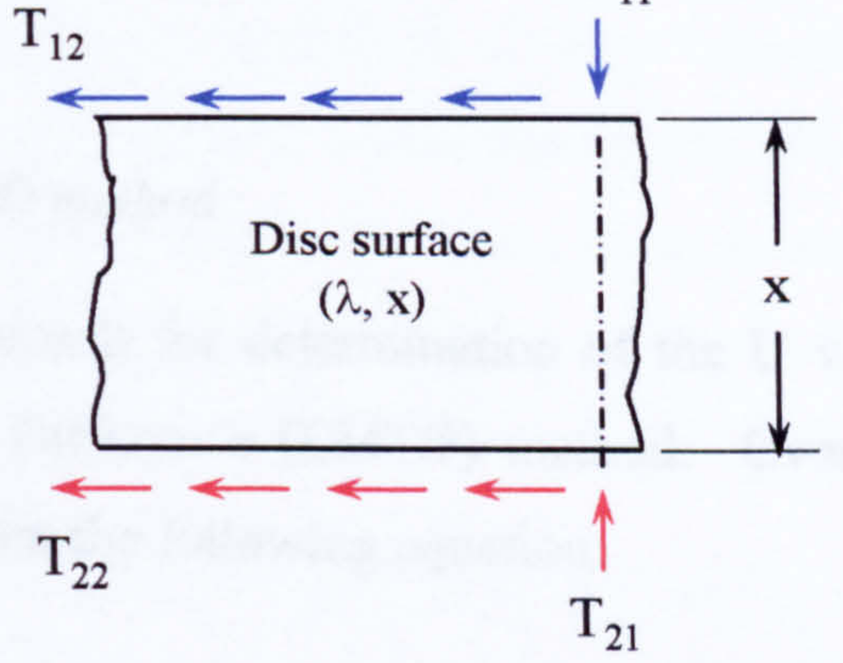


**Figure C.3. Co-current flows on the SDR**

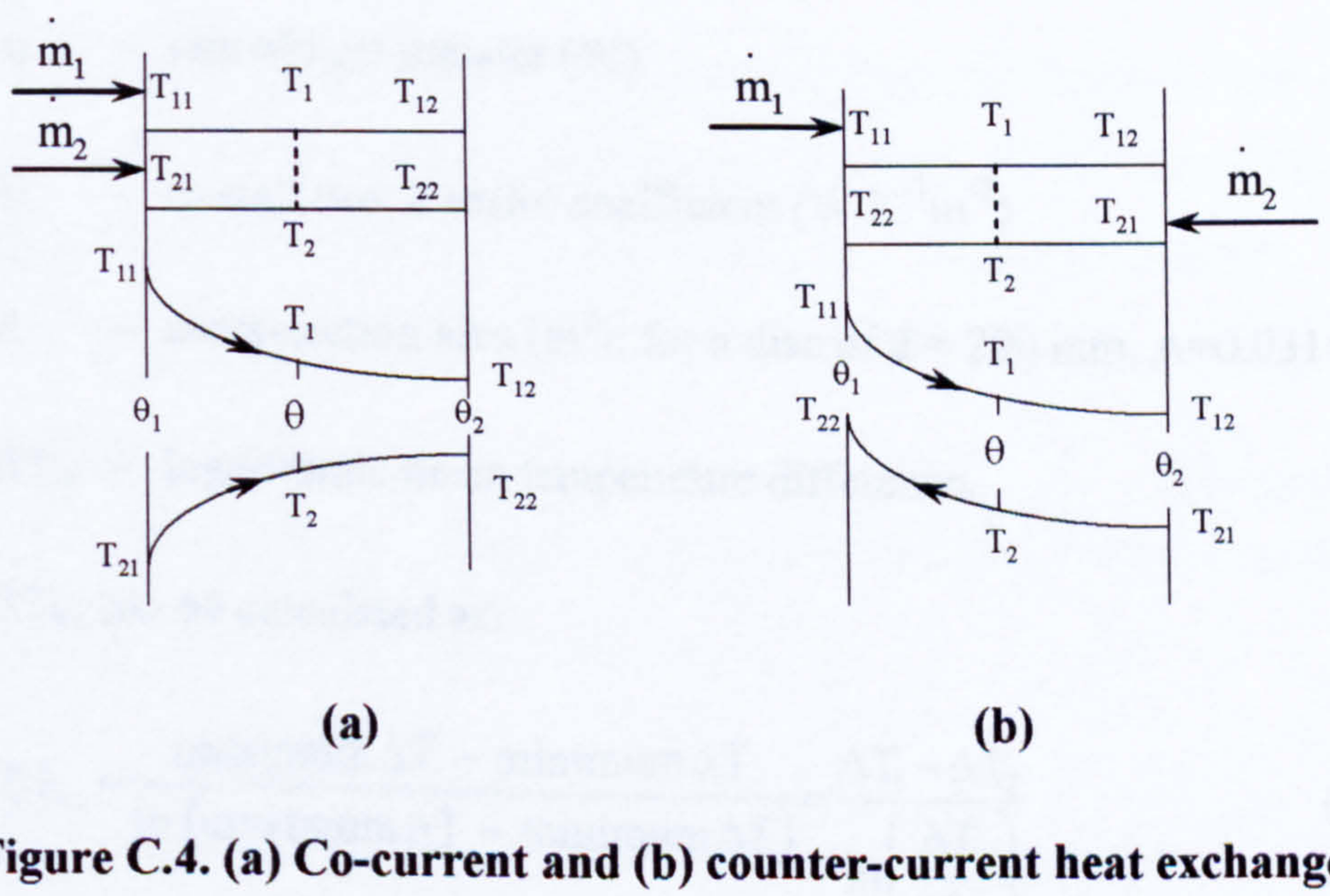


**Figure C.4. (a) Co-current and (b) counter-current heat exchanger**

The number of transfer units (**N**) can be calculated from the following equation (for a parallel flow single pass heat exchanger) [C1]:

$$\eta=\frac{1-\exp\left(-N\left(1+\frac{\dot{m}_1 c_{p,1}}{\dot{m}_2 c_{p,2}}\right)\right)}{1+\frac{\dot{m}_1 c_{p,1}}{\dot{m}_2 c_{p,2}}} \qquad \text{(c.21)}$$

Consequently, the overall heat transfer coefficient can be calculated from equation (c.17).

### *C.1.3.2 LMTD method*

Another approach for determination of the U value is using a Logarithmic Mean Temperature Difference (LMTD) method. Overall heat transfer coefficient can be calculated from the following equation:

$$\dot{q}=U A \Delta T_{lm} \qquad \text{(c.22)}$$

where:

$\dot{q}$ – rate of heat transfer (W)

U – overall heat transfer coefficient ($W K^{-1}m^{-2}$)

*A* – cross-section area ($m^2$); for a disc of d = 200 mm, A=0.0314 $m^2$

$\Delta T_{lm}$ – logarithmic mean temperature difference.

$\Delta T_{lm}$ can be calculated as:

$$\Delta T_{lm}=\frac{\text{maximum}\Delta T-\text{minimum}\Delta T}{\ln\left(\text{maximum}\Delta T-\text{minimum}\Delta T\right)}=\frac{\Delta T_1-\Delta T_2}{\ln\left(\frac{\Delta T_1}{\Delta T_2}\right)} \qquad \text{(c.23)}$$

Maximum temperatures are taken to be the temperature differences of the fluids at the ends of the exchanger. For co-current flow of heating (HTF) and process (PF) fluids, $\Delta T_1 = T_{21} - T_{11}$, $\Delta T_2 = T_{22} - T_{12}$.

When LMTD method is used, non-dimensional correction factor $F_G$ is included to determine the actual value of the overall heat transfer coefficient. The value of this correction factor is between 0 and 1; for counter flow heat exchangers value of $F_G$ is 1.

$$U_{act} = \frac{U}{F_G} \qquad \text{(c.24)}$$

Correction factor $F_G$ is defined as the proportion between areas needed for heat exchanger with counter flow which would work with the same heat transfer rate, same inlet temperatures and same flow rates as an actual investigated heat exchanger that with flow different than counter flow.

$$F_G = \frac{A_{counterflow}}{A} \leq 1 \qquad \text{(c.25)}$$

The LMTD method should not be used for heat exchangers in which there is a phase change, boiling or condensing of either fluid.

### C.1.4 HEAT BALANCE

It can be assumed that the heat removed from the heating fluid is partially used to heat up the liquid feed from the temperature of the feed inlet $T_i$ to the temperature of the feed outlet $T_o$, and partially lost to the environment. Hence an overall heat balance for the system can be presented as:

$$\left\{\begin{matrix}\text{Heat lost from}\\ \text{the heating fluid}\end{matrix}\right\} = \left\{\begin{matrix}\text{Heat used to heat}\\ \text{the liquid film on the disc}\end{matrix}\right\} + \left\{\begin{matrix}\text{Heat lost}\\ \text{to the environment}\end{matrix}\right\}$$

or:

$$\dot{q}_{int} = \dot{q}_{ext} + \dot{q}_{loss} ;$$

$$\dot{m}_{int}\, c_{p,int}\left(T_{HTF,i} - T_{HTF,o}\right) = \dot{m}_{ext}\, c_{p,ext}\left(T_{PF,o} - T_{PF,i}\right) + \dot{q}_{loss} \qquad \text{(c.26)}$$

The SDR system can be considered as a parallel flow single pass heat exchanger in which heat is transferred from one fluid stream to another without any direct contact or mixing of the fluids whose directions of flow are parallel. Very

often in the SDR heat transfer calculations, the heat lost to the environment is neglected as it is less than 10 % of the two other terms in (c.26).

Since the flow area is constantly changing with radial distance for both liquid on the disc and heating fluid under the disc, parallel flow single pass heat exchanger does not completely depict the flow in this system. The flow of both fluids satisfies parallel flow condition just in the area between the centre of the rotating surface and outer edge of it and ideally temperatures should be measured at these positions.

Heat balance for the SDR system on the fluid element in the small dr (Figure C.5) is given by:

$$\text{Rate of heat change} = \text{Heat out} - \text{Heat in}$$

$$\dot{m}\, c_p\, dT = \left[\pi (r + dr)^2\, \alpha\, (T_D - T)\right] - \pi r^2\, \alpha\, (T_D - T) \qquad \text{(c.27)}$$

or, simplified:

$$\dot{m}\, c_p\, dT = 2\, \pi\, r\, dr\, \alpha\, (T_D - T) \qquad \text{(c.28)}$$

where $\dot{m}$ – liquid mass flow rate;

$c_p$ – specific heat capacity of fluid;

$T$ – liquid film temperature;

$T_D$ – disc temperature (assumed constant);

$r$ – radial distance from centre of disc;

$\alpha$ – liquid film heat coefficient (ext).

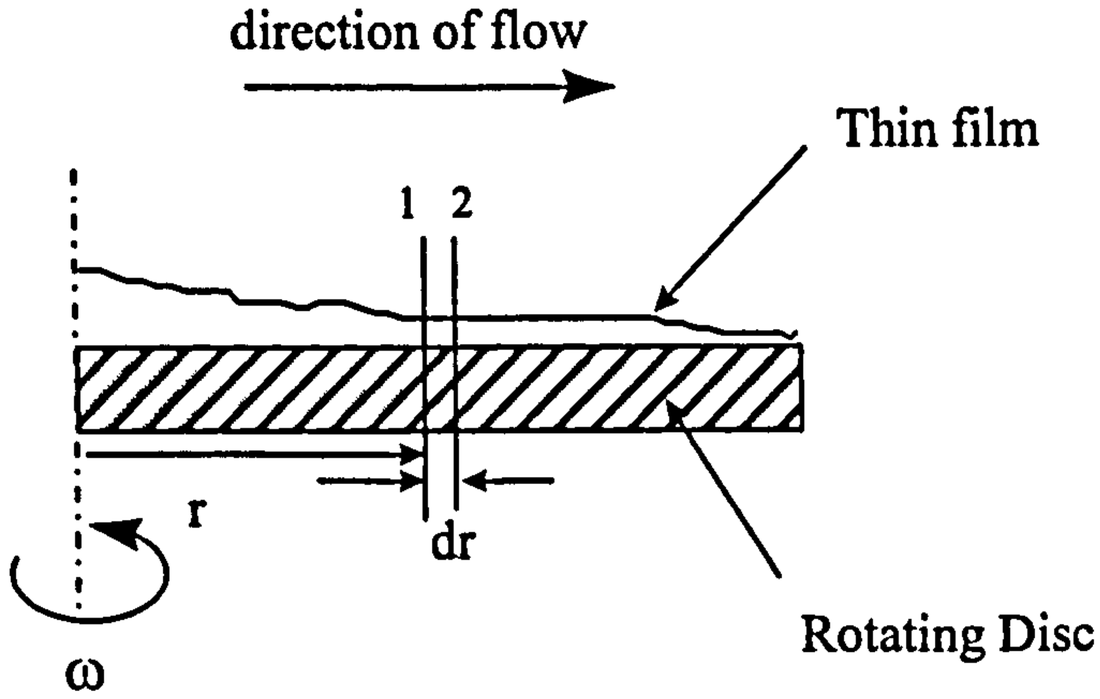


**Figure C.5. Heat balance on the SDR**

The derivation of the above equation is subject to the following simplifying assumptions: heat transfer occurs mainly by convection from the disc surface to the liquid film in a direction perpendicular to the plane surface of the disc; and that the thickness of the film is considered to be so small and mixing within the film is so intense that temperature variations across the height of the film are assumed to be negligible. Only temperature differences in the radial direction are significant.

The boundary conditions applicable in this case are as follows:

at $r = r_i$, $T = T_i$

and at $r = r_o$, $T = T_o$

where $r_i$ – inner radial feed point;

$r_o$ – outlet disc radius;

$T_i$ – inlet film temperature;

$T_o$ – outlet film temperature.

Integration of equation (c.28) within the above set of integral limits yields:

$$\frac{\pi\alpha}{\dot{m}c_p}\left(r_o^2 - r_i^2\right) = \ln\left(\frac{T_D - T_i}{T_D - T_o}\right) \qquad \text{(c.29)}$$

After rearrangement, equation (c.29) can be expressed as:

$$T_o = T_D - \frac{(T_D - T_i)}{\exp\left[\frac{\pi\alpha}{\dot{m}c_P}\left(r_o^2 - r_i^2\right)\right]} \qquad (c.30)$$

However, if the experiment is designed to obtain the values of internal/external heat transfer coefficients, following equations can be derived from equation (c.29):

$$\alpha_{int} = \frac{\dot{m}c_{p,int}\ln\left(\frac{T_D - T_i}{T_D - T_o}\right)}{\pi\left(r_o^2 - r_i^2\right)} \qquad (c.31)$$

$$\alpha_{ext} = \frac{\dot{m}c_{p,ext}\ln\left(\frac{T_D - T_i}{T_D - T_o}\right)}{\pi\left(r_o^2 - r_i^2\right)} \qquad (c.32)$$

Previous heat transfer work on the same spinning disc equipment has shown that an average film heat transfer coefficient as high as 10 kW/m$^2$K can be achieved along the rotating surface [C4, C5].

For the case of rearrangement of α–pinene oxide with an average flow of 4 cm$^3$/s, the following properties and conditions are applicable for the system considered in this investigation:

$\rho = 964$ kg/m$^3$ (see Appendix F for density calculation)

$\dot{m} = 4 \times 10^{-6} \times 964 = 0.003856$ kg/s

$r_i = 0.002$ m; $r_o = 0.1$ m

$T_i = 20^0$C; $T_D = 85^0$C

Temperature profile across the surface of the disc can be calculated using equation (c.30). This can be seen in Table C.1.

**Table C.1. Temperature profile across the disc surface (from 20$^0$C to 85$^0$C)**

| Radial Position (mm) | Radial Position (m) | T (K) | T ($^0$C) |
|---|---|---|---|
| 5 | 0.005 | 301.76 | 28.76 |
| 7.5 | 0.0075 | 312.67 | 39.67 |
| 10 | 0.01 | 324.47 | 51.47 |
| 12.5 | 0.0125 | 335.25 | 62.25 |
| 15 | 0.015 | 343.84 | 70.84 |
| 20 | 0.02 | 353.76 | 80.76 |
| 30 | 0.03 | 357.87 | 84.87 |
| 40 | 0.04 | 358.00 | 85.00 |
| 50 | 0.05 | 358.00 | 85.00 |
| 60 | 0.06 | 358.00 | 85.00 |
| 70 | 0.07 | 358.00 | 85.00 |
| 80 | 0.08 | 358.00 | 85.00 |
| 90 | 0.09 | 358.00 | 85.00 |
| 100 | 0.1 | 358.00 | 85.00 |

This implies that the film very quickly reaches the temperature of the disc as a result of the enhanced heat transfer from the disc surface to the liquid film.

## C.2 MASS TRANSFER

### C.2.1 INTRODUCTION

Mass transfer process can take place in a gas or a liquid as a result of molecular diffusion or eddy diffusion, or both. In most situations of technical importance, the molecular diffusion is of the type known as ordinary diffusion, which results from the thermal motion of the molecules. Eddy diffusion results from circulating (or eddy) currents present in a turbulent fluid. The driving force that produces movements of the molecules trough fluid is difference in concentrations between different regions. The rate of mass transfer is proportional to concentration gradient, which can be expressed in the following form:

$$\phi = K\, A\, \Delta C \tag{c.33}$$

where $\phi$ – rate of mass transfer (mol/s);

$A$ – area trough which is component A transferred (m$^2$);

$K$ – overall mass transfer coefficient (m/s);

$\Delta C$ – difference in concentrations between the regions in fluid ($mol/m^3$).

As mentioned above, diffusion can only occur in the presence of a concentration gradient and the diffusion coefficient D is defined by Fick's first law of diffusion [C6]:

$$-\frac{1}{A}\frac{dn_A}{dt}=D\frac{dc}{dx} \qquad (c.34)$$

where $-\frac{dn_A}{dt}$ is the flux of molecules across an area $A$ at which there is a concentration gradient of $\frac{dc}{dx}$.

Molecular diffusivity $D_{AB}$ is a physical property of the system and a function of its composition, pressure and temperature.

## C.2.2 MASS TRANSFER COEFFICIENT

Mass transfer coefficient is defined in either molar or mass diffusion form:

$$\alpha_m=\frac{G_{A\,int}}{(\rho_{A\,int}-\rho_{A\,j})}, \qquad (c.35)$$

where $G=\frac{\dot{m}}{A},\left(\frac{kg}{m^2 s}\right)$

By analogy with heat transfer it will correlate with flow parameters in the following dimensionless form:

$$\frac{\alpha_m L}{D_{AB}}=f\left(\frac{UL}{\nu},\frac{\nu}{D_{AB}},\text{geometry}\right) \qquad (c.36)$$

or

$Sh_L = f(Re_L, Sc, \text{geometry})$

Where $Sh = \frac{\alpha_m L}{D_{AB}}$ is called Sherwood number and is exactly analogous to the Nusselt number.

## C.2.3 FLAT DISC EQUATIONS

Axisymetric jet discharging from a nozzle and impinging perpendicularly at the centre of a solid circular disc heated by discrete sources, as shown in Figure C.6, is considered. For an incompressible fluid with the properties (density, viscosity, thermal conductivity and specific heat) dependent on temperature, the describing equations for the conservation of mass, momentum and energy in cylindrical coordinates can be written as [C7]:

$$\frac{1}{r}\frac{\partial}{\partial r}(\rho_f r \upsilon_r)+\frac{\partial}{\partial z}(\rho_f \upsilon_z)=0 \qquad \text{(c.37)}$$

$$\rho_f\left(\upsilon_r\frac{\partial \upsilon_r}{\partial r}+\upsilon_z\frac{\partial \upsilon_r}{\partial z}\right)=-\frac{\partial p}{\partial r}+\frac{1}{r}\frac{\partial}{\partial r}\left[\frac{2}{3}\mu r\left(2\frac{\partial \upsilon_r}{\partial r}-\frac{\upsilon_r}{r}-\frac{\partial \upsilon_r}{\partial z}\right)\right]+ +\frac{\partial}{\partial z}\left[\mu\left(\frac{\partial \upsilon_r}{\partial z}+\frac{\partial \upsilon_z}{\partial r}\right)\right] \qquad \text{(c.38)}$$

$$\rho_f\left(\upsilon_r\frac{\partial \upsilon_z}{\partial r}+\upsilon_z\frac{\partial \upsilon_z}{\partial z}\right)=-\rho_f g-\frac{\partial p}{\partial z}+\frac{1}{r}\frac{\partial}{\partial r}\left[\mu r\left(2\frac{\partial \upsilon_r}{\partial z}+\frac{\partial \upsilon_z}{\partial r}\right)\right]+ +\frac{\partial}{\partial z}\left[\frac{2}{3}\mu\left(\frac{\partial \upsilon_z}{\partial z}-\frac{\upsilon_r}{r}-\frac{\partial \upsilon_r}{\partial r}\right)\right] \qquad \text{(c.39)}$$

$$\rho_f\left(\upsilon_r\frac{\partial c_{p_f} T_f}{\partial r}+\upsilon_z\frac{\partial\left(c_{p_f} T_f\right)}{\partial z}\right)=\left[\frac{1}{r}\frac{\partial}{\partial r}\left(k_f r\frac{\partial T_f}{\partial r}\right)+\frac{\partial}{\partial z}\left(k_f\frac{\partial T_f}{\partial z}\right)\right]+\left(\upsilon_z\frac{\partial p}{\partial z}+\upsilon_r\frac{\partial p}{\partial r}\right)$$
$$+\mu_f\left\{2\left[\left(\frac{\partial \upsilon_r}{\partial r}\right)^2+\left(\frac{\upsilon_r}{r}\right)^2+\left(\frac{\partial \upsilon_z}{\partial z}\right)^2\right]+\left(\frac{\partial \upsilon_r}{\partial z}+\frac{\partial \upsilon_z}{\partial r}\right)^2-\frac{2}{3}\left[\frac{\partial \upsilon_r}{\partial r}+\frac{\upsilon_r}{r}+\frac{\partial \upsilon_z}{\partial z}\right]^2\right\} \qquad \text{(c.40)}$$

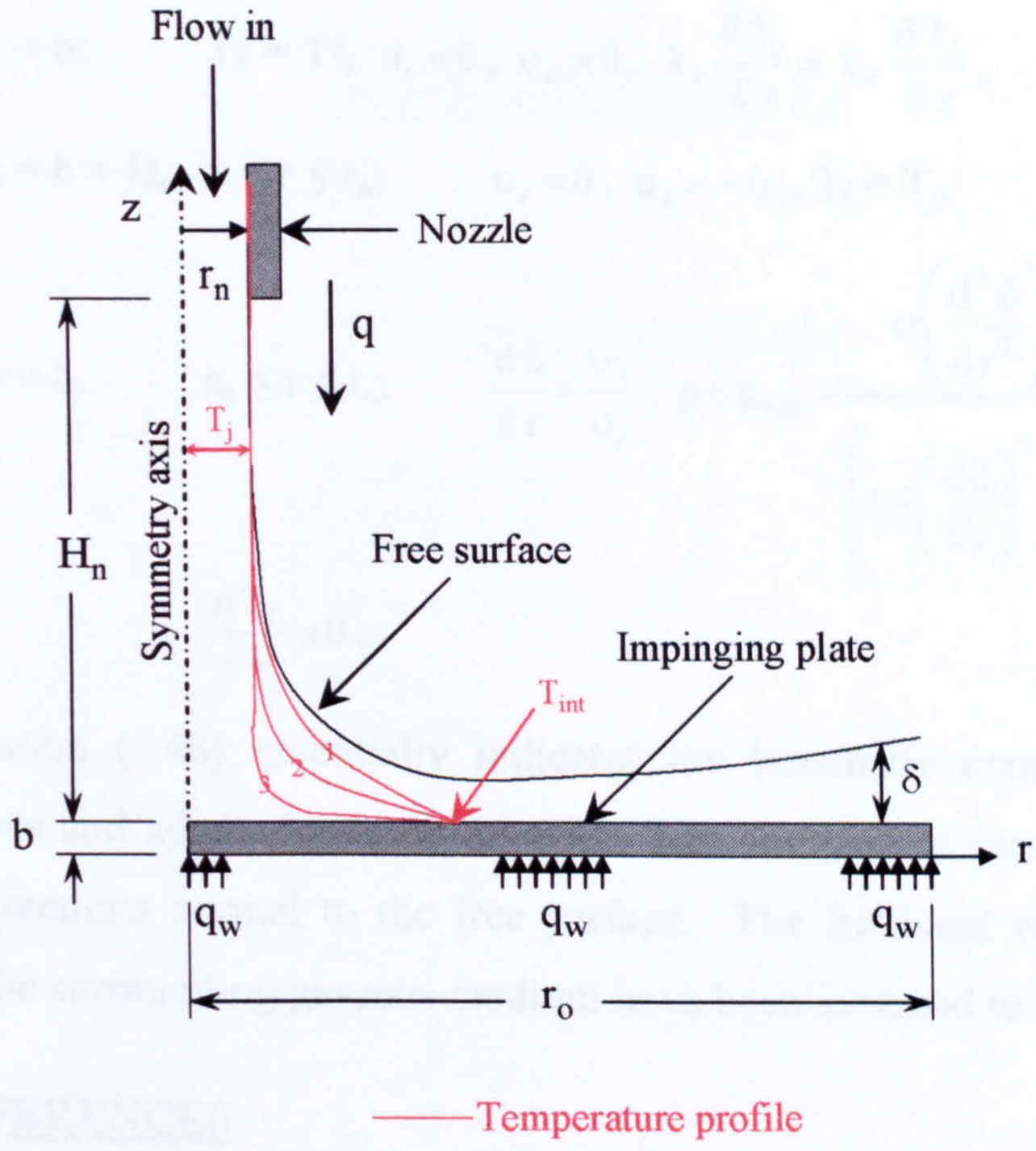


**Figure C.6. Schematic of a free axial jet impinging over a flat disc**

Considering variable thermal conductivity, the equation describing the conservation of energy inside the solid can be written as:

$$\frac{1}{r}\frac{\partial}{\partial r}\left(k_s\, r\frac{\partial T_s}{\partial r}\right)+\frac{\partial}{\partial z}\left(k_s\frac{\partial T}{\partial z}\right)=0 \qquad \text{(c.41)}$$

All the above equations (c.37-c.41) are subjected to the following boundary conditions:

$$\text{At } r=0, \qquad 0\le z\le b: \qquad \frac{\partial T_s}{\partial r}=0, \qquad \text{(c.42)}$$

$$\text{At } r=0, \qquad b\le z\le H_n: \qquad \upsilon_r=0,\ \frac{\partial \upsilon_z}{\partial r}=0,\ \frac{\partial T_f}{\partial r}=0, \qquad \text{(c.43)}$$

$$\text{At } r=r_o, \qquad 0\le z\le b: \qquad \frac{\partial T_s}{\partial r}=0, \qquad \text{(c.44)}$$

$$\text{At } r=r_o, \qquad b\le z\le \delta: \qquad p=0,\ \frac{\partial T_f}{\partial r}=0, \qquad \text{(c.45)}$$

$$\text{At } z = b: \qquad Ts = Tf,\ \upsilon_r = 0,\ \upsilon_z = 0,\ k_s \frac{\partial T_s}{\partial z} = k_f \frac{\partial T_f}{\partial z}, \tag{c.46}$$

$$\text{At } z = b + H_n,\ 0 \le r \le r_n: \qquad \upsilon_r = 0,\ \upsilon_z = -\upsilon_j,\ T_f = T_j, \tag{c.47}$$

$$\text{At } z = \delta,\quad r_n \le r \le r_o: \qquad \frac{d\delta}{dr} = \frac{\upsilon_z}{\upsilon_r},\ p = p_{atm} - \frac{\sigma\left(\frac{d^2\delta}{dr^2}\right)}{\left[1+\left(\frac{d\delta}{dr}\right)^2\right]^{\frac{3}{2}}},\ \frac{\partial \upsilon_t}{\partial n} = 0,$$

$$\frac{\partial T_f}{\partial n} = 0. \tag{c.48}$$

Equation (c.48) essentially indicates the kinematic condition, balance of normal forces and adiabatic condition at the free surface. It can be noted that "n" indicates directions normal to the free surface. The frictional resistance and heat transfer to the surrounding gaseous medium have been assumed to be negligible.

## C.3 REFERENCES


C1. Coulson, J.M. and J.F. Richardson, *Chemical Engineering, Vol. 1*. 1995, Oxford: Butterworth-Heinemann.

C2. White, F.M., *Heat and Mass Transfer*. Addison-Wesley Series in Mechanical Engineering. 1988: Addison-Wesley Publishing Company, Inc.

C3. Lydersen, A.L., *Fluid Flow and Heat Transfer*. 1979: John Wiley & Sons.

C4. Jachuck, R.J.J. and C. Ramshaw, *Process Intensification - Heat-Transfer Characteristics Of Tailored Rotating Surfaces*. Heat Recovery Systems & Chp, 1994. 14(5): p. 475-491.

C5. Johnstone, J.C., *Process intensification : thin film spinning disc reactor for controlled continuous photo-polymerisation of acrylates*. 2000, University of Newcastle upon Tyne.

C6. Burmeister, L.C., *Convective Heat Transfer*. 2nd ed. 1993, New York: Wiley.

# APPENDIX D

## DESIGN DRAWINGS

Drawing No. 1
EXPLOITED SECTION
Not to scale

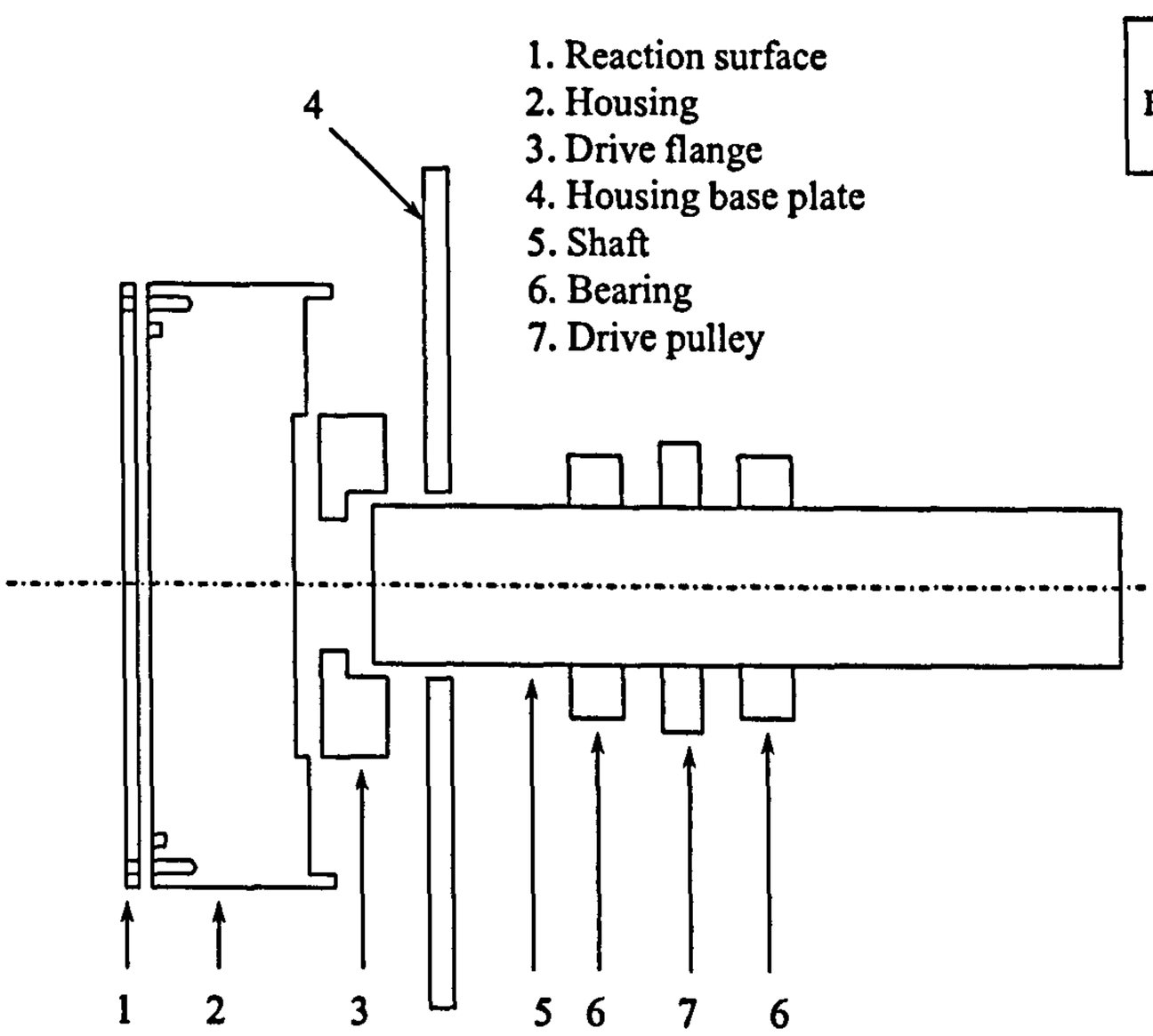


Drawing No. 2
SHAFT PIPE
Material: Stainless steel
Not to scale

TOP VIEW

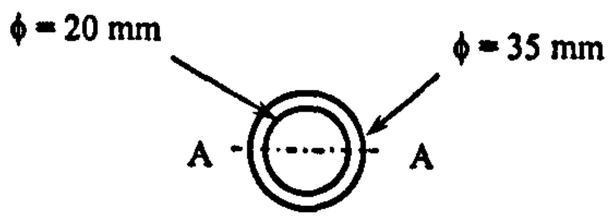


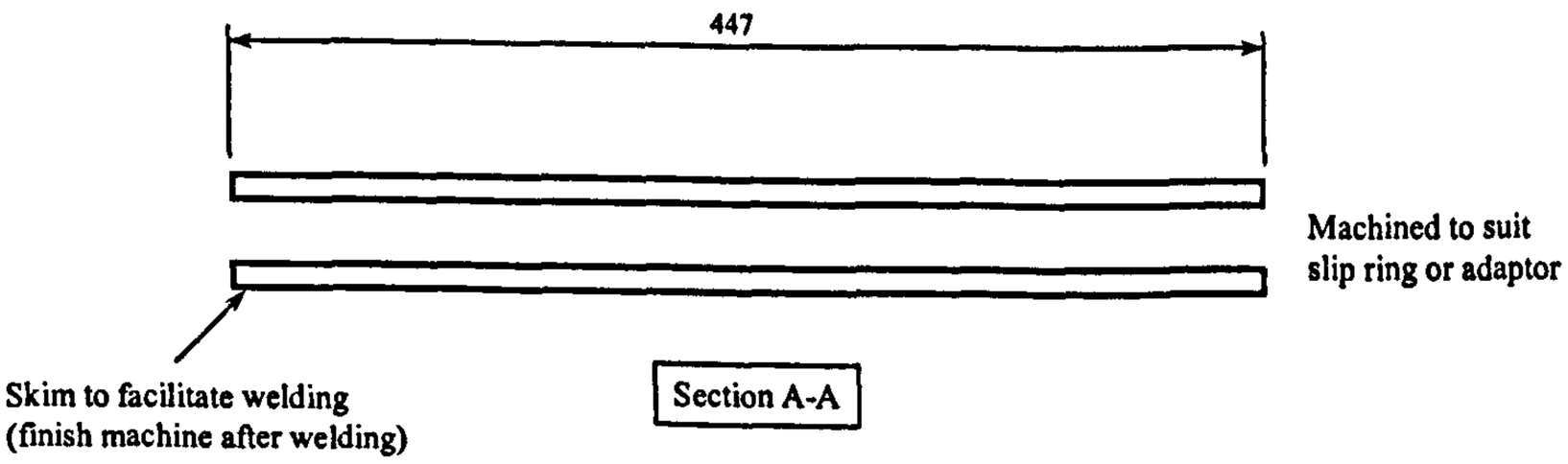


Section A-A

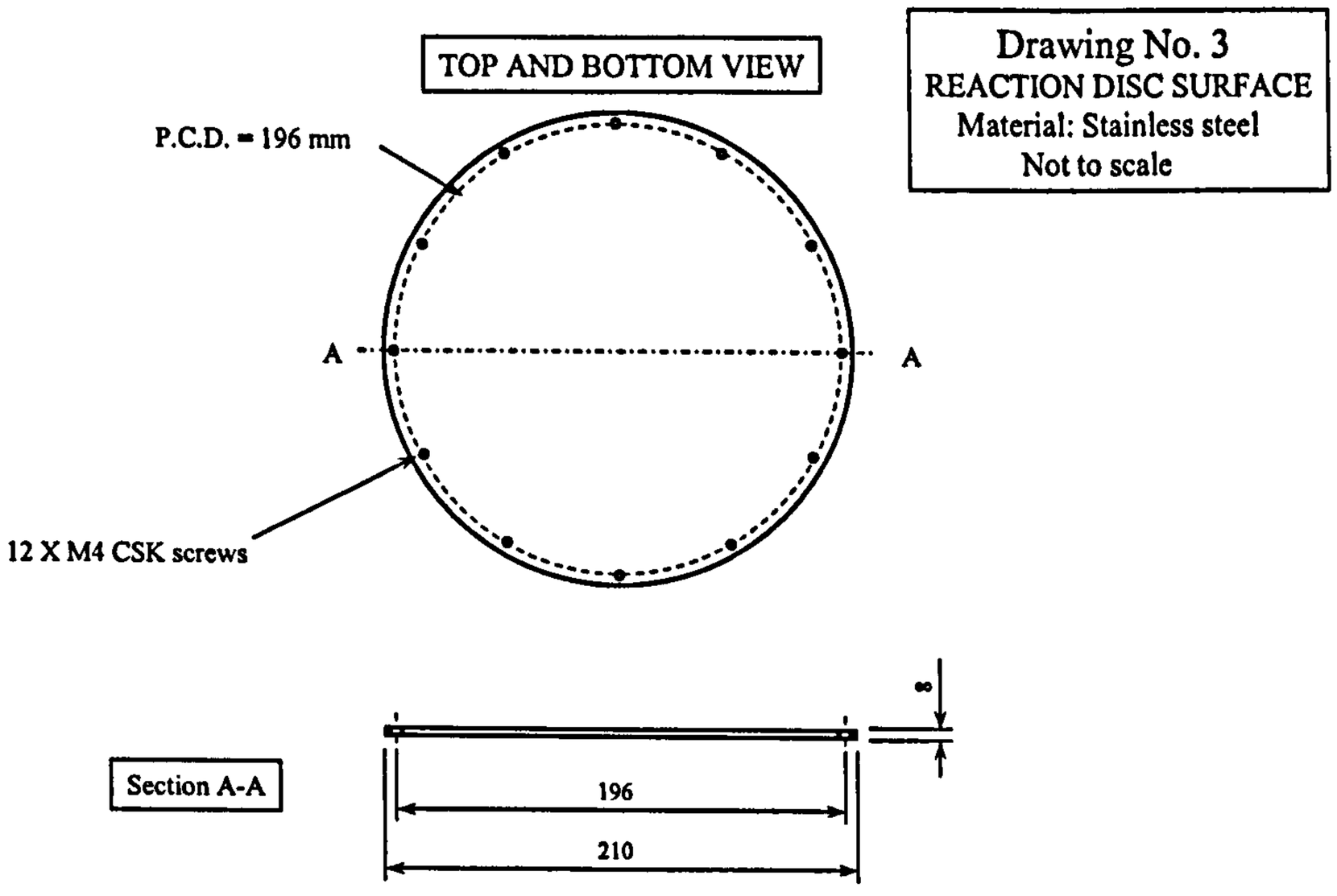
TOP AND BOTTOM VIEW
P.C.D. = 196 mm
A
A
12 X M4 CSK screws
Drawing No. 3
REACTION DISC SURFACE
Material: Stainless steel
Not to scale
Section A-A
8
196
210

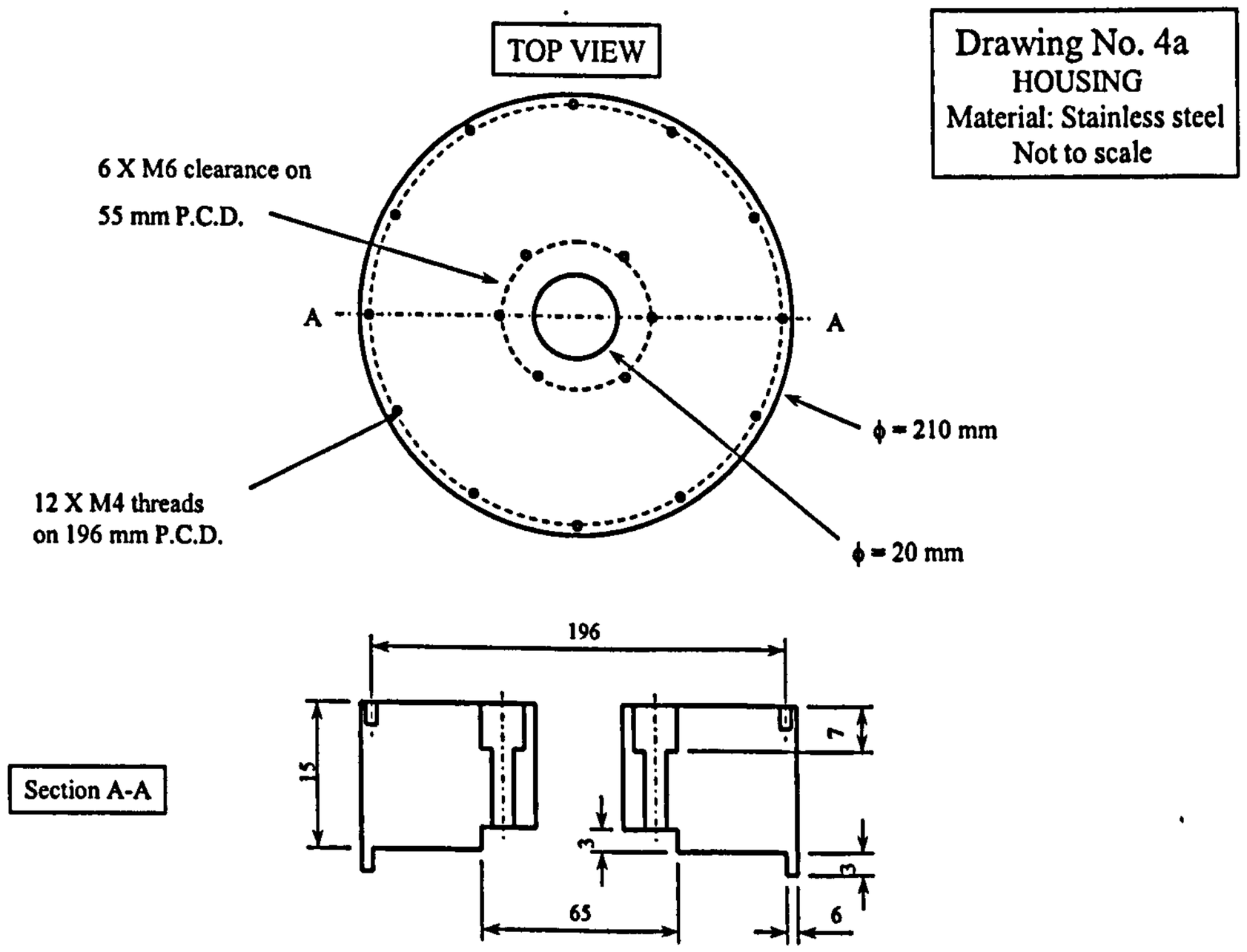
TOP VIEW
6 X M6 clearance on
55 mm P.C.D.
A
A
12 X M4 threads
on 196 mm P.C.D.
ϕ = 210 mm
ϕ = 20 mm
Drawing No. 4a
HOUSING
Material: Stainless steel
Not to scale
Section A-A
196
15
3
65
7
3
6

Drawing No. 4b
GROOVES FOR THERMOCOUPLES
Not to scale

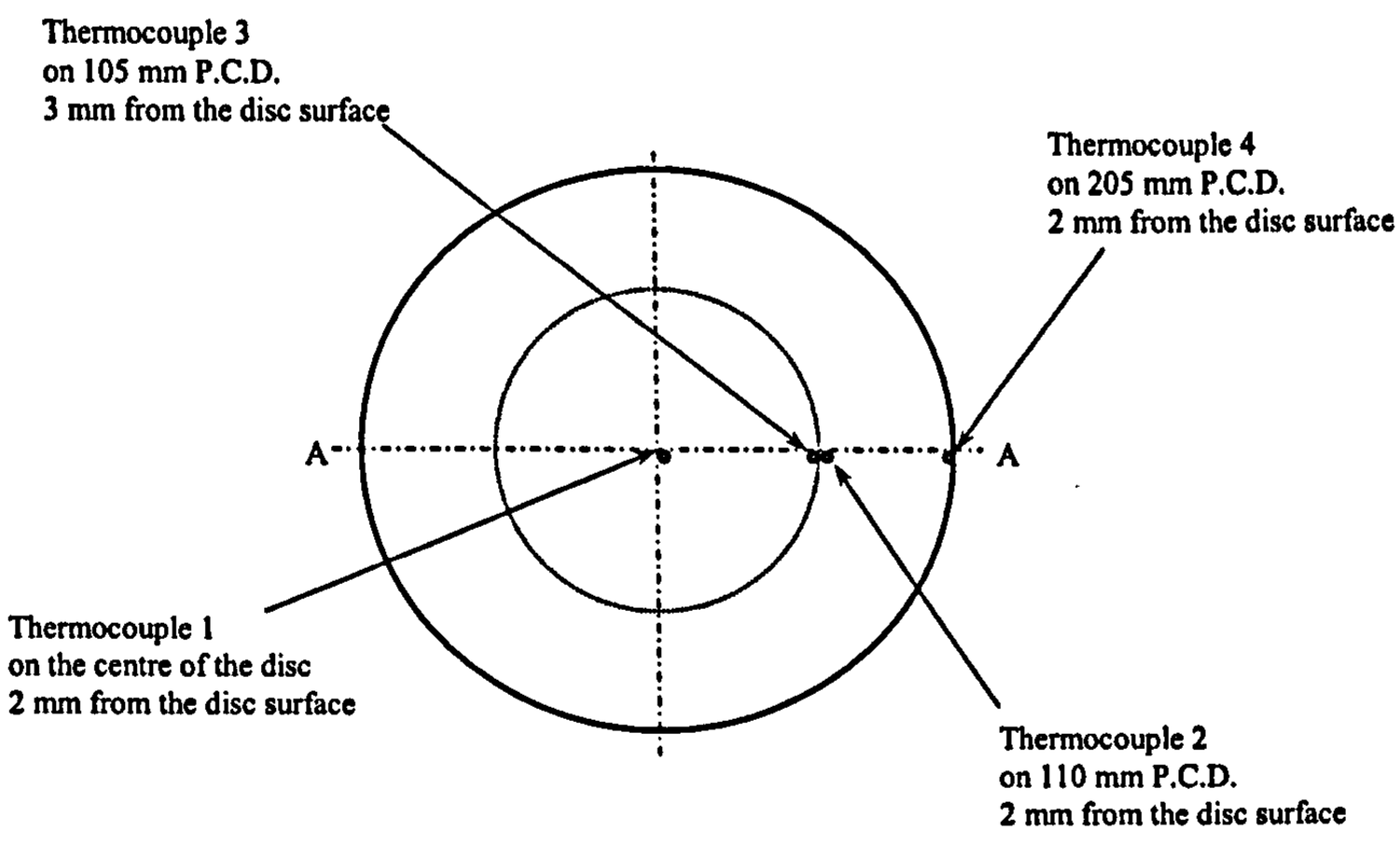


Drawing No. 4c
HOUSING
Material: Stainless steel
Not to scale

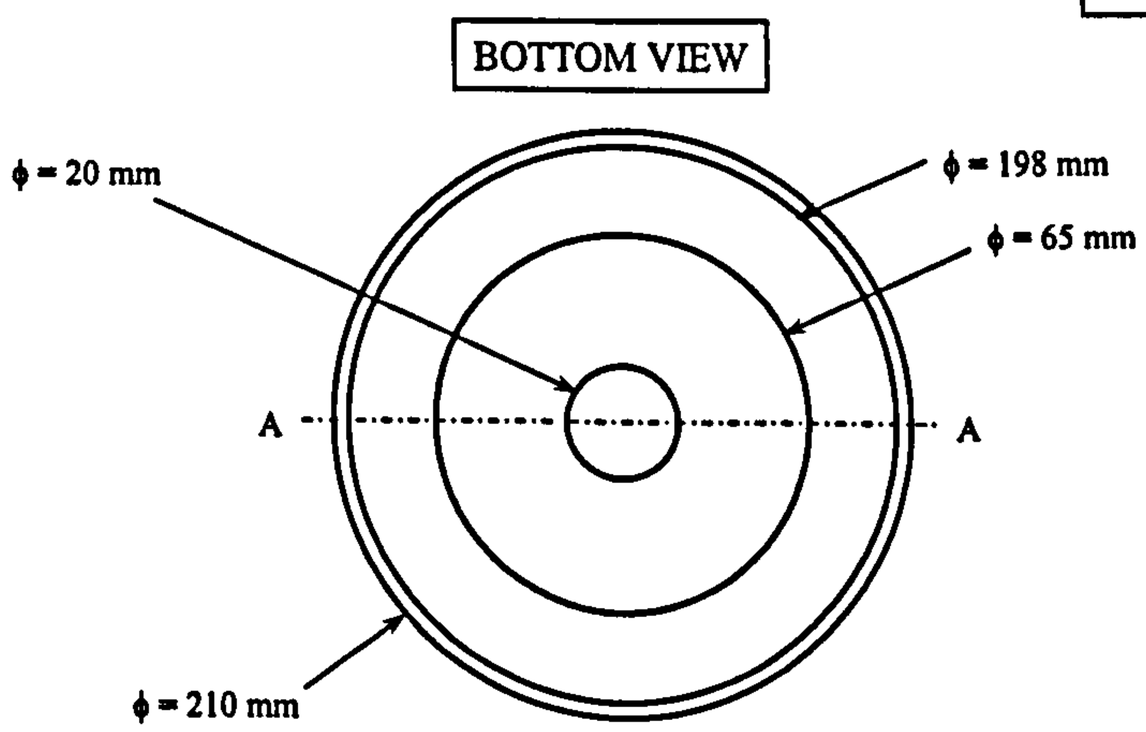

Drawing No. 5a
DRIVE FLANGE
Material: Stainless steel
Not to scale

TOP VIEW

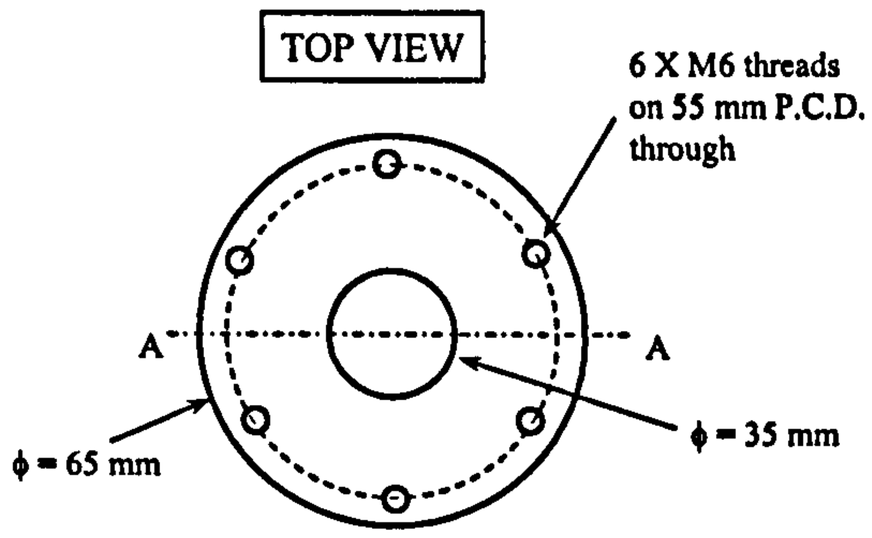


BOTTOM VIEW

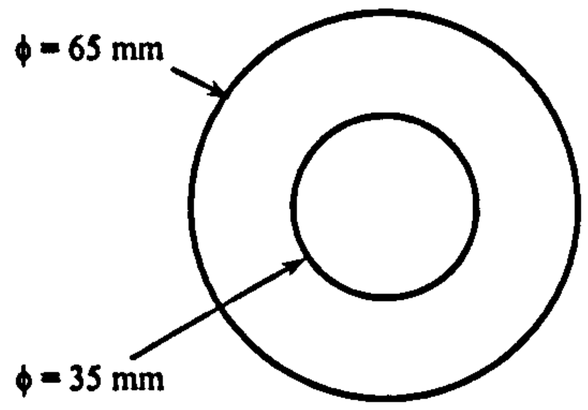


Section A-A

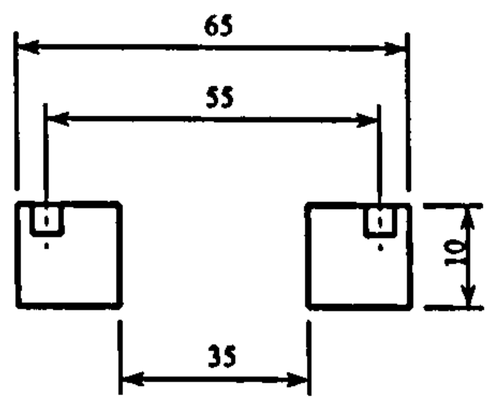


Machine thro with step on
shaft weld top and bottom

Drawing No. 5b
HOUSING, DRIVE FLANGE & SHAFT CONNECTION
Material: Stainless steel
Not to scale

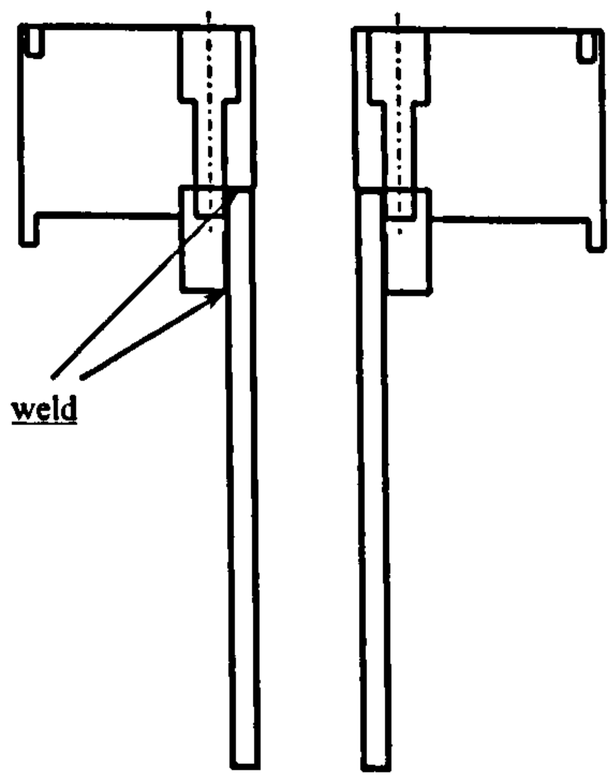

Drawing No. 6
EXPLOITED SECTION OF HOUSING
Not to scale

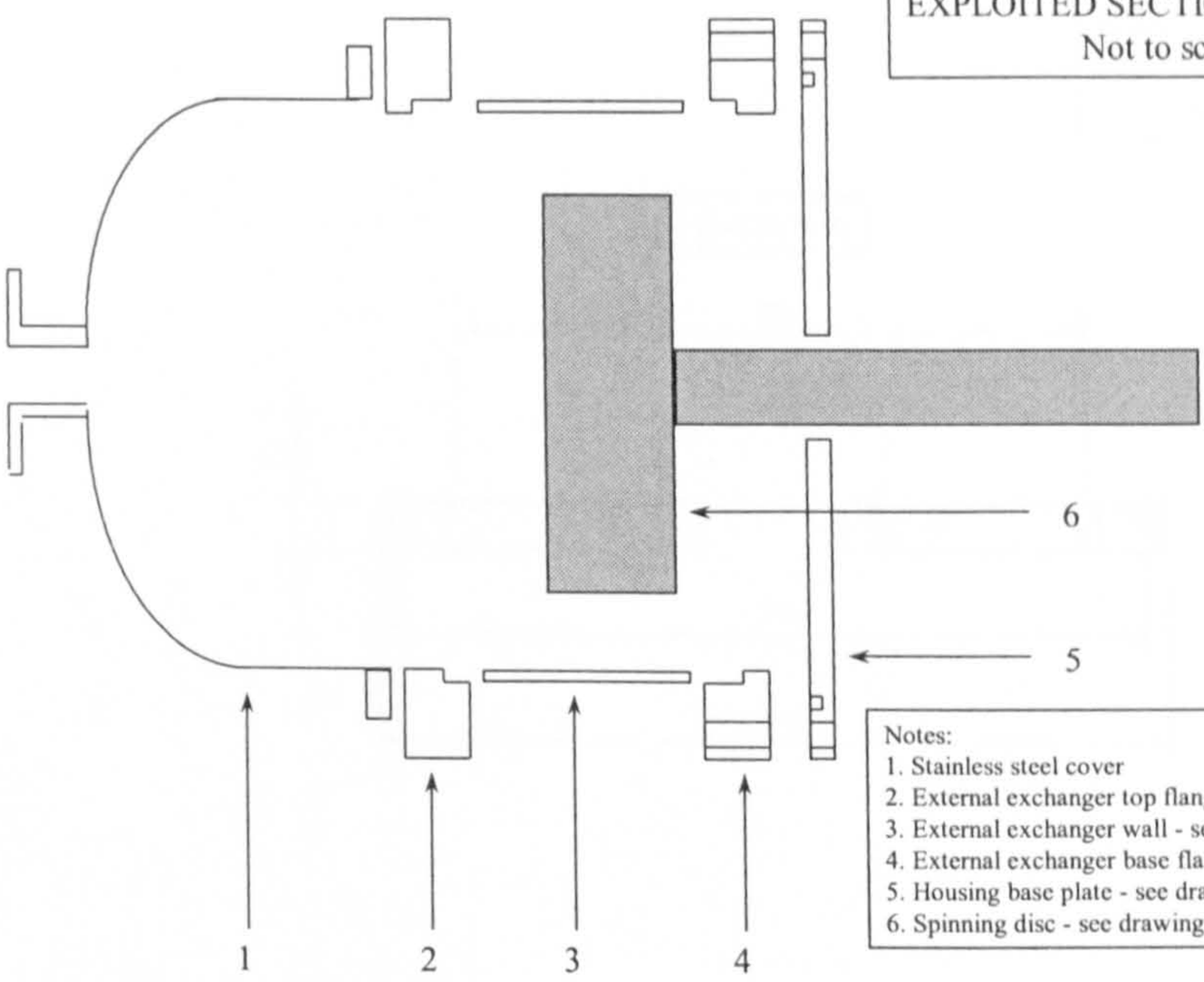


Notes:
1. Stainless steel cover
2. External exchanger top flange - see drawing No. 10
3. External exchanger wall - see drawing No. 9
4. External exchanger base flange - see drawing No. 8
5. Housing base plate - see drawing No. 7
6. Spinning disc - see drawings No. 3-5

Drawing No. 7a
HOUSING BASE PLATE
Material: Stainless steel
Not to scale

Order Number JW: 72-3193-57

TOP VIEW

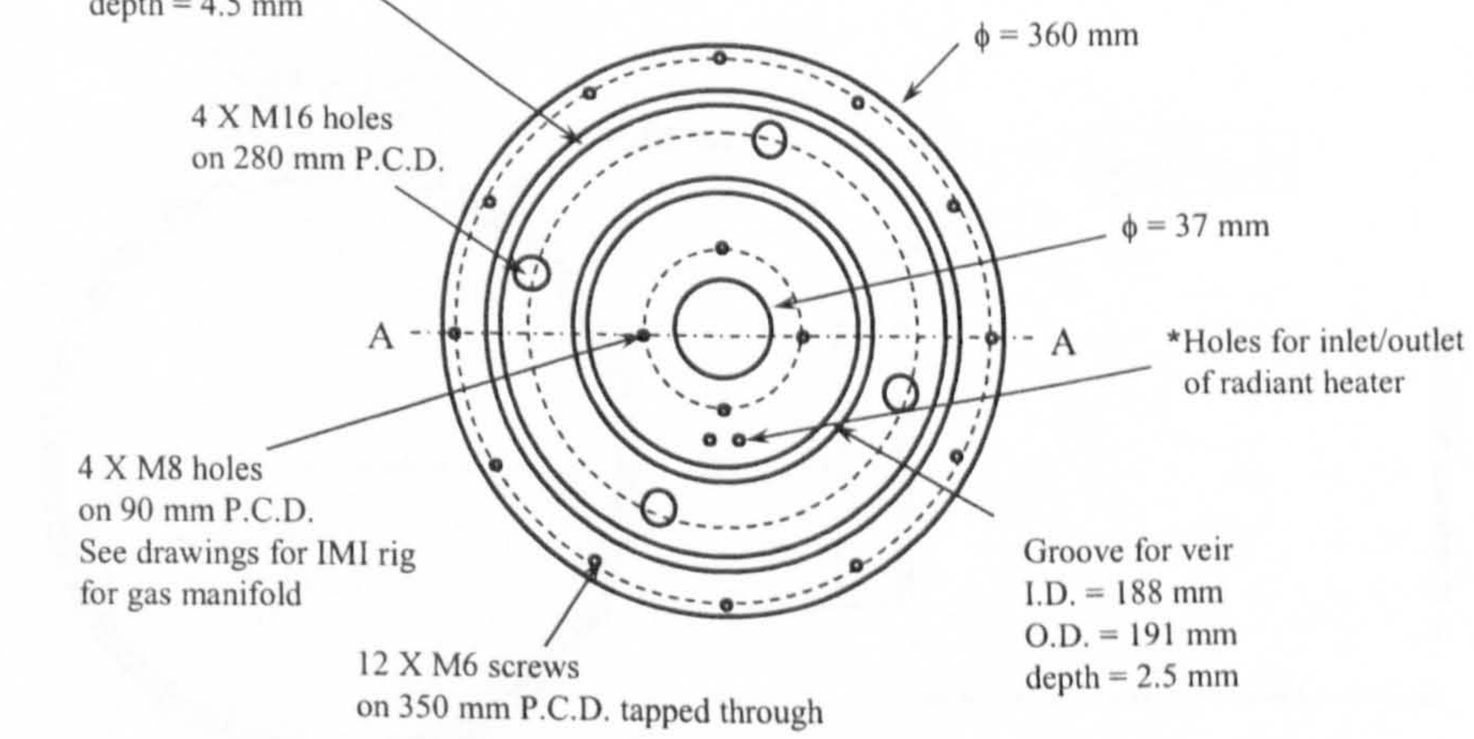

Drawing No. 7b
HOUSING BASE PLATE
Material: Stainless steel
Not to scale

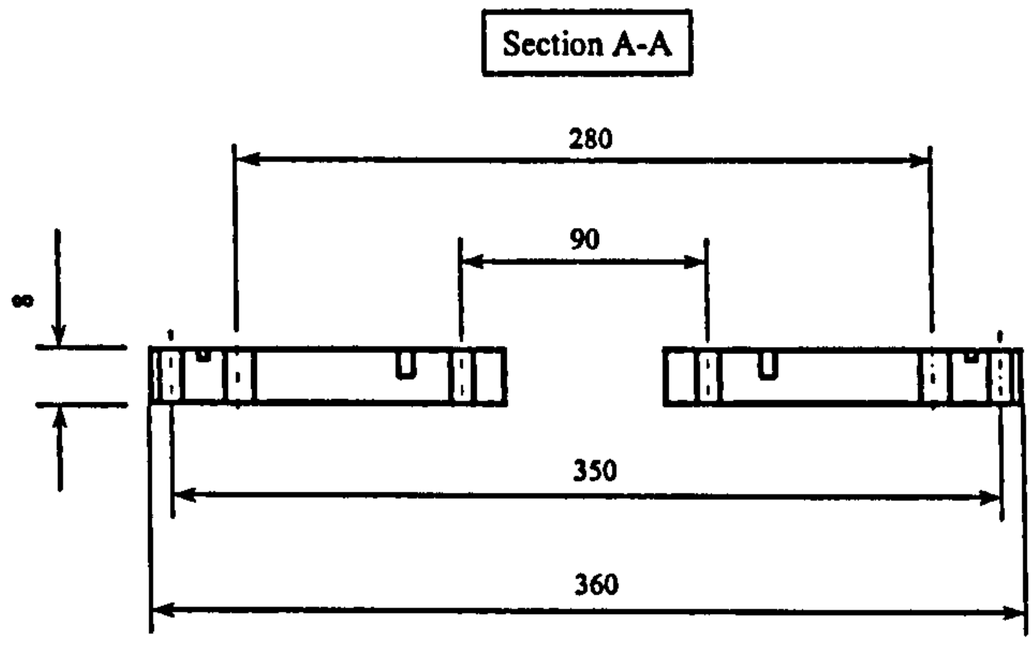


Drawing No. 7c
WEIR IN HOUSING BASE PLATE
Material: Stainless steel
Not to scale

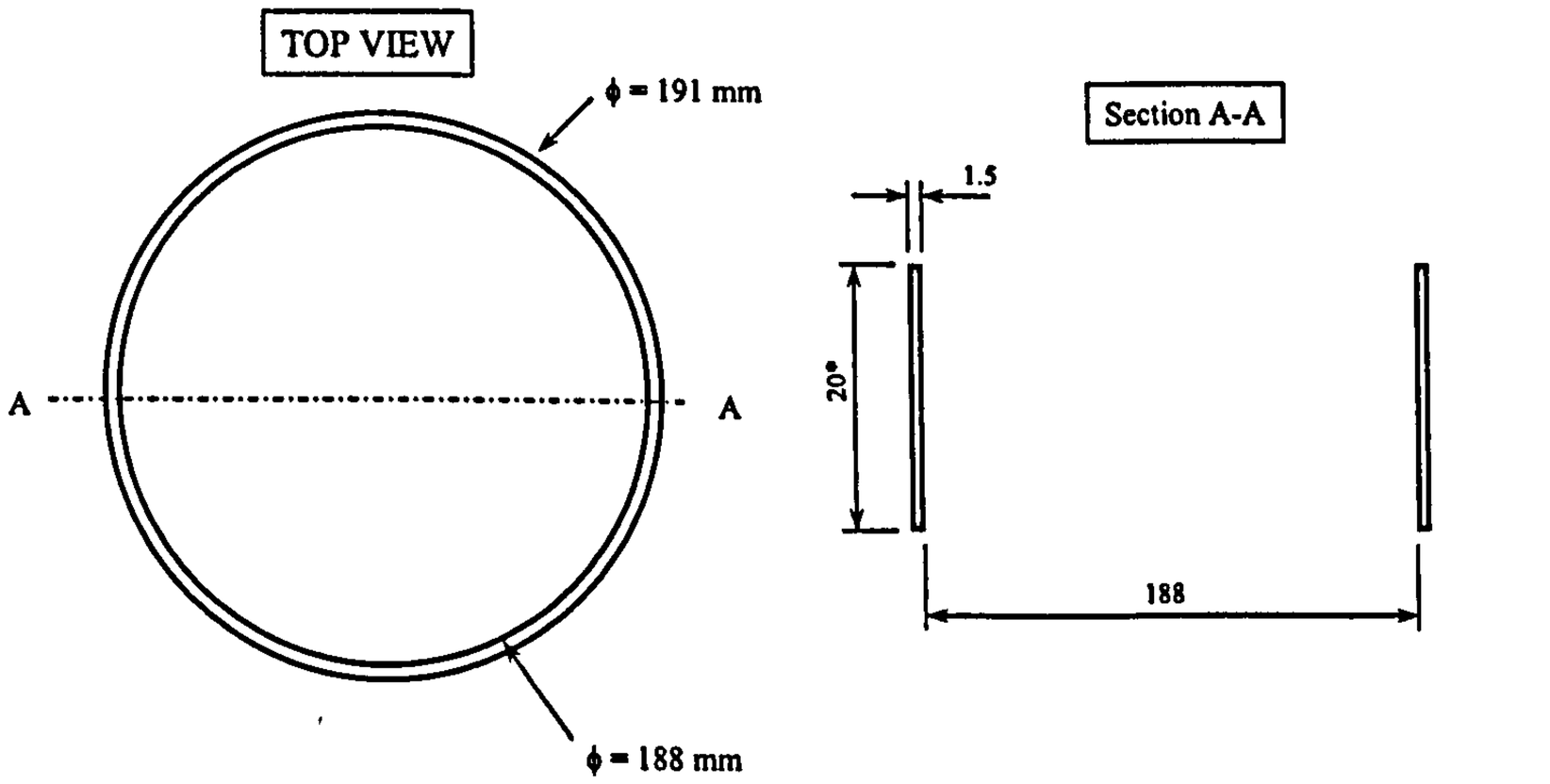

Drawing No. 8a
EXTERNAL EXCHANGER BASE FLANGE
Material: Stainless steel
Not to scale

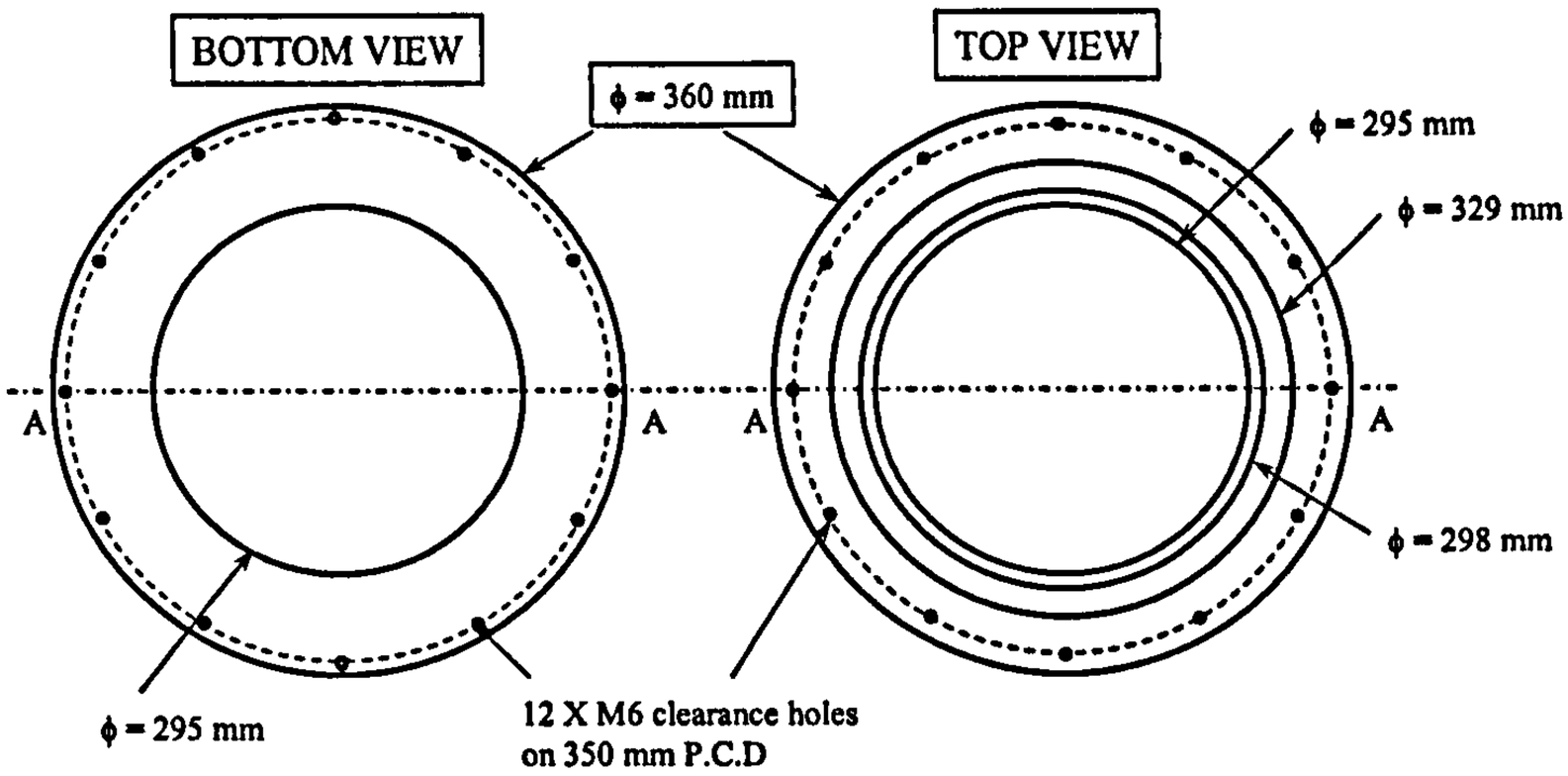


Drawing No. 8b
EXTERNAL EXCHANGER BASE FLANGE
Material: Stainless steel
Not to scale

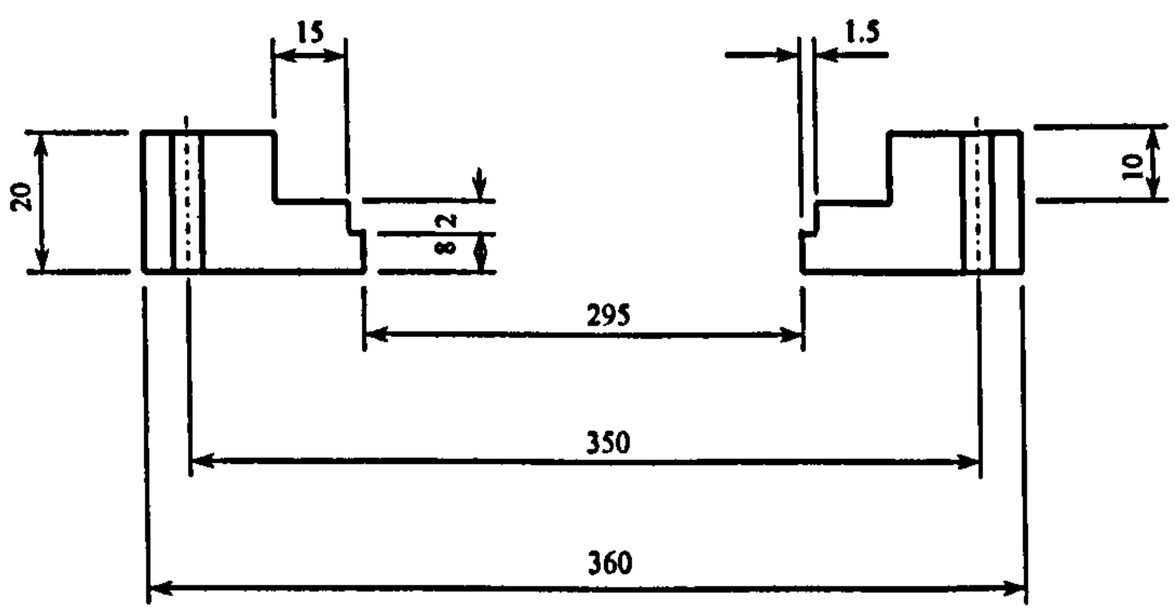


Section A-A

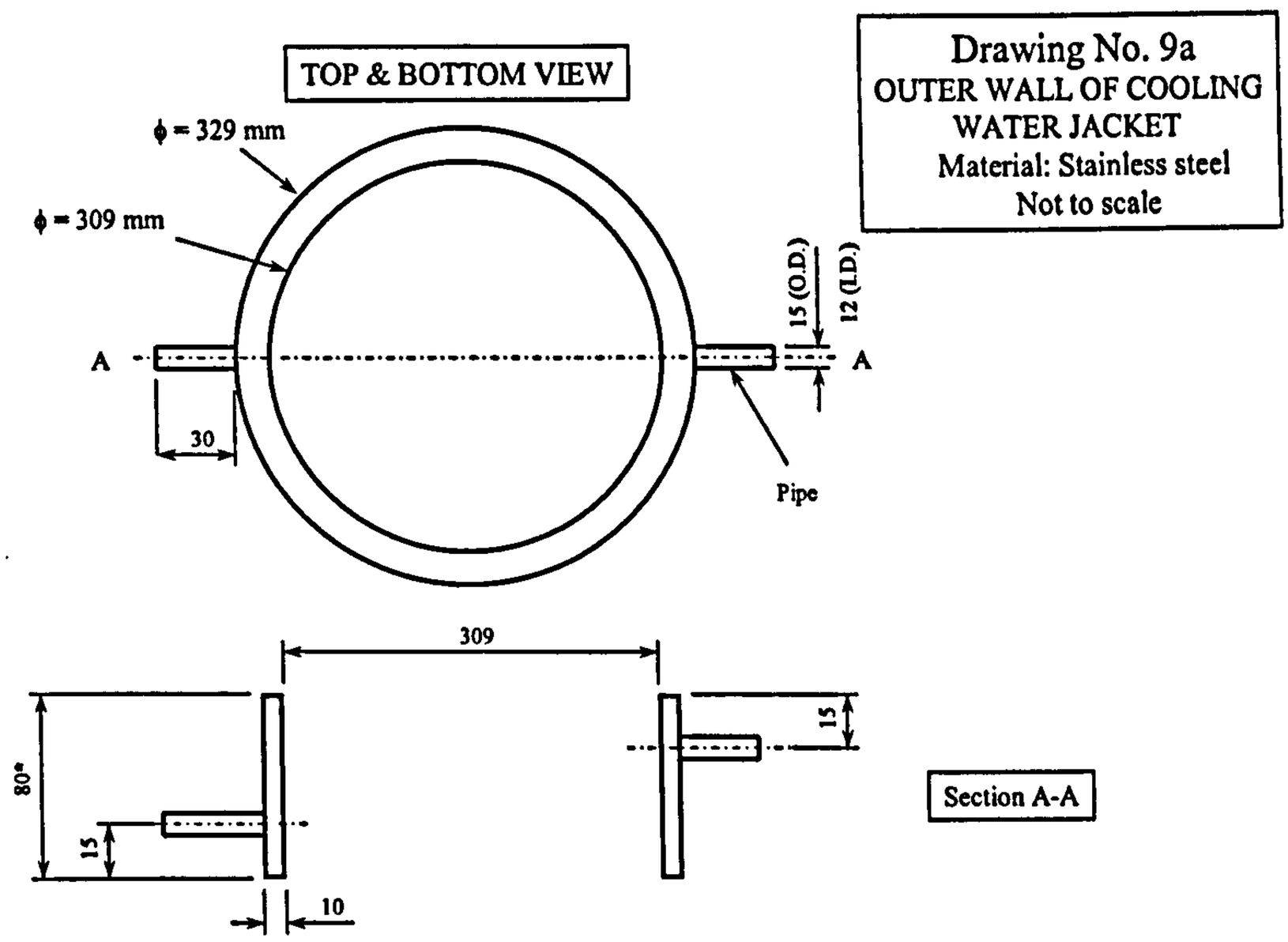


Drawing No. 9a
OUTER WALL OF COOLING WATER JACKET
Material: Stainless steel
Not to scale

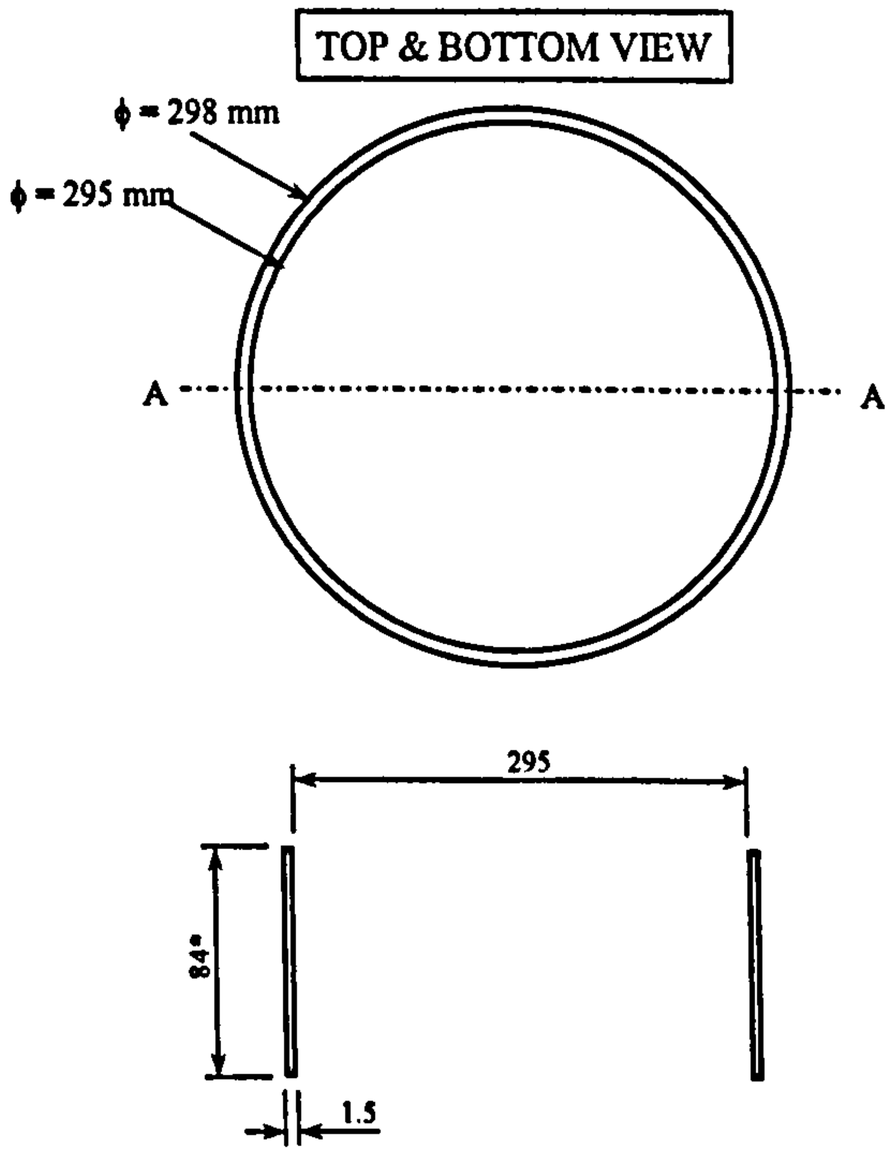


Drawing No. 9b
INNER WALL OF COOLING WATER JACKET
Material: Stainless steel
Not to scale

Drawing No. 9c
ASSEMBLY OF INNER & OUTER WALL
OF COOLING WATER JACKET
Not to scale

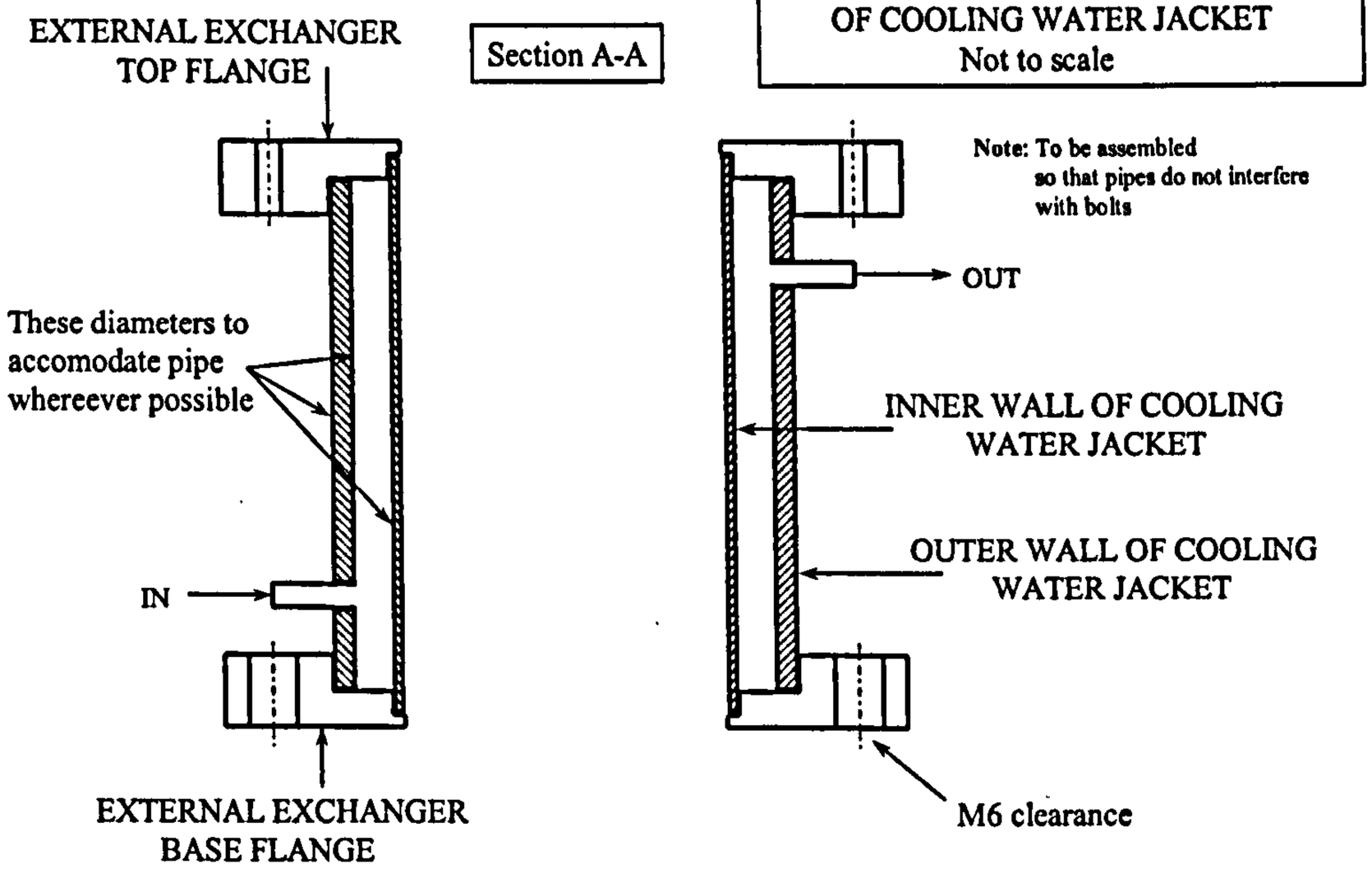


Drawing No. 10a
EXTERNAL EXCHANGER TOP FLANGE
Material: Stainless steel
Not to scale

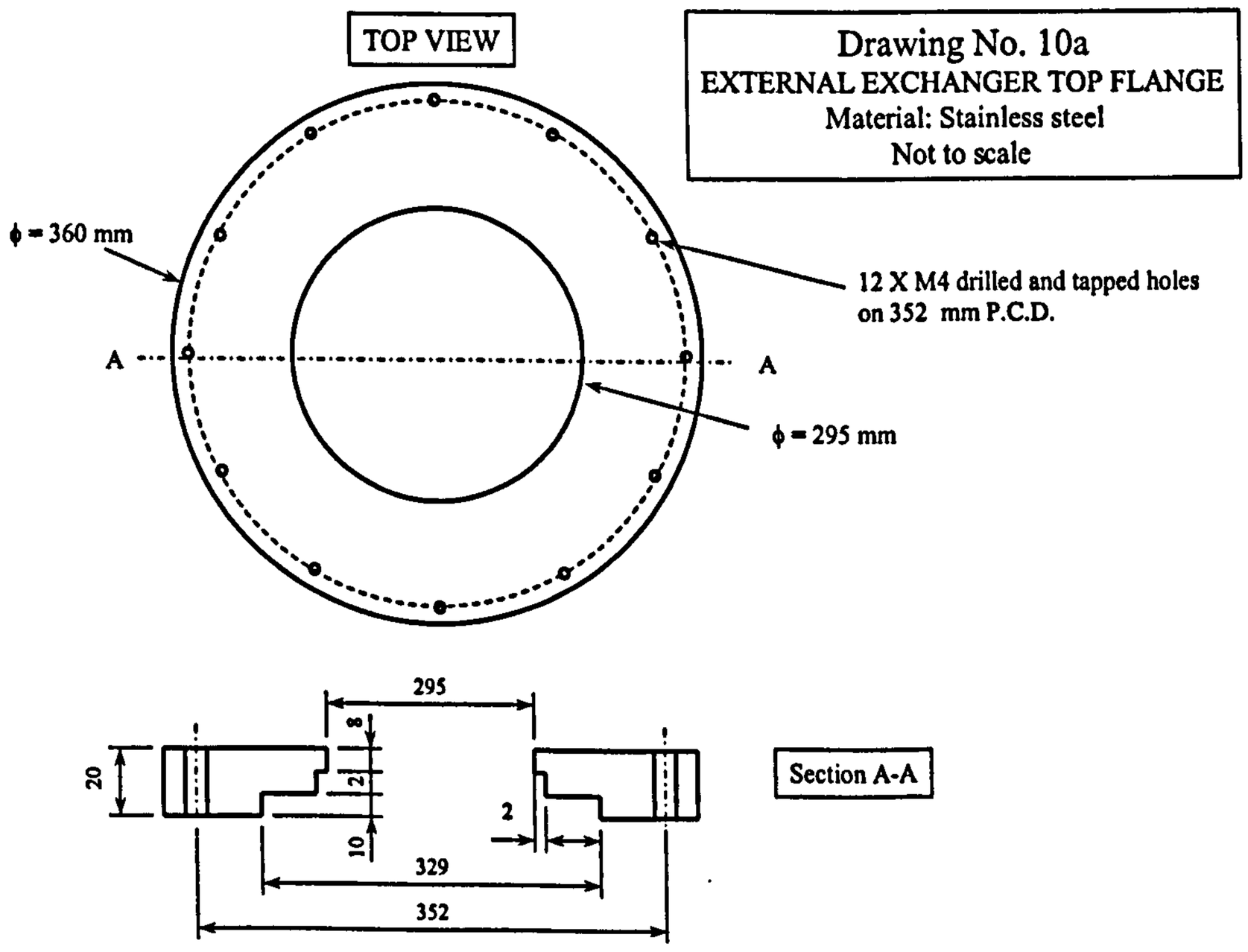

Drawing No. 10b
EXTERNAL EXCHANGER TOP FLANGE
Material: Stainless steel
Not to scale

BOTTOM VIEW

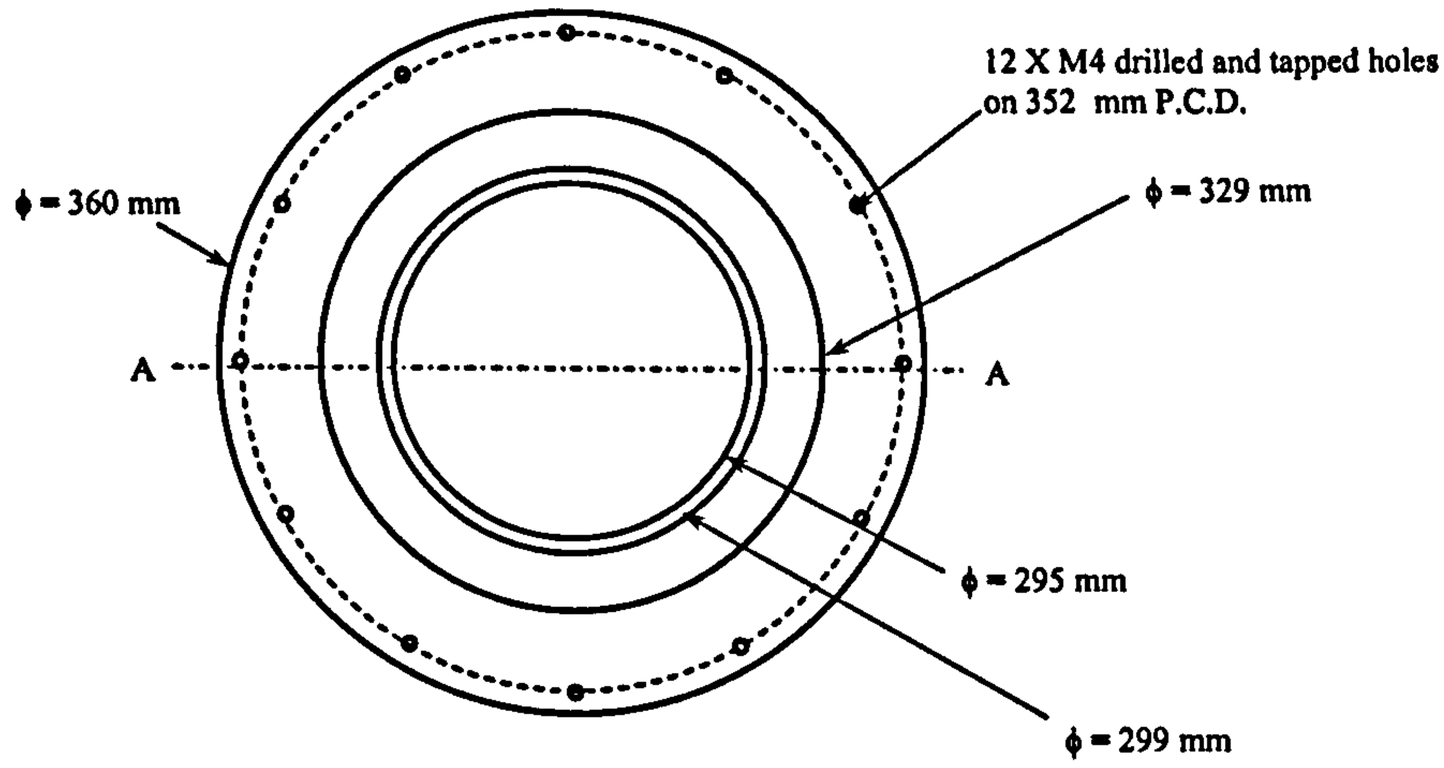

# APPENDIX E

## GAS/LIQUID CHROMATOGRAPHY

### E.1 INTRODUCTION

Few methods of chemical analysis are truly specific to a particular analyte. It is often found that the analyte of interest must be separated from the myriad of individual compounds that may be present in a sample. As well as providing the analytical scientist with methods of separation, chromatographic techniques can also provide methods of analysis.

Chromatography involves a sample (or sample extract) being dissolved in a mobile phase (which may be a gas, a liquid or a supercritical fluid). The mobile phase is then forced through an immobile, immiscible stationary phase. The phases are chosen such that components of the sample have differing solubilities in each phase. A component which is quite soluble in the stationary phase will take longer to travel through it than a component which is not very soluble in the stationary phase but very soluble in the mobile phase. As a result of these differences in mobilities, sample components will become separated from each other as they travel through the stationary phase.

Techniques such as H.P.L.C. (High Performance Liquid Chromatography) and G.C. (Gas Chromatography) use columns – narrow tubes packed with stationary phase, through which the mobile phase is forced. The sample is transported through the column by continuous addition of mobile phase. This process is called *elution*. The average rate at which an analyte moves through the column is determined by the time it spends in the mobile phase.

Schematic diagram of a gas chromatograph is presented in Figure E.1.

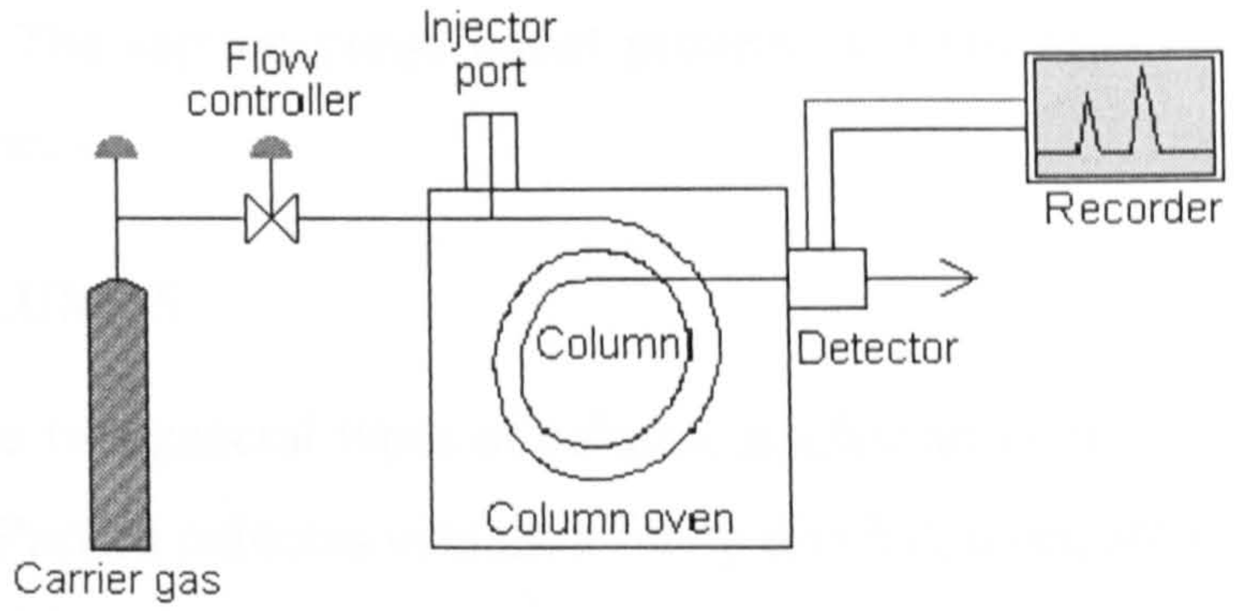


**Figure E.1. GC schematic diagram[1]**

## E.2 INSTRUMENTAL COMPONENTS

### E.2.1 CARRIER GAS

The carrier gas must be chemically inert. Commonly used gases include nitrogen, helium, argon, and carbon dioxide. The choice of carrier gas is often dependant upon the type of detector which is used. The carrier gas system also contains a molecular sieve to remove water and other impurities.

### E.2.2 SAMPLE INJECTION PORT

For optimum column efficiency, the sample should not be too large, and should be introduced onto the column as a "plug" of vapour – slow injection of large samples causes band broadening and loss of resolution. The most common injection method is where a microsyringe is used to inject sample through a rubber septum into a flash vapouriser port at the head of the column. The temperature of the sample port is usually about $50^0$C higher than the boiling point of the least volatile component of the sample. For packed columns, sample size ranges from tenths of a microlitre up to 20 microlitres. Capillary columns, on the other hand, need much less sample, typically around $10^{-3}$ µl. The injector can be used in one of two modes: split or splitless. The injector contains a heated chamber containing a glass liner into which the sample is injected through the septum. The carrier gas enters the chamber and can leave by three routes (when the injector is in split mode). The sample vapourises to form a mixture of carrier gas, vapourised solvent and vapourised solutes. A proportion of this mixture passes onto the column, but most exits through

[1] http://www.shu.ac.uk/schools/sci/chem/tutorials/chrom/gaschrm.htm

the split outlet. The septum purge outlet prevents septum bleed components from entering the column.

### E.2.3 COLUMNS

There are two general types of column, *packed* and *capillary* (also known as *open tubular*). Packed columns contain a finely divided, inert, solid support material coated with liquid stationary phase. Most packed columns are 1.5 – 10 m in length and have an internal diameter of 2 – 4 mm. Capillary columns have an internal diameter of a few tenths of a millimetre.

### E.2.4 DETECTORS

Detectors are either flow sensitive or mass sensitive depending on whether the mere presence of solute inside the detector cell is sufficient to create a response, or whether the solute is consumed in a chemical reaction, and it is the reaction or its products that create the response. Solutes pass unchanged through flow sensitive detectors which can therefore be linked in series.

The difference between the two detectors is highlighted by considering the effect of stopping the (single component) mobile phase as a solute passes through the detector cell.

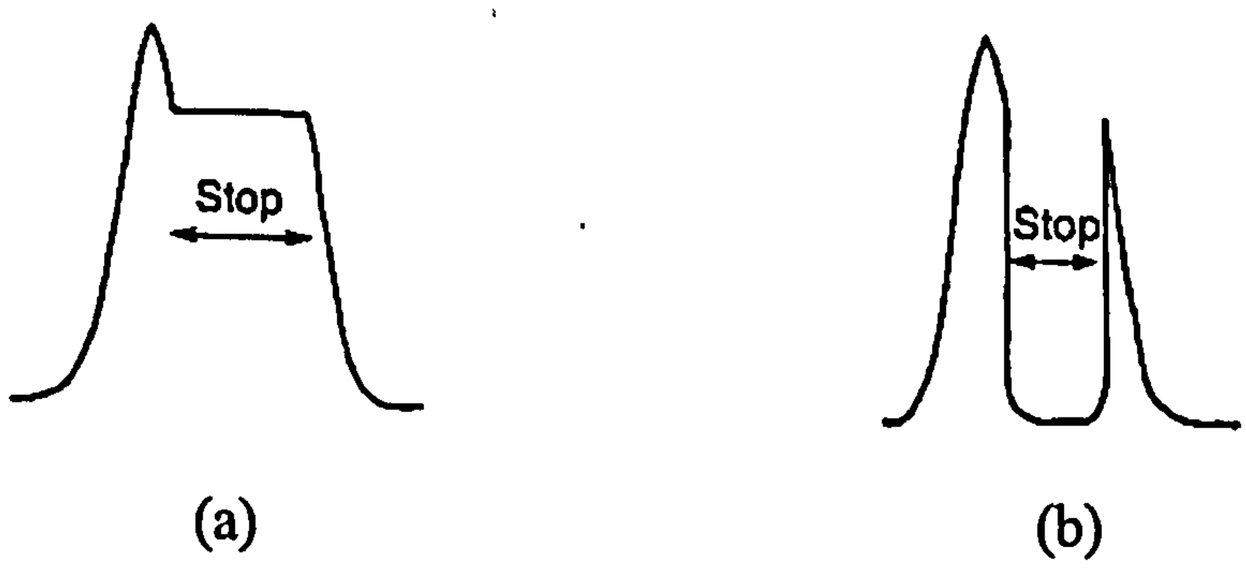


**Figure E.2. Effect of stopping mobile phase on detector signal. (a) Flow sensitive; (b) Mass sensitive**

In a flow sensitive detector, the detector signal is held constant and it will only change when the flow re-starts and sweeps the solute from the cell. The area of the solute peak is increased but the height remains nearly constant (in fact a 10% reduction in flow has been observed to produce a 1% increase in height).

In contrast, the signal level from a mass sensitive detector falls to zero (at a rate determined by the detector time constant) as a solute inside the cell is consumed and no more is delivered. When flow is continued the signal picks up again as the remaining solute is swept into the detector cell.

The peak area is split, but the sum of the two split areas is the same as the peak area if the flow had not stopped. Peak height is not preserved unless the maximum has eluted before the flow was interrupted.

The two types of detector are summarised in Table E.1.

**Table E.1. Types of detector**

| **Gas Chromatography** | | **Liquid Chromatography** | |
|---|---|---|---|
| FID | Mass | UV or UV/VIS detector | Flow |
| TCD | Flow | Refractive Index detector | Flow |
| ECD | Flow (Mass) | Fluorimetric detector | Flow |
| N/P FID | Mass | Electrochemical detector | Mass |
| FPD | Mass | Coulometric detector | Mass |
| Mass Spectrometer | Mass | | |
| Hall Detector | Flow | | |
| He ID | Mass | | |

When flow conditions are not rigorously controlled an ECD can behave as mass sensitive because the electron density (and so response) is a function of carrier flow rate.

### *E.2.4.1 The Flame Ionisation Detector (FID)*

The effluent from the column is mixed with hydrogen and air, and ignited. Organic compounds burning in the flame produce ions and electrons which can conduct electricity through the flame. A large electrical potential is applied at the burner tip, and a collector electrode is located above the flame. The current resulting from the pyrolysis of any organic compounds is measured. The FID is a useful general detector for the analysis of organic compounds; it has high sensitivity, a large linear response range, and low noise. It is also robust and easy to use, but unfortunately, it destroys the sample.

## E.3 STANDARD CALCULATIONS

Integrators offer three standard calculations; normalisation (area %), internal standard and external standard, and a variety of non-standard calculations, some of which are computer programs.

### E.3.1 AREA % OR NORMALISATION

The concentration, $C_i$, of a solute, i, is calculated from:

$$C_i = \frac{A_i}{\sum(A_i)} \cdot 100\% \qquad \text{(e.1)}$$

where $A_i$ is the peak area of solute i, and $\Sigma(A_i)$ is the total area of all the chromatogram peaks.

If response factors of each solute are included, last equation becomes:

$$C_i = \frac{A_i R_i}{\sum(A_i R_i)} \cdot 100\% \qquad \text{(e.2)}$$

where $R_i$ is absolute solute response factor, the quantity of matter to produce unit area count.

Area % as defined by equation (e.2) means percentage of solutes which are eluted and detected. This might only be fraction of what was injected. The analyst must be certain that nothing has been retained by the column or missed by the detector.

If solutes are known to be retained or not detected, and the measured fraction is known accurately, then instead of normalising to 100%, the results can be scaled to the fractional percentage by means of a scaling factor, *S*:

$$C_i = \frac{A_i R_i}{\sum(A_i R_i)} \cdot S\% \qquad \text{(e.3)}$$

For example, beer is typically analysed by GC using an FID which does not respond to water. If the beer is known to contain 94% water then it is more useful to normalise the analysis to 6% than 100%.

## E.3.2 INTERNAL STANDARD

The weight of solute in a sample is determined by comparing its area to the area of a known amount of standard added to the sample and analysed with it:

$$W_i = \frac{A_i R_{is}}{A_s} \cdot W_s \qquad \text{(e.4)}$$

where $W_i$ – solute quantity

$W_s$ – quantity of internal standard

$R_{is}$ – the relative response factor of solute to internal standard

= ratio of absolute response factors

The concentration of solute in the original sample ($W_{spl}$) is given by:

$$wt\% = \frac{W_i}{W_{spl}} \cdot 100 = \frac{A_i R_{is} W_s}{W_{spl}} \cdot 100\% \qquad \text{(e.5)}$$

If some solutes are retained by the column, or not detected, the sum of the detected solute weights will be less than the sample weight, or their concentrations will add to less than 100%.

Internal standard method allows absolute quantities of solute to be measured by compensating for variations in injected sample volume. It does not compensate for differences in peak shape between solute and standard if this indicates detector overloading. A good standard gives a peak that is the same size and shape as the peak it is to be compared with. It is a weakness of the internal standard technique that one peak serves as a standard for several others where these vary in shape and size.

## E.3.3 EXTERNAL STANDARD

The external standard method compares a solute peak area in an unknown sample with the area produced by a known amount of solute in a standard sample analysed under identical conditions.

Then:

$$W_i = \frac{A_i}{A_s} \cdot W_s \qquad \text{(e.6)}$$

No response factor is necessary because the sample and standard are the same species. If the peaks are similar in size, it will avoid peak shape/linearity problems. Equal sized injections of standard and unknown are essential. Manual injections are not normally accurate enough; sample valves or autosamplers are to be preferred.

Standard solutions are normally prepared containing a known amount of each of the solutes required from the unknown solution.

## E.4 SAMPLES OF CHROMATOGRAPHS USED IN THIS STUDY USING INTERNAL STANDARD METHOD

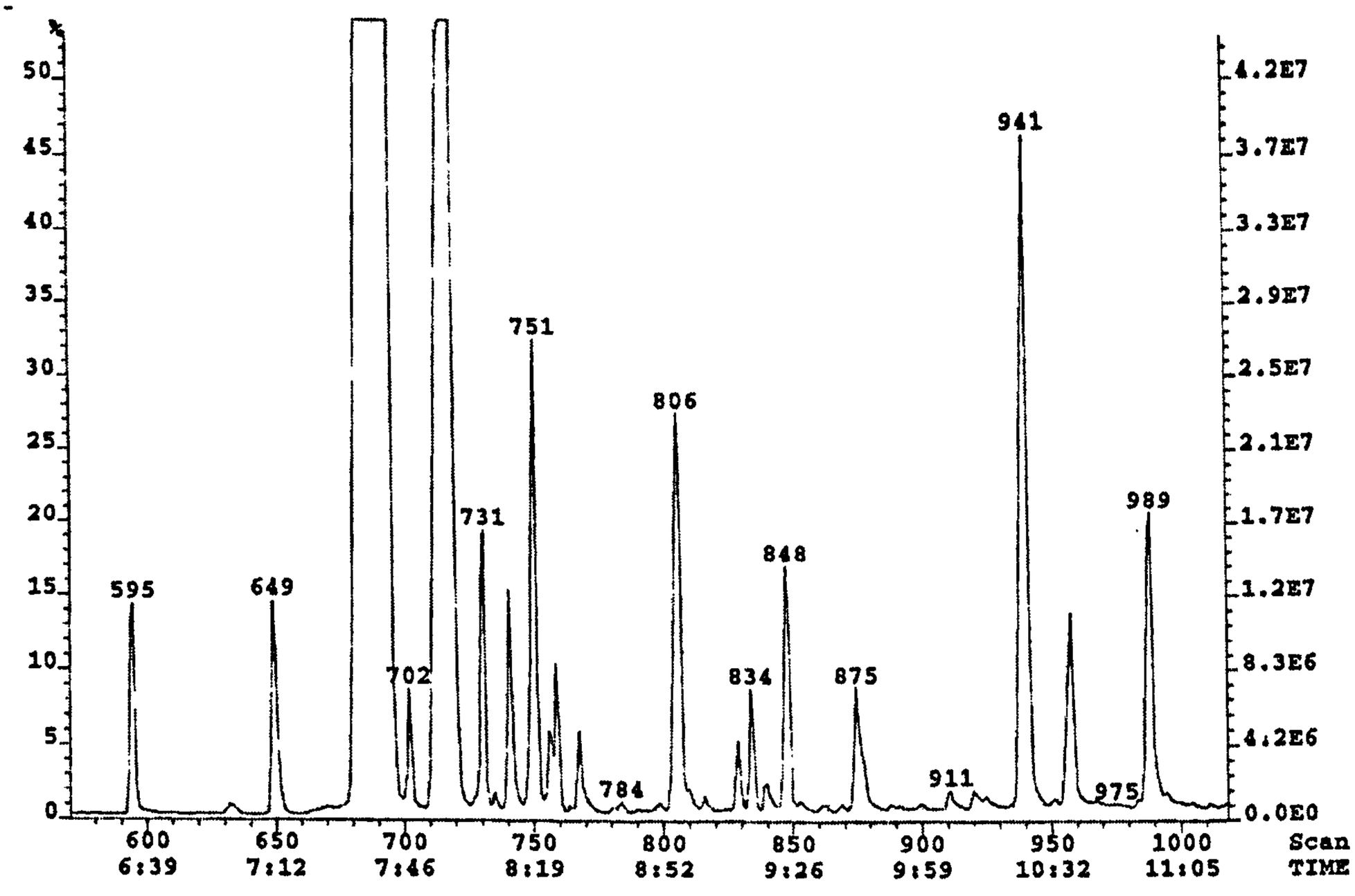


**Figure E.3. Septum Magnet AutoSpec (York)**

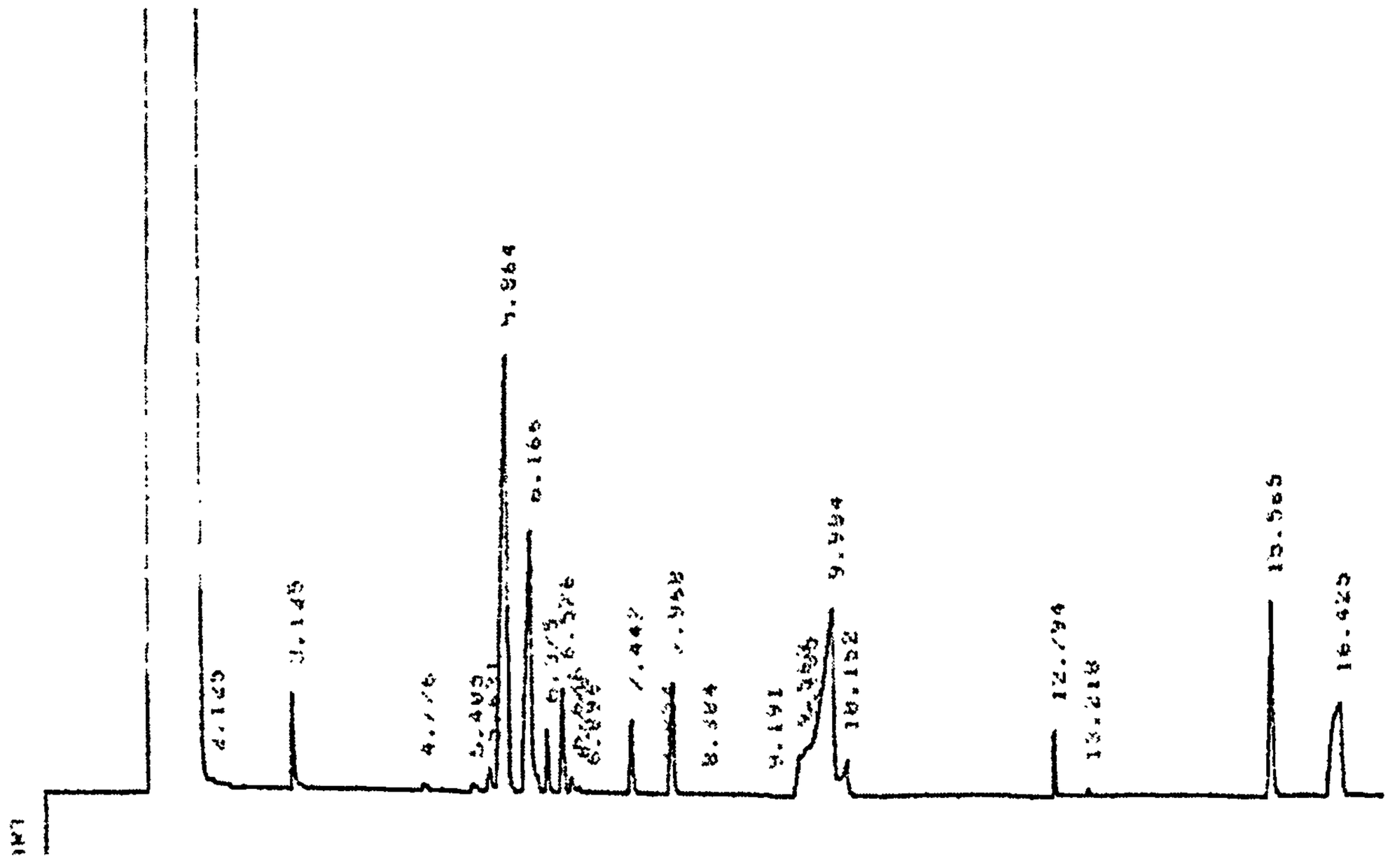

**Figure E.4. FID UNICAM Series 610 LC-GC, with a HP1 packed column**

# APPENDIX F

## PHYSICAL DATA

### F.1 DATA FOR α–PINENE OXIDE

**Table F.1. Physical data (α–pinene oxide)***

| | |
|---|---|
| **Viscosity (μ)** | $0.9 \cdot 10^{-3}$ Pa s |
| **Density** | As below calculated |
| **Molecular weight** | 152.24 g/mol |
| **Boiling point** | 102 – 103°C |

*From: http://www.fishersci.ca/msds2.nsf/EView1/33563/$file/msds-33563.html

#### F.1.1 DENSITY OF α–PINENE OXIDE

A known volume (1ml) of α–pinene oxide was weighed and density calculated as:

$$\rho\left(\frac{kg}{m^3}\right)=\frac{m(kg)}{V(m^3)}$$

Results are presented in Table F1.

**Table F.2. Density calculations**

| Sample | Mass · $10^3$ (kg) | Density (kg/m$^3$) |
|---|---|---|
| 1 | 0.964 | 964 |
| 2 | 0.965 | 965 |
| 3 | 0.964 | 964 |

### F.2 DATA FOR SOLVENT: 1,2–DICHLOROETHANE

**Table F.3. Physical data (1,2–dichloroethane)****

| | |
|---|---|
| **Viscosity (μ)** | $0.79 \cdot 10^{-3}$ Pa s |
| **Density** | $1.256 \cdot 10^3$ kg/m$^3$ |
| **Molecular weight** | 96.95 g/mol |
| **Refractive Index at 20°C** | 1.445 |
| **Boiling point** | 83°C |

**From: http://physchem.ox.ac.uk/MSDS/DI/1%2C2-dichloroethane.html

## F.3 PROPERTIES OF SILICA

**Table F.4. Physical, mechanical, thermal and electrical properties of fused silica*****

| Material | Fused Silica |
|---|---|
| Density ($g/cm^3$) | 2.2 |
| Thermal conductivity ($Wm^{-1}$ K) | 1.4 |
| Thermal expansion coeff. ($10^{-6}$ $K^{-1}$) | 0.4 |
| Tensile strength (MPa) | 110 |
| Compressive strength (MPa) | 690-1380 |
| Poisson's ratio | 0.165 |
| Fracture toughness (MPa) | 0.79 |
| Melting point (°C) | 1830 |
| Modulus of elasticity (GPa) | 73 |
| Thermal shock resistance | Excellent |
| Permittivity (ε') **** | 3.8 |
| Dielectric field strength (kV/mm) **** | 15.0-40.0 |
| Resistivity (Ωm) **** | $>10^{18}$ |

**** Dielectric Properties at 1 MHz 25°C

***From: http://www.azom.com/details.asp?ArticleID=1114

# APPENDIX G

## EXPERIMENTAL DATA

### G.1 CATALYST QUANTITY

**Table G.1. Quantity of catalyst used for coating of the disc**

| No. | Disc weight (g) | Disc+glue (g) | Disc+glue+catalyst (g) | Disc+glue+catalyst (dry) (g) | Catalyst (g) |
|---|---|---|---|---|---|
| 1 | 1238.6 | 1243.0 | 1243.8 | 1243.8 | 0.8 |
| 2 | 1238.6 | 1243.1 | 1243.9 | 1243.9 | 0.8 |
| 3 | 1238.6 | 1243.1 | 1243.9 | 1243.9 | 0.8 |
| 4 | 1238.6 | 1243.2 | 1244.0 | 1244.0 | 0.8 |
| 5 | 1238.6 | 1243.0 | 1243.8 | 1243.8 | 0.8 |
| 6 | 1238.6 | 1243.1 | 1243.9 | 1243.9 | 0.8 |
| 7 | 1238.6 | 1243.0 | 1243.8 | 1243.8 | 0.8 |
| 8 | 1238.6 | 1243.2 | 1244.0 | 1244.0 | 0.8 |
| 9 | 1238.6 | 1243.0 | 1243.8 | 1243.8 | 0.8 |
| 10 | 1238.6 | 1243.1 | 1243.9 | 1243.9 | 0.8 |
| 11 | 1238.6 | 1243.1 | 1243.9 | 1243.9 | 0.8 |
| 12 | 1238.6 | 1243.0 | 1243.8 | 1243.8 | 0.8 |
| 13 | 1238.6 | 1243.2 | 1244.0 | 1244.0 | 0.8 |
| 14 | 1238.6 | 1243.1 | 1243.9 | 1243.9 | 0.8 |

### G.1.1 CALCULATIONS

Conversion of α-pinene oxide and selectivity towards campholenic aldehyde are calculated as described in section 5.5 in Chapter 5. Conversion ($x_A$) can be calculated from concentration ($C_A$) and vice versa, using equations (g.1) and (g.2):

$$x_A(\%) = \frac{C_{A0} - C_A}{C_{A0}} \cdot 100 \qquad \text{(g.1)}$$

$$C_A = C_{A0}(1 - x_A) \qquad \text{(g.2)}$$

Residence time and film thickness are calculated as described in section 6.2 in Chapter 6. Concentration A in the following tables is the concentration of α-pinene oxide and Concentration B is the concentration of campholenic aldehyde in the product.

## G.2 CATALYST 1: 0.05 mmol/g $Zn(OTf)_2$ SUPPORTED ON $SiO_2$

### G.2.1 BATCH REACTION DATA

**Table G.2. Selectivity and conversion data for batch reaction ($85^0$C)**

| Time (min) | Concentration A ($kmol/m^3$) | Conversion (%) | Concentration B ($kmol/m^3$) | Selectivity (%) |
|---|---|---|---|---|
| 0 | 0.066 | 0 | 0 | 0 |
| 1 | 0.056 | 14.88 | 0.0038 | 39.20 |
| 2 | 0.039 | 40.80 | 0.0146 | 54.40 |
| 2.5 | 0.026 | 60.00 | 0.0241 | 61.00 |
| 3 | 0.020 | 69.80 | 0.0285 | 61.98 |
| 4 | 0.005 | 93.16 | 0.0389 | 63.52 |
| 5 | 0 | 100 | 0.0421 | 64.00 |
| 10 | 0 | 100 | 0.0414 | 63.00 |
| 15 | 0 | 100 | 0.0263 | 40.00 |
| 20 | 0 | 100 | 0.0151 | 23.00 |
| 25 | 0 | 100 | 0.0066 | 10.00 |
| 30 | 0 | 100 | 0.0039 | 6.00 |

### G.2.2 SDR DATA

**Table G.3. SDR runs data for catalyst activity study (flow rate 4 $cm^3/s$)**

| Run | Disc Temperature ($^o$C) | Disc Speed (rpm) | Concentration A ($kmol/m^3$) | Conversion (%) | Selectivity |
|---|---|---|---|---|---|
| **1** | 25 | 150 | 0.0525 | 20.2 | none |
| **2** | 25 | 150 | 0.0528 | 19.7 | none |
| **3** | 25 | 150 | 0.0526 | 20.0 | none |
| **4** | 25 | 150 | 0.0527 | 19.9 | none |
| **5** | 25 | 150 | 0.0526 | 20.0 | none |
| **6** | 25 | 150 | 0.0526 | 20.0 | none |
| **7** | 25 | 150 | 0.0526 | 20.0 | none |
| **8** | 25 | 150 | 0.0526 | 20.1 | none |
| **9** | 25 | 150 | 0.0528 | 19.8 | none |
| **10** | 25 | 150 | 0.0526 | 20.0 | none |
| **11** | 25 | 150 | 0.0527 | 19.9 | none |
| **12** | 25 | 150 | 0.0527 | 19.9 | none |
| **13** | 25 | 150 | 0.0526 | 20.0 | none |
| **14** | 25 | 150 | 0.0528 | 19.8 | none |
| **15** | 25 | 150 | 0.0526 | 20.0 | none |

## Table G.4. SDR runs at different temperatures (flow rate 4 $cm^3/s$)

| Run | Disc Temperature ($^0C$) | Disc Speed (rpm) | Concentration A ($kmol/m^3$) | Conversion (%) | Concentration B ($kmol/m^3$) | Selectivity (%) |
|---|---|---|---|---|---|---|
| 1 | 25 | 500 | 0.048 | 27.04 | 0 | 0.00 |
| 2 | 37 | 500 | 0.034 | 49.00 | 0.020 | 62.04 |
| 3 | 50 | 500 | 0.011 | 82.98 | 0.040 | 73.27 |
| 4 | 62 | 500 | 0.005 | 92.40 | 0.045 | 74.03 |
| 5 | 85 | 500 | 0 | 100 | 0 | 0.00 |

### G.2.3 VARIATIONS OF ROTATIONAL SPEED AND FLOW RATE

**Conditions (1)**

Disc temperature: $85^0C$

Flow rate: 4 $cm^3/s$

## Table G.5. Variations of disc speed at $85^0C$ and 4 $cm^3/s$

| Run | Disc speed (rpm) | Conversion (%) | Selectivity (%) | Residence time (s) | Film thickness (mm) |
|---|---|---|---|---|---|
| 1 | 100 | 100 | 0.00 | 1.21376 | 0.10325 |
| 2 | 151 | 100 | 0.00 | 0.92218 | 0.07844 |
| 3 | 200 | 100 | 0.00 | 0.76462 | 0.06504 |
| 4 | 250 | 100 | 0.00 | 0.65893 | 0.05605 |
| 5 | 312 | 100 | 0.00 | 0.56845 | 0.04836 |
| 6 | 399 | 100 | 0.00 | 0.48248 | 0.04104 |
| 7 | 450 | 100 | 0.00 | 0.44530 | 0.03788 |
| 8 | 501 | 100 | 0.00 | 0.41455 | 0.03526 |
| 9 | 550 | 100 | 0.00 | 0.38954 | 0.03314 |
| 10 | 615 | 100 | 0.00 | 0.36159 | 0.03076 |
| 11 | 760 | 100 | 1.06 | 0.31399 | 0.02671 |
| 12 | 785 | 100 | 1.22 | 0.30729 | 0.02614 |
| 13 | 805 | 100 | 1.22 | 0.30218 | 0.02570 |
| 14 | 799 | 100 | 0.91 | 0.30369 | 0.02583 |
| 15 | 845 | 100 | 1.20 | 0.29257 | 0.02489 |
| 16 | 912 | 100 | 1.52 | 0.27806 | 0.02365 |
| 17 | 1000 | 100 | 2.01 | 0.26150 | 0.02224 |
| 18 | 1095 | 100 | 5.62 | 0.24614 | 0.02094 |
| 19 | 1105 | 100 | 6.54 | 0.24466 | 0.02081 |
| 20 | 1100 | 100 | 6.08 | 0.24540 | 0.02087 |
| 21 | 1195 | 100 | 10.64 | 0.23221 | 0.01975 |
| 22 | 1215 | 100 | 12.92 | 0.22966 | 0.01954 |
| 23 | 1203 | 100 | 12.16 | 0.23118 | 0.01967 |
| 24 | 1299 | 100 | 20.98 | 0.21965 | 0.01868 |
| 25 | 1315 | 100 | 21.28 | 0.21786 | 0.01853 |
| 26 | 1285 | 100 | 20.37 | 0.22124 | 0.01882 |
| 27 | 1350 | 100 | 24.02 | 0.21408 | 0.01821 |
| 28 | 1402 | 100 | 30.40 | 0.20875 | 0.01776 |
| 29 | 1398 | 100 | 32.68 | 0.20915 | 0.01779 |
| 30 | 1405 | 100 | 31.92 | 0.20846 | 0.01773 |
| 31 | 1510 | 100 | 38.00 | 0.19868 | 0.01690 |
| 32 | 1500 | 100 | 39.52 | 0.19956 | 0.01698 |

**Conditions (2)**

Disc temperature: $85^0$C

Flow rate: 5 $cm^3/s$

**Table G.6. Variations of disc speed at $85^0$C and 5 $cm^3/s$**

| Run | Disc speed (rpm) | Conversion (%) | Selectivity (%) | Residence time (s) | Film thickness (mm) |
|---|---|---|---|---|---|
| 1 | 950 | 93.00 | 31.92 | 0.233190 | 0.024796 |
| 2 | 799 | 95.44 | 21.28 | 0.261714 | 0.027829 |
| 3 | 650 | 100 | 10.64 | 0.300319 | 0.031934 |
| 4 | 500 | 100 | 3.04 | 0.357721 | 0.038037 |
| 5 | 250 | 100 | 1.52 | 0.567847 | 0.060381 |
| 6 | 1100 | 91.5 | 39.52 | 0.211477 | 0.022487 |
| 7 | 1000 | 92.00 | 36.48 | 0.225350 | 0.023962 |
| 8 | 1200 | 91.00 | 41.04 | 0.199559 | 0.021220 |
| 9 | 1200 | 91.00 | 38.00 | 0.199559 | 0.021220 |
| 10 | 1400 | 89.80 | 47.12 | 0.180069 | 0.019147 |

**Conditions (3)**

Disc temperature: $85^0$C

Flow rate: 6$cm^3/s$

**Table G.7. Variations of disc speed at $85^0$C and 6 $cm^3/s$**

| Run | Disc speed (rpm) | Conversion (%) | Selectivity (%) | Residence time (s) | Film thickness (mm) |
|---|---|---|---|---|---|
| 1 | 800 | 89.36 | 38.00 | 0.231567 | 0.029548 |
| 2 | 901 | 86.30 | 50.16 | 0.213921 | 0.027296 |
| 3 | 750 | 95.40 | 36.48 | 0.241748 | 0.030847 |
| 4 | 611 | 100.0 | 25.84 | 0.277147 | 0.035364 |
| 5 | 552 | 100.0 | 21.28 | 0.296559 | 0.037841 |
| 6 | 300 | 100.0 | 7.60 | 0.445304 | 0.056820 |
| 7 | 800 | 89.40 | 39.52 | 0.231567 | 0.029548 |
| 8 | 1000 | 84.80 | 53.20 | 0.199559 | 0.025463 |
| 9 | 1200 | 81.80 | 57.76 | 0.176719 | 0.022549 |
| 10 | 1350 | 78.70 | 59.28 | 0.163373 | 0.020846 |
| 11 | 1500 | 77.20 | 62.32 | 0.152292 | 0.019432 |

**Conditions (4)**

Disc temperature: 85$^0$C

Disc speed: 800 rpm

**Table G.8. Variations of flow rates at 85$^0$C and 800 rpm**

| Run | Flow rate ($cm^3/s$) | Conversion (%) | Selectivity (%) | Residence time (s) | Film thickness (mm) |
|---|---|---|---|---|---|
| 1 | 3 | 100 | 0 | 0.367590 | 0.023452 |
| 2 | 4.5 | 100 | 12.16 | 0.280524 | 0.026846 |

## G.2.4 CASCADE SIMULATION

**Table G.9. Data from three passes on the disc (Flow rate 4 $cm^3/s$)**

| Run | Disc Temperature ($^0$C) | Disc Speed (rpm) | Concentration A ($kmol/m^3$) | Conversion (%) | Concentration B ($kmol/m^3$) | Selectivity (%) |
|---|---|---|---|---|---|---|
| 1 | 25 | 500 | 0.048 | 0.2704 | 27.04 | 0 |
| 2 | 25 | 500 | 0.040 | 0.3920 | 39.00 | 50 |
| 3 | 25 | 500 | 0.031 | 0.5212 | 52.00 | 76 |

## G.3 CATALYST 2: 0.01 mmol/g $Zn(OTf)_2$ SUPPORTED ON K100

## G.3.1 BATCH REACTION DATA

**Table G.10. Selectivity and conversion data for batch reaction (85$^0$C)**

| Time (min) | Concentration A ($kmol/m^3$) | Conversion (%) | Concentration B ($kmol/m^3$) | Selectivity (%) |
|---|---|---|---|---|
| 0 | 0.066 | 0 | 0 | 0 |
| 2.5 | 0.060 | 8.80 | 0.002 | 20.43 |
| 5 | 0.056 | 14.88 | 0.007 | 33.67 |
| 7.5 | 0.045 | 31.60 | 0.020 | 55.88 |
| 10 | 0.030 | 54.40 | 0.030 | 70.11 |
| 12.5 | 0.023 | 65.04 | 0.039 | 76.79 |
| 15 | 0.015 | 77.20 | 0.045 | 79.24 |
| 17.5 | 0.009 | 86.32 | 0.045 | 71.67 |
| 20 | 0.003 | 95.44 | 0.043 | 65.36 |
| 22.5 | 0 | 100 | 0.038 | 57.76 |
| 25 | 0 | 100 | 0.030 | 45.60 |
| 27.5 | 0 | 100 | 0.028 | 42.56 |
| 30 | 0 | 100 | 0.020 | 30.40 |

## G.3.2 SDR DATA

**Table G.11. SDR runs data for catalyst activity study (flow rate 4 $cm^3/s$)**

| Run | Disc Temperature (°C) | Disc Speed (rpm) | Concentration A ($kmol/m^3$) | Conversion (%) | Concentration B ($kmol/m^3$) | Selectivity (%) |
|---|---|---|---|---|---|---|
| 1 | 45 | 500 | 0.040 | 39.20 | 0.0180 | 69.80 |
| 2 | 45 | 500 | 0.038 | 42.24 | 0.0190 | 68.37 |
| 3 | 45 | 500 | 0.039 | 40.72 | 0.0182 | 67.94 |
| 4 | 45 | 500 | 0.039 | 40.72 | 0.0180 | 67.19 |
| 5 | 45 | 500 | 0.040 | 39.20 | 0.0180 | 69.80 |
| 6 | 45 | 500 | 0.038 | 42.24 | 0.0190 | 68.37 |
| 7 | 45 | 500 | 0.038 | 42.24 | 0.0190 | 68.37 |
| 8 | 45 | 500 | 0.040 | 39.20 | 0.0180 | 69.80 |
| 9 | 45 | 500 | 0.040 | 39.20 | 0.0182 | 70.57 |
| 10 | 45 | 500 | 0.040 | 39.20 | 0.0182 | 70.57 |
| 11 | 45 | 500 | 0.041 | 37.68 | 0.0182 | 73.42 |
| 12 | 45 | 500 | 0.040 | 39.20 | 0.0180 | 69.80 |
| 13 | 45 | 500 | 0.039 | 40.72 | 0.0191 | 71.30 |
| 14 | 45 | 500 | 0.040 | 39.20 | 0.0182 | 70.57 |
| 15 | 45 | 500 | 0.040 | 39.20 | 0.0180 | 69.80 |

**Table G.12. SDR runs at different temperatures (flow rate 4 $cm^3/s$)**

| Run | Disc Temperature (°C) | Disc Speed (rpm) | Concentration A ($kmol/m^3$) | Conversion (%) | Concentration B ($kmol/m^3$) | Selectivity (%) |
|---|---|---|---|---|---|---|
| 1 | 25 | 500 | 0.056 | 14.88 | 0.007 | 71.51 |
| 2 | 45 | 500 | 0.04 | 39.20 | 0.018 | 69.80 |
| 3 | 55 | 500 | 0.03 | 54.40 | 0.025 | 69.85 |
| 4 | 65 | 500 | 0.025 | 62.00 | 0.03 | 73.55 |
| 5 | 85 | 500 | 0.015 | 77.20 | 0.033 | 64.97 |

## G.3.3 VARIATIONS OF ROTATIONAL SPEED AND FLOW RATE

**Conditions (1)**

Disc temperature: $85^0$C

Flow rate: 4 $cm^3/s$

**Table G.13. Variations of disc speed at $85^0$C and 4 $cm^3/s$**

| Run | Disc speed (rpm) | Conversion (%) | Selectivity (%) | Residence time (s) | Film thickness (mm) |
|---|---|---|---|---|---|
| 1 | 200 | 90.88 | 50.18 | 0.764619 | 0.065043 |
| 2 | 251 | 86.32 | 54.59 | 0.657177 | 0.055903 |
| 3 | 398 | 84.8 | 57.36 | 0.483292 | 0.041112 |
| 4 | 502 | 77.20 | 64.97 | 0.413996 | 0.035217 |
| 5 | 550 | 74.16 | 65.59 | 0.389544 | 0.033137 |
| 6 | 610 | 71.12 | 68.39 | 0.363562 | 0.030927 |
| 7 | 752 | 68.08 | 71.45 | 0.316218 | 0.026899 |
| 8 | 801 | 65.04 | 74.78 | 0.303187 | 0.025791 |
| 9 | 798 | 62.00 | 78.45 | 0.303946 | 0.025855 |
| 10 | 849 | 58.96 | 82.50 | 0.291649 | 0.024809 |
| 11 | 1000 | 55.92 | 81.55 | 0.261496 | 0.022244 |
| 12 | 1099 | 54.40 | 75.44 | 0.245546 | 0.020888 |
| 13 | 1102 | 54.40 | 72.65 | 0.245100 | 0.020850 |
| 14 | 1200 | 51.36 | 73.99 | 0.231567 | 0.019698 |
| 15 | 1290 | 49.84 | 70.14 | 0.220668 | 0.018771 |
| 16 | 1350 | 48.32 | 62.91 | 0.214080 | 0.018211 |
| 17 | 1401 | 46.80 | 64.96 | 0.208852 | 0.017766 |
| 18 | 1500 | 43.76 | 69.47 | 0.199559 | 0.016976 |

**Conditions (2)**

Disc temperature: $85^0$C

Flow rate: 5 $cm^3/s$

**Table G.14. Variations of disc speed at $85^0$C and 5 $cm^3/s$**

| Run | Disc speed (rpm) | Conversion (%) | Selectivity (%) | Residence time (s) | Film thickness (mm) |
|---|---|---|---|---|---|
| 1 | 250 | 77.20 | 59.07 | 0.567847 | 0.060381 |
| 2 | 500 | 65.04 | 63.10 | 0.357721 | 0.038037 |
| 3 | 650 | 63.52 | 59.82 | 0.300319 | 0.031934 |
| 4 | 800 | 54.40 | 55.88 | 0.261496 | 0.027805 |
| 5 | 950 | 45.28 | 60.42 | 0.233190 | 0.024796 |
| 6 | 1000 | 42.24 | 53.98 | 0.225350 | 0.023962 |
| 7 | 1100 | 39.20 | 46.53 | 0.211477 | 0.022487 |
| 8 | 1200 | 36.16 | 50.44 | 0.199559 | 0.021220 |
| 9 | 1200 | 34.64 | 52.66 | 0.199559 | 0.021220 |
| 10 | 1400 | 33.12 | 55.07 | 0.180069 | 0.019147 |

**Conditions (3)**

Disc temperature: $85^0$C

Flow rate: 6 $cm^3/s$

**Table G.15. Variations of disc speed at $85^0$C and 6 $cm^3/s$**

| Run | Disc speed (rpm) | Conversion (%) | Selectivity (%) | Residence time (s) | Film thickness (mm) |
|---|---|---|---|---|---|
| 1 | 302 | 63.52 | 67.00 | 0.443336 | 0.056569 |
| 2 | 551 | 58.96 | 69.61 | 0.296918 | 0.037886 |
| 3 | 600 | 54.40 | 67.06 | 0.280524 | 0.035795 |
| 4 | 749 | 49.84 | 64.04 | 0.241963 | 0.030874 |
| 5 | 801 | 46.80 | 61.71 | 0.231375 | 0.029523 |
| 6 | 800 | 45.28 | 60.42 | 0.231567 | 0.029548 |
| 7 | 899 | 42.24 | 57.58 | 0.214239 | 0.027337 |
| 8 | 1000 | 39.20 | 54.29 | 0.199559 | 0.025463 |
| 9 | 1201 | 36.16 | 50.44 | 0.176621 | 0.022537 |
| 10 | 1350 | 33.12 | 45.89 | 0.163373 | 0.020846 |
| 11 | 1499 | 30.08 | 40.43 | 0.152360 | 0.019441 |

**Conditions (4)**

Disc temperature: $85^0$C

Disc speed: 800 rpm

**Table G.16. Variations of flow rates at $85^0$C and 800 rpm**

| Run | Flow rate ($cm^3/s$) | Conversion (%) | Selectivity (%) | Residence time (s) | Film thickness (mm) |
|---|---|---|---|---|---|
| 1 | 3 | 69.60 | 65.52 | 0.367590 | 0.023452 |
| 2 | 4.5 | 62.00 | 61.29 | 0.280524 | 0.026846 |

## G.3.4 CASCADE SIMULATION

**Table G.17. Data from three passes on the disc (Flow rate 4 $cm^3/s$)**

| Run | Disc Temperature ($^0$C) | Disc Speed (rpm) | Concentration A ($kmol/m^3$) | Conversion (%) | Concentration B ($kmol/m^3$) | Selectivity (%) |
|---|---|---|---|---|---|---|
| 1 | 25 | 500 | 0.056 | 14.88 | 0.007 | 71.51 |
| 2 | 25 | 500 | 0.044 | 33.12 | 0.017 | 78.02 |
| 3 | 25 | 500 | 0.030 | 54.40 | 0.029 | 81.03 |

## G.4 CATALYST 3: 0.05 mmol/g $Zn(OTf)_2$ SUPPORTED ON $HMS_{24}$

### G.4.1 BATCH REACTION DATA

**Table G.18. Selectivity and conversion data for batch reaction (45$^0$C)**

| Time (min) | Concentration A (kmol/m$^3$) | Conversion (%) | Concentration B (kmol/m$^3$) | Selectivity (%) |
|---|---|---|---|---|
| 0 | 0.066 | 0 | 0.040 | 39.20 |
| 0.5 | 0.061 | 7.280 | 0.030 | 54.40 |
| 1 | 0.058 | 11.84 | 0.027 | 58.96 |
| 1.5 | 0.054 | 17.92 | 0.025 | 62.00 |
| 2 | 0.05 | 24.00 | 0.023 | 65.04 |
| 2.5 | 0.047 | 28.56 | 0.019 | 71.12 |
| 3 | 0.042 | 36.16 | 0.015 | 77.20 |
| 3.5 | 0.038 | 42.24 | 0.013 | 80.24 |
| 4 | 0.032 | 51.36 | 0.010 | 84.80 |
| 4.5 | 0.029 | 55.92 | 0.012 | 81.76 |
| 5 | 0.026 | 60.48 | 0.017 | 74.16 |
| 5.5 | 0.021 | 68.08 | 0.020 | 69.60 |
| 6 | 0.017 | 74.16 | 0.023 | 65.04 |
| 6.5 | 0.012 | 81.76 | 0.026 | 60.48 |
| 7 | 0.007 | 89.36 | 0.029 | 55.92 |
| 7.5 | 0.001 | 98.48 | 0.034 | 48.32 |
| 8 | 0.0001 | 99.85 | 0.030 | 54.40 |
| 8.5 | 0 | 100 | 0.035 | 46.80 |
| 9 | 0 | 100 | 0.040 | 39.20 |

### G.4.2 SDR DATA

**Table G.19. SDR runs data for catalyst activity study (flow rate 4 cm$^3$/s)**

| Run | Disc Temperature ($^o$C) | Disc Speed (rpm) | Concentration A (kmol/m$^3$) | Conversion (%) | Concentration B (kmol/m$^3$) | Selectivity (%) |
|---|---|---|---|---|---|---|
| 1 | 25 | 500 | 0.020 | 69.60 | 0.0300 | 65.52 |
| 2 | 25 | 500 | 0.021 | 68.08 | 0.0301 | 67.20 |
| 3 | 25 | 500 | 0.020 | 69.75 | 0.0302 | 65.81 |
| 4 | 25 | 500 | 0.020 | 69.60 | 0.0309 | 67.48 |
| 5 | 25 | 500 | 0.021 | 68.08 | 0.0290 | 64.75 |
| 6 | 25 | 500 | 0.020 | 69.60 | 0.0300 | 65.52 |
| 7 | 25 | 500 | 0.020 | 69.90 | 0.0300 | 65.23 |
| 8 | 25 | 500 | 0.020 | 69.75 | 0.0300 | 65.37 |
| 9 | 25 | 500 | 0.020 | 69.60 | 0.0300 | 65.52 |
| 10 | 25 | 500 | 0.021 | 68.08 | 0.0300 | 66.98 |
| 11 | 25 | 500 | 0.020 | 69.60 | 0.0290 | 63.33 |
| 12 | 25 | 500 | 0.020 | 69.75 | 0.0300 | 65.37 |
| 13 | 25 | 500 | 0.020 | 69.60 | 0.0300 | 65.52 |
| 14 | 25 | 500 | 0.021 | 68.08 | 0.0300 | 66.98 |
| 15 | 25 | 500 | 0.020 | 69.60 | 0.0300 | 65.52 |

**Table G.20. SDR runs at different temperatures (flow rate 4 $cm^3/s$)**

| Run | Disc Temperature ($^oC$) | Disc Speed (rpm) | Concentration A ($kmol/m^3$) | Conversion (%) | Concentration B ($kmol/m^3$) | Selectivity (%) |
|---|---|---|---|---|---|---|
| 1 | 25 | 500 | 0.020 | 69.60 | 0.03 | 65.52 |
| 2 | 35 | 500 | 0.012 | 81.76 | 0.03 | 55.77 |
| 3 | 45 | 500 | 0 | 100.00 | 0.014 | 21.28 |
| 4 | 55 | 500 | 0.015 | 77.20 | 0.03 | 59.07 |
| 5 | 85 | 500 | 0.026 | 60.48 | 0.03 | 75.40 |

## G.4.3 VARIATIONS OF ROTATIONAL SPEED AND FLOW RATE

**Conditions (1)**

Disc temperature: $45^0C$

Flow rate: 4 $cm^3/s$

**Table G.21. Variations of disc speed at $45^0C$ and 4 $cm^3/s$**

| Run | Disc speed (rpm) | Conversion (%) | Selectivity (%) | Residence time (s) | Film thickness (mm) |
|---|---|---|---|---|---|
| 1 | 100 | 100 | 15.00 | 1.21376 | 0.10325 |
| 2 | 151 | 100 | 17.00 | 0.92218 | 0.07845 |
| 3 | 200 | 100 | 19.00 | 0.76462 | 0.06504 |
| 4 | 250 | 100 | 20.00 | 0.65893 | 0.05605 |
| 5 | 312 | 100 | 20.00 | 0.56845 | 0.04836 |
| 6 | 399 | 100 | 20.00 | 0.48248 | 0.04104 |
| 7 | 450 | 100 | 20.00 | 0.44530 | 0.03788 |
| 8 | 501 | 100 | 20.00 | 0.41455 | 0.03526 |
| 9 | 550 | 100 | 20.00 | 0.38954 | 0.03314 |
| 10 | 615 | 100 | 20.00 | 0.36159 | 0.03076 |
| 11 | 760 | 100 | 20.00 | 0.31399 | 0.02671 |
| 12 | 785 | 100 | 22.00 | 0.30729 | 0.02614 |
| 13 | 805 | 100 | 23.00 | 0.30218 | 0.02571 |
| 14 | 799 | 100 | 25.00 | 0.30369 | 0.02583 |
| 15 | 845 | 100 | 26.00 | 0.29257 | 0.02489 |
| 16 | 912 | 100 | 26.00 | 0.27806 | 0.02365 |
| 17 | 1000 | 100 | 27.00 | 0.26150 | 0.02224 |
| 18 | 1095 | 100 | 27.00 | 0.24614 | 0.02094 |
| 19 | 1105 | 100 | 30.00 | 0.24466 | 0.02081 |
| 20 | 1100 | 100 | 35.00 | 0.24540 | 0.02087 |
| 21 | 1195 | 100 | 35.00 | 0.23221 | 0.01975 |
| 22 | 1215 | 100 | 34.00 | 0.22966 | 0.01954 |
| 23 | 1203 | 100 | 36.00 | 0.23118 | 0.01967 |
| 24 | 1299 | 100 | 35.00 | 0.21965 | 0.01868 |
| 25 | 1315 | 100 | 38.00 | 0.21786 | 0.01853 |
| 26 | 1285 | 100 | 40.00 | 0.22124 | 0.01882 |
| 27 | 1350 | 100 | 44.00 | 0.21408 | 0.01821 |
| 28 | 1402 | 100 | 45.00 | 0.20875 | 0.01776 |
| 29 | 1398 | 100 | 47.00 | 0.20915 | 0.01779 |
| 30 | 1405 | 100 | 48.00 | 0.20846 | 0.01773 |
| 31 | 1510 | 100 | 50.00 | 0.19868 | 0.01690 |
| 32 | 1500 | 100 | 52.00 | 0.19956 | 0.01698 |

**Conditions (2)**

Disc temperature: 45$^0$C

Flow rate: 5 cm$^3$/s

**Table G.22. Variations of disc speed at 45$^0$C and 5 cm$^3$/s**

| Run | Disc speed (rpm) | Conversion (%) | Selectivity (%) | Residence time (s) | Film thickness (mm) |
|---|---|---|---|---|---|
| 1 | 250 | 100 | 20.00 | 0.23319 | 0.02480 |
| 2 | 500 | 100 | 25.00 | 0.26171 | 0.02783 |
| 3 | 650 | 100 | 30.00 | 0.30032 | 0.03193 |
| 4 | 799 | 98.48 | 35.00 | 0.35772 | 0.03804 |
| 5 | 950 | 100 | 45.00 | 0.56785 | 0.06038 |
| 6 | 1000 | 99.09 | 52.00 | 0.21148 | 0.02249 |
| 7 | 1100 | 98.48 | 50.00 | 0.22535 | 0.02396 |
| 8 | 1200 | 93.92 | 55.00 | 0.19956 | 0.02122 |
| 9 | 1200 | 93.92 | 54.00 | 0.19956 | 0.02122 |
| 10 | 1400 | 92.40 | 63.00 | 0.18007 | 0.01915 |

**Conditions (3)**

Disc temperature: 45$^0$C

Flow rate: 6 cm$^3$/s

**Table G.23. Variations of disc speed at 45$^0$C and 6 cm$^3$/s**

| Run | Disc speed (rpm) | Conversion (%) | Selectivity (%) | Residence time (s) | Film thickness (mm) |
|---|---|---|---|---|---|
| 1 | 900 | 97.72 | 65 | 0.21392 | 0.02730 |
| 2 | 750 | 100 | 46 | 0.24175 | 0.03085 |
| 3 | 605 | 100 | 40 | 0.27715 | 0.03536 |
| 4 | 551 | 100 | 38 | 0.29656 | 0.03784 |
| 5 | 301 | 100 | 28 | 0.44530 | 0.05682 |
| 6 | 800 | 98.48 | 50 | 0.23157 | 0.02955 |
| 7 | 1001 | 93.92 | 68 | 0.19956 | 0.02546 |
| 8 | 1199 | 90.88 | 70 | 0.17672 | 0.02255 |
| 9 | 1350 | 87.84 | 72 | 0.16337 | 0.02085 |
| 10 | 1500 | 84.8 | 75 | 0.15229 | 0.01943 |
| 11 | 900 | 97.72 | 65 | 0.21392 | 0.02730 |

**Conditions (4)**

Disc temperature: 45$^0$C

Disc speed: 800 rpm

**Table G.24. Variations of flow rates at 45$^0$C and 800 rpm**

| Run | Flow rate ($cm^3/s$) | Conversion (%) | Selectivity (%) | Residence time (s) | Film thickness (mm) |
|---|---|---|---|---|---|
| 1 | 3 | 100 | 20 | 1.5326934 | 0.036782 |
| 2 | 4.5 | 100 | 29 | 1.169664 | 0.0421049 |

## G.4.4 CASCADE SIMULATION

**Table G.25. Data from three passes on the disc (Flow rate 4 $cm^3/s$)**

| Run | Disc Temperature ($^0$C) | Disc Speed (rpm) | Concentration A ($kmol/m^3$) | Conversion (%) | Concentration B ($kmol/m^3$) | Selectivity (%) |
|---|---|---|---|---|---|---|
| 1 | 85 | 500 | 0.026 | 60 | 0.03 | 75 |
| 2 | 85 | 500 | 0.012 | 82 | 0.045 | 84 |
| 3 | 85 | 500 | 0 | 100 | 0.04 | 61 |

# APPENDIX H

## KINETIC DATA

### H.1 CATALYST 1

#### H.1.1 BATCH REACTION AT 25$^0$C

**Table H.1. Data for Catalyst 1 at 25$^0$C**

| Time (s) | Concentration (mol/dm$^3$) | Conversion | Conversion (%) | $C_A$ (mol/dm$^3$) | $\ln(C_A/C_{A0})$ | $1/C_A$ (dm$^3$/mol) |
|---|---|---|---|---|---|---|
| 0 | 0.066 | 0 | 0 | 0.0667 | 0 | 15.200 |
| 60 | 0.057 | 0.1336 | 13.36 | 0.0570 | -0.1434 | 17.545 |
| 120 | 0.0500 | 0.2476 | 24.76 | 0.0495 | -0.2845 | 20.202 |
| 180 | 0.0405 | 0.3844 | 38.44 | 0.0405 | -0.4852 | 24.691 |
| 240 | 0.0330 | 0.4984 | 49.84 | 0.0330 | -0.6900 | 30.303 |
| 300 | 0.0245 | 0.6276 | 62.76 | 0.0245 | -0.9878 | 40.816 |
| 360 | 0.0175 | 0.7340 | 73.40 | 0.0175 | -1.3242 | 57.143 |
| 420 | 0.0125 | 0.8100 | 81.00 | 0.0125 | -1.6607 | 80.000 |
| 480 | 0.0079 | 0.8799 | 87.99 | 0.0079 | -2.1196 | 126.58 |
| 540 | 0.0030 | 0.9544 | 95.44 | 0.0030 | -3.0878 | 333.33 |
| 600 | 0 | 1 | 100 | 0 | -34.120 | 1E+16 |
| 660 | 0 | 1 | 100 | 0 | -34.120 | 1E+16 |

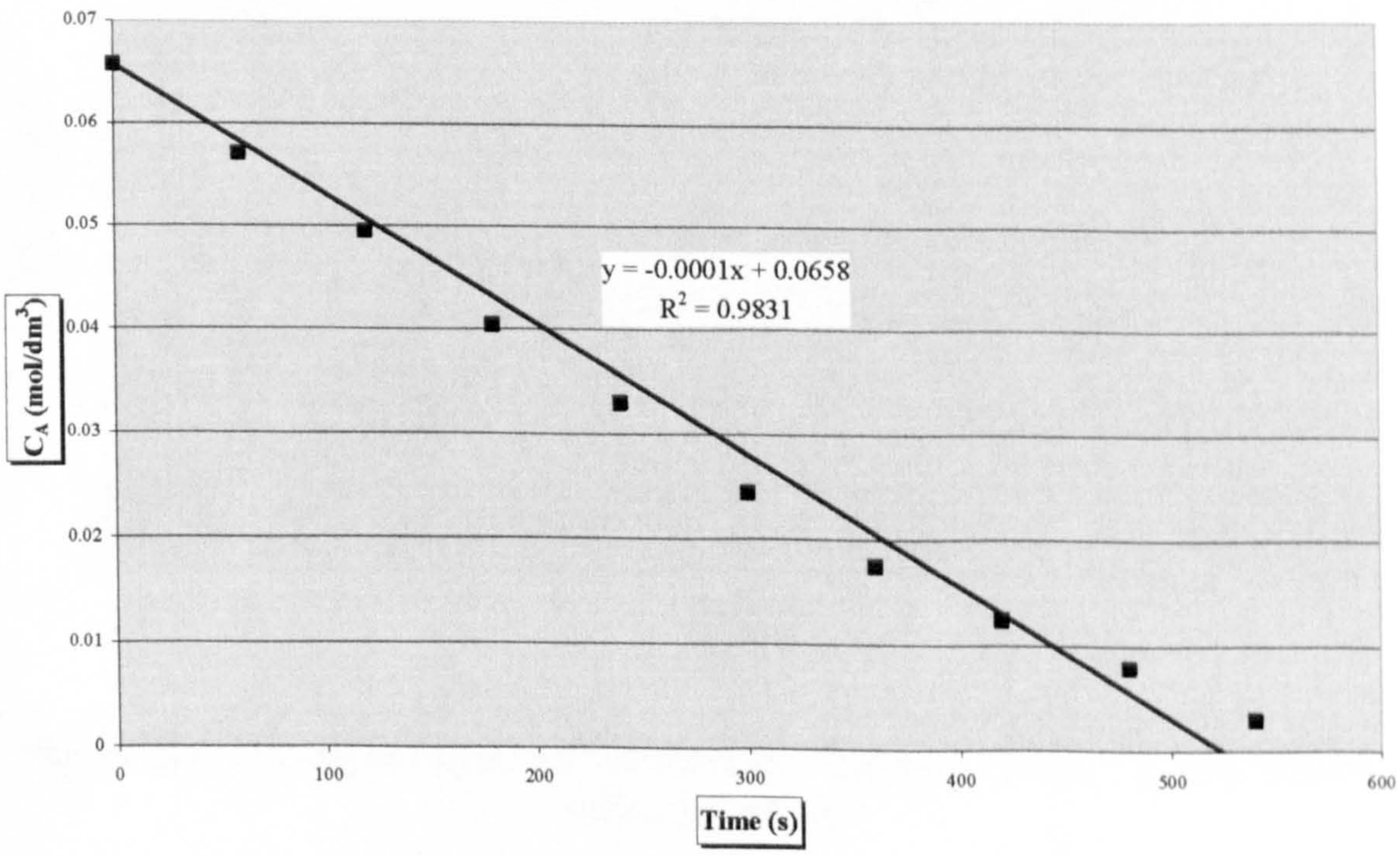


**Figure H.1. Fitting of experimental data for Catalyst 1 at 25$^0$C into a zero order equation**

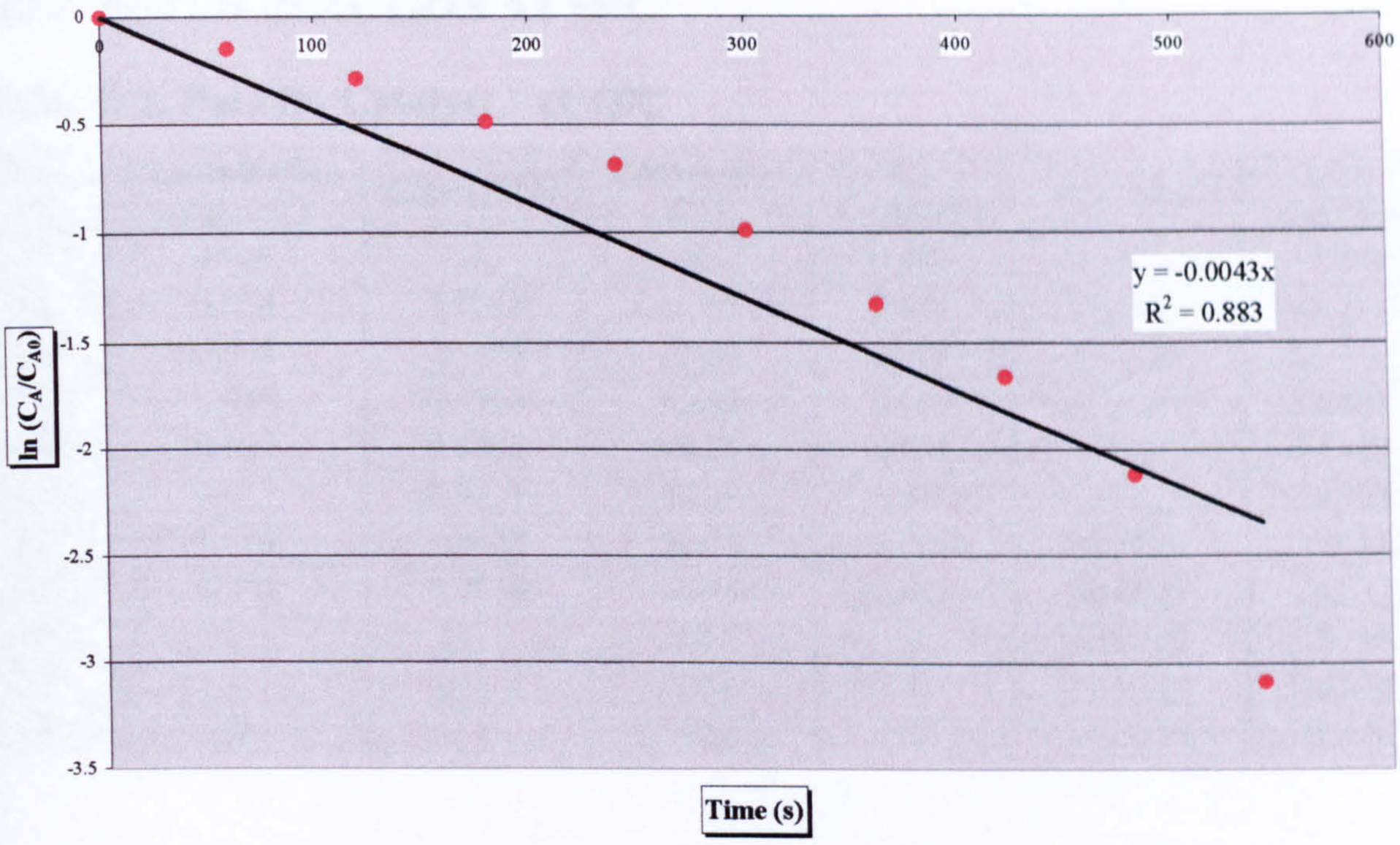


**Figure H.2. Fitting of experimental data for Catalyst 1 at 25$^0$C into a first order equation**

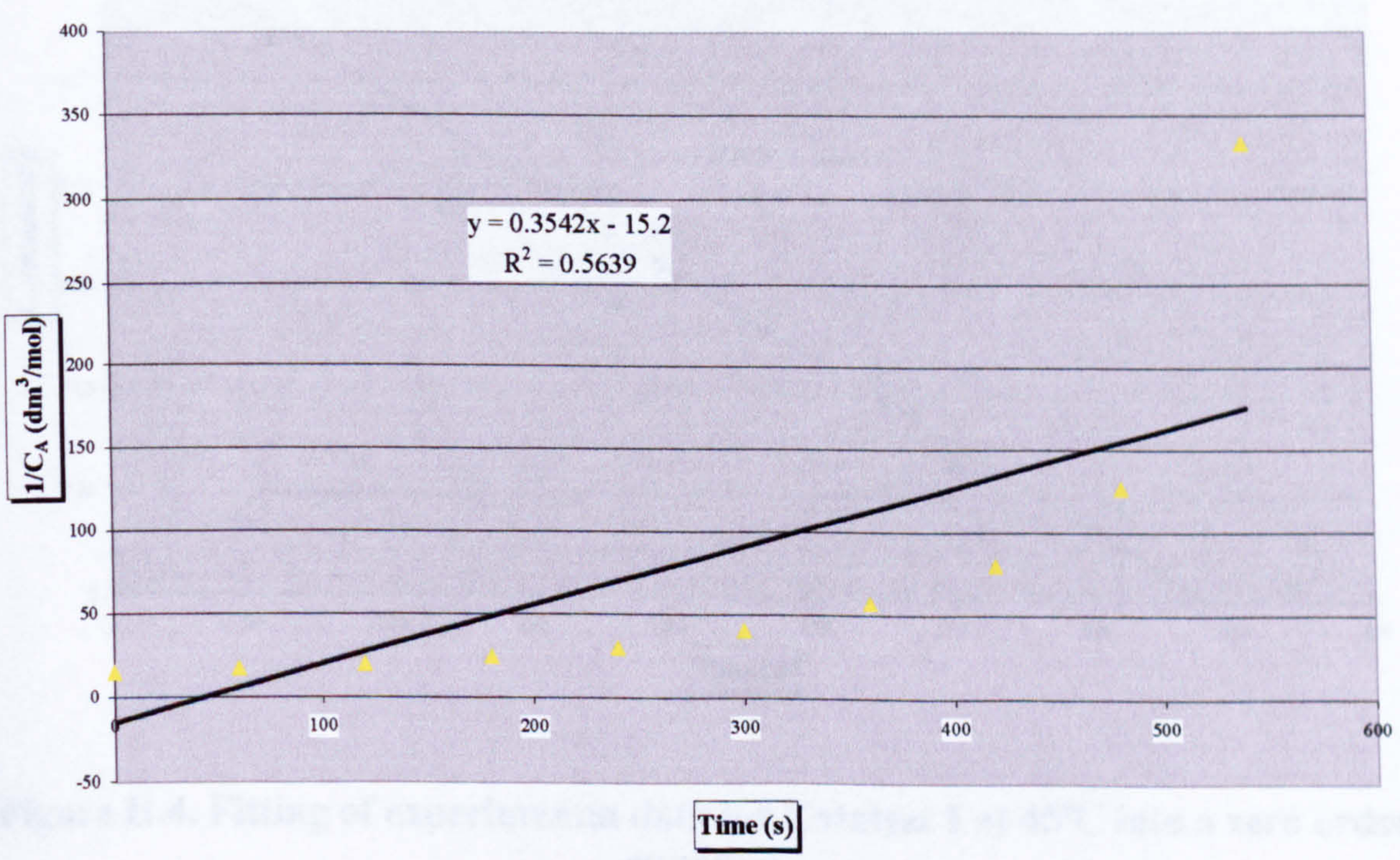


**Figure H.3. Fitting of experimental data for Catalyst 1 at 25$^0$C into a second order equation**

## H.1.2 BATCH REACTION AT 45$^0$C

**Table H.2. Data for Catalyst 1 at 45$^0$C**

| Time (s) | Concentration (mol/dm$^3$) | Conversion | Conversion (%) | $C_A$ (mol/dm$^3$) | ln($C_A/C_{A0}$) | 1/$C_A$ (dm$^3$/mol) |
|---|---|---|---|---|---|---|
| 0 | 0.066 | 0 | 0 | 0.066 | 0 | 15.200 |
| 60 | 0.054 | 0.1792 | 17.92 | 0.054 | -0.1975 | 18.518 |
| 120 | 0.038 | 0.4224 | 42.24 | 0.038 | -0.5489 | 26.316 |
| 180 | 0.029 | 0.5592 | 55.92 | 0.029 | -0.8191 | 34.483 |
| 240 | 0.021 | 0.6808 | 68.08 | 0.021 | -1.1419 | 47.619 |
| 300 | 0.013 | 0.8024 | 80.24 | 0.013 | -1.6215 | 76.923 |
| 360 | 0.009 | 0.8632 | 86.32 | 0.009 | -1.9892 | 111.11 |
| 420 | 0.001 | 0.9818 | 98.18 | 0.001 | -4.0041 | 833.33 |
| 480 | 0 | 1 | 100 | 0 | -34.120 | 1E+16 |
| 540 | 0 | 1 | 100 | 0 | -34.120 | 1E+16 |
| 600 | 0 | 1 | 100 | 0 | -34.120 | 1E+16 |

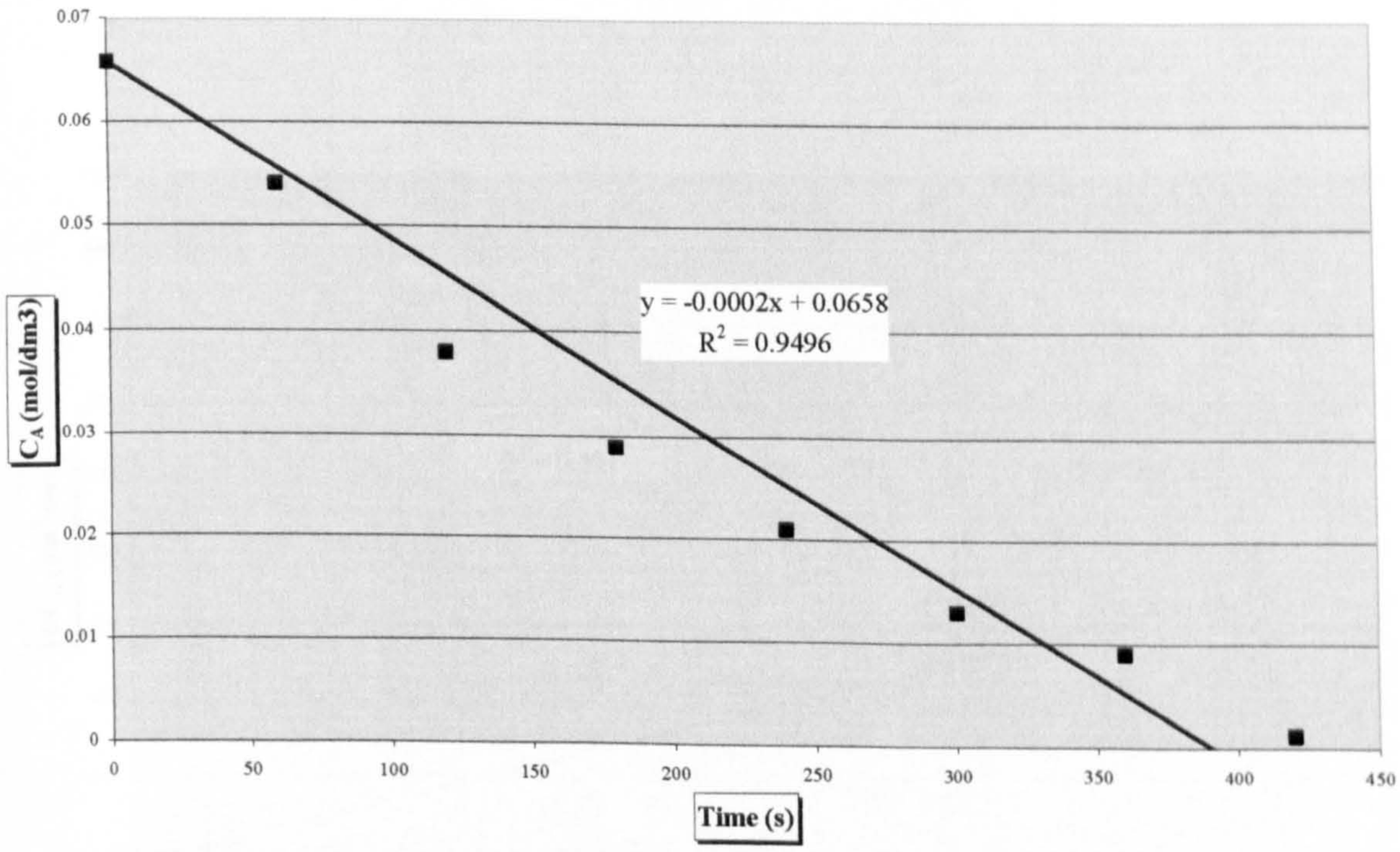


**Figure H.4. Fitting of experimental data for Catalyst 1 at 45$^0$C into a zero order equation**

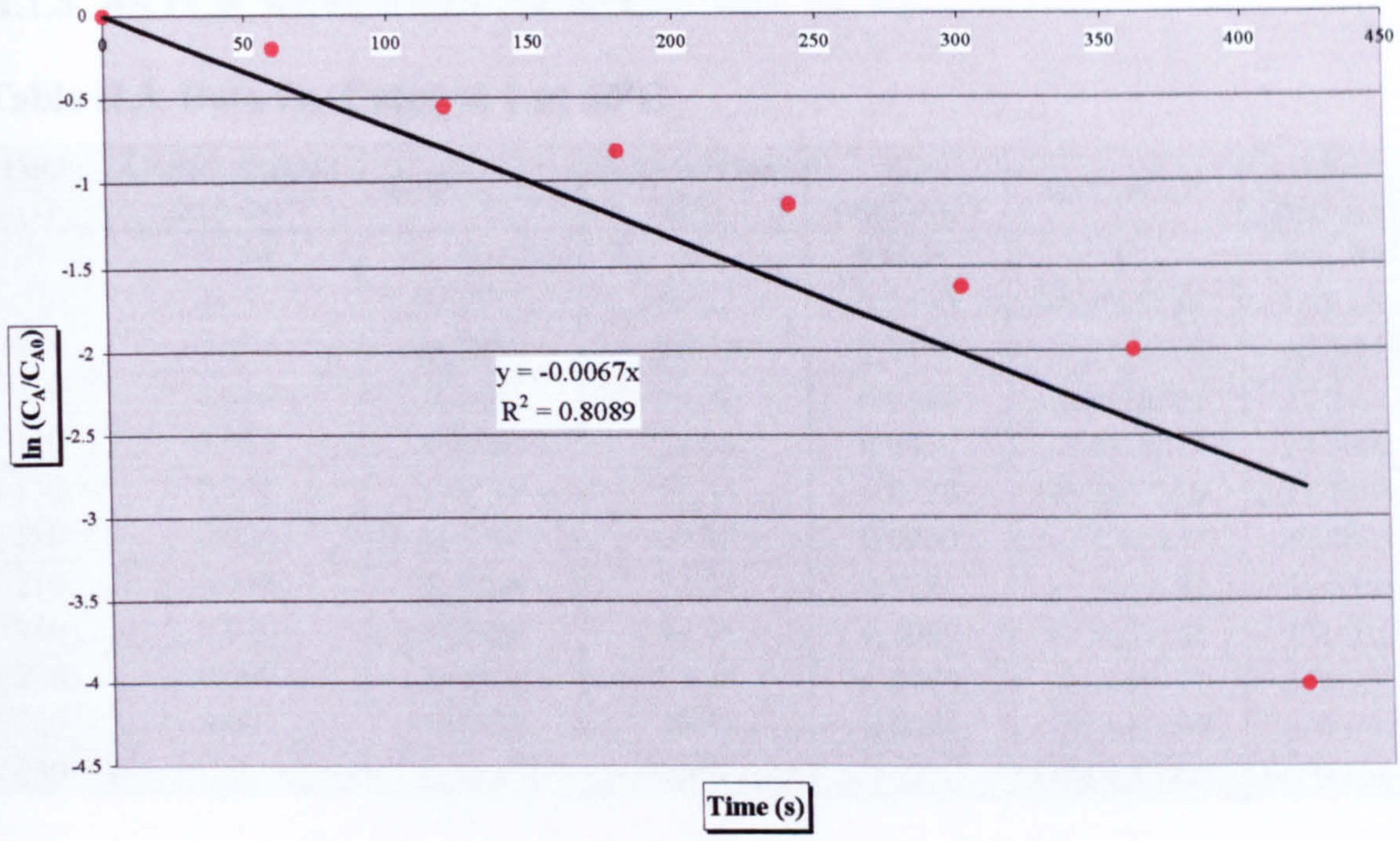


**Figure H.5. Fitting of experimental data for Catalyst 1 at 45$^0$C into a first order equation**

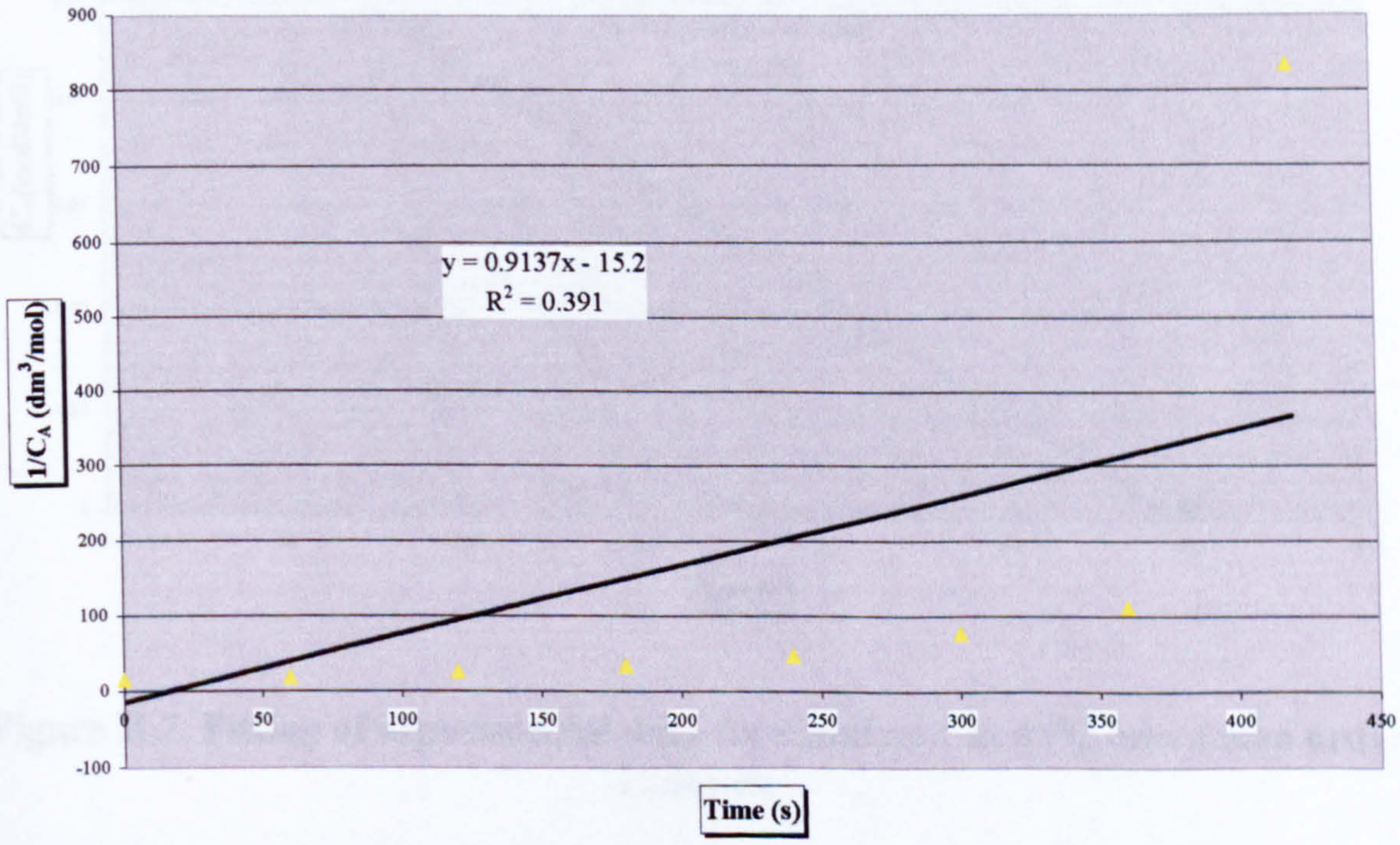


**Figure H.6. Fitting of experimental data for Catalyst 1 at 45$^0$C into a second order equation**

## H.1.3 BATCH REACTION AT 65$^0$C

**Table H.3. Data for Catalyst 1 at 65$^0$C**

| Time (s) | Concentration (mol/dm$^3$) | Conversion | Conversion (%) | $C_A$ (mol/dm$^3$) | ln($C_A/C_{A0}$) | 1/$C_A$ (dm$^3$/mol) |
|---|---|---|---|---|---|---|
| 0 | 0.066 | 0 | 0 | 0.0660 | 0 | 15.200 |
| 30 | 0.059 | 0.1032 | 10.32 | 0.0590 | -0.1089224 | 16.9491 |
| 60 | 0.050 | 0.2400 | 24.00 | 0.0500 | -0.2744368 | 20.0000 |
| 90 | 0.046 | 0.3008 | 30.08 | 0.0460 | -0.3578185 | 21.7391 |
| 120 | 0.041 | 0.3768 | 37.68 | 0.0410 | -0.4728878 | 24.3902 |
| 150 | 0.032 | 0.5136 | 51.36 | 0.0320 | -0.7207239 | 31.2500 |
| 180 | 0.026 | 0.6048 | 60.48 | 0.0260 | -0.9283633 | 38.4615 |
| 210 | 0.018 | 0.7264 | 72.64 | 0.0180 | -1.2960881 | 55.5556 |
| 240 | 0.010 | 0.8495 | 84.95 | 0.0099 | -1.8939251 | 101.010 |
| 270 | 0.007 | 0.8936 | 89.36 | 0.0070 | -2.2405497 | 142.857 |
| 300 | 0.001 | 0.9832 | 98.33 | 0.0011 | -4.0911497 | 909.090 |
| 330 | 0 | 1 | 100 | 0 | -34.120066 | 1E+16 |

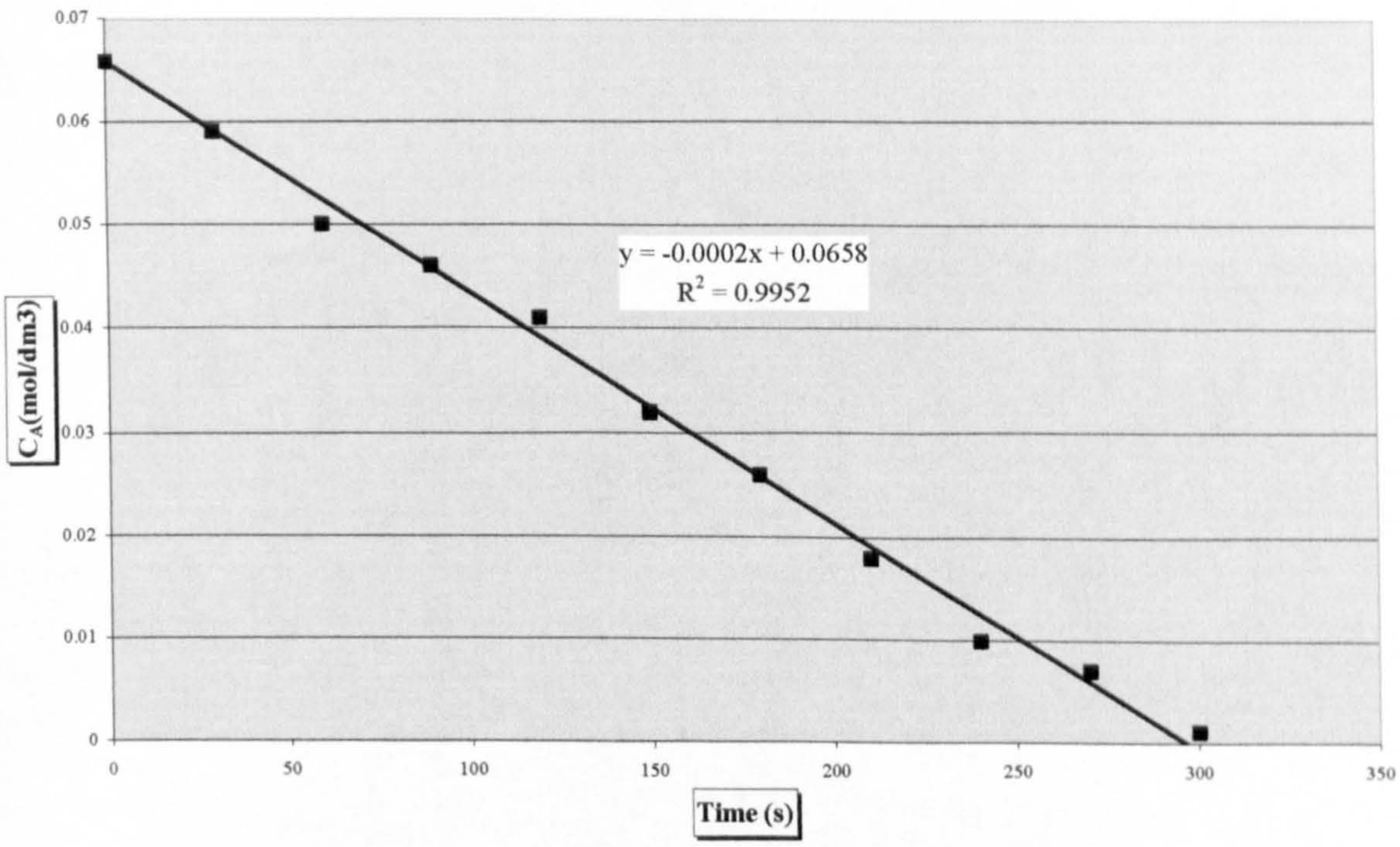


**Figure H.7. Fitting of experimental data for Catalyst 1 at 65$^0$C into a zero order equation**

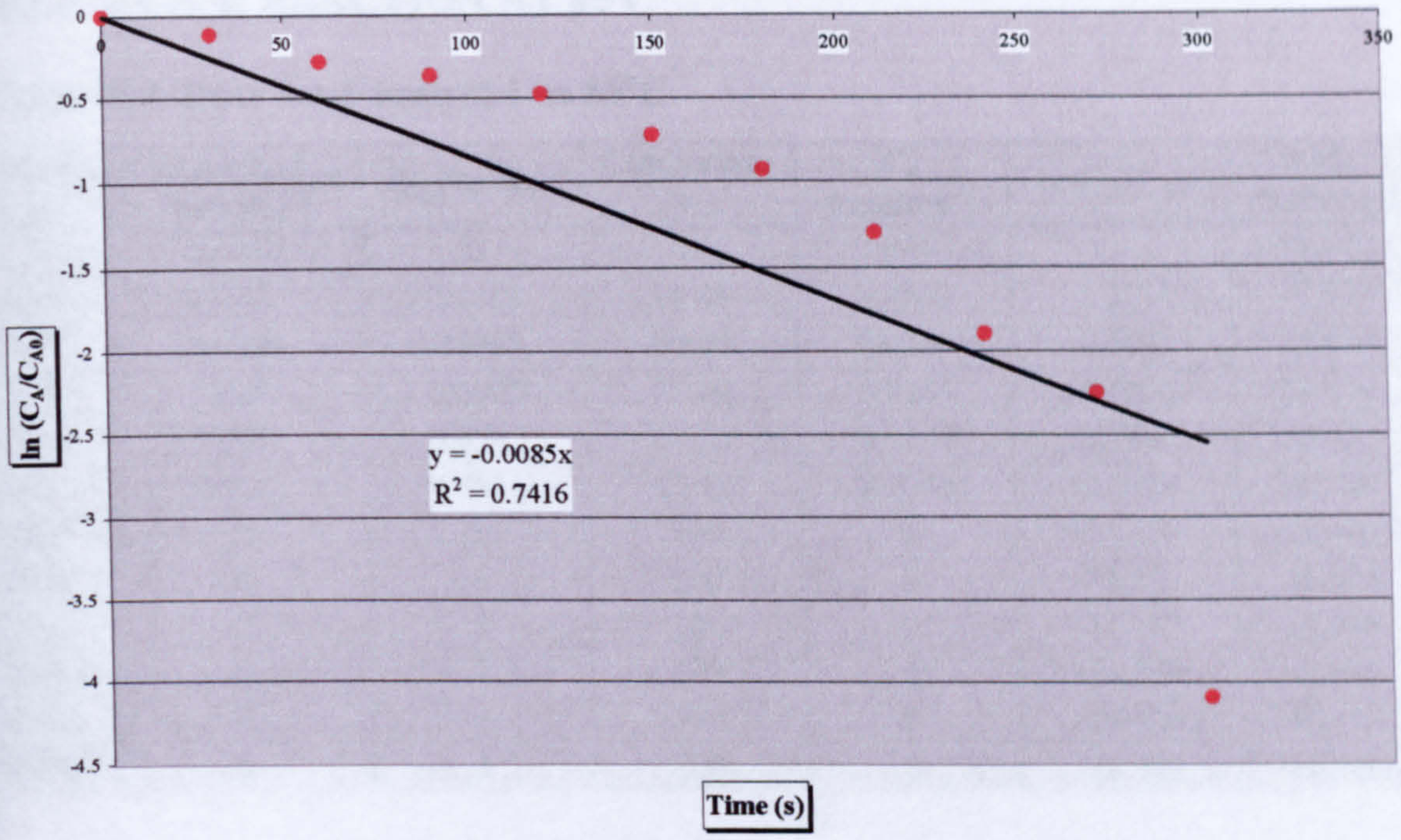


**Figure H.8. Fitting of experimental data for Catalyst 1 at 65$^0$C into a first order equation**

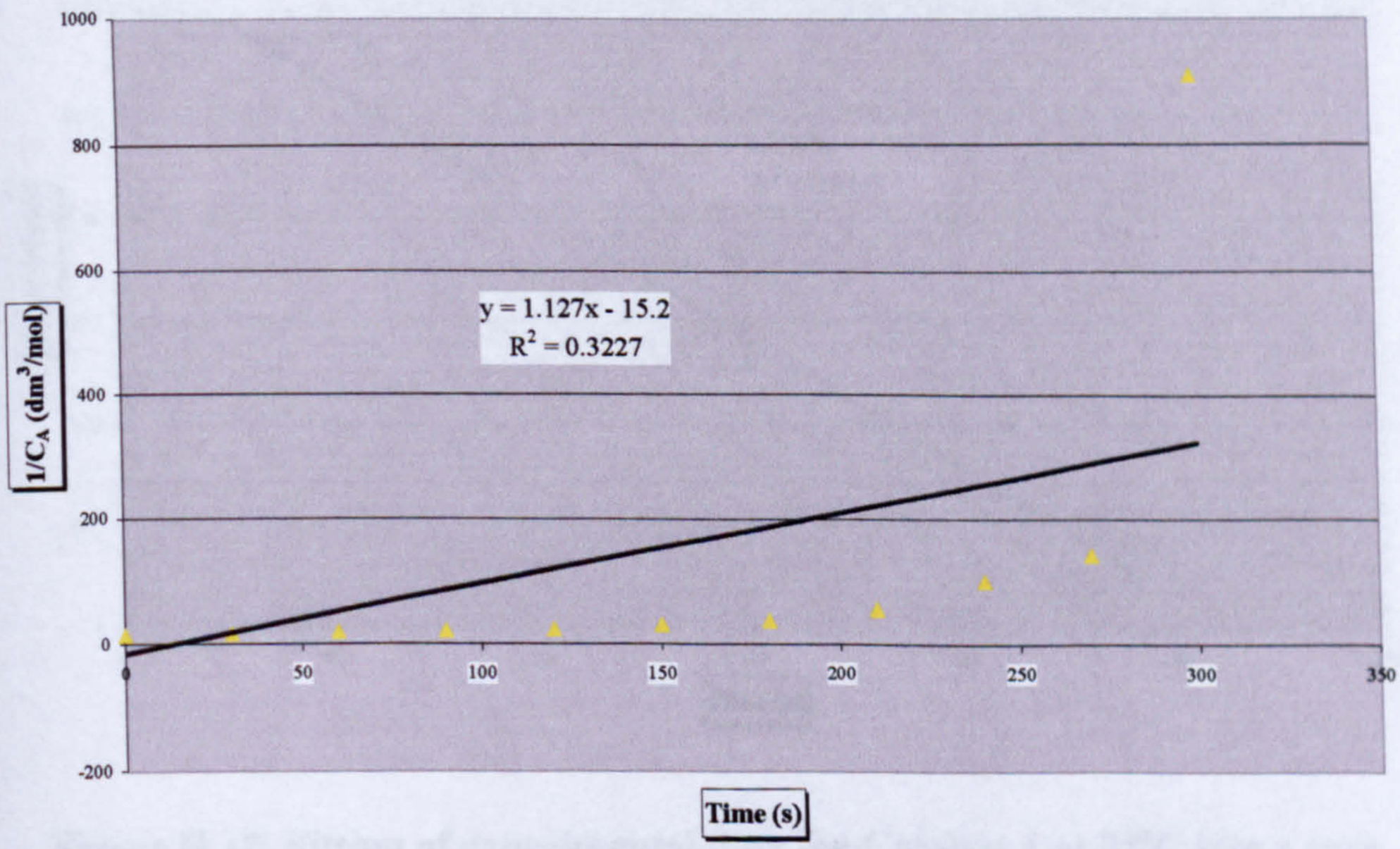


**Figure H.9. Fitting of experimental data for Catalyst 1 at 65$^0$C into a second order equation**

## H.1.4 BATCH REACTION AT 85$^0$C

**Table H.4. Data for Catalyst 1 at 85$^0$C**

| Time (s) | Concentration (mol/dm$^3$) | Conversion | Conversion (%) | $C_A$ (mol/dm$^3$) | $\ln(C_A/C_{A0})$ | $1/C_A$ (dm$^3$/mol) |
|---|---|---|---|---|---|---|
| 0 | 0.0660 | 0 | 0 | 0.0660 | 0 | 15.200 |
| 60 | 0.0560 | 0.1488 | 14.88 | 0.0560 | -0.1611 | 17.857 |
| 120 | 0.0389 | 0.4080 | 40.80 | 0.0389 | -0.5242 | 25.674 |
| 150 | 0.0263 | 0.6000 | 60.00 | 0.0263 | -0.9163 | 38.000 |
| 180 | 0.0199 | 0.6980 | 69.78 | 0.0199 | -1.1972 | 50.327 |
| 240 | 0.0045 | 0.9316 | 93.16 | 0.0045 | -2.6824 | 222.222 |
| 300 | 0 | 1 | 100 | 0 | -34.120 | 1E+16 |
| 600 | 0 | 1 | 100 | 0 | -34.120 | 1E+16 |
| 900 | 0 | 1 | 100 | 0 | -34.120 | 1E+16 |
| 1200 | 0 | 1 | 100 | 0 | -34.120 | 1E+16 |
| 1500 | 0 | 1 | 100 | 0 | -34.120 | 1E+16 |
| 1800 | 0 | 1 | 100 | 0 | -34.120 | 1E+16 |

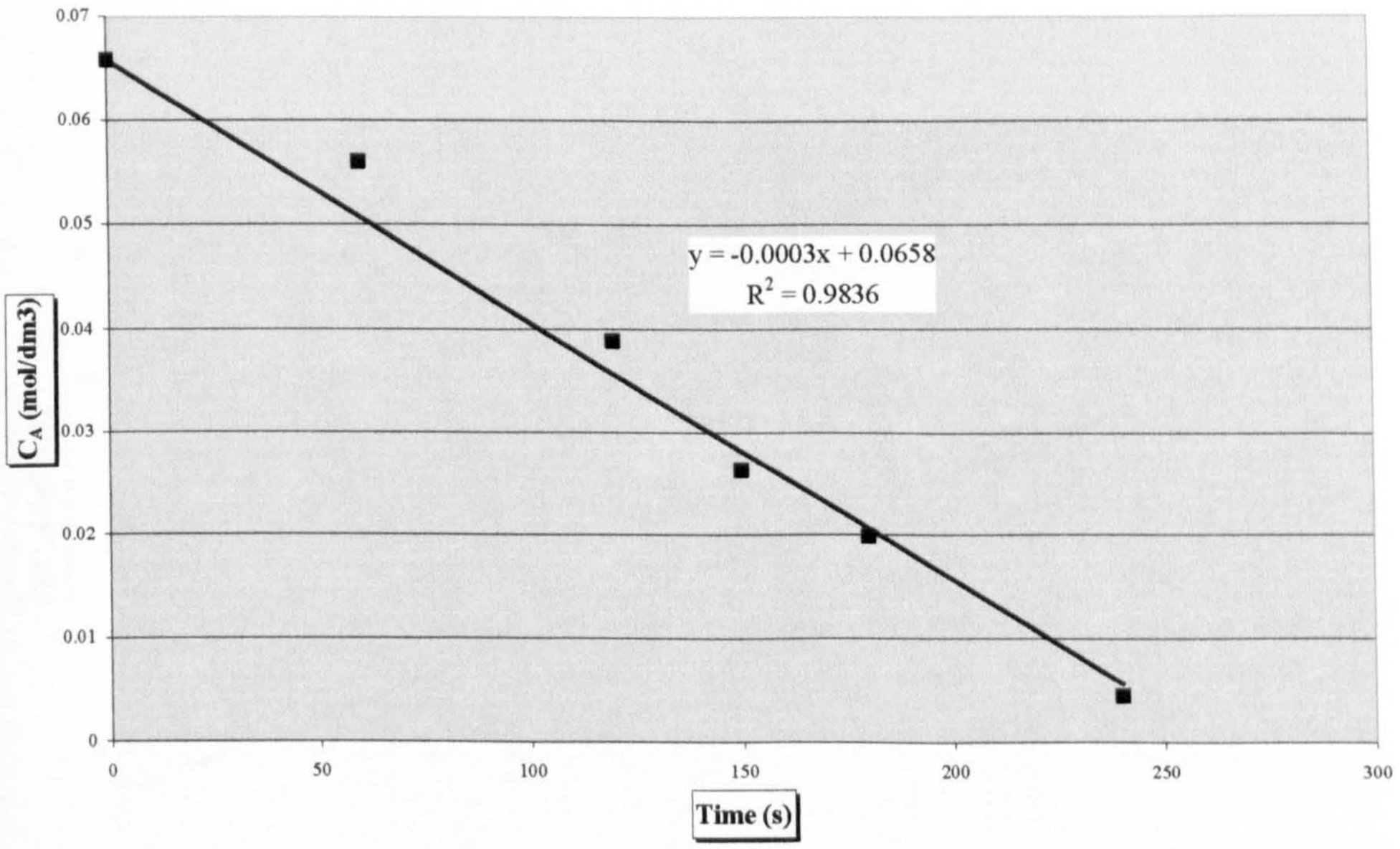


**Figure H.10. Fitting of experimental data for Catalyst 1 at 85$^0$C into a zero order equation**

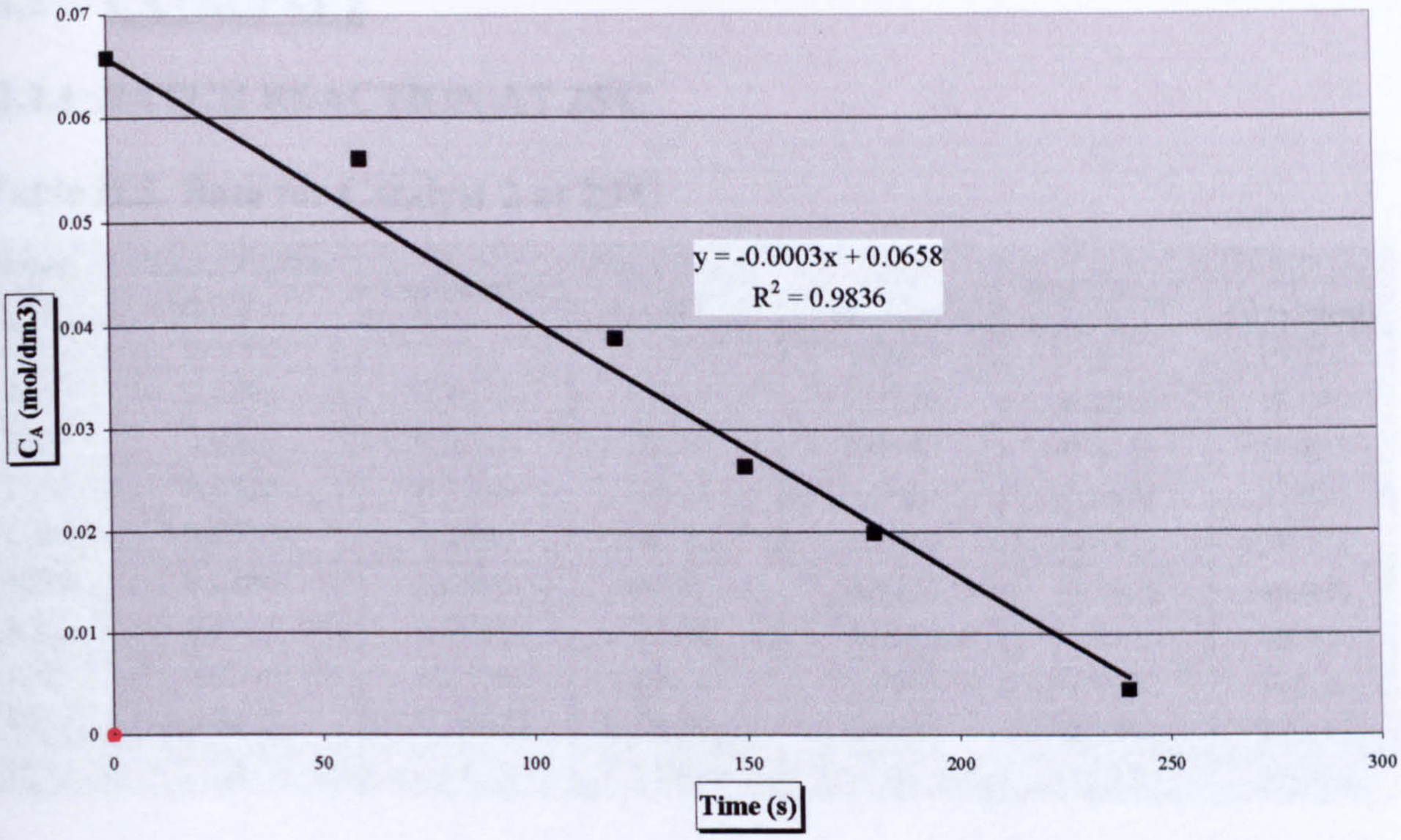


**Figure H.11. Fitting of experimental data for Catalyst 1 at 85$^0$C into a first order equation**

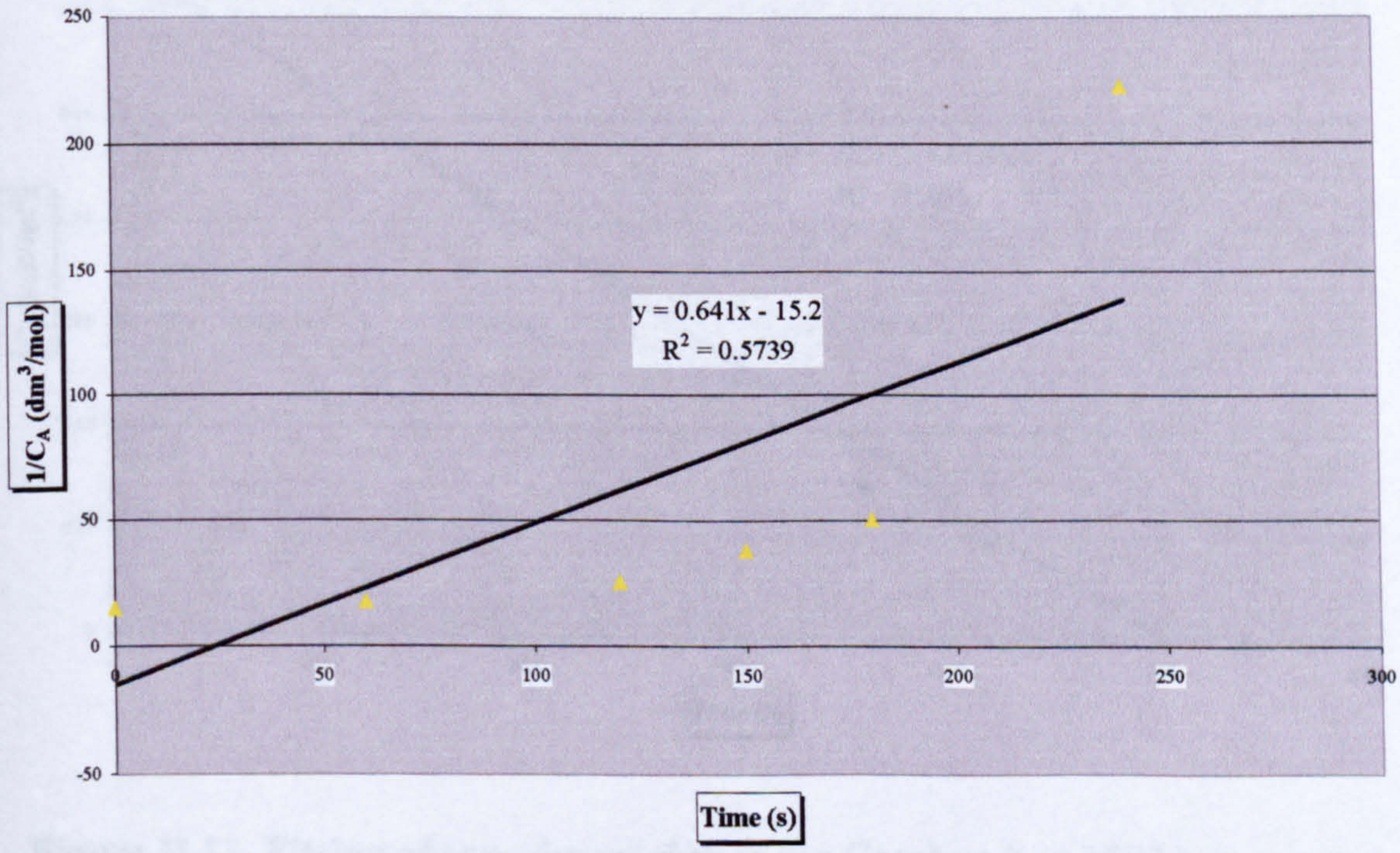


**Figure H.12. Fitting of experimental data for Catalyst 1 at 85$^0$C into a second order equation**

## H.2 CATALYST 2

### H.2.1 BATCH REACTION AT 25$^0$C

**Table H.5. Data for Catalyst 2 at 25$^0$C**

| Time (s) | Concentration (mol/dm$^3$) | Conversion | Conversion (%) | $C_A$ (mol/dm$^3$) | $\ln(C_A/C_{A0})$ | $1/C_A$ (dm$^3$/mol) |
|---|---|---|---|---|---|---|
| 0 | 0.0660 | 0 | 0 | 0.0665 | 0 | 15.200 |
| 600 | 0.0590 | 0.1032 | 10.32 | 0.0590 | -0.1089 | 16.949 |
| 1200 | 0.0480 | 0.2704 | 27.04 | 0.0480 | -0.3153 | 20.833 |
| 1800 | 0.0420 | 0.3616 | 36.16 | 0.0420 | -0.4488 | 23.809 |
| 2400 | 0.0350 | 0.4680 | 46.80 | 0.0350 | -0.6311 | 28.571 |
| 3000 | 0.0250 | 0.6200 | 62.00 | 0.0250 | -0.9676 | 40.000 |
| 3600 | 0.0145 | 0.7796 | 77.96 | 0.0145 | -1.5123 | 68.966 |
| 4200 | 0.0095 | 0.8556 | 85.56 | 0.0095 | -1.9352 | 105.26 |
| 4800 | 0.0035 | 0.9468 | 94.68 | 0.0035 | -2.9337 | 285.71 |
| 5400 | 0 | 1 | 100 | 0 | -34.120 | 1E+16 |

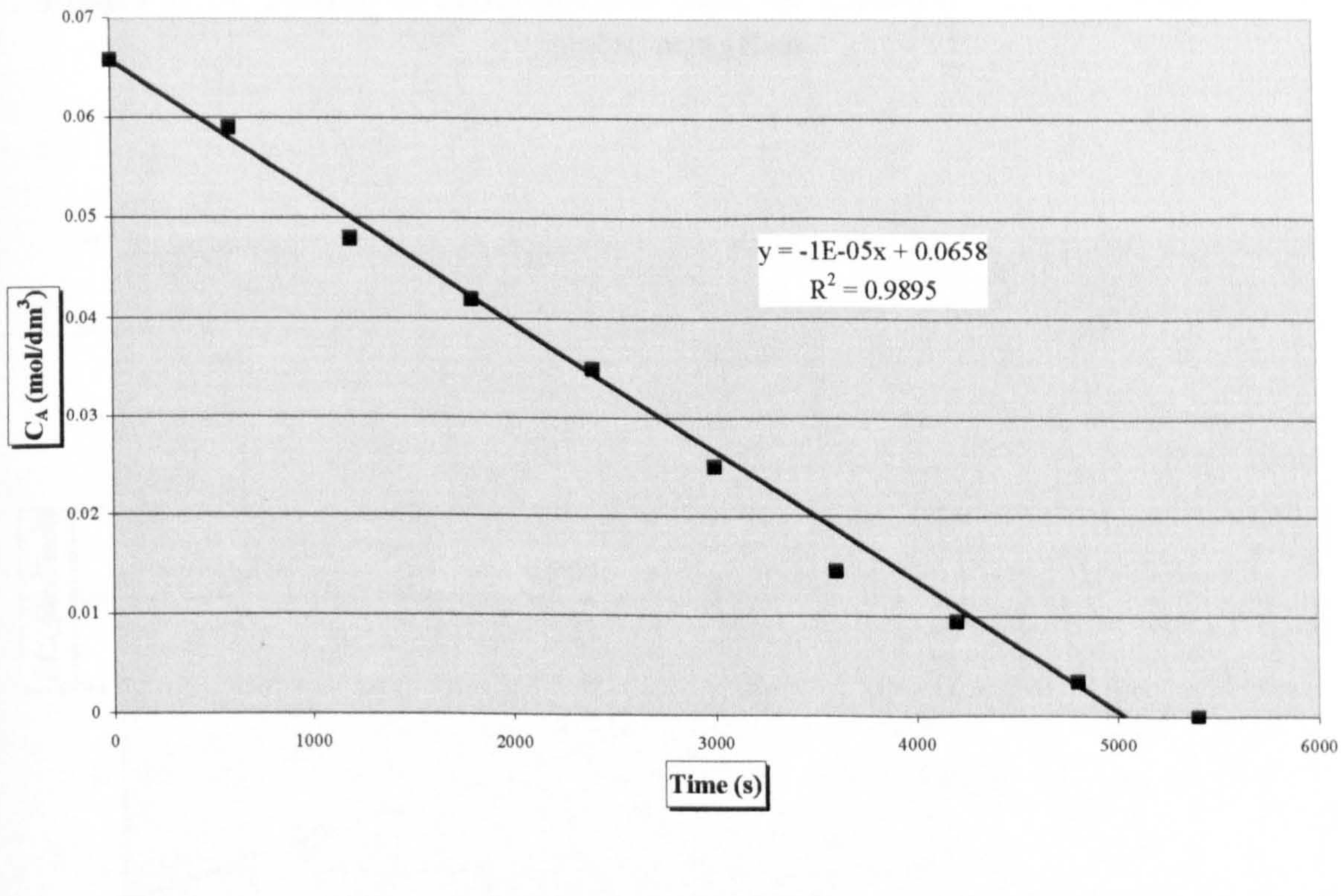


**Figure H.13. Fitting of experimental data for Catalyst 2 at 25$^0$C into a zero order equation**

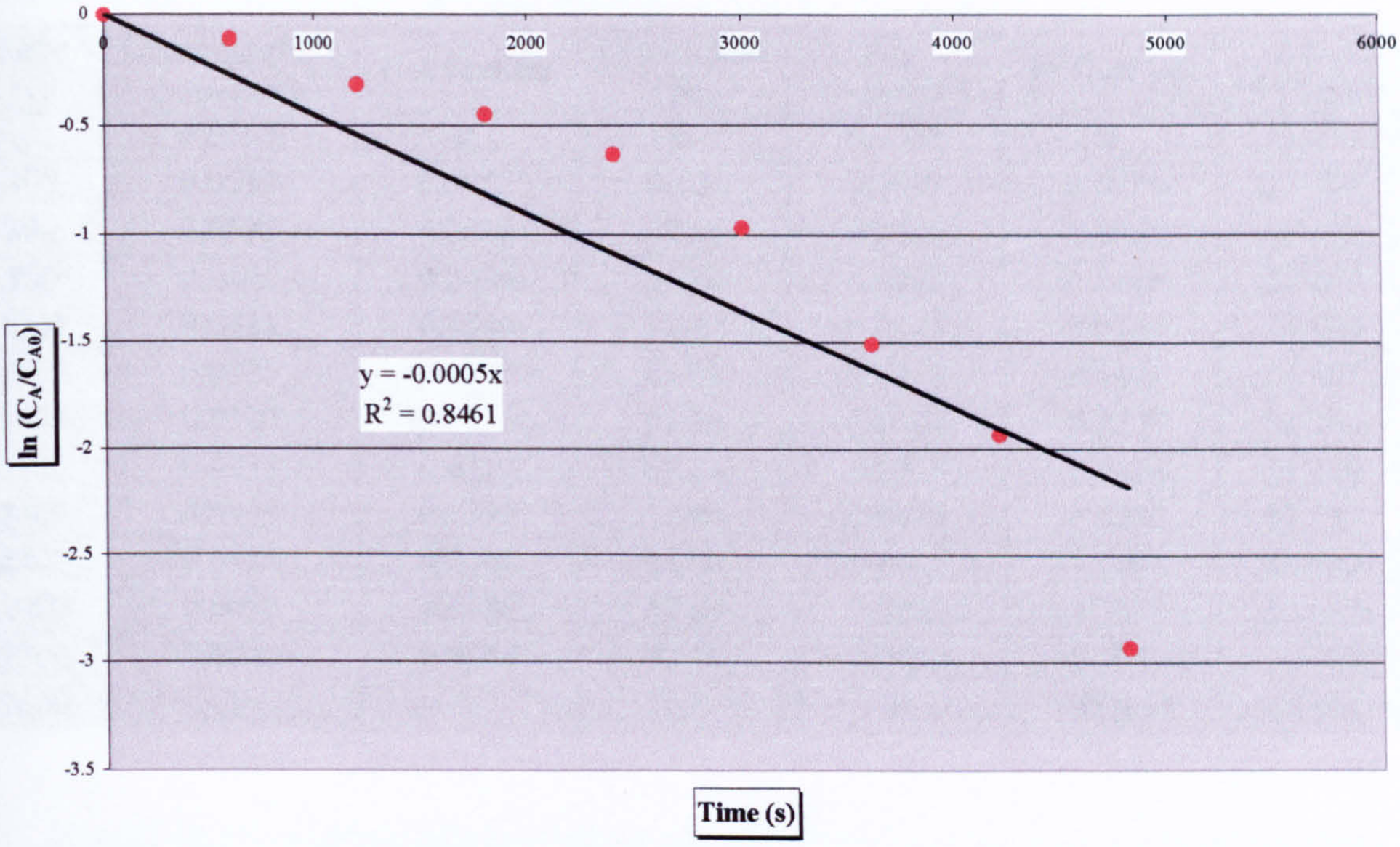


**Figure H.14. Fitting of experimental data for Catalyst 2 at 25$^0$C into a first order equation**

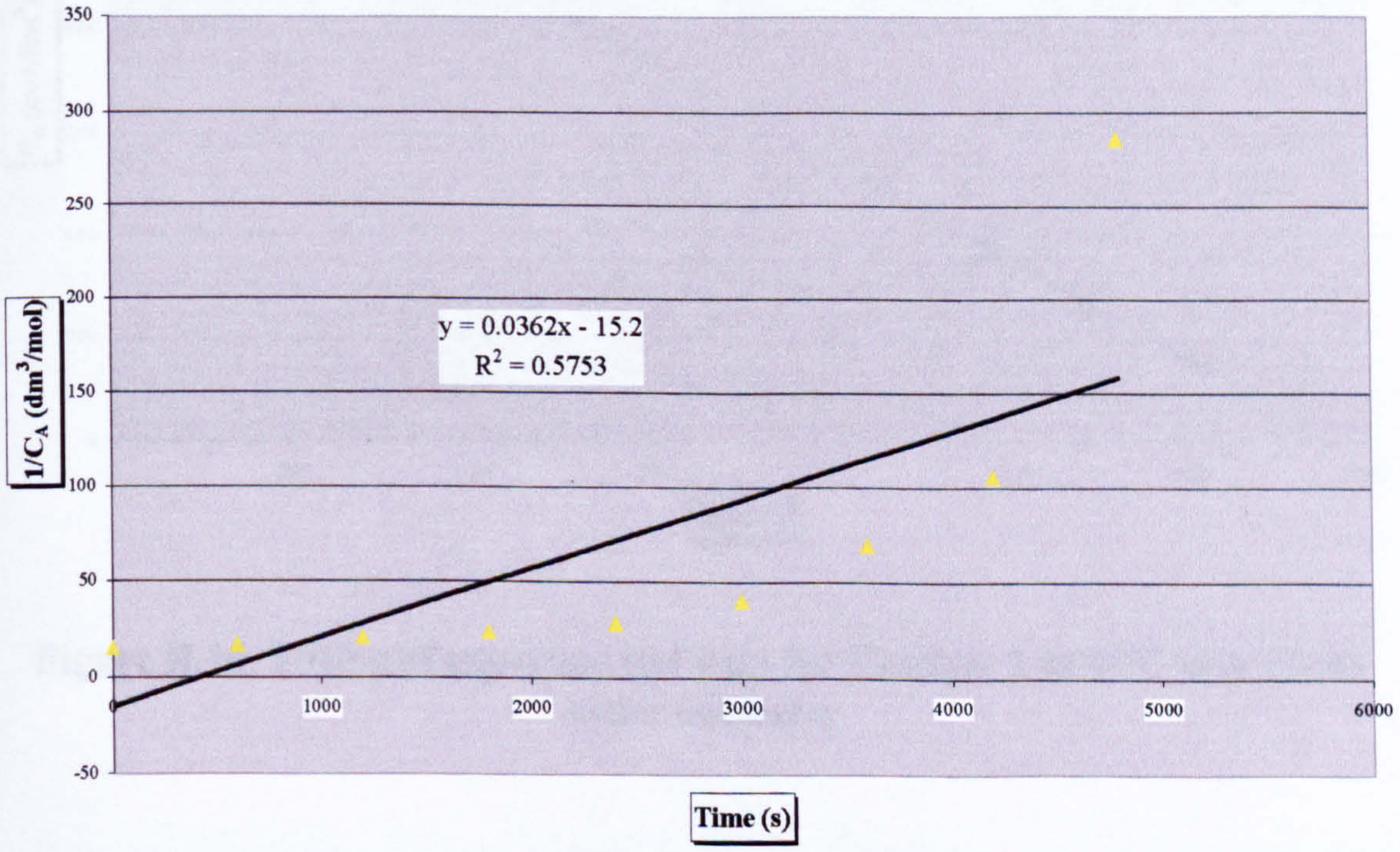


**Figure H.15. Fitting of experimental data for Catalyst 2 at 25$^0$C into a second order equation**

## H.2.2 BATCH REACTION AT 45$^0$C

**Table H.6. Data for Catalyst 2 at 45$^0$C**

| Time (s) | Concentration (mol/dm$^3$) | Conversion | Conversion (%) | $C_A$ (mol/dm$^3$) | $\ln(C_A/C_{A0})$ | $1/C_A$ (dm$^3$/mol) |
|---|---|---|---|---|---|---|
| 0 | 0.0660 | 0 | 0 | 0.0660 | 0 | 15.200 |
| 300 | 0.0615 | 0.0652 | 6.52 | 0.0615 | -0.0674 | 16.260 |
| 600 | 0.0535 | 0.1868 | 18.68 | 0.0535 | -0.2068 | 18.692 |
| 900 | 0.0495 | 0.2476 | 24.76 | 0.0495 | -0.2845 | 20.202 |
| 1200 | 0.0425 | 0.3540 | 35.40 | 0.0425 | -0.4370 | 23.529 |
| 1500 | 0.0375 | 0.4300 | 43.00 | 0.0375 | -0.5621 | 26.667 |
| 1800 | 0.0320 | 0.5136 | 51.36 | 0.0320 | -0.7207 | 31.250 |
| 2100 | 0.0255 | 0.6124 | 61.24 | 0.0255 | -0.9478 | 39.216 |
| 2400 | 0.0175 | 0.7340 | 73.40 | 0.0175 | -1.3242 | 57.143 |
| 2700 | 0.0125 | 0.8100 | 81.00 | 0.0125 | -1.6607 | 80.000 |
| 3000 | 0.0080 | 0.8784 | 87.84 | 0.0080 | -2.1070 | 125.00 |
| 3300 | 0.0050 | 0.9240 | 92.40 | 0.0050 | -2.5770 | 200.00 |
| 3600 | 0 | 1 | 100 | 0 | -31.817 | 1E+15 |

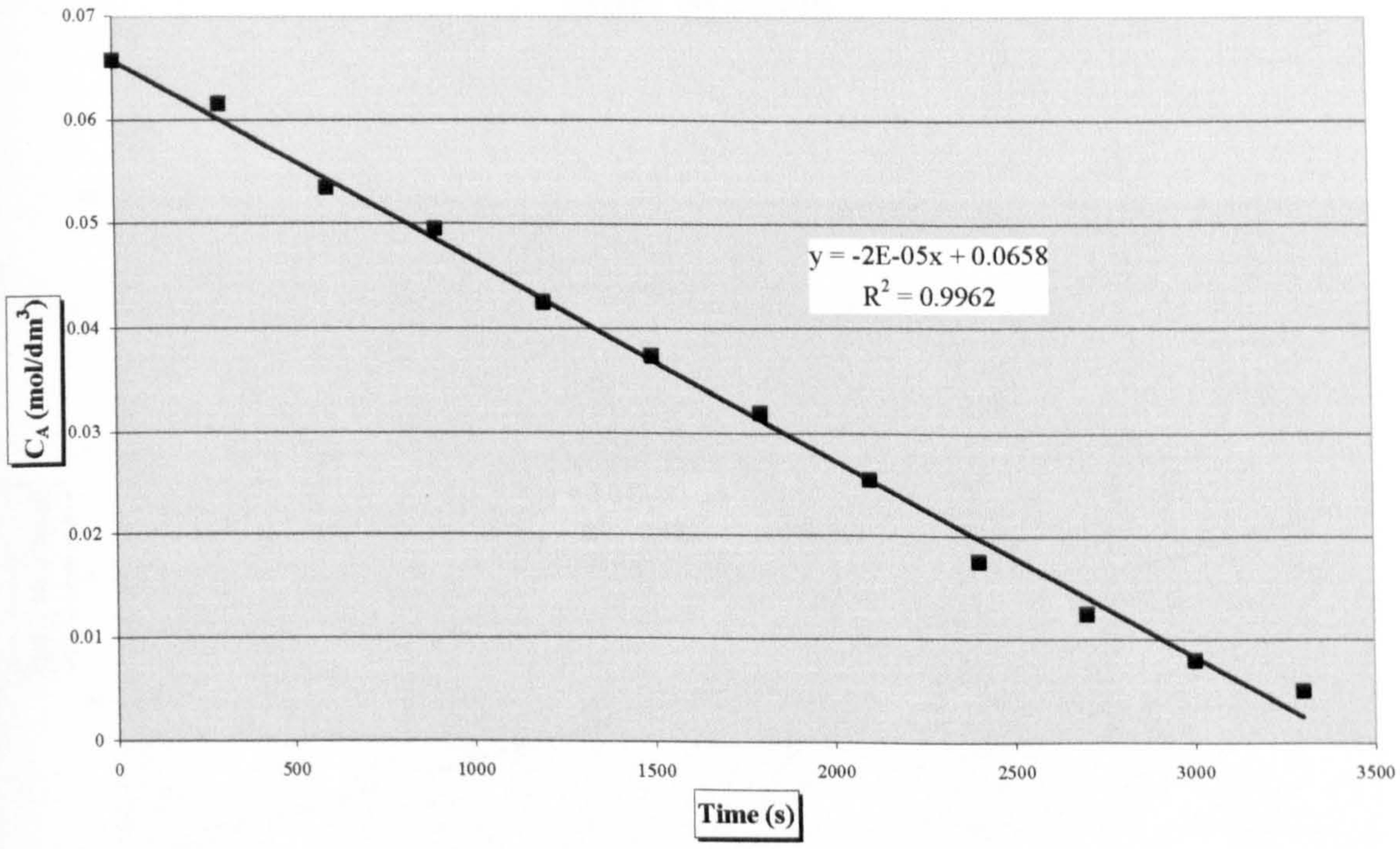


**Figure H.16. Fitting of experimental data for Catalyst 2 at 45$^0$C into a zero order equation**

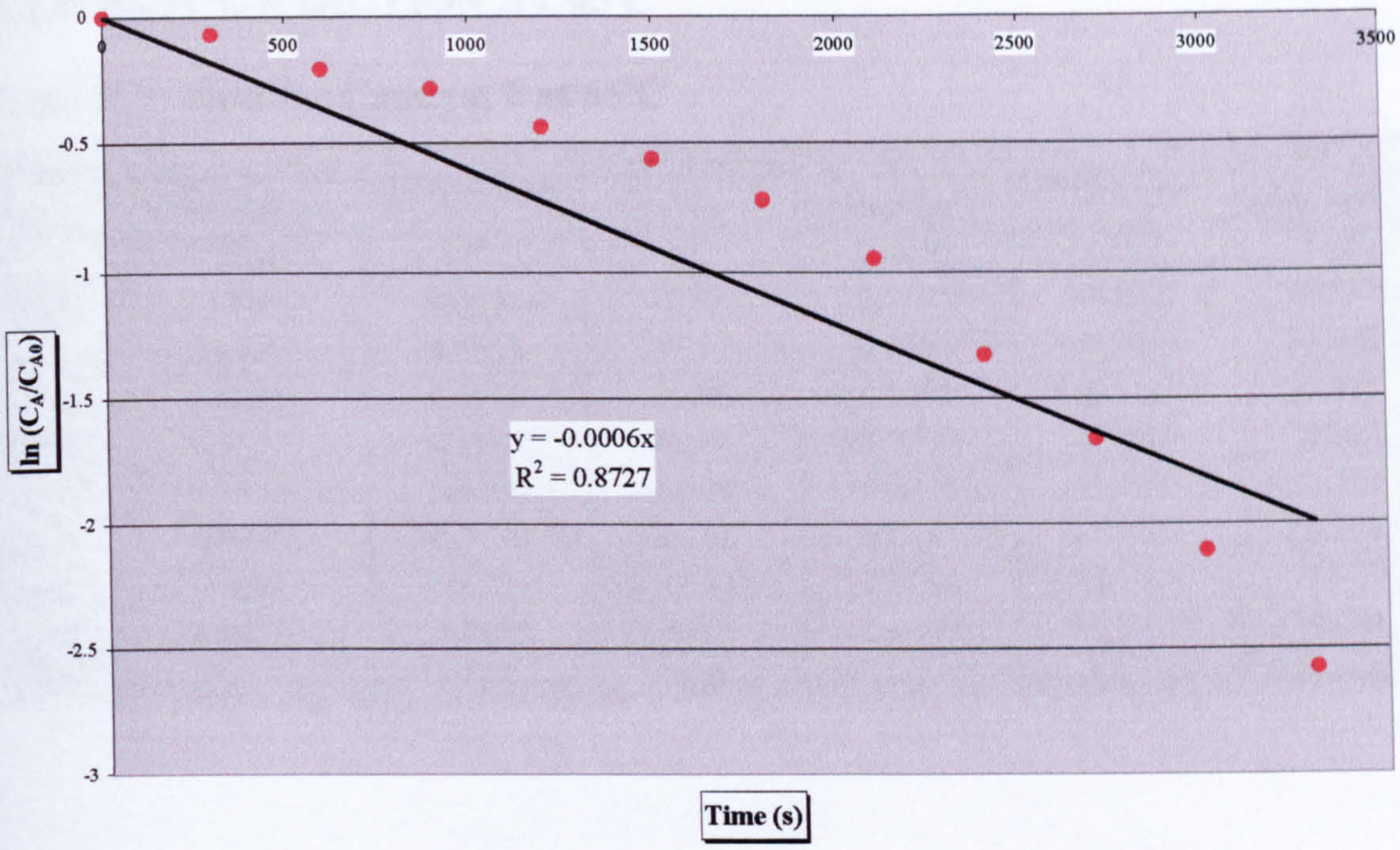


**Figure H.17. Fitting of experimental data for Catalyst 2 at 45$^0$C into a first order equation**

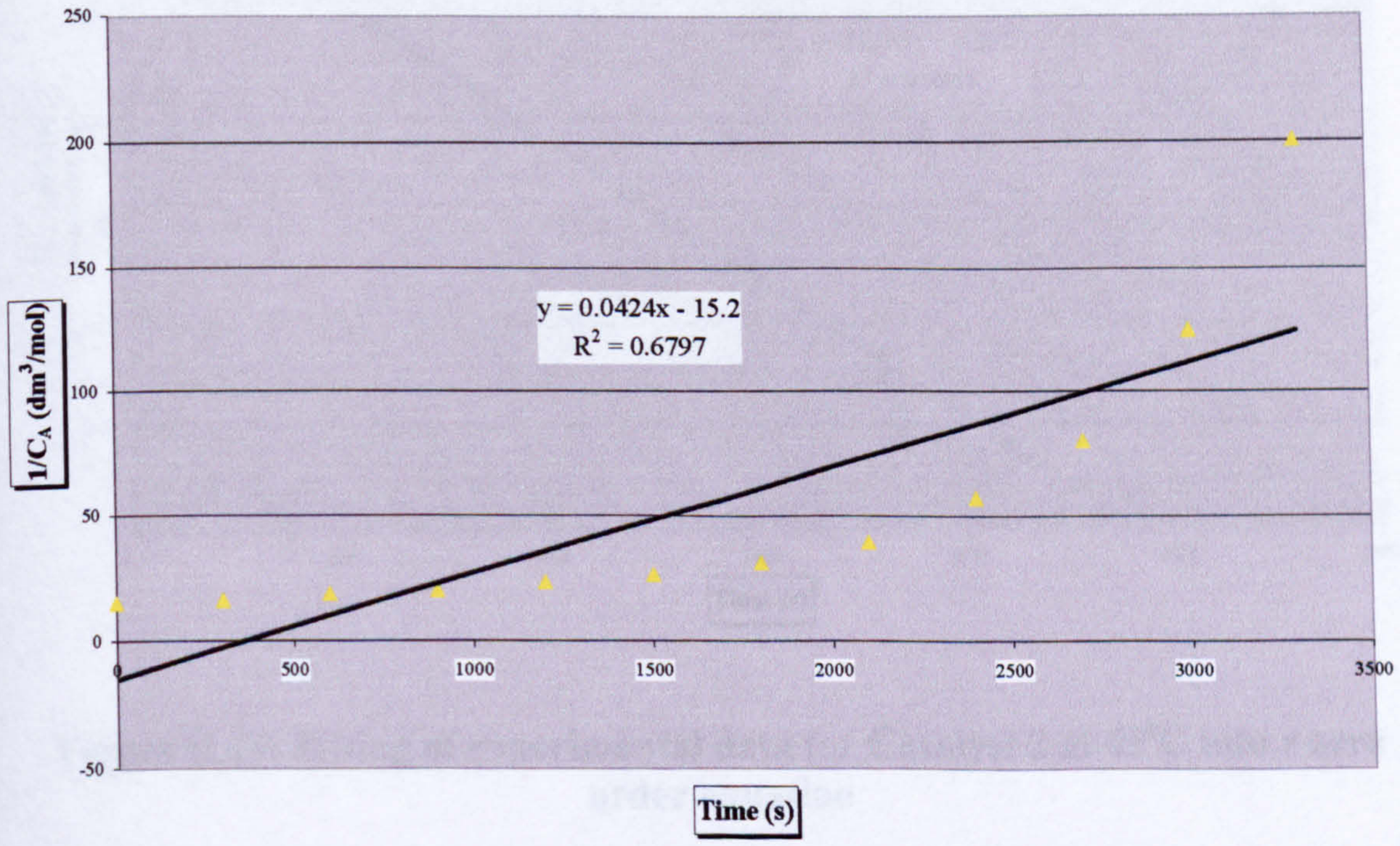


**Figure H.18. Fitting of experimental data for Catalyst 2 at 45$^0$C into a second order equation**

## H.2.3 BATCH REACTION AT 65$^0$C

### Table H.7. Data for Catalyst 2 at 65$^0$C

| Time (s) | Concentration (mol/dm$^3$) | Conversion | Conversion (%) | $C_A$ (mol/dm$^3$) | $\ln(C_A/C_{A0})$ | $1/C_A$ (dm$^3$/mol) |
|---|---|---|---|---|---|---|
| 0 | 0.0660 | 0 | 0 | 0.0660 | 0 | 15.200 |
| 300 | 0.0595 | 0.0956 | 9.56 | 0.0595 | -0.1005 | 16.807 |
| 600 | 0.0490 | 0.2552 | 25.52 | 0.0490 | -0.2946 | 20.408 |
| 900 | 0.0395 | 0.3996 | 39.96 | 0.0395 | -0.5102 | 25.316 |
| 1200 | 0.0330 | 0.4984 | 49.84 | 0.0330 | -0.6900 | 30.303 |
| 1500 | 0.0235 | 0.6428 | 64.28 | 0.0235 | -1.0295 | 42.553 |
| 1800 | 0.0145 | 0.7796 | 77.96 | 0.0145 | -1.5123 | 68.966 |
| 2100 | 0.0080 | 0.8784 | 87.84 | 0.0080 | -2.1070 | 125.00 |
| 2400 | 0.0026 | 0.9605 | 96.05 | 0.0026 | -3.2310 | 384.61 |
| 2700 | 0 | 1 | 100 | 0 | -34.120 | 1E+16 |

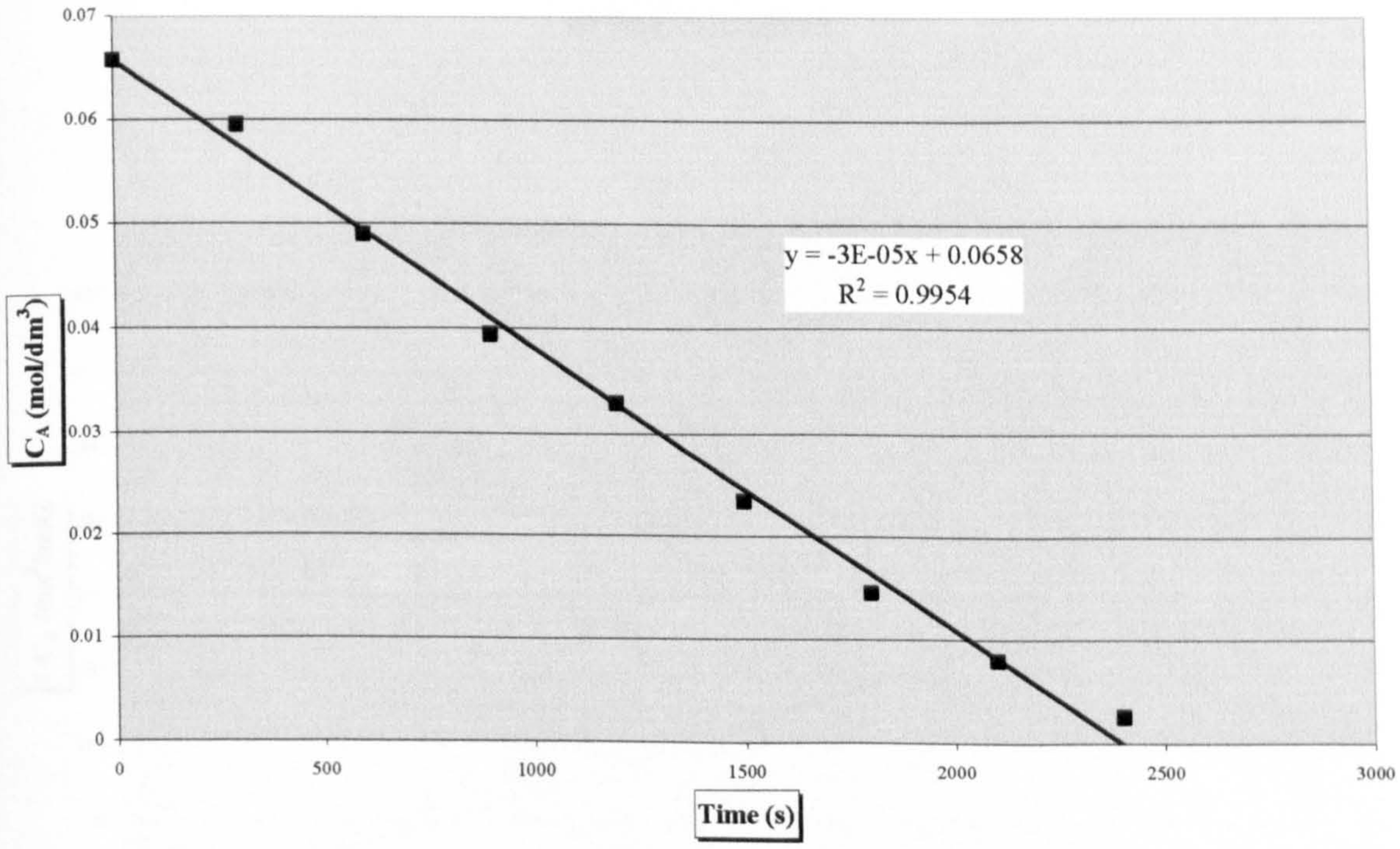


**Figure H.19. Fitting of experimental data for Catalyst 2 at 65$^0$C into a zero order equation**

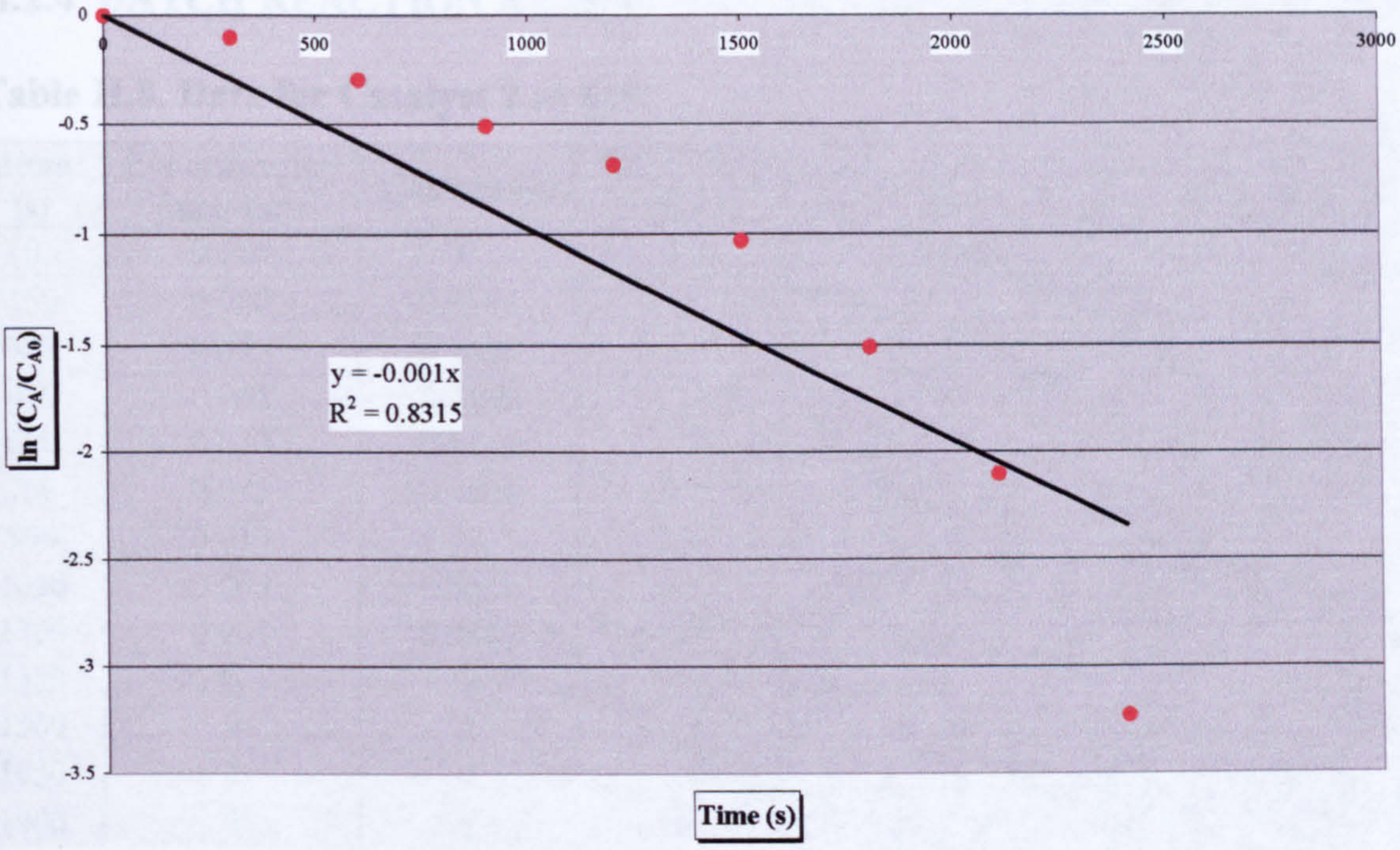


**Figure H.20. Fitting of experimental data for Catalyst 2 at 65$^0$C into a first order equation**

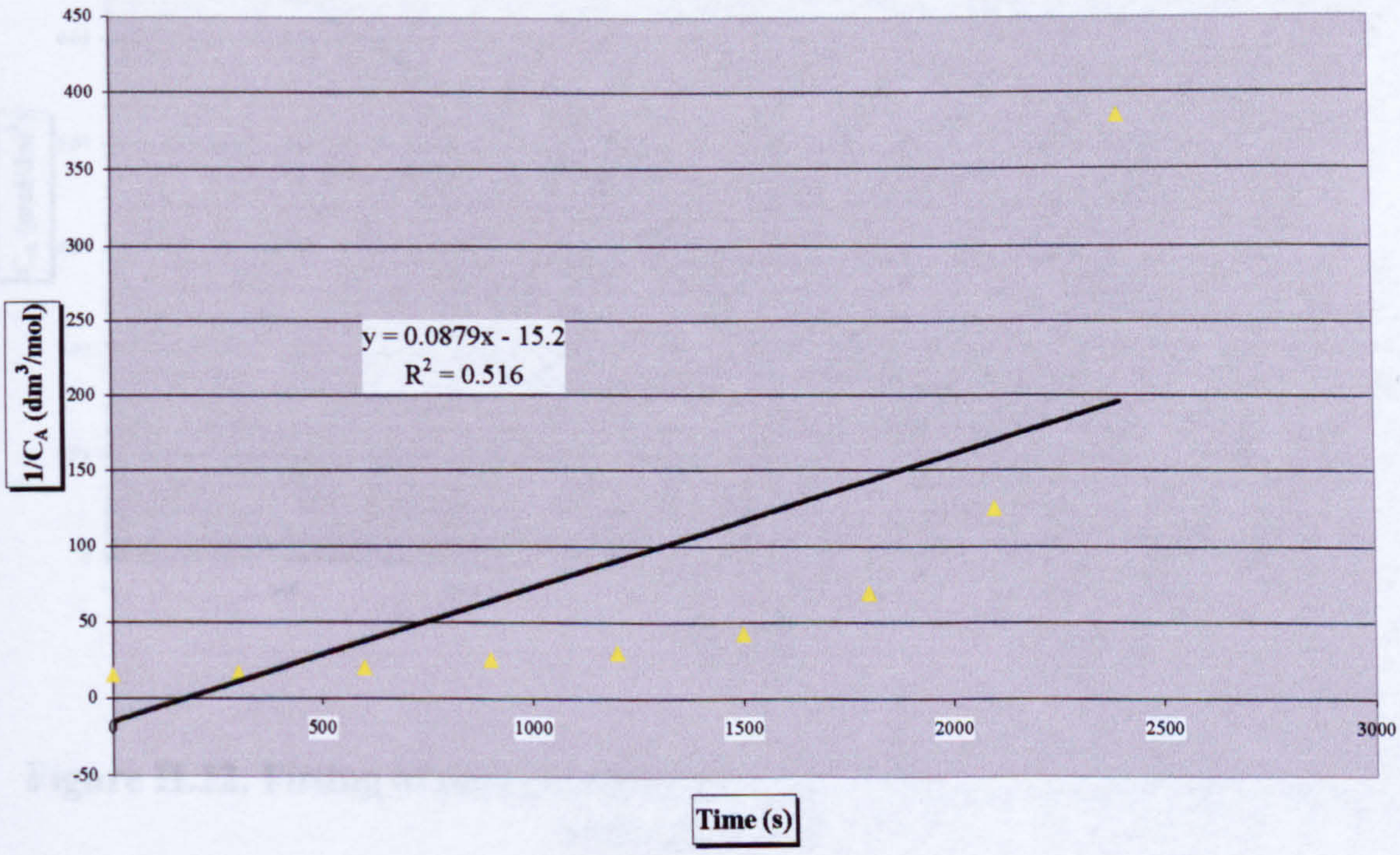


**Figure H.21. Fitting of experimental data for Catalyst 2 at 65$^0$C into a second order equation**

## H.2.4 BATCH REACTION AT 85$^0$C

### Table H.8. Data for Catalyst 2 at 85$^0$C

| Time (s) | Concentration (mol/dm$^3$) | Conversion | Conversion (%) | $C_A$ (mol/dm$^3$) | ln($C_A/C_{A0}$) | 1/$C_A$ (dm$^3$/mol) |
|---|---|---|---|---|---|---|
| 0 | 0.066 | 0 | 0 | 0.066 | 0 | 15.200 |
| 150 | 0.060 | 0.0880 | 8.80 | 0.060 | -0.0921 | 16.667 |
| 300 | 0.056 | 0.1488 | 14.88 | 0.056 | -0.1611 | 17.857 |
| 450 | 0.045 | 0.3160 | 31.60 | 0.045 | -0.3798 | 22.222 |
| 600 | 0.030 | 0.5440 | 54.40 | 0.030 | -0.7853 | 33.333 |
| 750 | 0.023 | 0.6504 | 65.04 | 0.023 | -1.0510 | 43.478 |
| 900 | 0.015 | 0.7720 | 77.20 | 0.015 | -1.4784 | 66.667 |
| 1050 | 0.009 | 0.8632 | 86.32 | 0.009 | -1.9892 | 111.11 |
| 1200 | 0.003 | 0.9544 | 95.44 | 0.003 | -3.0878 | 333.33 |
| 1350 | 0 | 1 | 100 | 0 | -34.120 | 1E+16 |
| 1500 | 0 | 1 | 100 | 0 | -34.120 | 1E+16 |
| 1650 | 0 | 1 | 100 | 0 | -34.120 | 1E+16 |
| 1800 | 0 | 1 | 100 | 0 | -34.120 | 1E+16 |

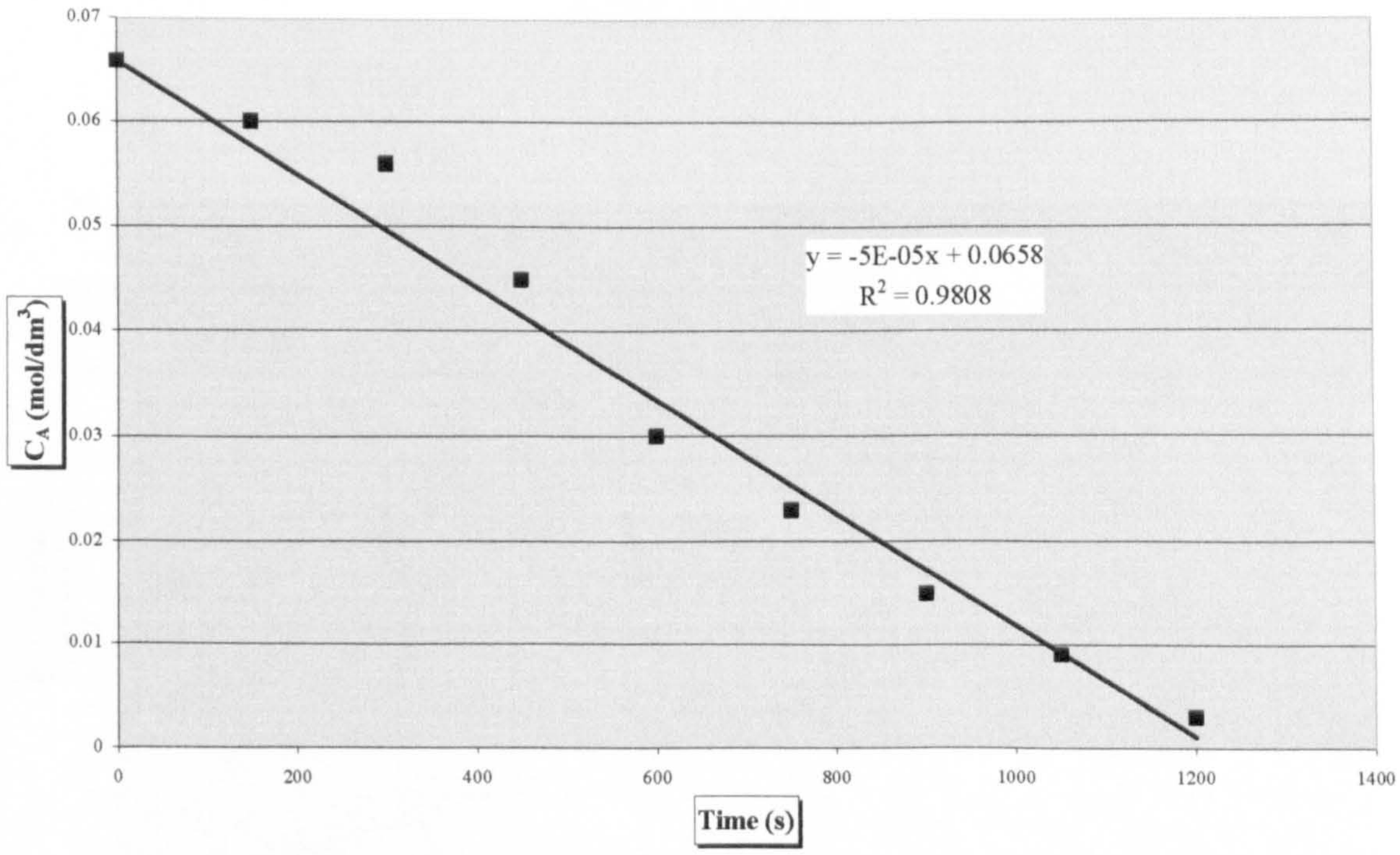


**Figure H.22. Fitting of experimental data for Catalyst 2 at 85$^0$C into a zero order equation**

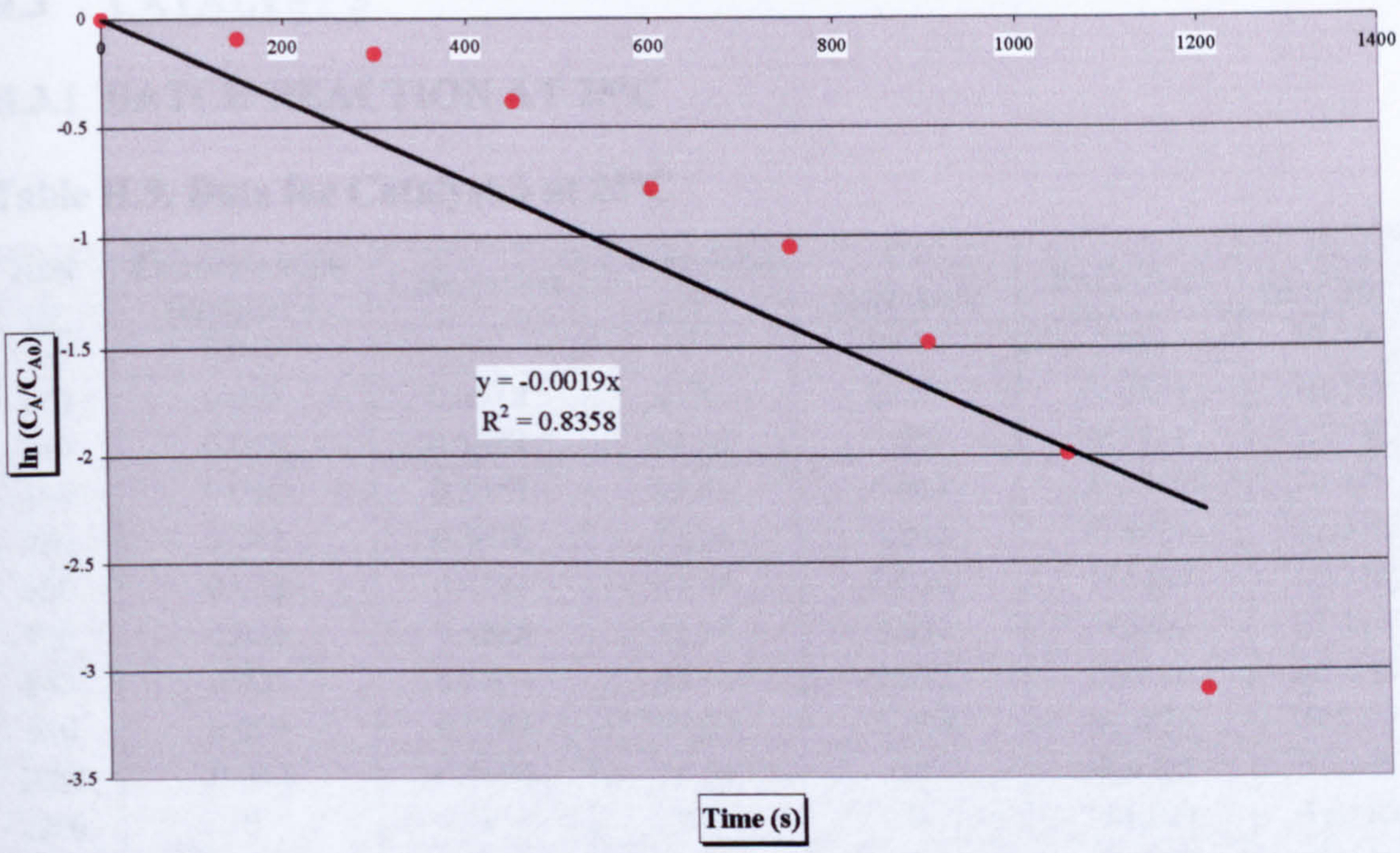


**Figure H.23. Fitting of experimental data for Catalyst 2 at 85$^0$C into a first order equation**

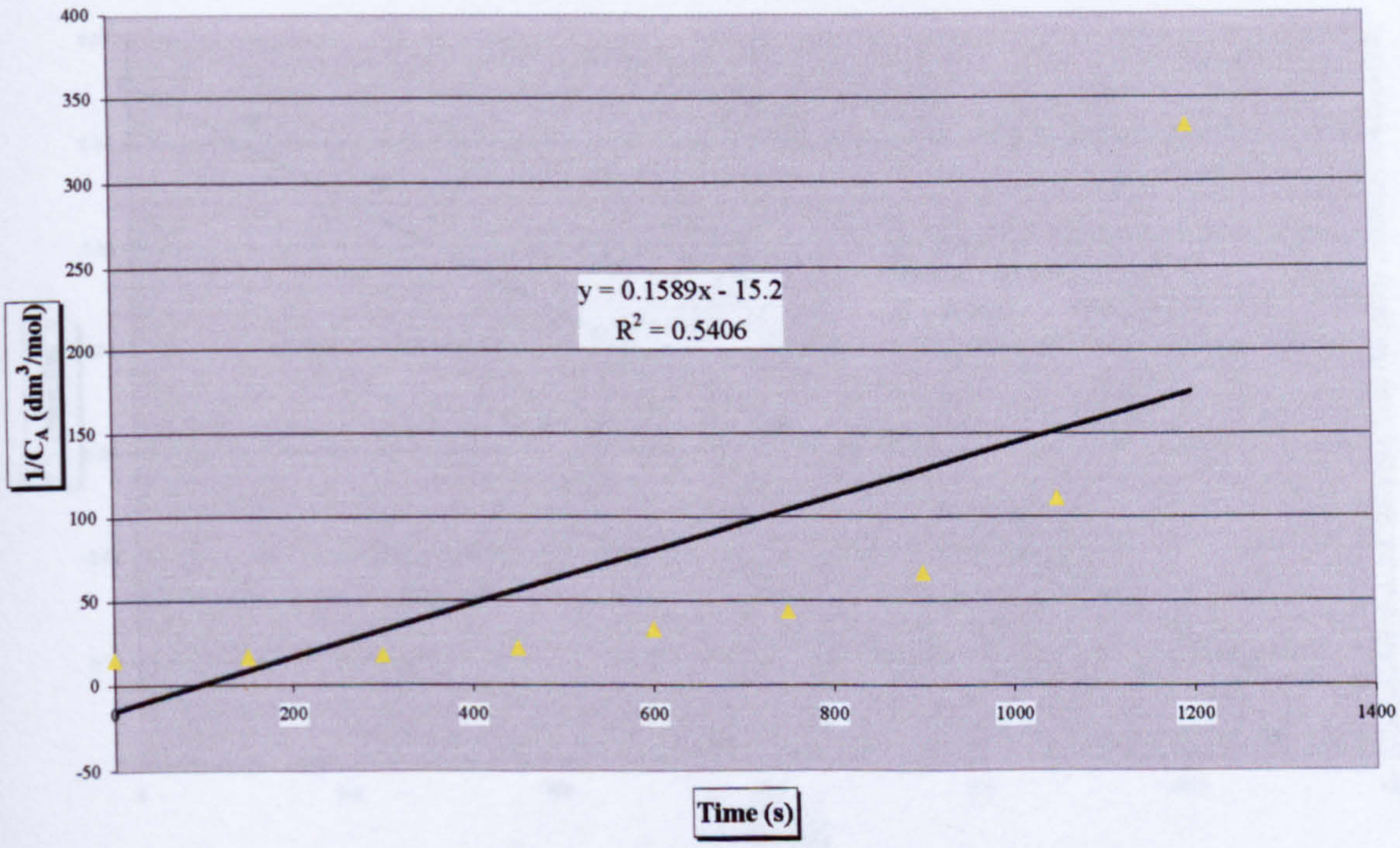


**Figure H.24. Fitting of experimental data for Catalyst 2 at 85$^0$C into a second order equation**

## H.3 CATALYST 3

### H.3.1 BATCH REACTION AT 25$^0$C

**Table H.9. Data for Catalyst 3 at 25$^0$C**

| Time (s) | Concentration (mol/dm$^3$) | Conversion | Conversion (%) | $C_A$ (mol/dm$^3$) | ln($C_A/C_{A0}$) | 1/$C_A$ (dm$^3$/mol) |
|---|---|---|---|---|---|---|
| 0 | 0.066 | 0 | 0 | 0.066 | 0 | 15.200 |
| 120 | 0.062 | 0.0576 | 5.76 | 0.062 | -0.0593 | 16.129 |
| 240 | 0.056 | 0.1488 | 14.88 | 0.056 | -0.1611 | 17.857 |
| 360 | 0.049 | 0.2552 | 25.52 | 0.049 | -0.2946 | 20.408 |
| 480 | 0.042 | 0.3616 | 36.16 | 0.042 | -0.4488 | 23.810 |
| 600 | 0.038 | 0.4224 | 42.24 | 0.038 | -0.5489 | 26.316 |
| 720 | 0.031 | 0.5288 | 52.88 | 0.031 | -0.7525 | 32.258 |
| 840 | 0.023 | 0.6504 | 65.04 | 0.023 | -1.0510 | 43.478 |
| 960 | 0.008 | 0.8784 | 87.84 | 0.008 | -2.1070 | 125.00 |
| 1080 | 0.002 | 0.9696 | 96.96 | 0.002 | -3.4933 | 500.00 |
| 1200 | 0 | 1 | 100 | 0 | -34.120 | 1E+16 |
| 1320 | 0 | 1 | 100 | 0 | -34.120 | 1E+16 |
| 1440 | 0 | 1 | 100 | 0 | -34.120 | 1E+16 |

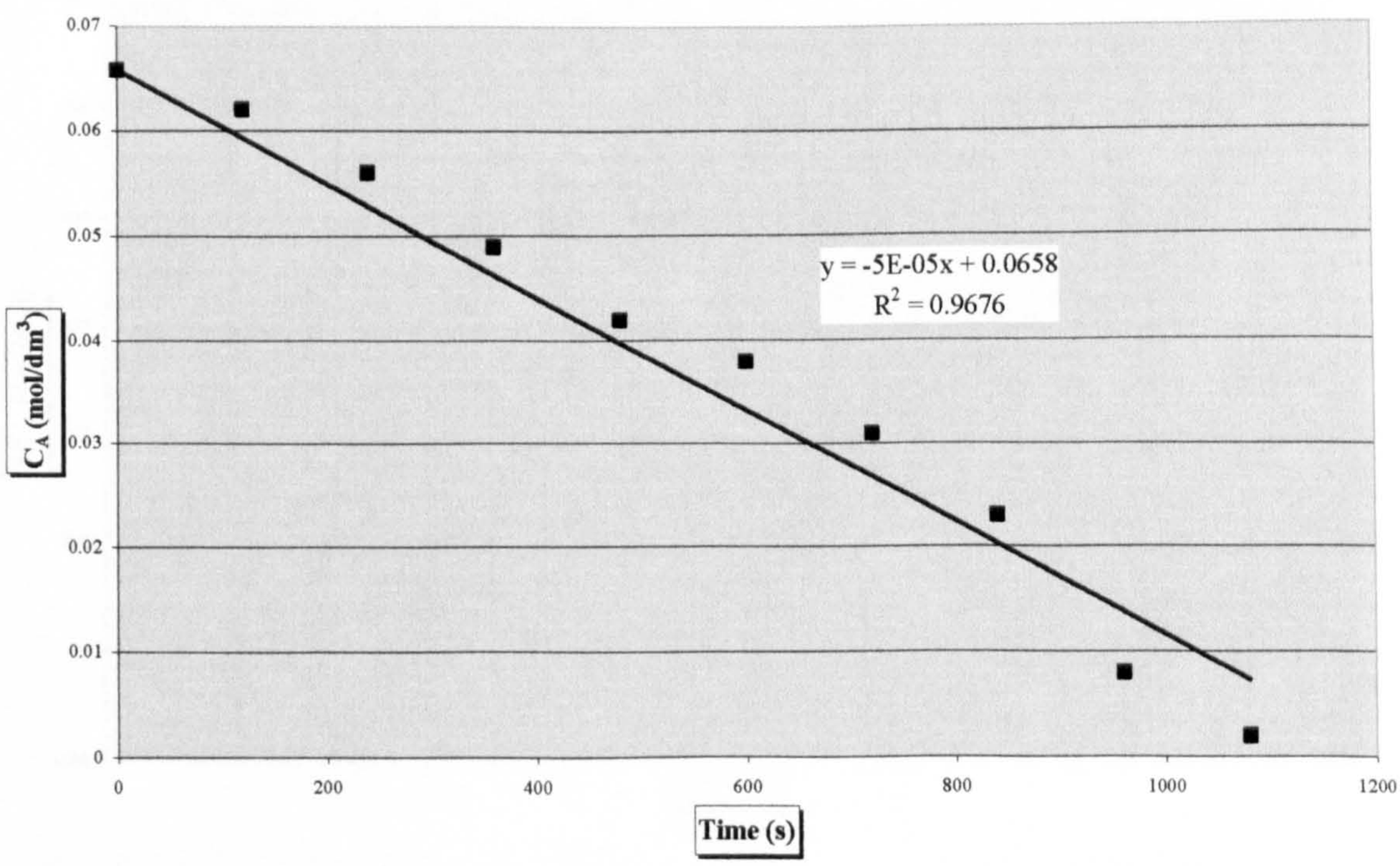


**Figure H.25. Fitting of experimental data for Catalyst 3 at 25$^0$C into a zero order equation**

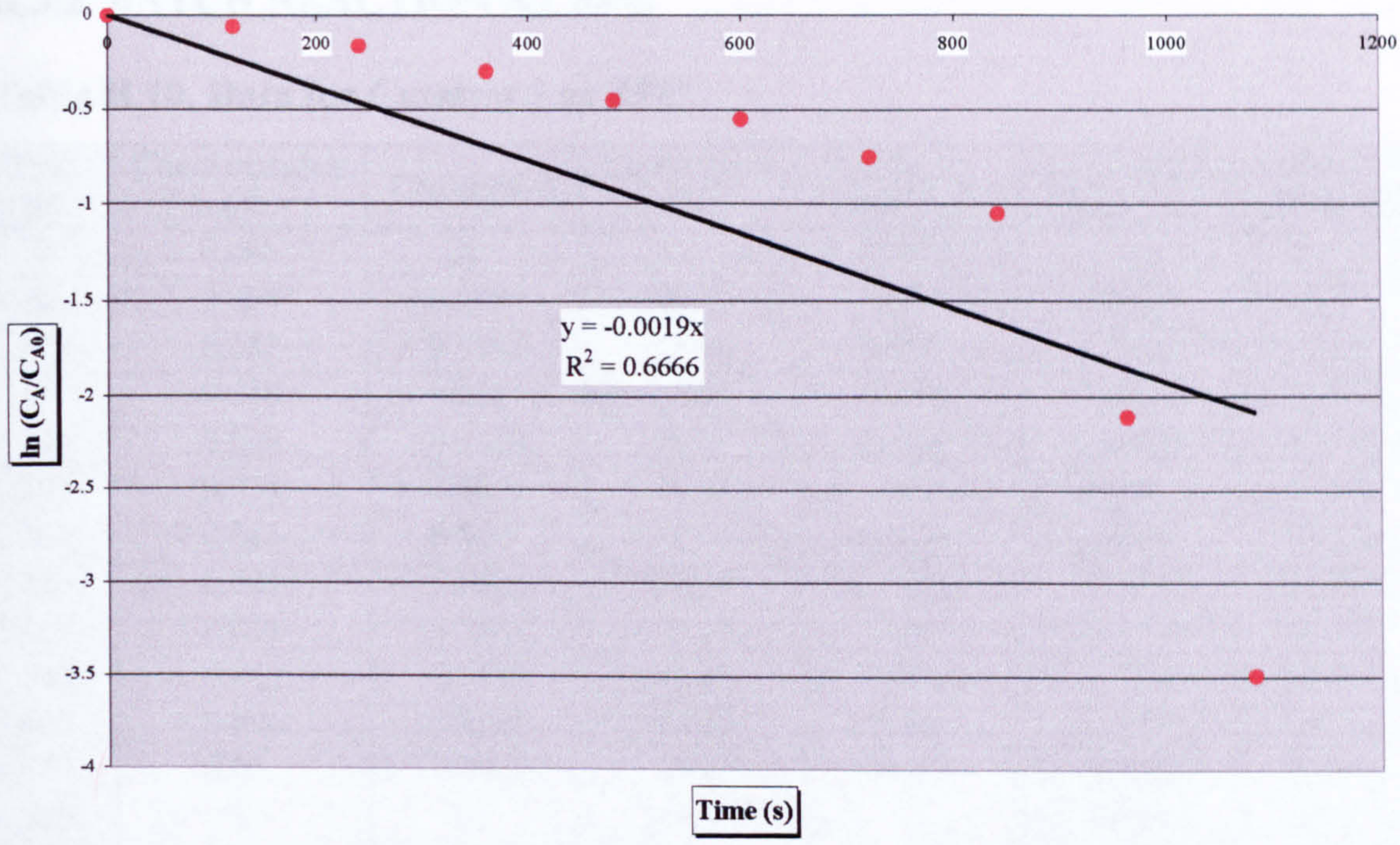


**Figure H.26. Fitting of experimental data for Catalyst 3 at 25$^0$C into a first order equation**

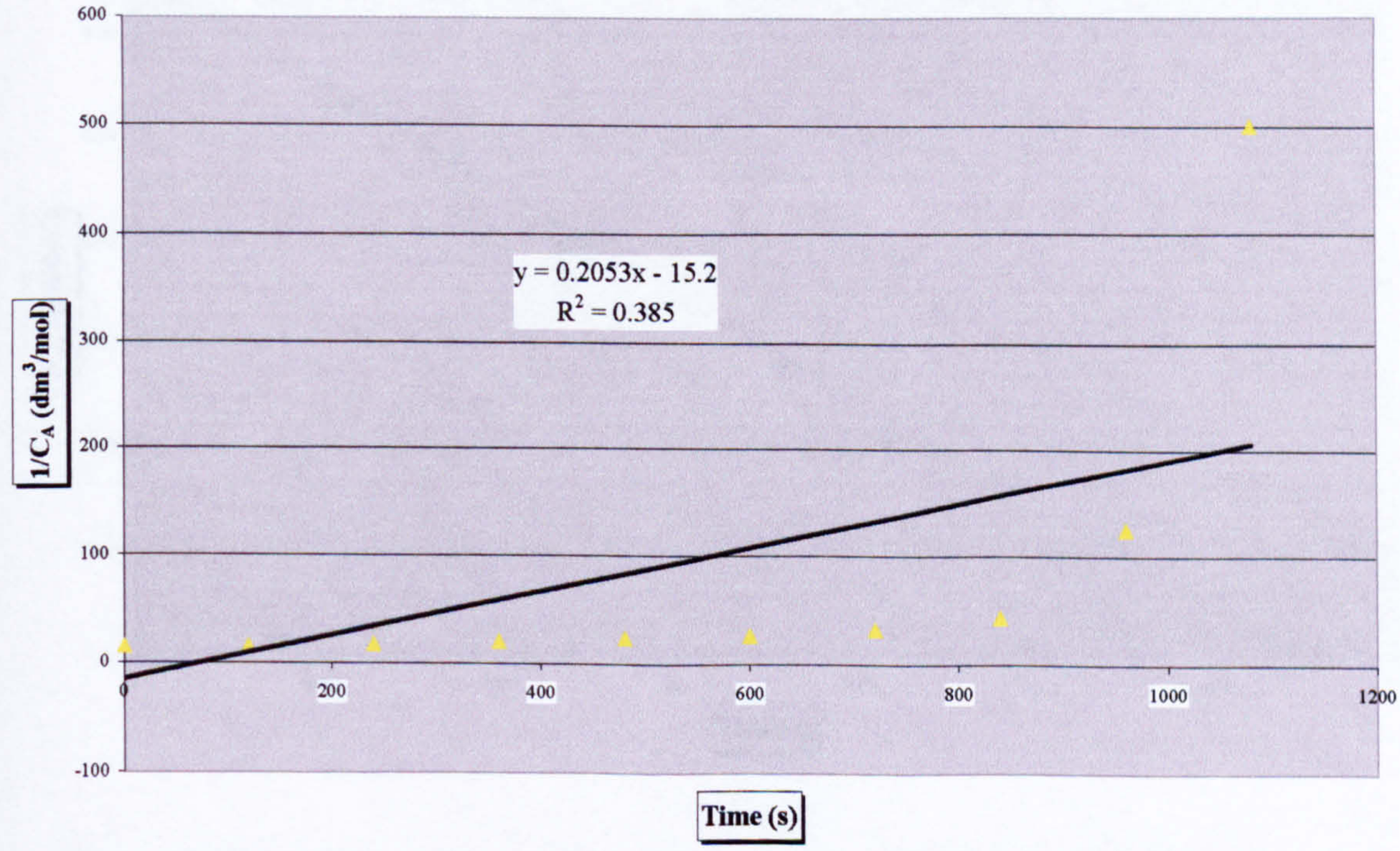


**Figure H.27. Fitting of experimental data for Catalyst 3 at 25$^0$C into a second order equation**

## H.3.2 BATCH REACTION AT 33$^0$C

**Table H.10. Data for Catalyst 3 at 33$^0$C**

| Time (s) | Concentration (mol/dm$^3$) | Conversion | Conversion (%) | $C_A$ (mol/dm$^3$) | $\ln(C_A/C_{A0})$ | $1/C_A$ (dm$^3$/mol) |
|---|---|---|---|---|---|---|
| 0 | 0.066 | 0 | 0 | 0.066 | 0 | 15.200 |
| 60 | 0.060 | 0.0880 | 8.80 | 0.060 | -0.0921 | 16.667 |
| 120 | 0.053 | 0.1944 | 19.44 | 0.053 | -0.2162 | 18.868 |
| 180 | 0.048 | 0.2704 | 27.04 | 0.048 | -0.3153 | 20.833 |
| 240 | 0.040 | 0.3920 | 39.20 | 0.040 | -0.4976 | 25.000 |
| 300 | 0.034 | 0.4832 | 48.32 | 0.034 | -0.6601 | 29.412 |
| 360 | 0.028 | 0.5744 | 57.44 | 0.028 | -0.8543 | 35.714 |
| 420 | 0.021 | 0.6808 | 68.08 | 0.021 | -1.1419 | 47.619 |
| 480 | 0.016 | 0.7568 | 75.68 | 0.016 | -1.4139 | 62.500 |
| 540 | 0.011 | 0.8328 | 83.28 | 0.011 | -1.7886 | 90.909 |
| 600 | 0.006 | 0.9088 | 90.88 | 0.006 | -2.3947 | 166.67 |
| 660 | 0.001 | 0.9848 | 98.48 | 0.001 | -4.1865 | 1000.0 |
| 720 | 0 | 1 | 100 | 0 | -34.120 | 1E+16 |
| 780 | 0 | 1 | 100 | 0 | -34.120 | 1E+16 |
| 840 | 0 | 1 | 100 | 0 | -34.120 | 1E+16 |

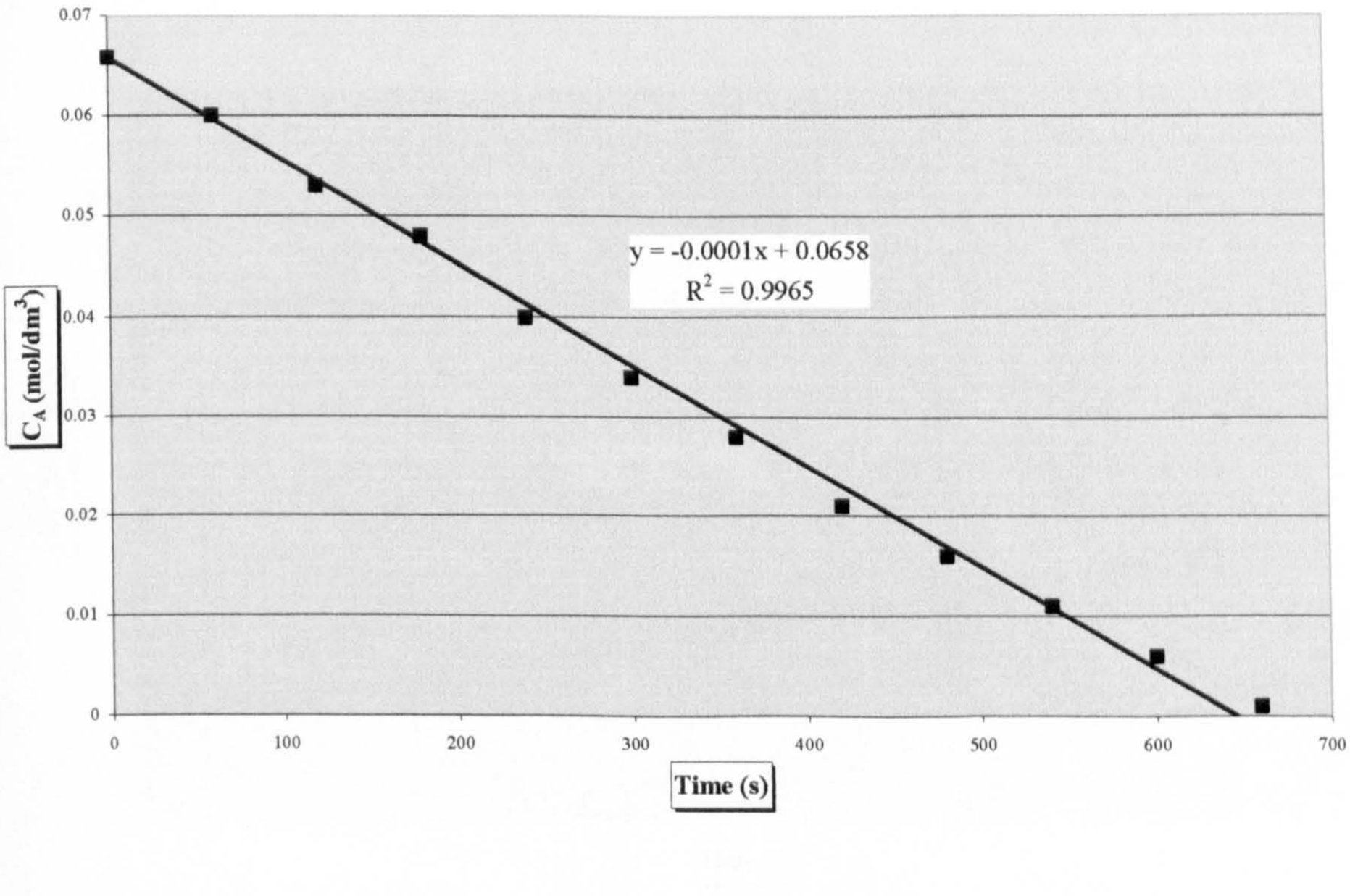


**Figure H.28. Fitting of experimental data for Catalyst 3 at 33$^0$C into a zero order equation**

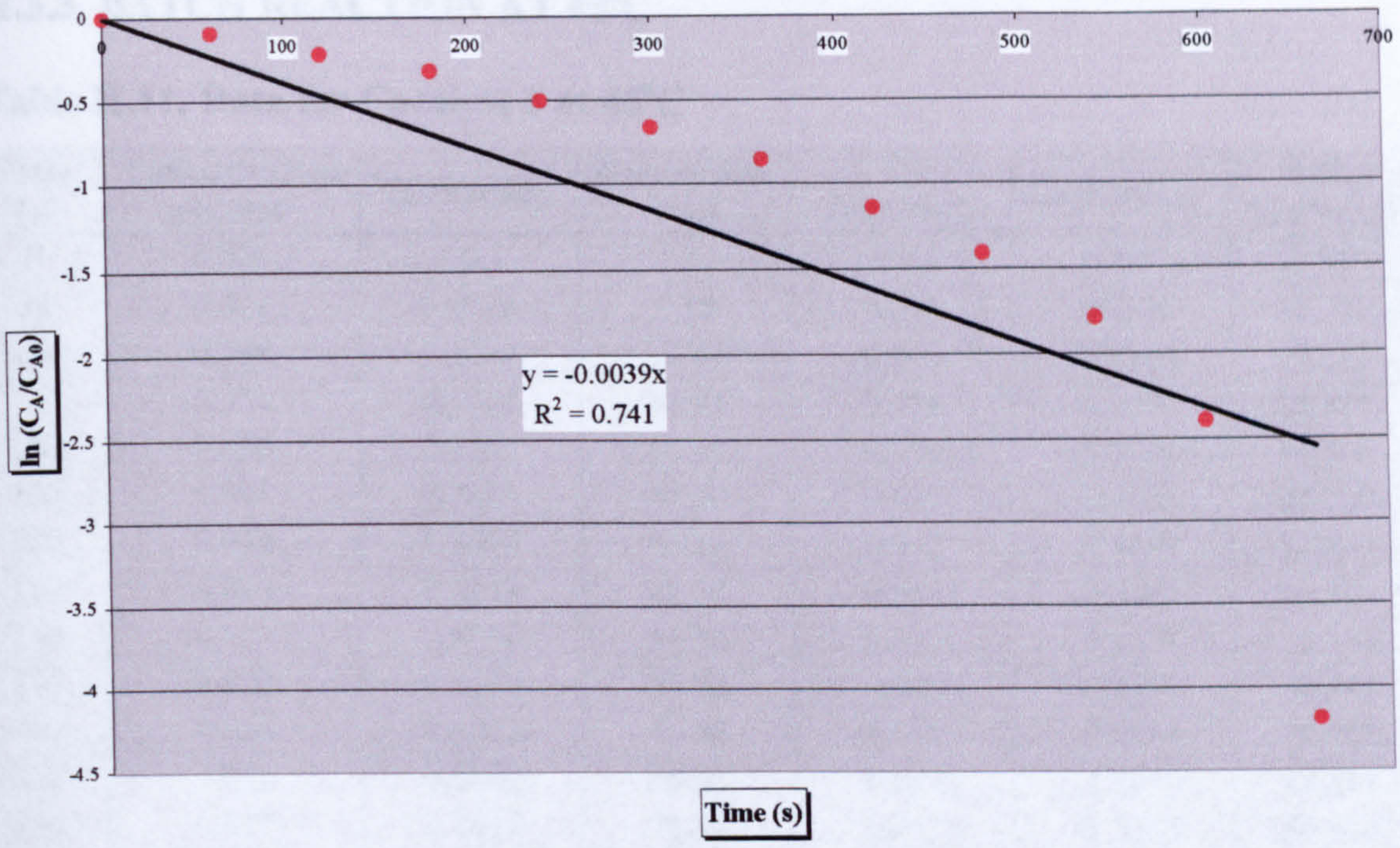


**Figure H.29. Fitting of experimental data for Catalyst 3 at 33$^0$C into a first order equation**

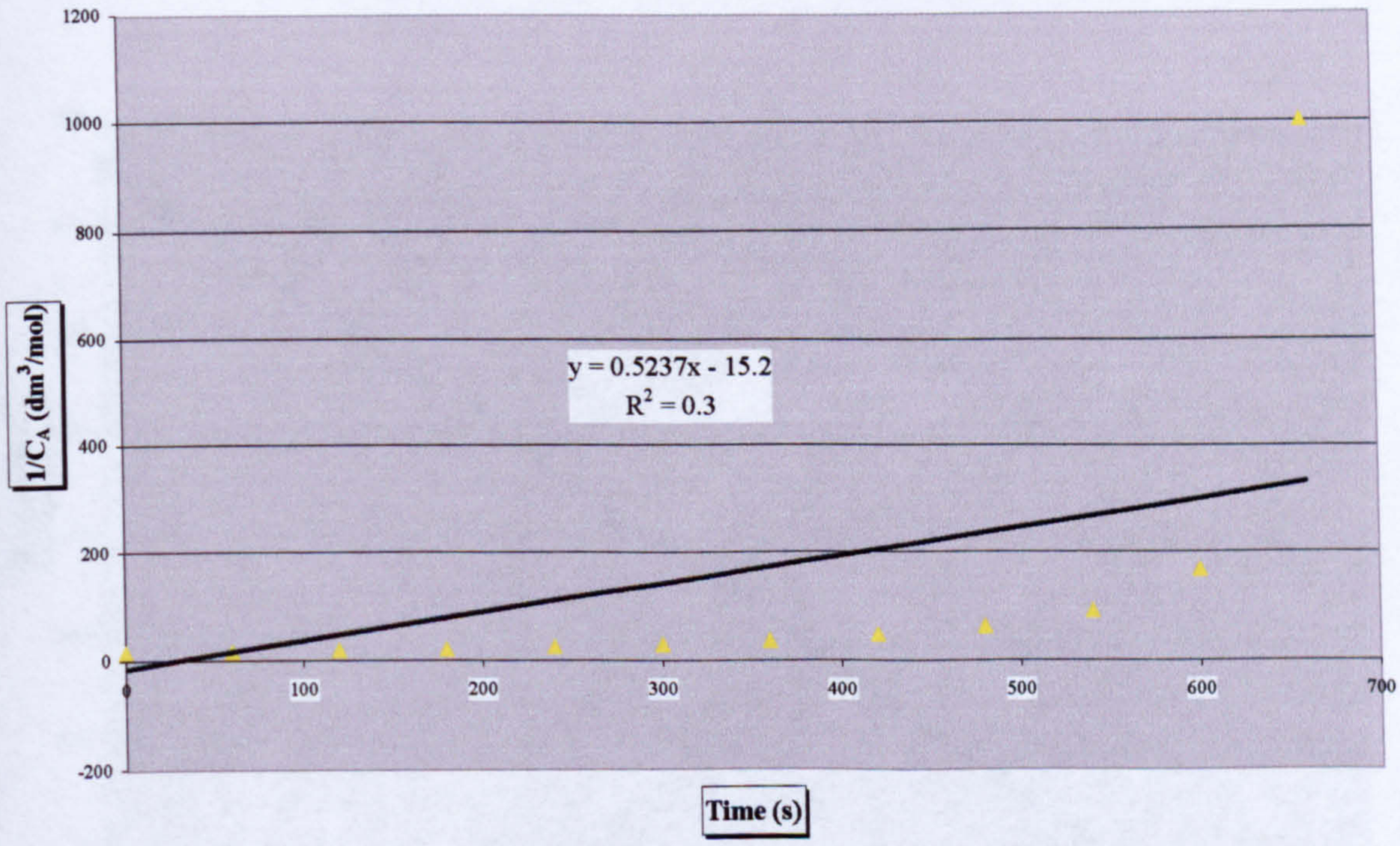


**Figure H.30. Fitting of experimental data for Catalyst 3 at 33$^0$C into a second order equation**

## H.3.3 BATCH REACTION AT 45$^0$C

### Table H.11. Data for Catalyst 3 at 45$^0$C

| Time (s) | Concentration (mol/dm$^3$) | Conversion | Conversion (%) | $C_A$ (mol/dm$^3$) | $\ln(C_A/C_{A0})$ | $1/C_A$ (dm$^3$/mol) |
|---|---|---|---|---|---|---|
| 0 | 0.066 | 0 | 0 | 0.066 | 0 | 15.200 |
| 30 | 0.061 | 0.0728 | 7.28 | 0.061 | -0.0756 | 16.393 |
| 60 | 0.058 | 0.1184 | 11.84 | 0.058 | -0.1260 | 17.241 |
| 90 | 0.054 | 0.1792 | 17.92 | 0.054 | -0.1975 | 18.518 |
| 120 | 0.050 | 0.2400 | 24.00 | 0.050 | -0.2744 | 20.000 |
| 150 | 0.047 | 0.2856 | 28.56 | 0.047 | -0.3363 | 21.277 |
| 180 | 0.042 | 0.3616 | 36.16 | 0.042 | -0.4488 | 23.809 |
| 210 | 0.038 | 0.4224 | 42.24 | 0.038 | -0.5489 | 26.316 |
| 240 | 0.032 | 0.5136 | 51.36 | 0.032 | -0.7207 | 31.250 |
| 270 | 0.029 | 0.5592 | 55.92 | 0.029 | -0.8190 | 34.483 |
| 300 | 0.026 | 0.6048 | 60.48 | 0.026 | -0.9284 | 38.462 |
| 330 | 0.021 | 0.6808 | 68.08 | 0.021 | -1.1419 | 47.619 |
| 360 | 0.017 | 0.7416 | 74.16 | 0.017 | -1.3532 | 58.824 |
| 390 | 0.012 | 0.8176 | 81.76 | 0.012 | -1.7016 | 83.333 |
| 420 | 0.007 | 0.8936 | 89.36 | 0.007 | -2.2405 | 142.86 |
| 450 | 0.001 | 0.9848 | 98.48 | 0.001 | -4.1865 | 1000.0 |
| 480 | 0.0001 | 0.9985 | 99.85 | 0.0001 | -6.4890 | 10000 |
| 510 | 0 | 1 | 100 | 0 | -34.120 | 1E+16 |
| 540 | 0 | 1 | 100 | 0 | -34.120 | 1E+16 |

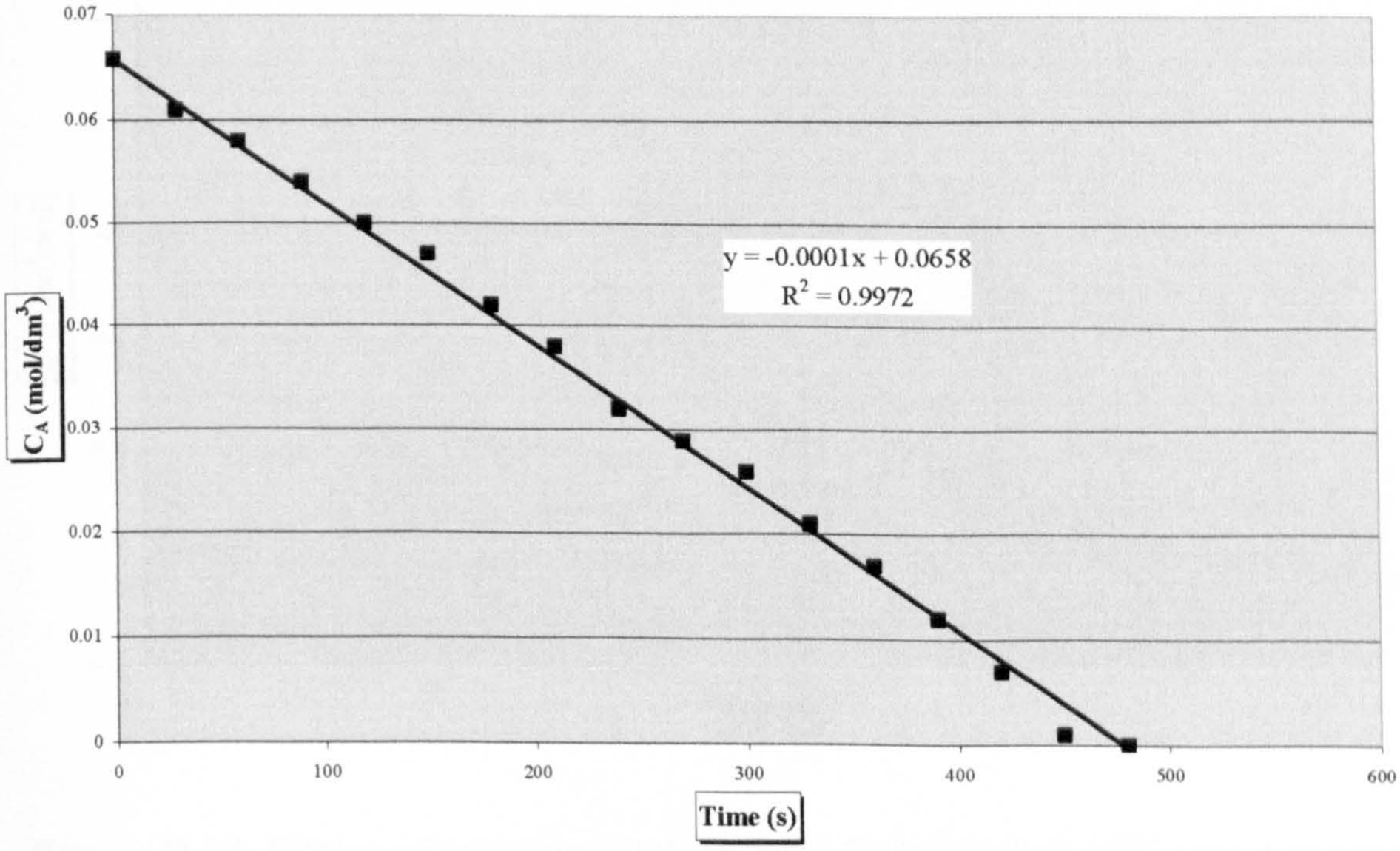


**Figure H.31. Fitting of experimental data for Catalyst 3 at 45$^0$C into a zero order equation**

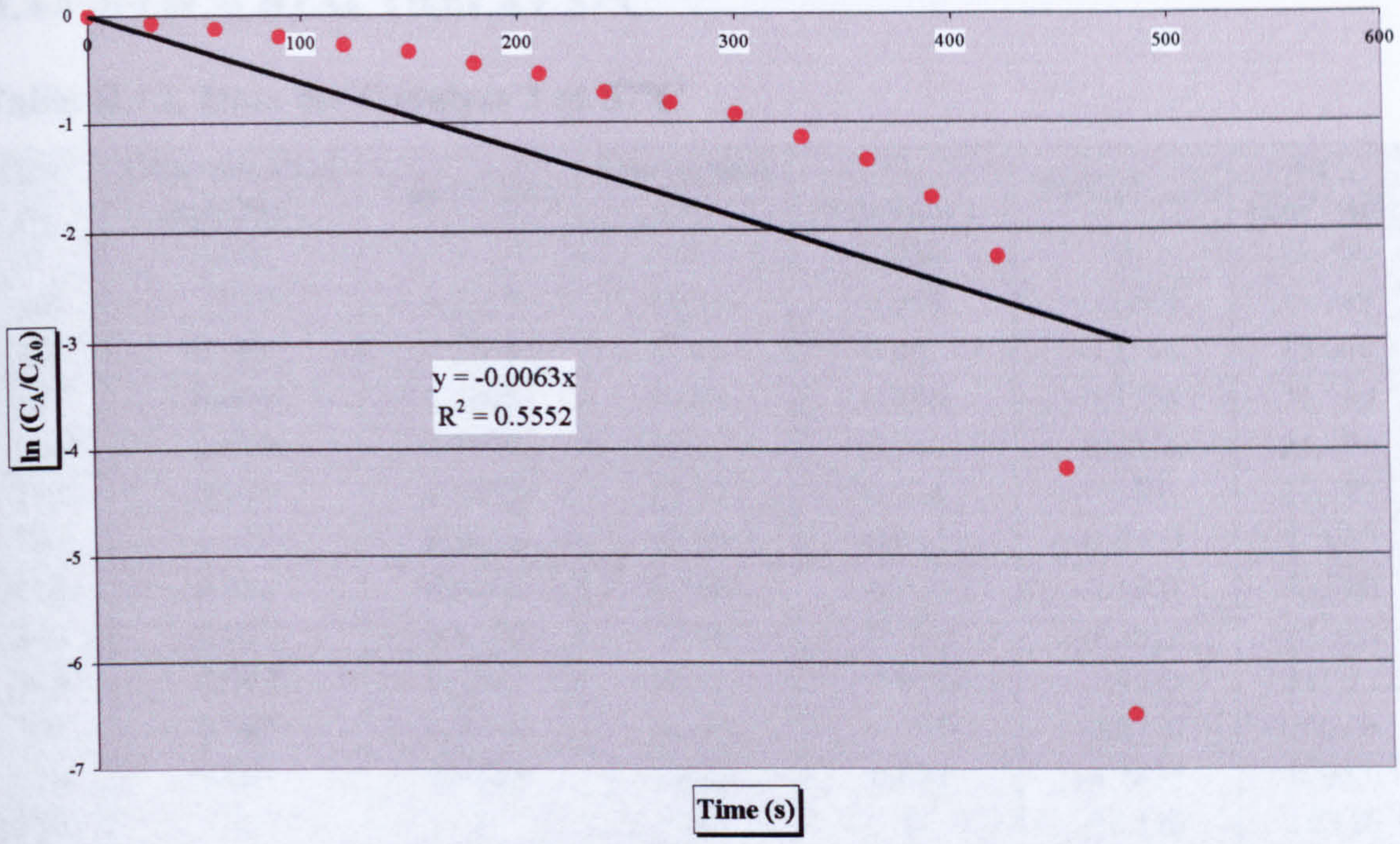


**Figure H.32. Fitting of experimental data for Catalyst 3 at 45$^0$C into a first order equation**

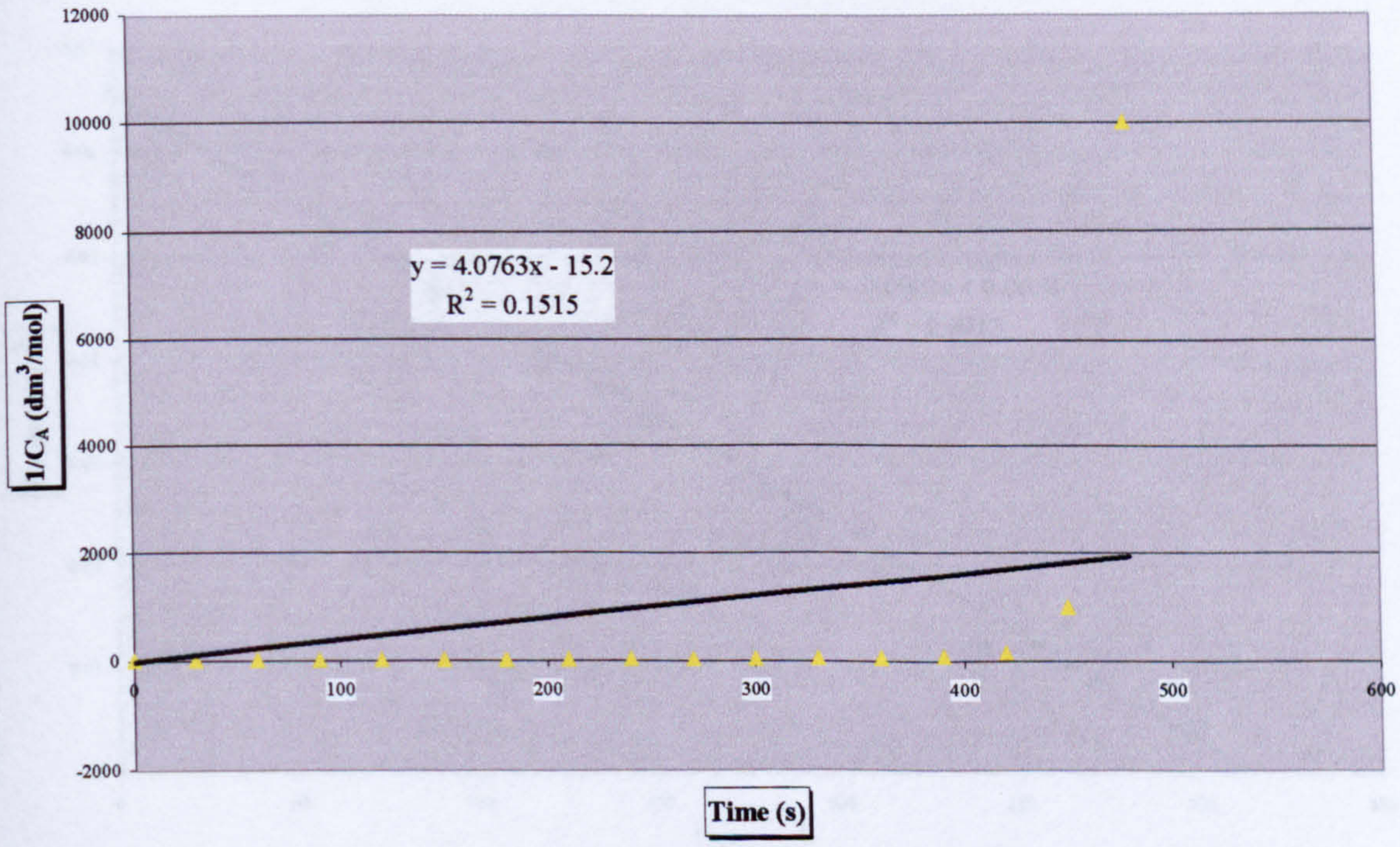


**Figure H.33. Fitting of experimental data for Catalyst 3 at 45$^0$C into a second order equation**

## H.3.4 BATCH REACTION AT 57$^0$C

### Table H.12. Data for Catalyst 3 at 57$^0$C

| Time (s) | Concentration (mol/dm$^3$) | Conversion | Conversion (%) | $C_A$ (mol/dm$^3$) | $\ln(C_A/C_{A0})$ | $1/C_A$ (dm$^3$/mol) |
|---|---|---|---|---|---|---|
| 0 | 0.066 | 0 | 0 | 0.066 | 0 | 15.200 |
| 30 | 0.059 | 0.1032 | 10.32 | 0.059 | -0.1089 | 16.949 |
| 60 | 0.051 | 0.2248 | 22.48 | 0.051 | -0.2546 | 19.608 |
| 90 | 0.046 | 0.3008 | 30.08 | 0.046 | -0.3578 | 21.739 |
| 120 | 0.040 | 0.3920 | 39.20 | 0.040 | -0.4976 | 25.000 |
| 150 | 0.034 | 0.4832 | 48.32 | 0.034 | -0.6601 | 29.412 |
| 180 | 0.027 | 0.5896 | 58.96 | 0.027 | -0.8900 | 37.037 |
| 210 | 0.020 | 0.6960 | 69.60 | 0.020 | -1.1907 | 50.000 |
| 240 | 0.012 | 0.8176 | 81.76 | 0.012 | -1.7015 | 83.333 |
| 270 | 0.009 | 0.8632 | 86.32 | 0.009 | -1.9892 | 111.11 |
| 300 | 0.005 | 0.9240 | 92.40 | 0.005 | -2.5770 | 200.00 |
| 330 | 0.001 | 0.9848 | 98.48 | 0.001 | -4.1865 | 1000.0 |
| 360 | 0 | 1 | 100 | 0 | -34.120 | 1E+16 |
| 390 | 0 | 1 | 100 | 0 | -34.120 | 1E+16 |
| 420 | 0 | 1 | 100 | 0 | -34.120 | 1E+16 |

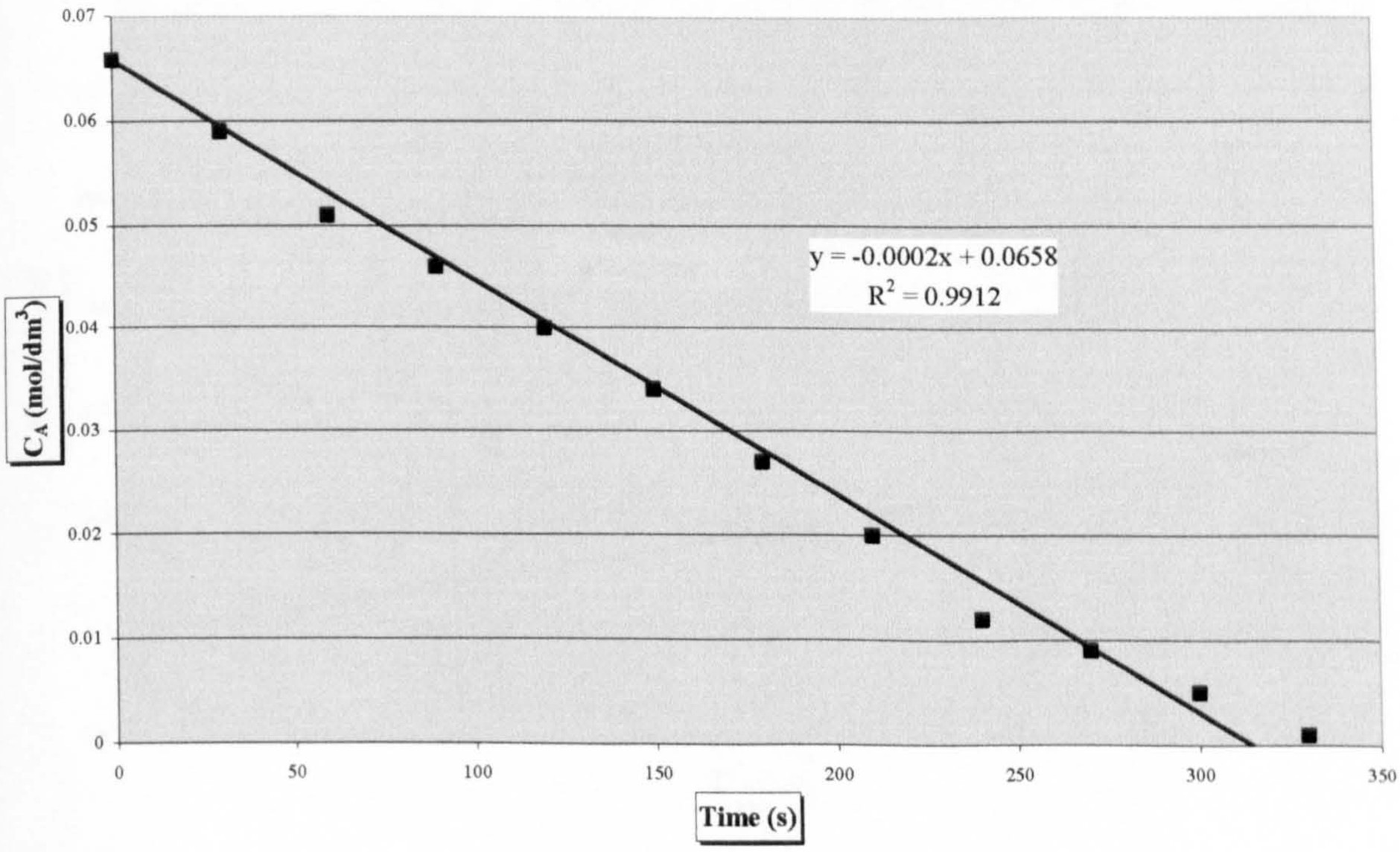


**Figure H.34. Fitting of experimental data for Catalyst 3 at 57$^0$C into a zero order equation**

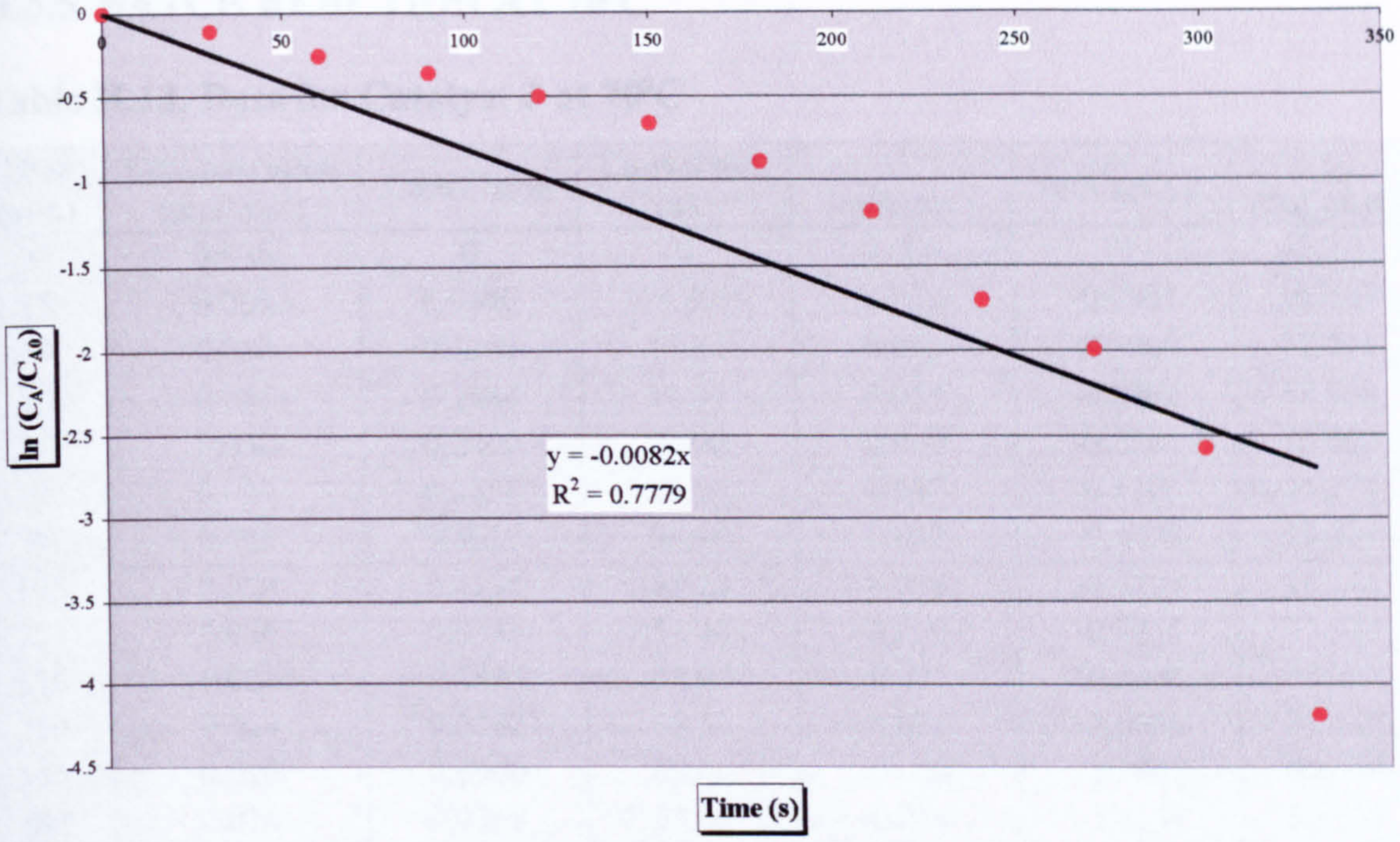


**Figure H.35. Fitting of experimental data for Catalyst 3 at 57$^0$C into a first order equation**

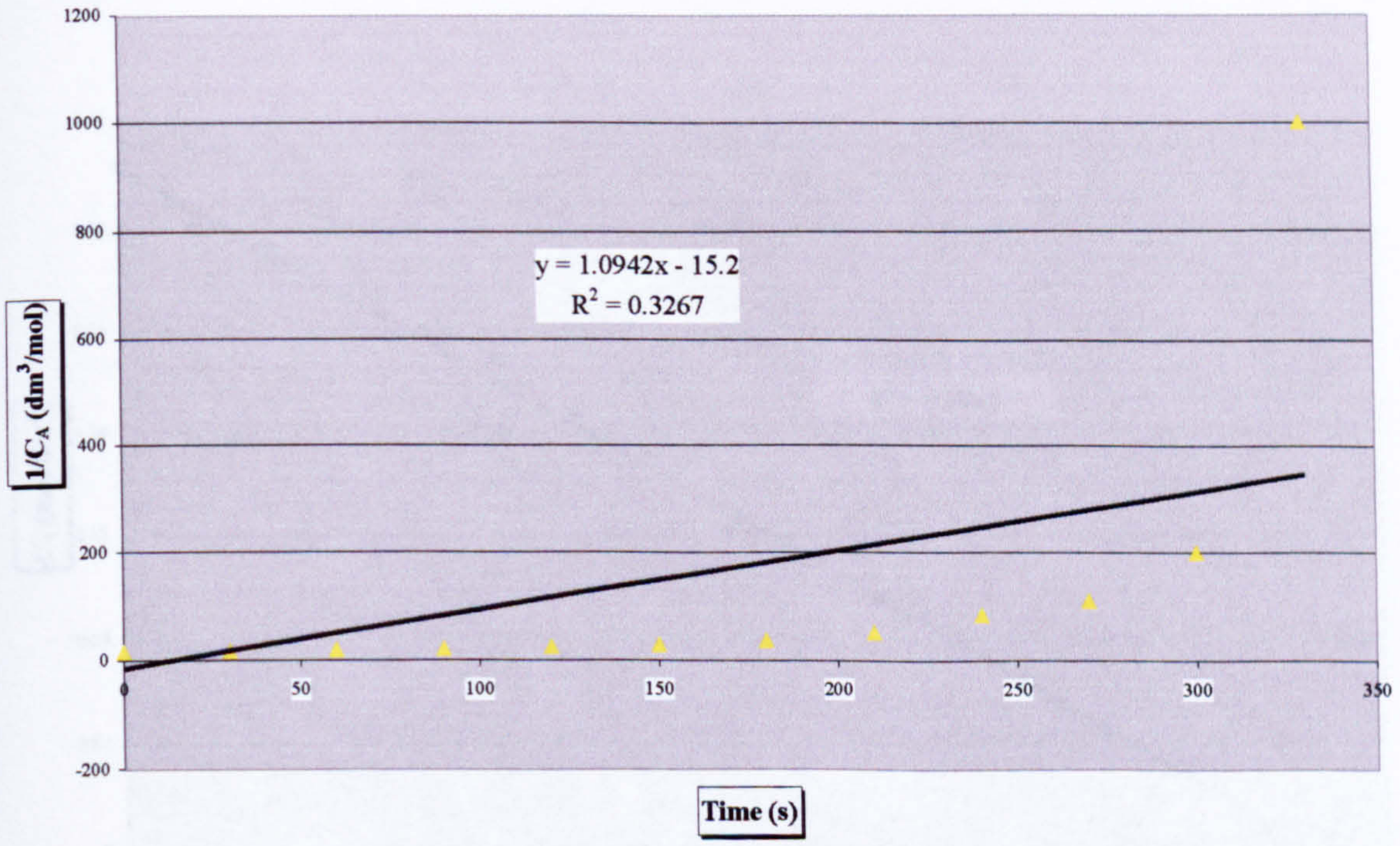


**Figure H.36. Fitting of experimental data for Catalyst 3 at 57$^0$C into a second order equation**

## H.3.5 BATCH REACTION AT 70$^0$C

### Table H.13. Data for Catalyst 3 at 70$^0$C

| Time (min) | Concentration (mol/dm$^3$) | Conversion | Conversion (%) | $C_A$ (mol/dm$^3$) | ln($C_A/C_{A0}$) | 1/$C_A$ (dm$^3$/mol) |
|---|---|---|---|---|---|---|
| 0 | 0.066 | 0 | 0 | 0.066 | 0 | 15.200 |
| 15 | 0.060 | 0.0880 | 8.80 | 0.060 | -0.0921 | 16.667 |
| 30 | 0.058 | 0.1184 | 11.84 | 0.058 | -0.1260 | 17.241 |
| 45 | 0.053 | 0.1944 | 19.44 | 0.053 | -0.2162 | 18.868 |
| 60 | 0.050 | 0.2400 | 24.00 | 0.050 | -0.2744 | 20.000 |
| 75 | 0.047 | 0.2856 | 28.56 | 0.047 | -0.3363 | 21.277 |
| 90 | 0.042 | 0.3616 | 36.16 | 0.042 | -0.4488 | 23.809 |
| 105 | 0.038 | 0.4224 | 42.24 | 0.038 | -0.5489 | 26.316 |
| 120 | 0.030 | 0.5440 | 54.40 | 0.030 | -0.7853 | 33.333 |
| 135 | 0.027 | 0.5896 | 58.96 | 0.027 | -0.8906 | 37.037 |
| 150 | 0.024 | 0.6352 | 63.52 | 0.024 | -1.0084 | 41.667 |
| 165 | 0.020 | 0.6960 | 69.60 | 0.020 | -1.1907 | 50.000 |
| 180 | 0.016 | 0.7568 | 75.68 | 0.016 | -1.4139 | 62.500 |
| 195 | 0.011 | 0.8328 | 83.28 | 0.011 | -1.7886 | 90.909 |
| 210 | 0.008 | 0.8784 | 87.84 | 0.008 | -2.1070 | 125.00 |
| 225 | 0.002 | 0.9696 | 96.96 | 0.002 | -3.4933 | 500.00 |
| 240 | 0 | 1 | 100 | 0 | -34.120 | 1E+16 |
| 255 | 0 | 1 | 100 | 0 | -34.120 | 1E+16 |
| 270 | 0 | 1 | 100 | 0 | -34.120 | 1E+16 |

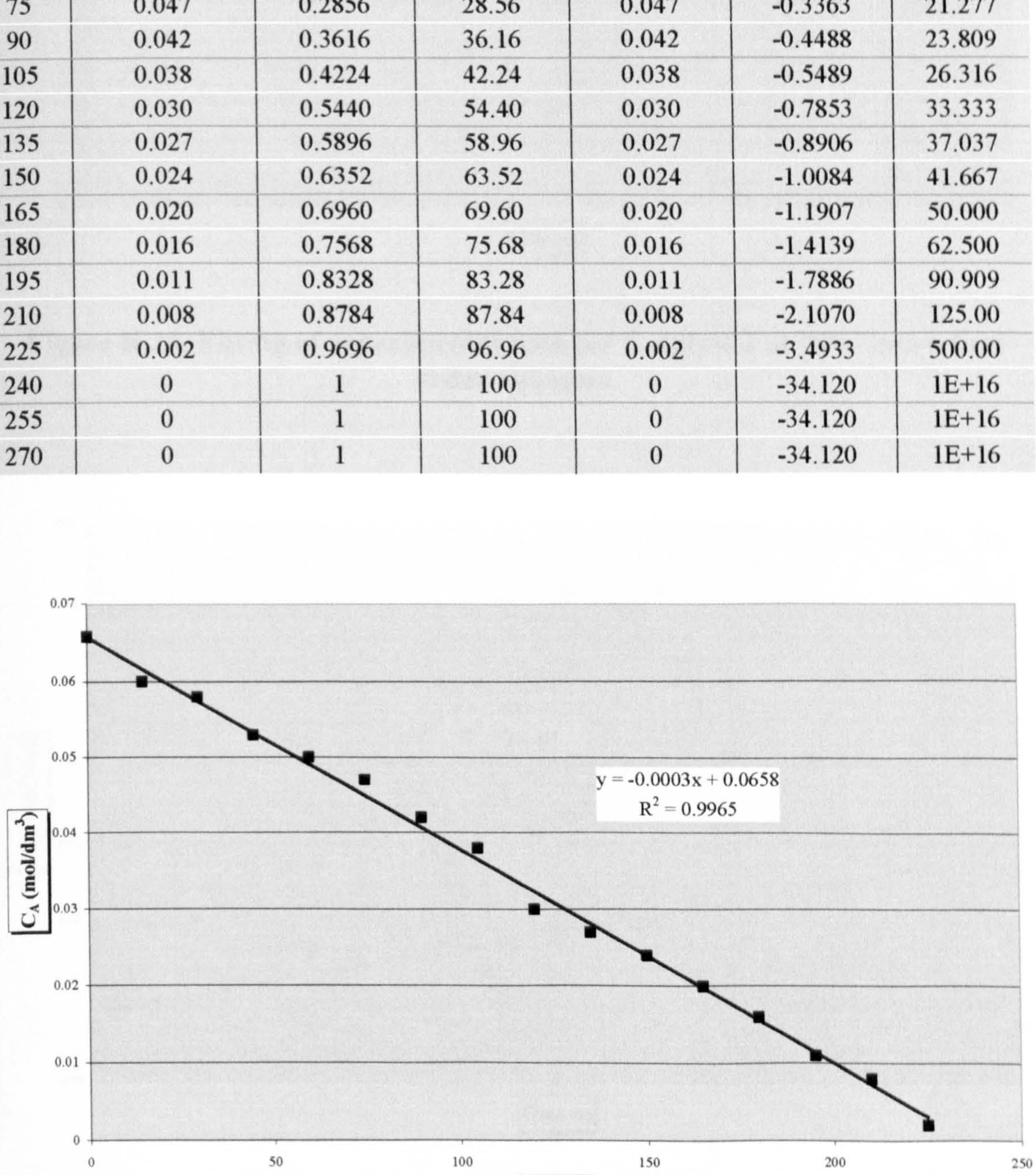


**Figure H.37. Fitting of experimental data for Catalyst 3 at 70$^0$C into a zero order equation**

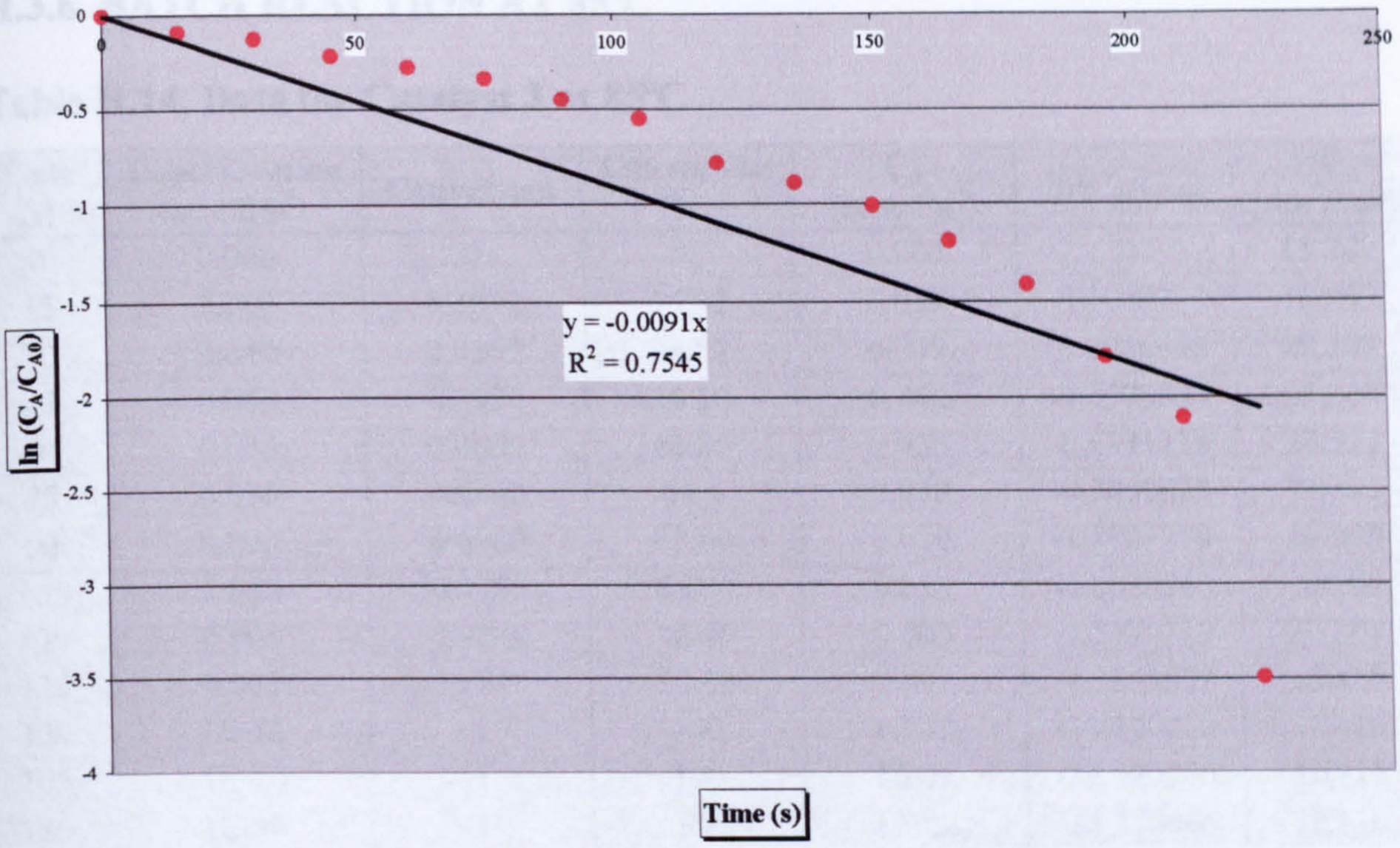


**Figure H.38. Fitting of experimental data for Catalyst 3 at 70$^0$C into a first order equation**

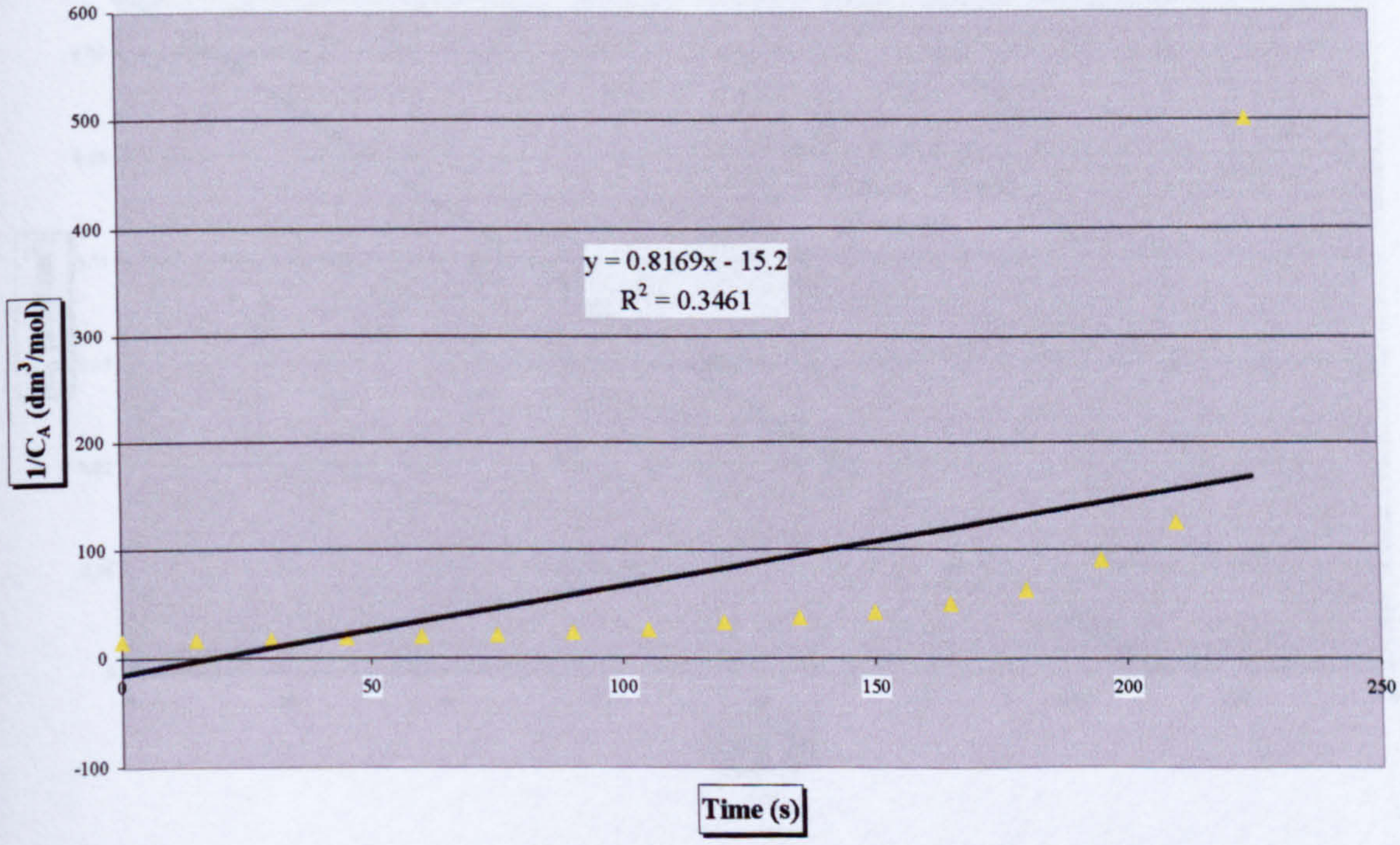


**Figure H.39. Fitting of experimental data for Catalyst 3 at 70$^0$C into a second order equation**

## H.3.6 BATCH REACTION AT 85$^0$C

### Table H.14. Data for Catalyst 3 at 85$^0$C

| Time (s) | Concentration (mol/dm$^3$) | Conversion | Conversion (%) | $C_A$ (mol/dm$^3$) | ln($C_A/C_{A0}$) | 1/$C_A$ (dm$^3$/mol) |
|---|---|---|---|---|---|---|
| 0 | 0.066 | 0 | 0 | 0.066 | 0 | 15.200 |
| 15 | 0.059 | 0.1032 | 10.32 | 0.059 | -0.1089224 | 16.949 |
| 30 | 0.049 | 0.2552 | 25.52 | 0.049 | -0.2946396 | 20.408 |
| 45 | 0.040 | 0.3920 | 39.20 | 0.040 | -0.4975804 | 25.000 |
| 60 | 0.035 | 0.4680 | 46.80 | 0.035 | -0.6311118 | 28.571 |
| 75 | 0.030 | 0.5440 | 54.4 | 0.030 | -0.7852625 | 33.333 |
| 90 | 0.020 | 0.6960 | 69.60 | 0.020 | -1.1907276 | 50.000 |
| 105 | 0.010 | 0.8480 | 84.80 | 0.010 | -1.8838748 | 100.00 |
| 120 | 0.005 | 0.9240 | 92.40 | 0.005 | -2.5770219 | 200.00 |
| 135 | 0.001 | 0.9848 | 98.48 | 0.001 | -4.1864599 | 1000.0 |
| 150 | 1E-16 | 1 | 100 | 1E-16 | -34.120066 | 1E+16 |
| 165 | 1E-16 | 1 | 100 | 1E-16 | -34.120066 | 1E+16 |
| 180 | 1E-16 | 1 | 100 | 1E-16 | -34.120066 | 1E+16 |

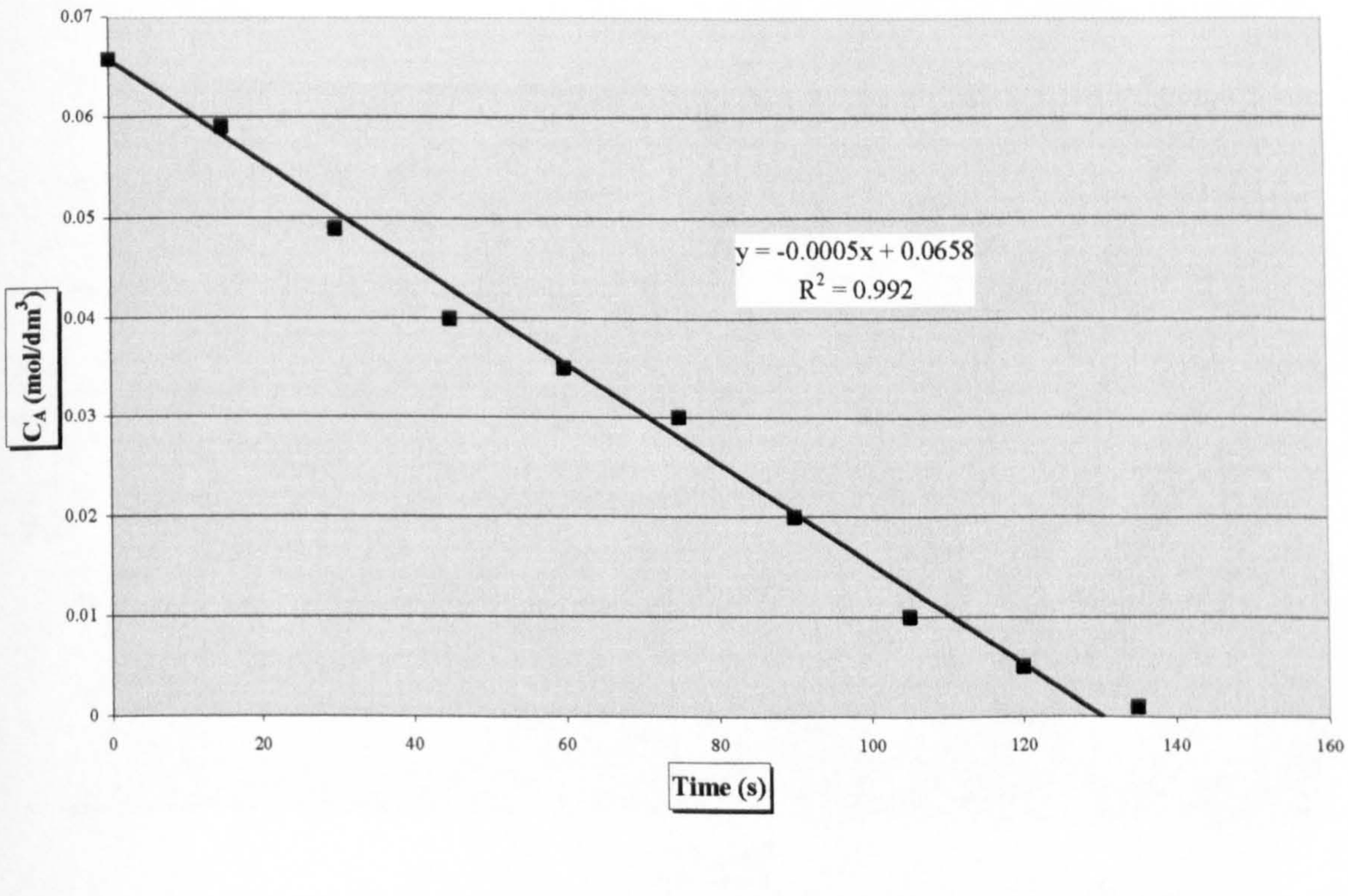


**Figure H.40. Fitting of experimental data for Catalyst 3 at 85$^0$C into a zero order equation**

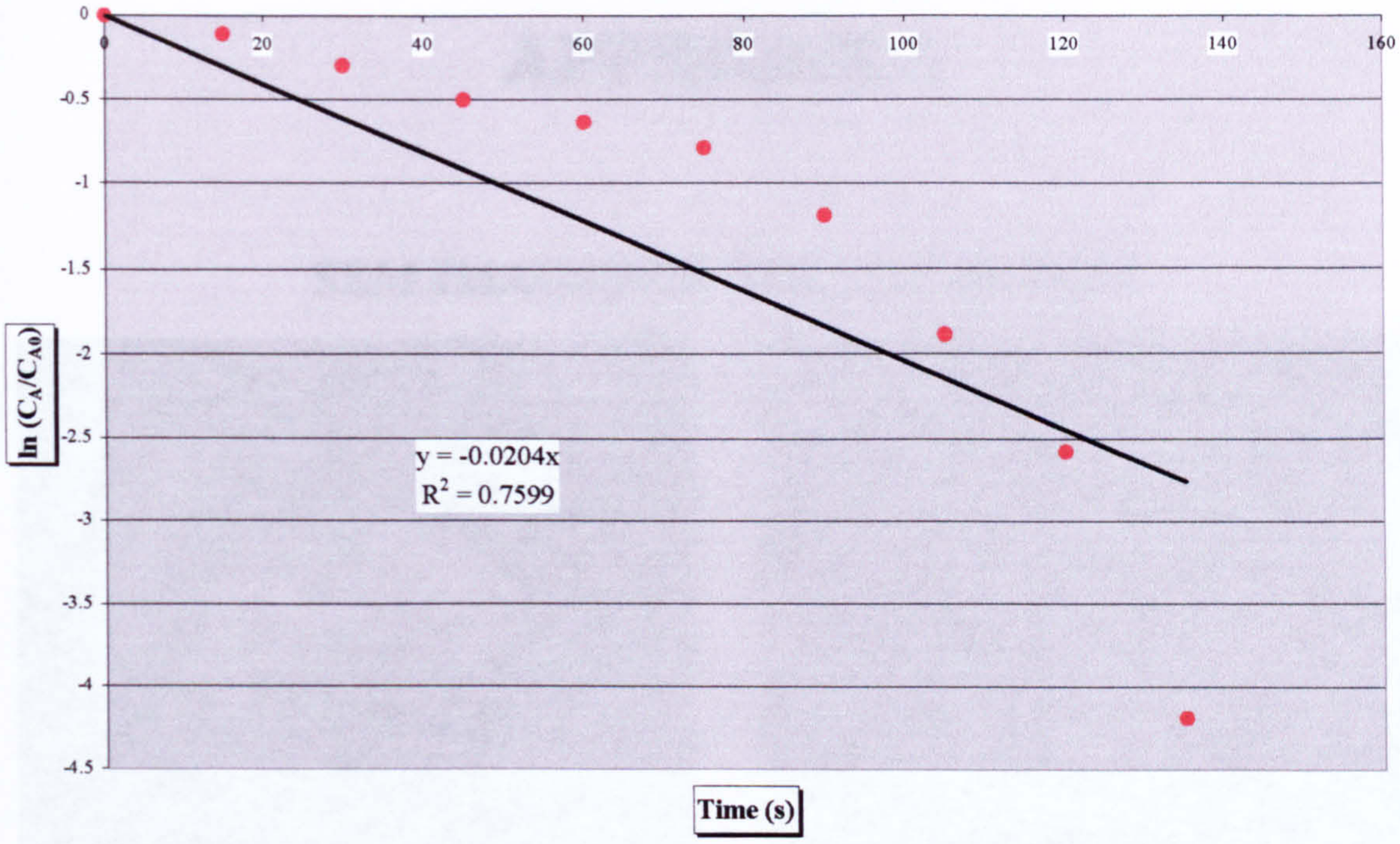


**Figure H.41. Fitting of experimental data for Catalyst 3 at 85$^0$C into a first order equation**

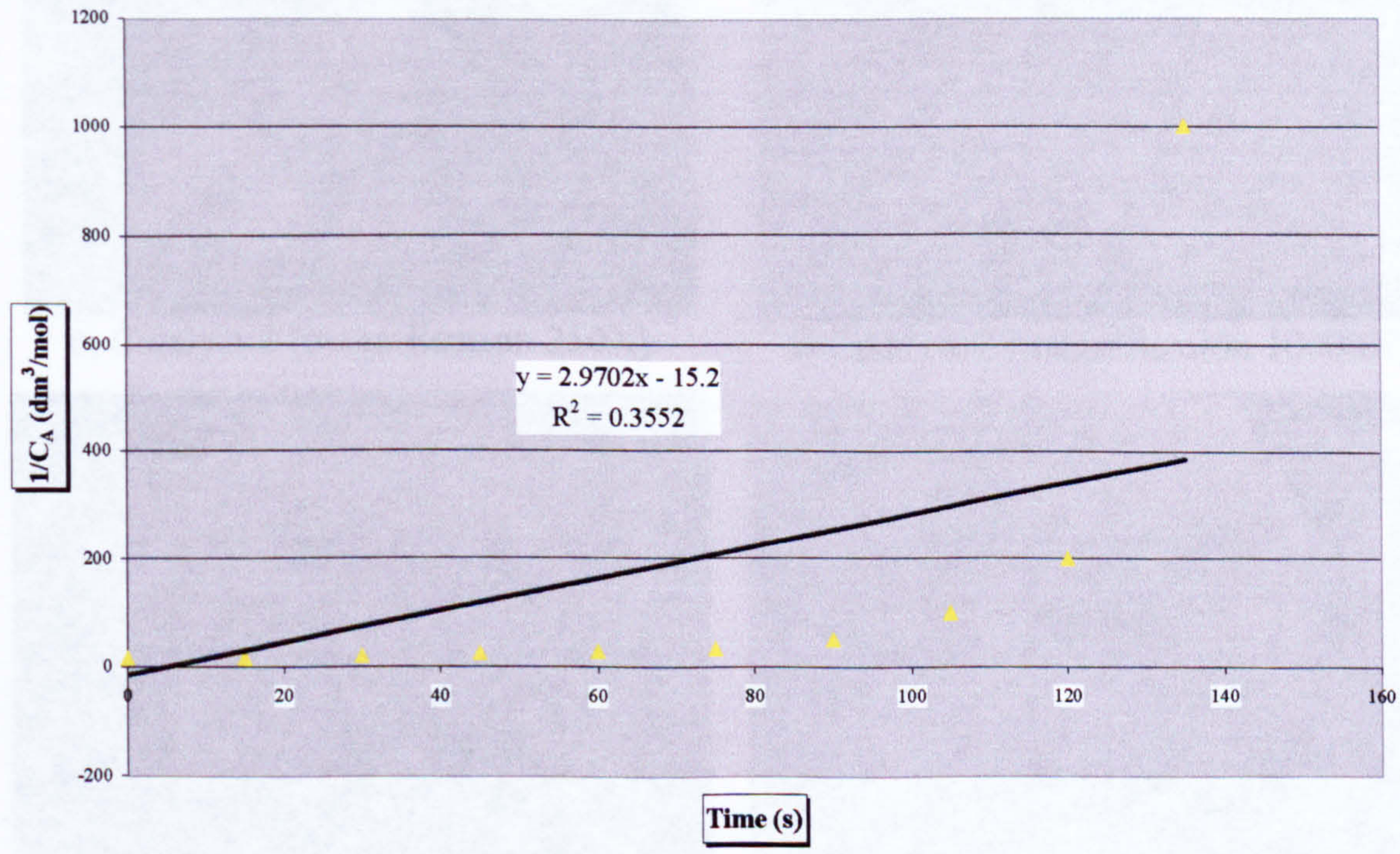


**Figure H.42. Fitting of experimental data for Catalyst 3 at 85$^0$C into a second order equation**

# APPENDIX I

## SEM IMAGES OF THE CATALYSTS

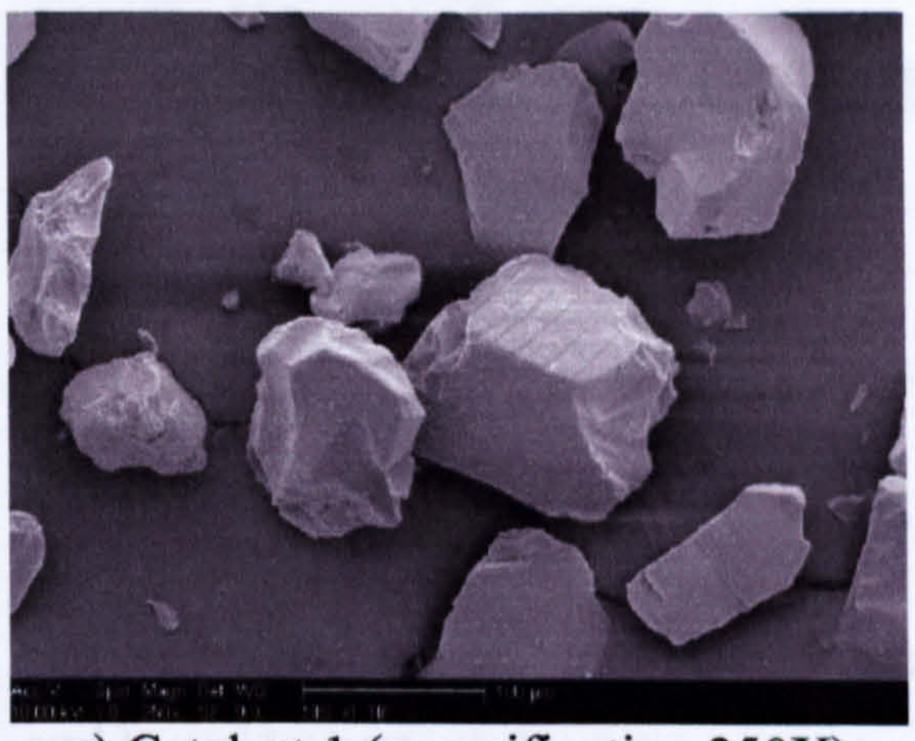

a) Catalyst 1 (magnification 250X)

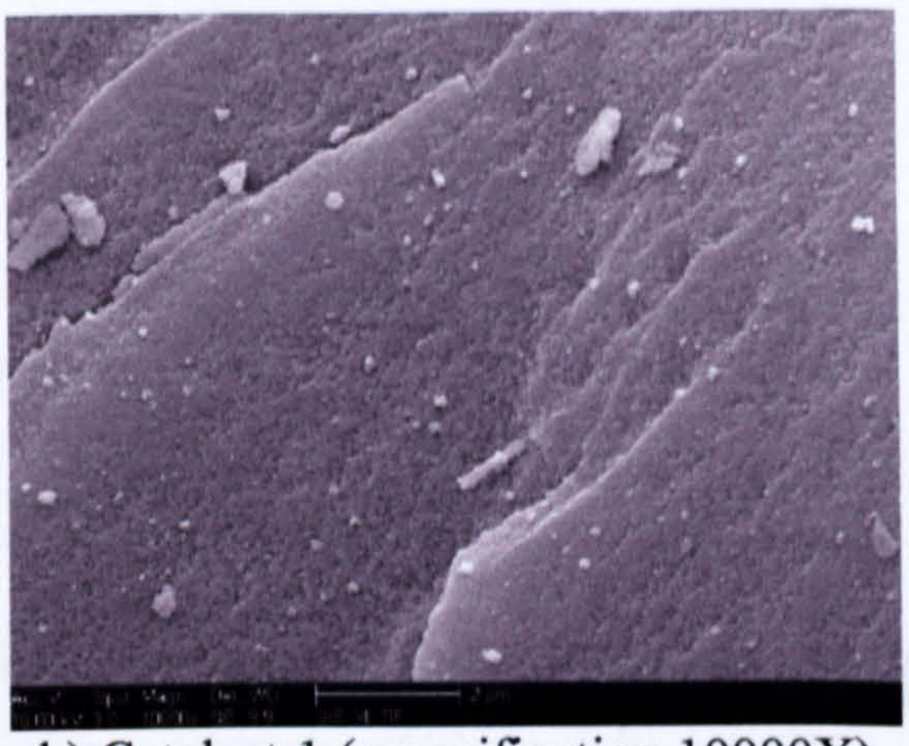

b) Catalyst 1 (magnification 10000X)

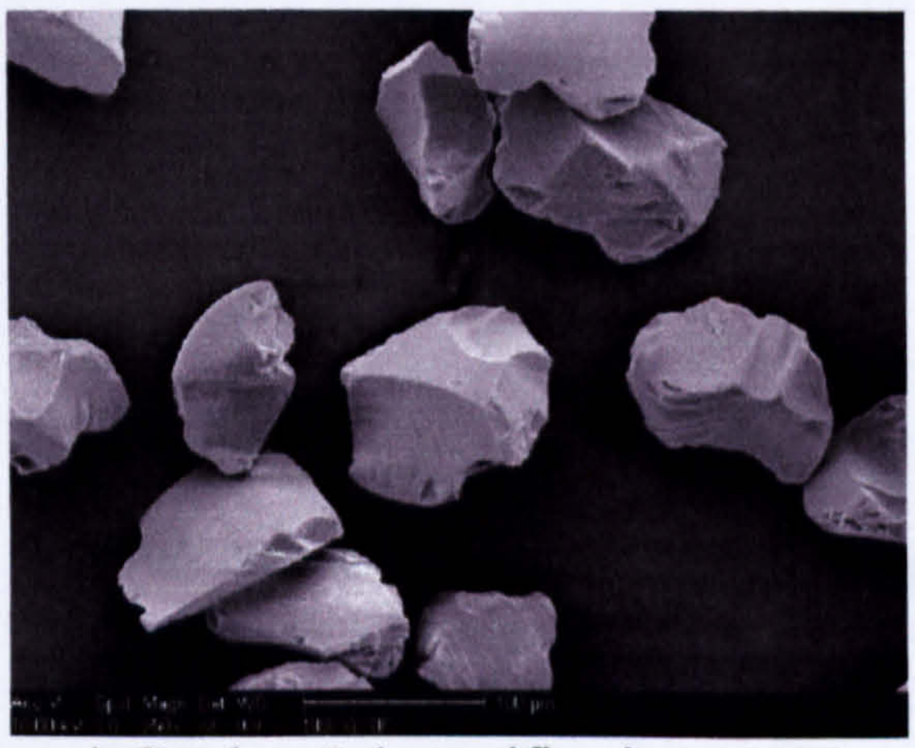

c) Catalyst 2 (magnification 250X)

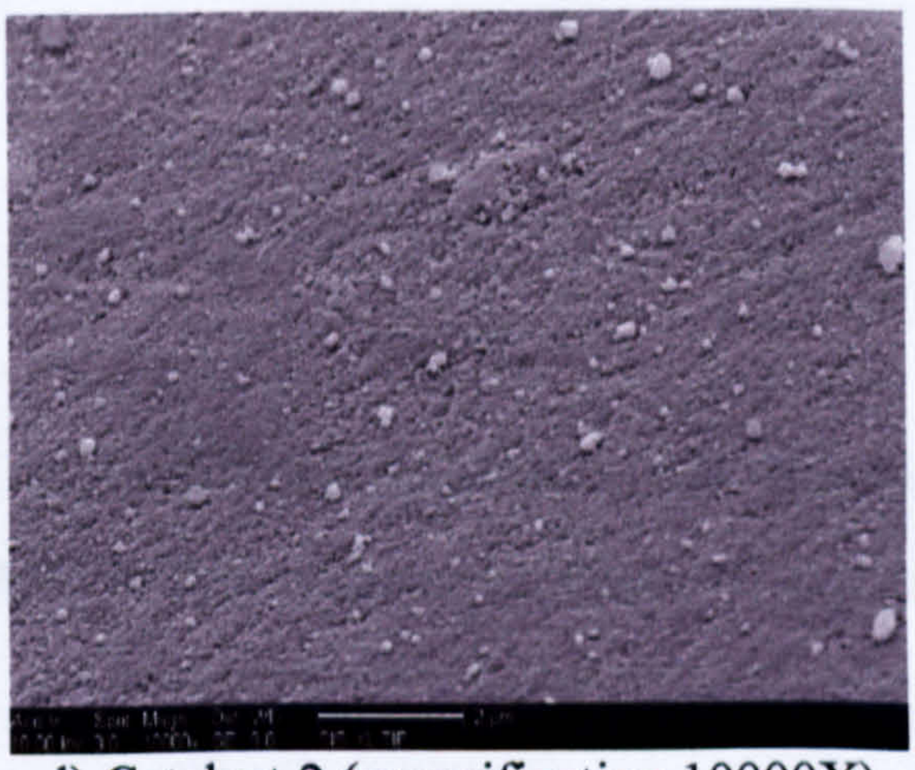

d) Catalyst 2 (magnification 10000X)

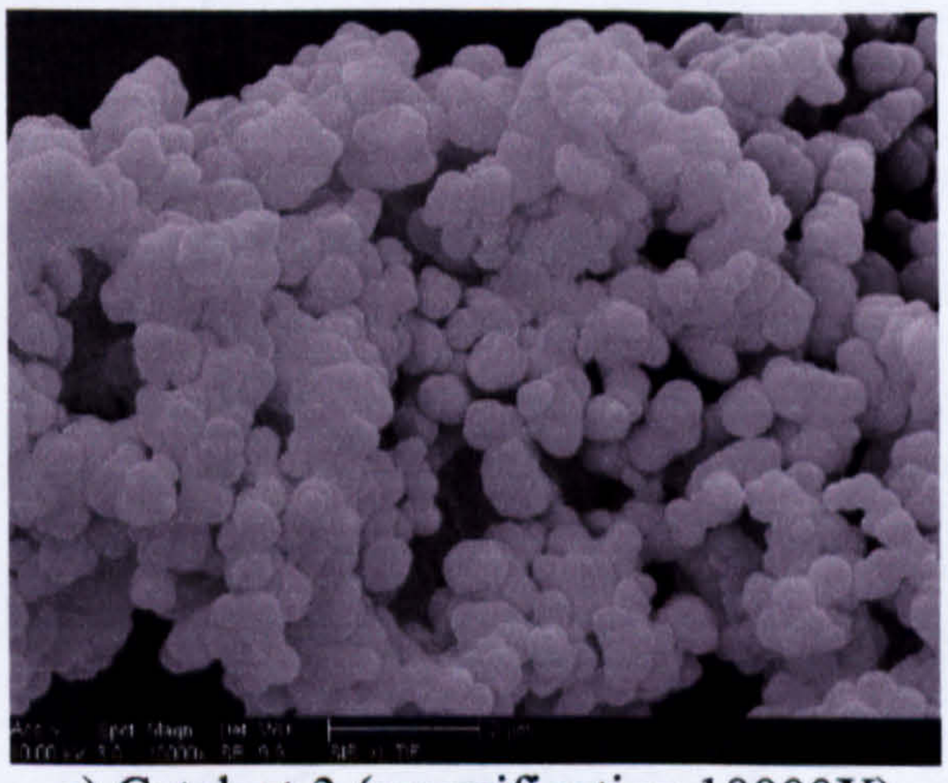

e) Catalyst 3 (magnification 10000X)

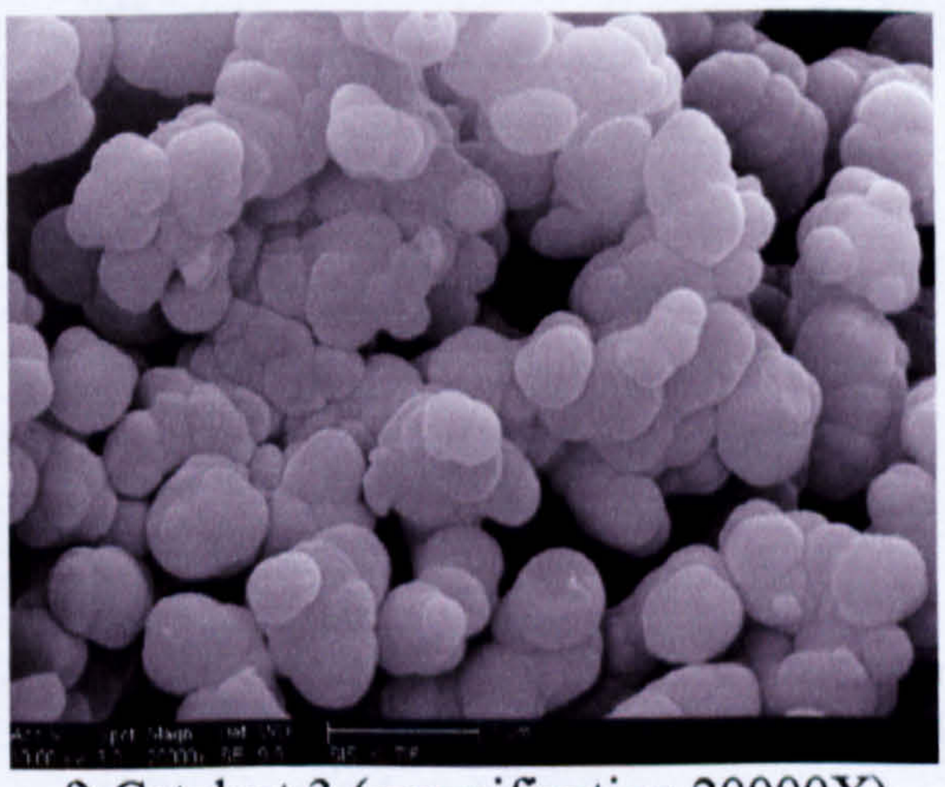

f) Catalyst 3 (magnification 20000X)

**Figure I.1. SEM images of all the catalysts**

# APPENDIX J

## SOLVING COMPLEX REACTIONS

### J.1 OPTIMUM CONTACT TIME

If a complex reaction:

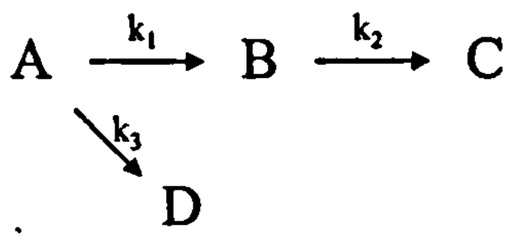


is considered for a maximum yield regarding component B and rate constants $k_1$, $k_2$ and $k_3$ are known, optimum contact time (residence time), $\tau_C$, can be found from the condition:

$$\frac{dC_B}{d\tau_C}=0 \qquad (j.1)$$

For the purpose of the exercise let us consider all the steps in this complex reaction are elementary, hence the rate expression regarding component A can be written as:

$$(-r_A)=k_1 C_A + k_3 C_A = (k_1+k_3)C_A = -\frac{dC_A}{d\tau_C} \qquad (j.2)$$

After rearrangement:

$$\frac{dC_A}{C_A}=-(k_1+k_3)d\tau_C \qquad (j.3)$$

$C_A$ can be expressed from (j.3) as:

$$C_A = C_{A0}\, e^{-(k_1+k_3)\tau_C}. \qquad (j.4)$$

Rate of forming of component B is:

$$(r_B) = k_1 C_A - k_2 C_B = \frac{dC_B}{d\tau_C} \qquad (j.5)$$

or, after rearrangement and integration:

$$\frac{dC_B}{d\tau_C} + k_2 C_B = k_1 C_{A0} e^{-(k_1+k_3)\tau_C} \qquad (j.6)$$

$$C_B = e^{-\int k_2 d\tau_C}\left[\left(\int k_1 C_{A0} e^{-(k_1+k_3)\tau_C}\right)\left(e^{\int k_2 d\tau_C} d\tau_C\right) + C\right] \qquad (j.7)$$

$$C_B = e^{-k_2\tau_C}\left[\left(\int k_1 C_{A0} e^{(k_2-k_1-k_3)\tau_C} d\tau_C\right) + C\right] \qquad (j.8)$$

$$C_B = e^{-k_2\tau_C}\left[\frac{k_1}{k_2-k_1-k_3} C_{A0} e^{(k_2-k_1-k_3)\tau_C} + C\right], \qquad (j.9)$$

where C is the integration constant and can be calculated from the boundary conditions; on the entry to the reactor $\tau_C = 0$; $C_A = C_{A0}$ and $C_B = C_{B0} = 0$, hence:

$$0 = \frac{k_1 C_{A0}}{k_2-k_1-k_3} + C \quad \Rightarrow \quad C = -\frac{k_1 C_{A0}}{k_2-k_1-k_3} \qquad (j.10)$$

Now we can replace the expression (j.10) in equation (j.9):

$$C_B = e^{-k_2\tau_C}\frac{k_1 C_{A0}}{k_2-k_1-k_3}\left[e^{(k_2-k_1-k_3)\tau_C} - 1\right] \qquad (j.11)$$

$$C_B = \frac{k_1 C_{A0}}{k_2-k_1-k_3}\left[e^{-(k_1+k_3)\tau_C} - e^{-k_2\tau_C}\right] \qquad (j.12)$$

$$\frac{dC_B}{d\tau_C} = 0 = \frac{k_1 C_{A0}}{k_2-k_1-k_3}\left[-(k_1+k_3) e^{-(k_1+k_3)\tau_C} + k_2 e^{-k_2\tau_C}\right] \qquad (j.13)$$

$$e^{(k_2-k_1-k_3)\tau_C} = \frac{k_2}{k_1+k_3} \qquad (j.14)$$

Finally, contact time can be calculated as:

$$\tau_{C,opt} = \frac{\ln \frac{k_2}{k_1 + k_3}}{k_2 - k_1 - k_3} \qquad \text{(j.15)}$$

# APPENDIX K

## SCALING CALCULATIONS

### K.1 INTRODUCTION

The following section provides description of scaling methods usually used to scale up/down SDR from the pilot operation to the industrial utilisation. Methods used for the scaling up are described by Burns in [K1].

### K.2 SCALING METHODS

Scaling-up is usually employed to analyse the size of the spinning disc needed to achieve same performance with different flow rate of the liquid and/or different disc rotational speed. In scaling-up of a SDR process it is assumed that liquid properties, such as density and viscosity are constant and that radius of the disc is altered. Parameters available for modification are liquid flow rate and rotational speed.

The scaling factor, *S*, for the system is defined as:

$$S = \frac{r_2}{r_1} \tag{k.1}$$

where:

$r_2$ – disc radius in an industrial plant;

$r_1$ – disc radius in a pilot plant.

The following sections provide scaling methods that link the two remaining parameters to the scaling factor *S*.

#### K.2.1 SCALING WITH RESIDENCE TIME AND FILM THICKNESS CONSTANT

Using the expressions for film thickness and residence time given by centrifugal model equations (3.16) and (3.18), and assuming that liquid properties do

not change, following equations can be developed in order to preserve residence time and average film thickness.

From the constant residence time condition:

$$\left(\frac{81\pi^2 \nu r_1^4}{16 Q_1^2 \omega_1^2}\right)=\left(\frac{81\pi^2 \nu r_2^4}{16 Q_2^2 \omega_2^2}\right) \quad \text{(k.2)}$$

$$\left(\frac{r_1^4}{Q_1^2 \omega_1^2}\right)=\left(\frac{r_2^4}{Q_2^2 \omega_2^2}\right) \quad \text{(k.3)}$$

Hence flow rate in an industrial plant can be expressed as:

$$Q_2 = S^2 \frac{\omega_1 Q_1}{\omega_2} \quad \text{(k.4)}$$

From the constant film thickness condition:

$$\left(\frac{3\nu Q_1}{2\pi \omega_1^2 r_1^2}\right)=\left(\frac{3\nu Q_2}{2\pi \omega_2^2 r_2^2}\right) \quad \text{(k.5)}$$

$$\left(\frac{Q_1}{r_1^2 \omega_1^2}\right)=\left(\frac{Q_2}{r_2^2 \omega_2^2}\right) \quad \text{(k.6)}$$

Substituting expression for $Q_2$ from the equation (k.4) into equation (k.6), following is derived:

$$\left(\frac{Q_1}{r_1^2 \omega_1^2}\right)=\left(\frac{S^2 \frac{\omega_1 Q_1}{\omega_2}}{r_2^2 \omega_2^2}\right) \quad \text{(k.7)}$$

$$\omega_2 = \omega_1 \quad \text{(k.8)}$$

And therefore equation (k.6) can be expressed as:

$$Q_2 = S^2 Q_1 \quad \text{(k.9)}$$

These expressions imply that in order to keep the same values for residence time and film thickness, rotational speed should remain constant but if disc radius is changed for factor *S*, liquid flow rate should be changed (increased/decreased) in proportion to the scaling factor (i.e. $S^2$).

### K.2.2 SCALING WITH HALF OF THE ORIGINAL RESIDENCE TIME AND CONSTANT FILM THICKNESS

For the rearrangement reaction of α-pinene oxide it would be appropriate to look into smaller residence times, as the reaction was promoted further than needed. Therefore following expressions can be derived.

From the half residence time condition:

$$\left(\frac{81\pi^2 \nu r_1^4}{16 Q_1^2 \omega_1^2}\right)=\frac{1}{2}\left(\frac{81\pi^2 \nu r_2^4}{16 Q_2^2 \omega_2^2}\right) \qquad \text{(k.10)}$$

$$\left(\frac{r_1^4}{Q_1^2 \omega_1^2}\right)=\frac{1}{2}\left(\frac{r_2^4}{Q_2^2 \omega_2^2}\right) \qquad \text{(k.11)}$$

The flow rate in an industrial plant can be presented as:

$$Q_2=\frac{1}{\sqrt{2}} S^2 \frac{\omega_1 Q_1}{\omega_2} \qquad \text{(k.12)}$$

From the constant film thickness condition:

$$\left(\frac{3\nu Q_1}{2\pi \omega_1^2 r_1^2}\right)=\left(\frac{3\nu Q_2}{2\pi \omega_2^2 r_2^2}\right) \qquad \text{(k.13)}$$

$$\left(\frac{Q_1}{r_1^2 \omega_1^2}\right)=\left(\frac{Q_2}{r_2^2 \omega_2^2}\right) \qquad \text{(k.14)}$$

Combining equations (k.12) and (k.14), following can be derived:

$$\left(\frac{Q_1}{r_1^2\,\omega_1^2}\right)=\left(\frac{\frac{1}{\sqrt{2}}S^2\,\frac{\omega_1 Q_1}{\omega_2}}{r_2^2\,\omega_2^2}\right) \qquad \text{(k.15)}$$

$$\omega_2 \quad = \quad \sqrt[6]{2}\,\omega_1 \qquad \text{(k.16)}$$

Hence equation (k.12) can be rewritten as:

$$Q_2 \quad = \quad \frac{\sqrt[6]{2}}{\sqrt{2}}S^2\,Q_1 \qquad \text{(k.17)}$$

## K.3 REFERENCES

K1. Burns, J.R., Spinning Disc – Engineering Handbook. 2002, University of Newcastle upon Tyne: Newcastle upon Tyne.